

**“Henri Coandă”
AIR FORCE ACADEMY**



ROMANIA

**“General M. R. Stefanik”
ARMED FORCES ACADEMY**



SLOVAK REPUBLIC

AFASES 2017

ISSN, ISSN-L:2247-3173
DOI:10.19062/2247-3173.2017.19.1

VOLUME I



EDITORIAL BOARD

LtCol Assoc Prof Eng **Laurian GHERMAN**, PhD

Assist Prof Eng **Liliana MIRON**, PhD

Col **Adam BONDARUK**, PhD

Prof Eng **Philippe DONDON**, PhD

Prof Eng **Constantin ROTARU**, PhD

Lecturer **Mihaela GURANDA**, PhD

WO **Sergiu OBREJA**

Eng. **Mariana GHINDAOANU**

Eng. **Daniela OBREJA**

Inf. **Adina DOBRITOIU**

Publishing House of "Henri Coanda" Air Force Academy Str. Mihai Viteazu 160, Brasov
500183, ROMANIA Phone: +40 268 423 421, Fax: +40 268 422 004 Webpage:
www.afahc.ro/ro/editura/editura.html
E-mail: editura@afahc.ro

COPYRIGHT© Publishing House of "Henri Coanda" Air Force Academy All rights reserved. No part of the contents of this volume may be reproduced or transmitted in any form or by any means without the written permission of the publisher.

INTERNATIONAL SCIENTIFIC COMMITTEE

President ship:

Air Flotilla General **Vasile BUCINSCHI**, PhD, Rector of “Henri Coandă” Air Force Academy, Romania

Doc.Ing. **Jozef PUTTERA**, CSc., Rector of Armed Forces Academy of General Milan Rastislav Štefánik, Slovakia

Members:

Brigadier General **Piotr KRAWCZYK**, PhD, Polish Air Force Academy, Poland

Brigadier General **Ghita BARSAN**, PhD, “Nicolae Balcescu” Land Forces Academy, Romania

Colonel **Iulian-Constantin VIZITIU**, PhD, Military Technical Academy, Romania

Colonel **Gheorghe CALOPĂREANU**, PhD, “Carol I” National Defense University, Romania

Captain (N) **Octavian TĂRĂBUTĂ**, PhD, “Mircea cel Batran” Naval Academy, Romania

Associate Professor Eng. **Marcel HARAKAL**, PhD, Armed Forces Academy of General Milan Rastislav Štefánik, Slovakia

Professor Eng. **Milan SOPÓCI**, PhD, Armed Forces Academy of General Milan Rastislav Štefánik, Slovakia

Associate Professor **Mária PETRUFOVÁ**, PhD, Armed Forces Academy of General Milan Rastislav Štefánik, Slovakia

Associate Professor Eng. **Jaroslav KOZUBA**, PhD, Polish Air Force Academy, Dęblin, Poland

Colonel **Grzegorz ROSLAN**, PhD, Polish Air Force Academy, Poland

Martin NASSUA, PhD, Helmut Schmidt University, Deutschland

Professor **Vladimir HORAK**, PhD, University of Defense, Czech Republic

Associate Professor **Juraj HUB**, PhD, University of Defense, Czech Republic

Professor **Robert SZABOLCSI**, PhD, Óbuda University, Budapest, Hungary

Associate Professor **Slawomir AUGUSTYN**, PhD, War Studies University, Poland

Colonel **Vasile CĂRUȚAȘU**, PhD, “Nicolae Balcescu” Land Forces Academy, Romania

Colonel **Constantin ENACHE**, PhD, Military Technical Academy, Romania

Colonel **Valentin DRAGOMIRESCU**, PhD, “Carol I” National Defense University, Romania

Captain (N) **Virgil ENE-VOICULESCU**, PhD, “Mircea cel Batran” Naval Academy, Romania

Associate Professor **Ludovic Dan LEMLE**, PhD, "Politehnica" University of Timisoara, Romania

Associate Professor **Maria Dorina PAȘCA**, PhD, University of Medicine and Pharmacy, Romania

Colonel **Bogdan GRENDA**, PhD, War Studies University, Warsaw, Poland

LTC **Andrzej SOBOŃ**, PhD, War Studies University, Warsaw, Poland

Colonel **Marin MARINOV**, PhD, “Vasil Levski” National Military University, Velico Tarnovo, Bulgaria

Vanya KATSARSKA, PhD, “Vasil Levski” National Military University, Velico Tarnovo, Bulgaria

Professor **Philippe DONDON**, PhD, ENSEIRB, France

Professor **Yann LEDOUX**, PhD, Université de Bordeaux, France

Professor Eng. **Juraj MIČEK**, PhD, University of Zilina, Slovakia

Professor **Patrick SEBASTIAN**, PhD, Université de Bordeaux, France

Professor **Thierry PALIN-LUC**, PhD, Institut de Mécanique et Ingénierie, France

Professor **Vitalijs PAVELKO**, PhD, Riga Technical University, Latvia

Associate Professor **Michael TODOROV**, PhD, Technical University of Sofia, Bulgaria

Associate Professor **Valentin ILIEV**, PhD, Technical University of Sofia, Bulgaria

Associate Professor **Berangere LARTIGUE**, PhD, “Paul Sabatier” University, Toulouse, France

Associate Professor **Ciprian Ioan RĂULEA**, PhD, “Lucian Blaga” University, Romania

Assistant Professor **Constantin Edmond CRACSNER**, PhD, Ecological University, Romania

Assistant Professor **Cătălin Marius GHERASIM**, PhD, Psychology Application Center, Romania

Associate Professor **Otilia TODOR**, PhD, “Spiru Haret” University, Romania

Associate Professor **Marius-Eleodor MILCU**, PhD, “Lucian Blaga” University, Sibiu, Romania

Professor Eng. **Alex ȘTEFAN**, PhD, Manhattan Institute of Management, USA

Professor Eng. **Marian PEARSICA**, PhD, “Henri Coandă” Air Force Academy, Romania

Associate Professor Eng. **Doru LUCULESCU**, PhD, “Henri Coandă” Air Force Academy, Romania

Professor Eng. **Ion DINESCU**, PhD, “Henri Coandă” Air Force Academy, Romania

Professor **Dorin BOCU**, PhD, ”Transilvania” University of Brașov, Romania

Professor **Daniela ROSCA**, PhD, University of Craiova, Romania

Professor **Adrian ROSCA**, PhD, University of Craiova, Romania

Professor **Maria DINESCU**, PhD, National Institute for Laser, Plasma and Radiation Physics, Romania

Professor **Sterian DĂNĂILĂ**, PhD, University “Politehnica” of Bucharest, Romania

Senior Researcher **Valentin SILIVESTRU**, PhD, Romanian Research & Development Institute for Gas Turbine

Scientific Researcher Eng. **Valeriu VILAG**, PhD, Romanian Research & Development Institute for Gas Turbine

Scientific Researcher Eng. **Cleopatra CUCIUMITA**, PhD, Romanian Research & Development Institute for Gas Turbine

Scientific Researcher Eng. **Jeni POPESCU**, PhD, Romanian Research & Development Institute for Gas Turbine

Professor Eng. **Adrian STOICA**, PhD, University “Politehnica” of Bucuresti, Romania

Professor Eng. **Gavrilă CALEFARIU**, PhD, “Transilvania” University of Brasov, Romania

Associate Professor Eng. **Aurelian Flavius SÎRBU**, PhD, “Transilvania” University of Brasov, Romania

Associate Professor **Daniela BELU**, PhD, “Henri Coandă” Air Force Academy, Romania

Associate Professor Eng. **Petrisor PÂRVU**, PhD, University “Politehnica” of Bucuresti, Romania

Associate Professor Eng. **Marius Cristian LUCULESCU**, PhD, “Transilvania” University of Brasov, Romania

Professor **Răzvan - Lucian ANDRONIC**, PhD, “Spiru Haret” University, Romania

Associate Professor **Anca-Olga ANDRONIC**, PhD, “Spiru Haret” University, Romania

Professor Eng. **Luciana CRISTEA**, PhD, “Transilvania” University of Brasov, Romania

Professor Phys. **Sorin Constantin ZAMFIRA**, PhD, “Transilvania” University of Brasov, Romania

Professor Eng. **Șerban BOBANCU**, PhD, “Transilvania” University of Brasov, Romania

Associate Professor Eng. **Răzvan UDROIU**, PhD, “Transilvania” University of Brasov, Romania

Associate Professor Eng. **Horațiu TEODORESCU-DRĂGICESCU**, PhD, “Transilvania” University of Brasov, Romania

Associate Professor Eng. **Cristin MORARIU**, PhD, “Transilvania” University of Brasov, Romania

Associate Professor Eng. **Mihai MIHĂILĂ-ANDRES**, PhD, Military Technical Academy, Romania

Scientific Researcher **Sorin CHEVAL**, PhD, National Meteorological Administration, Romania

Professor **Petrică VIZUREANU**, PhD, “Gheorghe Asachi” Technical University, Romania

Professor **Corneliu UDREA**, PhD, University of Pitesti, Romania

Professor **Ștefan-Gheorghe PENTIUC**, PhD, "Stefan cel Mare" University, Romania
Associate Professor **Marin VLADA**, PhD, University of Bucuresti, Romania
Scientific Researcher Eng. **Marius RĂDULESCU**, PhD, S.C. "Electromecanica"
Company of Ploiesti, Romania
Colonel **Gabriel RĂDUCANU**, PhD, Air Force Staff, Romania
Psychologist **Daniela HIERA**, PhD, Romanian College of Psychologist
Senior Researcher **Alexandru DUMITRACHE**, PhD, Institute of Mathematical
Statistics and Applied Mathematics
Professor **Romulus LUNGU**, PhD, University of Craiova, Romania
Mihai MACHEDON-PISU, PhD, "Transilvania" University of Brasov, Romania
Gheorghe RADU, PhD, "Henri Coandă" Air Force Academy, Romania
Mihai MIRON, PhD, "Transilvania" University of Brasov, Romania
Associate Professor **Alexandru Nicolae TUDOSIE**, PhD, University of Craiova,
Romania
Professor **Ioan NICOLAESCU**, PhD, Military Technical Academy, Romania
Associate Professor **Răzvan NECHIFOR**, PhD, Military Technical Academy,
Romania
Associate Professor **Cristian MOLDOVEANU**, PhD, Military Technical Academy,
Romania
Associate Professor **Ion PURICEL**, PhD, National Defense University "Carol I",
Romania

ORGANIZING COMMITTEE

CHAIR:

Lt.Col. **Laurian GHERMAN**, PhD

MEMBERS:

Col. **Ionică CÎRCIU**, PhD

Col. **Vasile ȘANDRU**, PhD

Cdor. **Marian BOBE**

Professor **Traian ANASTASIEI**, PhD

Professor Eng. **Constantin ROTARU**, PhD

Assistant Professor Eng. **Constantin STRÎMBU**, PhD

Assistant Professor Eng. **Liliana MIRON**, PhD

Assistant Professor **Mihaela SMEADĂ**, PhD

Assistant Professor **Mihaela GURANDA**, PhD

Assistant Professor Eng. **Vasile PRISĂCARIU**, PhD

Maj. **Alexandru-Iosif ROMAN**

Lt.Col. **Sorin VÂNT**

Ec. **Octavian ISĂILĂ**

Ec. **Sebastian POP**

LOGISTICS:

WO **Marian MIHALACHE**

WO **Marius TĂNASE**

WO **Călin DOBREAN**

WO **Deneș SZABO**

WO **Marius CODREANU**

SECRETARIAT:

WO **Sergiu OBREJA**

Eng. **Mariana GHINDĂOANU**

Eng. **Daniela OBREJA**

Inf. **Adina DOBRIȚOIU**

CONTENTS

VOLUME I

AERIAL SYSTEMS AND AEROSPACE ENGINEERING	Page
Marius ALEXA, Cătălin CIOACĂ <i>STUDY OF HIGH LEVEL ARCHITECTURE APLICABILITY IN AIR DEFENSE</i>	15
Irina Carmen ANDREI, Constantin ROTARU, Maria Cristina FADGYAS, Gabriela STROE, Mihai Leonida NICULESCU <i>NUMERICAL INVESTIGATION OF TURBOJET ENGINE THRUST CORRELATED WITH THE COMBUSTION CHAMBER'S PARAMETERS</i>	23
Irina Carmen ANDREI, Constantin ROTARU, Maria Cristina FADGYAS, Gabriela STROE, Mihai Leonida NICULESCU <i>NUMERICAL INVESTIGATION OF MIXED FLOWS TURBOFAN ENGINE THRUST CORRELATED WITH THE COMBUSTION CHAMBER'S PARAMETERS</i>	35
Ana-Maria BĂLDEA, Mihaela GARABET <i>INFORMATION MANAGEMENT IN UAS MULTIAGENT</i>	49
Bertold BÉKÉSI, Peter KORONVÁRY <i>ARE DRONES A BOON OR BANE?</i>	55
Viorel-Eugen BITAN, Valeriu CĂLIN <i>ASPECTS REGARDING SAFETY SYSTEM IN SURFACE-TO-AIR MISSILE FIRINGS</i>	65
Adam BONDARUK, Jarosław KOZUBA <i>EVALUATION OF TACTICAL MISSION EXECUTION</i>	71
Adam BONDARUK, Jarosław KOZUBA <i>SELECTED ASPECTS OF AVIATION COMMUNICATION</i>	79
Oliver CIUICĂ, Carmen ȘTEFAN, Serjii OBREJA, Nicolae CREȚU <i>ROMANIAN AIR FORCE AVIATION OCCURRENCES</i>	89
Ioan CURTA, Ileana Constanta ROSCA, Ciprian ENE, Marian Nicolae VELCEA, Ionel MOHIRTA <i>STRESS ASSESMENT USING MODERN MEASUREMENTS METODS</i>	99
Dumitru DINU <i>PSYCHOLOGICAL PROTECTION OF TROOPS WITHIN THE NEW CONTEXT OF THE MILITARY NORMATIVITY</i>	109
Alexandru DUMITRACHE, Mihai-Victor PRICOP, Mihai-Leonida NICULESCU, Marius-Gabriel COJOCARU, Tudor IONESCU <i>DESIGN AND ANALYSIS METHODS FOR UAV ROTOR BLADES</i>	115
Andrei-Mihai LUCHIAN, Mircea BOȘCOIANU, Elena-Corina BOȘCOIANU <i>NOISE REDUCTION IN MULTIPLE RFID SENSOR SYSTEMS USED IN AEROSPACE ENGINEERING</i>	127
Razvan-Viorel MIHAI, Alexandru RADU, Ovidiu TABAN <i>PROTOTYPING A LOW-COST EMBEDDED AIRSPEED SYSTEM</i>	133

Laurențiu MITITELU <i>SIMULATION TRAINING AND THEIR ROLE IN THE OPERATING INSTRUCTION OF FIGHTING SQUADRON</i>	141
Dinu PĂDURARIU, Nicolae CREȚU <i>HELICOPTERS DURING MARITIME MISSIONS</i>	145
Filip PANAYOTOV, Ivan DOBREV, Fawaz MASSOUH, Michael TODOROV <i>NUMERICAL STUDY ON THE INFLUENCE OF WAKE CONTRACTION ON THE COMPUTATIONAL ACCURACY AND RAPIDITY OF A MODEL OF A ROTOR IN HOVER</i>	153
Marius PANDELEA, Mircea BOȘCOIANU, Mădălina-Marina FRĂȚILĂ, Victor VLĂDĂREANU <i>CONCEPTUAL METHOD OF NAVIGATING AND CONTROLLING A DRONE</i>	165
Sebastian POP, Octavian ISAILĂ, Dragoș PREDA, Andrei-Mihai LUCHIAN <i>RISK MANAGEMENT REGARDING THE USE OF UAV IN THE MODERN AIR SPACE</i>	171
Mihai-Victor PRICOP, Mircea BOȘCOIANU, Cătălin NAE, Marius-Gabriel COJOCARU <i>MICROFIGHTER AS AN ALTERNATIVE TO FOURTH GENERATION FIGHTER PLANES</i>	177
Vasile PRISACARIU, Alexandru CIUBOTARU <i>ASPECT REGARDING OF THE PRATT & WHITNEY F100 JET ENGINE PERFORMANCES</i>	187
Marius RĂDULESCU <i>UNIFORMITY AND STANDARDIYATION OF THE AIR DEFENSE WEAPONS</i>	195
Mihai RADULESCU, Victor VLADAREANU <i>AERIAL PHOTOGRAPHY AND THE USE OF PHOTO CAMERAS ATTACHED TO DRONES</i>	201
Carmen ȘTEFAN, Oliver CIUICĂ <i>DISTANCE LEARNING SYSTEM FOR THEORETICAL TRAINING OF PILOTS</i>	207
Cornel STOICA, Dumitru PEPELEA, Mihai NICULESCU, Adrian TOADER <i>AERODYNAMIC DESIGN CONSIDERATIONS OF A FLYING WING TYPE UAV</i>	213
Peter SZEGEDI, Peter KORONVÁRY, Bertold BÉKÉSI <i>THE USE OF ROBOTS IN MILITARY OPERATIONS</i>	221
Alexandru Nicolae TUDOSIE <i>CONTROL LAWS FOR AN AIRCRAFT SUPERSONIC INLET WITH MOBILE PANEL</i>	231
Alexandru Nicolae TUDOSIE, Madalina-Luciana PAUNESCU <i>AUTOMATIC CONTROL SYSTEM FOR AN AIRCRAFT PLAN SUPERSONIC INLET WITH MOBILE PANEL</i>	243

ELECTRICAL AND ELECTRONIC ENGINEERING/ RENEWABLE ENERGY AND ENVIRONMENT

Bogdan Cornel BENEĂ <i>BIODIESEL PRODUCTION USING SOLAR ENERGY</i>	253
Mirela COMAN, Bogdan CIORUȚĂ <i>CONSIDERATIONS ABOUT THE INFLUENCE OF CLIMATE CHANGES AT BAIĂ MARE URBAN SYSTEM LEVEL</i>	257
Andreea DRĂGHICI, Titus BĂLAN <i>REMOTE DETECTION AND TRACKING OF ALCOHOL CONCENTRATION FOR CAR DRIVERS</i>	263
Laura Mihaela LELUȚIU, Marius Dan BENEĂ <i>STUDY AND CONSTRUCTION OF AN AMPEROMETRIC POTENTIOSTAT SUITABLE FOR USE IN ENVIRONMENTAL MONITORING</i>	269
Valentin MÜLLER, Monica SZABO <i>DETERMINING THE CAPACITY CONDENSER VALUE AT SINGLE-PHASE MOTOR SPEED CHANGE</i>	275
Cristian VIDAN, Daniel MĂRĂCINE <i>STUDYING THE POSSIBILITY OF INCREASING THE FLIGHT AUTONOMY OF A ROTARY-WING MUAV</i>	279
MECHANICAL ENGINEERING. MATERIALS AND TECHNOLOGY	
Cornel ARAMĂ, Lavinia ARAMĂ, Mariana ARAMĂ <i>A STUDY ON THE VEHICLE EVALUATION METHODS IN JUDICIAL TECHNICAL EXPERT REPORTS</i>	285
Ion DINESCU <i>EXPERIMENTAL RESEARCH ON POWDER PROPERTIES RESULTING IN BEARING RECTIFYING</i>	291
Linh DO DUC, Vladimír HORÁK, Tomáš LUKÁČ, Vladimír KULISH <i>DYNAMICS OF RECOIL SIMULATION DEVICE POWERED BY CARBON DIOXIDE</i>	295
Daniela Georgiana GOLEA, Lucian Ștefan COZMA <i>THE MAGNETIC PROPERTIES OF MATERIALS AND NEW MILITARY APPLICATIONS OF THEM</i>	305
Tomáš LUKÁČ, Roman VÍTEK, Linh DO DUC, Vladimír HORÁK <i>DYNAMICAL ANALYSIS OF THE GAS POWERED IMPULSE GENERATOR</i>	315
Ionel POPESCU, Lică FLORE, Albert ARNAU CUBILLO <i>DERIVATION OF MASS, STIFFNESS AND DAMPING MATRICES OF A MODEL WING FROM EXPERIMENTAL MODAL DATA</i>	323
Horatiu TEODORESCU-DRAGHICESCU, Mariana Domnica STANCIU, Florin TEODORESCU-DRAGHICESCU <i>NEW COMPOSITE SANDWICH WITH ALUMINUM CORE</i>	331
Béla VARGA, Gyula ÓVÁRI, László KAVAS <i>GAS TURBINE ENGINE COMBUSTORS AND THE ESTIMATION OF THEIR PRESSURE LOSS</i>	337

APPLIED MATHEMATICS, COMPUTER SCIENCE & IT	
Alexandra BĂLUȚĂ, Diana ROTARU, Mihaela ILIE, Dragoș FĂLIE, Eugen VASILE <i>TRANSITION PROBABILITY MODELING FOR QUANTUM OPTICS</i>	345
Costin ENE, Adrian-Mihail STOICA, Petrisor-Valentin PARVU <i>AUTOPILOT DESIGN DOR THE LATERAL-DIRECTIONAL MOTION OF AN UAV</i>	357
Bogdan GOHOREANU, Florin SANDU, Dan-Nicolae ROBU <i>SOLUTIONS FOR SECURITY ENHANCEMENTS IN DIGITAL NETWORKS</i>	365
Cosmin-Constantin IACOB, Gabriel BORSOS, Gavrilă CALEFARIU <i>THE MANAGAMENT OF BALLISTIC OPERATIONS USING MATLAB SOFTWARE</i>	371
Mircea LUPU, Gheorghe RADU, Cristian-George CONSTANTINESCU <i>ANALYTIC-NUMERIC METHODS IN THE VALIDATION OF ANY FLOW REGIMES IN HYDRO-AERODYNAMICS</i>	379
Ioan MILOSAN <i>APPLICATION OF THE CHAUVENET CRITERION TO DETECTION OF THE ABERRANT DATA OBTAINED IN THE INDUSTRIAL PROCESSES</i>	389
Bogdan CIORUȚA <i>REGARDING A CONTINUOUSLY DIFFERENTIABLE FRICTION MODEL USED FOR CONTROL OF DYNAMIC SYSTEMS DESIGN</i>	393

VOLUME II

MANAGEMENT & SOCIO-HUMANITIES	
Anca-Olga ANDRONIC, Răzvan-Lucian ANDRONIC <i>REGULATED AND ALTERNATIVE SERVICES ACTING IN MENTAL HEALTH</i>	15
Anca-Olga ANDRONIC, Răzvan-Lucian ANDRONIC <i>COMMUNITY-BASED MENTAL HEALTH SERVICES IN ROMANIA</i>	19
Cristiana BALAN <i>SCHOOL TODAY, BETWEEN LIMITS AND OPPORTUNITIES</i>	23
Cristiana BALAN <i>MEDIATIZED VIOLENCE AND ITS INFLUENCE ON YOUNG PEOPLE</i>	29
Daniela BELU <i>REASON VERSUS EMOTION IN THE INDIVIDUAL APPROACH OF STRESS MANAGEMENT</i>	35
Angela BLOGUȚ <i>SUBSTANTIATION OF THE OPPORTUNITY AND NEED OF PSYCHOLOGICAL EVALUATION OF THE AIRCREW PERSONNEL</i>	41
Ionel BOSTAN, Vasile Cosmin NICULA <i>INTERVENTIONS ON THE LEGAL FRAMEWORK OF FINANCIAL-BUDGETARY REASONS OF NATIONAL DEFENSE</i>	49
Cătălin CIOACĂ, Alexandru BRATU, Daniel ȘTEFĂNESCU <i>THE ANALYSIS OF BENCHMARKING APPLICATION IN CYBER SECURITY</i>	57
Georgeta Gabriela CORNEA <i>THE EFFICIENCY OF AEROBIC GYMNASTICS PATTERNS IN THE PHYSICAL EDUCATION ACTIVITIES AT PRESCHOOL CHILDREN</i>	63
Georgeta Gabriela CORNEA <i>FORMATIVE VALENCES OF LOGICAL-MATHEMATICAL GAMES FOR PRESCHOOLERS</i>	69
Gherasim Solovestru DOMIDE <i>10 YEARS OF INSURANCE BROKERAGE IN ROMANIA. EVOLUTION. PERSPECTIVES</i>	73
Ana Maria FURTUNA <i>THE CHILD WITH MOTOR DISABILITIES AND HIS RELATIONSHIP WITH THE FAMILY</i>	77
Ana Maria FURTUNA <i>ASPECTS OF PHYSICALLY DEFICIENT CHILDREN'S RELATIONS WITH THE FAMILY AND THE EDUCATIONAL ENVIRONMENT</i>	83
Doru GALAN, Gheorghe MIHALACHE <i>THE KNIFE - ATTACKING AND DEFENSIVE DANGEROUS WEAPON</i>	93
Doru GALAN, Gheorghe MIHALACHE <i>STUDY ABOUT THE USAGE OF BODYBUILDING ELEMENTS IN THE PSYCHO-PHYSICAL PREPARATION OF UNITS WITH SPECIAL STATUS</i>	101
Irina IOANA, Edmond CRACSNER <i>THE TERROR OF SUICIDE</i>	113

Diana Cristiana LUPU, Daniel Silviu NICULAE <i>THE BALKAN PACT – HISTORY AND MODERNITY</i>	123
Cristian PANAIT <i>EMOTIONAL INTELLIGENCE IN LEADERSHIP</i>	133
Alina PAPOI <i>THE PILOT TRAINING IN THE “MILITARY ROMANIA” JOURNAL</i>	139
Maria PETKOVA <i>PROBABILITY ASSESSMENT OF POSSIBLE VOLCANIC ASH CONTAMINATION FOR THE BULGARIAN AIRSPACE BY DEVELOPING OF EVENT TREE AND RISK MATRIX FOR HYPOTHETICAL VOLCANIC ERUPTION</i>	143
Maria PETKOVA <i>CASE-STUDY FOR A HYPOTHETICAL ERUPTION OF ETNA AND THE APPROPRIATE WEATHER CONDITIONS FOR DISPERSION OF VOLCANIC ASH TO BULGARIAN AIRSPACE</i>	149
Aureliana-Loredana PETRE <i>THE IMPACT OF ALTERNATIVE ASSESSMENT STRATEGIES ON STUDENTS</i>	157
Aureliana-Loredana PETRE <i>THE ROLE OF CONSTANT AND CONTINUOUS FEEDBACK ON STUDENTS’ LEARNING MOTIVATION</i>	161
Raluca RĂDUCEA <i>EVOLVING NORMS OF MILITARY INTERVENTION: BETWEEN LEGITIMIZING ACTIONS AND SHAPING STATE BEHAVIOUR</i>	167
Roxana MAIER, Marinela SÎRBU <i>STREAMLINING THE WORK OF SOCIAL WORKERS THROUGH THE OPTIMIZATION OF CERTAIN CHARACTERISTICS OF EMOTIONAL INTELLIGENCE</i>	175
Peter SZEGEDI <i>UAVs AND THE MILITARY LEADERSHIP</i>	179
Mirela TÂRNOVEANU, Monica PURCARU <i>CONSIDERATIONS UPON THE METHODS OF TEACHING MATHEMATICS IN PRIMARY SCHOOL</i>	189
Mirela TÂRNOVEANU, Monica PURCARU <i>SPECIFIC ASPECTS OF THE DIFFERENTIATED ASSESSMENT IN MATHEMATICS LESSONS IN SECONDARY SCHOOL</i>	195
Rodica ȚOCU <i>ADAPTATION TO THE STUDENTS’ EDUCATIVE REQUIREMENTS BY DEVELOPING TEACHER’S CREATIVITY</i>	207
Rodica ȚOCU <i>PEER VICTIMIZATION: FROM PRESCHOOL TO ADULTHOOD</i>	211
Mihaela Alina TOROK <i>PRACTICAL GUIDELINES FOR PRACTICING PSYCHOMOTRICITY</i>	217
Jozsef TOTH, Krisztina FEHÉR <i>METHODOLOGICAL QUESTIONS OF COST–BENEFIT ANALYSIS FOR PROJECTS CONNECTED WITH APPLICATION OF ALTERNATIVE FUELS IN PUBLIC AVIATION</i>	225
Florin VANCEA <i>THE BODY INTELLIGENCE - DESCRIPTION AND MEASUREMENT</i>	231

<p>Florin VANCEA <i>PSYCHOLOGICAL MATURITY AND INTEGRATIVE THREE-DIMENSIONAL STRUCTURE ANXIETY- DEPRESSION-SELF- DISSATISFACTION</i></p>	<p>235</p>
<p>Corina Mihaela ZAHARIA, Dumitru GRIGORE, Magda MOLDOVAN <i>DETERMINING PERSONALITY PROFILE THROUGH INFERENTIAL METHOD BY EDA NEUROSIGNALS</i></p>	<p>241</p>
<p>Andrei ZOTA <i>DEVELOPMENT OF THE INFORMATION MANAGEMENT WITHIN THE ROMANIAN MILITARY ENTITIES PARTICIPATING IN JOINT OPERATIONS</i></p>	<p>257</p>

STUDY OF HIGH LEVEL ARCHITECTURE APLICABILITY IN AIR DEFENSE

Marius ALEXA*, Cătălin CIOACĂ**

* Air Forces Simulation Training Center, Boboc, Romania (alexamarius@yahoo.com)

** „Henri Coandă” Air Force Academy, Braşov, Romania (catalin.cioaca@afahc.ro)

DOI: 10.19062/2247-3173.2017.19.1.1

Abstract: *Today we live in a complex world, in a complex environment; we are used to having a complex life, supported by a lot of technology, automatic tools, which is supposed to be sustained by more and more resources. In all domains of activities modeling and simulation are designated to resolve the problem of time spending and resources. In high technical domains, which involve well prepared operators, like air defense artillery and aviation, the main skills are formed and improved through many hours of theory and practice on a specific simulator. Virtual and constructive simulators had begun to play a main role and the users can't operate in real until they practice some hours on specific simulator. Serious games and multilevel simulator represent the key for the epistemic learning and in the present project we established another program simulation for Air Defense Artillery. This program is trying to connect two type of simulation (constructive and virtual simulation) and is designated to train command-control staff and Fire Control Unit users.*

Keywords: *high level architecture, simulation program, air defense, fire control system, serious games*

1. INTRODUCTION

Multilevel simulation is not a new concept, but it has new implications and applications in simulation training and is designated to train individual operators and Command and Control (C2) staff. In air defense artillery C2 staff and Fire Control Unit (FCU)/ gun operators work together like an individual entity and time is the main adversary for both. Working together they are supposed to respect the procedures and to do hours of rehearsals. The rehearsals have to be made on simulators and after that the staff and operators can operate in real [1].

For training, both staff and operators should connect constructive, virtual and real simulators in one physical model – multilevel simulation. Now the Romanian army has some individual simulators (aviation, naval, land and air defense), but that model works independently and trains the operator individually, in individual scenarios.

Multilevel simulation is a federation model, a connection between constructive, virtual and real simulations and that connection is done with High Level Architecture (HLA). HLA is a standard essential part of a multilevel simulation and is the key for models like that. Technically it is a procedure, a common language between different types of simulations [2,3].

Another essential part of training is represented by software and models designated to train real people, not only theoretically but also in practice and epistemic learning too. That kind of model is called serious games and is the future key for learning and training skills [4].

A serious game is a model which is almost similar with real model and is necessary to follow the same pattern, operation control and procedures like the original. The beneficiary has the opportunity to train in real-like conditions and the differences have to be almost zero, with some exception (eg. can't simulate the gravitational force).

Finally, the purpose of the multilevel simulator is to give a feedback to C2 staff representing the results of plans and planning, generating reports and training the staff in making decisions in the military process. The staff has the opportunity to restart one or more procedures if something is wrong with the execution of the plan.

After hundreds of hours of training on the multilevel simulator, the mission itself will not be anything other than training „somewhat serious”. This explains the success of NATO fighter-bomber aviation which plays out the tasks and missions with a very low rate of failure [5].

2. THE DESIGN OF HLA

The High Level Architecture (HLA) is a standard that enables all types of simulation systems to work together. The simulations systems need to work together in such a way that they can achieve an overarching goal by exchanging services.

According with the “Practical guide for developing distributed simulations”, there are five important concepts regarding HLA [6]:

1. The Runtime Infrastructure (RTI) is a part of software that provides the HLA services. The main service is to send and receive the right data to the right receiver.
2. The Federate is a system that connects a simulator to the RTI. Each federate can model any number of objects in a simulation; it can connect one aircraft simulator with one air defense simulator and both can be connected with a constructive simulator.
3. The Federation is all federates together with the RTI that they connect to and the FOM that they use. That is the group of system that interoperates.
4. The Federation Object Model (FOM) is a file that contains a description of the data exchange in the federation. This can be seen as the language of the federation.
5. The Federation Execution is a session when the federation runs. If you run the federation several times you will have several federation executions.

Runtime Infrastructure (RTI) is a basic topology formed by a number of simulations that have one single connection to a service bus (Fig. 1).

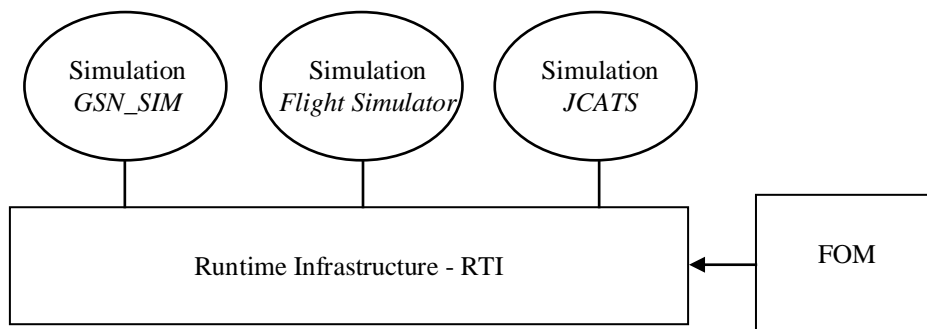


FIG. 1. The RTI architecture

Support Services are a number of utilities and here is the full list, in the order that the HLA standard describes them:

1. Federation Management (keep track of federation executions and federates, synchronization points, save/store);
2. Declaration Management (publish and subscribe of object and interaction classes);

3. Object Management (registering and discovering object instances, updating and reflecting attribute);
4. Ownership Management (transfer or modeling responsibilities);
5. Time Management (handling of logical time including delivery of time stamped data and advancing federate time);
6. Data Distribution Management (filtering based on data values);
7. Support Services (utility function);
8. Management Object Model (inspection and management of the federation).

For example, Simulation Generator (SimGe) is a fully-dressed HLA object model editor, simulation design and development environment, and a code generator that is intended to generate code automatically for HLA based distributed simulations [7]. The target platform for code generation is an HLA Runtime infrastructure abstraction layer called RTI abstraction component for .NET (RACoN). The architecture of the generated code by SimGe conforms to the layered architectural style.

3. SPECIFIC REQUIREMENTS

Oerlikon Contraves 35 mm caliber air defense system is an automated system designated to protect different objectives (eg. HQs, air bases). If the radar (SHORAR-TCP), Gun*Star Night and 35 mm Gun Air Defense System is engaged in a permanent position, according with the Drill Book a complete reconnaissance needs to be made only once [8].

Usually the position of Search Radar, FCUs, Guns and PSUs is fortified or protected in some way. Also the ammunition dump, first aid post and quarters can be constructed and perhaps coordinated with the installation of the defended critical asset or vital point.

The communication systems can be permanently installed. A typical critical asset of this type is an air-base or a land forces-base. In this case the defense system should be coordinated with the activities of the Air Force or Land Force. A lot of infrastructure can be used by air defense, too.

The Oerlikon Contraves 35 mm caliber air defense system is a complex one which works in a centralized mode and is mainly composed of [9]:

1. SHORAR TCP is designated for search, detection, identification and automatic target accompany. The SHORAR has the main role of managing the air space security and optimizing the air targets data to the fire control system Gun*Star Night.

2. Gun*Star Night is an automated subsystem designated to control two sets cannons. It is based on electro-optical tracking system and equipped with a computer to calculate ballistic trajectory and the timing of the fire release.

Fire control system Gun*Star Night provides the following main operations:

- a) receives data on air targets at SHORAR TCP or its digital optical viewfinder (DOS);
- b) evaluates the potential air attack in the area of responsibility (in decentralized mode);
- c) searches, finds and identifies the target;
- d) accompanying three-dimensional target (finders using laser and electron-optical system);
- e) calculates angles of sight for guns;
- f) forwards angles in gun sights.

3. Digital Optical Sight (DOS) is operated by a single operator and is designated to search air targets and send data to GSN. DOS is the main Intel sensor when GSN works in decentralized mode and receives data only from this subsystem.

4. Anti-aircraft automatic guns (AOKs) comprises two 35 mm caliber and are designated to fire directly against air targets or field targets, coordinated by GSN or by an individual.

A usual scenario looks like this: SHORAR-TCP radar is searching the air space and detects a target at 28 km; it identifies the target as friend/ non-friend and sends data to the GSN which has the best position in AOR or is ready to combat.

Sending data to one or more GSN is made according to the best course of action and according to the value of the target. This is a procedure that is one of the most important part of the military decision making process and is a quick and short one.

GSN is requiring the target and it follows it with infrared camera. The target's data are continuously updated by computer and laser telemeter and when the target is in the fire area, AOK can open fire against it conducted by FCU.

The output laser device wavelength is 1.54 μ m. In normal conditions of utilization, this laser device is considered eye safe as defined under class 3A in accordance with the EN 60825-1 classification. To prevent permanent injury to the human eye is strongly recommended never to view at the laser directly or with optical instruments (lenses, binoculars).

The whole system (two sets cannons and fire control system) is powered by electricity, with voltages of 220V AC and 110V DC. In order to work independently of the national electricity network in any place and time conditions, voltages are provided by two sets, running on leaded petrol, with a consumption of 24 l/h, and a generating set of low power, functional unleaded petrol, with a consumption of 1.5 l/h. Thus we can realize the costs involved in preparing a one-man operator, since the basic and advanced skills needed require at least three training phases, each phase taking place over a period of 2-3 weeks.

4. FIRE CONTROL SYSTEM GUN*STAR NIGHT SIMULATOR

GSN SIM is a simulation program for fire control Gun*Star Night system destined for learning and involvement of the operators and staff, for training and improving their skills in order to shorten the preparation time and training costs.

The model is a multilevel simulator. The FCU simulator (for individual operator) and the console (for staff or instructor) are connected and are working together, sending and receiving data and generating reports to staff about how the operator works.

Simulation software can be a way to train even when, for some reason, the technique is unable to be efficient. It also represents a necessary learning tool for the main menus and submenus and the presentation of the art verification algorithms. In current conditions, modern combat no longer leads through direct contact with the enemy, but it is based on information received from higher echelons or the discovery and tracking of its equipment.

Respecting the laws of modern conflict, fire control Gun*Star Night system flies over the target and gathers information from the research station (radar) to senior and displays them on the video display. Target data are displayed while the operator has selected the option of designating the target by radar and has been aligning with the radar.

If these operations are not performed the display will show data on the flight parameters of the target. Besides fire control interface device, the frame main menu, we created a help menu designed to facilitate the understanding of the operation of the simulator. Everything here may be introduced by the instructor or operator of the target flight and the parameters can evolve.

The success of operations depends not only by the operator, but the staff too; a good planning and a good management of forces will lead to success. If staff doesn't respect the procedures or if plans have some weaknesses, then it is possible to fail mission, even if the operators do everything in according with procedures. Failing a mission can be possible because the system counts all plan's details (location, points of view, no-go or slow-go zone) and too many weaknesses of planning affect the military operation.

The simulator respects the rules and principals of serious games, the rules of real systems simulation [10, 11]. For example, the background of FCU screen is represented by pictures tacked from Capu Midia, the camera can be moved from mouse, the fire trigger has two positions - FIRE/SAVE (Fig. 2).

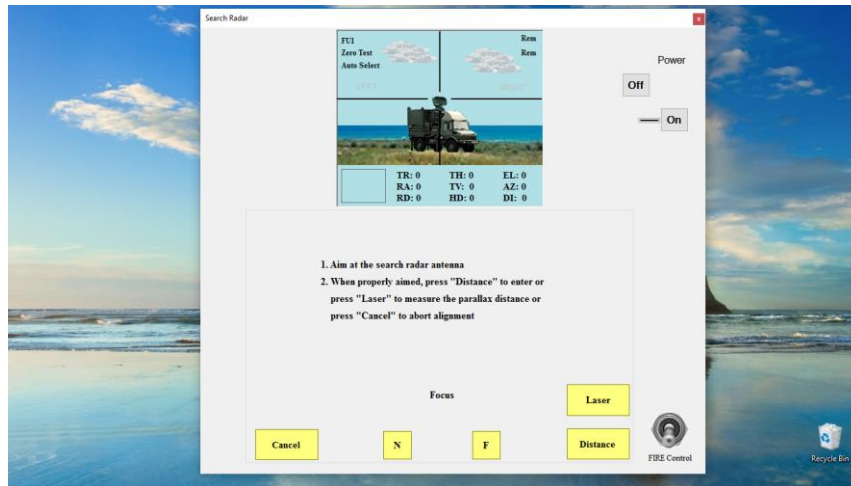


FIG. 2. Capture from GSN SIM

The operator or staff/instructor can operate in some different predefined scenarios, each scenario having a different location, weather and targets. Also the weather can be selected by operator or staff (instructor) and can affect the possibility of target combating.

The locations are the same with real locations. They respect the distances, the predefined point of view and the orientation points too, the Nord, no-go or slow-go zone.

Also, in the same idea of respecting principles of serious games, all procedures and activities have their roll in accomplishing the mission successfully.

For example, if the operator doesn't proceed to do the mount adjustment in according with procedures that will seriously affect the fire probability and it is possible to fail the mission.

Another essential point in respecting rules of a serious game is represented by left and right limits of the polygon, materialized on the field. Operators and the staff have to pay attention to the left and right limits of the polygon and these values must be operated from the *Firing menu*. Both – servo and fire sectors – have their roles in working in safety and in air security management. For staff is important to designate the right target to the right GSN and for operator is important not to fire in non-secure area.

It is important to know that the left and right limits have different values, in according with FCUs and AOKs position. The limits value depends of the point of view and the operators have to pay attention to that, because the computer automatically calculates the angles between FCUs, AOKs and limits.

In according with Romanian Army disposal about simulation training, to create a connection between virtual, real and constructive simulation in a multilevel simulation with HLA, in this model we constructed a set of values (data) that are necessary for RTI function, and here are only some examples:

SearchRadarAzimuthValoare, SearchRadarElevationValoare, FunctionalCheck, SearchRadarDistanceValoare, SearchRadarTiltValoare, GunStarEastValoare, GunStarNorthValoare, GunStarAltitudeValoare, CRPEastValoare, CRPNorthValoare, CRPAltitudeValoare, SearchRadarEastValoare, SearchRadarNorthValoare, GunStarEastTemp, SearchRadarAltitudeValoare, CRPNorthTemp, GunStarNorthTemp, GunStarAltitudeTemp, CRPEastTemp, CRPAltitudeTemp, NrSalve, SearchRadarEastTemp, SearchRadarNorthTemp, SearchRadarAltitudeTemp, ReferencesAzimuth, SearchRadarUnitValoare, ReferencesOrientation, MountElevation, ReferencesElevation, MountAzimuth.

On the video display device of fire control Gun*Star Night system there are displayed information about the target (Fig. 3).

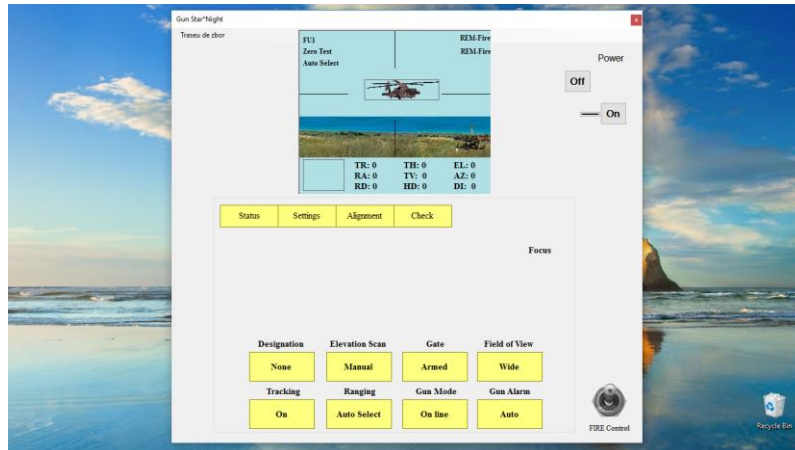


FIG. 3. Information about target

This information is vital in engaging the fight, so the operator needs to know and know how to interpret them very well. Next we will present information and their interpretation:

- TR / Track Number: number of targets designated by unit fire;
- AR / Radar Azimuth: angular position value SHORAR-TCP research station to the fire control system;
- RD / Radar Distance: parallax offset distance in feet from the research station;
- TH / Target Height: once target height in meters;
- TV / Target Velocity: target speed in m/s.

Information designated by the discovery and identification of its equipment:

- HD / HIT Distance: distance measured to the point of impact between the target and the projectile beam, calculated in meters;
- EL / Line of Sight Elevation: elevation angle of the target to fire control system;
- AZ / Line of Azimuth: azimuth angle of the target to fire control system;
- DI / Target Distance: distance inclined to direct fire control system to the target;
- T / Distance Tracing Mode: how to determine the distance to the target.

On the other side the simulator respects the number of fire, the probability on hit a target; if a target is in the fire area and the operator, with a well prepared system, succeeds to open fire against target with 6 to 8 shots, then there is a big probability to hit and accomplish the mission.

If the FCU's operator doesn't succeed to open fire or the number of shots is insufficient, then the target will fly away or can hit the system, and that means the mission is failed. We will exemplify that with some codes realized in VisualStudio focused on opened fire:

```
private void FireButton_MouseDown(object sender, MouseEventArgs e)
{
    if((NorthDirection == true)&&(OpticalSight == true)&&(AOKsGuns1 == true)&&(AOKsGuns2 ==true)&&(SearchRadar == true) &&(MountAdjustment == true))
```

```
{
  if ((NrSalve >= 6)|| (NrSalve <= 8))
  {
    Explosion.Visible = true;
    field.Location = new Point(flagX, flagY);
    nori.Location = new Point(70, 16);
    nori1.Location = new Point(204, 27);
    Target.Visible = false;
    difference = 0;
  }
  else
  {
    FireButton.Image = Image.FromFile(@"\\ON.gif");
    if((NorthDirection == true)&&(OpticalSight ==
true)&&(AOKsGuns1 == true)&&(AOKsGuns2
==true)&&(SearchRadar ==
true)&&(MountAdjustment == true))
    if (countpozitie < 700)
    {
      legaturatun1.Text = "REM-Fire";
      legaturatun2.Text = "REM-Fire";
      NrSalve = NrSalve + 1;
      System.Media.SoundPlayer player = new
System.Media.SoundPlayer(@"\\fire.wav");
      player.Play();
      difference = -1;
    }
    else
    {
      field.Location = new Point(flagX, flagY);
      nori.Location = new Point(70, 16);
      nori1.Location = new Point(204, 27);
      LeftButton.Visible = true;
      RightButton.Visible = true;
      Target.Visible = false;
      difference = 0;
    }
  }
}
```

In that new *GSN SIM* we implemented the rules of engagement: the target with the highest value is the most important target; more than that, the operator has the opportunity to combat a target and on command or by himself he can combat another target, according with the operation plans.

In order to test the way that an operator respects the rules of engagements, in *GSN SIM* there are present some air and field targets, in a check list. The operator or instructor has the possibility to choose one or more targets to be combated. Also one can select the order and time for action and these targets will respect the list.

This *GSN SIM* will be connected with another simulator model, like *Microsoft Flight Simulator* or *JCATS (Joint Conflict and Tactical Simulation)* in a multilevel simulator, via HLA standard.

This multilevel simulation model will train aviation, air defense artillery and radar, working together, and staff will be able to plan a joint operation, and more than that, will be able to see if these plans are available or not. The rehearsals, with minimum resources spending, will play the central role: what better.

CONCLUSIONS

Simulation can save financial resources, materials, time and, last but not least, human. Also, the diversity decision algorithms can be tested using the simulator, just respecting the initial conditions. In this way you can obtain optimal peak performance without spending any additional resources or alternative optimal algorithm.

Regardless of the number of hours the operators spend practicing in front of a simulator, regardless of their level of preparation (simple or advanced students) technique will not suffer as a result of “experiments” that could be taxed.

When the operator and staff are well prepared, when discovered, through experience, which is the best algorithm to follow and the best decision to be taken at a given time, then they can shift the actual equipment in the best conditions. Military educational institutions in the field do not have at the moment a simulation program of fire control Gun*Star Night system, so the present program could be a useful tool for training students or trainee officers.

Currently, in the Romanian army anti-aircraft artillery gun there is a program for simulation equipment operator’s anti-aircraft artillery, but the only occasions for training in real conditions are those of the polygon of drawdown conducted missions. This is an expensive method. Therefore, simulation software is intended as a first step in the field.

In the future, according with new simulation training doctrine in Ro. army, we intend to connect all individual simulators in a multilevel simulator and this is a first step in that direction. If we will be able to train a structure of the air defense battalion level (3 Air Defense Battery and C2 structure) with this simulator, definitely we will succeed to connect all simulators in one multilevel simulator.

The key for complex simulation training is represented by serious games, connected via HLA standard in multilevel simulators. Finally we will be able to say that the passion for air defense weapon, for the aviation, radar and air defense artillery has regained the place it deserves: a weapon of first-class, among weapons that can decide, in just the first two hours armed conflict, whether the fight is won or not.

REFERENCES

- [1] *** North Atlantic Treaty Organization. *NATO Modeling and Simulation Master Plan*, Draft v 0.2.2. NATO Working Paper AC/323-WP02, 1998;
- [2] R. M. Fujimoto, *The Management in The High Level Architecture*, Computational Science and Engineering Division, College of Computing, Georgia Institute of Technology, Atlanta, 1998;
- [3] *** IEEE New Standards Committee (NESCOM). *Standard for Modeling and Simulation (M&S) High Level Architecture (HLA) - Object Model Template (OMT) Specification*, IEEE Project Authorization Request (PAR) 1516.2, 1997;
- [4] B. P. Zeigler, H. Praehofer, and T. G. Kim, *Theory of modeling and simulation: integrating discrete event and continuous complex dynamic systems*, 2000;
- [5] *** NATO Modeling and Simulation (M&S) Orientation Course, ADL Course, Marshall PfP Consortium;
- [6] *** Pitch Technologies AB, *The HLA tutorial a practical guide for developing distributed simulations*, Sweden, 2012;
- [7] O. Topcu, *Simulation Generator (SimGe) – 0.2.6 user manual*, 2014. Available on: http://user.ceng.metu.edu.tr/~otopcu/simge/docs/SimGeUserManual_026.pdf;
- [8] *** Oerlikon Contraves, *GDF – 103 AA Drill book Oerlikon*, Oerlikon Contraves Publishing House, 2002;
- [9] *** *Air defence artillery operator’s training manual – Land Forces*, 35 mm Oerlikon System, MOD Publishing House, 2008;
- [10] Gh. Barbu and M. Miroiu, *Simulation Techniques*, Technical Publishing House, București, 2012;
- [11] K. Velten, *Mathematical Modeling and Simulation*, John Wiley and Sons, New York, 2009.

NUMERICAL INVESTIGATION OF TURBOJET ENGINE THRUST CORRELATED WITH THE COMBUSTION CHAMBER'S PARAMETERS

Irina-Carmen ANDREI^{*}, Constantin ROTARU^{**}, Maria-Cristina FADGYAS^{*},
Gabriela STROE^{***}, Mihai Leonida NICULESCU^{*}

^{*}National Institute for Aerospace Research “Elie Carafoli” (andrei.irina@incas.ro,
niculescu.mihai@incas.ro)

^{**}“Henri Coanda” Air Force Academy, Brasov, Romania (rotaru.constantin@yahoo.com)

^{***}“POLITEHNICA” University of Bucharest, Faculty of Aerospace Engineering,
(ing.Stroe@yao.com,)

DOI: 10.19062/2247-3173.2017.19.1.2

Abstract: *The purpose of this paper is to highlight the correlation between the thrust as the main performance of a turbojet engine and the parameters of the combustion chamber, e. g. the pressure losses and the influence of the perturbations in the turbine inlet temperature T_{3T} . The performances of the turbojet engine have been predicted by following the numerical simulation of the engine's operation, with an in-house developed code, based on a comprehensive mathematical model of the turbojet engine. The investigation is carried on at the engine's design point, which means 100% rotational speed, at sea level static standard atmosphere conditions. The most significant parameters of the combustion chamber, namely the combustion chamber's pressure losses and the perturbations in the turbine inlet temperature T_{3T} have been chosen such that to match the standpoint of the fighter pilot; the most relevant parameters is the turbine inlet temperature T_{3T} . The numerical results are summarized as graphs and charts, from which one can express new correlations and further, a new command and control law for the turbojet engine's operation can be concluded. The contributions of this study may prove to have practical applications, for being used both for training the pilot students and during flight operation, for contributing to a significant improvement in flight safety, which can be of real help for fighter pilots.*

Keywords: *turbojet engine, performance prediction, combustion chamber, numerical simulation, engine maps*

1. INTRODUCTION

The parameters of the combustion chamber, from the standpoint of a turbojet engine performances, are the turbine inlet temperature T_{3T} [K], the pressure loss coefficient, compressor exit temperature and the properties of the fuel, which for most of the cases are represented by the fuel specific power P_{ci} ; taking into account the following assumptions: 1/ that the combustion chamber is designed such that the pressure losses should be minimized, and therefore the pressure loss coefficient remains quasi constant, its magnitude being around 0.98; 2/ that the fuel specific power is with two orders of magnitude higher than the largest value of the stagnation specific enthalpy at turbine inlet, no matter that the fuel specific power is ranging from 40000 up to 45000 [kJ/kg];

3/ the variation of the compressor exit temperature is not so large and does not influence the turbojet performances, because the variation of the compressor pressure ratio (as shown by the compressor universal map) is limited; therefore, the investigation presented in this paper can be focused on the influence of the variation of the turbine inlet temperature, altitude and Mach number as flight parameters and speed as engine operating regime.

The study case is considered the VIPER 631 turbojet engine. For a large class of applications, the turbojet engine it is a optimized solution, due to the simplicity of construction (single-spool), ease of operating and maintenance and lower costs.

The **objectives** of the analysis of the turbojet engine are represented by modeling and simulation, in purpose to obtain the predicted engine performances, for different flight regimes and various operating regimes. Basically, the TURBOJET ENGINE Model supposes the completion of the steady state analysis, which supposes the calculation of the Brayton cycle at Sea Level Static SLS and ISA conditions, followed by the calculation of turbojet performances (thrust, specific thrust and fuel specific consumption, such that to build the engine's Operation Maps, which are: 1/ the Altitude Map, 2/ the Velocity Map, 3/ the Rotor Speed Map and 4/ the engine's Universal Map.

2. PERFORMANCE ANALYSIS OF TURBOJET ENGINE

2.1 Problem statement and framework

Performance Analysis of Turbojet Engine, also referred as **Thermodynamic Analysis** supposes the completion of three phases; thorough details are given in literature, Mattingly [1], as well as authors other researches, Andrei [8-15, 17-18], Rotaru [21-23] and Prisacariu [16].

The first phase consists in calculating at SLS, ISA conditions (i.e. "*fixed point*", which usually means altitude $H = 0$ [km] and flight velocity $V = 0$ [m/s]) of the engine's performances (*Thrust, Specific Thrust, Specific Fuel Consumption*) and the determination of the engine's thermodynamic cycle (i.e. Brayton cycle).

The second phase consists in calculating the engine's performances at different flight regimes and rotor speed, which usually are expressed by **ENGINE'S OPERATING MAPS** (i.e. **ALTITUDE MAP, VELOCITY MAP, SPEED MAP**).

The third phase, which consists in calculating of the **ENGINE'S UNIVERSAL MAP**, completes the performance analysis. The results obtained following the performance analysis of the engine allow to study the dynamic behaviour of the engine and to do the numerical simulations.

2.2 Identification of missing thermodynamic engine parameters

The main engine parameters of the VIPER 631 turbojet engine as the study case, must be input data (being given or determined) for the thermodynamic analysis.

Compressor Pressure Ratio π_c^* (1) defined as the ratio of stagnation pressures at compressor exit versus inlet.

$$\pi_c^* = \frac{p_2^*}{p_1^*} \tag{1}$$

$$\pi_c^* = 5.9 \tag{2}$$

Turbine inlet temperature T3T (also referred as T_3^*) is determined from the relation (8) expressing the specific work of turbine (3) as the specific enthalpy drop between turbine exit and turbine inlet; the operating law for the single-spool turbojet is (4), with the meaning that the specific work produced by the turbine is used to produce specific work on compression (5);

Compressor pressure ratio is defined as the ratio of stagnation pressures at compressor exit versus inlet (4); specific enthalpy is proportional with the temperature and constant pressure specific heat C_p , with different values for air (6.1) and mixture of burned gas (6.2); expressing the turbine specific work as a function (7) of the stagnation temperatures at turbine inlet T_3^* and turbine exit T_4^* , then relation (8) is deduced :

$$l_T^* = i_3^* - i_4^* \quad (3)$$

$$l_T^* = l_c^* \quad (4)$$

$$l_c^* = i_2^* - i_1^* = i_1^* \cdot \frac{\left((\pi_c^*)^{\frac{k-1}{k}} - 1 \right)}{\eta_c^*} \quad (5)$$

$$C_p = 1.005 \left[\frac{kJ}{kgK} \right] \quad (6.1)$$

$$C_{pg} = 1.165 \left[\frac{kJ}{kgK} \right] \quad (6.2)$$

$$l_T^* = i_3^* - i_4^* = C_{pg} \cdot (T_3^* - T_4^*) \quad (7)$$

$$T_3^* = T_4^* - \frac{l_T^*}{C_{pg}} \quad (8)$$

$$T_3^* = 1280 [K] \quad (9)$$

Note that for the specified operating regimes one can deduce also the **T3T operating control law**, expressing its variation with the % of the rotor speed regimes [%rpm]; next, the automatic controls of the engine/ fuel systems can be designed. E.g. Max starting = 105, Nominal -100, Cruising = 90, Cruising lowered = 85, Idle ground = 40.

Airflow rate \dot{M}_a [kg/s] is determined after a performing a number of iterations for the Brayton cycle, with the consequent calculation of the turbojet engine performances

(i.e. specific thrust $F_{sp} \left[\frac{Ns}{kg} \right]$, thrust F [N] and specific fuel consumption $C_{sp} \left[\frac{kg}{Nh} \right]$),

$$\dot{M}_a = 26.332 \left[\frac{kg}{s} \right] \quad (10)$$

Other engine parameters which must be determined before performing the thermodynamic analysis are listed downwards. These values have been trimmed such that to match the given thrust and specific fuel flow.

- **adiabatic efficiency on compression** η_c^* (11) defined as the ratio of specific work on compression and ideal specific work . From experience, centrifugal compressors have slightly lower values of adiabatic efficiencies with respect to axial flow compressor. In this case $\eta_c^* = 0.85$.

$$\eta_c^* = \frac{l_{c_{id}}^*}{l_c^*} \quad (11)$$

- **adiabatic efficiency on turbine expansion** η_t^* (12) defined as the ratio of ideal specific work of turbine and its specific work. In this case $\eta_t^* = 0.89$.

$$\eta_t^* = \frac{l_t^*}{l_{t_{id}}^*} \quad (12)$$

- **mechanical (shaft) efficiency** η_m (13) defined as the ratio of specific work consumed by compressor and specific work produced by turbine; in case of a single spool turbojet engine, $\eta_m = 1$. In, since there are no mechanical losses between compressor and turbine.

$$\eta_m = \frac{l_c^*}{l_t^*} \quad (13)$$

- **pressure loss at engine intake** σ_{da}^* (14) defined as the ratio of the stagnation pressures at intake exit versus inlet; $\sigma_{da}^* = 0.92$.

$$\sigma_{da}^* = \frac{p_1^*}{p_H^*} \quad (14)$$

- **pressure loss in combustor** σ_{ca}^* (15) defined as the ratio of the stagnation pressures at compressor exit versus combustor exit; $\sigma_{ca}^* = 0.98$.

$$\sigma_{ca}^* = \frac{p_3^*}{p_2^*} \quad (15)$$

- **combustion efficiency** $\xi_{ca} = 0.998$
- **exhaust nozzle velocity** $\varphi_{ar} = 0.940$

2.3 Purpose of calculations

a) the determination of **turbojet engines performances** (i.e. specific thrust $F_{sp} \left[\frac{Ns}{kg} \right]$ (47), thrust $F [N]$ (48), specific fuel consumption $C_{sp} \left[\frac{kg}{Nh} \right]$ (49), for all flight envelope and engine operating regimes;

b) the influence of altitude, flight Mach number and rotor speed [rpm] on inlet air flow rate (50) and compressor pressure ratio (55) - (58), was taken into account when calculating the turbojet engine performances, when operating at altitude, at specified flight velocity and engine regime [%rpm];

3. MATHEMATICAL MODEL

3.1 Hypothesis

The mathematical model of a turbojet engine describing its behavior as close to reality is based on the following **HYPOTHESIS**:

- the working fluid is considered perfect gas,
- two species:
 - A. // **air** // - from intake to compressor,
 - B. // **burned gas** // - within combustor, turbine and exhaust unit,
- fuel specific power, for JET A, JET A1 and/or JET B (aviation kerosene):

$$P_{CI} = 43500 \left[\frac{kJ}{kg} \right],$$

- ratio of specific heat $k = \frac{C_p}{C_v}$, see Table 1.

- constant pressure specific heat $C_p \left[\frac{kJ}{kgK} \right]$:

- gas constant $R \left[\frac{kJ}{kgK} \right]$; the relation between R and C_p is (16):

$$C_p = R \cdot \frac{k}{k-1} \quad (16)$$

Table 1 - Properties of the working fluids

Fluid	k	C_p [kJ/kg/K]	R [J/kg/K]
Air	1.4	1.005	287.3
Burned Gas	1.33	1.165	288.4

3.2. Basic equations

Basic equations (17) - (46) for computing the **turbojet engine performances** (algorithm defined by equations / relations ordered as entries in work flow):

- SLS, ISA conditions: $p_0 = 1.01325$ [bar] (17.1), $T_0 = 288$ [K] (17.2) and

$$i_0 = C_p \cdot T_0 \left[\frac{kJ}{kg} \right] \quad (18)$$

- conditions at engine inlet (intake) - station 0 (SLS) or H (flight):
 - if $H = 0$ [km] then $p_1^* = \sigma_{da}^* \cdot p_0$ [bar], (19.1), $T_1^* = T_0$ [K] (19.2), and

$$i_1^* = C_p \cdot T_1^* \left[\frac{kJ}{kg} \right] \quad (20)$$

- if $H > 0$ then $p_1^* = p_H^* \cdot p_0$ [bar] (21.1), $T_1^* = T_H^*$ [K] (21.2) and

$$i_1^* = C_p \cdot T_1^* \left[\frac{kJ}{kg} \right] \quad (22)$$

where $T_H = T_0 - 6.5 \cdot H$ [km], [K] (23)

and $p_H = p_0 \cdot \left(\frac{T_H}{T_0} \right)^{5.2558}$ (24)

and $T_H^* = T_H + \frac{V^2}{2 \cdot C_p}$ (25)

or $T_H^* = T_H \cdot \left(1 + \frac{(k-1)}{2} \cdot Mach^2 \right)$ (26)

and $p_H^* = p_H \cdot \left(1 + \frac{(k-1)}{2} \cdot Mach^2 \right)^{\frac{(k-1)}{k}}$ (27)

- dynamic pressure ratio:

$$\pi_d^* = \frac{p_H^*}{p_H} = \left(\frac{T_H^*}{T_H} \right)^{\frac{(k-1)}{k}} = \left(1 + \frac{(k-1)}{2} \cdot Mach^2 \right)^{\frac{(k-1)}{k}} = (\Theta(Mach))^{\frac{(k-1)}{k}} \quad (28)$$

- conditions at compressor inlet - station 1*: $p_1^* = \sigma_{da}^* \cdot p_H^*$ (29.1), $T_1^* = T_H^*$ (29.2), $i_1^* = i_H^*$ (30)

- conditions at combustor inlet - station 2*: $p_2^* = \pi_c^* \cdot p_1^*$ (31)

$$i_2^* = i_1^* \cdot \left(1 + \frac{\left((\pi_c^*)^{\frac{k-1}{k}} - 1 \right)}{\eta_c^*} \right) \quad (32)$$

$$T_2^* = \frac{i_2^*}{C_p} \quad (33)$$

- conditions at turbine inlet - station 3*: $p_3^* = \sigma_{ca}^* \cdot p_2^*$ (34)

- T_3^* from equation (8), $i_3^* = C_{pg} \cdot T_3^*$ (35)

- fuel flow coefficient (from energy balance eqn. in combustor):

$$m_c = \frac{(i_3^* - i_2^*)}{(\xi_{ca} \cdot P_{ci} - i_2^*)} \quad (36)$$

- burned gas flow coefficient (from mass balance eqn. in combustor):

$$m_g = 1 + m_c \quad (37)$$

- fuel flow coefficient:

$$m_c = \frac{\dot{M}_c}{\dot{M}_a} \quad (38)$$

- burned gas flow coefficient:

$$m_g = \frac{\dot{M}_g}{\dot{M}_a} \quad (39)$$

- conditions at turbine exit - station 4* : $i_4^* = i_3^* - l_t^*$ (40)

$$T_4^* = \frac{i_4^*}{C_{pg}} \quad (41)$$

$$p_4^* = \frac{\delta_t^*}{p_3^*} \quad (42)$$

- where δ_t^* is the pressure ratio in turbine, and it comes out from the expression of

$$\delta_t^* = \left(1 - \frac{l_{tid}^*}{i_3^*}\right)^{-\left(\frac{kg}{kg-1}\right)}$$

specific work in turbine. (43)

- conditions at nozzle exit - station 5 :

case: full exhaust nozzle expansion: $p_5 = p_H$ (44.1) , then the thrust obtained is maximum

case: partial exhaust nozzle expansion: $p_5 = p_{cr} < p_H$ (44.2),

$$p_{cr} = \left(\frac{2}{kg+1}\right)^{\left(\frac{kg}{kg-1}\right)} \cdot p_4^* \quad (45)$$

- velocity of expelled gas c_5 [m/s], (46):

$$c_5 = \varphi_{ar} \cdot \sqrt{2 \cdot \left\{ \left[i_3^* \cdot \left(1 - \pi_d^* \cdot \sigma_{da}^* \cdot \pi_c^* \cdot \sigma_{ca}^*\right)^{-\left(\frac{kg-1}{kg}\right)} \right] - i_1^* \cdot \left[\frac{(\pi_c^*)^{\frac{k-1}{k}} - 1}{\eta_c^* \cdot \eta_t^* \cdot \eta_m} \right] \right\}} \quad (46)$$

3.3. Definitions of turbojet engine performances

Relations (47) - (49) define the **turbojet engine performances** (i.e. thrust F [N],, specific thrust F_{sp} [Ns/kg] and specific fuel consumption C_{sp} [kg/Nh] or **TFC**,

- **specific thrust** $F_{sp} = m_g \cdot c_5 - V, \left[\frac{Ns}{kg}\right]$ (47)

- **thrust** $F = F_{sp} \cdot \dot{M}_a, [N]$ (48)

- **specific fuel consumption** $C_{sp} = \frac{3600 \cdot m_c}{F_{sp}}, \left[\frac{kg}{Nh}\right]$ (49)

3.4. The influence of altitude, flight mach number and rotor speed on airflow rate and compressor pressure ratio

Equations (50) - (58) express the **influence of altitude, flight Mach number** and **rotor speed** on inlet **air flow rate** (50) and **compressor pressure ratio** (55) - (58):

- Airflow rate (50) is influenced by the change of altitude and flight Mach number, by the means of the variation of compressor pressure ratio, dynamic pressure ratio and the ratio of static pressures al altitude H [km] versus SLS:

$$\dot{M}_a = \dot{M}_{a_0} \cdot \frac{\pi_c^*}{\pi_{c_0}^*} \cdot \pi_d^* \cdot \frac{p_H}{p_0} \quad (50)$$

- specific work on compression (51) changes with the square of rotor speed (52)
- $$l_c^* = l_{c_0}^* \cdot \bar{n}^2 \quad (51)$$
- rotor speed % (52) represents the ratio of speeds at operating versus nominal engine regime:

$$\bar{n} = \frac{n}{n_{NOMinal}} \quad (52)$$

- the relations between specific work of compressor, compressor pressure ratio, intake enthalpy and rotor speed, are (53) for SLS, ISA conditions and (54) for the flight at altitude:

$$l_{c_0}^* = i_0 \cdot \left(\frac{(\pi_{c_0}^*)^{\frac{k-1}{k}} - 1}{\eta_{c_0}^*} \right) \quad (53)$$

$$l_c^* = i_H^* \cdot \left(1 + \frac{(\pi_c^*)^{\frac{k-1}{k}} - 1}{\eta_c^*} \right) \quad (54)$$

- the influence of altitude, flight Mach number and rotor speed on compressor pressure ratio (55) - (58) is deduced from relations (53), (54) and (51); the ratio of compressor efficiencies at operating regime versus nominal can be taken about 1.0 (as initial approximation or in case that the universal compressor map is not available):

$$\pi_c^* = \left[1 + \left((\pi_{c_0}^*)^{\frac{k-1}{k}} - 1 \right) \cdot \frac{i_0}{i_H^*} \cdot \bar{n}^2 \cdot \frac{\eta_c^*}{\eta_{c_0}^*} \right]^{\frac{k}{k-1}} \quad (55)$$

$$\pi_c^* = \left[1 + \left((\pi_{c_0}^*)^{\frac{k-1}{k}} - 1 \right) \cdot \frac{i_0}{i_H^*} \cdot \bar{n}^2 \right]^{\frac{k}{k-1}} \quad (56)$$

$$\pi_c^* = \left[1 + \left((\pi_{c_0}^*)^{\frac{k-1}{k}} - 1 \right) \cdot \frac{i_0}{i_H^*} \cdot \bar{n}^2 \right]^{\frac{k}{k-1}} \quad (57)$$

$$\pi_c^* = \left[1 + \frac{l_{c_{id}}}{i_H^*} \cdot \bar{n}^2 \right]^{\frac{k}{k-1}} \quad (58)$$

3.5. The turbojet engine's operating maps

Definitions of turbojet engine's OPERATING MAPS, (i.e. the variation of the jet engine performances: thrust F [N], specific thrust F_{sp} [Ns/kg] and specific fuel consumption C_{sp} [kg/Nh] or TSFC, with altitude, flight velocity and engine rotational regime)

ENGINE OPERATING MAPS are represented by: 1/ **ALTITUDE MAP**, 2/ **VELOCITY MAP** and 3/ **SPEED MAP**

(1) - ALTITUDE MAP is defined as the variation of the jet engine's performances (i.e. thrust F [N],, specific thrust F_{sp} [Ns/kg] and specific fuel consumption C_{sp} [kg/Nh] or TSFC) with respect to altitude H [km], while the flight velocity and rotor speed [%rpm] are constant, their values being usually taken for SLS, ISA conditions

Thrust	$F = f(H) \Big _{\substack{V=0 \\ n\%=1}}$
Specific thrust	$F_{sp} = f(H) \Big _{\substack{V=0 \\ n\%=1}}$
Specific fuel consumption	$C_{sp} = f(H) \Big _{\substack{V=0 \\ n\%=1}}$
Altitude Map	

(2) - VELOCITY MAP is defined as the variation of the jet engine's performances (i.e. thrust F [N],, specific thrust F_{sp} [Ns/kg] and specific fuel consumption C_{sp} [kg/Nh] or TSFC) with respect to flight velocity V [m/s] or its equivalent, flight Mach number, while the altitude H [km] and rotor speed [%rpm] are constant, their values being usually taken for SLS, ISA conditions

Thrust	$F = f(V) \Big _{\substack{H=0 \\ n\%=1}}$	Thrust	$F = f(M) \Big _{\substack{H=0 \\ n\%=1}}$
Specific thrust	$F_{sp} = f(V) \Big _{\substack{H=0 \\ n\%=1}}$	Specific thrust	$F_{sp} = f(M) \Big _{\substack{H=0 \\ n\%=1}}$
Specific fuel consumption	$C_{sp} = f(V) \Big _{\substack{H=0 \\ n\%=1}}$	Specific fuel consumption	$C_{sp} = f(M) \Big _{\substack{H=0 \\ n\%=1}}$
Velocity Map		Velocity Map	

(3) - SPEED MAP is defined as the variation of the jet engine's performances (i.e. thrust F [N],, specific thrust F_{sp} [Ns/kg] and specific fuel consumption C_{sp} [kg/Nh] or TSFC) with respect to rotor speed [rpm] or its equivalent engine operational regime [%rpm], while the altitude H [km] and flight velocity V [m/s] are constant, their values being usually taken for SLS, ISA conditions

Thrust	$F = f(V) \Big _{\substack{H=0 \\ n\%=1}}$	Thrust	$F = f(M) \Big _{\substack{H=0 \\ n\%=1}}$
Specific thrust	$F_{sp} = f(V) \Big _{\substack{H=0 \\ n\%=1}}$	Specific thrust	$F_{sp} = f(M) \Big _{\substack{H=0 \\ n\%=1}}$
Specific fuel consumption	$C_{sp} = f(V) \Big _{\substack{H=0 \\ n\%=1}}$	Specific fuel consumption	$C_{sp} = f(M) \Big _{\substack{H=0 \\ n\%=1}}$
Speed Map		Speed Map	

3.6. The turbojet engine's universal map

Definitions of UNIVERSAL ENGINE MAP, (i.e. the variation of non-dimensional parameters of thrust F [N],, specific thrust F_{sp} [Ns/kg] and specific fuel consumption C_{sp} [kg/Nh] or TSFC, in case of a jet engine)

UNIVERSAL ENGINE MAPS are represented in coordinates **THRUST PARAMETER** and **SPECIFIC FUEL CONSUMPTION PARAMETER** versus either **flight Mach number** or **SPEED PARAMETER**. The **UNIVERSAL ENGINE MAP** is defined in two equivalent ways, expressing the variation of Thrust parameter and Specific fuel consumption parameter with respect to Mach number, for a constant Speed parameter, or vice-versa:

UNIVERSAL ENGINE MAP - definition # 1		UNIVERSAL ENGINE MAP - definition # 2	
$\frac{F}{p_1} = f(M) \Big _{\frac{n}{\sqrt{T_1}} = const.}$	Thrust parameter	$\frac{F}{p_1} = f\left(\frac{n}{\sqrt{T_1}}\right) \Big _{M = const.}$	Thrust parameter
$\frac{C_{sp}}{\sqrt{T_1}} = f(M) \Big _{\frac{n}{\sqrt{T_1}} = const.}$	Specific fuel consumption parameter	$\frac{C_{sp}}{\sqrt{T_1}} = f\left(\frac{n}{\sqrt{T_1}}\right) \Big _{M = const.}$	Specific fuel consumption parameter
$\frac{n}{\sqrt{T_1}} = constant$	Speed parameter	$M = constant$	Flight Mach number

Universal Map

4. RESULTS

This investigation is focused on highlighting the influence of the turbine inlet temperature, as the most significant parameters of the combustion chamber, upon the turbojet engine's performances. With respect to the engine's design point parameters, i.e. the turbine inlet temperature being 1280 [K], it was considered a ranging interval from 1230 [K] up to 1330 [K], which corresponds to a perturbation of temperature with 50 [K], up and down with respect to the reference value.

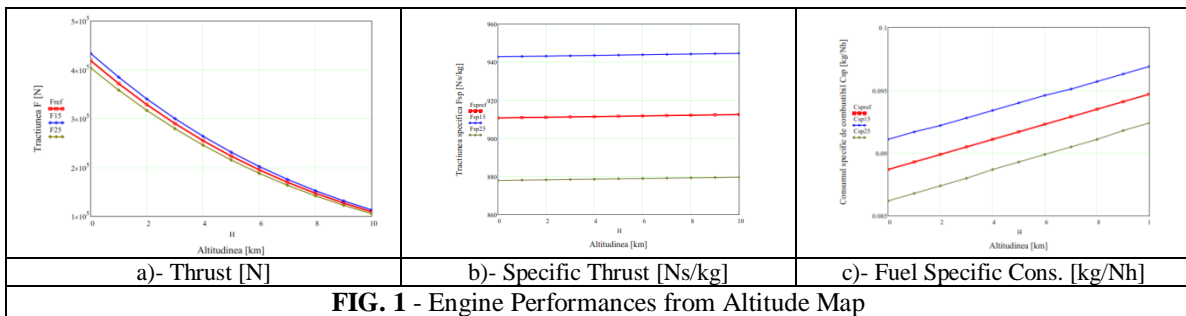


FIG. 1 - Engine Performances from Altitude Map

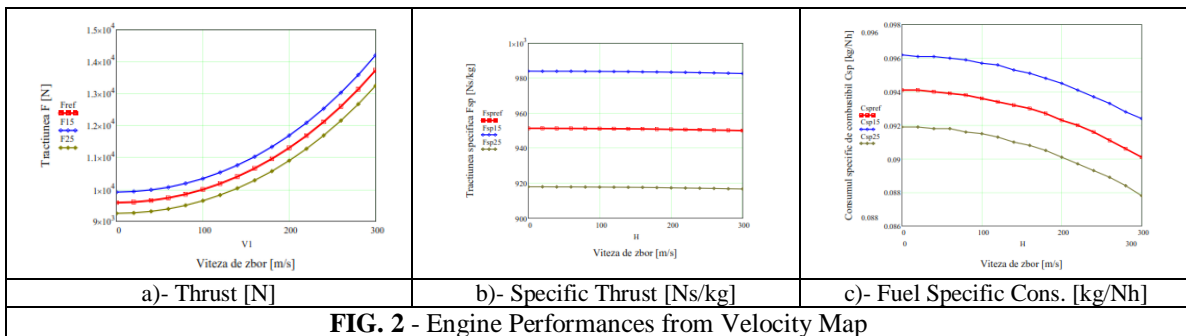


FIG. 2 - Engine Performances from Velocity Map

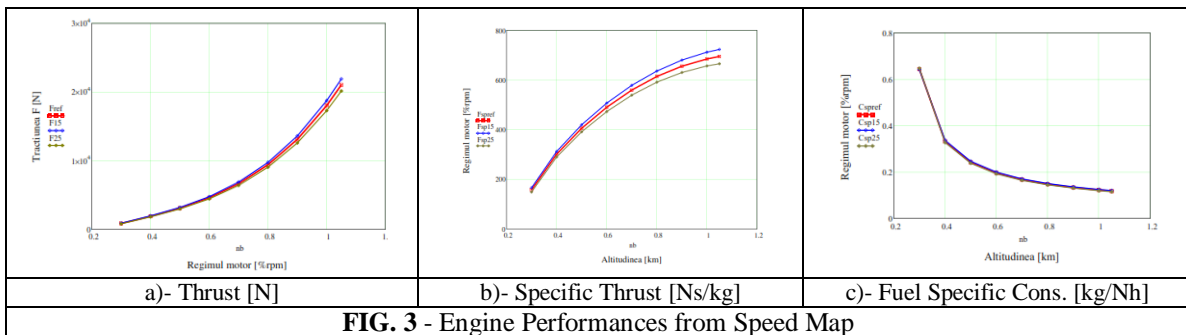


FIG. 3 - Engine Performances from Speed Map

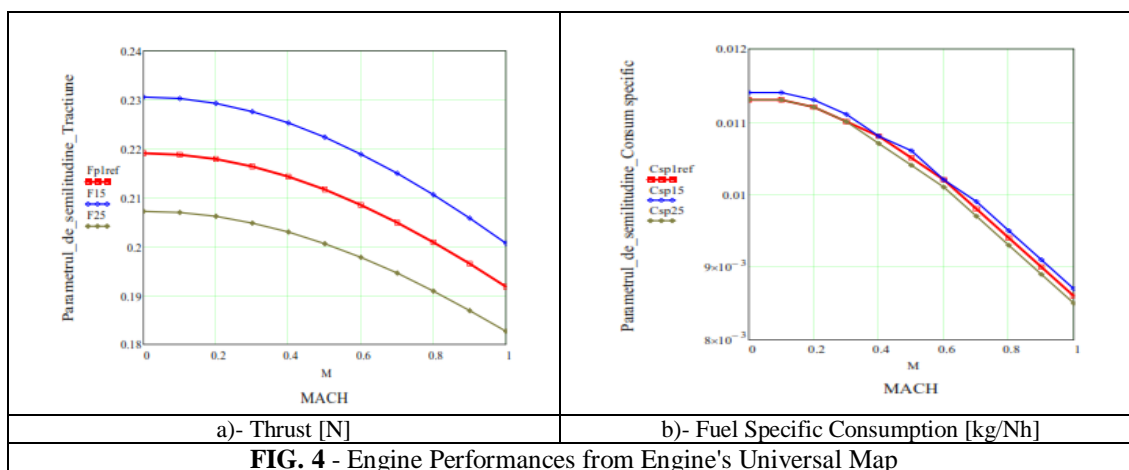


FIG. 4 - Engine Performances from Engine's Universal Map

5. CONCLUSIONS & ACKNOWLEDGMENT

The investigation presented in this paper is focused on the influence of the variation of the turbine inlet temperature, as perturbation of the engine's design parameter and altitude Mach number and speed as perturbations of the flight and engine operating regimes.

The objective of this study is to highlight the variation of engine's thrust for a given perturbation of the turbine inlet temperature. The turbine inlet temperature ranges between 1230 and 1330 [K], which corresponds to a perturbation of +/- 50 [K] with respect to the reference value, that is considered at the engine's design point.

The predicted performances of the turbojet engine (i.e. thrust, specific thrust and fuel specific consumption) are summarized in Fig. 1 ÷ Fig. 4.

Taking into account the variation of thrust (case a)- in Fig. 1 ÷ Fig. 3), one can note that the effect of the perturbation of turbine inlet temperature T3T on thrust is higher when the flight velocity changes Fig. 2-a; unlike this case, the cases when the flight altitude or engine speed change, the influence on thrust of the perturbations of T3T can be neglected, Fig. 1-a and Fig. 3-a. From the Universal Map, the thrust parameter is much more influenced by the perturbation of the turbine inlet temperature T3T.

Future developments of this study can aim to establish other correlations and further, a new command and control law for the turbojet engine's operation that might be concluded. The contributions of this study may prove to have practical applications, for being used both for training the pilot students and during flight operation, for contributing to a significant improvement in flight safety, which can be of real help for fighter pilots.

The authors would like to express their gratitude to the INCAS - National Institute of Aerospace Research "Elie Carafoli" Bucharest for the support while carrying on research activities within the Flow Physics Department, Numerical Simulations Unit, as well as the documentary research. The results presented in this paper are correlated to the current research activities regarding the jet propulsion systems, carried on within INCAS.

REFERENCES

- [1] J. D. Mattingly, *Elements of Propulsion and Gas Turbine and Rockets*, American Institute of Aeronautics and Astronautics Education Series, Inc. Reston, VA., 2006;
- [2] ***, Rolls Royce, *The Jet Engine*, fifth edition, ISBN 0 902121 2 35, The Technical Publications Department Rolls-Royce plc, Derby, England;
- [3] ***, Powerplant, JAA ATPL Training, JEPPESEN, Atlantic Flight Training Ltd ;
- [4] Wilfried Wisser, *Generic Analysis Methods for Gas Turbine Engine Performance, The development of the gas turbine simulation program GSP*, PhD Thesis, NLR and TU Delft, 2015;
- [5] ***, *Compressor and Turbine Maps for Gas Turbine Performance Computer Programs*, Issue 3, GasTurb GmbH, 2013;
- [6] NASA Technical Memorandum **TM X-3014**, *A generalized hybrid computer program for studying turbojet or turbofan engine dynamics*, John Szuch, Cleveland, Ohio, 1974;
- [7] S. M. Eastbourn, *Modeling and simulation study of a dynamic turbofan engine using Matlab Simulink*, M. Sc. A.E. Dissertation, Wright State University, 2012;
- [8] Pimsner V., *Motoare aeroreactoare*, Ed. Didactica si Pedagogica, Bucuresti, 1983;
- [9] Irina Andrei, Adrian Toader, Gabriela Stroe, Florin Frunzulica, *Performance Analysis and Dynamic Modeling of a Single-Spool Turbojet Engine*, International Conference in Nonlinear Problems in Aviation and Aerospace ICNPAA 2016, La Rochelle, France, AIP Conference Proceedings;
- [10] Gabriela Stroe, Irina Andrei, Florin Frunzulica, *Analysis of Control System Responses for Aircraft Stability and Efficient Numerical Techniques*, International Conference in Nonlinear Problems in Aviation and Aerospace ICNPAA 2016, La Rochelle, France, AIP Conference Proceedings;
- [11] Irina Andrei, Mihai Niculescu, Mihai Victor Pricop, Andreea Cernat, *Study of the Turbojet Engines as Propulsion Systems for the Unmanned Aerial Vehicles*, AFASES 2016, AFAHC Brasov, 2247-3173, Diseminare Proiect MASIM;
- [12] Alexandru Ionel, Stefan Palas, Irina Andrei, *Performance Analysis of the IAR 99 SOIM and IAR 99 TD*, AEROSPATIAL 2016, INCAS, ISSN 2067-8614;
- [13] Andreea Cernat, Alexandru Ionel, Irina Andrei, Stefan Palas, Adrian Mihai, *Simulation Tool for Predicting Ground Test Performances of a Turbofan Propulsion System Air Inlet*, AEROSPATIAL 2016, INCAS, ISSN 2067-8614;
- [14] Irina Andrei, Alexandru Ionel, Adrian Mihai, Stefan Palas, Tiberiu Salaoru, *Numerical Modeling Application for Simulating Engine Test Cell Validation Methodology of a Turbofan Exhaust System*, AEROSPATIAL 2016, INCAS, ISSN 2067-8614;
- [15] Irina Andrei, Alexandra Stanescu, Adrian Toader, *Issues on the completion of the mathematical model by Parameter Identification for Simulating a Jet Engine*, NMAS 2016, INCAS, ISSN 2360-1809;
- [16] Vasile Prisacariu, Ionica Circiu, *Considerations Regarding the Performances of the Combustion Chambers for Turbojet Engines*, Review of the Air Force Academy, No 2 (32) 2016 DOI: 10.19062/1842-9238.2016.14.2.7;
- [17] Irina Andrei, Adrian Toader, Ana Maria Neculaescu, *Numerical Simulations of Steady-State and Dynamic Analysis of a Single-Spool Turbojet Engine*, NMAS 2016, INCAS, ISSN 2360-1809;
- [18] Dr. I. Andrei, A. Stanescu, *Issues on modeling and simulation of a mixed flows turbofan*, Caius Iacob Conference, 2015;
- [19] Ciobotea V., *Teoria motoarelor de aviatie, vol. 1*, Editura Academiei Militare, Bucuresti, 1978;
- [20] Manole I., *Solutii constructive de turbomotoare de aviatie (album de scheme), vol. 1*, Editura Academiei Militare, Bucuresti, 1977;
- [21] Rotaru C., Mihaila-Andres M., Pericle G.M., Edu R. I., *Thermodynamic performances of the turbojet combustion chambers – numerical evaluation*, Proceedings of the 2014 International Conference on Mechanics, Fluid Mechanics, Heat and Mass Transfer, p. 86-91, 2014;
- [22] Rotaru C., Cîrciu I., Arama C., Constantinescu C., *Aspects regarding velocity distribution in the secondary zone of a gas turbine combustor*, Review of the Air Force Academy, 2/2015, DOI: 10.19062/1842-9238.2015.13.3.5, p. 33-38, 2015;
- [23] Rotaru C., Andres-Mihaila M., Pericle G.M., *An Extended Combustion Model for the Aircraft Turbojet Engine*, International Journal of Turbo & Jet-Engines, 3/2014, p.229-237, 2014;
- [24] Farokhi S., *Aircraft propulsion*, second edition, Wiley and sons, 2014;
- [25] Stefanescu I., *Advanced Training Aircraft IAR 99 (A) SOIM*, INCAS BULLETIN, vol. 4, Issue 2/2012, DOI: 10.13111/2066-8201.2012.4.2.13, pp. 125 – 135, 2012;
- [26] F. Zare, Dr. Arpad Veress, K. Beneda, *Simplified mathematical model for a single spool and no bypass jet engine*, RTK Conference, BME, 2013;
- [27] H. Asgari, X. Chen, R. Sainudin, *Modeling and simulation of gas turbines*, Intl. Journal Modelling, Simulation and Control, 2013;

- [28] S. C. Uysal, *High by-pass ratio turbofan engines aero-thermodynamic design and optimization*, PhD Thesis, The Graduate School of Natural and Applied Sciences, Middle East Technical University, 2014;
- [29] NASA Technical Memorandum 83446 (NASA - TM 83446), *Digital Computer Program for Generating Dynamic Turbofan Engine Models (DIGTEM)*, C.J. Daniele, S. M. Krosel, J. R. Szuch, E. J. Westerkamp, Lewis Research Center, Cleveland, Ohio, 1983.

NUMERICAL INVESTIGATION OF MIXED FLOWS TURBOFAN ENGINE THRUST CORRELATED WITH THE COMBUSTION CHAMBER'S PARAMETERS

Irina-Carmen ANDREI^{*}, Constantin ROTARU^{**}, Maria-Cristina FADGYAS^{*},
Gabriela STROE^{***}, Mihai Leonida NICULESCU^{*},

^{*}National Institute for Aerospace Research “Elie Carafoli” (andrei.irina@incas.ro,
niculescu.mihai@incas.ro)

^{**}“Henri Coanda” Air Force Academy, Brasov, Romania
(rotaru.constantin@yahoo.com)

^{***}“POLITEHNICA” University of Bucharest, Faculty of Aerospace Engineering,
(ing.Stroe@yao.com)

DOI: 10.19062/2247-3173.2017.19.1.3

Abstract: *The purpose of this paper is to show the influence of the most relevant parameters of the combustion chamber (e.g. perturbations in the turbine inlet temperature T3T and pressure losses) and the predicted performances of a mixed flows turbofan engine. The performances of the mixed flow turbofan engine have been predicted by following the numerical simulation of the engine's operation, with an in-house developed code, based on a comprehensive mathematical model of the mixed flow turbofan engine. The investigation is carried on at the engine's design point, which means 100% rotational speed, at sea level static standard atmosphere conditions. The most significant parameters of the combustion chamber, namely the combustion chamber's pressure losses and the perturbations in the turbine inlet temperature T3T have been chosen such that to match the standpoint of the fighter pilot; the most relevant parameter is the turbine inlet temperature T3T. The numerical results are summarized as graphs and charts, from which one can express new correlations and further, a new command and control law for the turbojet engine's operation can be concluded. The contributions of this study may prove to have practical applications, for being used both for training the pilot students and during flight operation, for contributing to a significant improvement in flight safety, which can be of real help for fighter pilots.*

Keywords: *mixed flows turbofan engine, performance prediction, combustion chamber, numerical simulation, engine maps*

1. INTRODUCTION

There are certain advantages provided by the use of the turbofan engines; the most important feature is that for twin- or triple-spool constructions, the engine operates much far from the surge line, for the entire flight envelope. The constructive differences between turbojet and turbofan engine can be noticed from the schematic diagram, Fig. 1.

Large bypass turbofans are shown in Fig. 1 - c, d, which are also referred as just turbofan; the object of this study is the mixed flows turbofan, presented in Fig. 1-a.

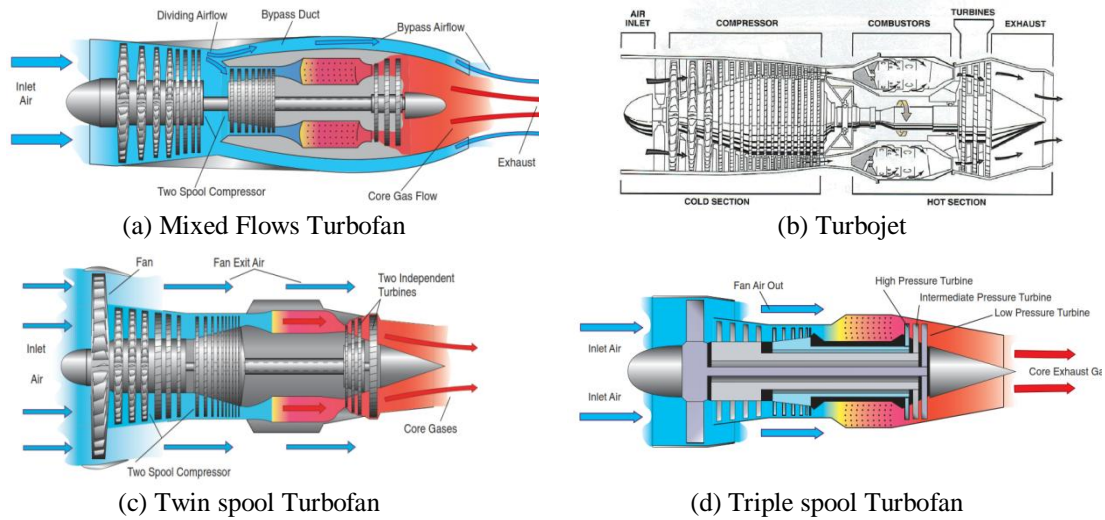


FIG. 1 - Schematic diagrams, [2-3]

The parameters of the combustion chamber, from the standpoint of the jet engine performances, are the turbine inlet temperature T_{3T} [K], the pressure loss coefficient, compressor exit temperature and the properties of the fuel, which for most of the cases are represented by the fuel specific power P_{ci} ; taking into account the following assumptions: 1/ that the combustion chamber is designed such that the pressure losses should be minimized, and therefore the pressure loss coefficient remains quasi constant, its magnitude being around 0.98, 2/ that the fuel specific power is with two orders of magnitude higher than the largest value of the stagnation specific enthalpy at turbine inlet, no matter that the fuel specific power is ranging from 40000 up to 45000 [kJ/kg], 3/ the variation of the compressor exit temperature is not so large and does not influence the turbojet performances, because the variation of the compressor pressure ratio (as shown by the compressor universal map) is limited; therefore, the investigation presented in this paper can be focused on the influence of the variation of the turbine inlet temperature, altitude and Mach number as flight parameters and speed as engine operating regime.

The **study case** is a mixed flows turbofan, as detailed in Fig. 1-a, defined by the main engine parameters: overall pressure ratio $\pi_c^* = 22$, by pass ratio $K = 2.9$, overall airflow rate $\dot{M}_a = 65.772$ [kg/s]; following the identification of missing design parameters, there have been determined, Andrei I. [15, 18], the Turbine inlet temperature $T_{3T} = 1410$ [K], then the fan pressure ratio $\pi_v^* = 1.76$, which corresponds to the optimum fan specific work $l_v^* = \underline{59.657}$ [kJ/kg]; eventually, at SLS level, ISA is calculated the maximum Thrust $F = 20.91$ [kN] (military thrust).

Other parameters required for calculating the performances of the engine are: air intake pressure loss, adiabatic efficiency on compression for compressor and for the fan, combustion chamber pressure loss, adiabatic efficiency on turbine expansion, velocity loss within nozzle exit, mechanical efficiency (i.e. shaft transmission efficiency). The specificity of the mixed flows turbofan is the mixing of the two streams, meaning the primary stream of burned gas and the secondary stream of compressed air; therefore, the parameters at fan exit and turbine exit are important for calculating the overall engine thrust; the parameters in question are: turbine exit stagnation pressure p_4^* and stagnation temperature T_4^* , fan air exit stagnation pressure p_{2v}^* and stagnation temperature T_{2v}^* and combustor fuel – air mixture ratio α .

The **objectives** of the analysis of the mixed flows turbofan MFTF engine are represented by modeling and simulation, in purpose to obtain the predicted engine performances, for different flight regimes and various operating regimes. Basically, the construction of a MFTF ENGINE Model supposes the completion of the steady state analysis, which supposes the calculation of the Brayton cycle at Sea Level Static SLS and ISA conditions, followed by the calculation of turbojet performances (thrust, specific thrust and fuel specific consumption, such that to build the engine's Operation Maps, which are: 1/ the Altitude Map, 2/ the Velocity Map, 3/ the Rotor Speed Map and 4/ the engine's Universal Map.

2. PERFORMANCE ANALYSIS OF MIXED FLOWS TURBOFAN ENGINE

2.1 Problem statement and framework

Performance Analysis of Mixed Flows Turbofan Engine, supposes the completion of three phases; thorough details are given in literature, Mattingly [1], as well as authors other researches, Andrei [8-15, 17-18], Rotaru [21-23] and Prisacariu [16].

The first phase consists in calculating at SLS, ISA conditions (i.e. "*fixed point*", which usually means altitude $H = 0$ [km] and flight velocity $V = 0$ [m/s]) of the engine's performances (*Thrust, Specific Thrust, Specific Fuel Consumption*) and the determination of the engine's thermodynamic cycle (i.e. Brayton cycle).

The second phase consists in calculating the engine's performances at different flight regimes and rotor speed, which usually are expressed by **ENGINE'S OPERATING MAPS** (i.e. **ALTITUDE MAP, VELOCITY MAP, SPEED MAP**).

The third phase, which consists in calculating of the **ENGINE'S UNIVERSAL MAP**, completes the performance analysis. The results obtained following the performance analysis of the engine allow to study the dynamic behaviour of the engine and to do the numerical simulations.

2.2 Mathematical support

The performances of the mixed flows turbofan can be calculated from relations (1) ÷ (9) presented below; the thrust of a mixed flows turbofan is expressed by the variation (1) of flow and velocity between the inlet and exit sections of the engine; the specific thrust is defined by relation (2), while the definition of specific fuel consumption is one of the equations (5-7,9). The order at calculating the performances of the mixed flows turbofan is that first is determined the specific thrust F_{sp} [Ns/kg], then the thrust F [N] and fuel specific consumption C_{sp} [kg/Nh]. The relations expressing the performances of the mixed flows turbofan engine are valid for all flight regimes and engine running conditions.

$$F = \dot{M}_{am} \cdot C_{5am} - \dot{M}_a \cdot V \quad (1)$$

$$F_{sp} = \frac{F}{\dot{M}_{a1}} \quad (2)$$

$$F = \dot{M}_{am} \cdot (1 + K) \cdot C_{5am} - \dot{M}_a \cdot (1 + K) \cdot V \quad (3)$$

$$F = \dot{M}_{am} \cdot (1 + K) \cdot (C_{5am} - V) \quad (4)$$

$$C_{sp} = 3600 \cdot \frac{\dot{M}_c}{F} \quad (5)$$

$$C_{sp} = 3600 \cdot \frac{\dot{M}_c}{\dot{M}_{a1}} \cdot \frac{1}{F_{sp}} \quad (6)$$

$$C_{sp} = 3600 \cdot \frac{m_c}{F_{sp}} \quad (7)$$

$$F_{sp} = (1 + K) \cdot (C_{5am} - V) \quad (8)$$

$$C_{sp} = 3600 \cdot \frac{m_c}{(1 + K) \cdot (C_{5am} - V)} \quad (9)$$

The airflow at mixing area \dot{M}_{4am} area results from the mainstream gas flow \dot{M}_g and the secondary stream airflow \dot{M}_{a2} ; taking into account that the gas flow results as a mixture of air and hot gas and after having neglected the fuel flow with respect to the airflow, then the airflow at mixing area becomes proportional with the bypass ratio and the mainstream airflow.

$$\dot{M}_c \ll \dot{M}_{a1} \quad (10)$$

$$\dot{M}_g = \dot{M}_{a1} + \dot{M}_c \quad (11)$$

$$\dot{M}_g \approx \dot{M}_{a1} \quad (12)$$

$$\dot{M}_{4am} = \dot{M}_g + \dot{M}_{a2} \quad (13)$$

$$\dot{M}_{4am} \approx \dot{M}_{a1} + \dot{M}_{a2} \quad (14)$$

$$\dot{M}_{4am} \approx \dot{M}_{a1} \cdot (1 + K) \quad (15)$$

For the particular case of the engine running at SLS, ISA conditions, which in literature is also referred as the "design point" or the "fixed point regime", the performances of the MFTF engine at fixed point conditions (SLS, ISA) are given by the simplified relations (16-18).

$$F_{sp0} = (1 + K_0) \cdot C_{5am_0} \quad (16) \quad F_0 = F_{sp0} \cdot \dot{M}_{a10} \quad (17) \quad C_{sp0} = 3600 \cdot \frac{m_{c0}}{F_{sp0}} \quad (18)$$

The expressions connecting the **air flowrates on main and secondary streams** are as follows: being given the airflow of both streams $\dot{M}_a = 65.772$ [kg/s] and the by-pass ratio, then the airflow of mainstream \dot{M}_{a1} and the airflow on secondary stream \dot{M}_{a2} are deduced as the solutions of a linear system of equations; the index "0" refers to the parameters values at fixed point condition.

$$K = \frac{\dot{M}_{a2}}{\dot{M}_{a1}} \quad (19)$$

$$\dot{M}_a = \dot{M}_{a1} + \dot{M}_{a2} \quad (20)$$

$$\dot{M}_{a1} = \frac{\dot{M}_a}{(1 + K)} \quad (21)$$

$$\dot{M}_{a10} = 16.865 \text{ [kg/s]} \quad (21.0)$$

$$\dot{M}_{a2} = \frac{K}{(1 + K)} \cdot \dot{M}_a \quad (22)$$

$$\dot{M}_{a20} = 48.907 \text{ [kg/s]} \quad (22.0)$$

The influence of the altitude, Mach number and speed variation has effects not just on the performances of the mixed flows turbofan engine, but on the specific work of the compressor and fan, on compressor pressure ratio and fan pressure ratio, on the fluid flow rates on both streams, on by-pass ratio and dynamic pressure ratio. An excerpt of the calculations are exposed in the following:

The variation of the specific work of compressor and fan with the flight regimes is expressed by the corresponding values at fixed point and the square of the ratio of the speeds \bar{n} at off-design versus design regimes. For computing the altitude map and velocity map and/ or the universal map of the engine, the ratio of the speeds \bar{n} is equal to the unity, meaning that the engine is running at the design regime speed.

$$\bar{n} = \frac{n_{off-design}[rpm]}{n_{design}[rpm]} \quad (23)$$

$$l_c^* = l_{c0}^* \cdot \bar{n}^2 \quad (24)$$

$$l_v^* = l_{v0}^* \cdot \bar{n}^2 \quad (25)$$

The relations between the **specific work** of compressor l_c^* [kJ/kg] and fan l_v^* [kJ/kg] and pressure ratio and specific stagnation enthalpy at air intake i_1^* [kJ/kg] are (25) and (26); for the fixed point regime, the relations (25.0) and (26.0) are likewise, but with different proportion factor, which is the specific enthalpy $i_0 \approx 288$ [kJ/kg].

$$l_c^* = i_1^* \cdot \frac{\left((\pi_c^*)^{\left(\frac{k}{k-1}\right)} - 1 \right)}{\eta_c^*} \quad (25)$$

$$l_v^* = i_1^* \cdot \frac{\left((\pi_v^*)^{\left(\frac{k}{k-1}\right)} - 1 \right)}{\eta_v^*} \quad (26)$$

From equation $\eta_m \cdot l_t^* = l_c^* + K \cdot l_v^*$ (27) which expresses the engine's work balance, the turbine specific work l_t^* [kJ/kg] is calculated. Therefore, at fixed point regime, the work balance shows $l_{c0}^* = 477$ [kJ/kg], $l_{v0}^* = 57.6$ [kJ/kg] and $l_{t0}^* = 645.3$ [kJ/kg].

$$l_{c0}^* = i_0 \cdot \frac{\left((\pi_{c0}^*)^{\left(\frac{k}{k-1}\right)} - 1 \right)}{\eta_{c0}^*} \quad (25.0)$$

$$l_{v0}^* = i_0 \cdot \frac{\left((\pi_{v0}^*)^{\left(\frac{k}{k-1}\right)} - 1 \right)}{\eta_{v0}^*} \quad (26.0)$$

The variation of the compressor pressure ratio (27) and fan pressure ratio (28) with the flying regime and engine speed.

$$\pi_c^* = \left(1 + \bar{n}^2 \cdot \left(\frac{i_0}{i_1^*} \right) \cdot \left(\frac{\eta_c}{\eta_{c0}} \right) \cdot \left[(\pi_{c0}^*)^{\left(\frac{k-1}{k}\right)} - 1 \right] \right)^{\left(\frac{k}{k-1}\right)} \quad (27)$$

$$\pi_v^* = \left(1 + \bar{n}^2 \cdot \left(\frac{i_0}{i_1^*} \right) \cdot \left(\frac{\eta_v}{\eta_{v0}} \right) \cdot \left[(\pi_{v0}^*)^{\left(\frac{k-1}{k}\right)} - 1 \right] \right)^{\left(\frac{k}{k-1}\right)} \quad (28)$$

The **dynamic pressure ratio** is defined (29) as the ratio of the stagnation versus static pressure at known altitude H [km]. After introducing the thermodynamic function $\theta(M)$ of argument being the Mach number, then other equations are deduced for the dynamic pressure ratio π_d^* .

$$\pi_d^* = \left(\frac{P_H^*}{P_H} \right) \quad (29)$$

$$\theta(M) = \left(\frac{T_H^*}{T_H} \right) \quad (30)$$

$$\theta(\lambda) = \left(\frac{T_H}{T_H^*} \right) \quad (31)$$

$$\theta(M) = \left(1 + \frac{k-1}{2} \cdot M^2 \right) \quad (32)$$

$$\theta(\lambda) = \left(1 - \frac{k-1}{k+1} \cdot \lambda^2 \right) \quad (33)$$

$$\left(\frac{P_H^*}{P_H} \right) = \left(\frac{T_H^*}{T_H} \right)^{\left(\frac{k}{k-1} \right)} \quad (34)$$

$$\pi_d^* = \left(\frac{T_H^*}{T_H} \right)^{\left(\frac{k}{k-1} \right)} \quad (35)$$

$$\pi_d^* = [\theta(M)]^{\left(\frac{k}{k-1} \right)} \quad (36)$$

$$\pi_d^* = [\theta(\lambda)]^{\left(\frac{k}{k-1} \right)} \quad (37)$$

The variation of the **bypass ratio** (38):

$$K = K_0 \cdot \left(\frac{\pi_v^*}{\pi_{v0}^*} \right) \left(\frac{\pi_{c0}^*}{\pi_c^*} \right) \cdot q(\bar{\lambda}_{s2}) \cdot \sqrt{\frac{(i_0 + l_{v0}^*)}{(i_1^* + l_{v0}^*)}} \quad (38)$$

This equation correlates the variation of the bypass ratio with the pressure ratios of fan and compressor, specific work of fan at fixed point l_{v0}^* , velocity coefficient λ and enthalpy at intake i_0 and i_1^* for fixed point and flight conditions respectively. With the thermodynamic flow function $q(\lambda)$, the dimensionless parameter $q(\bar{\lambda}_{s2})$ is obtained.

$$q(\bar{\lambda}_{s2}) = \frac{q(\lambda_{s2})}{q(\lambda_{s2_0})} \quad (39)$$

$$q(\lambda) = \lambda \cdot \left[\frac{k+1}{2} \cdot \left(1 - \left(\frac{k-1}{k+1} \right) \cdot \lambda^2 \right) \right]^{\frac{1}{k-1}} \quad (40)$$

$$\theta(\lambda) = \left(1 - \frac{k-1}{k+1} \cdot \lambda^2 \right) \quad (41)$$

$$a_{cr} = \sqrt{2 \cdot \frac{k}{k+1} \cdot R \cdot T^*} \quad (42)$$

$$i_1^* = i_H^* = i_H + \frac{V^2}{2} \quad (43)$$

$$i_H^* = i_H \cdot [\theta(M)] \quad (44)$$

The variation of **air flow on mainstream** is given by relation (45) and of airflow on secondary stream is then $\dot{M}_{a2} = K \cdot \dot{M}_{a1}$ (46), allowing to determine the airflow on both streams $\dot{M}_a = \dot{M}_{a1} + \dot{M}_{a2}$ (47); the variation of the both airflows with the flight regimes is influenced by the variation of the pressure ratio and bypass ratio with the flight regimes, the work done by the fan and inlet enthalpy for SLS, ISA and flight altitude, ISA.

$$\dot{M}_{a1} = \dot{M}_{a10} \cdot \frac{\pi_c^*}{\pi_{c0}^*} \cdot \pi_d^* \cdot \frac{p_H}{p_0} \quad (45)$$

The exhaust velocity of the mixed streams allows the calculation of specific thrust and thrust; it is defined by the drop of stagnation enthalpy between the mixing zone and engine' exhaust; the equivalent relation expresses the link between the exhaust velocity with the stagnation enthalpy in the mixing area and the ratio of stagnation pressures.

$$C_{5am} = \varphi_{ar_am} \cdot \sqrt{2 \cdot (i_{4am}^* - i_{5am_id})} \quad (48)$$

$$C_{5am} = \varphi_{ar_am} \cdot \sqrt{2 \cdot i_{4am}^* \cdot \left(1 - \left(\frac{p_5}{p_{4am}^*} \right)^{\frac{k_g-1}{k_g}} \right)} \quad (49)$$

$$C_{5am} = \varphi_{ar_am} \cdot \sqrt{2 \cdot i_{4am}^* \cdot \left(1 - \left(\frac{p_H}{p_{4am}^*} \right)^{\frac{k_g-1}{k_g}} \right)} \quad (50)$$

Usually, the exhaust velocity is calculated with the relation (49), which is valid for fully expansion, or with its equivalent (50) for partial expansion.

$$C_{5am} = \varphi_{ar_am} \cdot \sqrt{2 \cdot i_{4am}^* \cdot \left(1 - (0.543)^{\frac{k_g-1}{k_g}} \right)} \quad (51)$$

Fully expansion of core exhaust gases (down to ambient pressure) allows the obtaining of the maximum thrust, and occurs at take off; for the flight regimes, the core exhaust gases are partially expanded, down to the critical pressure.

$$p_{cr} \approx 0.543 \cdot p_{4am}^* \quad (52)$$

$$\left\{ \begin{array}{l} \text{if } (p_{cr} \leq p_H) \\ \text{then } (p_5 = p_H) \end{array} \right. \quad (53)$$

$$\left\{ \begin{array}{l} \text{if } (p_{cr} > p_H) \\ \text{then } (p_5 = p_{cr}) \end{array} \right. \quad (54)$$

The critical pressure aft turbine p_{cr} is an important parameter for determining the conditions for fully expansion (53) of partially expansion (54) of the mixing stream at exhaust. According to the nature of the expansion (i.e. fully versus partially), the exhaust velocity C_{5am} and then the performances of the engine (i.e. the specific thrust F_{sp} , thrust F and specific fuel consumption C_{sp}) can be calculated.

The critical pressure aft turbine p_{cr} (52) is calculated after the determination of the stagnation pressure at mixing area p_{4am}^* from the relation (55).

$$(1+K) \cdot \frac{\sqrt{T_{4am}^*}}{p_{4am}^*} \cdot \frac{1}{q(\lambda_{4am})} = \frac{\sqrt{T_4^*}}{p_4^*} \cdot \frac{1}{q(\lambda_4)} + K \cdot \frac{\sqrt{T_{2v}^*}}{p_{2v}^*} \cdot \frac{1}{q(\lambda_{2v})} \quad (55)$$

The calculation of the incoming and outgoing parameters from the mixing area is based on the mixing area model; from the condition that the velocities and pressures (static or stagnation) must be equal, is deduced, Andrei I. [15], a non linear equation (56) or (57) for the identification of the turbine inlet temperature T3T, which can be solved numerically.

$$\pi_c^* \cdot \sigma_{ca}^* \cdot \left(1 - \left(\frac{l_c^* + K \cdot l_v^*}{\eta_t^* \cdot i_3^*} \right) \right)^{\left(\frac{k_g}{k_g - 1} \right)} = \left(1 + \left(\frac{l_v^* \cdot \eta_v^*}{i_1^*} \right) \right)^{\left(\frac{k}{k-1} \right)} \quad (56)$$

$$\ln(\pi_c^* \cdot \sigma_{ca}^*) + \left(\frac{k_g}{k_g - 1} \right) \cdot \ln \left(1 - \left(\frac{l_c^* + K \cdot l_v^*}{\eta_t^* \cdot i_3^*} \right) \right) = \left(\frac{k}{k-1} \right) \cdot \ln \left(1 + \left(\frac{l_v^* \cdot \eta_v^*}{i_1^*} \right) \right) \quad (57)$$

Based on the conservation laws for mass, momentum and energy (58-60), the governing equations for the mixing area (61-62) are deduced:

$$\text{Mass conservation} \quad \dot{M}_{4am} = \dot{M}_{a1} \cdot (1+K) \quad (58)$$

$$\text{Momentum conservation} \quad (1+K) \cdot \sqrt{T_{4am}^*} \cdot z(\lambda_{4am}) = \sqrt{T_4^*} \cdot z(\lambda_4) + K \cdot \sqrt{T_{2v}^*} \cdot z(\lambda_{2v}) \quad (59)$$

$$\text{Energy conservation} \quad (1+K) \cdot i_{4am}^* = i_4^* + (1+K) \cdot i_{2v}^* \quad (60)$$

$$(1+K) \cdot \frac{\sqrt{T_{4am}^*}}{p_{4am}^*} \cdot \frac{1}{q(\lambda_{4am})} = \frac{\sqrt{T_4^*}}{p_4^*} \cdot \frac{1}{q(\lambda_4)} + K \cdot \frac{\sqrt{T_{2v}^*}}{p_{2v}^*} \cdot \frac{1}{q(\lambda_{2v})} \quad (61)$$

$$\lambda_4 \cdot (1+K) + \frac{1}{\lambda_4} \cdot \left(1 + K \cdot \frac{T_{2v}^*}{T_4^*} \right) = (1+K) \cdot \sqrt{\frac{T_{4am}^*}{T_4^*}} \cdot \left(\lambda_{4am} + \frac{1}{\lambda_{am}} \right) \quad (62)$$

The solutions are the roots (64) of the second order parabola (63); taking into account that the velocity coefficient (65) is always less than the unity, then there is only one valid value for the solution.

$$(\lambda_4)^2 \cdot (1+K) - (\lambda_4) \cdot (1+K) \cdot \sqrt{\frac{T_{4am}^*}{T_4^*}} + \left(1 + K \cdot \frac{T_{2v}^*}{T_4^*} \right) = 0 \quad (63)$$

$$(\lambda_4)_{1,2} = \frac{1}{2} \cdot \left(\sqrt{\frac{T_{4am}^*}{T_4^*}} \pm \sqrt{\frac{T_{4am}^*}{T_4^*} - \frac{4}{(1+K)} \cdot \left(1 + K \cdot \frac{T_{2v}^*}{T_4^*} \right)} \right) \quad (64)$$

$$\lambda \in [0,1] \subseteq \Re \quad (65)$$

$$\lambda_{2v} = \lambda_4 \cdot \sqrt{\frac{T_4^*}{T_{2v}^*}} \quad (66)$$

Therefore, the velocity coefficients for the main stream λ_4 (60) and secondary stream λ_{2v} (49) are determined analytically, both ranging the interval [0,1].

The mathematical model of a jet engine is completed by the assumptions regarding the properties of the fluids: 1/ the working fluid is considered perfect gas, 2/ two species:

A. // **air** // - from intake to compressor,

B. // **burned gas** // - within combustor, turbine and exhaust unit,

3/ fuel specific power, for JET A, JET A1 and/or JET B (aviation kerosene):

$P_{CI} = 43500 \left[\frac{kJ}{kg} \right]$, 4/ ratio of specific heat $k = \frac{C_p}{C_v}$, see Table 1; 5/ constant pressure specific heat $C_p \left[\frac{kJ}{kgK} \right]$; 6/ gas constant $R \left[\frac{kJ}{kgK} \right]$; the relation between R and C_p is (67):

$$C_p = R \cdot \frac{k}{k - 1} \quad (67)$$

Table 1 - Properties of the working fluids

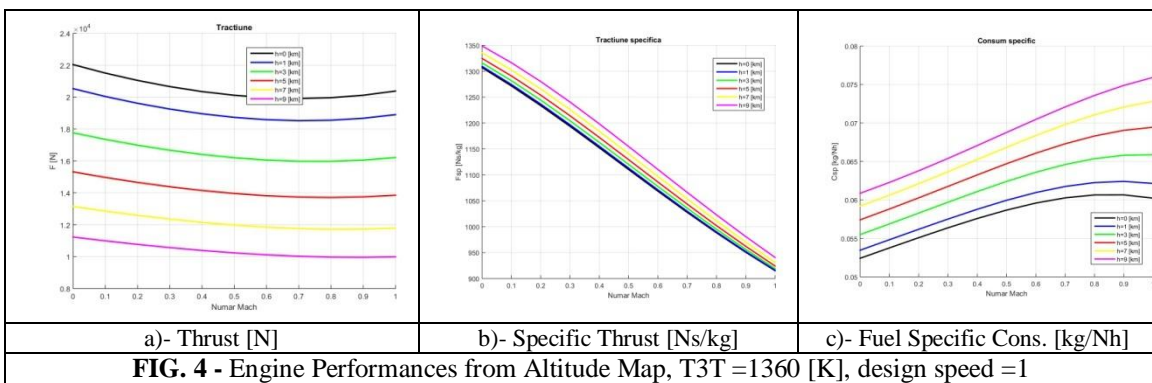
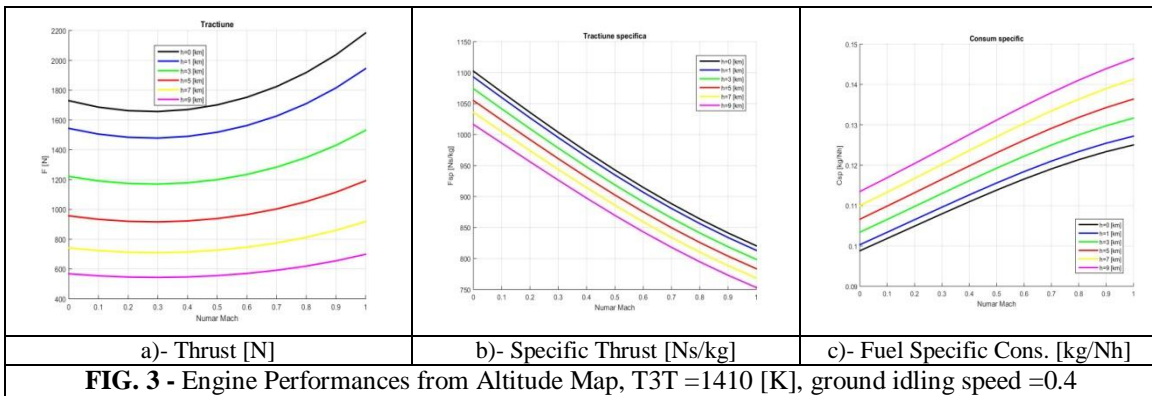
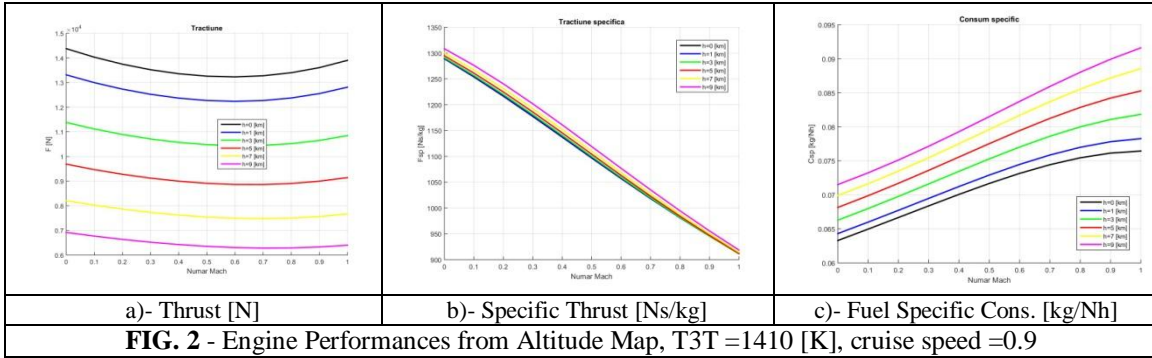
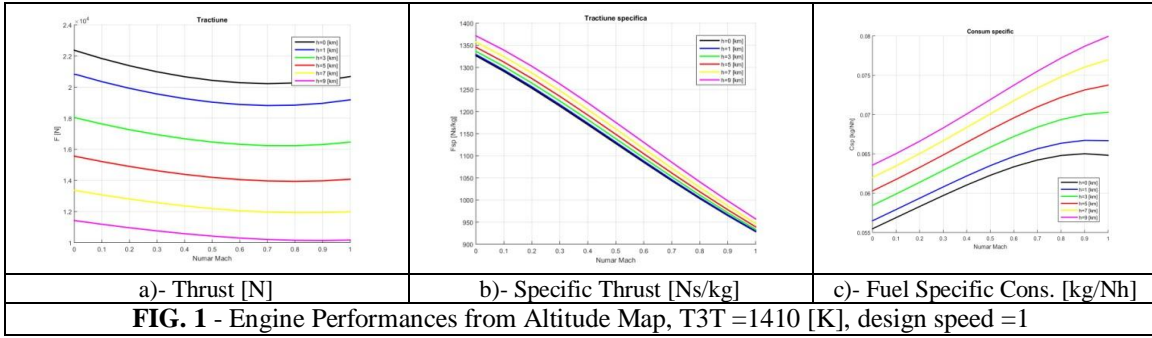
Fluid	k	C_p [kJ/kg/K]	R [J/kg/K]
Air	1.4	1.005	287.3
Burned Gas	1.33	1.165	288.4

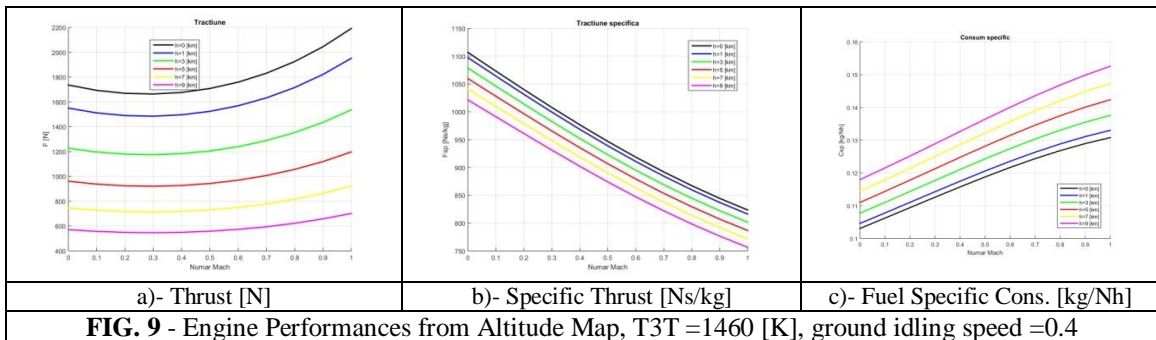
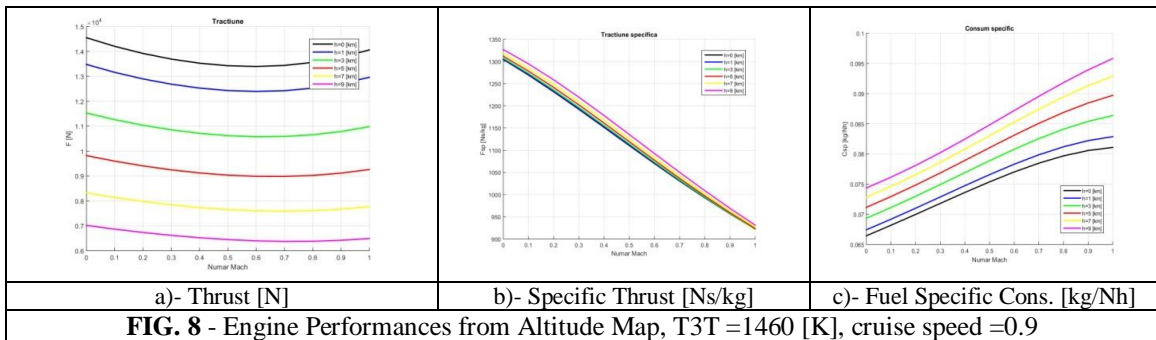
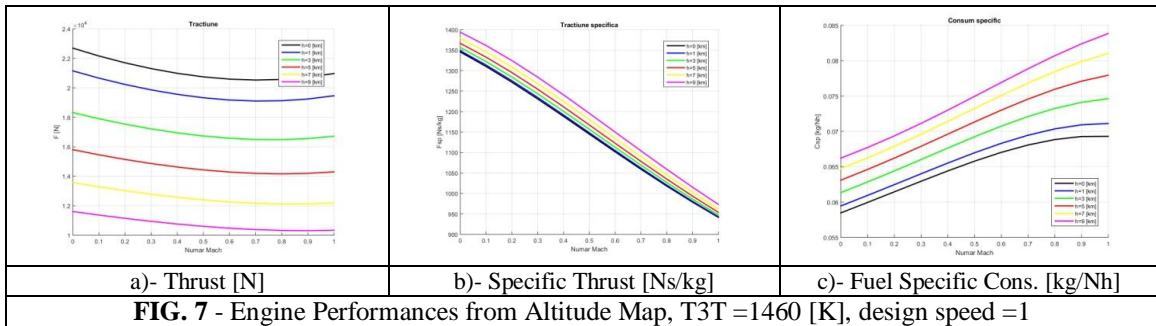
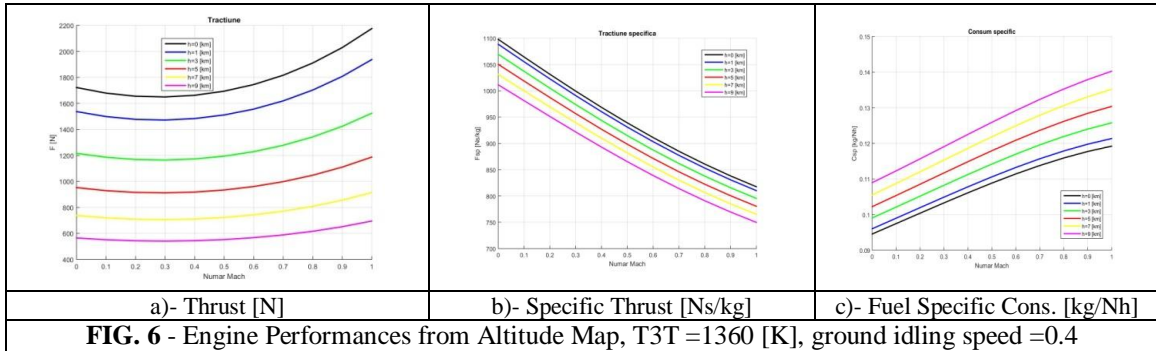
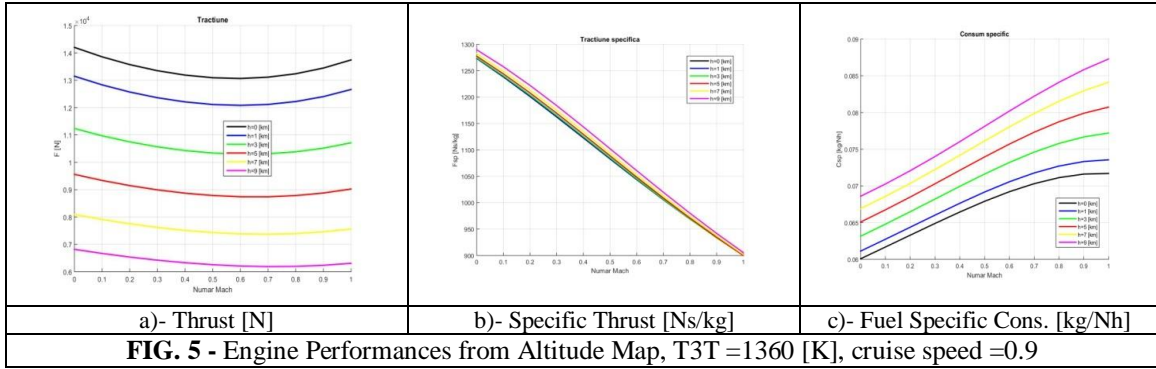
The mathematical model of a mixed flows turbofan includes the mathematical model of a turbojet engine, since the latter describes the mainstream fluid flow thermodynamical processes.

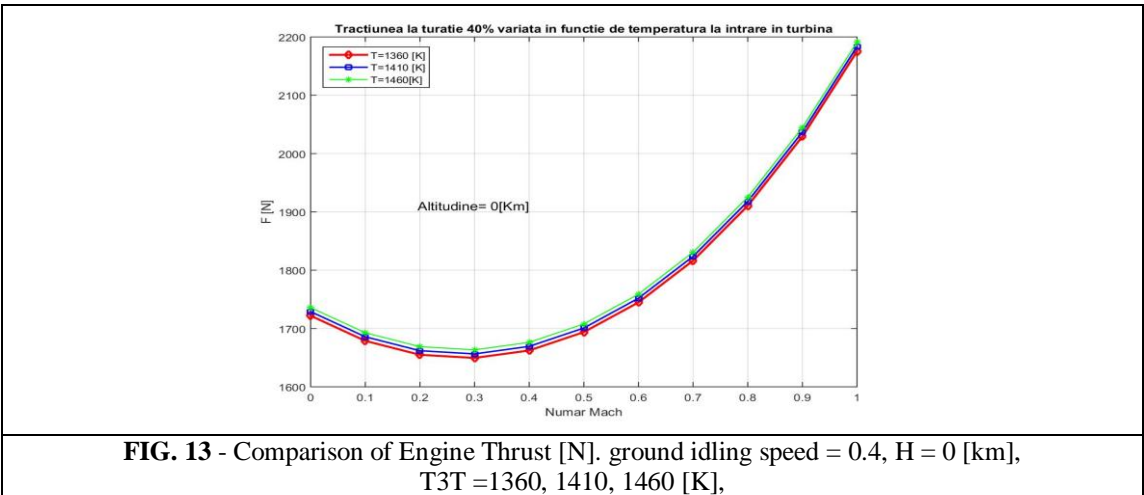
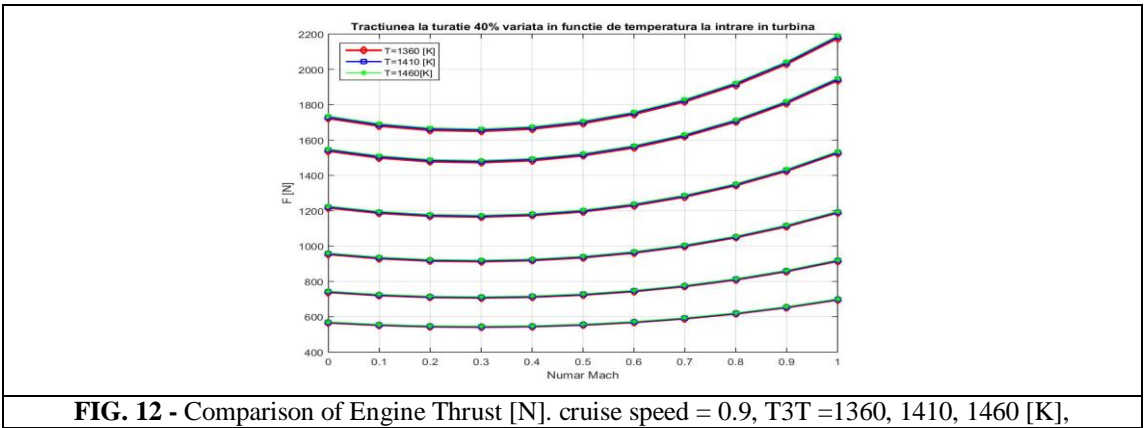
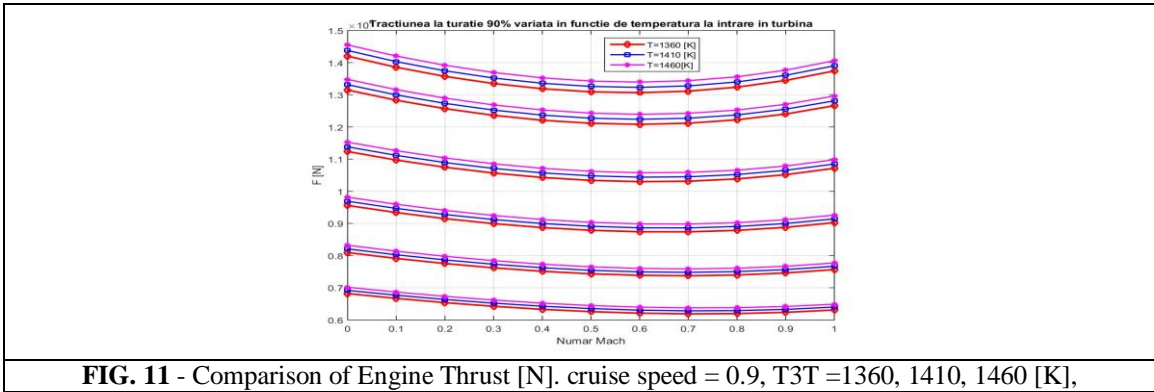
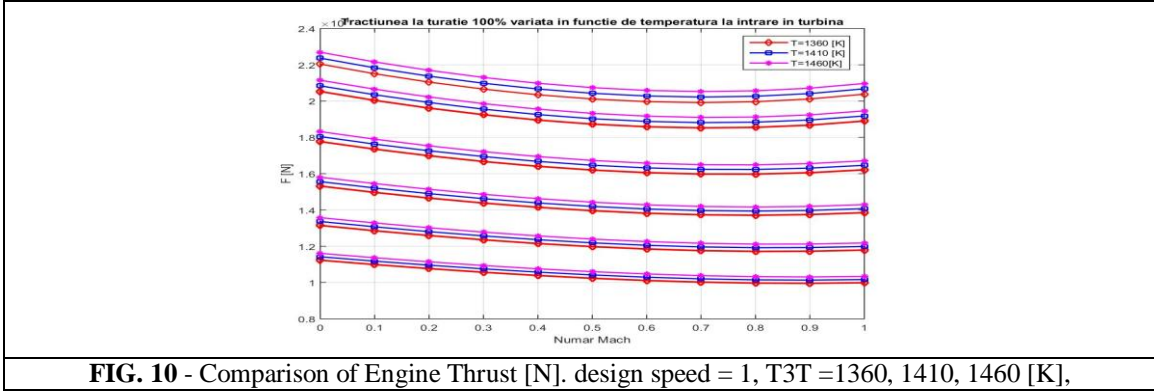
The results from the simulation the Mixed Flows Turbofan Engine are summarized and presented graphically as the engine operating maps (i.e. the altitude map, the velocity map, the rotor speed map) and the engine's universal map; their definitions are introduced in the following, taking into account that these maps express the variation of the jet engine performances: thrust F [N], specific thrust F_{sp} [Ns/kg] and specific fuel consumption C_{sp} [kg/Nh] or TSFC, with altitude, flight velocity and engine rotational regime)

4. RESULTS

This investigation is focused on highlighting the influence of the turbine inlet temperature, as the most significant parameters of the combustion chamber, upon the turbojet engine's performances. With respect to the engine's design point parameters, i.e. the turbine inlet temperature being 1410 [K], it was considered a ranging interval from 1360 [K] up to 1460 [K], which corresponds to a perturbation of temperature with 50 [K], up and down with respect to the reference value.







5. CONCLUSIONS & ACKNOWLEDGMENT

The investigation presented in this paper is focused on the influence of the variation of the turbine inlet temperature, as perturbation of the engine's design parameter and altitude Mach number and speed as perturbations of the flight and engine operating regimes.

The objective of this study is to highlight the variation of engine's thrust for a given perturbation of the turbine inlet temperature. The turbine inlet temperature ranges between 1360 and 1460 [K], which corresponds to a perturbation of +/- 50 [K] with respect to the reference value, that is considered at the engine's design point.

The predicted performances of the turbojet engine (i.e. thrust, specific thrust and fuel specific consumption) are summarized in Fig. 1 ÷ Fig. 9. In Fig. 10÷ Fig. 13 is summarized a comparison of the variation of thrust with the temperature T3T, for different rotor speed, flight Mach number and altitude. From Fig. 10÷ Fig. 13 comes out that the influence of T3T temperature perturbation on thrust is larger with the variation of rotor speed than with the flight velocity.

This observation can direct the future developments of this study towards the establishing of a new command and control law for the turbofan engine operation. Further, the practical applications of this study can be related to be used both for training the pilot students and during flight operation, for contributing to an improvement in flight safety, which can be of real help for fighter pilots.

The authors would like to express their gratitude to the INCAS - National Institute of Aerospace Research "Elie Carafoli" Bucharest for the support while carrying on research activities within the Flow Physics Department, Numerical Simulations Unit, as well as the documentary research. The results presented in this paper are correlated to the current research activities regarding the jet propulsion systems, carried on within INCAS.

REFERENCES

- [1] J. D. Mattingly, *Elements of Propulsion and Gas Turbine and Rockets*, American Institute of Aeronautics and Astronautics Education Series, Inc. Reston, VA., 2006
- [2] ***, Rolls Royce, *The Jet Engine*, fifth edition, ISBN 0 902121 2 35, The Technical Publications Department Rolls-Royce plc, Derby, England
- [3] ***, Powerplant, JAA ATPL Training, JEPPESEN, Atlantic Flight Training Ltd
- [4] Wilfried Wisser, *Generic Analysis Methods for Gas Turbine Engine Performance, The development of the gas turbine simulation program GSP*, PhD Thesis, NLR and TU Delft, 2015.
- [5] ***, *Compressor and Turbine Maps for Gas Turbine Performance Computer Programs*, Issue 3, GasTurb GmbH, 2013
- [6] NASA Technical Memorandum **TM X-3014**, *A generalized hybrid computer program for studying turbojet or turbofan engine dynamics*, John Szuch, Cleveland, Ohio, 1974
- [7] S. M. Eastbourn, *Modeling and simulation study of a dynamic turbofan engine using Matlab Simulink*, M. Sc. A.E. Dissertation, Wright State University, 2012
- [8] Pimsner V., *Motoare aeroreactoare*, Ed. Didactica si Pedagogica, Bucuresti, 1983
- [9] Irina Andrei, Adrian Toader, Gabriela Stroe, Florin Frunzulica, *Performance Analysis and Dynamic Modeling of a Single-Spool Turbojet Engine*, International Conference in Nonlinear Problems in Aviation and Aerospace ICNPAA 2016, La Rochelle, France, AIP Conference Proceedings,
- [10] Gabriela Stroe, Irina Andrei, Florin Frunzulica, *Analysis of Control System Responses for Aircraft Stability and Efficient Numerical Techniques*, International Conference in Nonlinear Problems in Aviation and Aerospace ICNPAA 2016, La Rochelle, France, AIP Conference Proceedings,
- [11] Irina Andrei, Mihai Niculescu, Mihai Victor Pricop, Andreea Cernat, *Study of the Turbojet Engines as Propulsion Systems for the Unmanned Aerial Vehicles*, AFASES 2016, AFAHC Brasov, 2247-3173, Diseminare Proiect MASIM
- [12] Alexandru Ionel, Stefan Palas, Irina Andrei, *Performance Analysis of the IAR 99 SOIM and IAR 99 TD*, AEROSPATIAL 2016, INCAS, ISSN 2067-8614

- [13] Andreea Cernat, Alexandru Ionel, Irina Andrei, Stefan Palas, Adrian Mihai, *Simulation Tool for Predicting Ground Test Performances of a Turbofan Propulsion System Air Inlet*, AEROSPATIAL 2016, INCAS, ISSN 2067-8614
- [14] Irina Andrei, Alexandru Ionel, Adrian Mihai, Stefan Palas, Tiberiu Salaoru, *Numerical Modeling Application for Simulating Engine Test Cell Validation Methodology of a Turbofan Exhaust System*, AEROSPATIAL 2016, INCAS, ISSN 2067-8614
- [15] Irina Andrei, Alexandra Stanescu, Adrian Toader, *Issues on the completion of the mathematical model by Parameter Identification for Simulating a Jet Engine*, NMAS 2016, INCAS, ISSN 2360-1809
- [16] Vasile Prisacariu, Ionica Cîrciu, *Considerations Regarding the Performances of the Combustion Chambers for Turbojet Engines*, Review of the Air Force Academy, No 2 (32) 2016 DOI: 10.19062/1842-9238.2016.14.2.7
- [17] Irina Andrei, Adrian Toader, Ana Maria Neculaescu, *Numerical Simulations of Steady-State and Dynamic Analysis of a Single-Spool Turbojet Engine*, NMAS 2016, INCAS, ISSN 2360-1809
- [18] Dr. I. Andrei, A. Stanescu, *Issues on modeling and simulation of a mixed flows turbofan*, Caius Iacob Conference, 2015
- [19] Ciobotea V., *Teoria motoarelor de aviatie, vol. 1*, Editura Academiei Militare, Bucuresti, 1978;
- [20] Manole I., *Solutii constructive de turbomotoare de aviatie (album de scheme), vol. 1*, Editura Academiei Militare, Bucuresti, 1977;
- [21] Rotaru C., Mihaila-Andres M., Pericle G.M., Edu R. I., *Thermodynamic performances of the turbojet combustion chambers – numerical evaluation*, Proceedings of the 2014 International Conference on Mechanics, Fluid Mechanics, Heat and Mass Transfer, p. 86-91, 2014;
- [22] Rotaru C., Cîrciu I., Arama C., Constantinescu C., *Aspects regarding velocity distribution in the secondary zone of a gas turbine combustor*, Review of the Air Force Academy, 2/2015, DOI: 10.19062/1842-9238.2015.13.3.5, p. 33-38, 2015;
- [23] Rotaru C., Andres-Mihaila M., Pericle G.M., *An Extended Combustion Model for the Aircraft Turbojet Engine*, International Journal of Turbo & Jet-Engines, 3/2014, p.229-237, 2014.
- [24] Farokhi S., *Aircraft propulsion*, second edition, Wiley and sons, 2014;
- [25] Stefanescu I., *Advanced Training Aircraft IAR 99 (A) SOIM*, INCAS BULLETIN, vol. 4, Issue 2/2012, DOI: 10.13111/2066-8201.2012.4.2.13, pp. 125 – 135, 2012;
- [26] F. Zare, Dr. Arpad Veress, K. Beneda, *Simplified mathematical model for a single spool and no by-pass jet engine*, RTK Conference, BME, 2013
- [27] H. Asgari, X. Chen, R. Sainudin, *Modeling and simulation of gas turbines*, Intl. Journal Modelling, Simulation and Control, 2013.
- [28] S. C. Uysal, *High by-pass ratio turbofan engines aero-thermodynamic design and optimization*, PhD Thesis, The Graduate School of Natural and Applied Sciences, Middle East Technical University, 2014
- [29] NASA Technical Memorandum 83446 (NASA - TM 83446), *Digital Computer Program for Generating Dynamic Turbofan Engine Models (DIGTEM)*, C.J. Daniele, S. M. Krosel, J. R. Szuch, E. J. Westerkamp, Lewis Research Center, Cleveland, Ohio, 1983

INFORMATION MANAGEMENT IN UAS MULTIAGENT

Ana-Maria BĂLDEA *, Mihaela GARABET**

*SIVECO București, Universitatea Transilvania din Brasov, Romania
(baldea_ana_maria@yahoo.com, ana.baldea@siveco.ro)

**SIVECO București, Romania (mihaela.garabet@siveco.ro)

DOI: 10.19062/2247-3173.2017.19.1.4

Summary: *Robotic aerial systems have seen a significant development in recent years, both due to technological development and the various missions that can be accomplished by the onboard equipment, leading to innovative approaches in inter and transdisciplinary fields due to technological and information management challenges, starting with concepts, materials, technologies, programming and ending with the educational and human resources area.*

The article wishes to present the UAS multi-agent systems from the perspective of information exploitation and sharing.

Keywords: UAV / UAS, multiagent system, ad-hoc network, flying wing, multicopter

Acronyms and symbols

UAV/UAS	Unmanned aerial vehicles/system	ISR	Intelligence, surveillance, reconnaissance
MAS	Multiagent system	WLAN	Wireless Local Area Network
NLS	Neutrosophic Logic System	GCS	Ground control station
MMAS	Max-Min Ant System	CACM	Clever Ant Colony Metaphor
EO-IR	Electro optic - infrared	WI-FI	wireless local area networking
STEM	Science, Technology, Engineering, Mathematics		
TCP-IP	Transmission Control Protocol - Internet Protocol		

1. INTRODUCTION

Robotic aerial systems have seen a significant development in recent years, both due to technological development and the various missions that can be accomplished by the onboard equipment, leading to innovative approaches in inter and transdisciplinary fields due to technological and information management challenges, starting with concepts, materials, technologies, programming and ending with the educational and human resources area. (STEM concept), [21, 23].

Specialized literature reveals a series of multiagent UAS in complex architectures that can carry out elaborate tasks and missions, sensor node networks on different locations [1, 2, 3, 19].

2. MULTIAGENT SYSTEM PROPOSAL

2.1. Information processing

The multiagent system consists of the following subsystems: the aerial system (both fixed and winged air vectors in modular design with flexible equipment, mission-adaptable), portable control station (portable platform, equipped with capabilities of command, control and maintenance), communications system, air-handling control platform and intelligent information management, see Figure 1, [3].

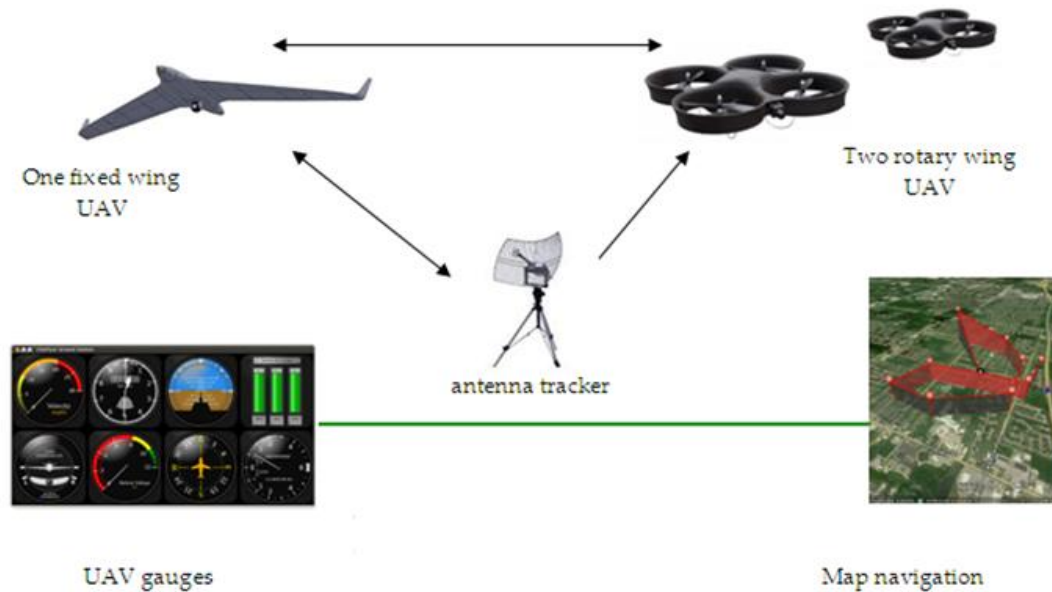


FIG.1. MASIM multiagent aerial system, [3]

2.2. Exploiting information

Unmanned aerial systems respond to any type of applications and missions carried out by classical aircraft and even an extension to the dangerous mission area, low life cycle costs, outstanding efficacy increasingly causing aerospace builders to turn to this type of research.

The ISR concept (*intelligence* – processed information, *surveillance* – information refinement through persistent observations and continuous collection, and *reconnaissance* - short-term coverage of a specific objective located in areas of interest) refers to the timely obtaining of accurate and relevant information at the same time as continuous and synchronized mission planning. ISR is based on the active use of wide-area sensors, information processing, exploitation and dissemination systems, providing full and effective decision support. ISR achieves a unique synergy that is based on the collection, provision, analysis of persistent and concentrated coverage, providing the ingredient for effective decisions in both urban and extra urban areas [5, 6].

The main missions specific to aerial platforms networks are: support in fire fighting, search-rescue, crash situations in crowded locations. The current state of the distributed vector-based control concept of air vector-type agents shows that a multi-agent system (MAS) is based on a concurrent, asynchronous, stochastic, and distributed computerized system architecture. These features of a multi-agent system provide the functions of a dynamic system with discrete events, which can be studied with analytical methodologies, especially with Petri networks [7, 8].

The main function of multi-agent control systems is the use of the concept of "agent coordination" to implement the "distributed control" concept. The ad-hoc network allows any two nodes to communicate, either directly or through an arbitrary number of other nodes acting as relays. The network protocol is an implementation of the dynamic ad-hoc network routing protocol. A monitoring architecture has been incorporated for detailed performance monitoring.

In order to establish a robust networking framework for aerial platforms, it is necessary to consider: the establishment of the architecture (the number and types of platforms according to with the mission); mission planning (feasibility, optimal trajectories); information exchange between component platforms; data merger to increase bandwidth efficiency; optimization of sensor arrangement; avoiding collisions and obstacles (sense and avoid), [9, 10, 11, 12].

The difficulty of reconfiguring such a hierarchical control system can be solved with the Multi-Agent System with reconfiguration potential. The use of a single central controller for a group of platforms is complicated by the increase in the number of agents because the central controller has to be informed of all the knowledge and intentions of the agents.

The proposed IT solution aims at implementing neutrosomic algorithms to optimize an overflow area and a network of UAVs required in overflight action, after a predetermined purpose and under specific surface conditions.

Pre-configuring the sensor quality parameters with which UAVs can be equipped (the distance from which they can detect, whether they can detect day and night, etc.), the application will automatically run the optimization algorithms, proposing one or more overflight solutions as output data, according to the purpose set:

- generating the number of optimal UAVs to be used (with the appropriate sensors);
- the flight path for each UAV (trajectory/waypoint) equipment, e.g. increasing the likelihood of finding the missing person in the shortest possible time. The flight path consists of sets of GPS coordinates that will be automatically transmitted by the piloting console application. The resulting flight path will have to meet the following essential conditions: the overflight area to be fully covered; covered areas may overlap or not; there is no collision risk; the cost of flying is optimal as time and energy consumption.

The Mobile Surveillance and Command Center is currently equipped with a UAV pilot solution based on an open-source web-based graphical targeting architecture using manual mapping (Google Earth). The solution can run on mobile devices such as tablets/notebooks to ensure mobility. This solution will be integrated at the database level through automated script-based transfer with the optimization solution proposed in this project to simplify the UAV operator's task of manually entering the overflight plan, eliminating any errors, and offering advantages regarding costs and time.

2.3. The IT application

The IT application will be developed in web technology under a Windows-based HTML5 /Javascript platform that involves the exclusive existence of a browser (IE, Chrome or Firefox) and a minimum resolution of 1024x & 68 with a local, internal database that can keep track of route paths or a possible history of changes. The application will be able to run a set of reports on covered areas, time necessary for overflight, estimated energy consumption, etc.

The portability level of the application implies the possibility of also running on operating systems dedicated to mobile devices with Java support (tablets or laptops).

The secondary functionalities of the application are: configuring various administrative or operational users, configuring automatic data transmission in TXT/XML format, archiving or restoring the database.

In the UAV system architecture, each node (multicopter, wing, GCS) will be equipped with wireless TCP / IP networking devices (WLANs) generally associated with communications in the IEEE 802.11 standard as follows, See figure 2:

- A. GCS 1: WI-FI modem and access point
- B. GCS 2: WI-FI Modem
- C. Multicopter 1: WI-FI modem and access point
- D. Multicopter 2: WI-FI modem and access point
- E. Flying wing: WI-FI modem.

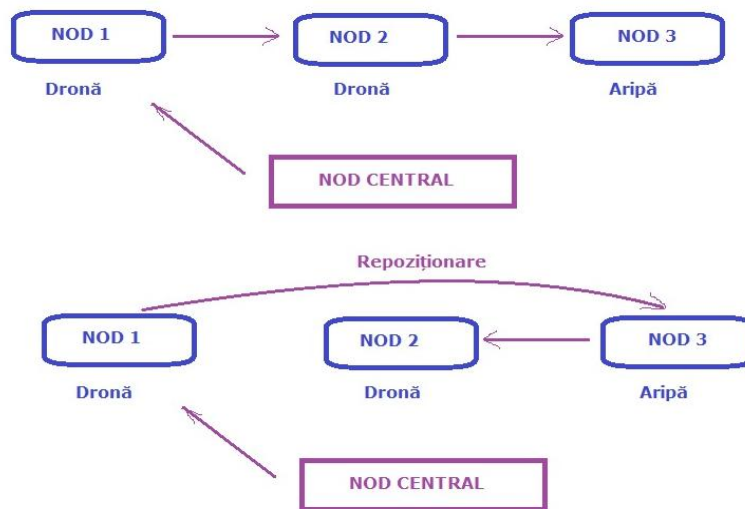


FIG.2 MASIM system architecture

3. AERIAL VECTORS

The master air vector is chosen in the fixed flying wing configuration (see figure 3), a configuration that was analyzed by numerical simulations and experimental tests in the subsonic sphere at INCAS Bucharest, the results being disseminated in a series of scientific references [13, 14, 17, 18].

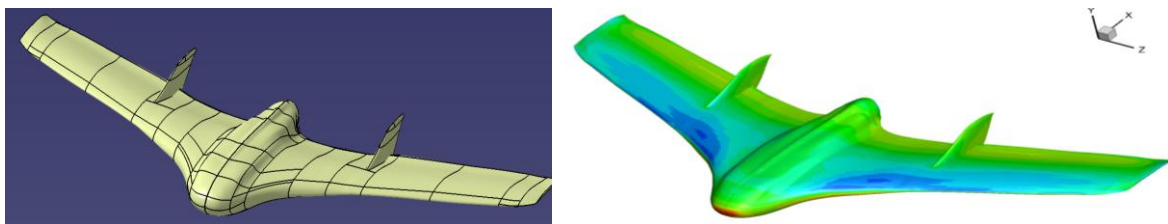


FIG.2 MASIM flying wing, [13]

The multicopters complete the aerial vector network by performing missions defined and selected by the high-speed vector (flying wing), data acquisition (EO-IR or biometric data) missions on delimited areas, see Figure 3.



FIG.2 MASIM Multicopter, (a. multicopter, b. precision agriculture map)

4. CONCLUSIONS AND FUTURE RESEARCH DIRECTIONS

The main future research directions include: identifying innovative technologies for tactical and operational decision support based on mobile sensor networks; developing strategies to increase the performance of air platforms (fixed wing and rotating wing) while miniaturizing them; designing special algorithms for miniaturized aerial platform missions; developing coordination strategies for the control of miniaturized aerial platforms (using a single autopilot for the formation head); developing "sense and avoid" strategies to avoid fixed or mobile obstacles.

With regard to the patenting of some of the innovative solutions within the project, the following are being taken into account: the solutions to increase the performances and capabilities of flying wing and rotary wing aerial platforms by modularity and the introduction of the morphing adaptability concept [15]; innovative mission planning algorithms under conditions of resource and airspace management restrictions based on the use of neutrosopic logic and NLS or social network analysis methods including CACM and MMAS solutions, [20, 24]; filtering and control algorithms that are specific to the models resulted for representation of the network of aerial platforms with sampled information; software implementation solutions for data control and distributed filtering algorithms.

STEM approaches [21], the UAV limits [22] and the experimental methods of assessing UAV performance [25] determine a conceptual propagation in the adjacent and interaction domains of robotic technical systems with the human resource that makes and uses this type of aerial vectors.

ACKNOWLEDGMENT

This work is supported by the Executive Agency for Higher Education, Research, Development and Innovation Funding (UEFISCDI) under MASIM project (PN-II-PT-PCCA-2013-4-1349).

REFERENCES

- [1] Maza, I., Kondak, K., Bernard, M. et al., *Multi-UAV Cooperation and Control for Load Transportation and Deployment*, J Intell Robot Syst (2010) 57: 417. , doi:10.1007/s10846-009-9352-8;
- [2] Ding, Xu Chu, Amir R. Rahmani, and Magnus Egerstedt. "Multi-UAV convoy protection: An optimal approach to path planning and coordination", IEEE Transactions on Robotics 26.2 (2010): 256-268;
- [3] Prisacariu V., Cîrciu I., Cioacă C., Boşcoianu M., Luchian A., *Multi aerial system stabilized in altitude for information management*, REVIEW OF THE AIR FORCE ACADEMY, 3(27)/2014, Braşov, Romania, ISSN 1842-9238; e-ISSN 2069-4733, p 89-94;

- [4] Barnhart R.K., Hottman S.B., Marshall D.M., Shappee E., *Introduction to unmanned aircraft systems*, CRC Press, 2012, ISBN 978-1-4398-3520-3, 215p;
- [5] Butler, Jeffrey T., *UAVs and ISR sensor technology*. No. AU/ACSC/033/2001-04. AIR COMMAND AND STAFF COLL MAXWELL AFB AL, 2001;
- [6] Eggers, J. W., and Mark H. Draper. "Multi-UAV control for tactical reconnaissance and close air support missions: operator perspectives and design challenges." Proc. NATO RTO Human Factors and Medicine Symp. HFM-135. NATO TRO, Neuilly-sur-Siene, CEDEX, Biarritz, France. 2006;
- [7] Love, Joshua Alan. *Network-Level Control of Collaborative UAVs*. Diss. University of California, Berkeley, 2011;
- [8] Love, Joshua, et al. "Csl: A language to specify and re-specify mobile sensor network behaviors." Real-Time and Embedded Technology and Applications Symposium, 2009. RTAS 2009. 15th IEEE. IEEE, 2009;
- [9] Muraru A., Cioaca C, Boscoianu M., *Modern Sense and Avoid Strategies for UAV*, la the 9th International Scientific Conference New Trends in Aviation Development, Technical University Kosice – Faculty of Aeronautics, Gerlachov-High Tatras, September 16-17, 2010, Slovak Republic, ISBN 978-80-553-0475-5;
- [10] Hutchings, Tim, Susan Jeffryes, and S. J. Farmer. "Architecting UAV sense & avoid systems." Autonomous Systems, 2007 Institution of Engineering and Technology Conference on. IET, 2007;
- [11] Prats, Xavier, et al. "Requirements, issues, and challenges for sense and avoid in unmanned aircraft systems." Journal of aircraft 49.3 (2012): 677-687;
- [12] Billingsley, Thomas B., Mykel J. Kochenderfer, and James P. Chryssanthacopoulos. "Collision avoidance for general aviation." IEEE Aerospace and Electronic Systems Magazine 27.7 (2012): 4-12;
- [13] Pepelea D. Cojocar M.G., Toader A., Niculescu M.L., *CFD analysis for UAV of flying wing*, SCIENTIFIC RESEARCH AND EDUCATION IN THE AIR FORCE-AFASES 2016, DOI: 10.19062/2247-3173.2016.18.1.22, p.171-176;
- [14] Prisacariu V., *CFD Analysis of UAV Flying Wing*, INCAS Bulletin, vol. 8, 3/2016, ISSN 2066 – 8201, DOI: 10.13111/2066-8201.2016.8.3.6, p 65-72;
- [15] Valasek J., *Morphing aerospace vehicles and structures*, Wiley, ISBN 978-0-470-97286-1, 2012, p286;
- [16] Fahlstrom P.G., Gleason T.J., *Introduction to UAV systems*, fourth edition, Aerospace Series, 2012 John Wiley & Sons Ltd., ISBN 978-1-119-97866-4, 280p;
- [17] Prisacariu V., Boşcoianu M., Cîrciu I., Lile Ramona, *Aspects Regarding the Performances of Small Swept Flying Wings Mini UAV-s in Aggressive Maneuvers*, Applied Mechanics and Materials, vol. 811, p. 157-161, Trans Tech Publications, 10.4028/www.scientific.net /AMM.811.157, ISSN: 1662-7482;
- [18] Prisacariu V., Boşcoianu Corina, Cîrciu I., Boşcoianu M., *The Limits of Downsizing –a Critical Analysis of the Limits of the Agile Flying Wing MiniUAV*, APPLIED MECHANICS AND MATERIALS Vol. 772 (2015) pp 424-429, © (2015) Trans Tech Publications, Switzerland, doi:10.4028/www.scientific.net /AMM.772.424, p. 424-429;
- [19] Ahmadzadeh, Ali, et al. "Multi-UAV cooperative surveillance with spatio-temporal specifications." Decision and Control, 2006 45th IEEE Conference on. IEEE, 2006;
- [20] Vladareanu V., et al. "Development Of Intelligent Algorithms For Uav Planning And Control." *Scientific Research & Education in the Air Force-AFASES 1* (2016), doi 10.19062/2247-3173.2016.18.1.29, p.221-226;
- [21] A.M. Baldea, M. Garabet, V. Prisacariu, I. Neacsu, *Educational approaches of the Romanian MASIM research project*, ICERI 2016 Proceedings, ISBN: 978-84-617-5895-1, ISSN: 2340-1095, doi: 10.21125/iceri.2016.2257, p.5201-5211;
- [22] Prisacariu V., Boşcoianu M., Luchian A., *Innovative solutions and UAS limits*, REVIEW OF THE AIR FORCE ACADEMY, 2(26)/2014, Braşov, Romania, ISSN 1842-9238; e-ISSN 2069-4733, p51-58;
- [23] F. X. Bogner, S. Schmid, O. Dieser, *Pathway – Predarea Ştiinţelor prin investigaţie*, Ghid pentru profesori, Creative Commons Attribution - NonCommercial-ShareAlike 3.0 Unported License, 2013;
- [24] Smarandache, Florentin. *Neutrosophic Theory and Its Applications, Vol. I: Collected Papers*. Infinite Study, 2014;
- [25] Anton S., Parvu P. "Experimental Methods for UAV Aerodynamic and Propulsion Performance Assessment." INCAS Bulletin, ISSN 2066–8201, Volume 7, Issue 2/ 2015, pp. 19–33.

ARE DRONES A BOON OR BANE?

Bertold BÉKÉSI*, **Peter KORONVÁRY****

*Faculty of Military Science and Officer Training, National University of Public Service, Budapest, Hungary (bekesi.bertold@uni-nke.hu)

**Faculty of Public Administration, National University of Public Service, Budapest, Hungary (koronvary.peter@uni-nke.hu)

DOI: 10.19062/2247-3173.2017.19.1.5

Abstract: *Every generation of humanity has inventions, which greatly influences our lifestyle, behavior and thinking. It's also true for security technologies. There is not a single year without any military conflicts, acts of terrorism or natural disaster. Not so long ago the UAVs were classified as military technology, however in the last 10 years civilian and industrial UAV developers and customers started to appear. In August 2013 the Association for Unmanned Vehicle Systems International (AUVSI) organized a conference in Washington with 80000 participants from 40 country. It was said that there will be approximately 10000 unmanned aerial vehicles in the US [6][7].*

In the article with some examples we show the UAV's fields of application and the complex challenges of their use.

Keywords: UAVs, drones, civilian-, military application

1. INTRODUCTION

According to the European Committee: "In 2050 civilian air traffic presumably will have different categories of flying vehicles, some with pilots, some without. That's why it's important to establish an European Market for RPASes or drones." A hundred years ago the transmission of electrical signals seemed to be unreal and fantastic, half century ago nobody heard of video monitoring systems. What will be the next phenomenon or device that will be able to influence our need in the information technology? One of this can be the unmanned aerial vehicles. The aerospace industry's small developments together with the successes of robotics greatly accelerated the development of drones. Not from far from now these robotic flying vehicles will (1) start to catch those who violate the speed limit on the roads (2) spread flyers (3) deliver packages or offer services for those who live far from cities. Not so long ago the UAVs were classified as military technology. But recently civilian developers and customers started to appear. Since the technology is developing rapidly and not only in the military field, "the RPASes will have to be able to fly in a not divided airspace, which means to take part in the normal civilian air traffic. Nowadays this technology is used for photographing and monitoring infrastructures, but in the future they may be able to transport people and cargo [33].

Since the development of the technologies and the marketing activities the market is growing steadily. The operation of drones which seems like toy planes are hard to understand for ordinary people. Most importantly using their unique ability of monitoring, equipped with a video- and heat sensing camera and other sensors they are able to transmit real-time information.

For example drones equipped with infra-red cameras do preplanned patrols over areas which are regularly affected by forest fires. They can be a cheap solution of minimizing the casualties [6][7][8][9][30][39].

2. THE SIZE OF THE DRONES ARE "LIMITLESS"

One of the most important parameters of flying vehicles, also for drones is the ability to fly, but the second to this is dependency to weather conditions (not only wind, but rain and ice too).

However for customers the main parameters to compare and choose which UAVs to use are: (1) flight duration and range (2) usability of payload, application and physical parameters.

The payload is one of the parameters on every flying vehicle, which customers are never satisfied with. In the past it seemed very impossible to build an unmanned aerial cargo vehicle. However Lockheed Martin and Piasecki Aircraft Corporation have been developing such vehicles for years, which will be able to lift and carry for a given distance a car. This vehicle will be able to take off and land vertically, maximum flight duration is only limited by the capabilities of the on-board electric power system. Assuming that the UAV's engine will use liquid fuel or batteries, operation time will be measured in minutes or hours instead of days [6][7].

Newer types of engines use solar panels, like the one developed by TitanAerospace, called Solara 50 which is planned to fly in the stratosphere (also called as aerial satellite). The wingspan is 50 m and it is able to carry 15 m long and 31 kg heavy payload, with a flight speed of 104 km/h. It will be able to fly for even a month in 15-20 km heights and will conduct military and civilian tasks. Primary the drone will be used for cartographic and meteorological purposes. The pictures about the surface of the Earth will be estimated to cost 5 dollars for every km² it is seven times less than the ones made by satellites [1][2][4].



FIG. 1. A TitanAerospace's Solara 50 UAV

Google with the Solara 50 (in Project Skybender) plans to establish 5G internet connection in areas where there were no internet, or where it would be very expensive to establish connection. The project is in the test phase now. The only problem is that the microwave signals that transmit the internet become very weak by the time they reach the surface transmission towers because of the great distances.

Further problem is the execution of continuous flight using only solar power. It is questionable that what happens when the plane fails, how fast they will be repair the error, and how long the area will be without internet. If these problems will be solved, the first real execution will be in the third world countries [5][6][7][37].

These stratospheric drones will look like storks, but there are drones that are cm long and resemble to mosquitoes or flies. These UAVs are able to lift a miniature camera and transmit real time information of the target object. The most important in development is to hold the balance between the own weight, payload, power supply and lifting power [6][7].

2.1 Nano Humming bird

Since 2006 DARPA contributed with 4 million dollars to AeroVironment to develop a nano size aerial vehicle (NAV). The new model, called the Hummingbird looks like a real hummingbird (Fig. 2.). The result is a hand made prototype, which has a wingspan of 160 mm and a weight of 19 g, making it lighter than an AA battery. This includes the systems necessary for flight: battery, engines, communication systems and a video camera.

The customers only has to to fly the robotic bird to the window of the target, which can monitor with its own camera [10][11][12][13][14][15].

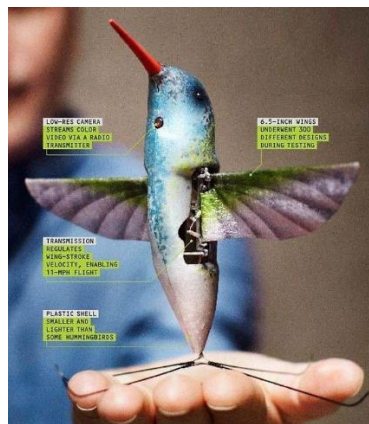


FIG. 2. Nano Air Vehicle „Hummingbird”

2.2 RoboRaven

Since 2007 the Robotics Centre of the University of Maryland (USA) is working on a fundamental different propulsion system for drones. This type of UAV can act like a bird, which enables it to covertly monitor the target [6][7].

The engineers in Maryland created a solar powered UAV called the RoboRaven III. The solar panels are on the upper part of the wing. The efficiency of the solar panels is 6%, but with the improvement of the solar technology this number will increase. The first versions of RoboRaven was presented in the spring of 2013 which then didn't had solar batteries, and had independent wing mechanisms, which all could be programmed differently. This enables the maintaining of flight stability [31][32][37].



FIG. 3. RoboRaven III

3. RECONNAISSANCE AND FIGHT DRONES

The first unmanned flight took place in 1916, when an American engineer, Elmer Sperry launched the flying torpedo, controlled by gyroscope systems. Working for the navy, Sperry soon started working on flying bombs - the prototypes of modern missiles.

Radio controlled UAVs are first made by the British, before the World War II, when the Queen Bee first flew. This airplane, which was first called to be a drone, was launched from a carrier with a catapult, and after it finished the mission landed on water [6][7][34].

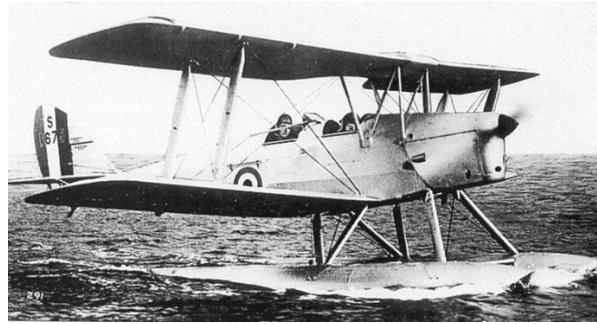


FIG. 4. Havilland Queen Bee

Today UAVs are being used on carriers, especially "stealth" drones like the American X-47B. It is not a separated unit, but a "flying system" with automatic take-off and landing, flight procedures and air refueling. This system is able to stay in air for even a week and if it's necessary they can refuel each other in the air. At the same time the on-board self-diagnostic systems can signal in time that the UAV needs repair.

The US Army's drones (Predators and Reapers) currently do patrol duties in Jemen, Somalia, Iraq, Pakistan and Afghanistan, so they test the technology in real environment. British UAVs in Afghanistan are controlled from the US. After it became public knowledge in May 2013 a campaign started against the use of drones, but the outrage stopped fast, because the PRs of the Department of Defense also started a marketing campaign.

A German UAV controlled by NATO operators almost collided with a passenger plane over Afghanistan. For the public it only became known because the videos made by the on-board cameras were uploaded to YouTube channels, which showed they only missed each other by a meter.

At the same time American drones still patrol over Kabul Airport, but the events must have shocked the Germans, because they refused to take part in the joint European development of the "Euro Hawk".

Drones can be the source of major problems in both the air and the ground. The laws which regulate the use of UAV systems are "immature" even in developed countries.

There is no evidence of fatal accident, but drones cause more and more problem in flying. There are lots of events tied to drones for example: (1) an old Soviet UAV with a red cross on its side scared to death the population of Balkuduk, a Kazakh village, when it crashed with a huge thump or (2) recently information come to light about a German UAV which crashed into a cargo plane on the ground in Afghanistan. According to the UAV's on-board camera, it seems that it's an "angry robot", because it accelerates toward a scared and fleeing crowd, than the profile of the cargo plane appears on the screen, and with a band the video ends. It later revealed that the UAV was controlled by an operator, who had no idea how to slow down the drone and shut off the propulsion system.

For the operators of the unmanned aerial vehicles the accusation and reservation of the qualification is getting more important. For the civilian population this is still new. A pilot who works in civilian aviation said about UAV operators: "Some generations has to pass until we can trust these operators in armchairs. Until that, I'm sorry but the air is ours".



FIG. 5. „Predator” UAV launching a missile

In the UN the Human Rights Committee, agreed that the minimum of using military robots in the field of operation is to not allow this electric equipment to be able to decide over the life of humans. Currently this law is about only ground equipment, but it would be logical to extend this to aerial vehicles too.

Thanks to the processing of the data from the on-board and other sensors, drones are able to distinguish objects from the air. Depending on the level of autonomy it is not a problem for the system to give an order about destroying the object, unless the first law of Asimov, which forbids the robots to kill anyone in any circumstance.

Asimov, the writer, never thought that robots can be susceptible to "illnesses". We can only hope that the operating systems and software which enables the controlling of the UAVs are robots and invulnerable. In reality however it's different, for example: in the Creech Airbase in Nevada one of the software which controls the movement of the Reapers and Predators in the Fall of 2011 was infected with a virus which monitors the order of the typed characters [6][7][8][9].

4. FRIENDLY AND NOT TOO FRIENDLY UAVS

In the civilian fields of use the military technology blends in between the peaceful equipments, as it happens with lots of technological fields the borderlines become blurry between the ability of regular and special systems.

The Parrot is equipped with an IP camera, a WiFi tool and a free iOS access, but it can be also equipped with high resolution camera and an RC tool with greater range.



FIG. 6. ParrotAR.Drone

The advanced AR. Drone 2.0 can be controlled with a remotely controlled quadcopter helicopter mobile or with a tablet, and has high resolution cameras and ultrasonic altimeter. During flight the on-board camera records HD video, that is transferred to the system in real time. The customer friendly tool enables to upload the video to the internet with just one click. With the pilot application everything is done easily without wires. The developers also thought about those who want to make longer videos, so a USB module is also present on the quadrotor [17][18][38]. For example: (1) the paparazzi no longer has to risk their health and safety, waiting in bushes or on fences, they just uplift the drone and they are already in the mansion of the celebrity. Or (2) the tendency of using drones also spreads in the media and news, there are examples of using drone-made photos and videos in protest movements in Poland, and Moscow. These are not made by the police, but the fans. The recordings uploaded to the internet we can see clearly what happened.

Nowadays, principally similar models to the Parrot patrol around German railways, checking the technological infrastructure. The MD4-100 Microdrone "helicopters" are currently doing their test flights over traffic roads. Their main use is to stop the increasing vandalism, to prevent the painting of buildings with aerosol paint.

"According to AUVSI in the future the tasks of RPAS will include precision agriculture, monitoring of the environment, protecting and other controlling tasks and security. Planes and helicopters responsible for controlling industrial tools, networks and works of art, along with the dangerous areas and plow lands will be taken over by RPASs." [33]

Drones used in forestry provide information about the spreading of plant pests, and monitor wild animals and locate forest fires. These and similar tasks require constant patrolling.



FIG. 7. Parrot AR 2.0 drone

To avoid the significant fuel and other costs University of Queensland in Australia has developed polyplane drones (Figure 8). These low cost, used once tools have good flying parameters, launching from the right altitude in the right direction they can be operated cheaply for example during fires [6][7][19][20].

Or imagine that a mobile service provider is located in the stratosphere, which makes it unnecessary for the networks provider to build network towers on the surface. A "network tower" flying on an altitude of 20.000 m can cover 45 000 km². If we could provide the slow speed flight of hovering of the UAV, this service could be sold as a good communication possibility, which doesn't need the public knowledge of the user's location.



FIG. 8. Polyplane UAV

One of the most interesting developments is thanks to the Japanese security company, Secom. It provides the customers the possibility to rent a quadcopter (Fig. 9.), which automatically flies to the air (starts its mission), if the alarm sets off and makes a high resolution recording to help the work of the detectives [21]. The drone makes pictures of the target - the face of men and the license plate of the vehicles - which is sent to the headquarters of the security company, where it is evaluated. More drone equipped with cameras save the customer the cost of deploying large numbers of monitoring system. The only drawback of the system is that the top speed is 10 km/h [19][22][23][35][36].

It is less fortunate that drones designed to hack systems are also starting to appear. The WASP UAV is came to life as a modification of the FQM-117B. It is equipped with electronic systems which makes it capable to detect the signals of GSM and WiFi networks and hack or disturb these signals [24][25].



FIG. 9. The world's first security drone

The length and wingspan of the drone is 1,8 m with a weight of 6,5 kg, including the high resolution camera, the GPS for the autonomous navigation and a computer which does the hacking. The matchbox sized computer has the full capability of a Linux operating system, the hard drive is 32 GB [6][7][26].

Another proof of the drones' wide area of use is that pizza delivering quadcopters are came to being. In urban cities, in peak time an UAV can deliver the food in minutes. This service is provided with a modified UAV, which had the original task as a monitoring drone. After the disarmament of the professional camera, the "Domicopter" delivered two pizzas in a thermobag for the customer [27].



FIG. 10. Pizza in the sky – more like marketing than a real service

The most obvious use for UAVs is police monitoring. For this a small, slow rotary winged aircraft is needed. For these tools a new name will appear in the near future - "Camcopters" [28][29].



FIG. 11. The Russian made S-100 UAV

5. SECURITY OR THREAT?

Since the price of UAVs is dropping from month to month, and the home use of radio-controlled models are increasing, the illegal use of these "flying toys" is starting to be a real threat. There is no better proof than (1) the protected witness Gaspare Spatuttsa claimed that 25 years ago the mafia was researching methods about carrying explosives in the airspace. The leaders of the "Cosa Nostra" Sicilian criminal organization the Graviano clan (brothers Filippo and Giuseppe) [16] personally ordered to Spatuttsa to make radio-controlled models, which can carry a small amount of explosives to a "destination"; (2) the German secret service identified a terrorist network, who were planning attacks using drones, which would carry explosives in the air. Imagine, what effects can a special mini-missile, classified as a "surface-drone", cause.

The user can use these tools for a "good cause" like the Belorussian forensics A.Vnukovich. In 2007 he planned and made a radio-controlled glider, equipped with a camera and launched it to find an illegal distillery, hiding in the woods [6][7][40].

CONCLUSION

Because of the increasing attention toward drones we can presume that there will be a "war" in the air. What should we do? Forbid the sell of these "toys"? It's like stopping the overusage of medicine or the sale of fuel.

Today an operating drone can be built at home. There is no guarantee that terrorists won't do the same.

The industry is growing steadily, and it is desired to regulate the use of UAVs as fast as possible, so we can take advantage of these equipment's services and don't suffer from the drawbacks.

REFERENCES

- [1] T. Singh, *TitanAerospaceDevelopingWorld'sFirstSolar-PoweredAtmosphericSatelliteDrones* (online) url: <http://inhabitat.com/titan-aerospace-developing-worlds-first-solar-powered-atmospheric-satellite-drones/> (2016.04.01);
- [2] *Солнечный беспилотник оставляют в воздухе напаять лет.* (online) url: <https://lenta.ru/news/2013/08/19/solar/> (2016.04.30);
- [3] B. Békési and M. Juhász, *Pilóta nélküli légitjárművek energia forrásai*, *Economica* (Szolnok), 2014/1, pp. 92–100;
- [4] Diamonds, *In The Sky*, (online) url: http://blog.ympact.me/diamonds-in-the-sky/#.V1Qzb_mLRdg (2016.05.13.);
- [5] Engadget: *Google plans to beam 5G internet from solardrones*, (online), url: <http://www.engadget.com/2016/01/30/google-project-skybender/> (2016.03.03.);
- [6] Анатолий Ермаченко, *Атака дронов. Беспилотные летательные аппараты – безопасность или угроза?* (online) url: <http://www.arms-expo.ru/articles/127/64596/> (2016.04.01);
- [7] Security Focus (Секьюрити Фокус), *Атака дронов. Беспилотные летательные аппараты-безопасность или угроза?* (online) url: <http://www.secnews.ru/articles/19210.htm#axzz43HYTU7pM> (2016.04.01);
- [8] Евгений Золотов, *Атака дронов*, (online) url: http://3d_print.jofo.ru/592584.html (2016.04.01);
- [9] Евгений Золотов: *Атака дронов. Рынок гражданских и коммерческих беспилотников готовится к взлету.* (online) url: <http://b-mag.ru/2014/russia/ataka-dronov/> (2016.04.01);
- [10] *Aero Vironment Nano Hummingbird*: (online) url: http://en.wikipedia.org/wiki/AeroVironment_Nano_Hummingbird (2013.05.26);
- [11] *A Pentagon kém kolibrije*, (online) url: <http://idokjelei.hu/2011/02/a-pentagon-kem-kolibrije/> (2013.05.26);
- [12] *Aero Vironment Develops World's First Fully Operational Life-Size Hummingbird-Like Unmanned Aircraft for DARPA*: (online) url: http://www.avinc.com/resources/press_release/aerovironment_develops_worlds_first_fully_operational_life-size_hummingbird (2013.05.26);
- [13] *Buch der Synergie Elektro- und Solarflugzeuge (2010–2012)*: (online) url: http://www.buch-der-synergie.de/c_neu_html/c_11_16_02_mobile_anwendungen_elektroflugzeuge_3.htm (2013.05.26);
- [14] Gy. Ritzinger, *Már nem csak a természet tudja!* (online) url: <http://www.mernokbazis.hu/cikkek/mar-nem-csak-a-termeszet-tudja> (2013.05.26);
- [15] B. Békési, *UAV fejlesztések, új alkalmazások*, In: Békési Bertold, Bottyán Zsolt, Dunai Pál, Halászné dr Tóth Alexandra, Makkay Imre, Palik Mátyás, Restás Ágoston, Wühl Tibor; Palik Mátyás (szerk.) *Pilóta nélküli repülés profioknak és amatőröknek*. 321 p. Második, javított kiadás. Budapest, Nemzeti Közzolgálati Egyetem, 2013. pp. 299-315. ISBN: 978-615-5057-64-9. (online) url: <https://opac.uni-nke.hu/webview?infile=&sobj=10140&source=webvd&cgimime=application%2Fpdf> (2016.04.01);
- [16] MTI: *A szicíliai maffiát is megviselte a válság* (online) url: http://hvg.hu/vilag/20121123_A_sziciliai_maffiat_is_megviselte_a_valsa (2016.04.25);
- [17] *ParrotAR.Drone 2.0 PowerEdition* (online) url: <https://xlo.hu/rc-jatekok-dronok/parrot-ardrone-20-power-edition?mf=5f-termek-tipus-szures> (2016.05.03);
- [18] *Parrot AR. Drone 2.0 EliteEdition*. (online) url: <http://www.arukereso.hu/taviranyitos-jatek-rc-jarmu-c4041/parrot/ar-drone-2-0-elite-edition-p216204408/?gclid=Cj0KEQjwx7u5BRC1lePz2biJpIYBEiQA-ZeDmtgHk-qQMql3huubtz1Of3H3hUje9MVV8wprYKziF0kaAjMk8P8HAQ#termek-leiras> (2016.05.03);
- [19] Maia Brown-Jackson: *Disposable Paper Plane UAV Prototype Designed to Help With Forest Fires*. (online), url: <http://www.themarysue.com/disposable-uav/> (2016.05.06);
- [20] *Steer able paper planes and maple seeds the basis for life-saving, disposable UAVs* (online), url: <http://www.gizmag.com/disposable-uav-paper-plane-maple-seed/28323/pictures#2> (2016.05.06);
- [21] P. Szűcs, *Drónok veszik el a biztonsági őr és kamera munkáját?* (online), url: <http://itcafe.hu/hir/dronok-veszik-el-a-biztonsagi-or-es-kamera-munkaja.html> (2016.05.06);
- [22] A. Adamu, *Japan has new security drones that can even chase suspects*, (online), url: <http://interestingengineering.com/japan-has-new-security-drones-that-can-even-chase-suspects/> (2016.05.03.);
- [23] K. Németh, *Japán drón, amely képes követni a gyanús személyeket.* (online), url: <http://videoanalytics.today/?p=16443> (2016.05.06);
- [24] Evgeny Zobnin, *WASP: беспилотный самолет с функциями взлома WiFi - сетей и перехвата GSM - сигнала.* (online), url: <https://www.opennet.ru/opennews/art.shtml?num=31347> (2016.05.06);
- [25] Pierluigi Paganini: *Vespid is amongst most the important espionage artifacts based on the Wireless Aerial Surveillance Platform for the for the construction of a DIY Spy Drone.* (online), url:

- <http://securityaffairs.co/wordpress/31190/hacking/wireless-aerial-surveillance-platform-diy-spy-drone.html> (2016.05.03.);
- [26] М. Карпов, *Беспилотник WASP взламывает сети Wi-Fi и GSM*. (online), url: <http://www.mobiledevice.ru/wasp-richard-perkins-besipilotnii-samolet-vzлом-seti-wi-fi-gsm.aspx> (2016.05.03);
- [27] H. Gye, *Now that's a special delivery: Domino's builds DRONE to deliver pizzas by air and beat the traffic*. (online), url: <http://www.dailymail.co.uk/news/article-2336324/Dominos-builds-DRONE-deliver-pizzas-air-beat-traffic.html> (2016.05.03);
- [28] *ФСБ России заказывает беспилотные вертолеты Siebel Camcopter S-100* (online), url: <http://bmpd.livejournal.com/309455.html> (2016.05.03);
- [29] *БАК Горизонт Эўр S-100*. (online), url: <http://www.gorizontrostov.ru/> (2016.05.03);
- [30] P. Szegedi, *A pilóta nélküli repüléshez kapcsolódva...Tanulmány a pilóta nélküli légijárművek működésével és üzembentartásával kapcsolatban*, p.: 80, ISBN 978-963-12-5224-8, 2016 http://m.ludita.uni-nke.hu/repozitorium/bitstream/handle/11410/10148/Tanulmany_Szegedi%20K%c3%a9sz_20160407.pdf?sequence=4&isAllowed=y (2017.04.02);
- [31] Jennifer Rooks, Rebecca Copeland: *Robo Raven III Harnesses Solar Power*. (online), url: <http://www.umdrighnow.umd.edu/news/robo-raven-iii-harnesses-solar-power> (2016.05.05);
- [32] *Американцы создали робота-ворона на солнечных батареях*. (online), url: <https://lenta.ru/news/2013/10/17/roboraven/> (2016.05.05);
- [33] Jan Simons, Marcel Philippe: *A légiközlekedési piac megnyitása a távirányított légijármű-rendszerek biztonságos és fenntartható polgári felhasználása előtt*. Brüsszel, 2014. (online), url: https://www.google.hu/url?sa=t&rct=j&q=&esrc=s&source=web&cd=1&cad=rja&uact=8&ved=0ahUKEwuj7Lb78tHMAhXF8ywKHSTbDiQQFggaMAA&url=https%3A%2F%2Fwebapi.eesc.europa.eu%2Fdocumentsanonymous%2Feesc-2014-03987-00-00-as-tra-hu.doc&usq=AFQjCNFqSGzWaOa12PkE3e_B-INSn043sA&sig2=brakfwypB01F0HSy42ZXog&bvm=bv.121658157,d.bGg (2016.05.05);
- [34] P. Szegedi, *Pilóta nélküli repülő eszközök*, Repüléstudományi Közlemények 16:(36/1) pp. 63-77. (2004);
- [35] *Japan security firm offers private drone*. (online), url: <http://www.news.com.au/technology/japan-security-firm-offers-private-drone/story-e6frfro0-1226544403160> (2016.05.05);
- [36] *Levadássza a behatólokat a biztonsági drón* (online), url: <http://computerworld.hu/computerworld/levadassza-a-behatolokat-a-biztonsagi-dron.html> (2016.05.06);
- [37] Ellie Zolfagharifard, *Is this the ultimate bird of prey?: 'Robo-Raven' so realistic it could become a weapon of war*. (online), url: <http://www.dailymail.co.uk/sciencetech/article-2335600/Robotic-bird-used-future-war-agent-Robo-Ravens-extreme-aerobatics-fool-real-birds-prey.html> (2016.05.05);
- [38] *Parrot AR Drone Quadricopter, 2.0 Edition* (online), url: http://www.amazon.com/Parrot-Drone-Quadricopter-Orange-Blue/dp/B007HZLLOK/ref=pd_sim_sbs_107_2?ie=UTF8&dpID=41tg12I-SIL&dpSrc=sims&preST=_AC_UL160_SR160%2C160_&refRID=19WYYBWDXYPMRCV9YHED (2016.05.03);
- [39] P. Szegedi, H. Tircsi, *Nanotechnológia a katonai vezetés új kihívása? Hadtudományi Szemle*, 2017. X. évfolyam, 1. szám pp.: 491-505;
- [40] B. Békési and P. Szegedi, *Pilóta nélküli légijárművek - biztonság vagy fenyegetés*, XV. Természet-, Műszaki és Gazdaságtudományok Alkalmazása Nemzetközi Konferencia, Nyugat-magyarországi Egyetem, Szombathely, 2016. pp. 130-141. (ISBN: 978-963-9871-61-8).

ASPECTS REGARDING SAFETY SYSTEM IN SURFACE-TO-AIR MISSILE FIRINGS

Viorel-Eugen BITAN, Valeriu CĂLIN

*Training Camp and Surface-to-Air Firing Range, Romania (vbitan@roaf.ro,
vcalin@roaf.ro)

DOI: 10.19062/2247-3173.2017.19.1.6

Abstract: *In present, the Air Defense Artillery & Missile branch became an essential component of Romania's air defense. In its history, Air Defense Artillery & Missile branch has evolved from modified field artillery to specialized antiaircraft artillery and complex surface-to-air missile systems and that evolution imposed setting up a specialized firing range to allow training firings in safe battlefield-like conditions. This role and mission was fulfilled by the Training Camp and Surface-to-Air Firing Range (TIPTSA), as a permanent firing range, large, open and complex, the only structure in the Romanian Armed Forces to organize and host firing activities that include the third dimension – the air. TIPTSA's activity is complex and includes mainly, to take every measure for the safety during live firing exercises, to provide the targets during the firing activities and to observe and evaluate the firing activities. The most important objective of range is named "No incident" objective, meaning that none of the participants, neighbors or equipment are injured/ damaged. During its evolution, the firing range was endowed with precise evaluation systems, able to measure the coordinates of every point in firing area. This paper presents how to highlight the precision of the evaluation systems using them in safety purposes during firing activities, and tries to offer an idea to modernize or develop new equipment to fulfill the safety issues in antiaircraft artillery and surface-to-air missile firings.*

Keywords: *antiaircraft missiles, surface-to-air missiles, antiaircraft firings, safety, evaluation systems*

1. INTRODUCTION

Firing range – generally, and Capu Midia firing range – particularly provides facilities for complex training exercises in the field with multiple targets available to engage. The most important challenge for range safety personnel is to assure that every activity can be performed in safety circumstances.

In order to totally remove the risks, there are performed trainings regarding safety issues with all personnel involved in activities.

General safety measures are measures to observe any entrance or exit in firing sector or safety sector, people, vehicles, boats or animals. There are grouped in TERESTRIAL, MARITIME and AERIAL measures and uses specific equipment like radar, binoculars, communication equipment, etc.

Immediate safety measures are depending on the air defense system used for firings and are applied in firing position. In addition, there are taken specific measures that reveal the position of the launched missile within the limits of the firing sector. The limits of the firing sector or safety sector are stipulated in regulations and depends on the type of the SAM system and the area available for shooting in every firing range. This are input data for every standing operating procedure applied in surface-to-air firings.

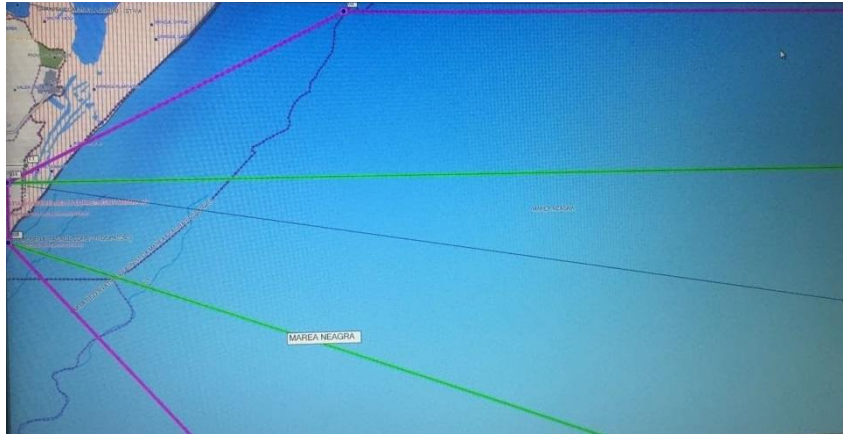


FIG. 1. Safety sector (pink) and firing sector (green) in the case of medium range SAM systems in Capu Midia firing range

It is obvious the need to know the position of the missile to decide when to destroy it, if necessary, as specific standing operating procedure requires. In the same time, no missile can be left to leave firing sector or pass the target in the case of no impact.

There are SAM systems that provide data about missile position by default, due to the homing method, but this task could be difficult in the case of SAM systems that use semi-active radar homing (SARH).

Semi-active radar homing (SARH) is a common type of missile guidance system, perhaps the most common type for longer-range air-to-air and surface-to-air missile systems. The name refers to the fact that the missile itself is only a passive detector of a radar signal – provided by an external source – as it reflects off the target[1]. Additionally, the missile will listen rearward to the launch platform's transmitted signal as a reference, enabling it to avoid some kinds of radar jamming distractions offered by the target. Therefore, we don't receive a signal from missile to determine its precise position. In a real combat this will be no disadvantage, but a firing range will need another system to get this information. Particularly, a such of system can be another radar, another weapon system that will track the launched missile without combat any target or a precise evaluation system, as it used in Capu Midia firing range.

2. EVALUATION SYSTEMS USED IN SAFETY PURPOSES

2.1 Optical and electro-optical evaluation system used in TIPTSA. For direct anti-aircraft artillery and V-SHORAD firing can be used the TZK binoculars or the Bosch binoculars, which are capable of observing targets and the results of the firing activities, measuring miss distances between the burst trails and the target, measuring horizontal angles (within the $n \times 360^\circ$ range) and vertical angles (within the $-18^\circ + 84^\circ$ range) and cueing the surface, air and water targets[2]. Due to their poor precision at big distances, these type of instruments can be used in safety purposes only for indication or can be used to cue objects entering the firing sector.

The electro-optical tracking system EOTS-F is meant to accurately determine the trajectories of the air targets, the errors between two air targets and between flares and an air target. Unlike the optical systems that are used, this is used for evaluating both anti-aircraft artillery firing and anti-aircraft/surface-to-air missile firing.

2.2 Electro-optical evaluation system used in TIPTSA. The EOTS-F system is primarily based on determining the angular coordinates of a point in space using bi-dimensional measuring instruments that have a highly accurate measuring system for the azimuth and elevation angles ($2 \cdot 10^{-4}$ gons $\equiv 3.14$ mm/km), set in accurately determined positions [3]. The cinetheodolite has either automatic infrared or visible tracking equipment to observe aerial targets by optical means and track them manually, automatically or by servicing at the central station, on a video signal (TV), or based on the radiated infrared (IR) signal. Output data of the EOTS-F cinetheodolites contains position information comprising coded azimuth and elevation angles (α, λ) and additional information, synchronized time, labels, etc. EOTS-F software uses mathematical triangulation method to process the spatial coordinates (x, y, z) of the tracked object, in its own Cartesian coordinate system.

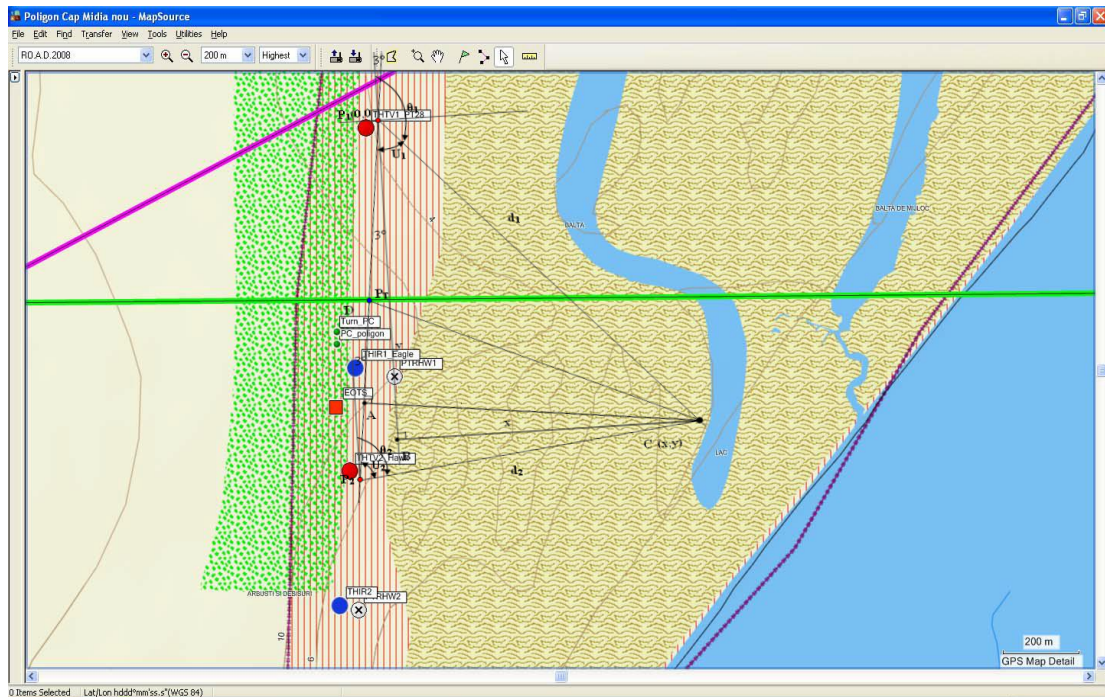


FIG. 2. Observation position of cinetheodolite TV (THTV1, THTV2) marked with red points and IR cinetheodolite (THIR1, THIR2) marked with blue points, in Capu Midia firing range; EOTS reference point, marked with red square

A target/object must be tracked by a pair of cinetheodolites of the same type (visual spectre or IR spectre) and the coordinates will be obtained using formulas above:

$$\begin{aligned}
 x &= x_1 + \frac{D \cdot \sin(183 - \theta_2) \cdot \sin \theta_1}{\sin(\theta_1 - \theta_2)}; \\
 y &= y_1 + \frac{D \cdot \sin(183 - \theta_2) \cdot \cos \theta_1}{\sin(\theta_1 - \theta_2)}; \\
 z &= z_1 + \frac{D \cdot \sin(183 - \theta_2) \cdot \text{tg} \gamma_1}{\sin(\theta_1 - \theta_2)}
 \end{aligned}
 \tag{1}$$

where (x_1, y_1, z_1) represents reference point of EOTS, marked with red square in Fig.2, D is the distance between cinetheodolites in TV or IR pair and $\theta_1, \theta_2, \gamma_1, \gamma_2$ represents determined azimuth and elevation angle determined by first and second cinetheodolite respectively.[4]

Considering that most of the trajectories are within the observation boundaries of the system the use of the EOTS-F for safety measures in the case of SAM with SARH guidance system.

3. AUTOMATIC AQUISITION, TRANSMISSION AND PROCESSING TARGET DATA FROM EOTS-F

As shown, EOTS-F determine precise coordinates of missiles/ targets but cannot determine if the missiles/ targets are within the boundaries of the firing sector/ safety sector. Those areas are defined considering every weapon system used and firing position so it is difficult to describe their limits in EOTS-F Cartesian coordinate system. In reverse, should be designed a method to convert the EOTS-F data in geographical coordinates.

Considering that the firing sector is defined as an angular sector pointed from the firing position, it appears that the problem is reduced at a method to convert the angle determined by EOTS-F in angular information usable from the firing position (to determine a correlation between this two angles) and to compare it with the angular limits of the sector.

Angular targeting / tracking data of the targets by the theodolites (azimuth and elevation angles) are transmitted by radio to central station (Master Station - MS), installed in the EOTS building, where it is performed post-mission analysis, so the extraction of the angle needs to identify a physical circuit from theodolite that contain angles information and the data format.

3.1 Real-time transmission of azimuth angle value originating from cinetheodolite, in Firing Control Center

The solution assumes that from the Angle Measurement System of one cinetheodolite with infrared tracking (THIR1), placed in position, to be taken the electrical signals in digital BCD format, which contain the azimuth angle value and the command signal for reading the angle. It is important to place the theodolite right in the back of the firing position to minimize the errors recorded in the first part of the missiles trajectory, otherwise the missile would be seen much outside the sector.

The electrical signals, after a preliminary hardware adjustments, are inserted into a data acquisition card (DAQ), which is coupled via a USB port with a laptop (LP_E) containing S/W of acquisition and processing signals, providing the instantaneous value of the angle. The azimuth angle value is transmitted in decimal format (gons and / or sexasimal grades) in the firing control center, downloaded to a laptop (LP_R), being displayed in real time and available to the officer in charge (**Fig.3**)

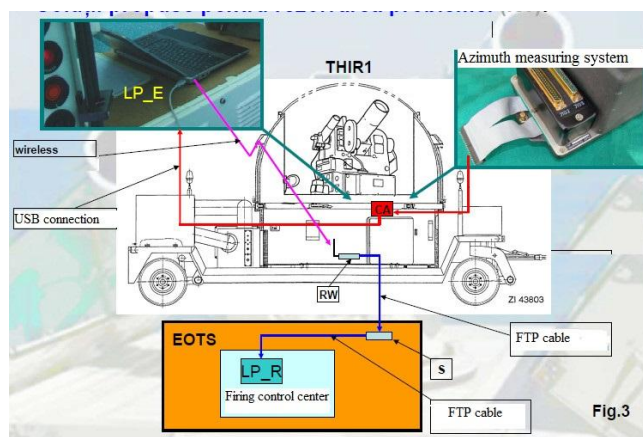


FIG. 4. Minimal configuration for acquisition, transmission and data processing system

Data transmission between LP_E (located in THIR1) and LP_R (located in the firing control center) is carried out in the proposed configuration via an FTP cable network provided with a wireless router (RW). The cable route will have the total length of 150 m, including the laying configuration to it. In the case of bigger distances it is necessary to enter a switch (S). From the switch, the FTP cable is brought directly to LP_R, in the firing control center (**Fig. 3**).

CA, LP_E will be located inside the THIR1, in the mobile part, and RW in its fixed part (**Fig. 3**).

3.2 Equipment used by automatic acquisition, transmission and data processing system. In this configuration are necessary materials and equipment as follows:

- data acquisition cards (NI DAQ 9174 modules with two NI 9425 cards).
- 2 laptops (LP_E, LP_R),
- wireless router,
- switch with power supply,
- FTP cable.

For scenarios with more than one missile launched there is necessary a configuration with more cinetheodolites, at bigger distances, connected using optic fiber channel (**Fig.4**).

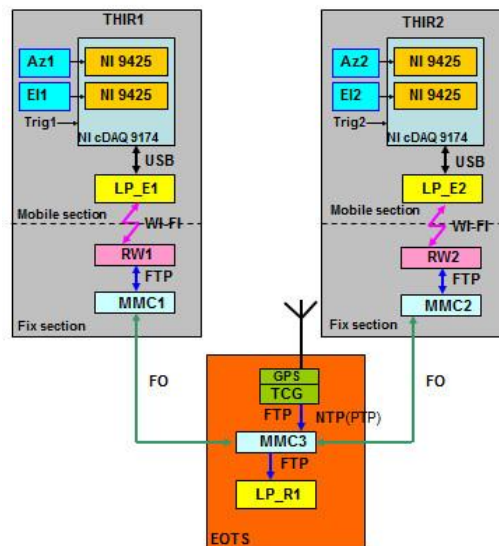


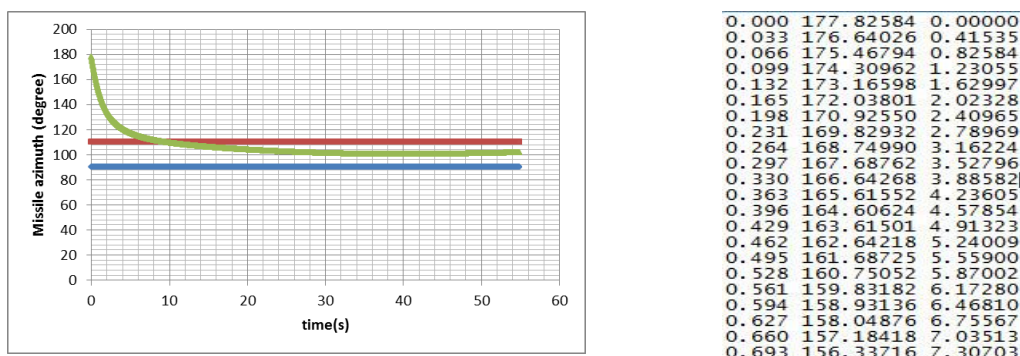
FIG. 4. Configuration for acquisition, transmission and data processing system for two cinetheodolites

Obvious, the equipment and materials will multiply to the number of missiles launched in the same time. The system needs a synchronized pulses for acquisition and transmission, so will be used a Time Code Generator with GPS time in the Master Station.

3.3 Results obtained. The minimal configuration used in testing activities proved to be satisfactory and reliable. Real time data used for making destroy missile decision are recorded for further evaluation.

One example of a missile's azimuth angle recorded is presented in **Fig.5 (a)**, marked with green. In the initial part of the trajectory, the missile is outside firing sector right and left boundaries, marked with red and blue respectively, and enters the sector after few seconds. In fact, the missile starts from firing position placed on the same alignment as the cinetheodolite (180^0 azimuth) and enters the 90 -110 degrees sector.

In **Fig.5 (b)**, is displayed a part of a recorded file with azimuth and elevation data information, sampled at every 33 milliseconds.



(a)

(b)

FIG. 5. (a) Example of the azimuth information of a missile fired in $90^{\circ} - 110^{\circ}$ firing sector; (b) Part of a file with azimuth and elevation automatically collected at every 33 milliseconds. In the first part of its trajectory, the missile is outside the limits of firing sector, marked with blue and red

Additionally, can be performed acoustic or visual alerts for the situation when a missile leaves the firing sector.

CONCLUSIONS

The safety of firings is the main objective during all activities in a firing range, so it is essential to adapt safety measures for all weapon systems. This very need and the absence of range radar for tracking missiles led to the use of the equipment used to evaluate the firing in order to achieve safety.

In future upgrades of such equipment or, in the case of new ones, is required the provision of a stand-alone mission in the field of firing safety. Including in S/W digital representations of allowed/forbidden areas from a firing range is a necessity for evaluation systems in order to increase the number of aspects evaluated in complex combat situations.

Until then the automatic acquisition, transmission and processing target data system described in this paper proves there are unexplored possibilities of actual systems that can solve temporarily safety issues.

REFERENCES

- [1] https://en.wikipedia.org/wiki/Semi-active_radar_homing, accessed on 24 Apr. 2017;
- [2] *** *Manual of TZK Device for control Air Defense Artillery Firings*, Capu Midia;
- [3] ***(1996). CB AAV 002 *EOTS-F cinetheodolite system – System description*, Part 1-2, Volume 1;
- [4] V. Bitan and V. Calin, *Evaluation systems for antiaircraft artillery and surface-to-air live firing activities*, Review of the Air Force Academy, Vol. XIV, No 2(32)/2016, pp. 31-39.

EVALUATION OF TACTICAL MISSION EXECUTION

Adam BONDARUK*, Jarosław KOZUBA**,

* Faculty of Aviation, Polish Air Force Academy, Deblin (a.bondaruk@wsosp.pl),

** Faculty of National Defence and Logistic, Polish Air Force Academy, Deblin
(j.kozuba@wsosp.pl)

DOI: 10.19062/2247-3173.2017.19.1.7

Abstract: *Training of flight crews, particularly in combat aviation is a complex and long term process. It requires the use of a standardized methodology in order to evaluate the mission execution in each of the training areas. Because of its complexity, tactical mission is the most difficult and demanding task to perform. It combines aircraft handling, procedural and tactical elements. Maintaining situational awareness at the minimum level required reflects the quality of preparedness (training) of the flight crew. Periodic inspection and ongoing evaluation are indispensable tools for confirming the correctness of the solutions adopted in tactical training of flight personnel.*

Keywords: *flight training, situational awareness, training methodology.*

1. INTRODUCTION

Training flight personnel in combat aviation is, due to their intended use, a process with a high degree of complexity, which increases with the application of new, technologically advanced tactical systems. Operational capabilities of the fourth and fifth generation multi-role aircraft undergo a continuous development. The factors which limit crossing the subsequent barriers are psychomotor (operator's) skills of the flight crew. Despite the automation of the decision-making processes in use, which ultimately provides the processed information, the sheer amount of that information often exceeds the pilot's perceptual capabilities. The main objective of the air training is to prepare flight crews, in the shortest time possible, to effectively execute combat missions in accordance with their intended purpose.

2. FLIGHT TRAINING AREAS

Flight training can be divided into three main areas [1]:

- flight maneuver training;
- procedural training;
- tactical training;

Flight training syllabus should ensure the implementation of training in the order specified yet the areas of training overlap at certain stages. The degree of their implementation depends on the main objective and the complexity of training, as well as on the level of training of a particular pilot. Training of emergency flight procedures is implemented throughout the entire flight training program, including simulator training.

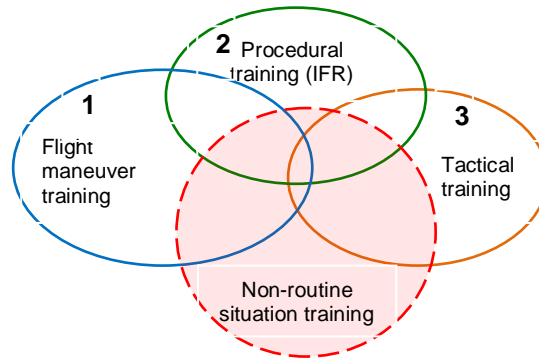


FIG. 1. Flight training areas.

The primary objective of the first area (flight maneuver training) is to master aircraft handling. Its purpose is to develop a "muscle memory" (habits) of the pilot and the multitasking skills appropriate in various flight phases (takeoff, climb, flight maneuvers, descent, landing). In the second area (procedural training), the pilot focuses on the procedures of performing the flight in the airspace according to the rules (regulations) applicable to all aircraft, and on the ability to interpret information coming from available sources describing the situation in the airspace (radio-navigation instruments, departure and arrival cards, information from the ATC, etc.). Its objective is to master the procedures and techniques applied in various phases of an IFR (procedural) flight.

The objective of the third area (tactical training) is to master the techniques of tactical maneuvering, mutual support in formation, data interpretation and the use of all tactical systems of the aircraft. In the course of that training, the pilot commences to build tactical situational awareness.

3. LEVELS OF SITUATIONAL AWARENESS.

Situational Awareness (SA) is the perception of the environment, adequate for the current status/phase of the flight, understanding the importance of elements perceived, and predicting the possibility of changes in their status in the nearest future [4].

According to M. Endsley [6], situational awareness has three levels, depending, among other things, on the degree of the pilot's training (operator's capabilities).

Level 1 is characterized by the pilot's ability to perceive (record) the current situation of the aircraft, as well as the changes of the flight, environmental (weather conditions), and operational parameters. This means that the pilot does not understand their interrelations and the resultant consequences. This is a very undesirable state, causing the deepening of the errors the correction of which exceeds the operator's skills (psychomotor) of the pilot.

At Level 2, the pilot understands the current situation, he is able to synthesize and analyze the information coming from all available sources, and to introduce changes (make a decision) in order to achieve the intended goal (the state of the flight), but in a very tight time margin. This means that the pilot sees, understands and corrects, the deviations from the desired state which occur, and his operator skills allow him to perform the flight (task) safely but with reduced efficiency (proficiency).

At Level 3, on the basis of an analysis of the available information, knowledge, and experience, the pilot is able to predict the development of the situation and to take the optimum decision in terms of achieving the objective of the main task.

This means that his operator's skills allow him to anticipate the consequences of the decision in the long time frame (at least several steps in advance). The mission is executed safely, efficiently, and with due proficiency.

4. MISSION EVALUATION

The evaluation of air mission execution is done on the basis of the standardization/evaluation instruction and other publications containing rating standards (training syllabi and methodologies) The program of flight crew evaluation verifies qualifications of personnel, and provides the efficient use of resources, and standardization of executing operational missions. Ongoing evaluation concerns each mission (flight) during the training process (e.g. primary flight training). Periodic evaluation is conducted in accordance with the relevant regulations.

Tactical training is the most difficult and demanding stage, which combines a wide range of skills from all areas of training. The objective of evaluating a tactical mission execution is to verify the correctness (in accordance with the accepted standard) of the tactical systems use. Periodic inspection of tactical mission applies to pilots, who maintain the CMR (Combat Mission Ready) and BMC (Basic Mission Capable) levels. During primary flight training, the pilot acquires the necessary tactical skills, which are verified on an ongoing basis by the instructor. The instructor assesses whether the trainee has achieved the level of tactical situational awareness which is required in a given training module.

In aviation, various rating scales are used in order to evaluate the mission execution. It is important that each instructor or evaluator understand the meaning of a particular grade identically. In periodic evaluation of tactical mission execution, a two or three-degree rating scale ("Q" qualified, "Q-" qualified minus, "U" unqualified) is adopted.

The particular grades shall be understood as follows [2, 3]:

- "Q" means that the pilot under evaluation both demonstrates the appropriate knowledge and also performs practical tasks in accordance with the accepted standard within the limits of the adopted (acceptable) tolerance;

- "Q-" indicates that the pilot under evaluation does not exceed the allowable tolerance in the individual areas, and does not breach either the conditions of the mission execution or safety. He requires, however, a detailed discussion or training, the scope of which is to be specified by the examiner;

- "U" means that the pilot exceeds the allowable parameters, resulting in a safety breach, or does not follow the accepted standards, which affects the performance of the task.

Combat mission execution evaluation is a mission whose scenario contains the tactics currently used by a given Air Force unit in accordance with its tasking/mission. The pilot under evaluation performs a formation flight in the position adequate to his level of training, e.g. the flight lead leads a four-aircraft formation. During the flight, the evaluator may change the formation, the master objective, however, is to evaluate the highest rating held by the pilot (the wingman may conduct a pre-flight briefing which will be evaluated). It is advisable to evaluate the tactical flight during an exercise or transfer to another airfield.

According to regulations adopted in Polish Air Force, while commencing the evaluation of a combat flight, the examiner must determine all the areas to be evaluated, including [2, 3]:

- tactical plan,
- tactical execution,
- radio use/tactical communications,
- visual lookout/radar mechanization,
- tactical navigation at high, medium, and low altitude,
- ingress/egress procedures,
- timing (preplanned time on target, etc.)
- threat reactions,
- onboard tactical system utilization.

Each of these elements has its own evaluation criteria, which are included in the general definition of grading criteria. For example, for tactical execution area:

"Q" - Applied tactics consistent with the threat and current standards is quickly adapted to changing environment. The pilot executed the plan and achieved mission goals. Maintained situational awareness (Level 3).

"Q-" - Minor deviations from tactical plan which did not result in an ineffective mission. Pilot makes slow and minor changes in the tactics to adapt the tactics to changing environment. Low situational awareness (Level 2).

"U" - The pilot is unable to accomplish the mission due to major errors during execution of the plan. Situational awareness lost (Level 1).

Another example may be radio use/tactical communications area, where:

"Q" - Radio communications were concise, accurate and effectively used to control (command) the formation or describe the tactical situation.

"Q-" - Minor terminology errors or omissions occurred, which did not significantly affect situational awareness, mutual support, or mission accomplishment.

"U" - Radio communications were inadequate (not precise enough or excessive) causing degradation of situational awareness and mutual support, and significantly reduced mission accomplishment effectiveness.

The grading criteria in the visual lookout/radar mechanization area are as follows:

"Q" - The pilot demonstrates thorough knowledge and effective application of visual lookout/radar search techniques for all phases of flight while maintaining deconfliction contracts.

"Q-" - The pilot demonstrates limited knowledge of visual lookout/radar search techniques and does not establish responsibilities for individual formation members in all flight phases. There are delays in task allocation and minor deviations in deconfliction contract adherence.

"U"- The pilot demonstrates unsatisfactory knowledge and skills of visual lookout/radar search responsibilities, due to which he allows undetected enemy to penetrate and commence a short range fight, and fails to maintain deconfliction contracts.

The above examples point out to the fact that each instructor (evaluator) must use the same conceptual apparatus, as otherwise double standards may be applied, which is an intolerable situation. Evaluation of the mission execution on the basis of countable values is relatively simple as it requires only the observation of the relevant parameters.

Table 1. An example of countable parameter evaluation criteria [3]

Q	Altitude	+/- 200
	Airspeed	+/- 5%
	Course	+/- 5 degrees/3 NM
	TACAN Arc	< 3 NM
Q-	Altitude	+/- 300
	Airspeed	+/- 10%
	Course	+/- 10 degrees/5 NM
	TACAN Arc	> 3 NM
U	Exceeded Q- limits	

A more difficult task is to evaluate the areas in which it is necessary to assess whether the pilot achieves the required degree (level) of knowledge or skills. In such a situation, it is necessary to introduce a hierarchy of training objectives. Taxonomy is a classification that is based on clear principles. The aim of taxonomy in training is to classify training objectives, and, what it involves, to use an evaluation standard for uncountable values. This allows to define the goals which may (should) be achieved in individual training modules.

The starting point is to define the basic components (categories) that create and systemize the process of learning. There are the following categories of learning [5,7]:

- knowledge,
- comprehension,
- skills.

Knowledge is understood as the ability to accumulate (memorize) the information and to recall it. Comprehension is a general term referring to the ability to organize knowledge in a conscious (deliberate) manner. We can distinguish five levels in this learning category. Skill is the ability to perform physical or mental tasks while maintaining a certain standard. Each organization which conducts flight personnel training has its own uniform system of performance evaluation (classification), which is a combination of categories and levels and which is based on a rating scale consisting of two to ten levels.

During the evaluation of tactical mission execution, both periodic and within the scope of a programmed training, a minimum acceptable performance level of individual mission elements is specified. An example might be an evaluation sheet used for TI (Tactical Interception) mission evaluation, which is performed during the multi-role F-16 aircraft training. The rating scale is composed of five levels:

- 0 – the pilot demonstrates lack of knowledge or skills;
- 1 – the pilot executes the mission safely, but with limited skill (proficiency), which causes the need of the instructor's intervention in order to correct the resulting errors;
- 2 – the pilot executes the mission correctly, recognizes the errors committed and corrects them;
- 3 – the pilot executes the mission correctly, effectively and efficiently, commits minor errors which do not significantly influence the quality of mission execution;
- 4 – the quality of mission execution points out to above-average degree of skill.

The most common scale of assessments used in the Polish Air Force is a digital scale from 2 to 5 which will serve as a basis for a discussion of a mutual relationship between such features as flight safety, the level of the operator's situational awareness as well as training objectives.

The most important criterion for the evaluation of the performance of the task by the air crew is the criterion of safety. Each task conducted in the air has its safety conditions and the execution conditions which are specifically defined in the training programme (training methodology). Any violation of the pre-defined safety conditions must result in receiving an "unsatisfactory" grade, which results in the implementation of an appropriate procedure with regard to the pilot - either by suspension in flights or performing an additional flight under supervision. An important element of the assessment is finding an answer to the question why the safety conditions have been violated. The cause is the degradation of the operator's situational awareness to an unacceptable level one. The reasons may vary, starting with the lack of basic knowledge and understanding of the processes of mutual correlation between essential elements which affect a flight, fatigue resulting in impaired psychomotor skills as well as improper division of attention in particular elements of the flight. Receiving a partial "unsatisfactory" grade (2) due to the breaching of safety conditions results in an overall assessment mark - 2.

The pilot can receive an "unsatisfactory" grade in relation to the evaluated element due to a breach of execution regulations caused by lack of knowledge or insufficient skills. This also means that the operator's situational awareness has been degraded to level one. Such a case does not result in the introduction of sanctions in relation to the operator if it is a new element in the training process (training module). The final evaluation is dependent on the training target specified in the briefing.

Another criterion for defining the assessment is to identify the operator's situational awareness in a given area of training. This is inseparably linked with specific training objectives. The training objectives during a tactical training apply to the operator's skills, that is to the execution of the operator's activities in accordance with the adopted standards. Specifying whether a pilot who undergoes training possesses the required knowledge and understands the factors, affecting a tactical job, is carried out during ground training and a pre-flight briefing.

The quality of the air task performance (proficiency) is determined by the instructor in the course of the mission and in detail at a debriefing. Each case, when the pilot is unable to predict the development of the tactical situation (lags “behind”) and requires the intervention of the instructor (although properly reacting to “codewords”) points to level one of the operator’s situational awareness in the area of tactical training caused by lack of experience. This situation corresponds to the assessment of a “satisfactory” grade (3). The training objective is not achieved, however, this is a normal condition during the implementation of the training module.

The implementation of the tactical task during which the trainee pilot performs solo (does not require the instructor’s intervention) all the measurable and immeasurable elements in terms of not exceeding the permissible margin of error (Q-) points to level two of the operator’s situational awareness. In other words, the pilot notices errors and corrects them, without exceeding the conditions of task execution. This is an acceptable level which is required on completion of the training module, and during periodic pilots’ inspection in continuous training (of the trained ones). Such a situation proves the achievement of detailed objectives of the tasks, and corresponds to the “good” grade (4).

The task execution with flying colours, where Q requirements are not exceeded points to level three of the operator’s situational awareness (the desired one) and corresponds to a “very good” grade (5). The specific objectives of the tasks have been achieved on a proficient level, confirming the mastery of the pilot’s experience.

CONCLUSION

The rating adopted for the evaluation of the tactical mission execution corresponds to the categories of learning and stages of operators situational awareness. This means that in the tactical area of flight training in each training module there is a specified minimum level (rating), which must be achieved by the pilot if they are to be allowed to move on to the subsequent stage. It is usually Level 2, at which the pilot has to demonstrate that he has the appropriate (required) knowledge, understands mutual relationships between all factors affecting the tasks within the mission, and is able to perform operator's actions in accordance with the accepted standard for a given element of the task. In any instance of safety breach the trainee will receive a "dangerous" rating, which means that he will fail the mission regardless of any partial results obtained.

The adoption of the minimum (required) rating level at the end of a training module comprising of several flights determines the pilot's assumed susceptibility to training actions (number of repetitions necessary to master operator actions).

Effective flight training requires a number of activities aimed at identifying an objective possible to achieve and the most optimal way to achieve it. Tactical mission is the most complex and demanding flight mission. Periodic inspection and the implementation of ongoing mission execution evaluation are the factors due to which training standards can be maintained.

REFERENCES

- [1] Bondaruk A., *“Kształtowanie świadomości sytuacyjnej pilotów na przykładzie praktycznego szkolenia IFR z zastosowaniem symulatora klasy BITD”*, Taktyka i dowodzenie w lotnictwie wojskowym, WSOSP Dęblin 2015;
- [2] Air Force Instruction 11-202, Vol. 2, *“Aircrew Standardization/Evaluation Program”*, 13 September 2010;
- [3] Air Force Instruction 11-2F-16, Vol. 2, *“F-16 Aircrew Evaluation Criteria”*, 10 December 2009;
- [4] Rash Clarence E., Adam Gina E., LeDuc Patricia A., Francis G. *“Pilot Attitudes on Glass and Traditional Cockpits in the U.S. Army’s AH-64 Apache helicopter”*, , Presented at the American Helicopter Society 59th Annual Forum, Phoenix, AZ, V. 2003;
- [5] Institute of Air Navigation Services *“Lesson Delivery Basics”*, Luxemburg 2013;
- [6] Endsley M., *“Toward a theory of situation awareness in dynamic systems”*, Human Factors 37. 1995.
- [7] Kozuba J., *„Selected aspects of forming pilot situational awareness”*, PAFA, Deblin 2013.

SELECTED ASPECTS OF AVIATION COMMUNICATION

Adam BONDARUK, Jarosław KOZUBA

Polish Air Force Academy, Dęblin, Poland (a.bondaruk@wsosp.pl, j.kozuba@wsosp.pl)

DOI: 10.19062/2247-3173.2017.19.1.8

Abstract: *The article refers to the selected aspects of conducting aviation communication by aviation personnel during daily activity. The characteristic of aviation communication was made by defining its kinds, types, and functions. The qualities required from aviation personnel engaged in the communication process were pointed out to, as well as the consequences of the failures in communication. It was emphasized that compliance with the principles of aviation communication by aviation personnel is one of the essential conditions for the success of any aviation mission. It was also noted that training in the field of aviation communication should be treated as a continuous process, regardless of the experience possessed by aviation personnel.*

Keywords: *aviation safety, aviation communication, communication functions*

1. INTRODUCTION

Communication has been treated as one of the most critical issues in all aspects of aviation and aviation safety, from the cockpit-to-controller interface to coordination in the cockpit-to-cockpit, and cockpit-to-cabin interaction to, finally, the management of safety and creation of a safety culture. This fact is clearly confirmed in the statistics of aviation accidents. According to a NASA survey, Aviation Safety Reporting System (ASRS) database identifies the causes of approx. 80% incidents or accidents as incorrect or incomplete communication between pilot and controller or pilot and another crew member. The main factors affecting aviation communication were found to be: incorrect communication – 80% of reports, absence of communication – 33% of reports, correct but late communication – 12% of reports. The same survey revealed which modus of communication is affected: listening – 45%, speaking – 30%, and reading or writing 25% [13]. Similar conclusions were reached by J.B. Sexton, R.L. Helmerich [8] and M. Krifka, S. Martens and S. Schwartz [7], who argue that factors associated with interpersonal communication underpinned about 70%-80% of aviation accidents over the past twenty years. They also believe that the high level of competence in the field of aviation technology is not a sufficient antidote that could prevent the catastrophic consequences of poor communication.

So what is the communication, what are the types of communication and what factors have a major impact on the communication quality in a complex aviation mission environment? Is it right to say, that the maintaining an effective communication, characterized by a high level of communicative quality, between members of the aviation personnel, with particular emphasis put on cabin crew, is essential for maintaining an acceptable level of safety during their operational activity? Among other things, a reader should find the answers to these questions in the article.

2. TYPES AND FUNCTIONS OF AVIATION COMMUNICATION

Communication is a form of exchanging information, thoughts and feelings. It should be done in legible manner, clear to understand. It is conducted in the two-way relationship between e.g. pilot and flight crew, cabin crew, air traffic controllers or ground handling staff. However, we should not forget about the important fact, that the pilot performs among others a communication process by means of a reception and entering specific data from instruments and other onboard equipment (e.g. systems). These devices are for him/her a source of essential information about the condition of the aircraft, the task environment, the status of an air mission etc. What should be recognized as particularly important is the correct process of information exchanging in the relationships described above. It should be treated as an essential condition for maintaining an acceptable level of situational awareness by aviation personnel.

Taking into consideration the way of the transfer/ exchange of information, we can distinguish the following types of communication:

1. Written communication. Usually, it is one-way communication for a pilot in which he/she acts as a recipient, for example: checklists, manualops, letters, memos etc. The advantages of this type of communication are undoubtedly the speed and range of distribution, as well as the possibility of making quick changes to the content of the message, and its re-distribution. However, that type of communication is characterized by a number of negative traits and the impersonal nature. Moreover, the rule of one-way communication significantly limits the opportunity to confirm the correctness of its understanding. Therefore, the information in written form shall be evolved in accordance with the specified structure, applicable to the specified aviation messages. They should be written using easy language and adhering to phrases and expressions used by aviation specialists.

2. Communication through visual perception. To put it simply, this process involves collecting images from the task environment (external and internal) and processing them into the information necessary to achieve an acceptable level of situational awareness. Human sensors and the linked systems of perception receive signals (including vision, hearing, taste, smell) as a result of the implementation of multiple physiological processes which allow us to receive a number of information items in real time. This information is one of the essential elements necessary for us to perform our activity in the task environment. At the same time, it should be emphasized that the process is complex and it functions in a manner not fully clear to us.

Taking into account the research in this area, it became clear that we can sometimes see the world in not an appropriate manner (real manner) [...]. Previous experience of pilots, their expectations, motivations and requirements may significantly affect the interpretation of their perceived "images" of the task environment. H.S. Smallman and St. John [9] described the process of perception of the task environment as follows: "imperfect interpretation (pictures acquired from the environment) which in effect gives imperfect approximation of the real state (task environment)." [3]

Therefore, a pilot who is working out a "snapshot" of the aircraft at a particular stage of the task should remember that each of the developed images of the task environment state is imperfect. Therefore, that status should be verified by using of his/ her knowledge in a given area.

3. A special type of visual perception is the so-called "body language". The fundamental methods of communication relating to the body language include: eye contact, facial expression, touch, body structure and posture, and physical distance between the communication participants.

It should be remembered that the arrangement of seats in the most of general aviation aircraft, transport aviation, and military aircraft(seats are located side by side or one after the other), is not favorable to conduct this type of communication.

4. Verbal communication - interpersonal communication, whose medium is the spoken language. Verbal communication is often accompanied by non-verbal communication (body language and perception communication). It finds particular application in aviation activities. Such factors as accent and speech modulation play a key role in verbal communication. They have a major influence on the reaction of an interlocutor, degree of spoken fluency or the content of expression. In this case the resource of the specialist content is based on the universally accepted language of aviation phraseology and related fixed phraseology phrases, as well as vowel production understood as the reduction or extension of the time in which a given word is spoken.. Special trainings in telecommunications and aviation phraseology are devoted to this type of communication. It should be emphasized that the way in which verbal communication is conducted is very important for the receiving party, for example the speed of speech, the height of tone or voice level may indicate the level of the sender's emotions. A factor which is essential for the proper transmission/ reception of verbal information by the participants of the correspondence is the level of mental load. As a rule the greater the mental load on one or both of the participants of verbal communication, the greater is the likelihood of error, which in turn may lead to an undesirable air event. Verbal communication consists of two main components which are applicable for the sender as well as for the recipient, i.e. listening and verbal response. It is estimated that every person spends about 40% of the daily time on listening, a similar situation occurs with aircraft crews. Therefore, it is believed that listening is one of the essential skills which determine the desired level of communication quality during the air mission execution, regardless of who a participant in that process will be. It should be also remembered that listening does not always mean hearing and understanding. Another element which is essential for the communication quality is an active response.

This division was presented to indicate that the communication process is extremely complex. In practical operation onboard the aircraft it is difficult to imagine a situation in the process of building the desired state of knowledge about the aircraft, in which the pilot would be using one of these types of communication, skipping the others. Practically, during the entire process of preparation and execution of the air tasks, the pilot/aircraft crew is using all forms of communication in parallel. In fact, they are complementary and constitute one of the key factors for achieving and maintaining the desired state of situational awareness by the pilot.

3. COMMUNICATION'S FUNCTIONS

W. B. Kanki and M. T. Palmer described a structure of communication functions in aviation and aviation safety, especially as it affects crew performance, as follows [6]:

1. Communication as a source of information – the lack of information, incomplete or incorrect information can be one of the essential causes of undesirable flight-related events from the point of view of the situation on board an aircraft. Therefore, providing timely information is essential in situations considered as normal/ predictable, as well as those critical from the point of view of safety and effective air mission execution.

As a result of the analysis of the pilot's decision-making process, we can conclude that solving problems related to achieving an acceptable state of situational awareness by the pilot, as well as the implementation of the pilot decision-making process, including the implementation of the decision taken, is largely based on the collection and exchange of information relevant from the point of view of solving the decision problem [14]. However, when we are talking about collecting and exchanging of any information, we should have in mind not just verbal communication, but also those nonverbal forms of communication mentioned above. We can find numerous sources of internal and external information in the cockpit of a modern aircraft, necessary for the proper execution of an aviation task, including, but not limited to, aircraft crew members, aviation services members, instruments, tools and onboard systems, onboard documentation, etc.

2. *Communication as the factor which establishes interpersonal relationships* – communication also has a social role, which is particularly important from the point of view of any aviation activity. It helps to create and improve areas connected with the board crew relationship, to improve the interpersonal relationships and the atmosphere among the crew members, which has a major impact on the quality and effectiveness of executing the tasks. Because of this fact that factor of communication can be considered as one of the essential factors for building the desired level of social climate within the air crew that encourages its members to share their knowledge/information in terms of preparation as well as performance of air missions. In addition, it is worth to point out that the manner of the verbal communication conducted by the crew commander can have a major impact on the efficiency of managing the crew of the aircraft. R. G. Ginetts presents in his report a number of determinants of the effective leadership in relation to the style of communication used by the leader of the group/aircraft crew commander, who should clearly confirm during the pre-flight briefing the creation of such safety elements as: the procedures, principles, norms, and task limitations which constitute the normative organizational model of the task execution. He/She should also establish clear rules of leadership in the crew as well as every crewmember's own technical, social and management competencies[4] .

3. *Communication as a factor which establishes predictable behavior patterns.* The crew of an aircraft who perform their tasks in a particularly complex and dynamically changing task environment must meet particularly high requirements. These include, among others, the need to integrate the actions of aircraft crew members in an organized manner, taking into account specific time constraints and maintaining an acceptable level of situational awareness at each stage of the task execution. This in turn allows them to maintain the required level of predictability of their aviation activities. One of the tools to support this goal is the coordination of actions between flight crew members, which in turn is accomplished through the use of the so-called Standard Operating Procedures (SOP). The correct implementation of communication by the flight crew is an important element supporting the SOP. For example in the so-called checklists, communication allows the crew to determine what tasks should be performed, who should perform them, in what order they should be performed, and what is their purpose. [2]. Furthermore, a high level of formalism in the way aviation information is transmitted allows the flight crew members to anticipate how and when the information will in fact be transmitted and thus a large proportion of flight crew behavior can be predictable. Another important factor in the establishment of behavior schemas by the flight crews is the time they spend together in preparation and tasks execution, regardless of whether it is the time spent in the flight preparation room, the simulator or the practical execution of aviation tasks.

Spending time together allows the aircraft crews to improve their ability to participate in common activities and to better understand how to communicate (verbally and non-verbally) and thereby it reduces the likelihood of misunderstanding the content being transmitted.

In conclusion, the achievement of the common way of communication that is acceptable by all crew members enables the on-board team to improve the air mission execution at a high level of safety and efficiency.

Thus, these actions become more predictable than they would be in the case of air crews who still begin flying together. [5]:

4. Communication maintains attention to executing the task and monitoring – communication process which is correctly conducted by the air crew allows full engagement of all crew members in the execution of the task. This requires the crew to be fully focused on assessing the situation on the basis of verbal and non-verbal communication, data and information received, and on making decisions based on that, enabling them to execute the air mission in accordance with the previously developed flight plan. Obtaining that data and information is possible by continuously monitoring onboard and external sources of information, and in the event of their being insufficient in quantity or doubts as to their validity, the air crew are forced to actively acquire data and information, supplement it or confirm the proper understanding thereof. Furthermore, keeping the attention of the crew members focused at a level which is from the perspective of the air mission execution stage allows the air crew to take corrective or emergency actions within the time limit which can be defined as the required response time. Furthermore, such behavior and conduct of the air crew is conducive to maintaining an acceptable level of situational awareness by all its members, and thus to remaining in constant readiness for making decisions relevant to situations arising on board the aircraft. In conclusion, in terms of communication, the crew is interested in how the mode of communication will promote maintaining the focus of the individual crew members continuously on the task, the effective monitoring of the task environment, and the maintenance of the desired situational awareness regardless of the situation on board the aircraft.

5. Communication is a management tool – communication is one of the essential tools which support the proper management of resources at the disposal of aircraft crews, including technical assets and onboard equipment and systems, airport equipment, ground navigation equipment, etc., as well as non-technical resources such as personnel, crew, air traffic and airport services, time, mental load, etc. This happens no matter whether the task is executed by a single aircraft crew, or the mission execution is assisted by other parallel components (e.g. air traffic services) that are focused on accomplishing the same task. All their activities must be subordinated to one objective, namely the efficient and safe execution of the air task. The proper coordination of the onboard crew and/or the support teams without a properly functioning communication process is hard to imagine.

A good air crew commander/manager knows when to take a complete control over the actions being taken on board and when to let crew members/support teams carry out activities in accordance with the situation. In other words, when to manage and when to monitor the situation onboard the aircraft.[5]:

It should be stressed that the crew resource management in a mission environment which is extremely complex and dynamically changing, with the ever increasing complexity of the missions themselves, is a task that demands high levels of competence from all crew members. A particular role in this team is played by the air crew commander, that is why his experience in the execution of air missions is so important.

In the area of communication, the essential role of the aircraft commander is to coordinate the activities of the crew, as well as to establish appropriate interpersonal relationships being the condition for the accomplishment of the desired multi-crew cooperation (MCC) level. These abilities should be constantly developed by attaching great importance to the quality of conducting verbal and non-verbal communication. This is especially important in the 21st century, when air crews are dealing with increasingly modern technologies. On the one hand, these technologies allow for executing increasingly complex air missions under environmental conditions critical from the point of view of aviation technology of the last century. On the other hand, these technologies are taking over more and more human performed tasks onboard the aircraft, which should also be considered as an advantage. However, in emergency situations, the crew of the aircraft must face challenges unprecedented in everyday flights. In this case, the achievement of the expected result in relation to air mission execution depends on the quality of the tasks performed by the entire air crew. Therefore, the knowledge and skills presented by the crew commander and other crew members in the areas related to communication have a major impact on the decisions and actions taken in order to prevent the risk of an undesirable flight-related event.

To sum up, in the 21st century, it is difficult to imagine the performance of aviation tasks at the desired quality and safety level. The key questions facing today's researchers dealing with broadly understood aviation communication is what factors determine the achievement of the desired level of communication by air crews.

4. SELECTED ASPECTS RELATED TO ENSURING THE DESIRED LEVEL OF VERBAL COMMUNICATION EFFECTIVENESS WITHIN AIR CREW

In the reference literature, we can also find the assertion that effective communication is one of the essential factors supporting error control. [12] The concept of communication skills expresses both social and interpersonal skills. According to K. Balawajder [1], communication is the transfer of information between any type of system/systems and the environment. If these systems are social, we talk about verbal/interpersonal communication, and if we talk about communication with the task environment (e.g. Earth atmosphere, weather, climate, equipment and technical systems, etc.), we speak about nonverbal communication. Regardless of the communication type, it should be treated as a process in which ten characteristic elements can be distinguished (Fig.1.).

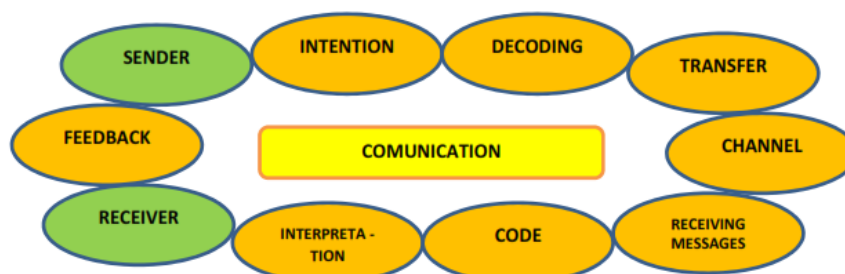


FIG.1. Characteristic elements related to interpersonal communication. Source: Author's own work, developed on the basis of: K. Balawajder, *Komunikacja, konflikty, negocjacje w organizacji*, UŚ, Katowice 1998.

No matter in which task environment we may be, those elements can be divided into two basic groups:

1. A group of elements that determines the emergence of communication (information transfer): the originator (sender), acting as a source of information, and the recipient acting as the addressee of the information.

2. A group of elements that allow for the characterizing/describing the information transfer medium, subject, efficiency and quality of the transfer, intention - treated as an objective, thought, feeling; information transfer code - translating intention, thought or feeling into information transfer in linguistic form, visualization, etc.; message - data, information transmitted in the form of a specific signal form such as speech, script, gesture, touch, image; physical channel: air, paper, electronic media, technical equipment, etc., reception of signals - active reception of data or information; decoding - translating the received signals into content and assigning them a specific meaning; interpretation - received data, information provided by the sender as understood by the recipient; feedback - recipient's response to the sender's message.

Onboard the aircraft, pilots need to maintain an effective level of data and information exchange at each stage of the mission execution. It should be emphasized that effective communication at a high quality level is the process of sending information in such a manner that the meaning of information received by the recipient is as close as possible to the intention of its sender. However, the effectiveness of communication depends not only on the sender but also on the recipient's competence to receive and understand the message. The reception of information is not equal to understanding it.

According to Z. Nęcki, the effectiveness of communication is dependent on such factors as:

- *the level of the recipient's awareness* of the sender's true intentions;
- *discrepancies between verbal and nonverbal communication* presented by the sender/recipient or both participants – differences in gestures and words;
- *lack of clearly defined purpose of communication* consisting in e.g. sudden change of the topic in a long-lasting correspondence between the sender and the recipient;
- *message code mismatch* - using a language that is too difficult or unfamiliar to the recipient, such as aviation communication codes which are country specific (e.g. Great Britain);
- *differences in perceiving (perception)* e.g. the same task situation by the communication participants;
- *differences in knowledge and skills* possessed by the sender and the receiver - the use of professional vocabulary or language (e.g. standard aviation phraseology) which is unfamiliar to one of the parties;
- *too difficult environmental conditions* that prevent effective communication
 - noise, lighting level, traffic density etc.;
- *excessive agitation* of the sender / receiver or both participants in the communication process - excessive agitation usually leads to stressful situations leading in turn to distortion of perception of reality and situation assessment, and thus it negatively affects rational thinking;
- *the tendency to over-interpretation* - searching for additional information and hidden meanings in the received message, information and/or data;
- *lack of mutual trust* between participants in the communication process or in one of them - creates uncertainty as to the quality of the data or information received and thus it evokes doubts about the applicability of that data or information, e.g. in the decision-making process.

The above-mentioned factors are particularly important when the sender, recipient or both of them perform tasks in a task environment subject to rapid changes, and the time that is at their disposal when making subsequent decisions is limited. As a rule, such is the task environment flight personnel has to deal with in their day-to-day operations. Regardless of the above, it should be stressed that in order to ensure that the information has been understood properly by the recipient, the recipient should confirm this each time. This should be done in a way assuring the sender that the recipient has received the information correctly, and what is more that the received information may be taken into account in the subsequent activities (Fig.2). The principles mentioned above are binding both in verbal and in non-verbal communication.

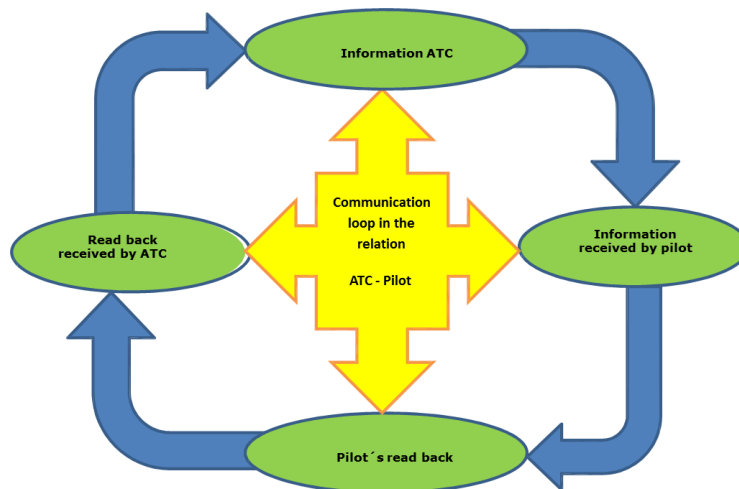


FIG. 2. The cycle determining the desired communication level exemplified by verbal communication in a pilot-air traffic controller relationship. Source: Author's own work.

J. Stewart [1], in turn, defined three essential barriers in verbal communication, namely:

1. **Judgment**, which can be expressed through such forms as: criticism (of the sender or the sender's opinions), interruption of the sender's communication, making a diagnosis with respect to the opinions presented, praising connected with the assessment of the interlocutor.

2. **Giving a solution**, which in the communication process is considered to be commanding, moralizing, asking too many questions, asking questions irrelevant to the message, unwarranted counseling.

3. **Low involvement in addressing the problem being the subject of communication** by diverting the attention from the point, lack of response to logical argumentation, lack of desire to pacify/rationalize the discussion.

The consequence of the emergence of this type of barriers in verbal communication can be the underlying factor for the lack of agreement among air personnel; create an atmosphere of anger and frustration, and, in extreme cases, create negative interpersonal relations, conflicts, misunderstandings, etc. What's worse, as a rule, they lead to a very low communication level, the result of which may be the misrepresentation in the information transmission or the lack of information transmission.

Taking into consideration the conclusions coming from the above communication theories and those resulting from the the analysis of the reference literature [11], we can distinguish a number of characteristics of the air personnel, which determine the desired level of communication in interpersonal relations, i.e. the relations among the air personnel members:

- *can communicate information clearly and in the manner easy to understand;*
- *communicates information when the participants in the communication process are ready to receive it;*
- *is aware of the fact that only receiving full information creates the conditions for its full understanding;*
- *is not afraid to ask questions;*
- *lets other participants in the communication process know his thoughts and feelings;*
- *presents the qualities of a good listener;*
- *presents the desired abilities to prevent conflicts in the cockpit, and once the conflict has arisen, he/she can solve it;*
- *presents the desirable ability to express and accept constructive criticism.*

Furthermore, air personnel involved in communication should be aware of their own strengths and weaknesses in that respect; pay attention to the little things; take into account the fluidity of the interlocutor's attention; not make premature evaluations; present willingness to admit own errors; take into consideration the feelings of the other person; not disregard any question; take into account that differences of opinion may be beneficial; try to take the listener's perspective, show respect to the partner in communication and speak in a clear and kind manner; they should avoid behavior that focuses too much on what one wants to say, and thus ignore what others want to say.

Taking into consideration the above, it should be stressed that only the knowledge of and the compliance with the above principles on the part of the air crew, combined with the presentation of the required level of expertise in aviation communication is a prerequisite for maintaining the desired state of situational awareness. Fulfillment of this condition is one of the essential elements which allow the air personnel to carry out the decision-making process properly and to implement its outcome correctly.

CONCLUSIONS

The fact that air personnel perform their tasks in an extremely complex and dynamically changing task environment causes a properly conducted process of verbal and/or nonverbal communication to often determine an air mission success. Therefore, air personnel, regardless of their function and tasks to accomplish, should be well prepared to carry out this process. Because of the degree of complexity and the aviation regulations, only systematic improvement of these skills may ensure the constant inflow of information and data that condition the correct air mission execution. Therefore, training in communication, both verbal and nonverbal, should be a continuous process independent of the professional experience of air personnel. That communication should become a specific part of the air safety culture. As is the case with safety rules in aviation, getting acquainted with them is not enough. They should be understood and willingly applied in everyday air operations. Otherwise, disruption in mission execution may cause an undesirable flight-related event.

REFERENCES

- [1] K. Balawajder, *Komunikacja, konflikty, negocjacje w organizacji*, UŚ, Katowice 1998.
- [2] A. S. Degani, E. L. Wiener, *Human factors of flight-deck checklist: the normal checklist* (NACAR 175449), NASA, Moffet Field, CA 1986.
- [3] R. Gibb, R. Gray, L. Scharff, *Aviation visual perception*, MPG Books Group, Farnham 2010, p.56.
- [4] R. G. Ginett, *The formation of airline flight crews*. Proceedings of the Fourth International Symposium on Aviation Psychology. Ohio State University Columbus 1987, pp. 399-405.
- [5] B. G. Kanki, R. Helmreich, J. Anca, *Crew Resource Management*, Elsevier, Burlington 2010, pp. 127-128.
- [6] B. G. Kanki, M. T. Palmer, *Communication and crew, resource management*. In E. Wiener, B. G. Kanki, R. Helmreich (Eds.), *Cockpit resource management*, CA: Academic Press, San Diego 1993, pp. 99-136
- [7] M. Krifka, S. Martens, S. Schwartz, *Group interaction in the cockpit: some linguistics factors*, Humbolt University, Berlin 2003.
- [8] J. B. Sexton, R. L. Helmerlich, *Analyzing cockpit communication the links between language, performance, error, and workload*, Human Performance in Extreme Environments Vol. 5, No 1/2000, pp. 63-68.
- [9] H. S. Smallman, M. St. John, Naïve realism: Misplaced faith in realistic display, Ergonomics design, Summer 2015, pp. 6-13 (p.8)
- [10] J. Stewart, *Mosty zamiast murów*. Podręcznik komunikacji interpersonalnej, PWN, Warszawa 2005, pp. 176-186.
- [11] S. R. Trollip, R. S. Jensen, *Human Factor for General Aviation*, Jeppesen Sandersen, Engelwood 1991, pp. 9-7
- [12] <http://www.rollanet.org/-mopilots/stlouis/now2005nws.htm>, on 27 July, 2016
- [13] Airbus Customer Services, *Flight Operations Briefing Notes, Human performance, Effective pilot/controller communication*, pp. 1-2. Electronic version retrieved August 19, 2016 from
- [14] J. Kozuba, *Selected aspects of forming pilot Situational Awareness*, PAFA, Dęblin 2013, pp. 55.

ROMANIAN AIR FORCE AVIATION OCCURRENCES

Oliver CIUICĂ*, Carmen ȘTEFAN**, Serjiu OBREJA*, Nicolae CREȚU***

*"Henri Coanda" Air Force Academy, Brasov, Romania (oliverciuca@yahoo.com, sergiuobreja@gmail.com)

**Romanian Aviation Academy, Bucharest, Romania (carmen.garnita@gmail.com)

***Romanian Air Force HQ, Bucharest, Romania (ncretu@roaf.ro)

DOI: 10.19062/2247-3173.2017.19.1.9

Abstract: *The history of modern aviation in Romania had its beginning in the period when the jet planes entered our logistics. It is well known that after World War II many of the aviators involved in war operations were grounded by the new political regime. In this way, the Romanian Air Force lost a lot of well trained personnel and it had to face challenges regarding new generations of airmen. After 1950, when the decision of Stalin was to strengthen the Eastern Europe air power by offering a new generation of aircraft, Romania started to train new young personnel, pilots, engineers, technicians and air traffic controllers under the Russians' supervision. The fast training process was meant to make Romanian Air Force to be ready for war in three years. Because of the intense practice and the number of new types of planes, the aviation events had multiple forms and causes. Looking back in history until nowadays it is essential for us to learn from mistakes and to set some lessons learned being aware of the most important resource, the human resource.*

Keywords: *history, flight safety, aviation occurrences, cause-chain, factors, errors.*

1. INTRODUCTION

Aviation occurrences, incidents or accidents, include a variety of unwanted events in which aircraft and crew are involved. They may be air collisions, ground collisions or collision with the ground, air or ground explosions (fire), in-flight canopy depressurization or opening and, not the least, careless exploitation of the technique, resulting in involuntary accidents, sometimes with tragic ending. Learning from others mistakes is essential for all organization. That is why, the conclusions of aviation occurrences must be disseminated in the real form to the entire personnel. Our research is meant to be a draft material to all airmen and to all those who are linked to aviation activities.

2. HISTORY TYPES OF ACCIDENTS

Surveying the air occurrences of the period 1950-2014 [1, 6], we can mention some of the most important ones:

a. Air collisions

-1952, Craiova airdrome. Four MiG 15 aircraft took off in formation of twos, at an interval of 20 seconds after each other, for later on to fly together on the circle circuit. During their coming closer, the leader of the first formation hit the leader of the second formation upon a too steep turn.

-As a result of this maneuver, the aircraft became uncontrollable and because of the low altitude they were flying, the ejection could not be executed in due time; the two planes crashed to the ground and the two pilots lost their lives.

These are, in fact, the first recorded victims of the jet aviation in our country, and also the first air collision between two flying apparatuses.

- 1993, Deveselu airdrome. Two fighter aircraft MiG 21 were involved in an air collision while executing two different missions. One of them, two seats, was executing a classical flight to approach, while the other, single seat, was executing its takeoff maneuvers for a flight on route. At the altitude of 3100 m, the two aircraft crashed into each other; consequently, the two seater crew died and the single seat aircraft pilot performed the ejection.

This case is unique in the history of aviation, being the first and the only one to occur between different flight missions (different from the previous one, of the flight in formation).

- 2004, Câmpia Turzii airdrome. An intercept training mission by the quick reaction alert formation, made up of MiG 21 LanceR aircraft, of the aircraft that flew unauthorized over the Romanian airspace, the target aircraft being another MiG 21 LanceR. During the escort flight of the target aircraft, the two aircraft collided, the pilots managing to save themselves by ejection.

This represented the tenth and last air collision in the history of our national military aviation.

b. Ground collisions

- 1953, Craiova airdrome. During a night flight, an aircraft, type MiG 15, while taxiing on the runway, got seriously damaged by a truck at high speed and having its headlights turned off. As a result of this incident, the aircraft was removed from use.

- 1992, Boboc airdrome. During a day flight an aircraft, type L 29, while taxiing toward the runway holding point hit with its right wing and fuselage the startup machine of the airdrome. As a result, the aircraft was removed from the operational use and it was exhibited on base.

c. Collisions into terrain

- 1952, Deveselu airdrome. During a training flight mission on route, under instrument meteorological conditions, in formation of two, two aircraft, type MiG 15 hit the ground attempting a forced landing on unknown terrain/ outside the runway, due to a sudden worsening of visibility, disorientation and fuel consumption aboard, one of them colliding into a river bank and the other into a hill top.

- 1972, Ianca airdrome. During a training flight for learning the low height maneuvers, an aircraft, type L 29 crashed, the two pilots (the instructor and a trainee of the aviation school) lost their lives. Witnesses declared afterward that the instructor had deviated from the mission's profile, executing a low pass over a lake and not managing to establish the real height.

- 2006, Otopeni airdrome. During a training flight on route, at low altitude, the crew of a helicopter, type IAR 330 Puma, flew over a lake, at very low altitude. The sun shine and the lack of any possibility of determining the height following landscape contour led to the helicopter collision into the body of water. As a result of this catastrophe, the three members of the crew lost their lives.

The reminding of the two cases of interdicted very low passes is not at all randomly. This is one of the very frequent causes for collision into terrain.

- 1997, Giarmata (Timișoara) airdrome. In order to perform the flight trainings preliminary to the Aviation Day (June, 17), during the meteorological flight in the proximity of the airdrome, the crew of a fighter/ training aircraft L 39 executed a skew flip at a too low altitude, the recovery not being possible the aircraft hit the ground, causing the death of the two members of the crew.

This event is the only aviation catastrophe of this type and the only loss of a General that the Military Aviation experienced.

The cases presented previously represent classical situations of CFIT - Controlled Flight into Terrain, occurrences that are quite frequent and typical for both national and international environments.

-2010, Tuzla airdrome. During a training flight for parachute dropping, upon takingoff, an An 2 aircraft lost lift and hit the ground, falling from an approximate height of 50-60 meters. The catastrophe left two survivors (one of the pilots and a paratrooper), the other 12 occupants of the aircraft being deceased after the crash. Following this air tragedy the An 2 aircraft was withdrawn from exploitation, but it remained stored on Boboc airdrome.

- 2012, Boboc airdrome. During flight training for acclimatization and observation of the aircraft controls under various flight regimes, a helicopter, type IAR 316 B Alouette hit the ground from a height of under 50 m. The crew made up of the instructor pilot, the student-pilot (student of the Air Force Academy, in his first year) and two board technics lost their lives following the crash.

Again, this is one of the unique cases in history resulting in the death of the youngest military trainee pilot, the student aged 19.

The last two cases invoked are different from the first two, because on the descending trajectory of aircraft to approach the pilots lost control of their aircraft (Loss of Control In - flight – LOC-I).

c. Explosion (fire) in the air or on the ground

- 1972, Borcea airdrome. During the takeoff for a night training flight under visual meteorological conditions, the pilot of an aircraft, type MiG 21, was force to perform the ejection maneuver after the aircraft explosion and break in the air, at an altitude of approximately 800 m.

- 1997, Craiova airdrome. A mixed technical crew was assuring the arming and preparation of an aircraft, type IAR 93, which was to execute a real firing testing flight. During the preliminary steps of the aircraft's arming there was an explosion that led to 16 fatalities, including technical and flight engineering staff.

d. Cockpit depressurization or canopy opening en route

- 1953, Craiova airdrome. During a training flight with an aircraft, type MiG 15 two seats, the canopy opened from its lock mechanisms and, under the air flow hit the head of front occupant, leaving him dead. The aircraft was landed by the instructor, the occupant of the rear seat.

- 2007, Câmpia Turzii airdrome. On a post-maintenance flight of a MiG 21 LanceR, during the climb toward the indicated area, at the altitude of 6500 m, the pilot noticed the broken glass canopy. He interrupted his mission immediately, announced the air traffic controller and came to approach, under safety conditions.

e. Careless exploitation of the technique

- 1986, Craiova airdrome. The accident occurred during the flight mission, toward the end of a solo flight, when the pilot was ready to exit the cockpit. He opened the canopy, released himself from the seat safety belts and involuntarily pressed the ejection. Consequently, the system came in operation, the ejection took place and the seat and pilot were ejected at 32 m away from the plane. Because of the injuries, the pilot died.

- 1994, Mihail Kogălniceanu airdrome. During the arming process of the MiG 29 aircraft with unguided reactive projectiles, at one moment, one of the projectiles was armed and exploded. The result was the death of the load officer and the serious injury of another.

3. FACTORS THAT INFLUENCE THE AVIATION OCCURRENCES

Rarely does an accident or catastrophe hold just a unique cause. In most of the cases, we may speak of a primary cause, to which one or more secondary ones are added. For example, a critical situation, initially produced due to a technical defect, may become worse because of the pilot's wrong action. Or, an initial error, the generating factor for a critical situation, may be followed by new errors which can deteriorate the situation even worse, [2].

The Romanian Explanatory Dictionary defines the 'cause' as "a phenomenon or a set of phenomena which precede something and, under definite conditions, determine the appearance of another phenomenon, named effect, to which it serves as a starting point". In "Instructions regarding the manner of technical investigation of aviation occurrences involving military aircraft", causes are defined as the "actions, omissions, events, conditions or any combination of these diverse elements that produced or could have produced an air occurrence", [3].

The causes of aviation occurrences are included within three major groups, as follows:

- human factors;
- technical factors;
- environmental factors.

By environmental factors one should understand atmospheric conditions in their totality (reduced visibility, ceiling, turbulence, strong wind, icing, precipitations, thunderstorms, storms, fog, bird activity etc.). However, we should not ignore the artificial environment, either, because it has direct effects on the human factor.

In the specialized literature, [7, 8], there is also mentioned a fourth group, named "operational factors" or "organizational factors", a group that may be integrated in that of the human factors, since it refers to the organization of activities and deficiencies that may appear throughout their process. Taken individually, each of these causes, in most of the times, do not hold extreme relevance, but when combined, they may generate a long range of events, apparently without any relationship between one another, still which result in an accident.

In the attempt of clarifying the air occurrences in the military aviation throughout time, there were taken into account (only) the three factors (human, technical, environmental) and their derivatives.

Thus, the investigation commissions release their conclusions mentioning as the main factors the following, [1]:

- human error;
- technical flaw;
- indiscipline;
- material wearout;
- piloting error;
- bird strikes;
- meteo conditions;
- unknown causes;
- Other causes.

From the studied analyses, there resulted that out of 296 catastrophes and accidents these were attributed to the following factors (Figure 1):

- Human factor/ HF 152;
- Technical factor/ TF 87;
- Environmental factor/ EF 32;
- Undetermined/unknown causes/ UNK 25.

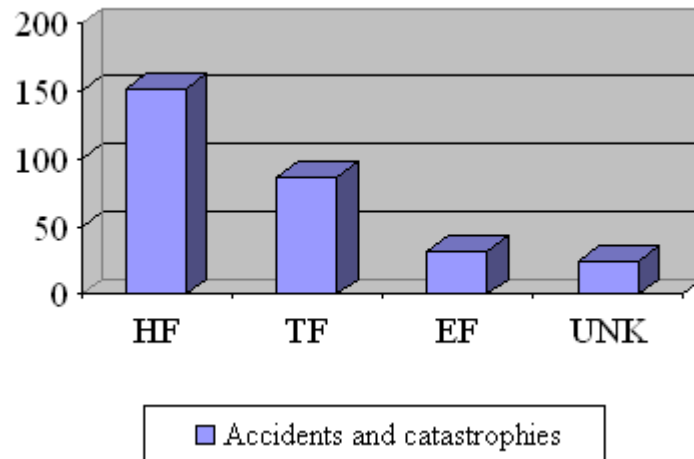


FIG. 1 – Accidents determining factors

As it is noticeable from the block chart above, the main reasons of the air occurrences and implicitly of the human and material resource losses are those of technical and human nature. We will further detail on the aircraft components subjected to material wearouts/failures as well as on the human factor's contributions to the occurrence of accidents, so as they resulted from the conclusions released by the investigation commissions.

From the analysis of the technical factors contributing to the serious aviation events, there turns out that the main systems of aircraft such as the power installation (engine) or material wearout/failure led to the occurrence of most of the serious aviation events. Irrespective of the pilots' level of training or professional experience, the appearance of one of the enumerated system defects places the crew in the impossibility of maneuvering the aircraft and implicitly it requires the choice of the optimal solution. If the time at the crew's disposal is reduced, or if the rescuing option by leaving the cockpit is excluded based on aircraft construction reasons, then disaster is almost imminent.

Referring to the human factor, the most present cause in aviation occurrences (and in other domains) worldwide, it is also the basis for the greatest human losses among pilots. Why? The answer is simple: the crew is taken by surprise and does not have the time to react (low pass flight, aerobatics at low altitude) or, wishing to repair their mistake (voluntary or involuntary, based on perceptions) the crew tries its best to save the aircraft, hoping for a happy ending, thus managing to "hide" itself from the punitive repercussions of the system.

As a result of the serious occurrences, the number of lost or removed from exploitation aircraft as well as the situation of the flying personnel are in Table 1.

Out of 304 lost aircraft throughout this period of time, starting with 1950, their types and numbers were the following:

Table 1 – Aircraft losses and flying personnel fatalities

Aircraft type	Exploited	Destroyed	Crew fatalities	Aircraft type	Exploited	Destroyed	Crew fatalities
IAK 23	62	15	3	IAR 330	106	28	35
MiG15/S 102	470	84	58	IAR 93	86	11	2
MiG 17	24	5	3	IAR 99	28	8	3
MiG 19	27	11	7	Il 28/H5	28	8	11
MiG 21	350	86	46	Mi8/17	41	5	9
MiG 23	46	7	1	IAR 823	58	4	8
MiG 29	21	4	3	IAK 18	20	2	2
L 29	52	7	5	IAK 52	24	2	1
L 39	32	1	2	An 2	26	1	4
IAR 316B	127	15	16				

Although an impressive number of aircraft were lost, the fact that there were survivors to share from their experience and sensations lived from the very incipient stage of the events up to the safe landing, by means of parachute or as a result of a forced landing, makes the number of the avoided events to be never found out. It is certain that among pilots there are many ‘talks’. This sharing of occurrences, sometimes slightly nuanced, leads to a decrease in the number of air events, but it does not make them disappear for good.

By far, the top three aviation events include three types: aircraft MiG 15 and MiG 21, and helicopter IAR 330. The multitude of missions that are possible to execute in the tactical field under all meteorological conditions made the three types of aircraft to be purchased and used intensely for the flying personnel’s training and carrying out of combat orders. In the incipient phases of starting using those types of aircraft, their use for training missions was applied under normal meteorological conditions, especially during the daylight. Out of easy to understand reasons, not all the flying personnel designated to be trained on these types of aircraft got to the performance of using the technique at its maximum capacity. Thus, a selection of crews, based on their skills, performance, and, not the least, intellectual capacity was performed. The more efficient the technique is, the more the crews’ capacity of data synthesis and analysis must be and implicitly the time for decision making in a coordinated and adequate manner is shorter.

Taking into account the previous specifications, many of the pilots had to, out of their own initiative (or forced by the military system), admit their limits and to select another inferior category of aircraft, or even specializations that did not include flight activities. We not at all wrong to affirm that some of those pilots displaying reduced capacities of exploiting and using aircraft were ‘excluded’ by them.

Our viewpoint with regard to the personnel that managed to face difficult situations, while putting their experienced facts and events into the lessons learned chapter of their professional lives, is that they are ready to exploit their given aircraft. Even though they made mistakes that led to a series of events, their capacity and expertise made them not degenerate and succeed in managing difficult moments in a unique manner, many times reducing resources loss.

For comparison purposes, the number of destroyed aircraft, of losses and survivals of the flying personnel, is represented on decades, in Table 2.

Table 2 – Situation of lost aircraft and flying personnel involved on decades

Destroyed aircraft	1950-1959	1960-1969	1970-1979	1980-1989	1990-1999	2000-2014	Total
Without ejection system	-	-	6	18	15	7	46
With ejection system	75	39	43	34	48	22	261
Total aircraft	75	39	49	52	63	29	307
Fatalities	46	22	39	49	33	33	222
Ejections	8	10	18	15	20	7	78
Survivals	27	9	6	22	23	6	93
Total rescues	35	19	24	37	43	13	171

4. CHARACTERIZATION OF THE AVIATION ACTIVITY BETWEEN 1950 AND 2014

By analyzing the percentages of collected and analyzed data, we found the following facts:

- Out of 1628 aircraft, 19 different types, to which we refer, there were 304 aircraft lost, representing 18.6% of the total;
- Out of the total number of helicopters equipping the Romanian Air Force (207), there were 48 lost, representing 17.5%.
- The number of airplanes taken out of use, 256, represents a percentage of 19% of the total of 1354 items.
- A number of 219 people that lost their lives (pilots, technical crew, navigators, shooters and radiotelegraphists) were part of the 298 serious accidents (6 helicopters were lost on the ground, as a result of fire in one of the hangars, in Sibiu).
- Out of these 298 accidents, a number of 171 flying personnel was rescued, 73 of whom managing to save their lives by ejection procedures.

Note: out of the 78 successful ejections, a number of 3 pilots executed two ejections, only 2 of whom are still alive today.

Starting from the number of fatalities from the period 1950-1959, 46, we notice that the number of life losses decreases suddenly, by almost 52%, in the period 1960-1969, up to 22.

The years of 1970 recorded an increase of 77% fatalities, a number of 39 human losses among the flying personnel, compared to the previous decade, the ascendant trend being in place for the '80s, as well, when 49 people lost their lives, approximately with 30% higher level.

For the next two decades, the value of human resource loss remained the same, counting 33 pilots, which represents a decrease with 33%, as compared to the years of '70-'79.

By analyzing the existent data with regard to the survival percentages in contrast with the human lives losses, we can reach the following conclusions (Figure 2):

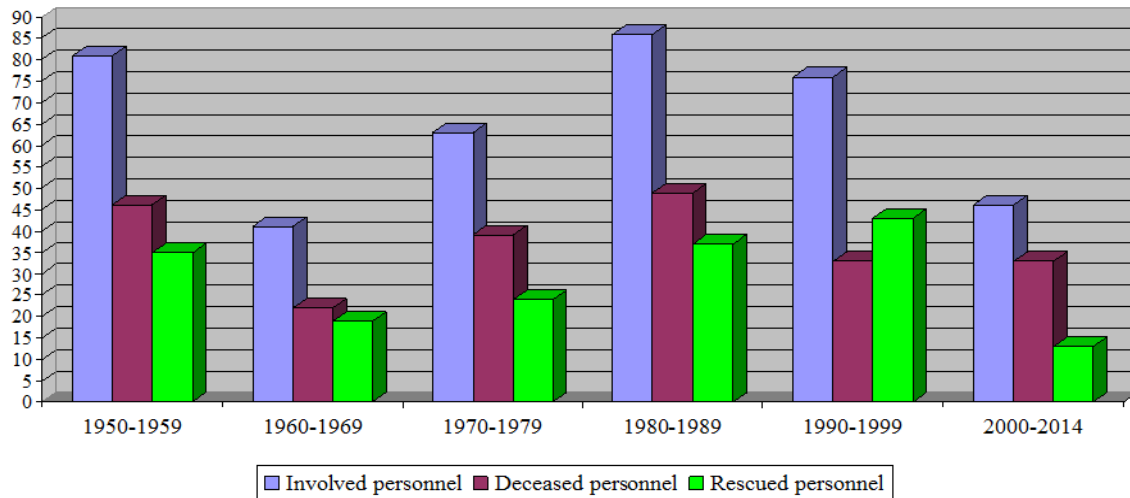


FIG. 2 – Personnel involved in accidents

- Between 1950-1959 – out of 81 aviators involved in flight events, 46 (57%) of them died and 35 (43%) saved their lives;
- Between 1960-1969 – out of 41 aviators involved in flight events, 22 (54%) of them died and 19 (46%) saved their lives;
- Between 1970-1979 – out of 63 aviators involved in flight events, 39 (62%) of them died and 24 (38%) saved their lives;
- Between 1980-1989 – out of 86 aviators involved in flight events, 49 (57%) of them died and 37 (43%) saved their lives;
- Between 1990-1999 – out of 76 aviators involved in flight events, 33 (43%) of them died and 43 (57%) saved their lives;
- Between 2000-2014 – out of 46 aviators involved in flight events, 33 (72%) of them died and 13 (28%) saved their lives.

Comparing the six decades, we can divide them into three distinct periods:

1. Years of '50-'89, when the ratio of survivals held an average percentage of 42.5% (**under the percentage of fatalities** of 57.5%);
2. Years of '90-'99, when the values are exactly the opposite. The ratio of survivals held the value of 57% (**above the percentage of fatalities** of 43%);
3. Years of 2000-2014, when, unfortunately, the ration of survivals decreases a lot beneath fatalities – 28% of survival compared to 72% fatalities!!!

The first period falls under the influence of the beginning of use of a great number of types and variants of aviation equipment purchased from the former USSR and other member states of the Warsaw treaty, in large amounts. The lack of flight experience, but also the alert pace in the training of the flying personnel is tightly connected to the numbers shown above.

The little experience acquired on double-seater aircraft, tremendously different from the one that were used for regular training in solo flights, led to discovering the secrets of flying progressively, through repeated attempt, which were many times disastrous, [4, 5].

The period between 1990 and 1999 is one of social relaxation, which its presence felt in all areas of human activity.

The massive growth in the number of flying hours allotted to flying training, the hunger for the continuation of training being evident for each member of the military aeronautical organization, led to an increase in the number of air accidents survivors and all these denote, first of all, an increase in the awareness regarding the importance of the human resource and equally, trust in the capacity of rescuing means found aboard of aircrafts. Moreover, the participation in joint exercise with other NATO member states and other states influenced the approach to training the personnel belonging to the Air Force.

With regard to the period of time before Romania's joining the NATO structures, there was the time for implementing tactics and techniques of forming, training and using the Air Force based on the principle "not many, but best". The massive leaving of the military environment, starting with the year of 1998, by a large number of professionals, conducted to the disappearance of experts in the area of aeronautical activities' planning and execution.

The minimal acquisition of equipment and new technique and budgetary limitations led to abandoning many types of aircraft, considered "inadequate for the training of flying personnel based on the NATO standards", but also to the adopted solution, that of crisis time, of modernization and expansion of the lifetime of a number of aircraft equipping the air fleet, in order to maintain the minimum level of national defense of our air space and to meet the minimum standards required by the alliance. The training of crew is thus tremendously influenced by the level of allocated financial resources for the aviation bases but also by the massive exodus of the personnel with a high level of expertise.

5. CONCLUSIONS

There are known problems, and, more seriously than that, they are sometimes accepted.

Why should we discover them when we can prevent them? The current paper aims to bring up new elements in the traditional field of aviation safety and to eliminate vulnerabilities regarding it.

The diverse causality draws our attention toward an essential fact: at any time, deficiencies in the aeronautical system, which were previously ignored, will be able to generate, through different combinations, a series of more or less visible and serious events. It is relevant in this respect the "iceberg" model (Figure 3), which highlights:

- a) a continuum of events, from the simple deficiencies to accidents and catastrophes;
- b) the frequency of errors representing the visible part of the iceberg is much smaller than that of 'inoffensive' errors, in first place;
- c) the possibility of interrupting the undesirable event's evolution through the detection and recovery in due time of errors at all decision making levels.

The cause-chain of critical events progresses from bottom to top, which means that the chances of early prevention of an air accident decrease as we get closer to the top. The event analysis tries to decrease as much as possible toward the bottom of the pyramid, in order to find a large spectrum of primary causes.

This approach to an air disaster analysis allows the identification of dysfunctions in the air system under analysis and which may drag about other air incidents or accidents.

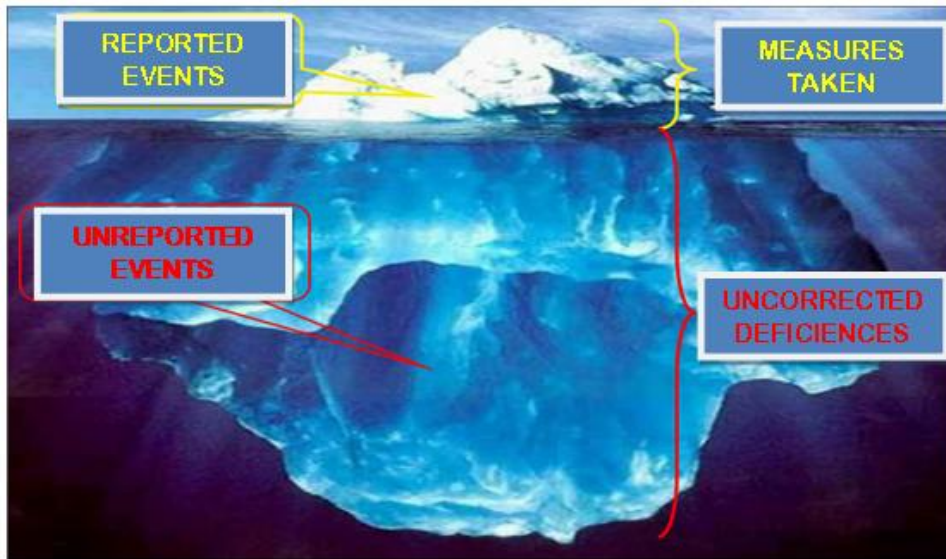


FIG. 3 – Visual exemplification of latent errors

By analyzing this photography let's try to identify, at least, those uncorrected deficiencies, whereas the decision making fora are left with the duty of eliminating as many factors as possible.

REFERENCES

- [1] Romanian Air Force HQ – archive.
- [2] Ceaușu, V., *Psihologia zborului*, Military Publishing House, Bucharest, 1976, p.227
- [3] *Instrucțiuni privind modul de investigare tehnică a evenimentelor de aviație produse cu aeronave militare*, Bucharest, Air Force Staff, 2007, p.34;
- [4] *Istoria aviației române*, Scientific and Enciclopedic Publishing House, Bucharest, 1984.
- [5] Avram, V., *S-a furat aviația*, Host models Publishing House, Brașov, 2011.
- [6] Ionescu, A. C., *Eroii erei reactive*, RBA Media Publishing House, Bucharest, 2014.
- [7] Perrow, C., *Normal accidents*, Basic Books, New York, 1984.
- [8] Reason, J., *Managing the Risks of Organizational Accident*, Ashgate, England: Aldershot, 1997.

STRESS ASSESSMENT USING MODERN MEASUREMENT METHODS

Ioan CURTA^{*}, Ionel MOHIRTA^{**}, Ciprian ENE^{*}, Marian Nicolae VELCEA^{***},
Ileana Constanta ROSCA^{****}

^{*}“Quantum Therapy” Integrative Medical Centre, Bucharest, Romania
(icurta@yahoo.com, drciprianene@gmail.com)

^{**}Romanian Transpersonal Psychology Association, Bucharest, Romania
(imohirta@tanatopsihologie.ro)

^{***}University of Agricultural Sciences and Veterinary Medicine, Bucharest, Romania
(marian.nicolae.velcea@gmail.com)

^{****}“Transilvania” University, Brasov, Romania (ilcrosca@unitbv.ro)

DOI: 10.19062/2247-3173.2017.19.1.10

Abstract: *Stress is an adaptive and subjective reaction of an individual to the exposure to environmental factors. The main objective of this paper is to determine a methodology of assessing the level of anxiety/stress of aviation personnel by using state-of-the-art measuring equipment such as the GDV (Gas Discharge Visualization) device and the Rofes device. The second objective of this paper is to take a first step towards creating a stress resistance profile that could be useful in testing candidates for a career in aviation. This research aims to make repeated measurements on different people, in both laboratory conditions - using a flight simulator - and in real conditions – using a light aircraft. The working hypothesis is that no adjustment to stress can lead to diminished attention, which in turn can determine human errors with severe consequences.*

Keywords: *stress assessment, anxiety, GDV, aviation, pilot*

1. INTRODUCTION

1.1 Stress, general information, beneficial and non-beneficial aspects.

The current technical and scientific process requires a high level of adaptation of the organism. This is the first time in human history that we have access to so much information, that we have to “process” so much “new information” in so little time. We can foresee that this evolution will continue and will amplify in the future. However, there is a price to pay for the progress and the challenges that we are subjected to in order to keep up the pace and this price is mainly represented by stress.

1.2 Theoretical aspects regarding stress in aircraft pilots

Stress, which is sometimes defined as the “disease of the century” represents a manner in which the body adapts to the environmental changes. another definition is: “*stress is a complex factor that consists of both an emotional component (anxiety) and a somatic component that results from prolonged exposure to constant anxiety.*” [1].

A special aspect is represented by stress during aeronautical activities (maintenance, ground and air operation). In an interview for *Adevarul* newspaper, a pilot stated that:

“No matter how much you fly and no matter how used to piloting you are, the stress of flying is still there. Any pilot sitting before the steering wheel of an aircraft is aware of the fact that stress is there and will always be there, even if he/she does not realize it.” [2]

The pilot of the ultralight aircraft (motor-hang-glider/microlite, **Fig. 7**) used in the test flight stated that with this type of aircraft (and probably with all types of aircrafts) the hardest and most stressful part is the landing.

It is for this reason that the authors of this paper aim to measure/investigate the evolution of this important parameter through a new approach, using state-of-the-art equipment.

2. THEORETICAL CONSIDERATIONS ON THE METHODS AND INSTRUMENTS USED IN MEASURING THE LEVEL OF STRESS IN AIRCRAFT PILOTS

2.1. Methods of assessing stress

One of the classic methods used in assessing stress is *POMS (Profile of Mood States)*, a laborious method that involves filling in surveys and interpreting them from a statistical point of view. The instruments, techniques and methods used in measuring and investigating various parameter values of the human body have evolved in direct contact with the technical and scientific developments. New measuring methods and devices were developed using two resources: the principles of quantum mechanics and the rediscovery of Oriental medicine, namely the Traditional Chinese Medicine (TCM).

A new research approach was implemented once the Kirlian photography/effect was discovered at the middle of the previous century. The devices created based on the Kirlian effects enabled the visualisation and study of an “unseen” field, i.e. the human Biofield.

The definition of the biofield is no longer unanimous. Herein under are two definitions: the first one is provided by Prof. K. Korotkov [3], while the second, which we consider to be more comprehensive and explicit, is provided by Prof. PhD. Corneliu Moldovan.

Biofield Definition

- “a type of field that occurs as a consequence of the complex interactions between the physical body and radiations of known or unknown energy, including electromagnetic fields, gravitational fields, acoustic fields etc. It is distributed in space around biological organisms and it is created by the emissions of the body when it interacts with environmental processes. It represents an information exchange interface between a certain organism, the environment and other organisms”. [3]

“The human body is an assembly of cells that are constantly growing, developing, diversifying, regenerating and dying. In an adult person, 25 million cells divide in only one second and the blood cells renew themselves at a rate of 100 million per minute. During the cell division and growth electromagnetic waves are constantly emitted. These signals vary depending on sex, age, genetics, nutrition, health status or illness, pathological processes present or on-going.”[4]

The majority of authors that conducted studies on the Biofield (W. Tiller [5], Inyusin [6], Cornelia Guja [7][8][9], K.Korotkov [3][10][11]) consider it a communication interface between living organisms and the environment. Said interface is believed to contain many of or all of the information regarding that particular organism.

If we consider the above hypothesis to be correct, the study of the Biofield is the most recommended and fast method of investigating anxiety and stress.

We have conducted a research on PhD theses that study stress using GDV devices. According to the dissertations presented at Holos University in the USA [12],[13], in Slovenia [14], and in Romania, [1], [15],[16], various methods have been used to decrease this parameter, i.e. Art of Living Programme, dance therapy, music, sounds emitted by specially tuned crystal balls, modified states of consciousness, ingestion of colloidal solutions, etc.

An important aspect that needs to be mentioned is described in the thesis of Psychologist Manolea, M.D. This aspect represents one of the factors that led the authors of this paper to conduct their research. Following a statistical study, Manolea, M.D. found that in neither of the cases of stress analysed during pre-testing (also using POMS tests) “there was no homogeneity in the groups in what concerns the self-perception of the state of depression and the level of stress.” The conclusion was that the subjects – the students (and by extension other people that live in similar conditions) – *were not aware of the fact that they were living in a state of stress!*

3. EXPERIMENTAL CAMPAIGN ON THE STRESS OF AIRCRAFT PILOTS

The aim of this research is to assess the stress to which a pilot is subjected in simulated conditions and the stress to which a pilot and a passenger are subjected in real conditions, using a light aircraft. The assessment will be performed using various methods – video monitoring, pulse and cardiac rhythm monitoring, measurement of the Biofield changes highlighted by the *BioWell* and *Rofes* devices – that are described in detail herein under. The purpose is to assess the level of stress and the resistance to stress during a flight and to determine a set of reliable parameters that would help in assessing the pilot before flying.

3.1 Experimental conditions. Methodology. Eexperimental stages

All the measurements will be performed in the same location, by the same operator, with the same subjects and in the same order, in compliance with the measuring protocol considered optimal by the inventor of the device and procedure, Prof. K. Korotkov [2], in order to minimise the systematic errors.

Stress generates important changes in the energy field. *The images presented herein under are eloquent and have been taken from the article “Measuring Human Energy Field” [2]*

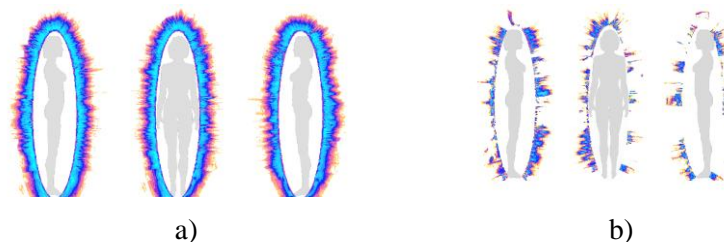


FIG. 1. Biofield distribution of a person: normal, healthy (a), stressed (b).

In Fig. 1 a) a healthy person has a uniformly distributed field, without any interruptions, holes, explosions or irregularities, while in Fig. 4 b) the person is extremely stressed.

GDV (Technique) – “The method used to visualise the biological emissions and optical radiations (living or non-living) by means of stimulating the amplified electromagnetic field through photographic capturing of the gas discharges (usually in the air), followed by processing using a computer”. [2]

The GDV devices are well-known by the authors due to their years of experience.

4. MOTIVATION OF THE CHOICE FOR MEASURING DEVICES

The measuring devices recommended for these tests are *BioWell* and *Rofes*. Both devices were created and developed in the Russian Federation, as stated by the investors and have also been used in the military field. The reasons for which said devices were chosen are the following: the devices enable the assessment of the emotional tension and the stress level; they are non-invasive, user friendly and the examination of a subject lasts less than 2-3 minutes; they take measurements using non-invasive, simple, painless and clean procedures, without risk of infection, without collection of bodily substances or fluids; they do not require injection of contrast solution or previous preparation (e.g. undressing) of the subject and do not require special conditions. Moreover, each device obtains a series of parameters, from only one measurement, that can be subsequently selected for comparative studies.

5. DESCRIPTION OF THE DEVICES CHOSEN/SELECTED FOR THE TESTS

5.1. The BioWell device

a. Description

The GDV (Gas Discharge Visualization) device called BioWell is the newest system created by Prof. Korotkov’s team and it is accompanied by a strong software that has replaced all the other models of GDV devices (compact, express etc.). The same as the other devices in the GDV series, BioWell is based on the Kirlian effect.



Fig. 2. The BioWell device Test procedure <http://www.the-colors.ch/gdv-biowell.php?view=12>

The method of use of the *BioWell* device is very simple (information taken from the device’s user manual). All 10 fingers of the hands are inserted into the device hole, which is protected from ambient lighting, one by one, in a predetermined order. Once the tip of the finger touches firmly the positioning plate, the operator orders the stimulation of the high voltage field using the computer (for 10 milliseconds), which is linked to the camera that captures the brightness of the air discharge around each finger. Subsequently, the images obtained are sent via internet to the producer’s website that includes the software that enables the quick analysis, almost the real-time analysis of the changes caused to the energy of the human body.

Since the results are obtained so fast, this device can also be called an “express method” of detecting anomalies that require more detailed investigations.

b. The parameters that can be highlighted by the Biowell device

The images obtained show the distribution of the energy field in sections (front, back, lateral, 2D and 3D), the size and positioning of the chakras, a circular diagram of the energy level of each organ and system, a graphic (bar chart) showing the level of stress and the levels of energy inside the body.[17]

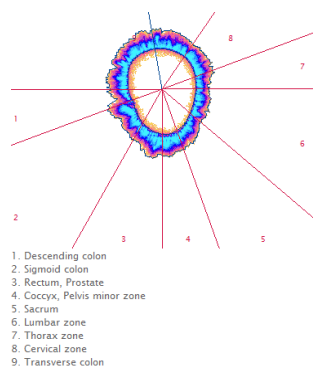


FIG. 3 The ring finger – the image of various organ sectors

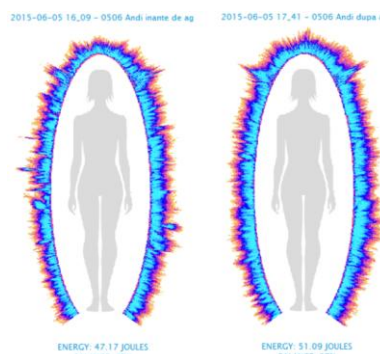


FIG. 4 Field distribution (2D) around the body.

The software enables the comparison of two (or more) measurements taken from the same person, at different times or from different persons. The software also enables the user to print a page of all the parameters measured for archiving purposes.

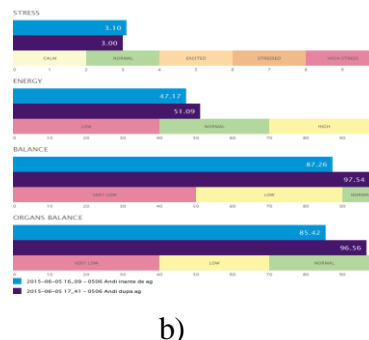
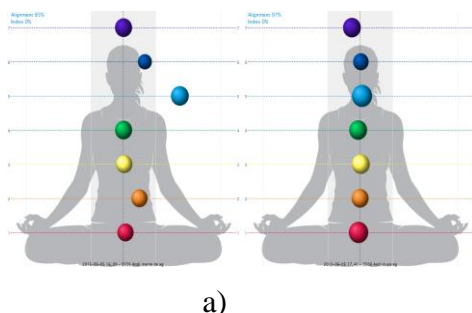


FIG. 5. The synoptic presentation of the main parameters that can be measured with BioWell GDV: the size and position of the chakras (a); the distribution and intensity of the energy field, the level of stress, the general energy balance and the organ energy balance (b).

The most important parameter that can be measured using the GDV devices is emotional pressure (the level of stress).

Emotional Pressure (Stress)

By using special software, it is possible to make a quantitative assessment of the anxiety and health index on a 10-point scale

- **0 - 2** - very calm, relaxed people; at the same time it may be the case of chronic depression
- **2 - 3** - normal calm quiescent state.
- **3 - 4** - the state of anxiety. The state of permanent anxiety without relaxation can cause serious problems.
- **4 - 6** - the excited stress state characteristic of active work, excitement, intense activity.
- **6 - 8** - at least four possible situations:

The reaction to a previous stressful situation (an unpleasant conversation, illness, failure in the training process, driving in stressful conditions, etc.), increased nervousness accumulated over long periods of time, stress, emotional stress, autonomic dysfunction, athletes in the moment of competition, actors during performances, students at exams, etc.

• **8 - 10** - a very high level of stress, the peak of emotional excitement. If a patient with activation level 8-10 appears calm, this could indicate a dangerous situation, i.e. the person is on the verge of a nervous breakdown, so be aware and exercise caution.

Important note by the official BioWell User Manual. [17]: Stress level assessment with the Bio-Well device gives you an indication of a stress level. This assessment should not be used as a medical assessment.

c. The advantages of the Biowell device and method

An important advantage of the BioWell device is its price, which is relatively low and the availability for fast delivery. Other advantages consist of:

- simplified use due to the software that includes an intuitive interface that is user friendly;

- the parameters that are to be highlighted are predetermined for measuring and are presented synoptically on the same graphic, i.e. emotional tension/stress index, energy and balance, organ balance;

- the software enables the comparison of the measured parameters obtained from the same subject or from different subjects;

- the software provides a .pdf document of all the measured parameters that can be printed or sent via email;

- the device can be equipped with a platinum sensor/electrode, that can be used for an energy analysis of various liquids.

d. Limitation of the Biowell device and method

The two main limitations of the device consist of:

- the work method requires internet connection in order for the electrophotonic images created by the device to be sent on a dedicated website where they are processed in order to obtain the results;

- access to the website for data processing is provided by means of monthly subscription. The device can also provide offline measuring, but the data will only be processed after the internet connection has been restored.

5.2. The Rofes device

a. Description

The *Rofes* device (registrar of the functional-emotional state assessment) was created during the early '70s when Soviet scientists were concerned with assessing the health status of astronauts during long orbital flights. The researchers at the Institute of Scientific Research in the field of medicine and biology of the USSR Scientific Academy, that dealt with all the medical aspects regarding spatial programs, started developing the idea of "prenosological diagnosis". The aim of this diagnosis was to identify health issues before the occurrence of the symptoms. This allowed them to provide medical interventions upon commencement of the disease and help the patient avoid serious problems by using fewer, cheaper and non-invasive means. Operating and Service Instruction Manual.[18]

Soon afterwards, this method was transferred from spatial medicine to army medicine. Here it was mainly used to assess the psycho-emotional state of soldiers and officers, to avoid suicides, the violation of the military discipline and various accidents caused by the level of stress of the managers and operators of military equipment.

ROFES is constantly improved based on the practical results of its application in medical and treatment centres in Russia. This device is at its fourth generation and it is also available in the civilian version, “for home use”.

b. How does Rofes work?

The device is put on the left arm in order for the active electrode to be put on the active biological point Daling (MC-7) [19][20] of the left wrist. Once the device is started, it will emit a weak electrical signal and it will register the manner in which said signal changes/modifies. Afterwards, the software installed on the computer will compare the result obtained with the standard (what is typical for a healthy person of that age). The results of the comparison can be observed on the screen in the shape of figures, according to the scale graded in 5 steps. Five is excellent, while one is bad. For a better visualisation, the figures are coloured from dark green to bright red [18].

This is to assess the general health status and the 17 organs and systems, as well as the degree of exposure to stress, fatigue or nerve demand.

Generally, testing with the ROFES device represents an easy method of dynamic control of the health status that is aimed at maintaining health by creating the necessary conditions for a good physical, mental and social state.

The contradictions in the use of the ROFES device:

a. *The electrical cardiostimulator (pacemaker).*

b. *Pregnant women.* Since there was no research conducted to prove that the ROFES device is safe for pregnant women, for safety purposes, we recommend you avoid testing it on pregnant women.

c. *Active oncologic diseases.* In this case, if the patient is undergoing treatment, we shall not use this test. The research on the influence of the ROFES device on tumours has not yet been completed; therefore, we prefer to be cautious.

d. *The absence of the left arm.*

The entire testing algorithm was created for the PC-7 point of the left wrist. If a patient is missing his/her left arm, testing is impossible. If the left arm presents lesions, this does not represent an obstacle for testing.

c. Testing

The active electrode of the device will be placed above the active biological point PC-7 (named “Daling” according to TCM) (Fig.7) after the area has been wiped using a wet tissue. Then, the measuring will begin and the results will be available within 3 minutes. Said results will be presented in a table (Fig. 8) that can be printed or sent via email.



FIG. 6. Rofes device-Test procedure

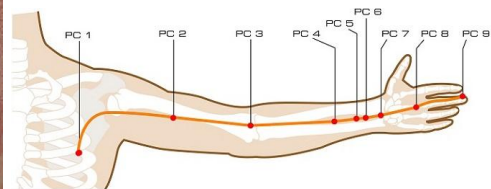


FIG. 7. Daling (TCM) –PC-7 biological point

The advantages of the Rofes test (pre-clinical test of the organ and system functioning; test of the psycho-emotional state)

- *Fast:* lasts for only 3 minutes. The testing frequency should not exceed once every 20 minutes.

- *Easy:* only one point on the wrist is being tested. It does not require special preparation or training. The ROFES devices only needs to be connected to a computer or a tablet and then you press start.

Important: the date of birth and sex must be correctly filled in. The precision of the test depends on this data because the software compares the electrical point indicators of the patient to the standard database for the same age and sex. If the sex is filled in incorrectly, the results will be absurd. If the date of birth is filled in incorrectly, the results will be false.

The device tests the following: The general level of health, the psycho-emotional state, the functioning of the 17 organs and systems, the level of stress/fatigue/neurosis/the heart and the blood vessels/the immune system/the spine (Fig. 8).

Program Rofes 2.0.1.1 Account nik nik (Male , 52 Years) Test 4/1/2017 9:13:17 PM			
General functional state:		Thyroid	5 3
General functional state		Adrenals	4 5
High level of health. High energy resource, providing the mechanisms of body self-regulation.		Kidneys	4 4
		Bladder	5 4
		Prostate	5 4
		Functional state - FS	
		Energetic resource - RR	
Organs and systems:		Psycho-emotional characteristics:	
Immune system	5 4	Stressful condition	2
Cardiovascular system	5 4	Signs of fatigue / Internal emotional strain	4
Cervical spine	5 4	Signs of nervousness, irritability	4
Thoracic spine	5 5	Attention! This rofogram shows the state of your organism only at present moment. Deviations from the norm on the rofogram may be caused by physical and emotional load, stress, influence of environment or food. In order to get the results, which are free from the influence of external factors, it is advisable to conduct not less than 5 tests during a week (in a relaxed atmosphere, better in the morning before breakfast, shower and medications). The results tendency should then be analysed.	
Lumbar spine	4 4	Software developer INFERUM, LLC www.inferum.ru	
Bronchi	5 5		
Lungs	5 4		
Liver	5 5		
Stomach	5 4		
Colon	4 4		
Pancreas	4 4		

FIG. 8. The synoptic presentation table of the Rofes parameters

The interpretation of the results is also simple: the higher the values (equal to or near 5) the better adapted the body and the better equipped to deal with environmental challenges.

6. DISCUSSIONS

The authors aim to perform several sets of measurements under various conditions. The first set of measurements will be performed in laboratory conditions, using a flight simulator. The main hypothesis is that even though the flight simulator (Fig. 9) enables the programming of extremely difficult conditions for the pilot, he/she will not perceive them as stressful.

For this reason, a second set of measurements is scheduled. As far as possible, the same subjects will be used for testing, but in this case, the measurements will be performed in conditions that are closer to reality, by using a ultralight aircraft. (Fig. 10)

On April 29, 2017, one of the authors took a first short experimental flight (22 minutes), as passenger aboard a two-passenger ultralight trike that took off and landed on Ilfoveni aerodrome, in Dambovita County. During this flight (Fig.10) no measurements were taken, the aim was only to assess the available space for the measuring devices of physiological parameters. The flight conditions were of low difficulty – light wind 8-10 km/h, with brief gusts over 250 m altitude, approx. 18°C temperature, partially clouded sky and rain here and there.



FIG. 9. Flight simulator



FIG.10. pilot accompanied by the take-off and landing assistant

The conclusion of this flight was that the measurements will be performed on the ground, before taking off and after landing due to the very limited space on board that does not allow placing and operating measuring equipment. Only small devices can be used to monitor the pulse and cardiac rhythm.

7. CONCLUSIONS

The parameter changes that can be highlighted using the devices described herein enable the assessment of the evolution of the level of anxiety (stress).[21] After the analysis and interpretation of a large number of measurements performed under various conditions we will be able to obtain some threshold values for the level of anxiety. Any value that exceeds the threshold would mean that any strenuous activity in the field of aviation, such as piloting or flight controlling, should be avoided (at least on that day). These tests are even more important, since according to Psychiatrist A. Manolea, M.D. [1] many of the people involved in these activities might not even be aware of or might ignore their own level of stress.

The aim of this research is to increase the level of safety of the people involved in the field of aviation.[22]

REFERENCES

- [1] A. Manolea, *Condiționarea psihosomatică, psihodiagnoza și intervenție psihoterapeutică folosind stările modificate de conștiință [Psychosomatic conditioning, psychodiagnosis and psychotherapeutic intervention using modified consciousness states]*, Abstract thesis. Bucuresti 2012, Universitatea Bucuresti, Facultatea de psihologie si stiintele Educatiei
- [2] adevarul.ro/life-style/stil-de-viata/Serban-capitan-oricat-pilota-stresul-zborului-inca-exista-1_50ace6747c42d5a6638b7bd3/index.html, accessed on 4 May 2017;
- [3] K. Korotkov, *Human Energy Field. Study with GDV Bioelectronography*, 2002
- [4] C. Moldovan, <http://www.clinicaqi.ro/media/uploads/3D-NLS-DIACOM-Metatron.pdf>, accessed on 04 May 2017
- [5] W.Tiller, *Energy fields and the human body*, in White, J. (ed.), *Frontiers of Consciousness. The Meeting Ground between Inner and Outer Reality*, New York, Julian Press, 229-242
- [6] V.M Inyushin, *Bioplasma geoplasma-Și structura psiho-energetică a omului [Bioplasma, geoplasma and the psychoenergetic structure of the human body]* - http://www.newhumanity.ru/nauchnaya_mysl/inushin/inushin_bioplazma_struktury.htm accessed on 04 May 2017
- [7] C. Guja, *Aurele Corpurilor. Interfețe cu Cosmosul [Body aureoles. Interfaces with the Cosmos.]*, vol. I, Editura Enciclopedică, București, 1993, ISBN 973-45-0050-3
- [8] C. Guja, *Aurele Corpurilor. Interfețe cu Cosmosul [Body aureoles. Interfaces with the Cosmos.]*, vol II, Editura Polirom, 2000, ISBN 973-683-394-1, ISBN 973-683-404-2
- [9] C. Guja, *Aura Corpului Uman. Introducere în antropologia individului [Human body aureole. Introduction into the anthropology of the individual]*, Ed. Polirom, Iași, 2000, ISBN 973-683-394-1, ISBN 973-683-405-0
- [10] C. Korotkov, C., E. JAKOVLEVA, *Electrophotonic Analysis in medicine*, 2013
- [11] C. Korotkov, PHD, PROF., *Energy of Consciousness*, Lexington, NY, 2013
- [12] S. Gibson, S., *The effect of music and focused meditation on the human energy field as measured by the gas discharge visualisation (GDV) technique and profile of mood states*, Thesis of a dissertation submitted to the faculty of HOLOS university graduate seminary, April 2002
- [13] N. Cowan M., B.Nunley, *The Effects of Crystal Bowl Toning on the Chakras as Measured by the Gas Discharge Visualization Technique (GDV) and Scores on the Profile of Mood States Scale*, *Subtle Energies and Energy Medicine*. V.16, N 9, pp 37-40, 2005
- [14] P. Dobson, E. O’Keffe., *Investigations into Stress and it’s Management using the Gas Discharge Visualisation Technique*, *International J of Alternative and Complementary Medicine*. June 2000

- [15] I. Mohîrță, *Psihologia Sonoluminică [Sensation and perception psychology]*, Ed. Ars Docendi, 2011, ISBN978-973-558-599-0
- [16] I. Curta, et al., *Summary of the methods used to lower the anxiety parameter-stress index (T) – according to the measurements made with the GDV Camera*, Second International Conference on Radiation and Dosimetry in Various Fields of Research RAD 2014, Conference, pag 81, Book of abstracts, <http://www.rad2014.elfak.rs/program.php>
- [17] *** *The BioWell User Manual*, http://biowell.eu/assets/files/biowell_user_manual_1.pdf
- [18] *** *Operation and Service Instruction manual*, http://carlaine.com/assets/download/rofes/manual_en.pdf
- [19] F.I. Dumitrescu, D. Constantin, *Acupunctură științifică modernă [Modern scientific acupuncture]*, Editura Junimea, Iași, 1977
- [20] C. Ionescu-Târgoviște, *Acupunctura și bioenergetica umană [Human acupuncture and bioenergy]*, Ed Sport-Turism, 1986
- [21] <http://www.csid.ro/boli-afectiuni/psihiatrice/stresul-definitie-cauze-factori-de-stres-si-metode-de-combatere-13763206/>
- [22] M. Schwarz, et al., *Safety culture. Resilient Behaviour and Stress in Air traffic Management*, Aviation Psychology and Applied Human Factors (2016), 6, pp. 12-23. DOI: 10.1027/2192-0923/a000091. © 2016 Hogrefe Publishing

PSYCHOLOGICAL PROTECTION OF TROOPS WITHIN THE NEW CONTEXT OF THE MILITARY NORMATIVITY

Dumitru DINU

„Henri Coanda” Air Force Academy, Brasov, Romania

DOI: 10.19062/2247-3173.2017.19.1.11

Abstract: *This study deals with the issue of psychological protection, in a comparative way, in terms of operational doctrines of forces categories, fighting manuals and doctrines of force protection, highlighting a number of discrepancies and inconsistencies in the analyzed subject treatment, and concluding, by useful proposals to structures responsible in this field.*

Keywords: *psychological warfare, psychological protection, counteracting psychological influences, mental stability, moral*

1. INTRODUCTION

Nowadays, we speak more and more about a new kind of war, characterized by asymmetries in the areas of objectives, methods and means used by the opponents, about the hybrid warfare, a compilation of classic and unconventional at all levels of military action. Moreover, the vast majority of armed conflicts in the past 50 years revealed a mixture of conventional and unconventional symmetry and asymmetry, the end of confrontations usually resulting in producing significant changes politically, economically and socially, but also in a record of deaths and awfully injured people, physically and mentally.

On the other hand, the contemporary military conflict, the modern military action involves engaging in specific confrontations of a new type of soldier, intelligent, physically and mentally strong, balanced, mobile, flexible in thinking, able to make decisions in a short time and in extreme situations, good manager of cyberspace, of database and of modern systems of decisions expertise, able to act in isolation, under any circumstances, in a hostile, disproportionate and hybrid environment.

The Romanian military specialists in the areas of doctrine and instruction consider that, in order to be fit to combat and to test the ability to combat, the individual / soldier must have at least three qualities, as the result of carrying out the educational process:

- ***the technical and tactical training***, as the consequence of knowledge specific skills training and development and of the use of the provided equipment, in accordance with technical and tactical military operation norms, established by the military normatively;

- ***physical training***, defined as education and physical and sports culture, based on a biological, anatomical and physiological structure, intended to provide the psychophysical training support to the fighter, necessary to his development and improving his general motor and fighting capacity;

- ***psychological training***, based on a clinically normal mental, enabling the individual, from the psycho-moral and behavioral perspective, to act effectively in the tactical field; it is expressed self-confidence, confidence in commanders, in the armament and combat equipment, in the degree of the sub-unit cohesion, by the actional motivation level and by his personal satisfaction.

The three dimensions, related synergistically, confer, par excellence to the military, the fighter status. Fluctuations concerning the power and the prevailing trend of one or of another within the synergistic model, will be determined by the reality of the battlefield, but it is important that the result of their dynamics to provide to the fighter, the psycho-behavioral and actional harmony, necessary to perform his mission.

A closer research, based on experience gained in studying the phenomenon "war", demonstrates with the power of evidence, that the psychophysical dyad still is the most vulnerable and it presents amplitude oscillations of a high dramatism. Exactly this aspect determines with necessity the general military training orientation, in a significant part, in shaping and developing specific psychological and physical characteristics, allowing the military to face the current danger on the battlefield.

Studying the phenomenon of "war", Clausewitz noted that there were "*four components that constitute the atmosphere in which the war moves - danger, physical exertion, uncertainty and chance*" [1], and the General Marshall in his book entitled suggestively "Soldiers in fire" noted that "*We do not want to admit that war means essentially dead, although it is the simplest possible truth.*"

2. PREMISES OF THE MILITARY PSYCHOLOGICAL PROTECTION

Considering some "surprise" aspects occurred in recent wars (Arab-Israeli wars, in the Malvinas / Falkland wars, the conflicts in the Persian Gulf, armed conflicts in the former Yugoslavia, the war in Afghanistan, Syria, etc.) as well as the polymorphic manifestations of the international terrorism, the military experts in psycho-sociological orientation approached more carefully the deconstructed factors of the individuals psycho-moral stability, taking into account, however, a number of findings such as:

The first is that "front line" has faded, that "*the confrontation environment has grown dramatically*" [2], that the war has been "widespread" and has taken in its mechanism not only armies but also civilians of the countries in conflict.

The second finding points out the technology used, the sophisticated weaponry, the ammunition destructive power, the accuracy of shots based on laser and infrared equipment, the graphite and unfortified uranium bombs etc., which have a non-discriminatory effect upon the combatants and non-combatants or civilians.

A final finding presented could be that in perspective, a new war is prefigured, generically called the "special war". This would include all forms of non-classical, non-typical (atypical) training and warfare in which, without considering this presentation as an exhaustive one, there can be listed the following: the psychological warfare, the information warfare, the holotropic war etc. Their general feature is the "humanism", based on "non-lethal" (soft-kill) component, which would reduce the aberrant "consumption" of people, equipment, weapons and materials, while facilitating political and military objectives through "*economical*" logistics [3].

These assessments have raised new problems to the military specialists, who most of them, advocate for the implementation of a national psychological preparation of the population against any aggression, but without falling into the trap of so-called "nationalist hysteria". A negative presentation of our future war could give us a terrific image, presented not without some truth, only by the science-fiction literature. Thus, after the first days of battle, it may be noticed that the military would wander erratically, would be overwhelmed by the massive traffic jams, by destructions and fires on a large scale, would be dehumanized by the suffering and troubles that would partake;

few people would be able to withstand such an intense stress; physical casualties, but mainly mental casualties, especially where there are no specialized services for medical, psychological and social assistance, can reach very high levels.

Such a possible hallucinating array has generated the idea of establishing, since peacetime, a troops' psychological preparation system for combat, starting from the principle that the army is a tool designed exclusively to wage war and preparing fighters must be made during those periods and under those conditions when the "war" takes place by other means, less violent physically and / or more subtle.

The military's psycho-moral preparation must take into account that fighting will be in a permanent dynamic, continuous and of a high-intensity, with high-index mobility and fluidity that will involve massive destructions and a very high mortality rate. In the above-mentioned context, the overestimation by the new "hi-tech", which are growing rapidly and asymptotically toward the "artificial intelligence" expected by cybernetics, genetic engineering and cognitive psychology adds to the existential anguish new barriers that the man must overcome in his perpetual adaptation. Trying to approach the concept of psychological protection, it is necessary to start from the motives (premises) that require protection, from the causes circumscribed within the psychological aggression area, with the two elements of its functional components:

- **stimuli** (physical and mental stress, stress factors, operational stress), specific to the action environment / confrontation;
- **messages** prepared and submitted by the opponent, usually through the media and other dissemination channels (internet, social networking, correspondence).

3. MILITARY'S PSYCHOLOGICAL PROTECTION UNDER THE NEW REGULATORY CONTEXT

The transition to the new century and millennium has brought profound changes in the Romanian Army, not only in terms of achieving the political-military objectives of Romania but also with regard to developing doctrines specific to the military system, changes required by the adhering process to NATO, as well as the further participation of Romanian military detachments to the actions of the Multinational Forces in the operation theaters.

This is the period that takes shape and the concept of psychological operations / actions (PSYOPS) gets increased amplitude, almost eclipsing it, in terms of their promotion, over the psychological protection, even if their field of expression should intersect in a very little manner.

Remaining in the same period and studying the three operational doctrines of the categories of force, we find that only two of them insert psychological protection among the types of actions insurance schemes and of forces protection, while the Operational Doctrine of the Army (FT-1) substitutes it by "*counteracting the effects of psychological actions of the enemy*". And, in order to apprehend how much commonality of thinking and, at the same time, how much diversity of approaches there are in this area, I will try to get your attention to a few details of the previously mentioned doctrines, conducted by responsible operations structures, within the period of 2004-2016.

The theorist specialists of the Navy argue that **psychological protection** is represented by a set of measures and actions of real complexity, which are organized and conducted in a unitary to "*develop mental strength and stability of troops; maintaining a high moral thereof; identifying and countering psychological pressures that affect combat capability; recovering and restoring forces; reducing potential psychological , weakening the willingness to combat and the enemy's capacity of resistance* . "[4].

In other words, it is the goal of the troops' protection process, psychically speaking, aiming the own military, fighters / combatants, a process which should be implemented within the military structures according to the commander's *concept*, in accordance with that one specified by the upper echelon, with support of the staff of the unit, under psychological and medical *counseling, regardless* of the period in which action is taken or the military activities.

To achieve timely and efficiently the psychological protection of the military, the Navy recommended consistently, both in 2006 and also in 2012, a rather wide range of actionable approaches to be taken by commanders and responsible structures in the domain, among which we can mention :

- increasing the psycho-physical strength and the process and mental products stability of fighters, in order to mitigate and defeat the adverse effects of stressful factors;
- developing and building confidence of the troops in their own ability to fight successfully against any opponent;
- developing the military capacity to overcome various forms of physical and mental stress, to make correct decisions under pressure, to adapt to the military actions that follow;
- training and developing to the combatants their capability to apprehend and to resist to the hostile psychological and propaganda influence, deliberately carried out, and also to unmask them appropriately and counteract them;
- developing to the commanders the skills to lead men in battle, to strengthen their morale and to achieve combat teams cohesion.

The military Air Force theorists have approached the *psychological protection* both in 2007 and later in 2016 in the context of the reaction against the enemy's non-lethal actions, quite briefly, in a phrase where there are no essential deviations from the definition addressed by the Navy. They stated that it "*represents a set of measures and actions undertaken within the Air Force into a unified concept, for the development of the troops' moral resistance and stability, maintaining their high morale, identifying and counteracting the mental pressure that affect the combat capability, the forces' recovery and restoration, reducing the psychological potential, weakening their will to struggle and the enemy's capacity of resilience*".[5]

Within the same categories of forces, the concept is approached broader, fairer and more realistic way, in textbooks for use in the combat of various military structures, particularly fire / combative structures, where the psychological protection is defined as a set of measures and actions "*carried out in order to develop the troops' psychological resistance, to bring up their moral, to identify and to counteract the psychological pressures and to eliminate the stress effects*" [6].

The psychological protection is governed directly by the commandant of the big unit / units with the psychologist's support and general staff's support, usually during the warfare preparations, between the enemy's attacks and it insures: consolidation of the fighters' trust in their own forces, in commanders and in the fighting technique; learning and obeying the military values and norms in order to maintain vigilance, the spirit of order and discipline; preventing and combating state of fear, insecurity and panic; development of military strength and mental stability to cope with the modern battle space and with the psychological influence from the opponent.

Analyzing the concept of "**Counteraction of the enemy's psychological action effects**" approached by the Operational Doctrine of the Army (FT-1) – edition of 2004, compared to the *psychological protection* previously described, we can make more precisions and speculations, at the same.

Starting from the definition given to the **counteracting** as representing "*the entire set of measures and activities meant to maintain or alter perceptions, attitudes and behaviors of individuals or human groups in order to achieve the intended goals as well as to prevent the use of this kind of actions by the enemy. This involves measures, techniques and procedures initiated and applied in a unitary conception to protect their own forces and population in the area of the operation against hostile messages or to reduce their impact*, it can be noticed some conceptual slippage toward the problem of psychological actions / operations, but also their expansion to multiple recipients, such as "population in the areas of the military actions".

The same aspect is also maintained when formulating the missions of counteracting the effects of enemy's psychological operations, respectively "*maintaining the stability of opinions, feelings, attitudes and behavior of the military personnel and civilians, so that the accomplishment of the objectives should not be affected; the rejection and neutralization of enemy's propaganda and maintaining a predominantly offensive-preventive character of the own counter-propaganda activity; strengthening the morale, the confidence of the military personnel and the public opinion in the ability of our forces capability to defeat; undermining the favorable image, real or fictitious, promoted by the enemy's propaganda about their own potential*" [7].

The missions established are fulfilled by preparatory and preventive actions and counteractions and the process of counteraction the effects of the enemy's psychological actions is expected to be achieved through: mental training of staff; protection against the enemy's psychological actions influences; its psychological influence; to ensure psychological support to the stability and assistance operations.

Otherwise, these are part of the forms of achieving troops' psychological protection, and the wording "**counteract the opponent's psychological influence**" [8], identified in several specialty papers, appears to be the result of the conceptual mixing between **counteracting the effects of the enemy's psychological actions and the protection against the enemy's psychological actions influences**.

The creators / authors of the combat textbooks of various military structures within the Army Forces, published after 2012, provoked even more violent controversy in the thinking of those destined to achieve the actions insurance and the troops' protection, whereas even if they took the doctrine provisions concerning the definition, the purpose and the mission of the counteracting of the enemy's effects of psychological actions, they also supplement the theoretical-action approach with objectives of psychological protection of the military, namely: "*the development of psychical resistance of the military at the action of disturbing factors in struggle, strengthen their confidence in their own forces, in commanders and weaponry; preventing and fighting, among their own forces, against psycho-moral deterrence, states of fear... and panic; limitation and annihilation of the effects of influencing actions, taken by the enemy; psychological recovery and rebuilding troops' morale, affected psychically; reducing the psychological potential, undermining the will of struggle and resilience of the enemy*" [9].

In a closer context, studying the provisions of the Manual for Combat of the Mixed Artillery Regiment, the nebula becomes greater, on one hand as a result of considering "psychological operations" as a form of actions insurance and of troops' protection, not as a force multiplier in operation and, on the other hand, that they have the same goals and missions as counteracting the effects of enemy's psychological actions influence, stipulated in other use of forces manuals.

This type of inconsistency within the theoretical approaches extends also in treating the general area of operations insurance and force protection, especially after the emergence of the doctrinal provisions on "force protection", taken, nearly identically, from to regulations with the same topic of the American army. But, as always, we forget that we are not Americans and that we cannot compare the Romanian army to the US army.

And thus, in the draft of the Doctrine for operations of the Army, Chapter concerning the field that we mentioned above does not appear anymore and the concept of "force protection" is, in a great measure, an approach in a new vision regarding the operational efficiency issues, in order to achieve in an optimum way, the combat missions, taking into account the threats and risks generated by enemy's actions.

We also notice that, even if the psychological protection is not listed as embodiment of the force protection, within the fields and the fundamental elements of passive nature, we rediscover those proactive measures that are intended to identify the risks and to protect the military forces of all operational and psychological consequences resulting from the use of various types of weapons with high lethality, and within the recovery, those necessary to restore the essential operational capabilities which permit further task achievement.

4. CONCLUSIONS AND SUGGESTIONS

At the end, we consider that the psychological protection should constitute, for all forces, one of the forms of operations insurance and of troops' protection, whose definition shall be in conformity with the Operational Doctrines of the Air Force and the Navy, and the action measures for its achievement, taken into consideration by the commanders, shall be in conformity with the specificity of each category of forces/big units/units. At the same time, it should be considered as one of the embodiments of achieving the force protection, as a dimension / component of medical protection.

REFERENCES

- [1] Carl von Clausewitz, *About War*, Editura Militară, București, 1982
- [2] Mihail Orzeață, *Continuous War*, Editura Militară, București, 2011
- [3] Alvin și Heidi Toffler, *War and Antiwar*, Editura Antet, București, 1995
- [4] *** *Operations Doctrine Operațiilor of the Navy*, București, 2006 și 2012
- [5] *** *Operations Doctrine of the Air Force*, București, 2007 și 2016
- [6] *** *Combat Manual of Surface-to-Air Missiles Brigade*, București, 2014
- [7] *** *Operations Doctrine of the Army*, București, 2004
- [8] *** *Psychological Actions beyond Myth and Legend*, Editura CTMI, București, 2000
- [9] *** F.T. /V.M. – 2, *Combat Manual for the Mountain Huntsmen Batallion*, București, 2014

DESIGN AND ANALYSIS METHODS FOR UAV ROTOR BLADES

Alexandru DUMITRACHE*, Mihai-Victor PRICOP**, Mihai-Leonida NICULESCU**, Marius-Gabriel COJOCARU**, Tudor IONESCU***

*Institute of Mathematical Statistics and Applied Mathematics, Bucharest, Romania
(alexandru.dumitrache@ima.ro)

**National Institute for Aerospace Research “Elie Carafoli”, Bucharest,
Romania (pricop.victor@incas.ro, niculescu.mihai@incas.ro,
cojocaru.gabriel@incas.ro)

***Politehnica University of Bucharest, Romania (tudor.ionescu@acse.pub.ro)

DOI: 10.19062/2247-3173.2017.19.1.48

Abstract: A design method and analysis tool of an UAV propeller based on Blade Element Momentum Theory (BEMT) for low-Reynolds number flow is presented. BEMT is completed with 3D equilibrium- implementation, a post-stall model and swirl velocity considerations to improve the accuracy of the results. An open-source code, JBlade, based on BEMT is used to obtain performance curves in off-design cases for a given propeller. Finally, the results are analyzed for a UAV Hirrus propeller. This methodology can be used successfully in the preliminary design phase of an UAV propeller, whose data can then be used as input in an optimization method.

Keywords: combustion chamber, CFD, methane combustion, turbulent flow

1. INTRODUCTION

The propeller has several application areas, but the most spectacular application is its use as a propeller propulsion system, particularly for aircraft. It has been found that the use of propeller engines driving becoming more improved is not enough without the improved propeller efficiency, requiring theoretical and experimental studies [1], [2].

The procedure used in aerodynamic design of a propeller is essential to determine aerodynamic loads on the basis of which the required thrust and torque are then determined. The most important aerodynamic characteristics of the propeller, the efficiency and the power required are then obtained from the values of thrust and torque. Since these loads must be accurately determined for different operating conditions of the propeller, the choice of the calculation method is an important issue.



FIG. 1. Small UAV launch from an air-powered catapult.

In recent years more researches on unmanned aircraft (UAV) have been carried out, especially for those of small size, since they are less observable and they can be exploring in smaller spaces. In these conditions the study of suitable profiles of rotor blades used in propelling of these aircrafts. i.e. at low Reynolds numbers, has been imposed. Although UAV systems are composed of several elements apart from air vehicle, they are usually classified based on the capacity of air vehicle to perform the required tasks [3].

The development of advanced small or micro- UAVs is hampered by a number of technology gaps including: insufficient analysis methods for low Reynolds number aerodynamics, combined battery-motor-propeller propulsion, control effectiveness estimation, and weight estimation.

It is known that the main task during the introduction stage of aeroplane design is to determine the basic aeroplane performance. The thrust curve of the power plant is one of the input data, i.e., available thrust versus flight velocity. That means it is necessary to obtain this characteristics curve for a propelled aeroplane.

2. OVERVIEW ON THE AERODYNAMIC CALCULUS OF A PROPULSIVE PROPELLER

Depending on the design stage of the airplane (preliminary or final), the aerodynamic calculus of a propeller can be carried out using empirical methods, theoretical methods or a combination of those (the hybrid method).

Since the propeller plane is powered by a reference propeller, the propeller plane theory has been chosen as the basis of the theory propeller for UAVs. The speed of movement mentioned above must be sufficient to provide a lifting force on the UAV's wing, which is equal to the weight of the plane. The propulsion propeller can be defined as consisting of a number of blades which are identical and arranged radially, and equiangular, forming the rotor. By means of an engine, these blades are rotated around the axis of the impeller.

The thrust required to move an UAV is produced by one or more UAV propellers.

It is considered that any blade cross-section has the shape of an airfoil. By his movement through the fluid, on any element of the blade, the drag and lift forces are exerted.

The blade, like the profiles, executes a rotating motion with angular velocity Ω and a translatory speed V_∞ , the resultant motion velocity is the velocity W of the profile considered at rest air from the upstream infinity.

The design of an airplane propeller and a given engine has three phases:

1) the establishment of the basic kinematic parameters of the propeller (usually as basic kinematic parameters the flight speed and rotational speed of the propeller are selected);

2) the establishment of the basic geometric parameters of the propeller (as the basic geometric parameters of the propeller, the diameter and the number of blades are chosen);

3) the aerodynamic calculus that includes 2 stages [1], [4]-[6]:

- determination of the propeller geometry, i.e. the variation of chord, thickness, and the twisting of the blade depending on the radius, to obtain maximum efficiency for most important operation regime of the airplane (preliminary propeller design);

- determination of the aerodynamic characteristics of the propeller.

Usually this calculation requires several iterations to obtain required performance characteristics. In general, basic kinematic parameters of the propeller are imposed by the design theme, being specific to the aircraft to be equipped with the propeller and to engine have to spin it.

Rotational speed is determined by engine power and, once chosen, determines the size of the transmission which also realizes the link between engine and propeller. By knowing the operational conditions of the propeller (the flight speed, the engine characteristic, the rotational speed of the engine and of the propeller and the maximum weight at takeoff of the plane) one can solve the indirect problem for the basic geometric characteristics of the propeller (the second stage in sequence of the aerodynamic design of the propeller plane).

The most important parameter which occurs in the design of a propeller is the diameter. The diameter of the propeller depends on several factors: the required performance of the propeller in various operating conditions, the maximum blade tip speed (which affects performance and the noise levels of the propeller), the weight of the propeller, the distance from the ground to the propeller axis.

If neglecting the influence of the induced velocity, the blade tip speed is

$$W_{\max} = \sqrt{V_{\infty}^2 + (\pi ND)^2} \quad (1)$$

or dimensionless, Mach number, M :

$$M_{\max} = M_{\infty} \sqrt{1 + (C_P/C_T)^2} \quad (2)$$

Usually, taking into account the noise level, the permissible limit is $M_{\max} = 0.85-0.9$. However, even in operating conditions, using the Mach number, M_{\max} can be considered acceptable at values of 250-300 m/s, however, due to high noise levels the values are limited to 250 m/s.

The influence of the diameter on the propeller efficiency is determined based on the aerodynamic characteristics of the propeller. It is necessary to choose the cruise speed of the UAV corresponding to the calculation.

The number of blades is a very important parameter in the design process of a propeller. It is chosen according to the product of the blades and propeller total activity factor. In general, activity factor (AF) for a blade has values between 80 and 180.

$$AF_{propeller} = B \cdot AF_{blade} = B \cdot (10^5/16) \int_{TD}^1 \bar{c} \cdot \bar{r}^3 d\bar{r} \quad (3)$$

These methods belong to a class of indirect solving problems to determine the geometry of the rotor, i.e. the diameter and the number of blades of the propeller

After solving the indirect problem, solving the direct problem follows, reaching the third design stage of the propeller, namely calculus of the aerodynamic characteristics of the propeller.

Blade Element Momentum Theory (BEMT).

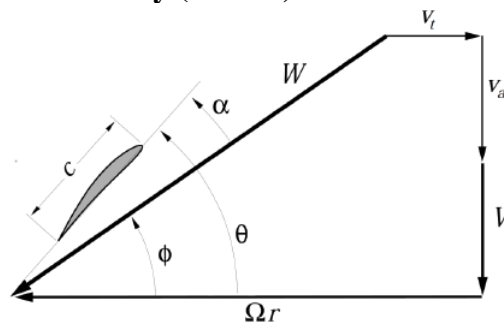


FIG. 2. Velocities at a blade element.

Combining the classical momentum theory, introduced by Froude [7] with the blade element theory enables a model of the performance of a propeller whose airfoil properties, size, and twist distribution are known. This analysis is based on the differential propeller thrust, dT , and torque, dQ , derived from momentum theory and blade element theory, being equivalent [1].

$$\left. \begin{aligned} C_a &= C_L \cos \phi - C_D \sin \phi \\ C_w &= C_L \sin \phi + C_D \cos \phi \end{aligned} \right\} F_x = \frac{1}{2} \rho W^2 c C_x \quad \left\{ \begin{aligned} T &= B \int_{R_{root}}^{R_{tip}} F_a dr \\ Q &= B \int_{R_{root}}^{R_{tip}} F_t r dr \end{aligned} \right. \quad (4)$$

To find ϕ and W , the iteration variables of the classical BEM for each blade element are the axial, a_a and the tangential induction factor, a_t :

$$a_a = (W_a - V)/V \quad a_t = (W_t - \Omega r)/\Omega r \quad (5)$$

These are derived from momentum theory as:

$$a_a = \left(\frac{\sigma C_a}{4k \sin^2 \phi - \sigma C_a} \right) \quad a_t = \left(\frac{\sigma C_t}{4k \sin \phi \cos \phi + \sigma C_t} \right) \quad (6)$$

where σ is the local rotor solidity ratio, $\sigma = cB/(2\pi r)$ and k is the Prandtl's correction factor that allows the blades 3D correction to the induced velocity field. The Prandtl's correction factor can be expressed simply by the following

$$k = \frac{2}{\pi} \arccos(e^{-f}). \quad (7)$$

The correction factor is used to modify the momentum segment of the BEM equations. Because for a given element, the local aerodynamics may be affected by both the tip- and hub-loss, the two correction factors are multiplied to create the total loss factor. In this case f can be expressed as:

$$f_{tip} = \frac{B}{2} \left(\frac{R-r}{r \sin \phi} \right); \quad f_{root} = \frac{B}{2} \left(\frac{r-R_{root}}{r \sin \phi} \right). \quad (8)$$

Including two-dimensional airfoil tables of lift and drag, $C_L = C_L(\alpha, Re)$ and $C_D = C_D(\alpha, Re)$ a set of equation is obtained that can be iteratively solved for the induced velocities and forces on each blade element.

Low Reynolds Airfoils. To design a propeller suitable for a UAV it is necessary, first, to know which is the size of UAV's, which is the mission to accomplished, and at what height is performed.

In the case of small UAVs, it is obvious that we are in the case of low Reynolds numbers, with some drawbacks from aerodynamics point of view. Flight at these Reynolds numbers is much less efficient than at higher Reynolds numbers and available power is a limiting technological factor at small scales. It is important to operate the airfoil at its maximum L/D operating point, but this requires operating close to the maximum steady-state lift coefficient.

We know that the most important to achieve a good performance propeller, its blade profiles must be analyzed and selected carefully.

There are now airfoils, studied (numerical or experimental) for various classes of flows at low Reynolds numbers, but not enough for small to micro UAVs.

Flow at low Reynolds numbers is dominated by viscosity, and as the Reynolds number is reduced, the effects of increasing boundary layer thickness become more pronounced.

A numerical experiment has been performed, using CFD (Fluent) [18], on a profile from known class – NACA, to obtain an airfoil polar, for a given Reynolds number (Table 1).

Leading edge separation is delayed in thin sections, with trailing edge separation delayed in thicker sections (Fig. 3). The results are higher attainable angles of attack and higher maximum steady-state lift coefficients.

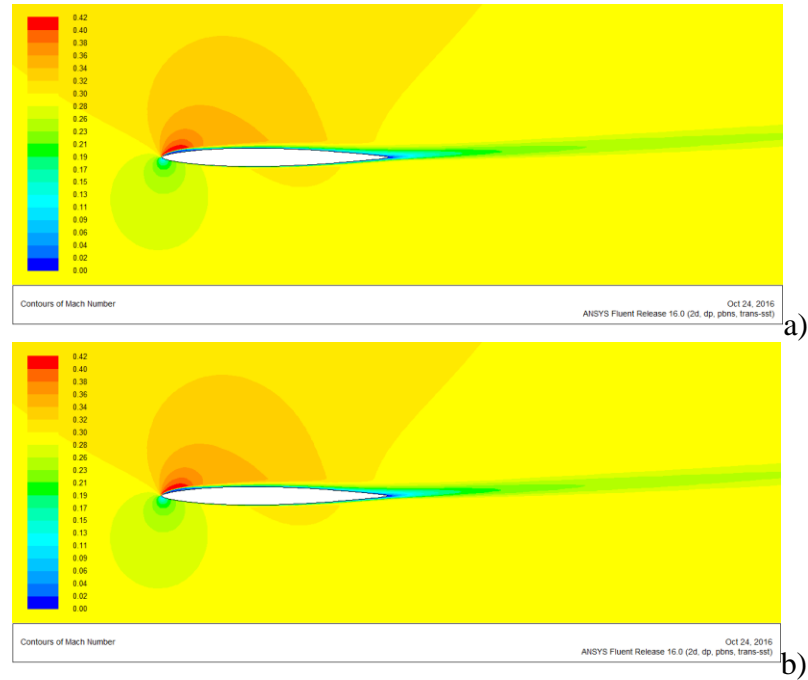


Fig. 3. Contours of Mach number for 4 deg (a) and 6 deg AOA (b) (Re = 80000)

Table 1 – Aerodynamic characteristics ($C_L(\alpha)$ and $C_d(\alpha)$) for NACA008 (Re = 80000)

alpha (deg)	C_L	C_d
0	0	1.36E-02
2	0.1125	1.54E-02
4	0.4269	2.24E-02
6	0.55	3.80E-02

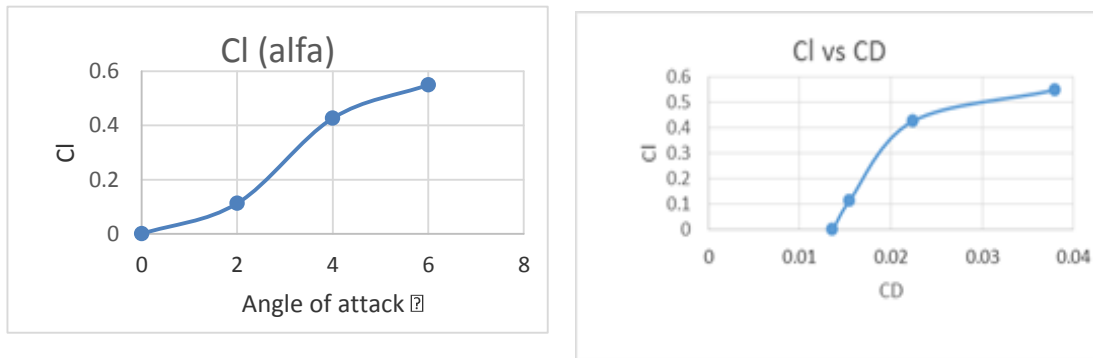


FIG. 4. $C_L(\alpha)$ and $C_L(C_D)$ for NACA008 at Re=80000. (CFD - Ansys FLUENT)

As can be seen in Fig. 4, aerodynamic characteristics (airfoil polars) for an airfoil of a blade may be obtained using computational methods CFD (such as Ansys Fluent), but they are expensive and not justified in a preliminary design stage.

An alternative, cheaper method to obtain an airfoil polars is using the XFLR5 [16]. XFLR5 is an analysis tool for airfoils, wings and planes operating at low Reynolds numbers. It includes:

1. XFOil's Direct and Inverse Analysis capabilities.
2. Wing design and analysis capabilities based on the Lifting Line Theory, on the Vortex Lattice Method, and on a 3D Panel Method.

It is known that the Reynolds number varies along the blade and it is therefore necessary to analyze its influence on the aerodynamic characteristics for an airfoil. Using XFOIL code this influence for NACA008 is obtained, with Reynolds number varying between 60000 and 100000 (Fig. 5).

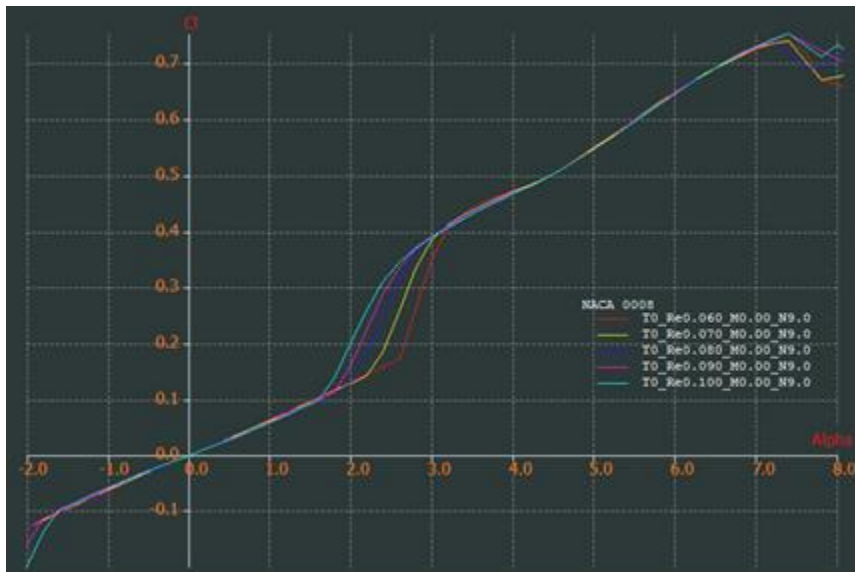


FIG. 5. Influence of Reynolds number on aerodynamic characteristics for NACA0008 ($60000 < Re < 100000$)

The effects of camber do not differ significantly from those at much higher Reynolds numbers, but the fact that the detailed geometry is still an effective driver of performance at such low Reynolds numbers is itself a useful conclusion (Fig. 6).

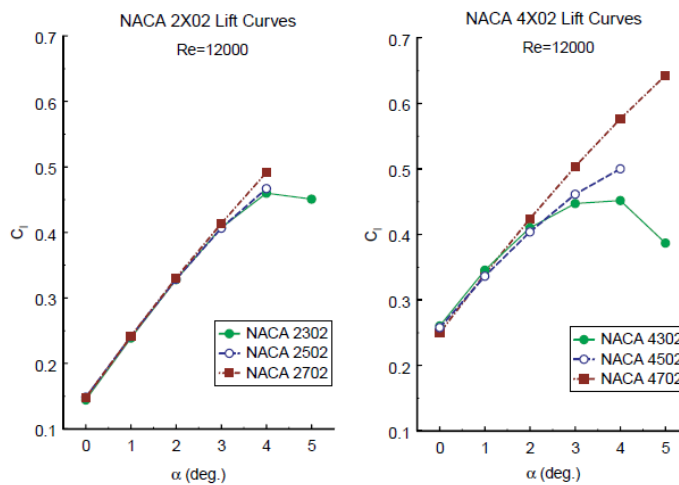


FIG. 6. Lift curves for 2% and 4% cambered NACA 4-digit airfoils at $Re=12000$.

It is possible to use an optimization method to obtain an airfoil with the optimum camber line and/or the thicknesses. The lack of experience at low Reynolds numbers makes optimizers an effective and important tool, not only for design, but also for enhancing our understanding of this flight regime. In the optimization design process, XFOIL can be employed for the calculation of the airfoil aerodynamic characteristics at low-speed and low Reynolds numbers, and estimate the chord-wise location of transition from laminar to turbulent flow. Thus, one can obtain an optimized version of an Eppler E387 airfoil, which already has a C_L/C_D ratio superior to other profiles, suitable for the design process of an UAV propeller blade [8].

Finally, wind-tunnel testing of low Reynolds number airfoils is, however, still needed to provide engineers with a necessary level of confidence required to make important engineering decisions.

BEMT is completed with 3D equilibrium- implementation, a post-stall model [9] and swirl velocity considerations to improve the accuracy of the results.

Swirl Velocity Considerations. The formulation, at this stage, incorporates only the inviscid induced tangential velocity, also referred to as inviscid swirl. In most conventional large scale, high Reynolds number applications, this is sufficient. For the small scale, very low Reynolds number applications of interest here, the viscous flow entrainment is an important consideration.

The thick wake regions generated by each blade produce a significant ‘viscous swirl’ effect. For the purpose of formulating the equations this term is incorporated by separating the tangential velocity into v_{inviscid} (v_i) and v_{viscous} (v_v). No viscous correction is applied to the vertical induced velocity. The viscous swirl is proportional to $\cos(\phi)$ while any viscous downwash term would be proportional to $\sin(\phi)$ and roughly an order of magnitude smaller than the swirl correction.

The viscous swirl is incorporated in all terms of the formulation except in the inviscid portion of the actuator ring equation for torque. The viscous losses are already accounted for in the viscous drag portion of that equation. These substitutions result in the final versions of the four basic relations:

Actuator Ring:

$$dT = 2k\rho u(u + U_\infty)(2\pi r)dr - B(C_d/C_l)(u + U_\infty)\rho\Gamma dr \quad (9)$$

$$dQ = 2k\rho v_i(u + U_\infty)(2\pi r)rdr - B(C_d/C_l)(\Omega r - v_v - v_i)\rho\Gamma rdr \quad (10)$$

where k is the Prandtl tip loss factor.

Blade Element:

$$dT = B\rho(\Omega r - v_v - v_i)\Gamma dr - B(C_d/C_l)(u + U_\infty)\rho\Gamma dr \quad (11)$$

$$dQ = B\rho(u + U_\infty)\Gamma rdr + B(C_d/C_l)(\Omega r - v_v - v_i)\rho\Gamma rdr \quad (12)$$

These four relations for thrust and torque (Eqs. 9 - 12) yield two equations for two unknowns (u , v_i) for each differential blade element. The other three unknown quantities (Γ , κ , and v_v) are treated as dependent functions of the input parameters: the lift distribution, rotor speed, ascent rate, number of blades, and chord distribution.

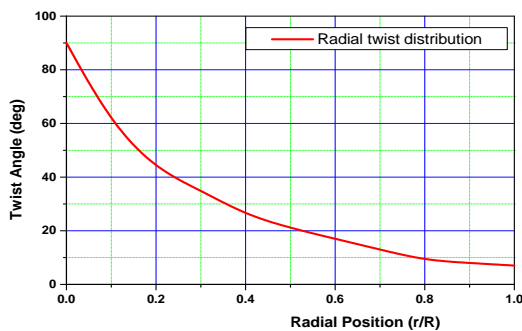
With values for u and v_i , the required blade pitch distribution, $\theta(r)$ may be found as:

$$\theta(r) = \alpha_{geo} + \text{atan}\left(\frac{U_\infty + u}{\Omega r - v_i - v_v}\right) \quad (13)$$

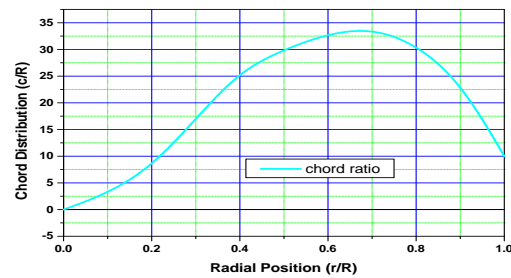
The determination of angle $\theta(r)$ distribution is the last step in what can be described as the design case (Table 2, Fig. 7 a,b).

Table 2 – Initial geometry of propeller

r/R	0.2	0.3	0.4	0.5	0.6	0.7	0.8	0.9	1.0		
Chord [mm]	8	17	26	30	33	34	31	24	10	D Diameter [mm]	380
θ [deg]	43	35	26	21	18	13	9	8	7	B Number of blades	3



a)



b)

FIG. 7. Radial twist (a) and chord (b) distribution of the blade

3. PERFORMANCE CHARACTERISTICS OF THE PROPELLER

3.1 Analysis Tools

As mentioned before, for the first phase of the propeller design it is adequate to use computational methods based on the blade element momentum theory. Currently, there exist few available open sources, such as JBLADE [11], JAVAPROP [12], QPROP [13], or XROTOR [14] that can be used for this purpose. To analyze the aerodynamic characteristics of the given geometric configuration of the UAV propeller, in this study, the open source JBLADE is used.

JBLADE is an open-source propeller design and analysis code written in programming language. The code is based on David Marten’s QBLADE [15] and André Deperrois’ XFLR5 [16].

The airfoil performance figures needed for the blades simulation come from QBLADE’s coupling with the open-source code XFOIL [17]. This integration, which is also being improved, allows for the fast design of custom airfoils and computation of their polars.

JBLADE uses the classical Blade Element Momentum (BEM) theory modified to account for the 3D flow equilibrium, already presented in the previous sections.

The code can estimate the performance curves of a given propeller design for off-design analysis. The software has a graphical interface making it easier to build and analyze the propeller simulations. The code structure is presented in Figure 8.

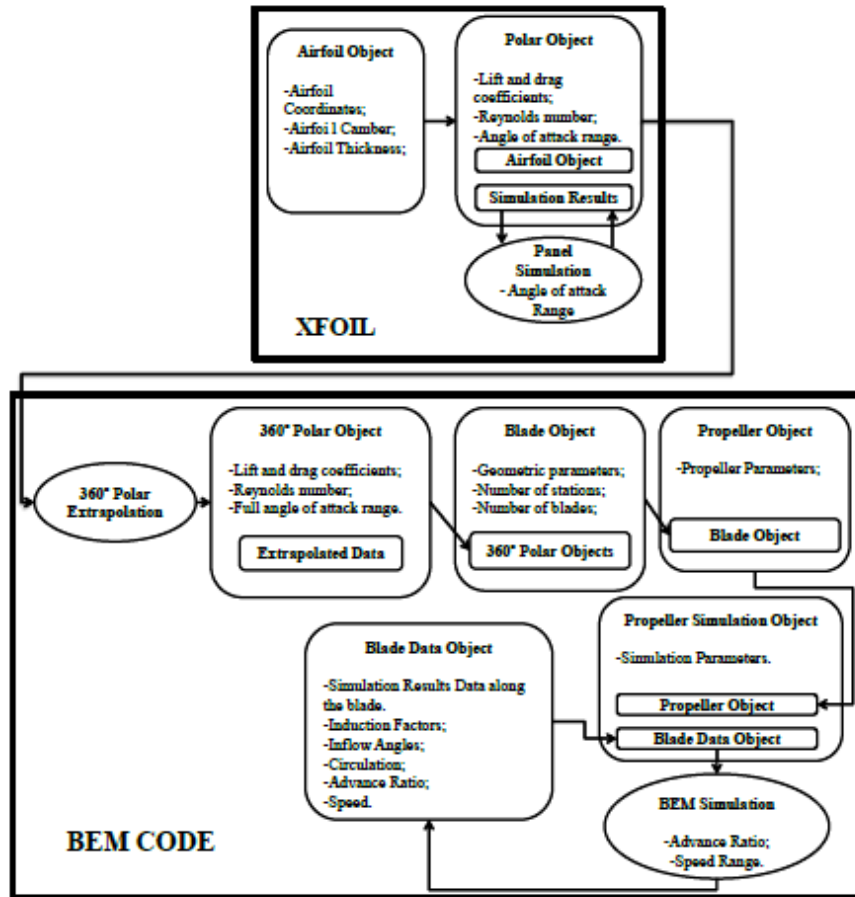


FIG. 8. JBLADE code structure [11]

Comparing with JAVAPROP and QPROP, JBLADE gives the best overall results.

3.2 Input Data

It has been considered that the investigated propeller propels a Hirus UAV, having the characteristics given in Fig. 9. It has been mentioned that when beginning to design a propeller one must know which is the motor that rotates it and what is the flight mission of the UAV.

Wingspan	2,35 m
Length	1,1 m
MTOW	7 kg
Maximum speed	130 km/h
Cruise speed	90 km/h
Radius of operation:	15 km
Ceiling height	3000 m
Propulsion	electric
Endurance	180 min
Launch system	<u>autorun</u>
Recovery system –	parachute
Maximum payload	0,9 kg




FIG. 9. Characteristics data of Hirus UAV

The blade geometry can be introduced as an arbitrary number of sections characterized by their radial position, chord, twist, length and airfoil coordinates. The propeller number of blades and hub radius must be specified as well.

The given geometry of the investigated propeller (Fig.10) consists of:

- Blade airfoil : Eppler 387 (it can be optimized in XFOIL)
- Blade radius: $R=0.190$ m
- Hub radius: $r_h=0.017$ m
- Number of blade: $B=3$
- Number of blade elements: $n_e=20$
- Chord distribution, $c(r)$: see Table 3
- Pitch distribution, $\theta(r)$: see Table 3

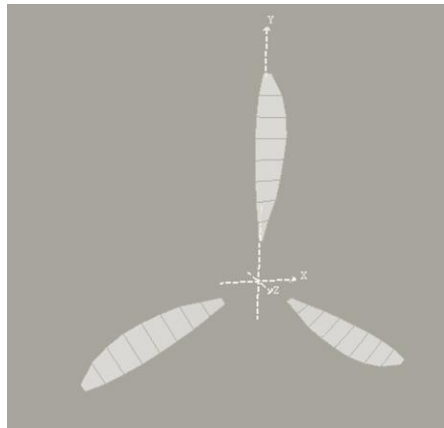
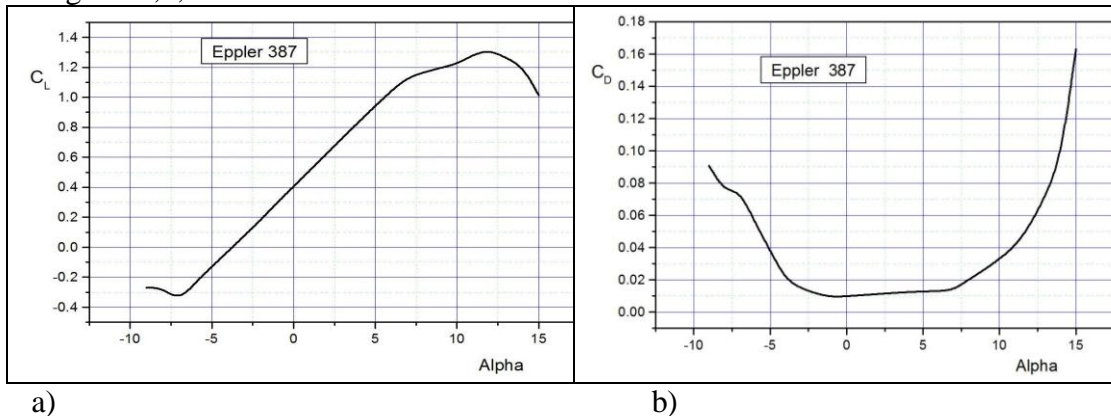


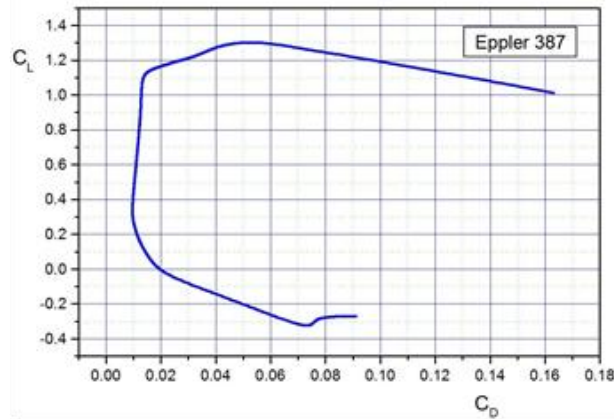
FIG. 10. The geometry of the 3-blade rotor

Additional input data:

- Altitude: $h = 200$ m
- Density: $\rho = 1.21$ kg/m³
- Cruise speed: $V = 25$ m/s
- Rotation speed: $N = 5500$ r.p.m.
 $\Omega = 576$ rad/s
 $n = 92$ r.p.s.

The Eppler 387 polar data, obtained in Sub-Module XFOIL, are presented graphically in Fig. 11 a,b,c.





c)

FIG. 11. Eppler 387 Polar : a) $C_L(\alpha)$, b) $C_D(\alpha)$ and c) $C_L(C_D)$, ($Re=200000$).

4. NUMERICAL RESULTS AND DISCUSSIONS

Given the advance ratio J , the geometric description of the propeller: the diameter D , the number of blades B , the pitch angle distribution $\theta(\bar{r})$, chord distribution $c(\bar{r})$, sectional aerodynamic characteristics, the lift (C_L) and drag (C_D) coefficients and another input data (section 3.2), using open source JBLADE, based on BEMT, off-design performance characteristics curves of this propeller have been obtained: power coefficient (Fig. 12), thrust coefficient (Fig. 13), propeller efficiency versus advance ratio (Fig. 14), as well as values for thrust, power or torque (Fig. 15).

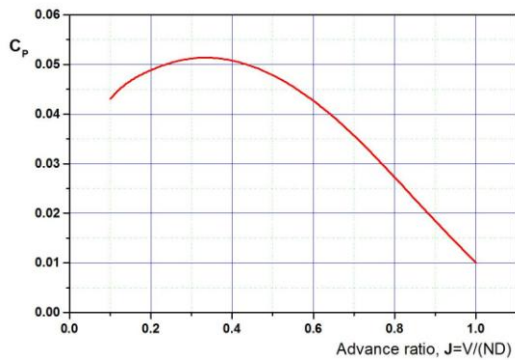


FIG. 12. Power coefficient versus advance ratio

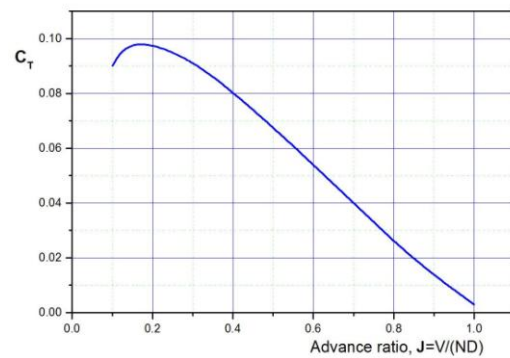


FIG. 13. Thrust coefficient versus advance ratio

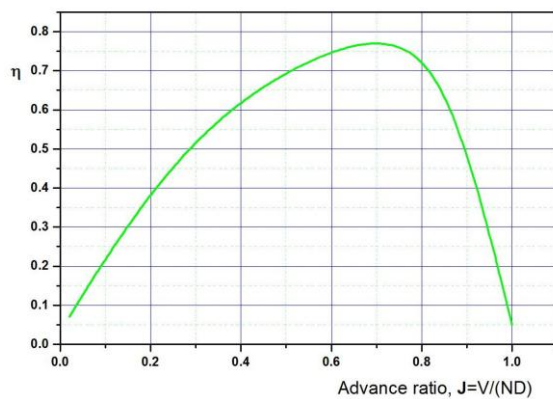


FIG. 14. Propeller efficiency versus advance ratio

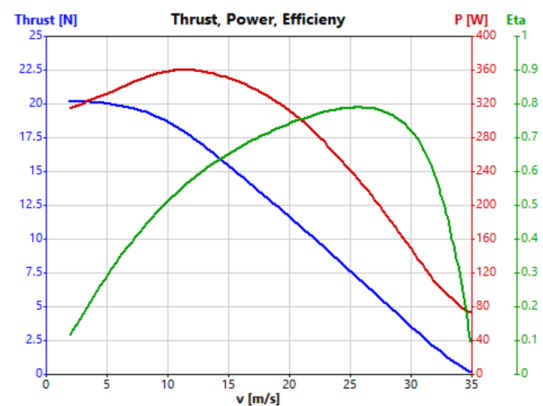


FIG. 15. Thrust, power and propeller efficiency versus cruise speed

There is no experimental data for this configuration of the propeller, but in previous calibration investigations and comparisons of different methods of computing it was noticed that JBLADE predicts closely the thrust coefficient. However, the power coefficient is under predicted at low advance ratios and slightly overestimated at higher final advance ratio values.

A first reason for these differences can be attributed to the airfoil's 360° angle of attack range airfoil polar obtained by extrapolation in XFOIL (3D rotational effect in the root portion of the blade is not enough quantified) and, furthermore, the constant axial induced velocity across the propeller disk is not seen to be the best assumption.

However, these results can be considered useful for a first design stage and can be considered as initial data in a subsequent optimization process. This is possible because it can be analyzed several configurations and regimes operating in a short time and at a reduced cost.

5. CONCLUSIONS

A method of preliminary design and analysis of propellers for small UAVs has been proposed, based on BEM theory. The design procedure has created the blade geometry in terms of the chord distribution along the radius as well as the distribution of the blade angle.

A case study on the profiles used for low Reynolds numbers has been carried out.

The used analysis method, less expensive, can be successfully used in a program to optimize the initial solution.

In the follow-up, other methods can be used to calculate more accurate solutions (CFDs) and experimental tests for the wind tunnel and even the flight tests will be required to ensure that the solution is optimal and the product may be passed into manufacturing.

REFERENCES

- [1] H. Dumitrescu, A. Georgescu, A. Dumitrache, V. Ceanga, J.S. Popovici, Gh. Ghita, B. Nicolescu, *Calculus of propellers, / (Calculul elicei)*, Romanian Academy Publishing House, Bucharest, 1990;
- [2] H. Dumitrache, V. Cardos, A. Dumitrache, *Aerodynamics for wind turbines / (Aerodinamica turbinelor de vânt)*, Romanian Academy Publishing House, Bucharest, 2001;
- [3] A. Altman, *A Conceptual Design Methodology for Low Speed High Altitude Long Endurance Unmanned Aerial Vehicles*, Thesis, Cranfield University, 2000;
- [4] Glauert, H., "Airplane propellers," *Aerodynamic theory*, Durand WF, ed., Berlin: 1935;
- [5] I.P. Tracy, *Propeller Design and Analysis for a Small, Autonomous UAV, Methodology for Low Speed High Altitude Long Endurance Unmanned Aerial Vehicles*, Thesis, Massachusetts Institute of Technology, 2011;
- [6] M.F. Shariff, *Propeller Aerodynamic Analysis and Design*, AERO2365 Thesis, RMIT University, 2007
- [7] W. M. J., Rankine, and R. E., Froude, *On the Mechanical Principles of the Action of the Propellers*, Trans Inst Naval Architects (British), 1889;
- [8] Ma, R., Zhong, B. & Liu, Optimization design study of low-Reynolds-number high-lift airfoils for the high-efficiency propeller of low-dynamic vehicles in stratosphere, P. Sci. China Technol. Sci., 53: 2792, 2010;
- [9] J. Corrigan, and J. Schillings, Empirical Model for Blade Stall Delay Due to Rotation, *American Helicopter Society Aeromechanics Specialists*, San Francisco: 1994;
- [10] J. L. Tangier, M. S. Selig, An evaluation of an empirical model for stall delay due to rotation for HAWTs. NREL/CP-440-23258, 1997;
- [11] Silvestre, M. A. R., Morgado, J. and Páscoa, J. C., JBLADE: a Propeller Design and Analysis Code, AIAA 2013-4220, 2013 International Powered Lift Conference, August 12-14, Los Angeles, CA., 2013;
- [12] M. Hepperle, JAVAPROP-User Guide , Last Revision January 2015;
- [13] M. Drela, *QPROP Formulation*, 2006;
- [14] M. Drela, XROTOR Propeller and Windmill Design/Analysis software. [Online]. Massachusetts Institute of Technology Home Page. Available: <http://web.mit.edu/drela/Public/web/xrotor> ;
- [15] D. Marten, and J. Wendler, *QBlade Guidelines v0.6*, Berlin: 2013;
- [16] A. Deperrois, *Analysis of Foils and Wings Operating at Low Reynolds Numbers - Guidelines for XFLR5 v6.03*, 2011;
- [17] Drela, M., XFOIL - An Analysis and Design System for Low Reynolds Number Airfoils, *Low Reynolds Number Aerodynamics*, T.J. Mueller, ed., Berlin: Springer-Velag, pp. 1–12, 1989;
- [18] *** Ansys Fluent Theory Guide.

NOISE REDUCTION IN MULTIPLE RFID SENSOR SYSTEMS USED IN AEROSPACE ENGINEERING

Andrei-Mihai LUCHIAN*, Mircea BOȘCOIANU**, Elena-Corina BOȘCOIANU***

*Transilvania University, Brașov, Romania

**„Henri Coanda” Air Force Academy, Brașov, Romania

***National Institute for Aerospace Research “Elie Carofoli”, Bucharest, Romania

DOI: 10.19062/2247-3173.2017.19.1.12

Abstract: *In the recent years, Radio Frequency Identification (RFID) has included smart tags which can monitor the various surroundings of an area. To create such a tag one must have an accurate measurement system. Sometimes, noisy signals are generated because of the surrounding changes. In the following paper we will propose an improved Kalman filter to obtain a better noise reduction and a more precise data acknowledgement. The Kalman filter performance stand in their noise covariance's which are called R and Q variables. These variables are found in the Kalman filter algorithm. Still, to obtain the best results we must choose the correct R and Q variables. More specifically, the main purpose of the paper is to propose an improved Kalman filter to locate an aircraft. The covariance is used only for a simple architecture and could be adjusted using neural networks. Using this method, we can obtain a more detailed database from the RFID tags. In a simulation, the proposed improved Kalman filter will show a more précised location of an aircraft compared to the old gain amplifier, due to the multitude of sensors which are being used. The performance of the Kalman filter will be demonstrated in a simulation program.*

1. INTRODUCTION

In the technology field of Radio Frequency Identification (RFID), an enormous variety of RFID sensors have emerged. RFID Sensor Labels are also known as RFID intelligent tags, which measure and calculate data. Intelligent RFID tags functions can be combined to form a single small-size device. These functions are: detection, computing and communication. The need for solutions regarding detection and localization is highlighted in legislative and regulatory demands. Here we have requirements for certain industries such as: dangerous goods transport, pharmaceuticals, explosives, etc. Low temperatures is a key requirement for pharmaceutical products and perishable items. [1]

Modern RFID systems become incredibly complex, thus intelligent system demands keep rising, as well as one-sensor RFID tag monitoring systems. Often they are unable to meet the new needs of society. Intelligent RFID tags combined with multiple sensors and container with various products can provide integrated services and information to managers and customers. This can be achieved by combining different sensor data from its detection materials.

For example, the information provided by temperature, humidity and oxygen sensors from an RFID tag attached can provide conditions for an item/product and protect customers. So far, an intelligent single sensor RFID tag provides the information using

multiple labels. Finally, by integrating multiple sensors into an RFID tag, we can imply a low-cost, high-power RFID system with an adequate radius [2].

Multiple sensors can be combined to form a smart RFID tag. These sensors: resistive, capacitive or inductive can extract important data which represents various states, such as: freshness or vitality. In a multi-sensor environment, RFID tags obtain data using one or more ports.

The Kalman filter has been widely applied to solve the problem of measuring system noise. The Kalman filter optimally estimates model states with known parameters. However, variations of measurement noise should be evaluated from empirical noise data, as it is difficult to obtain data in most cases. If the measurement noise statistics are unknown, the Kalman filter can not guarantee optimal resolution of the problem [3]. To solve this problem, we propose an adaptive filtering method based on the Kalman filter using neural networks.

2. SENSITIVE ENVIRONMENT

When system designers organize multi-sensor system, it is not sure that each sensor will work properly due to factors that disrupt their activity. These factors: noise and interference are caused by the measurement system in a multi-sensor environment. The RFID Multi-Sensor System is composed of a multi-electron system and a sensor board combined with sensors, as shown in Figure 1. The multi-electronics system is a RFID detection platform and is connected to a PC via a USB port to measure and compile data.

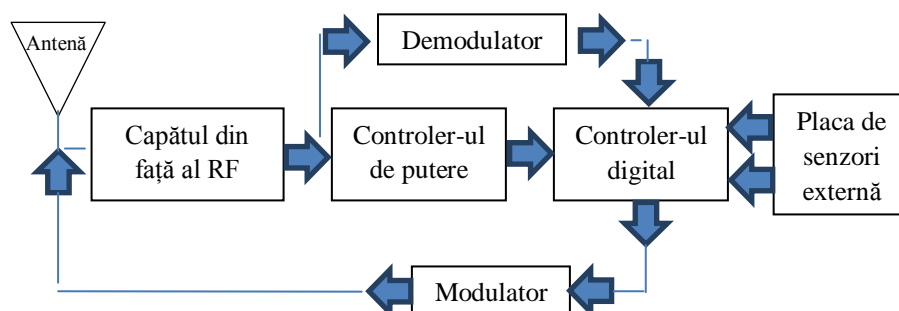


FIG. 1. Block diagram of the measurement system configuration

3. IMPROVEMENTS FOR KALMAN FILTERS

The Kalman filter requires accurate knowledge of all dynamic processes and noise, even when the noise processes are zero, meaning there is white noise. If the theoretical and the actual behavior do not match, there will be a divergence problem. When the error covariance is calculated using data from the current measurement error, we will obtain satisfactory results, without divergence. Kalman filter noise acts as a bandwidth controller and modulates Kalman gain.

The abnormal choice of noise covariance is one of the most important factors that make the difference between Kalman filters. The objective of this method is to estimate the noise covariance. Thus, by using neural networks we will try to prevent Kalman filter divergence.

The variables w_k and v_k represent, respectively, the process and the noise measurement. They are supposed to be independent of each other, and with normal probability distributions [4,5]:

$$x_{k+1} = Ax_k + Bu_k + w_k \quad (1)$$

$$z_k = Hx_k + v_k \quad (2)$$

Matrix A in an differential equation (1) relates the state to the previous $k-1$ state with the state at the current k stage. Matrix B makes reference to the optional control input, while matrix H correlates the state with the z_k in the measurement equation (2):

$$P(w) \sim N(0, Q) \quad (3)$$

$$P(v) \sim N(0, R) \quad (4)$$

Q represents the process noise covariance and R is the covariance of the measurement noise. Derivating the Kalman filtering formula, we start with an equation that calculates a state estimate of previous results. Simultaneously we calculate a linear combination of an a priori estimate and a weighted difference between a real and a prediction measurement [4,6].

Time equations are responsible for moving the current state and error covariance estimates. This will be done so that we can obtain a priori estimates for the next step. Measurement update equations are responsible for the feedback, and they also incorporate a new measurement in a priori estimation so that we can obtain an improved posterior development:

$$\hat{x}_{k/k} = \hat{x}_{k/k-1} + K_k \{z_k - H\hat{x}_{k/k-1}\} \quad (5)$$

$\hat{x}_{k/k-1}$ is an a priori estimation of k, and x_k , and $\hat{x}_{k/k}$ to be our posterior state estimate for the measured k-stage. z_k is the noisy observation vector. $H\hat{x}_{k/k-1}$ is a presumption for the pre-measurement value. $\hat{x}_{k/k}$ can be presented (6):

$$\hat{x}_{k/k-1} = A\hat{x}_{k-1/k-1} + Bu_k \quad (6)$$

The Kalman gain K_k minimizez a posterior state estimate by incorporating measurements. Here $E\{e_{k/k}e_{k/k}^T\}$ is the Kalman filter equation. The purpose of this equation is to find a Kalman gain K_k . Equation (7) expresses the posteriori estimative errors:

$$e_{k/k} = x_k - \hat{x}_{k-k} \quad (7)$$

The derivation of the covariance equation is shown by equation (8):

$$E\{e_{k/k} e_{k/k}^T\} = P_{k/k-1} + K_k H P_{k/k-1} H^T K_k^T + K_k R K_k^T - P_{k/k-1} H^T K_k^T - K_k H P_{k/k-1} \quad (8)$$

The value above is equivalent to minimizing traces of the a posteriori estimative covariance matrix. The trace is minimized when the matrix derivative is zero, as in equation (9). Solving equation (9) for K_k leads to Kalman's gain, which is the optimal gain (10):

$$\frac{\partial E\{e_{k/k} e_{k/k}^T\}}{\partial K_k} = 2 H P_{k/k-1} H^T K_k^T + 2 R K_k^T - H P_{k/k-1} - \left\{ P_{k/k-1} H^T \right\}^T = 0 \quad (9)$$

$$K_k = P_{k/k-1} H^T \{ H P_{k/k-1} H^T + R \}^{-1} \quad (10)$$

Kalman filters estimate a process by using a form of feedback control. In other words the filter evaluates the state of the process, while at the same time obtains a feedback. In common parts, we can divide the Kalman filter equations into two groups: time update equations and measurement update equations. Time updating equations can also be considered as predictive equations, while equations for measuring updates can be considered as correcting equations [7]. Still, in the final estimation algorithm we can resemble the correct predictors or algorithms for solving numerical problems.

3.1. Kalman Filter Improvements

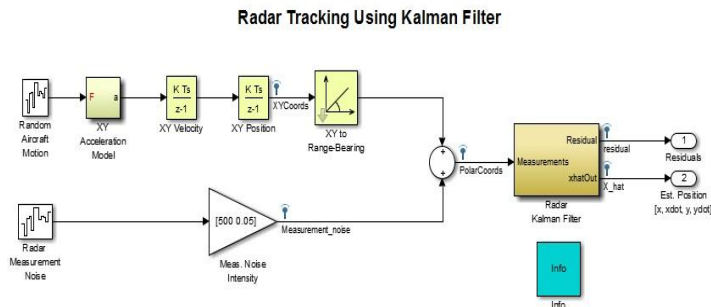


FIG. 2. Using a Kalman filter to improve radar data

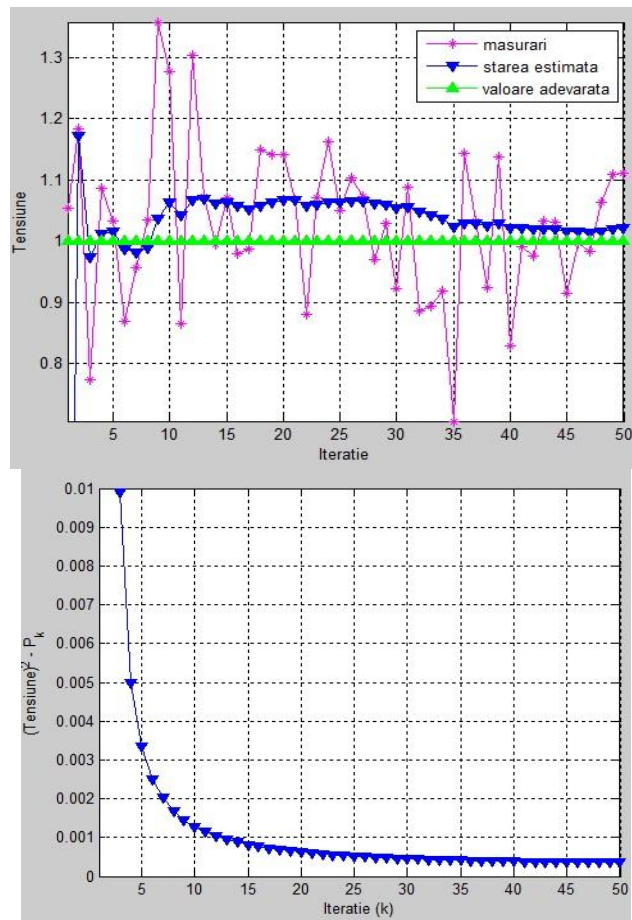


FIG.3. The results of the Kalman filter for radars

Comparing the results of the Kalman Joint Method and the Kalman Enhanced Filter, we examined the simulations with an assumed measured covariance. The Kalman filter can offer optimal solutions, if the system model is correctly defined and if the measurement and system noise statistics are fully acknowledge [8]. Figure 3 presents the simulation results with the assumed measured tension of the Kalman filter. This is done so we can evaluate the performance of the Kalman joint filter.

4. CONCLUSIONS

These results show that the Kalman filtering method is good for reducing measurement noise. The previous method for determining the measurement noise covariance (R) for the Kalman filter depends on the analysis of the empirical data of each sensor and its modification. Because there are no perfect sensors, their performance are reduced with time. This determines the uncertainty in the previous Kalman filter method, which has a considerable impact on the performance of the Kalman filter [10].

The Kalman filter R value affects the weight on which the filter applies between existing process information and the most recent measurements. Failure in any of them may result in the filter being suboptimal or even cause divergences.

5. ACKNOWLEDGEMENTS

The authors wish to thank the “*Transilvania*” University of Braşov and “*Henri Coandă*” Air Force Academy of Braşov for supporting the research necessary for writing this article.

REFERENCES

- [1] Pesonen, N.; Jaakkola, K.; Lamy, J.; Nummila, K.; Marjonen, J. Smart RFID Tags. In *Development and Implementation of RFID Technology*; Turcu, C., Ed.; InTech: Rijeka, Croatia, 2009; pp. 159-178;
- [2] Ho, L.; Moh, M.; Walker, Z.; Hamada, T.; Su, C. A Prototype on RFID and Sensor Networks for Elder Healthcare: Progress Report. In *Proceedings of ACM SIGCOMM Workshop on Experimental Approaches to Wireless Network Design and Analysis*, Philadelphia, PA, USA, 22 August 2005; pp. 70-75;
- [3] Gibson, J.D.; Koo, B.; Gray, S.D. Filtering of Colored Noise for Speech Enhancement and Coding. *IEEE Trans. Sign. Process.* 1991, 39, 1732-1742;
- [4] Hagan, M.; Demuth, H.; Beale, M. *Neural Network Design*; PWS Publishing: Boston, MA, USA, 1996;
- [5] Yu, D.L.; Chang, T.K.; Yu, D.W. Adaptive Neural Model-Based Fault Tolerant Control for Multi-Variable Processes. *Eng. Appl. Artif. Intell.* 2005, 18, 393-411. *Sensors* 2011, 1110282;
- [6] Wang, J.; Ding, W.; Wang, J. Improving Adaptive Kalman Filter in GPS/SDINS Integration with Neural Network. In *Proceedings of ION GNSS 2007*, Fort Worth, TX, USA, 25–28 September 2007;
- [7] Haykin, S. *Neural Networks (A Comprehensive Foundation)*; Prentice-Hall International: Upper Saddle River, NJ, USA, 1999;
- [8] Kalman, R.E. A New Approach to Linear Filtering and Prediction Problems. *Trans. ASME J. Basic Eng.* 1960, 82, 35-45.

PROTOTYPING A LOW-COST EMBEDDED AIRSPEED SYSTEM

Razvan-Viorel MIHAI, Alexandru RADU, Ovidiu TABAN

Military Technical Academy, Bucharest, Romania (razvan.mihai@mta.ro)

DOI: 10.19062/2247-3173.2017.19.1.13

Abstract: Velocity is one of the main parameters that must be known during the flight of an aircraft. In aeronautics a pitot-static system is used.. In this paper we present the implementation of a low cost embedded system design to measure in real-time the airspeed of the aircraft and a graphical user interface to provide the possibility to change density of the air and the speed of a DC motor used as a fan to produce a fluid flow to verify the performance of our system. In modern aircraft, an air data computer computes air speed based on the digital results obtained after extracting the static pressure from the total pressure. We use a two in one sensor that directly provides the difference of pressure, under the form of an analog signal.

Keywords: pitot tube, embedded system, low cost, Graphical User Interface

1. INTRODUCTION

Airplane's speed is measured in knots or miles per hour and it is displayed inside the cockpit of the aircraft. The airspeed indicator is one of the basic aircraft instruments and is of importance to pilots because adherence to safe operating speeds is imperative.

Pilots need to know the speed during some critical phases of the flight, when taking off, landing, stalling.

The airspeed indicator works by subtracting the static pressure from the total pressure. This article presents the transition from conventional airspeed instruments to the computerized systems found on today's airplanes. Airspeed can also be obtained from a GPS unit, even though the data has significant errors that must be corrected. The best option is the differential GPS which requires a beacon fixed at some known coordinates, which provides corrections to the data that is obtained from the satellites. Unfortunately these systems are quite expensive for what we aimed to achieve in this research.

The airspeed indicator is part of the pitot-static system, used to provide the dynamic pressure. This parameter is used to measure the true airspeed obtained from an analogue device, using the following formula:

$$TAS = a_0 \sqrt{\frac{5T}{T_0} \left[\left(\frac{q_c}{P} + 1 \right)^{\frac{2}{7}} - 1 \right]} \quad (1)$$

q_c - impact pressure

P - static pressure

T - temperature

T_0 – temperature at the standard sea level

a_0 – speed of sound at the standard sea level

We chose to build an embedded system which is able to calculate and display the true airspeed at low speeds and altitudes, so we had to use the following formula for this case:

$$TAS = EAS \sqrt{\frac{\rho_0}{\rho}} \quad (2)$$

where:

ρ is the actual air density

ρ_0 is the standard sea level density (1.225 kg/m³)

$$EAS = \sqrt{\frac{2q}{\rho_0}} \quad (3)$$

$$q = \frac{1}{2} \rho v^2 \quad (4)$$

where:

q is the dynamic pressure

v is the flow speed

Youngshin Kang et. all propose the Kalman filter setup to calibrate static pressure, or airspeed and barometric altitude using GPS ground velocity [1]. And also Kalman filter based AOS calibration method is proposed using flight data. Proposed methods are verified by simulation and real flight data of Smart UAV.

The next paper [2] claims that the coefficient α must be calibrated to correct the measurement result. The authors suggest to use a Doppler laser anemometer to calibrate Pitot-tube to acquire the coefficient α .

2. HARDWARE DESIGN

We tried to design a simple board on which we should be able to develop new features in a modular fashion. Figure 1 illustrates the resulted board:

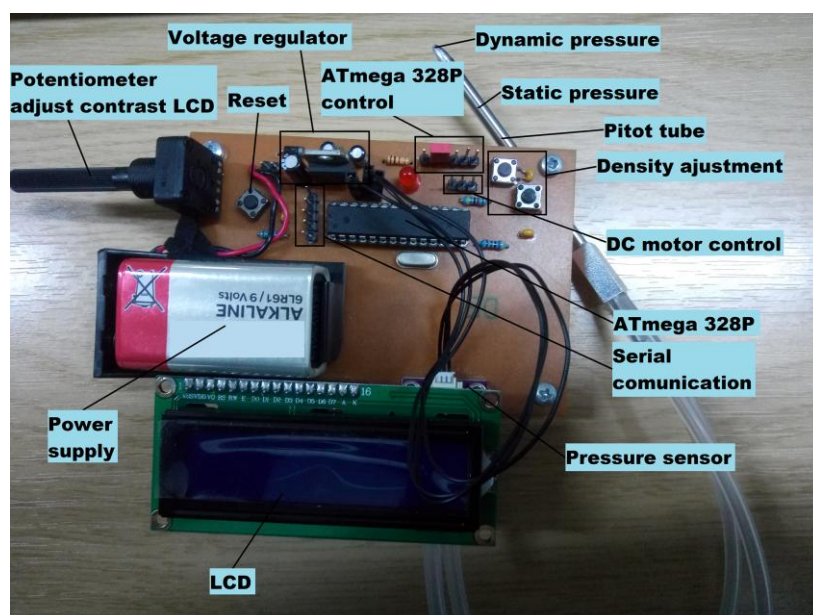


FIG. 1

In terms of data display, the aviation industry is moving from cathode ray tubes to the lighter and more reliable LCD (Liquid Crystal Displays). CRTs require high voltages—up to 50,000 volts—and generate a lot of heat, while LCDs, like large chips, can use power in the 5-volt range. The advantages of the LED (Light Emitting Diodes) over the incandescent lamps are longer life, lower voltage, faster on and off operations, and less heat. The LCD has an advantage over the LED in that it requires less power to operate. Where LEDs commonly operate in the milli-watt range, the LCD operates in the microwatt range. In order to keep a low power consumption we chose to use a 32 characters on two lines LCD, because we decided to display the density of the air and the true air speed.

The core component responsible with data conversion, processing and communication is a CMOS (Complementary Metal-Oxide Semiconductor) 8-bit AVR Atmel chip, respectively ATmega328p. This microcontroller is integrated in the well known Arduino Uno board which has a lot of features that we need to particularly configure them in our application. Thus we designed a prototype board aiming to minimize costs, comparing with Arduino Uno.

Because of the great variety of conditions, ranges, and materials for which pressure must be measured, there are many different types of pressure sensor designs. Often pressure can be converted to some intermediate form, such as displacement. The sensor then converts this displacement into an electrical output such as voltage or current. The three most universal types of pressure transducers of this form are the strain gage, variable capacitance, and piezoelectric.

Piezoelectric pressure transducer take advantage of the electrical properties of naturally occurring crystals such as quartz. These crystals generate an electrical charge when they are strained. We chose to use the differential pressure sensor – CJMCU-36, which is based on the component MPX5010 presented in Fig. 2. The MPxx5010 series piezo resistive transducers are state-of-the-art monolithic silicon pressure sensors designed for a wide range of applications, but particularly those employing a microcontroller or microprocessor with A/D inputs.



FIG. 2

The nominal transfer value is hardware calibrated under the following formula:

$$V_{out} = V_s * (0.09 * P + 0.04) \pm (Pressure\ Error * TempFactor * 0.09 * V_s) \quad (5)$$

V_s - Supply Voltage

V_{out} - Output Voltage

We used this sensor because it directly outputs the dynamic pressure analogue quantity, therefore helping us to avoid the usage of two analogue to digital channels and also decreasing the probable error.

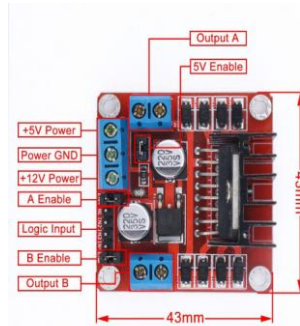


FIG. 3

One simple and easy way to control the speed of a motor is to regulate the amount of voltage across its terminals and this can be achieved using “Pulse Width Modulation” or PWM. As its name suggests, pulse width modulation speed control works by varying the duty cycle, of the pulses while keeping the frequency constant.

The power applied to the motor can be controlled by varying the width of these applied pulses and thereby varying the average DC voltage applied to the motors terminals. To be able to control the speed of the motor we used a motor driver – L298N, as depicted in “Fig.3”.

“ Figure 4” and “Figure 5” show the implementation of a Graphical User Interface in python to be able to check all USB ports from PC and recognize our board if is connected, on which port and what baud rate, in order to provide the possibility to change air density and to control the speed of the motor through serial communication with the microcontroller ATmega328p which will give a modifiable PWM signal to the motor driver.

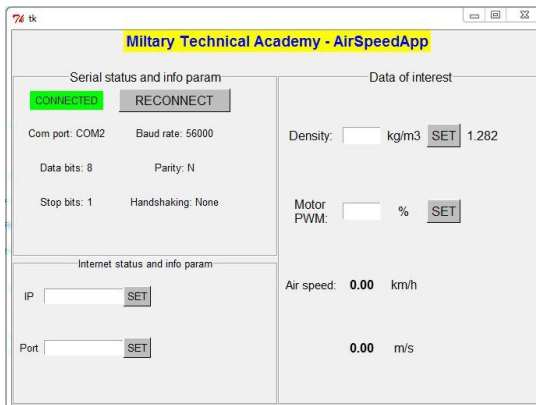


FIG. 4

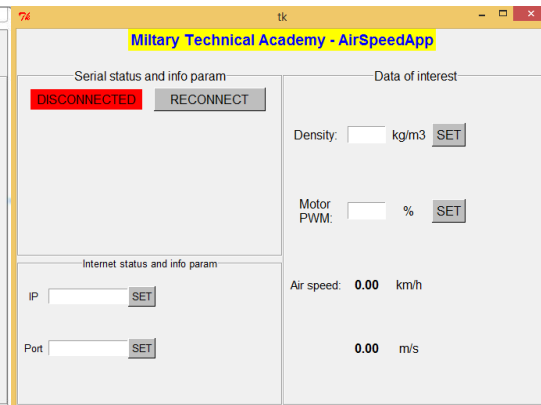


FIG. 5

Schematic capture or schematic entry is a step in the design cycle of electronic design automation (EDA) at which the electronic diagram, or electronic schematic of the designed electronic circuit is created by a designer.

The most known software programs for PCB design are OrCAD, EAGLE, Altium. Taking into account that we don’t have a big budget or a large project, we chose to use EAGLE, for his friendly environment and low cost price, to design the printed circuit board which is presented in “Fig. 6”.

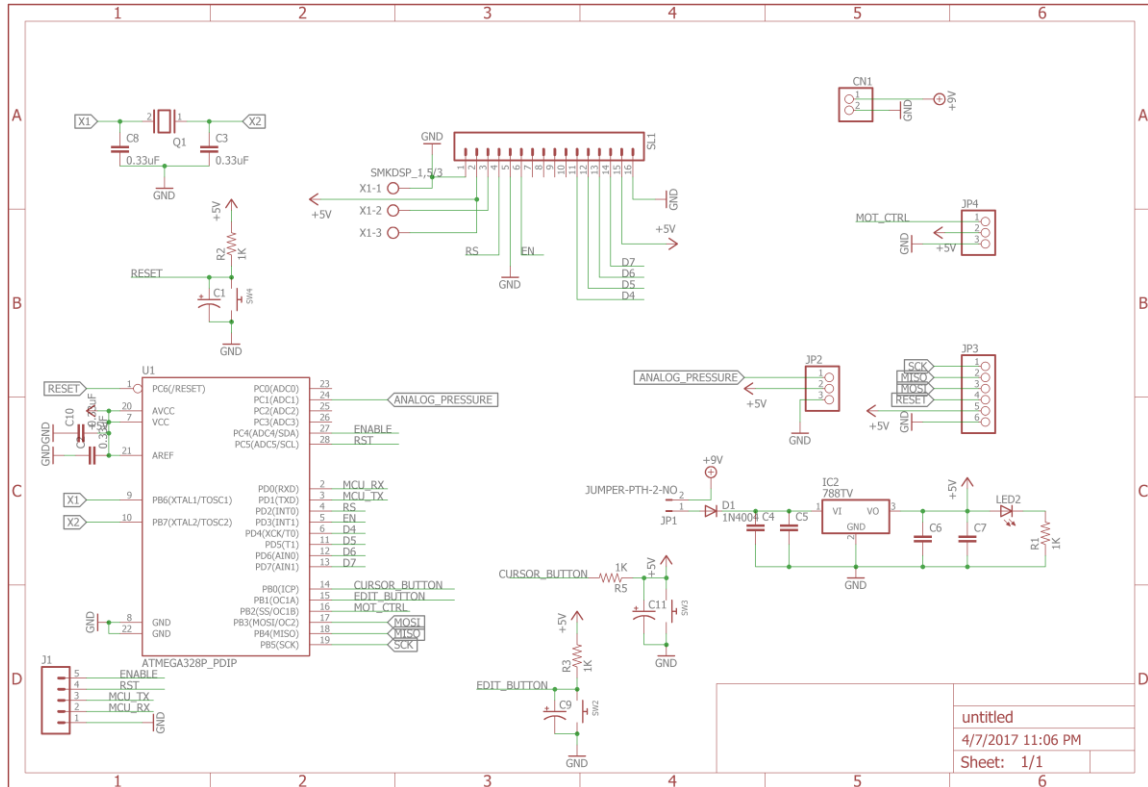


FIG. 6

3. SOFTWARE IMPLEMENTATION

The software we chose to work is Atmel Studio 7. Atmel Studio is an integrated development platform for developing and debugging all AVR microcontroller applications. The Atmel Studio integrated development platform gives you an easy-to-use environment to write, build and debug your applications written in C/C++ or assembly code. Studio 7 can also seamlessly import your Arduino sketches as C++ projects.

Another software we could chose was Arduino in which a program may be written in any programming language for a compiler that produces binary machine code for the target processor. The biggest lack of this software is that you cannot debug your program and it is really hard to determinate your flaws. In addition to that it offers a slower response time to register access.

The main loop in the software implementation:

```
while(1)
{
    switch(StateMachine)
    {
        case CALIBRATION:
            //dis_data('C');
            start_calibration();
            //dis_data('a');
        break;
        case PRIMARY_SCREEN:
            //dis_data('B');
            primary_screen();
            ADC_START_CONV;
            StateMachine = FREE_RUN;
        break;
    }
}
```



```

    case FREE_RUN:
        get_adc_chunk();
        get_msg();
    break;
    case EDIT_DENS:
        incrVal = '0';
        dens = 0.0;
        start_to_edit_screen();
        //dis_cmd();
        StateMachine = INSERT_VAL;
    break;
    case INSERT_VAL:
        if (flag_digit_incr)
        {
            if (incrVal > '9')        incrVal = '0';
            user_input_screen(incrVal++);
            flag_digit_incr = FALSE;
        }
    break;
}
}
}

```

The program that we developed consists in a main loop in which it is executed one of the 5 states of this software. Those 5 states consist in: calibration, primary screen, free run, edit density and insert value.

The first state is calibration in which the message that will be displayed on LCD is made intelligible by calibrating the data received from ADC connected to the pitot tube using a mediation of 1000 values. This calibration method is not the best because inserts critical errors when the velocity of the flow is quick changed.

This method of calibration can be improved by reducing the values that are mediated, but reducing these values can change the way in which the data are displayed, making them appear quicker on the LCD resulting in an hazy display.

The second state primary screen represent the communication of the microcontroller with the LCD. With the help of this state the data received from ADC and compiled by the microcontroller is displayed on LCD, but first is displayed an introduction message. Aside from displaying velocity it also display the density value which can be changed.

The free run state refers to the nominal state of our application, during which we simply get data from ADC and display it on the LCD, but also in this state we expect a message from GUI to change the PWM of the DC motor control resulting in the change of the velocity flow through the Pitot tube.

The edit density state is called when the user press the edit density button and change the message displayed on the LCD to resemble a new density to be introduced. Because density varies with altitude it is essential to be able to insert updated values. The edit state can also be accessed through GUI.

Lastly the insert value refers to the moment when the edit density is pressed and is expected to be introduced the new value. This state help you to change the value of the density displayed on LCD.

Our code use the following formula to calculate the airspeed which depends on the two pressures that the sensor is measuring and density.

$$V = \sqrt{\frac{2P}{\rho}} \tag{6}$$

4. RESULTS AND CONCLUSION

In this paper we presented the design of a low-cost embedded system design to measure in real-time the airspeed of the aircraft which was tested in a wind tunnel at Clinceni presented in “Fig. 7” and “Fig. 8”. After we analyzed the results we discovered that our module have small errors introduced by the air density which was not measured very accurate with our equipment.

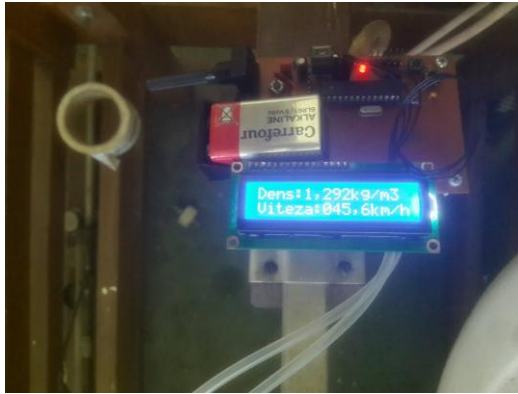


FIG. 6



FIG. 7

When the wind tunnel reached a flow velocity of 60-70 km/h, the tested system crashed and started to show false data, “Fig. 9”. One major reason for this malfunction could be the usage of an simplified formula (5) which does not take into account all the parameters needed for high flow velocities (1). In order to solve this issue we will take in consideration the static pressure in the future.

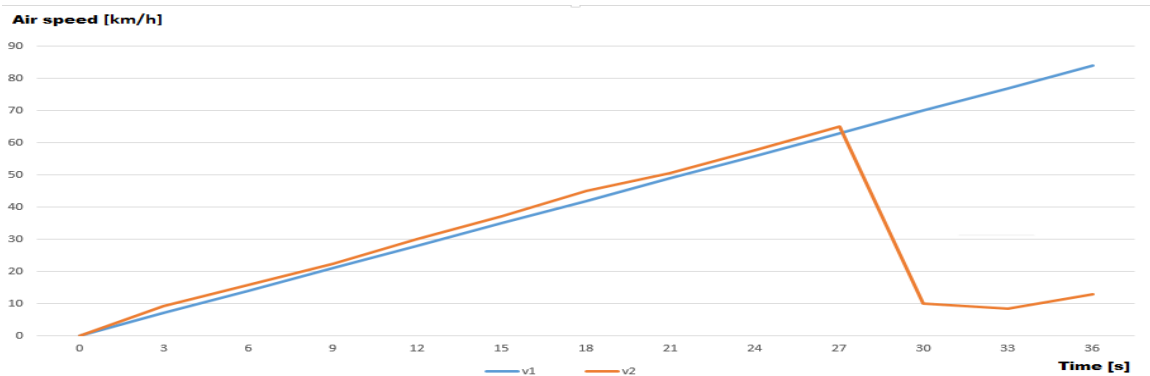


FIG. 8

The system is easy to use thanks to the graphical user interface which is design to accept new features. The future work assumes to equip our board with an wireless module and internet connection in order to be able to update in real-time and autonomous the density of the air and temperature depending on the altitude.

REFERENCES

- [1] *Air data system calibration using GPS velocity information*, written by: Youngshin Kang, Sam-Ok Koo, Bum-Jin Park.
- [2] *Experimental investigation to calibrate pitot-tube by laser doppler anemometer*, written by: L.-S. Cui, H.-M. Hu, C.-H. Li
- [3] <https://www.thebalance.com/basic-flight-instruments-the-airspeed-indicator-282607>
- [4] <https://www.engineersgarage.com/articles/pressure-sensors-types-working>
- [5] <http://www.experimentalaircraft.info/flight-planning/aircraft-navigation-speed.php>

SIMULATION TRAINING AND THEIR ROLE IN THE OPERATING INSTRUCTION OF FIGHTING SQUADRON

Laurențiu MITITELU

Air Force HQ, Bucharest, Romania (lmititelu@roaf.ro)

DOI: 10.19062/2247-3173.2017.19.1.14

Abstract: *„If network simulators and its inherent value is appreciated quickly, then today`s (current) and tomorrow`s (future) warriors will step into potential battles with the great advantage of improved flying ability, reflexes and „seeing” the big picture while working their own luck along the way. The network simulators has a future and is destined to be cornerstone of air and space dominance in the future”, Michael R Oakes*

Keywords: *simulators, network, training, program, learning.*

1. INTRODUCTION

A continuing concern of the military aeronautical community is how to improve pilots training programs from the perspective of using flight simulators or simulator networks to develop and improve pilots' combat capabilities and to develop new tactics to use in air combat.

The recent development of the battle technique has led to the emergence of new tasks during missions and, implicitly, to new challenges in the formulation of pilots' training programs.

If in the past flight simulators were used only to improve piloting techniques or to learn how to operate systems and equipment on board the aircraft, it has recently become insignificant in relation to the training needs required by the new conditions and tactics opponent's struggle.

The training opportunities offered by the virtual environment, the technical capabilities of reproduction of the modern battlefield, characterized by a multitude of both terrestrial and airborne threats and the need to train pilots to operate in more and more crowded airspace, Approaching a new vision whereby training given to combat aircraft pilots must ensure the success but at the same time survival in the battlefield.

2. THE IMPACT OF TRAINING SIMULATION ON THE OPERATIONAL ENVIRONMENT

Under the conditions of modern wars, the actions performed with isolated aircraft are almost excluded, and the new battle tactics of aviation are addressed to the formations of at least two aircraft, which has led to the emergence of new training needs for the pilots, to develop their ability to understand responsibilities In the struggle structures to ensure the success of the mission.

These new training challenges have resolved with the networking of advanced simulators and represent a new step in the field of virtual training that offers unlimited possibilities to generate highly complex scenarios designed to reproduce the environment as faithfully as possible real flight and develop pilots' skills in making the best decisions to accomplish their missions.

Flight simulator interconnection and simulator network development has facilitated the development of new tactics, techniques, or procedures for aviation use in combat, and allowed them to be validated before being used in real combat, and last but not least, provided solutions for remodeling the pilot training programs in line with the new requirements.

However, the simulators also have some limitations, determined by the graphical possibilities of visual representation, the quality of the sensors and the accuracy of the information received from them, the number of variables processed for real flight simulation, the realism of the scenarios used, the lack of environmental psychological factors Real flight, the fidelity with which the aircraft cabin is reproduced, and, last but not least, the software / hardware capabilities. All these limitations can have a negative effect on the training processes on how to carry out tasks and missions, or may prove to be critical in the development of misconceptions that are difficult to identify and corrected later on.

Analyzing both the benefits and limitations set forth above, and judging each task or mission according to its peculiarities, the decision on the need for virtual training, complementary to in-flight training, ultimately belongs to the comrades and is based on the analysis of the following indicators:

- Utility of simulator training;
- Effectiveness in acquiring the knowledge required to operate on-board systems and equipment, interpreting sensor input and decision making, tactical situation management, weapon use, etc.
- Influence of simulator training on pilots' performance in real flight.

In order to demonstrate the usefulness of simulator training, the study by the US Air Force Research Laboratory, involving pilots qualified for the mission and using a network of two F-15 simulators (full view) and two tactical simulators (for Simulation of opponents / interactive threats) as well as a Weapons Director. In addition to the interactive threats, controlled by the two tactical simulators, the scenario was complemented by constructively generated threats, increasing in this way the degree of complexity and realism.

After one training week, pilots were asked to assess the usefulness of the simulator training relative to the flight instruction in the base units. The outcome of the study not only demonstrated the usefulness of simulation training but also highlighted many tasks for which it proved to be more beneficial but also more efficient due to the following:

- Training costs much lower than those generated by in-flight training;
- The advantage of repeating certain tasks or assignments for a better student understanding without additional fuel or time;
- The possibility of analyzing an event immediately after it has occurred gives the opportunity for immediate feedback, and it is not necessary to complete the debriefing mission;
- It is possible to record the mission performed and can be used later as a reference in assessing progress in training or as a future scenario.

Thus, two categories of tasks were identified, differentiated according to the assessments received, as shown in the table:

Better Trained in Simulator	Highly Valuable Simulator Training
Multibogey selection Reaction to SAM Better Trained in Simulator	All-aspect Defense BVR Employment Highly Valuable Simulator Training
Dissimilar Air Combat Tactics All-Weather Employment Communication Jamming Chaff&Flare Employment Escort Tactics ECM Employment Tactical Electronic Warfare System Assessment Work with WD	Radar Sorting Reaction to Air Interceptors Missile Employment Egress Tactics

[1] **Source:** Adapted from Michael R. Houck, Gary S. Thomas, and Herbert H. Bell, *Training Evaluation of the F-15 Advanced Air Combat Simulation* (Williams Air Force Base, AZ: Armstrong Laboratory, Aircrew Training Research Division, September 1991), table 6,10.

To identify the contribution of the simulator instruction to improving pilots performance, according to the results of the study conducted by AMSTRONG LABORATORY at AFB Williams, Arizona, where 40 MR and FL pilots and 23 wing man pilots were tested Through the 36 exits executed in advanced network-connected simulators, there was a significant improvement in pilots performance in 2v2 missions and less for 2v4 missions (due to the increased complexity of missions performance improvement was not so obvious). The study was conducted in the framework of a comprehensive research program to "identify the potential of simulator networks in piloting a Situational Awareness (SA) pilot during combat operations. To measure pilot performance, 22 indicators were used, grouped as follows:

Category	Behavioral Indicators
Tactical Game Plan	Developing plan Executing plan Adjusting plan on-the-fly
System Operation	Radar Tactical electronic warfare system Overall weapons system proficiency
Communication	Quality (brevity, accuracy, timeliness) Ability to use controller information
Information Interpretation	Interpreting vertical situation display Interpreting threat warning system Ability to use controller information Integrating overall information Radar sorting
Information Interpretation	Analyzing engagement geometry Threat prioritization
Tactical Employment-BVR	Targeting decisions Fire-point selection

Tactical Employment- General	Assessing offensiveness/defensiveness Lookout Defensive reaction Mutual support
---------------------------------	--

[2] **Source:** Adapted from Wayne L. Waag et al, “Use of Multiship Simulation as a Tool for Measuring and Training Situation Awareness,” in AGARD-CP-575, *Situation Awareness: Limitations and Enhancement in the Aviation Environment*, (Neuilly-Sur-Seine, France: Advisory Group for Aerospace Research and Development, January 1996), table 1, 20-2.

3. CONCLUSIONS

Despite the fact that the virtual training environment imposes certain limitations on the reproduction of the flight environment and the real battlefield, these limitations can not prevent the development of well-designed training programs where combining flight and simulation training can provide training Efficient use of all the benefits offered by flight simulators and eliminating the potential negative effects of virtual training in flight training.

Simulator training can significantly improve pilot training if it is properly integrated and effectively complements flight instruction.

For future combat pilots, information processing skills will be more important than motor skills. New emerging combat planes in the United States and Europe will be easy to fly but hard to manage, so pilots will have to be trained to carry out tasks different from those during the Cold War.

The qualities of older generations, such as flying skills, though still relevant, will be less important in new aircraft that will have a digital environment and require situational and tactical capabilities to manage the available information. Information management in digital cabinets will be much more complex, with much more information, and a larger volume than it does today.

REFERENCES

- [1] Michael R. Houck, Gary S. Thomas, and Herbert H. Bell, *Training Evaluation of the F-15 Advanced Air Combat Simulation* (Williams Air Force Base, AZ: Armstrong Laboratory, Aircrew Training Research Division, September 1991),
- [2] Wayne L. Waag et al, “Use of Multiship Simulation as a Tool for Measuring and Training Situation Awareness,” in AGARD-CP-575, *Situation Awareness: Limitations and Enhancement in the Aviation Environment*, (Neuilly-Sur-Seine, France: Advisory Group for Aerospace Research and Development, January 1996)

HELICOPTERS DURING MARITIME MISSIONS

Dinu PĂDURARIU, Nicolae CREȚU

National Defense University “Carol I” București, Romania (dinupadurariu@yahoo.com, shimu_nae@yahoo.com)

DOI: 10.19062/2247-3173.2017.19.1.15

Abstract: By maritime power we understand the state’s political, economical and military abilities to impose its national interests to and from the sea. The emergence of helicopters and their further development diversified the missions that aviation can execute in the naval aviation service; they will provide operational capabilities necessary for the efficient execution of combat missions. The article highlights the use of helicopters for naval missions as platforms designed and constructed in accordance with certain standards so that they can meet the users of maritime security having an impact on the defense industry and military acquisitions.

Keywords: Maritime Power, helicopters, antisurface, surveillance

Acronyms:

ASW	- antisubmarin warfare	VERTREP	- vertical replenishment
CASEVAC	- casualty evacuation	ASuW	- antisurface warfare
SAR	- search and rescue	UAV/S	- unmanned aerial vehicle/system
MIO	-mision interdiction operation	MSO	-maritime surveillance operations
CNSAS	- Corpul Național pentru Relief Alpin și Speleologic		

1. GENERAL CONSIDERATIONS REGARDING THE MARITIME DEVELOPMENT POWER

According to specialized references [1], through maritime power we understand the state’s political, economical and military abilities to impose its national interests to and from the sea.

Using aircraft in aerial-maritime actions since World War I, led to the exploitation of maritime domain with implications for the exercise of rights of air supremacy. The first aircraft were seaplanes (1914) used in research assignments and then they were used to arrange and conduct vessels used for air vectors (carriers), see figures 1 și 2, [2, 3].

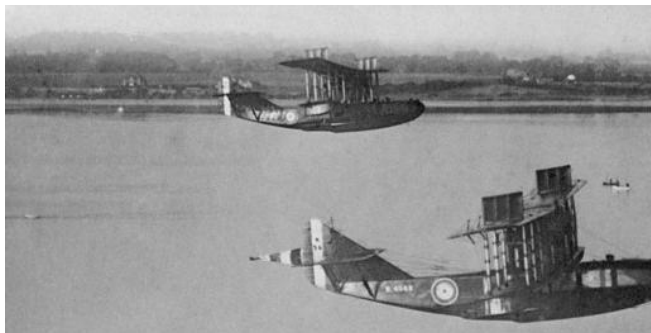


FIG.1. Hidroavion Felixstowe F5s

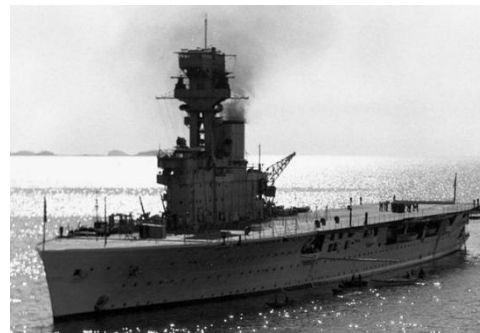


FIG. 2. HMS Furious (British Aircraft Carrier, 1917-1948), [3]

The first mission of a seaplane was executed on 31 May 1916 by the English squadron at Jutland, in research missions at sea and to discover the fleet and the actions of the German army, and the English are the first to release on water, in 1919, "Hermes", the first operational aircraft carrier during weather conditions specially built for this purpose, see figure 3. Aircraft carrier will consolidate its position among the already existing battleships during the second world war.

During the Second World War, the aviation was used in the complete range of missions: from the mission of neutralizing the enemy ships to the support of landing actions, missions independently executed and rarely in cooperation with forces whom benefits were acting.

Romanian hidroaviation was developed since 1920 in Constanța where seaplanes were (included in the structure of the Sea Division) catches of war, but which were requiring overhaul. Constanța Port had two depots equipped with ramps for launching and for raising to the shore of the acvatorium's seaplanes. First Romanian SAR seaplane 1 Getta was conducted at August 15, 1925 in Constanta Transport Society factory for air surveillance of the territorial waters, and the first flight took place on August 15, 1925, when it celebrates "Navy Day", see figure 3, [4, 5].



Fig. 3. RAS 1 *Getta*

During the Second World War hidroaviation had as main mission offshore exploration to discover enemy naval movements and close and distant escorting of ships.

After the Second World War, the use of joint air and naval forces changed the concepts regarding military power of maritime States. Current carriers are experiencing a considerable increase in their share, being able to achieve important strategic missions by destroying targets deep in the enemy territory. Naval forces are the aggregation element of naval power, and maritime navigation, river navigation, port infrastructure and the access to ports, submarines resources (oil and gas), fishing, maritime trade and submarine communications, all have to be seen as a unit, as a part of sea power [6, 7].

The emergence of helicopters and their further development diversified even more the missions that aviation service can execute for the benefit of naval forces, they will provide operational capabilities necessary for the efficient execution of combat missions against submarine threats (ASW) against surface ships (ASuW), in search and rescue missions (SAR), vertical replenishment (VERTREP) and casualty evacuation (CASEVAC).

Unlike terrestrial power, which generally can be defined only by military terms, maritime and aviation power cannot be separated from the economical, commercial or diplomatic elements.

Air power, as well as naval power, of a state or non-state actor, includes all Air Force military (which operates weapon systems which acts in/from the airspace), civil aviation (commercial and recreational), the aeronautical/radiocommunication manufacturing industry, aeronautical education and research, raw material resources necessary for aeronautical manufacturing, international research and procurement of equipment/weapon systems and munitions partnerships, thereby increasing the ability of a country to use its airspace for other non-military purposes, [7].

2. HELICOPTERS DURING NAVAL MISSIONS

2.1. Tactical helicopter group

Due to their technico-tactical characteristics, helicopters have become extremely flexible means that can be integrally utilized in the air, on land and at sea. The article highlights the use of helicopters for naval missions as air platforms created and designed according to different standards in such a manner that they can satisfy the maritime security users that influence the defence and military acquisitions industry.

At the moment there is a debate on military technologies with multiple utilization in order to develop system equipments capable of executing terrestrial and naval missions with both military and civil purposes.

The strategic helicopter grouping is the deployable structure used for executing various missions during operations; the grouping must be flexible and must focus on positioning their own units in the most favourable background when confronting their opponent.

In the beginning helicopters have been used only for transportation, search and rescue and MEDEVAC (the US military infantry in Nicaragua – 1932 and in Korea – 1950) missions; then the helicopter's role in the new concept of air mobility made it possible for the helicopter to become, for the Terrestrial Forces, an air mean used in air support missions as important as the airplane, see figure 4, [8, 9].



FIG. 4. Sikorsky H-19, [9].



FIG. 4. SH-3 Sea King, [10].

As of 1961, the marine infantry and naval forces of the USA have been equipped with SH-3 Sea King helicopters in order to be utilized in amphibious, anti-submarine and search-rescue operations, see figure 5, [10].

The use of helicopters in amphibious operations had as purpose the increase of mobility and fighting capability of the marine infantry, the helicopters being utilized mainly for: transport, for the unfolding and recovery of the seek-diversion grouping, the unfolding of the maritime assault in delta areas or on the opponent's depth for conquering some districts or deterring the opponent to regroup his defenses on the shore, for air support, for supplying and recovering landed units, as well for the excuting aeromedical evacuation operation.

In anti-submarine operations, the helicopter use increases investigation possibilities of submarine-hunting surface ships, by searching for and discovering submarines at long-distance, and by striking the submarines with torpedoes. The convenience of using helicopters in anti-submarine operations is also due to the fact that they are more mobile and faster than surface ships and they are less vulnerable at the attack of the submarines that they discover.

In SAR operations, helicopters are used for rescuing the crew of the sinking ships, and for searching for and rescuing the crew of the aircrafts stricken above the sea. As of 1979, naval forces and the coast guard of the USA started to replace their search-rescue helicopters with Sikorsky S-70 SeaHawk, [17].

Despite all the advantages, it remains the most expensive weapon operated by human force that requires the most complex logistics and continual procurement with new technologies and has the longest training that human factor uses.

2.2. UAV during naval missions. Cooperation with UAV

UAVs air vectors were used by the US military in 1922 when there was the first release of an unmanned air target (RAE 1921) carried aboard HMS Argus, and in 1927 the British fleet used drones for shooting exercises [11, 12, 14].

The first use of a helicopter type UAV took place in 1962 when the naval version DASH (Drone Antisubmarine helicopters) for QH-50A entered into operational service of the US Navy, [13, 14].

To increase efficiency of the helicopter maritime missions there have been adopted a series of strategies for technological development and cooperation with other types of forces and combat equipment, an interesting cooperation that is worth mentioning is performed using unmanned vehicles (UAVs) that can provide real-time data in areas of interest without the risk of casualties, UAVs which have proven their capabilities, maturity and high degree of integration in a number of conflicts, [15, 16]. Currently, helicopter type UAS have been successfully used by the Australian Navy FOTEA, [21] and U.S.Navy [22], see figure 5.



FIG. 5. Landing RQ-8A unmanned elicopter [23]

3. CONSIDERATIONS REGARDING HELICOPTERS DURING MARITIME MISSIONS

3.1. Italy

Italian Naval Forces describe its own Naval Air Force features as a "weapon system for naval unit" which is rather an operational "long arm" than a system of autonomous weapons.

Italian Navy refers to the concept of maritime-air power and not the concept of air power, given the dimensions of air and sea are indivisible and Navy amplifies not only the capability of recognizing and observing the fleet but also the employment capacity. Navy Aircraft is used to carry out three main types of missions: anti-submarine warfare (ASW), against surface ships (ASuW) and fight amphibious (support forces amphibious / special "operations assault helicopters" [18]), see figure 6.



FIG. 6 Forțele Navale Italiene

Moreover, Navy helicopters contributes to maritime security and maritime interdiction operations (MIO), search and rescue missions at sea (SAR) in the context of counter piracy efforts.

A good example is the operation Nostrum Sea [19] started in October 2013 in which naval mission was conducted in parallel with humanitarian assistance operations and the maritime security. In course of action, the navy used five ships and 920 men. Regarding the use of helicopters, it is worth mentioning the participation of four AB-212 aircraft, an HH-139 aircraft for search and rescue and two EH-101 equipped with infrared optics and surface search radars.

In the context of operations that are not strictly military, but can still have a dual nature (civil and military) aircrafts are used both in support of the Department of Civil Protection and saving people affected by natural disasters or interventions in mountain areas with CNSAS . (The national body for alpine relief and Speleology) [20].

3.2. France

The most important feature of the French National Navy is to permanently cover the following two areas: combative (combat missions offshore) and non-combative (out surveillance, reconnaissance, research and its proximity to the coast).

In all cases, helicopters are not considered to be consistent operational tools capable of being carried out without naval support. They do nothing but to intensify the combat capability of the ship to which they are assigned.

In France, the helicopters are employed in four types of operation for maritime security: fight against threats submarine (ASW) against surface ships (ASuW) operations, maritime surveillance (MSO) and operations procedures at sea (MWO), see figure 7.



FIG. 7 Operațiuni de securitate maritimă

For attack operations at sea, helicopters are used in close cooperation with the ships, both independently and in coordination with other ships or aircraft. Navy helicopters are under the command of the Navy, but when they are in action at sea, they are under operational command of the ship captain to whom he was assigned.

MSO maritime surveillance operations are the responsibility of the Coast Guard, carried out by the Navy with the support of frontier police and even the constabulary in some cases. It is coordinated by the charge d'its navy "maritime prefect" - a high-ranking admiral [24].

Military equipment involved in carrying out these operations consists of helicopters aboard surveillance frigates and ground-based helicopters. These missions have a wide range of tasks such as monitoring territorial waters, SAR, internal security operations (drugs). These missions can extend over into international waters, especially those designed to prevent drug trafficking, in which Navy helicopters are noted in tracking and capturing monitored fast boats.

Fleet armed forces will be numerical reduced from 481 equipped helicopters in 2013 to 392 in 2019. At the end of the six years program is intended as a third of the fleet to be made up of new generation helicopters (Tiger and NH - 90) [25], see figure 8.



FIG. 8. NH-90 helicopter [27]

3.3. United Kingdom

At the moment Royal Navy benefits modern helicopters both for training: Squirell, Wilcat HMA2 and for the usage for naval support operations (reconnaissance, surveillance, anti-submarine warfare) HT1 / HT2, Lynx HMA 8, Merlin HM 2, Merlin HC 3, Sea King MK7, AW159 Wildcat, [28], see figure 9.



FIG. 9 AW 159 Wildcat, [29]

According to the "British Navy Doctrine" [26] Air corps is an essential element of maritime power with the primary task ASW, AsuW, ASAC (Airborne Surveillance and Control Area), SAR and troop transport. In the near future Royal Navy will rely mainly on two Regina Elisabeta class carriers because the British Government believes that the United Kingdom must stick to military facilities which can provide rapid deployment of air forces anywhere on earth, the carriers being the only able of it.

The first aircraft carrier will start being tested in 2017 and will board helicopters with the capabilities necessary for reconnaissance missions, reconnaissance, SAR, ASW, AsuW.

Unlike the Italian and French model, British case shows a clear paradigm shift. The introduction of new Regina Elisabeta class aircraft carriers will serve to make these two ships the principal operating platforms at sea for aircrafts with fixed wing and rotary wing. Despite some controversy aroused among military doctrine specialists, the decision seems to have a deeper political motivation and important financial reasons. Participation in international waters on a planetary scale compels the UK Royal Navy forces in a pragmatic and modern approach. London's decision is understandable in the context of the growing role that aviation plays in maritime military operations. The sale of frigates and corvettes seems not only to solve financial problems, but rather be the sign of a new approach to marine British military presence in the world.

4. CONCLUSIONS

Sustained progress over the past century in aviation, especially in the last 20 years, has brought the aircraft at the heart of the military. We could not talk about removing the land and naval forces, but rather about a culmination of the military evolution and of the occupation of its naturally role by the aviation. Both on land and at sea starting from the ground or ship, rotary wing aircraft have become a mandatory attendance at theaters for nations which regard their own safety seriously.

Looking at the approaches from different point of views, we can observe the larger fighting power for the model with the carrier, but more easily bearable costs and greater adequacy to the modest needs of the second and amid the growing role of aviation is required an appropriate situation for the new situation, either to increase boarding capacity of the helicopters (2-3 helicopters) either to create tactical groups of two or more ships each with a helicopter on board.

After analyzing the use of the helicopters for naval missions in terms of realities, perspectives and missions in which they participate, it can be interpreted as follows: countries with access to enclosed seas with maritime ambitions confined to national security are those for which the binomial frigate/ corvette/ helicopter remains by far the most suitable unlike states with emphasized involvement with the planetary ocean and with ample resources are more inclined to adopt a different model: the aircraft carrier (and helicopters) together with corvettes and frigates without helicopters.

THANKS

The article was written with documentary support from the National Defense University "Carol I" Bucharest and the Air Force Academy "Henri Coandă" Braşov.

REFERENCES

- [1] Marin G., Hâldan R., *Forțele Navale ale lumii în secolul XXI*, Editura C.T.E.A., București, 2009;
- [2] https://en.wikipedia.org/wiki/Flying_boat#World_War_I, consultat la 02.02.2017;
- [3] [https://en.wikipedia.org/wiki/HMS_Hermes_\(95\)](https://en.wikipedia.org/wiki/HMS_Hermes_(95)), consultat la 02.02.2017
- [4] Guđju I., Iacobescu G., Ionescu O. *Construcđii aeronautice românești 1905-1970*, Editura Militară, 334p;
- [5] Prisacariu V., Ciucă O.E., *Aeronave de școală și antrenament*, Editura Academiei Forțelor Aeriene “Henri Coandă” 2015 Brașov, ISBN 978-606-8356-35-8, 142p;
- [6] Iordache C., *Aviația maritimă necesitate stringentă a Forțelor Navale Române*, Editura Centrului Tehnic – Editorial al Armatei, București, 2012;
- [7] Puricel I., *Puterea Aeriană în mișcare – Dimensiunea aeriană a conflictualității contemporane în Regiunea Mării Negre*, Editura U.N.Ap., București, p.15;
- [8] <http://www.globalsecurity.org/military/systems/aircraft/rotary-usmc.htm>, consultat la 02.02.2017;
- [9] FLIGHT, may 1954, p.568, disponibil la <https://www.flightglobal.com/FlightPDFArchive/1954/1954%20-%201281.PDF>;
- [10] *Westland SH-3 D Sea King*, Flight International, 30.11.1967, p.911, disponibil la <https://www.flightglobal.com/FlightPDFArchive/1967/1967%20-%202319.PDF>;
- [11] *Automatic flight The Forty-Sixth Wilbur Wright Memorial Lecture*, Flight 16 mai 1958, p58;
- [12] Barnhart R.K., Hottman S.B., Marshall D.M., Shappee E., *Introduction to unmanned aircraft systems*, CRC Press, 2012, ISBN 978-1-4398-3520-3, 215p;
- [13] Evans S.S., *The Incredible Story of the QH-50 DASH – The First Unmanned Helicopter Turns 50*, Vertiflyght Magazine, vol.57 1/2011, p 36-39;
- [14] Prisacariu V. *Managementul integrării soluțiilor tehnice inovative la sisteme aeriene robotizate*, teză de doctorat, Universitatea Transilvania Brașov, 2014;
- [15] Prisacariu V., Muraru A., *Unmanned aerial system (UAS) in the context of modern warfare*, SCIENTIFIC RESEARCH AND EDUCATION IN THE AIR FORCE-AFASES 2016, Brasov, DOI: 10.19062/2247-3173.2016.18.1.23, ISSN 2247-3173, p. 177-183;
- [16] Prisacariu V., *The UAVs in the theatre of operations and the modern airspace system*, RECENT Journal, 3 (39)/2013, ISSN 1582-0246, p. 169-180;
- [17] https://en.wikipedia.org/wiki/Sikorsky_SH-60_Seahawk, consultat la 12.02.2017;
- [18] Paolo Treu, interview, *Coccarde Tricolori*, 2010, pp.82-91.;
- [19] http://www.europarl.europa.eu/meetdocs/2014_2019/plmrep/COMMITTEES/PETI/CM/2016/04-18/1088112RO.pdf, consultat la 12.02.2017;
- [20] <http://www.soccorsospeleo.it/en/about-us/introduction/>;
- [21] Ashworth P., *Unmanned aerial vehicles and the future Navy*, 2001, Royal Australian Navy Sea Power Centre, 28p., disponibil la www.navy.gov.au/sites/default/files/documents/Working_Paper_6.pdf;
- [22] Jacobsen D.M., *Master of military studies unmanned aerial vehicles – the key to effective situational awareness in littoral operations*, United States Marine Corps Command and Staff College Marine Corps University, Marine Corps Combat Development Command Quantico, Virginia 22134-5068, 2002, 51p, disponibil la <http://www.dtic.mil/dtic/tr/fulltext/u2/a401156.pdf>;
- [23] http://www.bluebird-electric.net/oceanography/Ocean_Plastic_International_Rescue/ , consultat la 19.02.2017;
- [24] Jean-Claude Allard, *The French Case Study*, in vol. *The Role of Dual-Use Helicopters in the Security and Defence Field*, 2015, p. 84.;
- [25] *Projet de Loi relatif à la programmation militaire pour les années 2009 à 2014 et portant diverses dispositions concernant la défense*, No. 1216, 29 October 2008, disponibil la <http://www.assemblee-nationale.fr/13/projets/pl1216.asp>;
- [26] UK Ministry of Defence, *British Maritime Doctrine (JDP 0-10 Fourth Edition)*, August 2011, par. 333 ss., disponibil la [https://www.gov.uk/government/publications/jdp-0-10-british-maritime-doctrine.;](https://www.gov.uk/government/publications/jdp-0-10-british-maritime-doctrine;)
- [27] http://www.airrecognition.com/images/stories/europe/france/helicopter/nh90_nfh/NH90_NFH_NATO_Frigate_Helicopter_maritime_weapon_system_surface_fleet_defence_640.jpg, consultat la 07.02.2017;
- [28] https://en.wikipedia.org/wiki/Fleet_Air_Arm#Flying_squadrons, consultat la 27.02.2017;
- [29] https://en.wikipedia.org/wiki/AgustaWestland_AW159_Wildcat , consultat la 27.02.2017.

NUMERICAL STUDY ON THE INFLUENCE OF WAKE CONTRACTION ON THE COMPUTATIONAL ACCURACY AND RAPIDITY OF A MODEL OF A ROTOR IN HOVER

Filip PANAYOTOV*, Ivan DOBREV**, Fawaz MASSOUH**, Michael TODOROV*

*Technical University of Sofia, Bulgaria (michael.todorov@tu-sofia.bg)

**Arts et Métiers - ParisTech, Paris, France (fawaz.massouh@ensam.eu)

DOI: 10.19062/2247-3173.2017.19.1.16

Abstract: *In the present article, the authors are performing a comparison study between two vortex models for the numerical computation of the static thrust of a model helicopter rotor in hover. The aim of this study is to access the rapidity and accuracy of the vortex models, comprised of a series of vortex rings and a single semi-infinite vortex cylinder. The first model has a cylindrical arrangement of the vortex elements, while the second model has a contracting arrangement of its vortex elements. Studies are performed for the optimal positioning and spacing of the vortex elements, in order to provide both rapid computation and good agreement with the experimental data, obtained from a wind tunnel test of the model rotor. The results of the study show a slight increase in the required computational time for the case of the contracting wake, while offering a significantly better accuracy than the cylindrical wake. Another interesting result from the numerical study is that in the case of the contracting wake model there is a reduction of the spacing (compression) between the vortex rings in the near wake, which results in the reduction of the overall length of the vortex system trailing downstream of the rotor.*

Keywords: *model rotor; hover; induced velocity; vortex ring; vortex cylinder; cylindrical wake; contracting wake,*

1. INTRODUCTION

The rotors of drones operate in unsteady operational conditions, as they are rarely performing long lasting hovers in zero wind conditions. Most of the time their utility is such that they are constantly maneuvering or performing thrust adjustments, in order to maintain stable flight or hover, while compensating for atmospheric disturbances. Thus of great interest is the rotor performance during transient or unsteady operational regimes.

The authors are aimed at the development of a numerical model, capable of rapid and accurate computation of the thrust of a hovering rotor. Such tool will allow the possibility to study the rotor performance in unsteady flow conditions, resulting from the transition from one operational regime to another or from phenomenons, such as the tip vortex aperiodicity of a hovering rotor [1].

Nowadays, widespread is the use of CFD and BEM models for studies on UAV rotor performance and optimization of the blade geometry. Although their accuracy, the CFD models are computationally expensive and slow to perform when modeling the complete rotor geometry and the entire computational domain of the flow-field around it. This is due to the computation of Navier-Stokes equations for typically a few hundred-thousand up to a few million cells.

In [2] are summarized all major possibilities to speed up the computation with a CFD model, without losing any significant degree of accuracy. The most common solution is to couple the CFD simulation with other models, which allow for significant reduction of the required amount of numerical computations. In most cases, the CFD models are coupled with BEM or vortex models, which allow for the rapid determination of the aerodynamic loads on the blades or the induced velocity field around the rotor. This allows to save a significant amount of computational resources that contributes to the overall reduction of the computational time, although that the volume of required computations remains significant.

The BEM models can rapidly estimate the forces, acting on the blades of a rotor, as well as the radial distribution of the induced velocity. This allows for rapid evaluation of the overall rotor performance. However, the BEM models do not provide an insight for the flow-field outside the plane of the rotor.

Due to the aforementioned disadvantages of the CFD and BEM models, the authors chose to use the vortex theory for the development of a numerical model for the rapid computation of the thrust, produced by a rotor in transient or unsteady operational condition.

2. STATE OF THE ART OF HOVERING ROTOR MODELS

According to [3], Joukovsky performed a series of theoretical studies on propellers, which established the mathematical foundations for the vortex theory such as applied to rotors. Those works were followed by numerous flow visualization experimental studies on small scale and full scale helicopter rotors in both forward flight and hover. They added more clarity on the structure of the flow-field around a helicopter rotor. These studies also provided the first semi-empirical numerical models for hovering rotors, derived from the obtained experimental performance data and the geometry of the trailing wake.

Jenny et al. [4] and Landgrebe [5] proposed vortex models for the prediction of the hovering performance of helicopter rotors. These models consist of a helical wake, composed of helical vortex sheets, trailing from each one of the rotor blades. Simplifying assumptions are introduced, which allow the representation of the helical wake with a finite number of discrete vortex filaments, namely straight-line segmentation of the tip trailing helical vortex. The induced velocity field is computed with the use of the Biot-Savart law. These numerical models are capable to adequately predict the performance of a hovering rotor, although the simplifying assumption for a rigid helical wake introduces a significant error when the rotor is operating in too light or too heavy load conditions, corresponding to values of the coefficients of thrust C_T smaller than 0.0025 and bigger than 0.01. Another inconvenience is that for higher degree of accuracy a greater number of straight-line segments per complete helical turn must be considered and a greater number of complete helical turns must be taken into account, which significantly increases the volume of the required numerical computations.

Landgrebe [6], Miller et al. [7, 8] and Reddy [9] proposed an alternative approach for modeling the hovering rotor by decomposing the trailing wake into several parts, namely: near, intermediate and far. Each of those parts is modeled with a different type and amount of vortex elements with the aim to achieve greater accuracy, while offering significant numerical simplification. In the aforementioned papers demonstrated is the ability to obtain a significant degree of accuracy for the evaluation of the performance of hovering rotors with vortex systems, which comprise of less than 30 vortex elements in total.

Karpatne et al. [1] demonstrated the capabilities of a vortex model, in which the wake of the hovering rotor is modeled entirely with a system of vortex rings. In their model the vortex rings are emitted with a specific time-step, depending on the angular velocity of the rotor and are allowed to move freely under the induced velocities, resulting from the interaction with the remainder part of the previously emitted vortex rings. Reference [1] showed that the vortex models are capable to adequately simulate unsteady flow phenomena, thus allowing their study.

3. THE MILLER MODEL

Modeling the wake of a hovering rotor with a combination of different types of vortex elements for different segments of the wake is demonstrated in [1], [8] and [9]. The comparison study is performed with the vortex model proposed by Miller et al. in [8]. In the remainder part of the article it will be referred as the Miller model.

The wake of the Miller model consists of two parts: a near wake composed of 20 circular vortex rings arranged in series downstream of the rotor; and a far wake modeled by a single semi-infinite vortex cylinder, placed behind the last vortex ring of the near wake. Thus the model consists of only 21 vortex elements to be accounted for the computation of the entire flow-field around the rotor.

The semi-infinite vortex cylinder allows the model to compensate for the velocity deficit formed downstream of a wake when modeled with a series of vortex rings. It allows to stabilize the numerical computation and ensures that the induced velocities in the far wake double those induced in the rotor plane, such as per the theory for the hovering rotor.

Key for the degree of accuracy and the adequate operation of the model is the proper setup of the parameters d_0 , d_1 and d_2 , shown on Fig. 1.

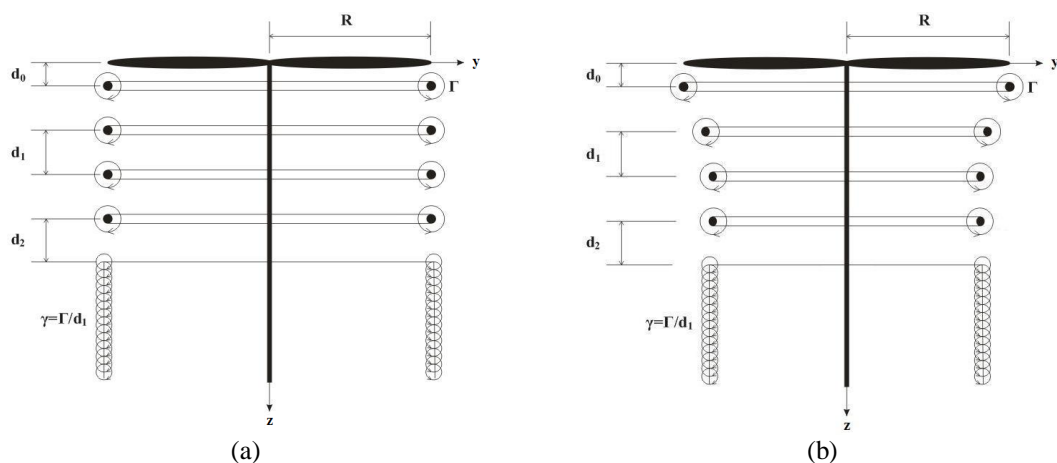


FIG. 1. The Miller model, composed of a series of vortex rings and a semi-infinite vortex cylinder. On Fig. 1 a) is presented the cylindrical arrangement of the vortex system. On Fig 1 b) is presented the initial prescribed position of the contracting wake, from which the computation is initialized.

The distance d_0 , at which the first vortex ring is placed behind the rotor, has a key role for the distribution of the induced velocities along the blade. It is referred in [8] as the first blade-vortex encounter position, which represents the distance between the vortex ring emitted by the preceding blade and the following blade. This parameter can be varied, in order to study its influence on the induced velocity distribution on the blades and in the near wake downstream of the rotor.

The vortex rings are spaced between one another with $d_1 = p/N_b$, where p is the pitch of the helical wake, produced when the same operational conditions of the rotor are applied to the helical wake model and N_b is the number of the blades of the rotor. The distance d_2 is the spacing between the last vortex ring of the near wake and the semi-infinite vortex cylinder, which models the far wake. The optimal values of the parameters d_0 and d_2 are estimated in a comparison between numerical and experimental data for multiple operational regimes of the rotor.

The Miller model offers the potential for rapid numerical computation when compared to CFD and BEM models due to the necessity to compute for significantly less amount of vortex elements. An additional reduction of the volume of numerical computations is possible for hover and vertical flight regimes due to the presence of axis-symmetric flow condition for the rotor. For the studied rotor with two blades, only half of the flow-field can be computed in order to visualize the entire flow around the rotor.

4. NUMERICAL STUDIES

Performed are two numerical studies. The first one is aimed to find the optimal spacing parameters of the vortex elements in both wake models, namely:

- The best positioning of the initial vortex of the series of vortex rings d_0 .
- The best positioning of the semi-infinite vortex cylinder after the last vortex ring of the near wake d_2 .

The near wake is modeled with 20 vortex rings for both the cylindrical and the contracting arrangement of the vortex elements of the Miller model. The parameters d_0 and d_2 are varied as a percentage of the amplitude p , which represents the distance between two vortex rings, emitted by the same blade of the rotor.

The second numerical study compares the two vortex models with the aim to evaluate the accuracy and computational rapidity of the contracting wake model against the cylindrical wake model, thus benchmarking its performance capabilities. Studied is the distribution of the induced velocity along the blades of the model rotor for a specific set of operational regimes, namely for different combinations of angular velocity of the rotor Ω and pitch angle of the blades θ .

The results from the first study are presented in section 5 “Results from the numerical studies” sub-section 5.1 “Optimal parameter study”, while the results from the second study are presented in sub-section 5.2 “Comparison study”.

The model rotor, which is used as reference geometry in those studies, has two rectangular untwisted blades of NACA0012 profile. The tip radius R of the blades is 288mm, the root radius at the hub mounting r_0 is 65mm and the chord length c is 25mm. The pitch angle of the blades is adjustable and thus can be varied between wind tunnel experiments.

Shown on Fig. 2 is the velocity triangle in a typical cross-section of the blade. The velocity of the axial flow through the plane of rotation of the rotor, resulting from the work of the rotor, is denoted with V_z . In the literature it is referred as the axial induced velocity and is a function of the operational parameters of the rotor, namely the angular velocity Ω and the pitch angle of the blade θ . The speed of rotation of the section in the plane of the rotor is denoted with $U = \Omega y$, where y is the blade station radius, which varies from r_0 to R . For the tip of the blade $y = R$ and $U = \Omega R = V_{tip}$. The relative air speed for the cross-section of the blade W is computed with (1):

$$W = \sqrt{U^2 + V_z^2} . \tag{1}$$

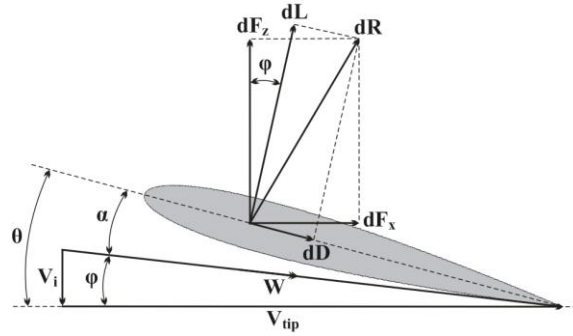


FIG. 2. Triangle of velocities in the cross-section of the rotor

4.1 Assumptions

According to Miller et al. [8] for simplification purposes the wake may be considered as steady and its displacement can be limited in one of the three dimensions. Therefore, in order to reduce the numerical computations to a two-dimensional case, the following assumptions are taken:

- Hover flight is considered, thus the only axial velocity component, computed along the axis z , is the induced axial velocity V_z at that point.
- The wake is considered to be rigid, thus fixing a constant speed of displacement of the trailing vortices, equal to the induced velocity at the trailing edge of the blades [7, 8].
- The wake is steady, thus the induced velocity field of the rotor is independent from time.

These assumptions allow predetermining the exact positions of the trailing vortices, which technically is referred in the literature as a prescribed wake [7, 8].

4.2 Numerical approach

According to [1], by assuming uniform bound circulation and a single tip-trailing vortex per blade, the vortex strength can be computed with:

$$\Gamma = \frac{2T}{\rho N_b R V_{tip}}, \quad (2)$$

where T is the total thrust produced by the model rotor at a fixed angular velocity Ω and pitch angle of the blades θ . R is the tip radius of the blades, $V_{tip} = \Omega R$ is the velocity at the tip of the blades, N_b is the number of blades of the rotor and ρ is the density of the air.

For every change in either the angular velocity Ω or the pitch angle of the blades θ , the total thrust of the rotor T and the bound circulation Γ are also changed. Equation (2) is used for the computation of the bound circulation Γ .

In [13] the coefficient of thrust C_T is defined as:

$$C_T = \frac{T}{\rho A \Omega^2 R^2}, \quad (3)$$

where T is the total thrust produced by the rotor; ρ is the density of the air; Ω is the angular velocity of the rotor; R is the radius of the rotor and $A = \pi R^2$ is the area of the rotor disc. Equation (4) is used for the computation of the coefficient of thrust C_T .

From Fig. 2 it can be observed that for an increase of the axial induced velocity V_z there is a decrease of the angle of attack α . The smaller is the angle of attack of the cross-sectional airfoil, the smaller is the local thrust increment ΔF_z . Thus the total thrust of the rotor T reduces and with it reduces the coefficient of thrust C_T .

On Fig. 3 are shown the key dimensions, used in the computation of the induced velocity in a point of the flow-field. The dimensions y_m , y_n , z_m and z_n are universal for both the cylindrical and contracting wake models. Those are the coordinates of two points, namely M and N. It is considered that the induction happens in point M by a vortex element, situated at point N.

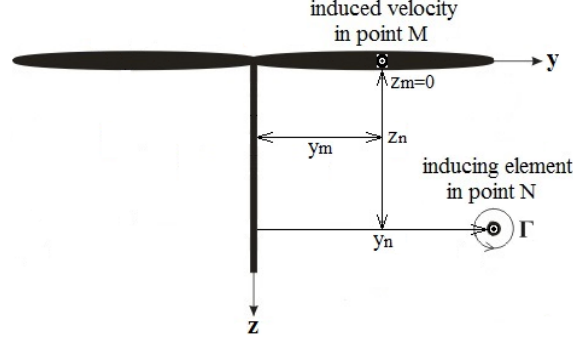


FIG. 3. Dimensions used in the computation of the induced velocity field of the rotor

Lewis [14] introduces the dimensionless parameters y and z with (4) and (5):

$$z = \frac{z_m - z_n}{y_n}, \quad (4)$$

$$y = \frac{y_m}{y_n}. \quad (5)$$

Those are used for the derivation of the equations for the axial V_z and radial V_y induced velocities. For the case of the semi-infinite vortex cylinder, the axial velocity is computed with (6) and for the case of $y = 1$, (7) is used:

$$V_{z,cyl} = \frac{\Gamma}{4\pi} \left\{ B + \frac{z}{\sqrt{z^2 + (y+1)^2}} \left[K(k^2) - \frac{y-1}{y+1} \Pi(n, k^2) \right] \right\}, \quad (6)$$

$$V_{z,cyl(y=1)} = \Gamma \left(\frac{1}{4} + \frac{z K(k^2)}{2\pi\sqrt{z^2 + 4}} \right). \quad (7)$$

For the case of a semi-infinite vortex cylinder, the radial induced velocity is computed with (8):

$$V_{y,cyl} = \frac{2\Gamma}{\pi k^2 \sqrt{z^2 + (y+1)^2}} \left[E(k^2) - \left(1 - \frac{k^2}{2} \right) K(k^2) \right]. \quad (8)$$

The constant B in (6) depends from the ratio between the outer radius of the vortex cylinder and the radius of the rotor. For the case of $y = 1$ it is:

$$B_{(y=1)} = \frac{\pi}{2}. \quad (9)$$

For the case of the system of vortex rings, the axial induced velocity is computed with (10) and for the radial induced velocity (11) is used:

$$V_{z,cyl} = \frac{\Gamma}{4\pi} \left\{ B + \frac{z}{\sqrt{z^2 + (y+1)^2}} \left[K(k^2) - \frac{y-1}{y+1} \Pi(n, k^2) \right] \right\}, \quad (10)$$

$$V_{z,cyl(y=1)} = \Gamma \left(\frac{1}{4} + \frac{z K(k^2)}{2\pi\sqrt{z^2 + 4}} \right). \quad (11)$$

Equations (6), (7), (8), (10) and (11) contain complete elliptic integrals of the first $E(k^2)$, second $K(k^2)$ and third order $\Pi(n, k^2)$. The elliptic parameters n and k are introduced with (12) and (13).

$$k = \sqrt{\frac{4y}{z^2 + (y+1)^2}}, \quad (12)$$

$$n = \frac{4y}{(y+1)^2}. \quad (13)$$

The amplitude p between two consecutive vortex rings, produced by the same blade is calculated with (14):

$$p = 2\pi R \tan(\varphi). \quad (14)$$

For a rotor with N_b number of blades the step between the vortex rings in the near wake d_l is calculated with (15):

$$d_l = \frac{p}{N_b}. \quad (15)$$

Equations (16) and (17) are introducing the initial contraction of the wake for the case of the Miller model with contracting arrangement of the vortex elements.

$$\frac{y}{R} = A + (1-A)e^{-ki2\pi}, \quad (16)$$

$$k = 0.145 + 27C_T. \quad (17)$$

The parameter A in (16) represents the ration between the radius of the flow-field in the far wake R_{fw} and the radius R of the hovering rotor. According to Leishman [13] most experimental studies confirm that $A=0.78$ and not the theoretical value of 0.707.

For the Miller model the parameter i in (16) represents the number of the vortex elements that modify the trailing wake downstream of the rotor in hover.

The parameter k in (17) is introduced in order to modify the rate of contraction of the wake in function of the coefficient of thrust C_T of the hovering rotor. It is introduced for the first time by Landgrebe in [6]. In [9], Reddy uses the linear approximation for k such as proposed by Landgrebe, although that alternative non-linear equation do exist. However those alternative formulas for k are shown to give adequate results for a small range of values for C_T .

5. RESULTS FROM THE NUMERICAL STUDIES

5.1 Optimal parameters study

On Fig. 4 are shown six computational cases for the flow field of the model rotor in hover, computed with the Miller model. The numerical computations are performed for 2000 RPM and $\theta=12\text{deg}$ for three different values of the parameter d_2 , namely $0.25p$ for case a) and d); $0.5p$ for case b) and e); and $0.75p$ for case c) and f). In all six cases d_0 is set to $0.1p$. Situated in the left section of Fig. 4 are the computational cases a), b) and c), produced with the cylindrical wake model, while in the right section of Fig. 4 are situated computational cases d), e) and f), which are produced with the contracting wake model.

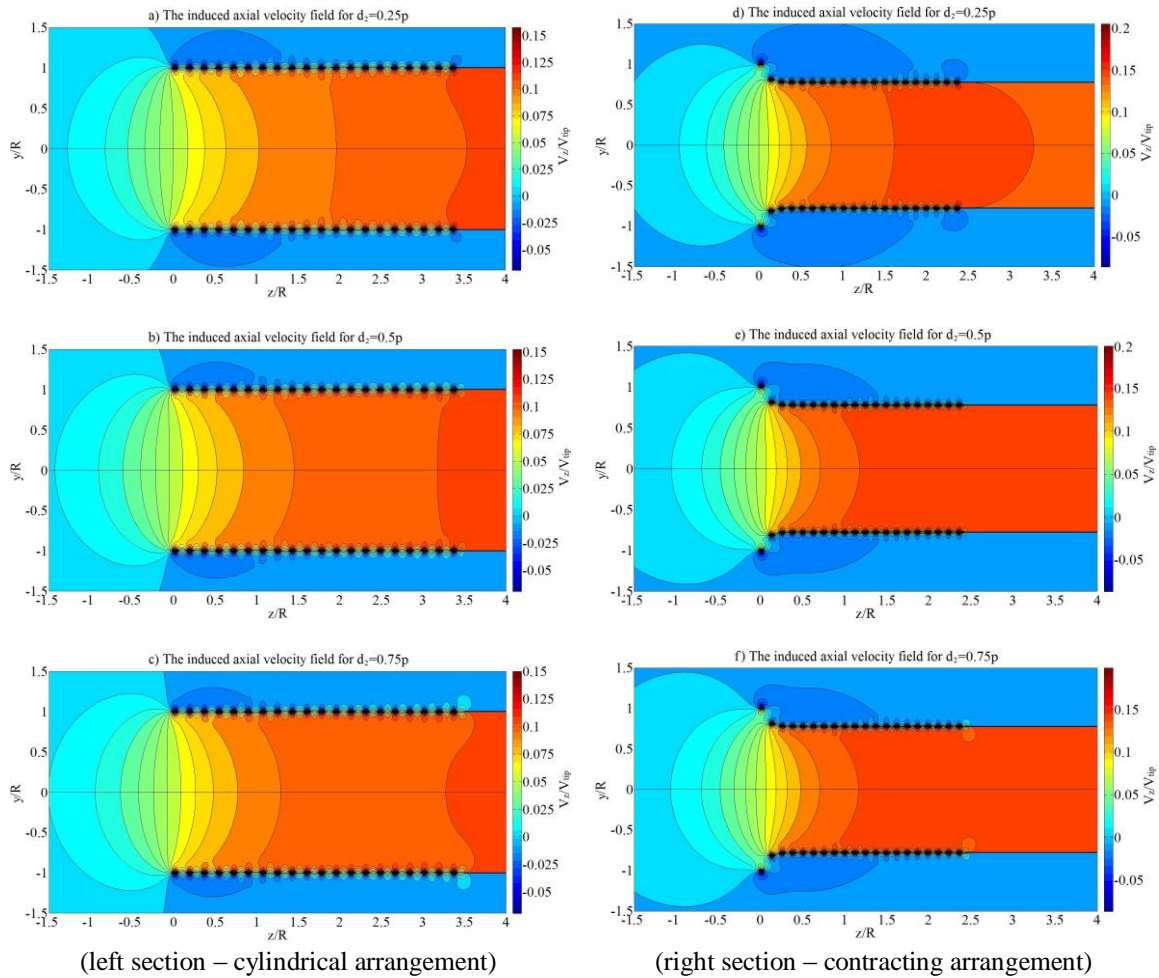


FIG. 4. The flow-field of the rotor computed with the Miller model for 2000 RPM and $\theta=12\text{deg}$ for dimensions $d_0=0.1p$ and $d_2=\text{var}$. On the left section of Fig. 4 are presented three computational cases for three value of d_2 for the cylindrical arrangement of the vortex elements, while on the right section of Fig. 4 are presented the same three computational cases for the contracting arrangement.

On Fig. 5 a) is presented the optimal initial relative displacement d_0/R of the first vortex ring of the near wake of the rotor in function of the pitch angle of the blades θ . On Fig. 5 b) is presented the optimal relative displacement d_1/R between the vortex rings in the near wake in function of the pitch angle of the blades θ .

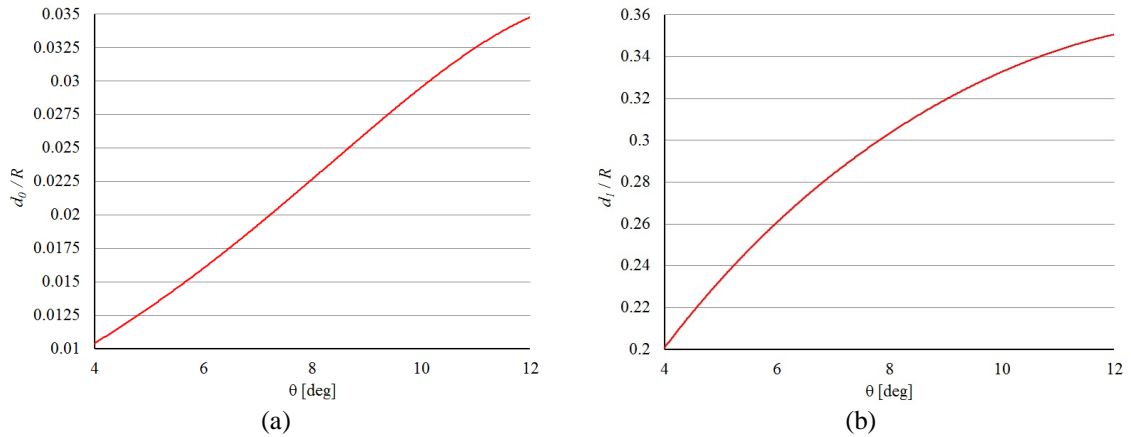


FIG. 5. The optimal values of the spacing parameters for the vortex system, non-dimensioned with the radius of the rotor R . On Fig. 5 a) is presented the function of the initial relative displacement of the first vortex ring d_0/R in function of the pitch angle of the blades of the rotor. On Fig. 5 b) is presented the relative spacing between the vortex rings d_1/R of the near wake in function of the pitch angle of the blades.

5.2 Comparison study

On Fig 6 a) is presented the relative axial induced velocity V_z/V_{tip} , computed with both models for 2000 RPM at blade-station $y/R=0.75$ for pitch angle settings varying from 4 to 10 deg. The near wake is modeled with 20 vortex rings. The spacing parameters for both models are set to be $d_0=0.1p$ and $d_2=0.5p$. The results from the numerical simulations are compared with the wind tunnel experimental data.

On Fig. 6 b) is presented the distribution of the relative induced axial velocity V_z/V_{tip} along the blade for the Miller model for 2000 RPM and $\theta=10$ deg for both the cylindrical and the contracting wake. The near wake is modeled with 20 vortex rings. The spacing parameters for both models are set to be $d_0=0.1p$ and $d_2=0.5p$.

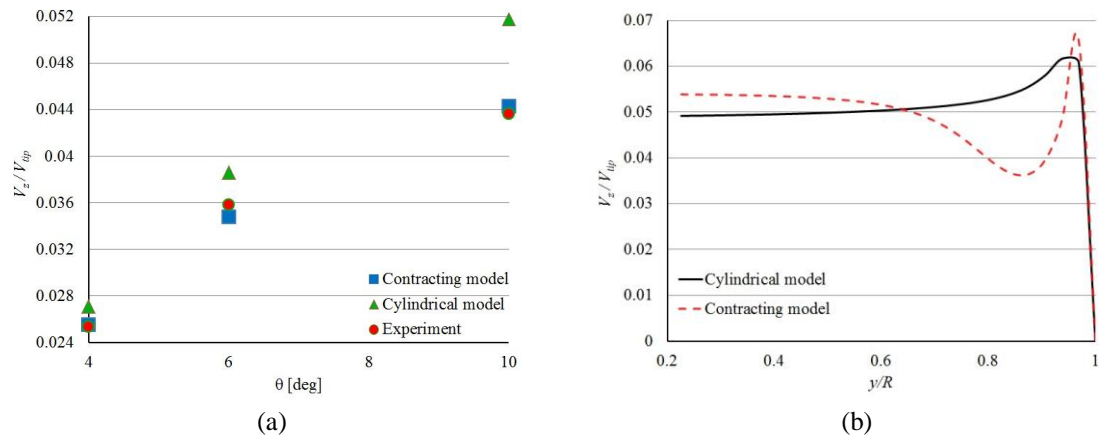


FIG. 6. The relative axial induced velocity V_z/V_{tip} . On Fig. 6 a) is presented the relative axial induced velocity V_z/V_{tip} , computed for 2000 RPM at blade-station $y/R=0.75$, in function of the pitch angle of the blades. On Fig. 6 b) is presented a comparison of the results for the relative axial induced velocity V_z/V_{tip} , computed along the blade for the cases of a cylindrical and contracting arrangement of the vortex elements.

In Table 1 are compared the relative axial induced velocity V_z/V_{tip} and the coefficient of thrust C_T for both arrangements of the vortex elements of the Miller model and the wind tunnel experiment for 2000 RPM and $\theta=6$ deg at blade station $y/R = 0.75$. Presented are also the percentage error $|\Delta|$ and the required computational time t_{comp} for both

simulations. The near wake is modeled with 20 vortex rings. The spacing parameters for both computations are set as follows: $d_0=0.1p$ and $d_2=0.5p$.

Table 1. Comparison of the results obtained with both arrangement of the vortex elements of the Miller model, against the wind-tunnel experiment data

Models	<i>Cylindrical wake arrangement</i>	<i>Contracting wake arrangement</i>	<i>Wind tunnel experiment</i>
V_z/V_{tip} [-]	0.03858	0.03479	0.03584
C_T [10^{-3}]	2.977	2.421	2.569
$ \Delta $ [%]	15.88	5.76	-
t_{comp} [s]	0.18	0.22	-

6. DISCUSSIONS ON THE RESULTS

From the numerical results for the flow-field, presented on Fig. 4, it becomes apparent that the optimal value for the placement of the semi-infinite vortex cylinder behind the last vortex ring d_2 , is the same as the spacing of the vortex rings in the near wake d_1 . This is due to the fact that the most uniform velocity field is formed for $d_2 = d_1$, which can be observed on Fig. 4 b) for $z/R = 3.3$ and on Fig. 4 e) for $z/R = 2.5$. It is also the only setting, for which the average computed value of the axial induced velocity V_z in the plane of the rotor $z/R = 0$ double its value in the far wake beyond $z/R = 5$, such as predicted by the theory for a rotor in hover.

Such as shown on Fig. 5 a), the optimal value of the initial displacement of the first vortex ring d_0 is found to vary approximately linearly with the pitch angle of the blades. Its value is approximately 1% of R for $\theta=4\text{deg}$ and rises up to about 3.5% of R for $\theta=12\text{deg}$. The non-linear nature of the spacing between the vortex rings modeling the near wake is shown on Fig. 5 b).

From the results, presented on Fig. 6 a), it becomes apparent that the contracting wake model provides a better accuracy over the entire range of studied pitch angle settings. However, the accuracy of the numerical results, obtained with both wake models, depends significantly from the correct choice of the spacing parameters d_0 and d_2 . When the near wake is modeled with 20 vortex rings the average value of the required computational time for the cylindrical wake model is $t_{comp} = 0.19$ s, while for the case of the contracting wake model t_{comp} increases slightly to 0.22 s.

From the results, presented on Fig. 6 b), it can be observed that the profile of the axial induced velocity distribution differs significantly between the two wake models. The contracting model induces slightly higher axial induced velocities inboard of the blade between sections $y/R=0.2$ and 0.6 , followed by a slight drop around blade station $y/R=0.8$ before rising again to form a peak toward the tip. In contrast, the cylindrical model induces an axial induced velocity distribution, which gradually increases from the root to the tip of the blade, while achieving a similar peak in both magnitude and position along the blade.

CONCLUSION

The accuracy and rapidity of the numerical approach for the computation of the performance of a model rotor in hover was evaluated with two vortex based models.

Based on the results from the performed studies, it can be concluded that the Miller model with contracting arrangement of the vortex elements is only slightly slower than the cylindrical wake model in terms of computational speed, while providing significantly higher degree of accuracy.

The existing percentage error $|\Delta|$ between the computational results and the experimental data for the axial induced velocity V_z is acceptable. Therefore, the contracting wake model can be used for preliminary studies and simulations of the expected thrust and overall performance of newly designed rotors.

FUTURE WORK

The results from the conducted studies, presented in this paper, encouraged the authors to use the Miller model with the contracting arrangement of the vortex elements, in order to study the thrust of small UAV rotors in unsteady operational condition. The intent is to perform a series of studies on the rotor performance during transient operational regimes, produced by both big and small rates of change in the angular velocity of the rotor Ω ; and for both positive and negative rates of change.

Of special interest is to study the changes in the thrust, resulting from a rapid change of the pitch angle of the blades θ for a constant angular velocity of the rotor Ω . Such a study will provide greater insights into the rotor performance during the transition period, in which the flow-field is adjusting to the new operational conditions of the rotor.

The future work on the model includes:

- To allow the numerical model to take into account the self-induced velocities of the vortex rings, which will in turn change the axial induced velocity V_z on the blade sections, thus redistributing the blade loads and affecting the bound circulation Γ .
- To allow the numerical model to dynamically change both the angular velocity of the rotor Ω and the blade pitch angle θ , thus allowing for the study of the dynamics of the rotor wake in the transition between different operational regimes of the rotor.
- To allow the possibility to vary dynamically d_0 in function of the computed blade loading and the pitch angle of the blades of the rotor.
- To introduce the real fluid viscosity effects by taking into account the actual vortex core radius r_{vc} , which will vary in function of both the axial and radial displacements of the vortex elements in the free wake.

REFERENCES

- [1] A. Karpatne, J. Sirohi, S. Mula and C. Tinney, "Vortex ring model of tip vortex aperiodicity in a hovering helicopter rotor", *Journal of Fluids Engineering, ASME*, vol. 136, 2014;
- [2] C. V. Velkova, *Modeling the Dynamic Behavior of Helicopter Rotors*, 2013-ENAM-0055, Paris, France, 2013;
- [3] V. I. Okulov, J. N. Soerensen and D. H. Wood, "The rotor theories by professor Joukowski: Vortex Theories", *Progress in Aerospace Sciences*, vol 73, 2015, pp. 19-46;
- [4] D. S. Jenney, J. R. Olson and A. J. Landgrebe, "A reassessment of rotor hovering performance prediction methods", *Journal of the American Helicopter Society*, Vol. 13, No. 2, April 1968, pp. 1-26;
- [5] A. J. Landgrebe, "An analytical and experimental investigation of helicopter rotor hover performance and wake geometry characteristics", *US Army Air Mobility Research and Development Laboratory, Technical Report 71-14*, Fort Eustis, Virginia, USA, June 1971;

- [6] A. J. Landgrebe, "An analytical method for predicting rotor wake geometry", *Journal of the American Helicopter Society*, Vol. 14, No. 4, October 1969, pp. 20-32;
- [7] R. H. Miller, "Rotor hovering performance using the method of fast free wake analysis", *Journal of Aircrafts*, vol. 20, 1983;
- [8] R. H. Miller, T. W. Roberts and E. M. Murman, "Computational methods for wake modeling and blade airload determination in hover and forward flight", *Computers and Mathematics with Applications*, vol. 12A, 1986;
- [9] K. R. Reddy, "The vortex flow-field generated by a hovering helicopter", 7th Australasian Hydraulics and Fluid Mechanics Conference, Brisbane, Australia, 18-22 August 1980;
- [10] J. Chattot and M. E. Braaten, "Wind turbine pitch change simulation with helicoidal vortex model", ASME, Turbo Expo 2012: Turbine Technical Conference and Exposition, Volume 6: Oil and Gas Applications; Concentrating Solar Power Plants; Steam Turbines; Wind Energy, pp. 789-796, June 2012, Copenhagen, Denmark, doi:10.1115/GT2012-68294;
- [11] S. Gupta and J. G. Leishman, "Accuracy of the induced velocity from helicoidal vortices using straight-line segmentation", *AIAA Journal*, Vol. 43, 2005;
- [12] W. Johnson, "Comparison of Calculated and Measured Model Rotor Loading and Wake Geometry", NASA, TM 81189, USA, 1980;
- [13] J. G. Leishman, *Principles of Helicopter Aerodynamics*, 1st ed., New York: Cambridge University Press, 2000, pp. 43-44;
- [14] R. I. Lewis, *Vortex Element Methods for Fluid Dynamic Analysis of Engineering Systems*. New York: Cambridge University Press, 1991, pp. 147-170.

CONCEPTUAL METHOD OF NAVIGATING AND CONTROLLING A DRONE

Marius PANDELEA^{*}, Mircea BOȘCOIANU^{**}, Mădălina-Marina FRĂȚILĂ^{*},
Victor VLĂDĂREANU^{*}

^{*}IMSAR, Bucharest, Romania (marpius65@yahoo.com)

^{**}”Henri Coandă” Air Force Academy, Brașov, Romania (boscoianu.mircea@yahoo.com)

DOI: 10.19062/2247-3173.2017.19.1.17

Abstract: *The main purpose of this paper is to present a conceptual method of navigating and controlling a quadcopter that aims to reach its destination, avoiding obstacles in the workspace. Another objective is to test the efficiency of the method on a simulator. Drone flight control is a major action that determines the safety and the accomplishment of the missions. The method involves setting the flight altitude by comparison with the height of the obstacle, and avoiding it, in the case of detection of an obstacle on the flight path. All drone subsystems must receive and transmit information so that the interaction between them be fully coordinated in order to increase the working capacity of the drone. In the case of a drone fleet, their interoperability is of utmost importance alongside the knowledge of the real situation in the workspace. Efficient cooperation implies that the information gathered by one of the drones to be readily known by all fleet drones, and so along with the strategic level information, the capacity of the entire military structure to have a greater degree of autonomy and mobility.*

Keywords: *drone; navigating and controlling method; workspace; obstacles.*

1. INTRODUCTION

In the world we live, the rationale human being involves scientific knowledge, control and also the management of the action plans, so that the performances achieved to ensure the progress of the society and the individual life.

Integrating scientific research into the processes of existential action is a mean and a priority, as well, determined by the proposed goal and without which we will not be able to live better [1]. In a society dominated by technology, where humanity's demands are growing, ideas are merging and developing in an accelerating rate, which requires a balance between existing natural capacities and needs. Drones become more and more frequent in our life and as a result the field is of interest and must be treated with much responsibility and attention [2,3].

The proposed method is part of the research directions assumed by report no. 1 of 2015 of the MASIM project, respectively, from the miniaturized aerial platforms algorithms, whose concept belongs to "sense and avoid" strategies for avoiding fixed obstacles [4].

The MASIM project - "Multi-Agent Aerial System with Mobile Land Information Management Station" proposes an innovative solution for finding the necessary information to solve in real-time a situation by means of a fleet of autonomous mini-platforms, coordinated from the ground by a mobile station with command and control function.

The complexity and novelty of the MASIM system is determined by the innovative concept, the architectural structure and the complexity of the components, combined with smart management. At the same time, the testing of the research results at the integrated system level offers value to the MASIM project. [4]

2. DRONE NAVIGATION AND CONTROL

Drone is the popular name of unmanned multi-rotor aircraft, being considered in modern literature as the modern version of the hot air balloon. The scientific term of these complex systems is the UAV, comes from the English (Unmanned Aerial Vehicle) and defines unmanned aerial vehicles driven from a distance by human beings or capable of autonomous operation by a digital automatic pilot.

The main using areas of the drones are: military (security and safety, recognition etc.) and non-military or civil (commercial, health, agriculture, logistics, entertainment etc.). Thus, at present there are drones used for shooting, product delivery, surveillance, mapping etc.

The general architecture of a drone is presented in fig. 1 and the typical flight control loops for a multi-rotor are presented in fig. 2 [5].

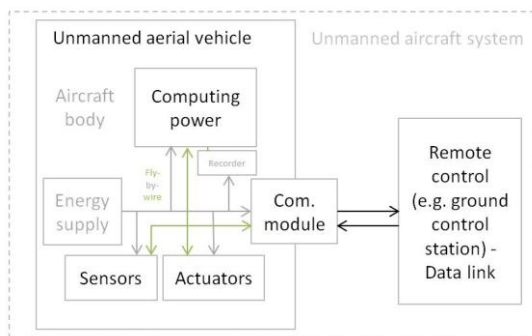


FIG. 1 General physical structure of an UAV

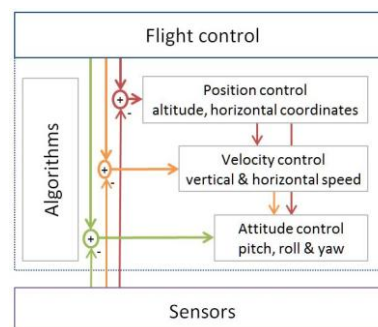


FIG. 2 Typical flight-control loops for a multi-rotor

The Federal Aviation Administration (FAA) of the US Department of Transportation announced at the end of March 2017 over 770,000 drone owners for hobby, estimating more than 1.1 million units. In the future, by 2021, this number is expected to reach 3.55 million, with an annual average growth rate of about 26.4%.

Regarding non-hobby models, the FAA has much higher expectations that the fleet would grow at an even faster rate. If in 2016 the number of drones was rather low due to strict regulations, about 42,000 units, the fleet is expected to grow at an annual average of 58.6% by 2021 (442,000 units), given that the regulations have been improved.[6]

The navigation system of a drone is divided into three main modules:

- research, detection and determination of initial parameters;
- route planning;
- movement control.

There are numerous experiments that have clearly indicated that the error of measuring the distance between the drone and the obstacle depends on the size, shape, physical structure of the obstacle material, the ability to reflect light, the degree of finishing of the outer surface/roughness or environmental parameters.

Flight controller is one of the most important part of the drone, being basically the element that reads all the sensor data, organizes and conducts the flight, continuously calculating according to an algorithm and passing the best commands to the other components so that the drone can successfully complete its mission. Remote sensors are indispensable components of a drone to fulfil the mission and the safety requirements.

Distance sensor orientation is made in several directions, respectively vertically downwards as the drone flight involves, on the one hand, altitude to eliminate impact with the ground, but also horizontally, on the other hand, for the detection of the fixed obstacles situated on the flight route, to avoid them.

The workspace is framed into a three-dimensional axe system comprising three elements: the starting position of the drone, the fixed obstacle (elementary geometric object) and the end position of the drone (finishing point).

In our case study, we will neglect air friction and all environmental factors, and the flight will be considered horizontally parallel with the ground after the drone reached the necessary altitude.

The drone will be considered as a point that has to move from the starting position to the final position. The dimensions are virtually reduced to its mass centre. Its mission does not end to the final position and the drone has to return to the starting position. The back route is not the subject of the present study.

The fixed obstacle can have a multitude of shapes, whether convex or concave. In this paper we will study the parallelepiped rectangular obstacle, with a convex body, whose dimensions are comparable to each other.

3. THE CONTROL ALGORITHM

The logic scheme of the flight algorithm of the drone moving into the three-dimensional workspace is shown in fig. 3.

The algorithm compares the z_B value of the destination point with the L_3 value of the obstacle, ie the altitude of the target point with the obstacle height.

If $z_B > L_3$ the drone rises to the z_B altitude and flies in a right line parallel to the ground to the point B (target).

If $z_B \leq L_3$ the conceptual navigation scheme of fig. 4 will be used because there is an obstacle on the drone route. In this case, the control algorithm of a plane flight is reported to a two-dimensional reference system and the drone route can be seen in fig. 5.

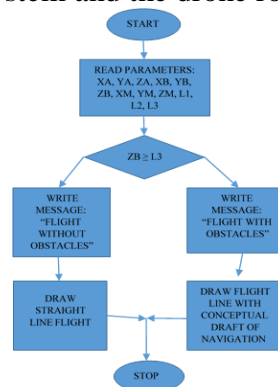


FIG. 3 Schematic block diagram of the drone flight

Navigation and control conceptual scheme in case of an existing obstacle has the following graphic representation [7,8]:

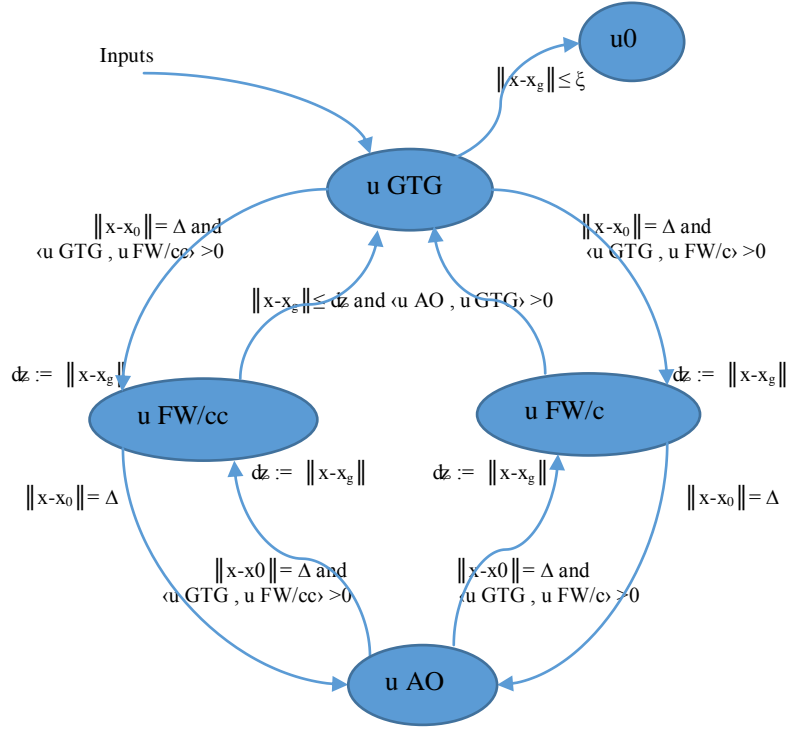


FIG. 4 Navigation and control conceptual scheme in case of an existing obstacle

where: u_{GTG} is the vector from the starting point of the drone to the goal, u_{AO} is the vector to avoid obstacle, $u_{FW/c}$ is the vector follow wall in clockwise direction, $u_{FW/cc}$ is the vector follow wall in counter clockwise direction, u_0 is the vector STOP when the drone arrives to the goal ($u = 0$), x_0 = initial position, x_g = position of the goal, d_z is the distance to the goal.

Behaviour of a the drone flight towards a goal is represented by a schema of a hybrid automaton with many guard conditions.

The flight stages include several commands:

- stage 1: go to goal,
- stage 2: navigating avoiding obstacle,
- stage 3: follow wall in clockwise or counter clockwise direction,
- stage 4: continue to the goal after avoiding obstacle,
- stage 5: repeat stage 2, 3 and 4 in case that another obstacle appears.

Around the obstacle we consider a line at Δ distance away from the obstacle, at which the drone need to change its trajectory and navigate avoiding obstacle.

The movement parameters are:

$$\begin{aligned}
 u_{GTG} &= K_{GTG} (x_{goal} - x), \\
 u_{AO} &= K_{AO} (x - x_{obst}), \\
 u_{FW} &= \alpha R_{(\pm\pi/2)} u_{AO}, \\
 R(\theta) &= \begin{bmatrix} \cos \theta & -\sin \theta \\ \sin \theta & \cos \theta \end{bmatrix} - \text{rotation matrix.}
 \end{aligned}$$

The drone trajectory meets Δ line and now the automaton schema starts working.

These two formula of inner product represents control laws to avoid obstacle clockwise or counter clockwise:

$$\langle u_{GTG}, u_{FW}^C \rangle = \|u_{GTG}\| \|u_{FW}^C\| \cos(\theta_{GTG,FW})$$

$$\langle u_{GTG}, u_{FW}^{CC} \rangle = \|u_{GTG}\| \|u_{FW}^{CC}\| \cos(\theta_{GTG,FW}).$$

The point where the drone meets the Δ line is represented in the next figure.

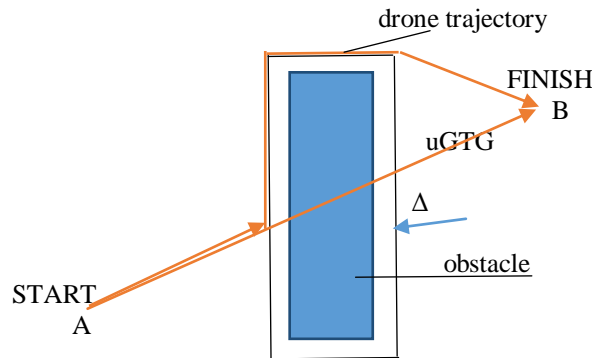


FIG. 5 Drone trajectory

The main term of this equation is the angle θ between the two vectors u_{GTG} and u_{FW} , which determines the clockwise or counter clockwise direction in which the drone flight will follow wall to avoid the obstacle.

Going closer to the goal determines the return to the automaton and restarting the stages of the schema.

When the two conditions are satisfied:

$$\|x - x_g\| \leq d_z \text{ and } \langle u_{AO}, u_{GTG} \rangle > 0$$

the drone will switch back from follow wall to go to goal, where d_z is the distance to the goal.

In case of encountering another obstacle the drone will start the whole process again.

4. SIMULATION RESULTS AND CONCLUSIONS

However to get a better result, an experimental method is preferable and we will use a simulation environment in which to test and view the results of various inputs and controllers.

In our case we will use DroneKit-Python, which is an open-source project and communicates with vehicle autopilots using the MAVLink protocol. The kit version 2.9.0 offers the opportunities which we need to test the proposed conceptual method [9].

In the MASIM project, communication between the aerial vectors and the base (or between them) is done by radio transmission, MavLink protocol. Transmission of feeds (video, sensors etc.) is done through an industrial power WI-FI network, in which base and drones are access points. [3]

On Quick Start the application and then we launches the simulator. Vehicle state information is exposed through vehicle attributes which can be read and observed (and in some cases written) and vehicle settings which can be read, written, iterated and observed using parameters (a special attribute). The proposed method is a simple one and the results legitimize its use.

This paper illustrates a simple way of navigating and controlling a drone. The drones will definitely be more and more present in our everyday life and will occupy an important place taking into account the current trends.

Our research will continue aiming a better understanding of the phenomenon, as well as an increasing progress in this area. The current application also presents ample opportunities for future research in a wide array of connected fields, of which several possibilities, such as virtualisation, terrestrial robot cooperation and complex decision systems [10,11], are already being investigated.

That is why, in the near future, we will model and simulate cases where the fixed obstacle will be: a cylinder, an ellipsoid, a pyramid or a rigid in suspension. We can say very sincerely that we, the research team, have found a model and its algorithm for a drone flight from the start point to a final target avoiding a fixed rectangular parallelepiped obstacle.

These things must be presented and communicated in order to be known hoping that they will be appreciated and developed in the future, so that the results can provide a real breakthrough to the problems faced in this field nowadays.

ACKNOWLEDGMENT

This work was accomplished through the Partnerships Program in priority fields - PN II, developed with the support of MEN-UEFISCDI, PN-II-PT-PCCA-2013-4-1349, MASIM project no. 255/2014.

REFERENCES

- [1] G. Chamayou, *A Theory of the Drone*, The New Press, 2015;
- [2] Bevacqua, G., Cacace, J., Finzi, A., & Lippiello, V. (2015, April). *Mixed-Initiative Planning and Execution for Multiple Drones in Search and Rescue Missions*. In ICAPS (pp. 315-323).
- [3] Gregory, D. (2011). *From a view to a kill: Drones and late modern war*. Theory, Culture & Society, 28(7-8), 188-215.
- [4] MASIM project - "Multi-Agent Airsystem with Mobile Land Information Management Station";
- [5] https://en.wikipedia.org/wiki/Unmanned_aerial_vehicle
- [6] <https://www.faa.gov/> .
- [7] *Control of Mobile Robots* - Course, Georgia Institute of Technology, 2017;
- [8] B. Siciliano, O. Khatib - *Springer Handbook of Robotics*, 2nd Edition, Springer-Verlag, 2016;
- [9] <http://python.dronekit.io/> ;
- [10] Şandru, OI; Vlădăreanu, L; Şchiopu, P; Vlădăreanu, V; Şandru, A, *Multidimensional Extensics Theory*, University Politehnica Of Bucharest Scientific Bulletin-Series A-Applied Mathematics And Physics, Vol 75 /1, pg: 3-12, 2013
- [11] Vlădăreanu, V; Dumitrache, I; Vlădăreanu, L; Sacală, IS; Tonţ, G; Moisescu, MA, *Versatile Intelligent Portable Robot Control Platform Based on Cyber Physical Systems Principles*, Studies In Informatics And Control, Vol 24 /4, pg: 409-418, 2015

RISK MANAGEMENT REGARDING THE USE OF UAV IN THE MODERN AIR SPACE

Sebastian POP*, Octavian ISAILĂ**, Dragoș PREDA**, Andrei-Mihai LUCHIAN*

*Transilvania University of Brașov, Romania (aerodrone.uav@gmail.com,
riesigen@gmail.com)

**ITSC-SVFP of Mediaș, Romania, (office@vehiculefarapilot.ro, dragos.preda@
vehiculefarapilot.ro)

DOI: 10.19062/2247-3173.2017.19.1.18

Summary: Aviation is the domain with one of the greatest technical developments. Thus the emergence and development at the consumer level of commercial UAVs has put the entire aerospace industry and national security system in front of a fulfilled fact. These unmanned human onboard systems and the continuous development of hardware and software systems are currently creating one of the biggest challenges: integration in airspace.

The article reviews the risks, threats and concepts of illegal use of the drones.

Key words: UAV, air space, risk management, NOTAM

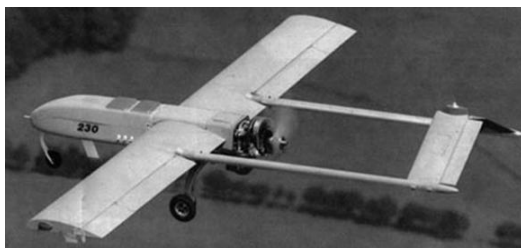
Acronyms and symbols

RPAS	- remotely piloted aerial system	NOTAM	- Notice To Air Man
UAV	- unmanned aerial vehicle	SAR	- synthetic aperture radar
E/VLOS	- extended/ visual line of site	ATC	- air traffic control
BVLOS	- behind visual line of site	ADSB	-Automatic Dependent Surveillance, Broadcast
NBC	- nuclear, biological and chemical	IED	- Improvised Explosive Device

1. INTRODUCTION

1.1. Theoretical landmarks on UAV.

Technological advances in aeronautics, particularly through system miniaturization, have led to a new system-level approach, generating innovative solutions for the technical and management part. According to the references, the UAV field at national [1, 4] and international level, [5, 6, 7, 8] for both civil and military [2, 3] offers a number of modern technical solutions, see Figure 1.



(a)



(b)

FIG. 1 The UAVs, a. AAI RQ- 7 Shadow 200, b. Altair (NASA) [8]

1.2. Air space classification

The use of UAVs in airspace involves aviation safety issues and optimal air traffic management, so it is necessary for UAV operators to know the classification of airspace and the existing restrictions. Depending on the altitude and the distance from the airport, airspace is spread over several areas as shown in Figure 2.

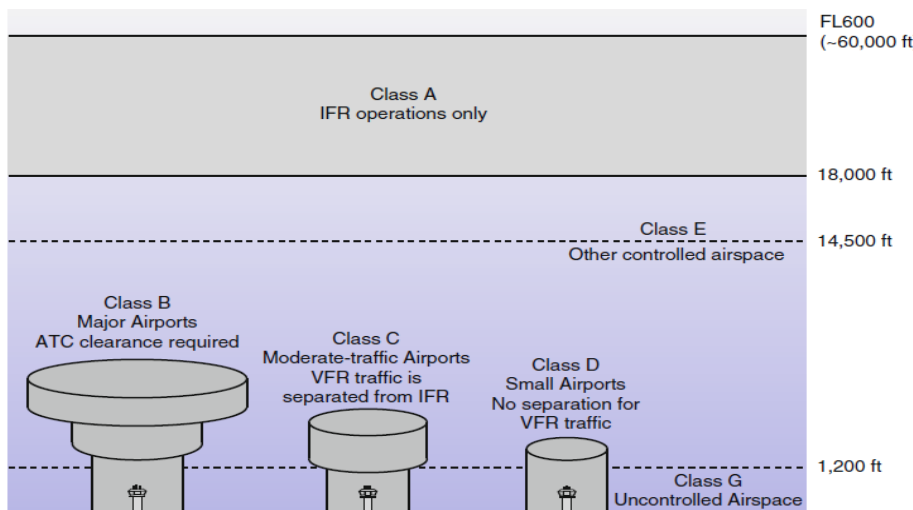


FIG. 2. Air space classification

2. RISKS AND POSSIBLE THREATS IN USING UAV'S

The field of aviation is one of the greatest technical developments. Thus the emergence and development at the consumer level of commercial UAVs has put the entire aerospace industry and national security system in front of a fulfilled fact.

These unmanned human onboard systems and the continuous development of hardware and software systems are currently creating one of the biggest challenges: integration in airspace. The benefits of using UAVs have been demonstrated in a variety of areas: Critical Infrastructure Inspection and Surveillance, Agriculture applications, SAR, law enforcement, and applications that would normally be considered too dangerous to be operated by aircrafts with a human pilot on board.

In addition, the implementation of any technical system, in addition to its benefits, cannot be free of both technical and human risks, so UAV incidents will occur irrespective of the measures taken, requiring a number of regulations and technical solutions to limit the risks [10, 11, 12].

2.1 Collision with an aircraft with human staff on board or UAV

One of the most common problems that may arise in operating the UAVs in the airspace is the possibility of collision with an aircraft carrying personnel on board or the collision between two UAVs. Depending on the impact force, the masses of the aircraft and their structure (fixed wing or rotating wing), this can materialize by destroying one or both aircraft. The fact that a UAV can be in flight in one of three situations: VLOS (visual line of site) is operated in the visual range; EVLOS (extended line of site) where the operator is assisted by an external operator at the limit of the visual range; BVLOS (behind visual line of site) where the UAV is only piloted instrumentally and far exceeds the visual range. These situations call for a set of measures both on the part of the authorities and on the part of the UAV operators as follows: announcement of the flight to the Air Operations Center as well as establishing a link with the traffic unit if the flight takes place in the classroom B, C, D.

In the case of VLOS flights, it is necessary: an observer to monitor airspace visually; the deployment of ADSB (Automatic Dependent Surveillance - Broadcast) systems that connects to the UAV's Fail Safe system which can make decisions to correct the trajectory much faster than the operator response.

In the case of BVLOS flights, it is essential to set up TSA segregated areas whose presence is announced for at least 24 hours via the NOTAM (Notice to Air Man) system.

2.2 Impact on soil with an object on the ground or with people

This event may occur for several reasons, such as: an air collision between a UAV and another aircraft or birds; the release of material or electronic elements; deliberate destruction by anti-aircraft combat means; terrorist attacks.

In the diagram below you can see the components that lead to a ground impact and impact result. The frequency of incidents can be calculated using the following equation:

$$f_F = A_{exp} \cdot \rho \cdot p \cdot f_{GIA} \cdot f_{shelter} \tag{1}$$

Where:

f_F – represents the frequency of incidents;

A_{exp} - The area in which the incident occurred;

ρ – Population density in the area;

p (*fatality/exposure*) – depends on the strength of the human body at impact as well as the resistance of shelters;

f_{GIA} – Rate of ground impact;

$f_{shelter}$ – are marked with values from 0 to 1 where 0 represents the fact that all persons are housed and 1 represents that no person is housed.

Following the conducted studies, it has been established that a minimum level of ground impact safety would correspond to a value of 95 KJ. For the kinetic energy limits and the end of flight method, two collapse scenarios, depending on the type of UAV, should be considered as follows:

-for UAVs (fixed wing or multi-copter type) capable of developing a high horizontal travel velocity, the kinetic energy assessment will be performed for the maximum impact velocity (established as $1.4 \times V_{max}$ that can be achieved in flight horizontally);

-for all multi-copter UAVs, the kinetic impact energy will be evaluated for a free fall of 400 ft. Thus, for the above data and the weight of the aircraft, the kinetic energy of the impact can be calculated, see Table 1.

Table 1 Kinetic energy

Weight RPA	Max speed - Hconst (Vmax)	Impact speed 1.4 x Vmax	Cinetic energy of impact speed	Weight RPA	Max speed - Hconst (Vmax)	Impact speed 1.4 x Vmax	Cinetic energy of impact speed
Kg	Kts	m/s	KJ	Kg	Kts	m/s	KJ
1	70	50	1	50	70	50	64
2	70	50	3	60	70	50	76
3	70	50	4	70	70	50	89
4	70	50	5	75	70	50	95
5	70	50	6	80	68	49	95
10	70	50	13	90	64	46	95
15	70	50	19	100	60	44	95
20	70	50	25	110	58	42	95
25	70	50	32	120	55	40	95
30	70	50	38	130	53	38	95
40	70	50	51	150	49	36	95

2.3 The possibility of carrying out terrorist and smuggling acts (illicit shipments):

The availability of the general public to the constructive elements of a UAV, as well as some incidents that have taken place lately, jeopardize the use of these systems for committing terrorist attacks. Thus we can list some incidents as follows:

- USA 2011 - 26-year-old Rezwan Ferdaus is arrested for planning an attack on the Pentagon building with a radio commanded model [13];
- In January 2015, a Phantom DJI multi-copter collapses on the white house's lawn. Fortunately, the incident was due to a technical failure known as flyaway, [14]
- USA 2015 - ElMehdi Semlali Fahti is arrested for planning an attack on a school and on a governmental institution, [15]
- September 2013 a Parrot drone succeeds to approach German Chancellor Angela Merkel, [16];

3. CONCEPTS ON ILLEGAL USE OF DRONES

Public disorder: It is manifested by violation of private property, the emergence of UAV's at various public events, and is manifested by a low risk, in most cases being done by "terrible" people or by children.

Airspace interference: The lack of clear and applicable legislation at the moment creates the prerequisites for the use of the drones in different airspaces, thereby endangering air traffic. In recent years, a number of incidents have been reported in which there was an assumption of an air accident between UAVs and onboard aircraft.

Illegal monitoring: One of the most notable threats is the use of UAV's for illegal monitoring in various areas of private or governmental interest. The current capabilities of the hobby platforms (DJI, 3DR) 4k camcorder, zoom, live HD transmission, full autonomous flight have brought this technology from the prohibitive area of information structures to the public area, making it very difficult to identify what the mission is Each system and the information that collects them.

Accident risk: UAV is a real danger to people and goods on the ground. In addition to the human or material damage that can be generated by the impact, there is also the risk of fires due to the Lithium-Polymer batteries used by these flight systems, see Figure 3.



FIG. 3 Damage caused by UAVs



FIG. 4 Taser drone [17]

Contraband and transport of illicit materials: UAVs can be used as a smuggling cargo transportation system. Their use allows criminal groups or terrorist organizations to avoid classical security systems. Often, attempts to place goods with drone in prison are reported.

Non-lethal weapons: While non-lethal weapon use is not associated with criminal activities, it is already used by security structures. The provision of drones with rubber bullets, tear gas, or electro-shock weapons are applications that can be used by the police or the gendarmerie. An example is the Chaotic Moon drones that were equipped with a 80000V Taser type system, see Figure 4, [17].

Dead weapons: With a minimum of effort, these drones can be equipped with a lethal weapon like a gun, a flame thrower. The electronics with which they are equipped allows for the realization of different control systems, and the association with visual recognition software can create a threat to be considered, see figure 5, [18].



FIG. 5 UAV equipped with UZI machine guns, [18].

NBC (Nuclear - Biological - Chemical): Weapons of mass destruction are a real danger in today's geopolitical context. Thus, a UAV equipped for the transport of such substances can become very "effective" at this time for terrorist structures. Failure to be immediately detected as a dangerous system, as well as the distances that can be traversed, creates a security issue at the moment.

IED (Improvised Explosive Device): Terrorist structures have so far shown enough ingenuity in the placement of explosive material. So using a drone for an assault becomes a viable thing and you can ask yourself: when and where this will happen, [20].

Radio electronic attack: A particular case of criminal use of UAVs is to equip them with electronic devices that can connect to WIFI or GSM systems and collect data. These equipment are called Snoopy can penetrate any radio data system, [19].

4. CONCLUSIONS

The article addresses a new field of interest, an area that until recently was exclusively the prestige of the specialized military structures for anti-aircraft defense. To deepen the scope of my own research I propose to study a miniaturized airborne robot recovery system that meets current security requirements and addresses the micro UAV category for civilian use. For this I will go through the following steps: analysis of target acquisition methods represented by miniaturized airborne robots both wing-type wing systems and fixed wing systems; analysis and simulation of methods of intercepting aerial targets such as miniaturized aerial robots; the development of an airframe model with a fixed wing interceptor; analysis of the interception phase; the realization of an experimental model (for launching a recovery net and a recovery parachute).

ACKNOWLEDGEMENT

The National Authority for Scientific Research, Romania supported this work – CNCS-UEFISCDI: PN-II-PT-PCCA-2013-4-1349, MASIM project “*Multi Agent Aerial System with Mobile Ground Control Station for Information Management*”, contract 255/2014.

REFERENCES

- [1] Prisacariu V., Cîrciu I., Luchian A., *Unmanned aircraft vehicle (UAV) in the Romanian airspace. An overview*. Journal Of Defense Resources Management, vol.4 issue 1(8)/2014, ISSN:2068-9403, eISSN:2247-6466, ISSN-L: 2247-6466, p123-128;
- [2] Prisacariu V., *The UAVs in the theatre of operations and the modern airspace system*, RECENT Journal, 3 (39)/2013, Transilvania University of Brasov, Romania, ISSN 1582-0246, p. 169-180;
- [3] Prisacariu V., Muraru A., *Unmanned aerial system (UAS) in the context of modern warfare*, Scientific Research And Education In The Air Force-AFASES 2016, Brasov, DOI: 10.19062/2247-3173.2016.18.1.23, ISSN 2247-3173, p. 177-183;
- [4] Prisacariu V., Cîrciu I., Cioacă C., Boşcoianu M., Luchian A., *Multi aerial system stabilized in altitude for information management*, REVIEW OF THE AIR FORCE ACADEMY, 3(27)/2014, Braşov, Romania, ISSN 1842-9238; e-ISSN 2069-4733, p 89-94;
- [5] Reg Austin, *Unmanned Aircraft Systems UAVs design, development and deployment*, Aerospace Series, ISBN 978-0-470-05819-0, 2010, 365p;
- [6] UAS Yearbook, *Unmanned aircraft systems – The Global Perspective 2011/2012*, Blyenburg & Co, june 2011, Paris, ISSN 1967-1709, 216 p., available at www.uvs-info.com;
- [7] Suraj G. Gupta, Mangesh M. Ghonge, Dr. P. M. Jawandhiya, *Review of Unmanned Aircraft System (UAS)*, International Journal of Advanced Research in Computer Engineering & Technology (IJARCET), Volume 2, Issue 4, April 2013, ISSN: 2278 – 1323, p1646-1658;
- [8] <http://www.trade.gov/td/otm/assets/aero/UAS2011.pdf>, accessed at 12.05.2017;
- [9] <https://www.unmannedtechshop.co.uk/ping-rx-ads-b-receiver-for-uavs/>, accessed at 12.05.2017
- [10] EASA, Introduction of a regulatory framework for the operation of unmanned aircraft, Technical opinion, Related A-NPA: 2015-10 —RMT.0230—18.12.2015, 50p, available at <https://www.easa.europa.eu/system/files/dfu/Introduction%20of%20a%20regulatory%20framework%20for%20the%20operation%20of%20unmanned%20aircraft.pdf>
- [11] Global Aerospace, UNMANNED AVIATION RISK MANAGEMENT, ACCIDENT PREVENTION AND INSURANCE, available at http://www.global-aero.com/wp-content/uploads/2015/10/GA135_Whitpaper_Template_Screen_Version_r9.pdf;
- [12] Prisacariu V., Pop S., Cîrciu I., *Recovery system of the multi-helicopter UAV*, REVIEW OF THE AIR FORCE ACADEMY, 1(31)/2016, Braşov, Romania, DOI: 10.19062/1842-9238.2016.14.1.13, ISSN 1842-9238; e-ISSN 2069-4733, p 92-98;
- [13] <https://www.theguardian.com/world/2011/sep/29/fbi-entrapment-rezwan-ferdaus>, accessed at 14.05.2017;
- [14] <http://www.bbc.com/news/technology-31023750>, accessed at 15.05.2017;
- [15] <https://www.investigativeproject.org/case/662/us-v-fathi> , accessed at 15.05.2017;
- [16] <https://arstechnica.com/information-technology/2013/09/german-chancellors-drone-attack-shows-the-threat-of-weaponized-uavs> , accessed at 15.05.2017;
- [17] <http://pix11.com/2014/03/09/texas-company-creates-a-drone-with-a-80000-volt-stun-gun>, accessed at 17.05.2017;
- [18] <http://www.dailymail.co.uk/sciencetech/article-2134024/FPSRussia-shows-flying-drone-fitted-machine-gun.html>, accessed at 17.05.2017;
- [19] Mears M.J., *Cooperative Electronic Attack using Unmanned Air Vehicles*, Wright-Patterson Air Force Base, AFRL/VACA, WPAFB, OH 45433-7531, USA, 2006, 10p, available at <http://www.dtic.mil/dtic/tr/fulltext/u2/a444985.pdf>;
- [20] Wallace R.J., Loffi J.M., *Examining Unmanned Aerial System Threats & Defenses: A Conceptual Analysis*, International Journal of Aviation, Aeronautics and Aerospace, vol.2, issue 4., 2005, p34.

MICROFIGHTER AS AN ALTERNATIVE TO FOURTH GENERATION FIGHTER PLANES

Mihai-Victor PRICOP^{*}, Mircea BOȘCOIANU^{**}, Cătălin NAE^{***}, Marius-Gabriel COJOCARU^{***}

^{*}Transilvania University of Brașov and National Institute for Aerospace Research, Bucharest, Romania, (pricop.victor@incas.ro)

^{**}”Henri Coandă” Air Force Academy, Brașov, Romania (boscoianu.mircea@yahoo.com)

^{***} National Institute for Aerospace Research, Bucharest, Romania, (nae.catalin@incas.ro, cojocaru.gabriel@incas.ro)

DOI: 10.19062/2247-3173.2017.19.1.19

Abstract: *The paper presents an affordable low observable concept for a very light strike-fighter plane, using a mixture of high and low tech. Currently for a small defense budget, trying to comply with leading military standards enables a small number of fourth generation warplanes, typically degraded with respect to essential capabilities such as air defense and deep strike, due to the restrictions in purchase of high performance weaponry. A solution is to eliminate standard compliance and adopt cost effective solutions, based on a mix of proven items and newly emerging technologies, in an attempt to obtain better solutions than degraded fourth generation warplane as available on the market.*

Keywords: *microfighter, super cruise*

1. NATIONAL HISTORICAL BACKGROUND

Romania was one of the few countries producing fighter planes during the Second World War, namely IAR-80. Although the general performance has been decent around 1941, there has been no significant upgrade during the production/operation. Other warplanes benefited from a significant power/armour/weapons growth during their production life, increasing the effectiveness, so that at the end of the production, around 1944, IAR-80 and its dive bombing variant IAR-81 have become largely obsolete for air defense, while the lack of armour made ground attack a hazardous mission, although the firepower proved to be very good. Around 350 have been produced and were flown until 1952 as trainers. The attempt to install a larger engine failed due to war related procurement constraints, while technically was achievable, **FIG. 1** (a).

During the cold war a joint development/production process took place with Yugoslavia, resulting in IAR-93/J-22, which essentially is a ground strike fighter. For the Romanian version the weapon system was poor, somehow at the level of Mig-17 which IAR-93 was supposed to replace. Unguided only munitions were planned and the reliability of the hydraulic system was low, although this was eventually solved. About 80 airplanes were inducted into service and they have been mothballed in 1998 after a crash and phased out in 2000 under difficult economic-political conditions [1].

The decision to axe such a large number of essentially new airplanes was largely wrong and today such a plane would still be valuable given the new generation of smaller precision guided munitions and the small price of up to date avionics systems. A “scientific” justification has been carefully prepared [4] in order to upgrade Mig-21 to what is known today as Lancer. The author of [4] seems to judge airplane performance with invented numbers as measure of their efficiency, being unaware about the outcome of Falkland and Bekaa Valley aerial battles already a decade before the report issuing date. The effectiveness of Mig-21/32 or Mirage III/Dagger, with rear aspect launching IR missiles was essentially zero against fourth generation fighters armed with all aspect IR missiles. Therefore, a cost effective solution at that time was the simple replacement of the old missiles, keeping the line of sight aiming procedure, as described in [5]. The author of [4] paved the way of upgrading 75 Mig-21 as ground strikers, eliminating IAR-93 from the air force and sending to scrapyard all related human/hardware investments. The ground strike capabilities of IAR-93 and its low level behavior were much beyond those of Mig-21, as proven in a number of exercises [1], not to mention the 2.5 times larger payload. In contrast with IAR-93, the Serbian program Orao 2.0 is a good example of what this warplane would become under a good management **FIG. 2** (b).

The inheritance from IAR-80 and IAR-93/99 programs consists in a number of five manufacturing companies (three state owned, two private) and a number of research establishments covering aerodynamics, propulsion (state owned) plus avionics (private), having the potential to resume the development of an indigenous very small fighter plane. In addition there are a number of RR-Viper 632 engines left from IAR-93 program, which are to be cleared of the afterburner system for the potential micro fighter.

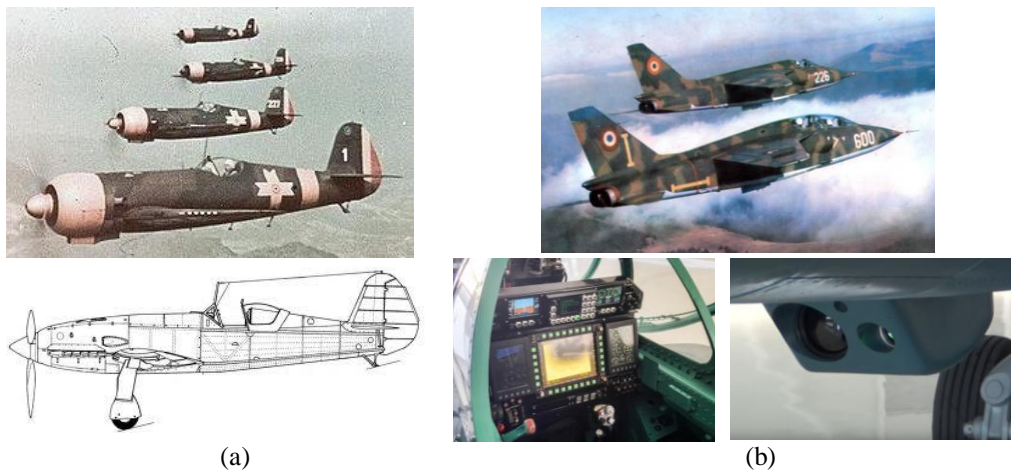


FIG. 1 IAR-80 standard top, upgraded down (a), IAR-93 top, upgraded Orao 2.0, down (b)

2. GENERAL REQUIREMENTS

The most stringent requirement is to come up with a solution that would preserve the air force existence, its mass, its flight academy and resolve the shortcomings of Mig-21 and F-16 platforms. A partial solution is the adoption of second hand F-16 AM/BM, which as they are equipped are obsolete when compared with up to date Russian warplanes (Su-30, 34, 35, Mig-35), all employing advanced electronically scanned radars and electronic warfare capabilities [12,13,14]. This purchase represents a typical degraded fourth generation package, criticized as cost ineffective in [2], backed by a tiny amount of almost obsolete weapons.

Although a very limited platform, Mig-21 maintenance is mastered at national level, making the airplane supportable in significant numbers, in contrast with F-16, for which there is no national maintenance/upgrade capability, but has much longer lifecycle.

The national air force lost the mass from 350 warplanes (most at very small effectiveness) at the end of the cold war to about 10% of that [3], which is not acceptable.

Considering Mig-21 as the airplane to replace, its main weakness is the combat persistence: range/endurance plus very small payload, specifically in air defense. In realistic conditions it is operated with two under wing tanks and two IR AAM missiles, which by today's standards is not acceptable.

A notional sensor system should be based on: low power/small size mechanical/AESA/hybrid radar, EO turret ventral placed for air to air and air to ground, optical distributed aperture system plus modems to support data exchange with other platforms and weapons in *lock after launch mode*. Such a system would provide an intrinsic reconnaissance capability of moderate performance, since it is not possible to accommodate a large diameter optical system.

A notional weapons package consists in a single outer shape weapon family, covering air to air and air to surface. Two main weapons could be developed: missile and bomb. They use the same foldable rear control fins, actuation, part of navigation system and only exhibit different homers and warheads.

A review of the jet age local wars and war games (Red Flag) shows what was basically learned in WWII. Victories are obtained mostly because of victims' lack of situational awareness. When the technical disparity is very large, in a low density environment (F-14/AIM-54 vs Mig-21/R-13 as in Iran-Iraq war), results are in the favor of technical superiority. If the smaller fighter would have LO and RF awareness capabilities, the BVR engagement would be mostly denied, bringing the fight to close distance, on more equal terms. In a high density environment the technical superiority advantages are largely denied.

A decent radar (in the class of ELTA-2032), as it is part of current inventory is ruled out from the current concept, because of size, weight, cooling requirements, radio frequency noisy operation. Modern radar warning systems and data links could in part compensate for a radar. A radar should provide just enough range to enable full envelope exploitation of the AAMs, since an integrated RWR/modem could provide the tactical picture to reduce radar performance/cost, added constraints. Given the fact that the AAMs on the current platform are in between R-60 and AIM-9X Sidewinder, the tracking range for a fighter like target (F-16, RCS 3m^2) should not be larger than 20 Km. The notional AAM will rely on a combination of IR homing system and INS/modem for *lock after launch* procedure, in order to maximize the range and probability of kill. For this purpose do contribute the aerodynamic cleanliness of the weapon, as there are no rail jugs, there is a pyramidal optical dome, there are only rear fins.

Given the existing engine (RR-Viper 632) with its high fuel consumption, it only makes sense to have a fast aircraft, ideally a super cruiser. The specific thrust of the engine is just high enough to enable super cruise. Its afterburning device (long tube, variable section nozzle, hydraulics) weights around 120 Kg, produces additionally 400 daN, has an unacceptable impact on the airplane design and therefore cannot be used. The largest inconvenient is the length it adds, which compromises the design. Another candidate engine is the GE J-85, although the maximum thrust is even smaller. However, its nominal thrust is smaller than Viper's, which remains the first option.

Functionality	Mig-21 Lancer	F-16 Block 15	Microfighter
Low observability	fairly good, due to small size	decent	high
Supercruise	no	combat irrelevant	yes
Manoeuvrability	decent	excellent	decent deliberately, to increase combat persistence
Climbing speed	decent	excellent	decent
After burner engine	yes	yes	no
Endurance	low	middle	middle
Capability to fight at supersonic speeds	not practical, over 5000m, severe buffet in transonic	yes, limited time	yes, by definition

Functionality	Mig-21 Lancer	F-16 Block 15	Microfighter
Pilot interface	decent, HMS	decent	5th generation, HMS tbd, windshield projection
Ejection seat	good	excellent, 0-0 capability	tbd, standard solutions not applicable
G-load system	good	good	tbd, for weight saving and correlated with moderate g load capability

Functionality	Mig-21 Lancer	F-16 Block 15	Microfighter
Radar	fairly good	good	low power PESA, tbd
Ground targeting EO	external, barely used	external, good usage	internal, permanent, lower optical performance, higher integration by design
Distributed EO	no	no	yes
Ground/sea radio sources detection	basic RWR	basic RWR plus external pods, not for Ro	native, by large, integrated RWR arrays and integration with EO and radar
RWR	generic	generic	custom designed
Integration RWR-radar-EO	no	no	yes
Data link	no	no for Ro	desired by definition
Reconnaissance pod	yes, barely used	not for Ro	native, by integrated EO system, lacking panoramic view

Functionality	Mig-21 Lancer	F-16 Block 15	Microfighter
Max. Air-Air weapons	4	6	6
BVR weapons	no	4	no
Air-Air payload plus external fuel tanks	2	4	6, no fuel tanks
Cannon	yes	yes	no, by definition
Unguided munition	yes	yes	no
Small caliber guided or unguided rockets	yes	yes	no
Anti-ship missile	use air-ground munition, up to 250 Kg	use air-ground munition for Ro, no specific weapon	small format weapons
Anti radar missile	no	not for Ro	no

FIG. 2 Capabilities/requirements for existing fighters and microfighter

EngineSim from NASA has been used to compute engine charts of Viper and GE J-85. The first engine has been modeled and calibrated (cross area) according to known data to match the nominal thrust and corresponding consumption. The GE J-85 is already modeled in the code and there is no need to calibrate.

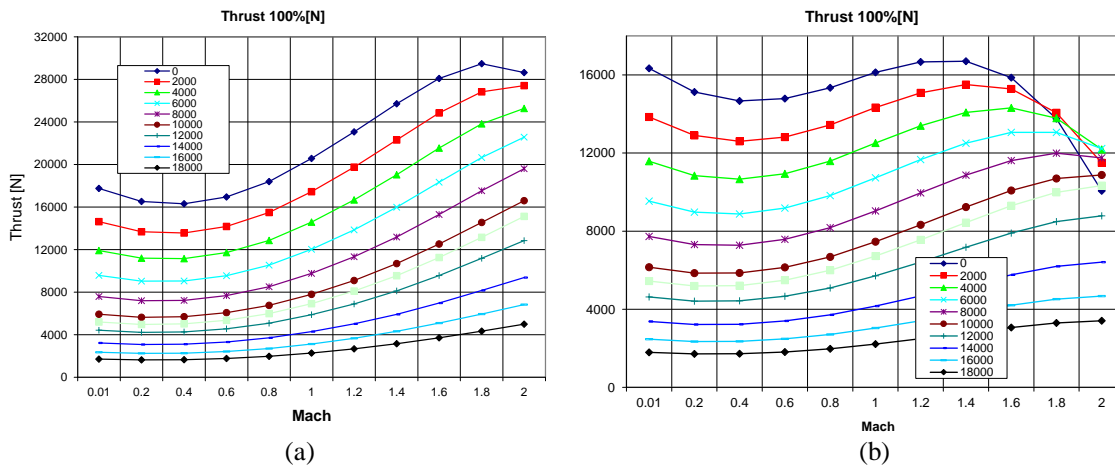


FIG. 3 Thrust characteristics of RR Viper 632 (a) and GE J-85 (b)




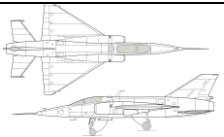

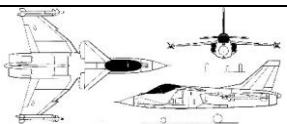


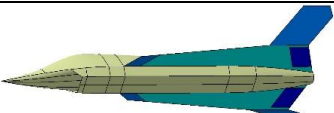
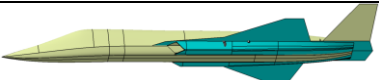
3. MICROFIGHTER ATTEMPTS

In the jet age there was a considerable effort devoted to microfighters and small fighters development as in [9]. Yak-1000 has been converted to the first successful anti shipping missile after an unsuccessful take-off, SNCASO Deltaviex exhibited modest performance due to the small engine, Boeing Quiet Bird was more a ground demonstrator incorporating RF LO features, HA-300 did not achieved the expected performance, P-900 has advanced features for the '80s, but remained a concept and is not a microfighter, Piranha was a sound design, Bird of Prey was a technology demonstrator with advanced manufacturability and LO capabilities at low dynamic performance.

Industry risk management made microfighter attempts fail. Two small fighters were anyway successful: Mig-21 plus derivatives and F-5 Tiger.

They lack those features that would enable their further upgrade: supercruise, LO and internal weapon carriage, plus they are old airplanes and have to be simply replaced. Political pressure from super powers disabled some of the national initiatives in the microfighter field.

Table 1. Small and microfighters

No.	Name		Remarks
1	Yakovlev Yak-1000 1951		Promising concept, poor controllability, redesign needed
2	SNCASO Deltaviex 1954		Promising concept, innovative controls, poor performance due to lack of proper engine
3	Boeing Quiet Bird 1963		Promising concept, the earliest LO, both RF and acoustic
4	Helwan HA-300 1964		Overestimated performance, never proven, lacking supersonic flight aerodynamic features, or credible weapon system
5	Northrop P-900 Advanced Fighter Concept, 1982		Credible concept, relatively large, very small
6	ALR-Aerospace 1979, Piranha		Credible concept, limited payload, no LO features, limited supersonic performance
7	McDonnell Douglas and Boeing, Bird of Prey, 1996		Proof of concept, advanced manufacturing technology and LO, no payload, subsonic
8	McDonnell Douglas, X-36, 1997		Unmanned, very agile, proven, low speed, no weapon system
9	INCAS 2016		Radio frequency & supercruise shaped, 8 weapons, ventral semi-recessed
10	INCAS 2017		Flatter shape for RCS reduction, smaller ref. area, less controls, 6 weapons

3. AVIONICS & WEAPON SYSTEM

Radar must be hybrid PESA (abandoned in western Europe or US for combat aircraft) or AESA (under development and production), with a mechanical repositioning system for larger aperture. It must be fully integrated with the RWR system and must provide targeting updates for the air-air and air-ground weapons in order to maximize range and probability of kill for missiles.

Low probability of intercept mode is a must for such a system. Antenna reflection is to be minimized versus the identified threats by an adaptive repositioning.

LO management must enable deep penetration with respect to all adversary sensors. Therefore passive detection and optimal navigation/exposure versus adverse sensors must be part of the working procedure.

Two sets of IR instruments are foreseen: one set is dedicated to the accurate detection and attack of aerial and surface targets and one set is dedicated to defense plus targeting assistance in high off boresight weapon delivery modes.

The accurate attack IR suite consists in two IR turrets: one integrated with the windshield with rear and upper field of view, one under the nose with full horizon and down field of view. Affordable IR sensor arrays are available at small price on the market. They can be integrated with normal optics to develop high performance turrets or fixed detectors with high aperture.

Man-machine interface must be very simple due to the small cockpit and for operation simplicity, since there is no double sitter. Two control sticks and two touch screens plus HMS would make for the whole interface. Other control panels are included to be used as mission preparation and technical checks on the ground. Voice command is envisaged, since the technology matured, enabling a simple cockpit layout.

A light ejection seat as a Martin Baker MK-15 derivative is available on the market. A normal fighter seat is beyond the mass budget of such a small aircraft.

3. POSSIBLE MISSIONS

The small platform only allows small weapons delivery. Therefore, accuracy is greatly needed in all possible modes. Since small AA missiles are proven (unique class of R-60), it is the surface/sea attack where larger warheads need to be employed. The most critical would be to antishipping strike, while for the land the assumption is to target military equipment only as vehicles or radars. The size of the platform excludes an internal cannon, which needs special care for the development/integration, in order to minimize interference with engine, structure and sensors. Elimination of the cannon would significantly reduce the amount of flight training and ground crew preparation. Cannon use is also risky in all types of missions and requires hard mechanical loadings at break-away.

A single target acquisition method is foreseen, making use of the data fusion, regardless of the target's type: aerial, land or sea based. Weapons are to be supported during their flight via guiding modems, when possible. Snap-shot target acquisition/attack is mandatory for all possible targets in visual range, using the HMS/EO turrets, distributed optical system and weapon guidance modems. Fast surface target geolocation is to be used in a second pass or for network distribution.

Reconnaissance and post-strike damage assessment are intrinsic functions of the targeting EO/optical distributed system.

One-ship or multiple-ship surface based radio frequency emitting sources is also a must, under hypothesis of low observability. Therefore SEAD missions are achievable in both kinematic striking or close-range harassing for adversary munition depletion and snap-shot attacks. Weapon shaped external jamming pods may be part of the inventory, enabling better cover/defense.

For long endurance subsonic missions a conformal fuel tank with dorsal mounting is the solution.

Asymmetry with conventional warplanes (small size, LO and super-cruise) must be exploited in air to air, by denying BVR weapons employment.

4. CONCEPT AND APPLICABLE TECHNOLOGIES

A number of configurations have been studied in order to find feasible architectures that would enable accommodation of engine, weapons, pilot, landing gear, offer volume for fuel and still provide LO and super-cruise, [6,7,8,9]. COTS weapons like AIM-9X or AGM-114 are impossible to be accommodated, although currently part of the alliance. They make for a good match, since the length and mass of a single AIM-9X are double to the length and mass of AGM-114. Such a weapon payload as in **FIG. 4** may be integrated in a larger aircraft, having as disadvantage a small payload mass in a large weapon bay. Both weapons in their most modern variants can be used in air to air and air to surface engagements. The no foldable fins makes them impossible to be ventral integrated for LO and therefore a new weapon is required.

The development program is dual: aircraft and weapons package, making use of all existing capabilities at national level.

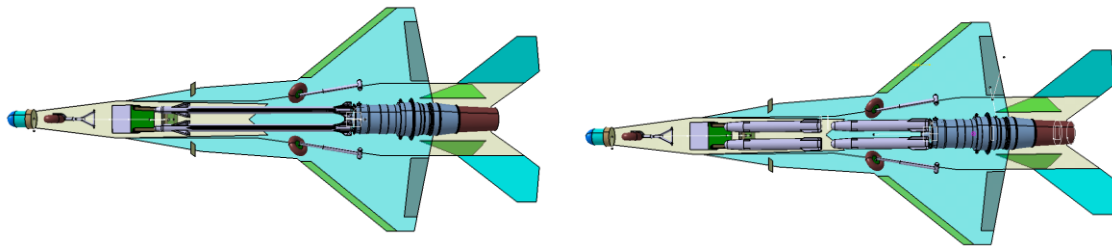


FIG. 4 Configuration relying on existing weapons, unfeasible, 2014

The weapon package consists in a common weapon format as in **FIG. 4**, intended to be used as universal missile (air to air and air to surface) or bomb. Common features are parts of the sensor, optical dome, computer + IMU, fins and their actuators, modem. Motor and warheads are different, while the bomb is expected to be heavier than missile, although with a modest impact in aircraft flight performance. Pyramidal optical nose is used as a mean to reduce aerodynamic drag. An innovative release system eliminates rail/jugs, while rear only foldable fins are provided.



FIG. 5 Universal weapon configuration

Additional COTS weapons may be installed, like 70 and 80mm laser guided projectiles: APKWS, Roketsan Cirit or Electromecanica LRDL.

The airplane in any configuration needs to be a flat platform, with side edge and leading/trailing edge alignment as a set of minimal LO features.

The more or less classical fuselage contains two strakes, providing volume for the landing gear and support for the V-tail. Weapons number has been optimistically considered 8 as in **FIG. 6** and **FIG. 7**, but after some engineering iterations it is now considered at 6, as in **FIG. 8**. This also brings a mass reduction, plus more space for weapon extraction systems as risk management measure.

A droop nose airfoil family is used instead of a complex leading edge flap as a compromise for high AoA and for mass/cost reduction, considering that dog-fighting and strafing are ruled out.

Fixed geometry lateral intakes are chosen instead of dorsal or ventral ones, because of the most promising LO impact as S-duct and as they do not enlarge the side contour, good compromise as functionality as they are under the strakes in a high pressure area at high angle of attack and as good engine protection in foreign object damage.

V-tail is the solution as it offers the smallest wetted area, best promising LO capability, while emphasize is not put on high maneuverability. Also the number of control surfaces and their corresponding actuators is minimized with respect to a standard twin fin tail.

A very long, thin nose, although attractive for a low boom supersonic flight, may bring difficulties with nose sensors integration, as well as with the mechanical loadings. Another way to decrease the acoustic signature is coming from the rear fuselage architecture, which offers an acoustic shielding capability by the use of V-tail and relative engine nozzle positioning. This configuration also provide some IR low observability capabilities, as existing in A-10 aircraft.

Hydraulic control surfaces actuation can be performed with available designs from IAR-93, IAR-95 and IAR-99 programs. Experience with IAR-93 evidenced a large number of technical weaknesses, which have been much better solved in IAR-99. This shows that some parts of the hydraulic system may be replaced from the design with electric systems. The same can be stated about the fuel system, where a safe and simple system is considered from an early stage of development. Due to the available volume in the fuselage, there is no need of wing tanks. Therefore, classic tanks can be accommodated in the fuselage.

Manufacturing relies in large molds, large structural parts, for mass and cost reduction. This is enabled by large milling machines available at national level and the proven way to manufacture molds in high density polyurethane.

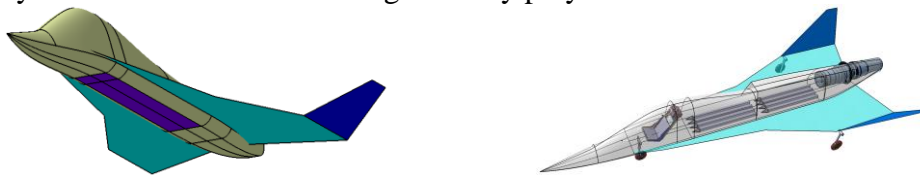


FIG. 6 Configuration 2015

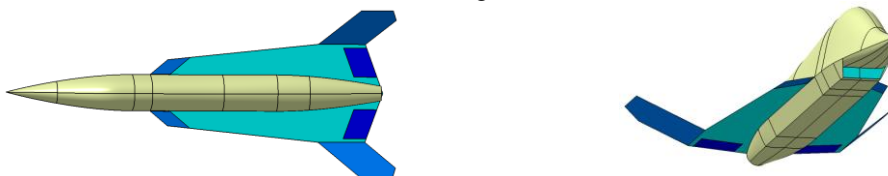


FIG. 7 Configuration 2016

Aircraft shaping is performed in CATIA, using a script organized as a collection of procedures for all main parts. A small set of global variables are used, while most of the defining parameters are introduced at procedure level. Simple splines with analytic definitions for their points and tangent vectors are used for all but wings and tail surfaces, where typical analytic formulations are considered for airfoils.

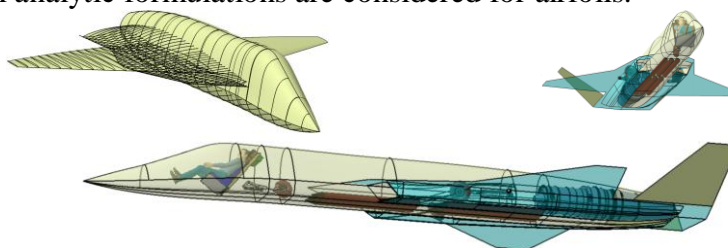


FIG. 8 Configuration 2017

Preliminary performance estimation

The flight envelope is the most desirable chart in an early design stage. Therefore, a routine in VBScript under Excel is used to make this computation. Existing aerodynamic data are considered as for a somehow similar platform, introduced in [6], as trimmed drag polars. The data covers essentially all flight regimes, as they are computed with semi-analytic tools.

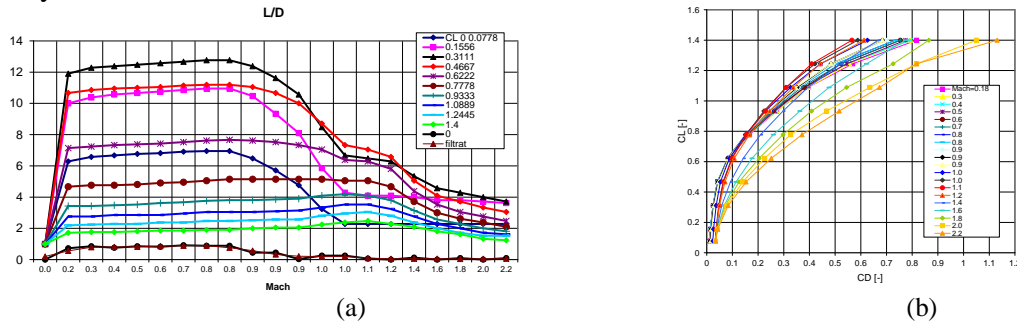


FIG. 9 Notional fighter aerodynamic characteristics [10]

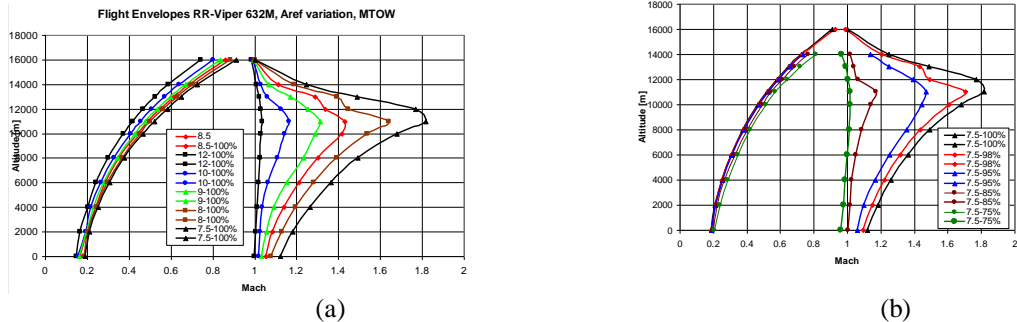


FIG. 10 Flight envelopes with RR-Viper at 100% rate, various reference areas (a), Flight envelopes with smallest reference area (b)

Reference area, as well as wetted area have a strong impact on the flight envelope, when aiming for super-cruise capability. There is a threshold value for the planform reference area, such that when the design is beyond, supersonic flight is no longer possible, even with significant weight reduction. The supersonic performance sensitivity comes from the fact that the aircraft in [6] is essentially not a super-cruiser. This is going to be further investigated after a complete CAD model is worked and numerical flow analyses are performed.

The required super-cruise engine setting is also important mainly because of thermal constraints. The current engine allows an operating time of 5 minutes at 100%, 30 minutes at 98% and unlimited at 95% of the nominal setting. The best super-cruiser of today can only sustain 30 minutes.

4. CONCLUSIONS AND FUTURE WORK

The study shows that for the given figures super cruise performance is achievable, as the main goal, even at MTOW. LO features are considered as basic, since a computing tool is still under development. However, given the difficulties in training missions of fourth generation fighters with small fighters like Mig-21 or T-38, we are highly optimistic that a simple LO shaping can produce very good results and can make BVR engagements very challenging. Further refinement of LO can completely deny BVR engagements. A comparison with F-5 shows a large difference in the side profile, with greatest impact in LO under normal flight operation (attitude) FIG. 11.

A unified target engagement with missile/bomb, plus the lack of cannon with its own skill requirements/aircraft loadings is very attractive for an air force with small allocated resources for training. The national defense system of today has a very small mass of fighter planes. Since the air force shrinking process is ongoing, the forecast is that in few years the military flight academy will be dissolved. Therefore a microfighter solution is possible and can lead to the recovery of capability and beyond, at a cost fraction of the force as it is being foreseen today. Its sustainability would be equivalent to that of a trainer fleet as IAR-99. A microfighter program would help recover the industry at a significant scale, and should be initiated as soon as possible, while the lessons in the development of IAR-93 and IAR-99 are still living through part of the involved engineers and pilots.

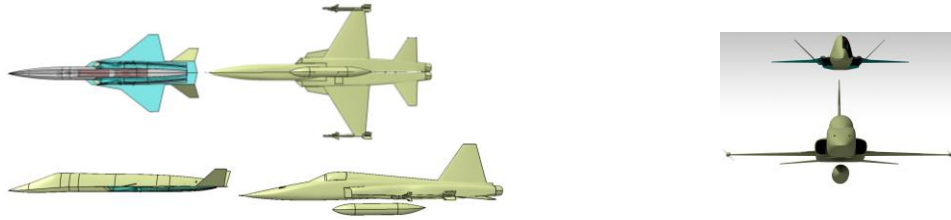


FIG. 11 Comparison with F-5 Tiger

The simple/unified technical and mission requirements, under the mentioned notional weapon system with targeting oriented automation may lead to lean pilot learning/training, lean ground support, lean fighting, lean operation and a new paradigm from the classical “Train as you fight, Fight as you train” straight to “Fight as you play”. Achieving good training for the existing platform ensures success, versus low training on excellent platform [10,11].

Future work is considering the numerical aerodynamic assessment, RCS numerical tool development and endurance/range assessment. Mig-21 R-13 engine without reheat would be a major candidate for a larger design, with greater capabilities.

Results of this study are obtained without funding, as pure volunteering work. The authors thank to student Martin Barthelemy from IUT/Toulouse for its contribution in CAD modeling, during its internship at INCAS, under ERASMUS.

REFERENCES

- [1] Gheorghe – Ion Vaida, Avionul IAR-93 Oameni și fapte, Editura Global Media Sibiu, ISBN 978-606-8809-08-3, 2016
- [2] Nowa Technika Wojskowa, May Nr 5/2017, ISSN 1230-1655
- [3] Wojsko I Technika, 4/2017, ISSN 2450-1301 INDEKS 407445
- [4] Stefan Voian, STUDIU DE SINTEZA privind MODERNIZAREA AVIOANELOR DE LUPTA DIN GENERATIA ANILOR 1965-'75 (generatia a III-a) LA NIVELUL CERINTELOR ACTUALE, 1992
- [5] Sea Harrier Over The Falklands: A Maverick at War, Commander Sharkey Ward, 2007
- [6] Daniel P. Raymer, Next-Generation Attack Fighter, Design Tradeoffs and Notional System Concepts, RAND, 1996, ISBN 0-8330-2406-X
- [7] Daniel P. Raymer, Aircraft Design: A Conceptual Approach, AIAA Education Series, 1992, ISBN 0-930403-51-7
- [8] Special Course on Fundamentals of Fighter Aircraft Design, AGARD-R-740, 1987, ISBN 92-835-1560-9
- [9] Bill Gunston, Future fighters and combat aircraft, Salamanders Book Limited London 1984, ISBN 0 86101 163 5
- [10] Robert E. Ball, The Fundamentals of Aircraft Combat Survivability Analysis and Design, Second Edition, AIAA Education Series, ISBN 1-56347-582-0, 2003
- [11] Robert L. Shaw, The art and science of air-to-air combat, Patrick Stephens Ltd; 2nd edition edition (November 21, 1988), ISBN 1852602015
- [12] Complete collection of Take-off Magazine, <http://en.take-off.ru/>
- [13] Collection of Combat Aircraft, Key Publishing
- [14] Collection of Air Forces Monthly, Key Publishing

ASPECT REGARDING OF THE PRATT & WHITNEY F100 JET ENGINE PERFORMANCES

Vasile PRISACARIU, Alexandru CIUBOTARU

“Henri Coandă” Air Force Academy of Braşov, Romania (aerosavelli73@yahoo.com, aleczvasile@yahoo.ro)

DOI: 10.19062/2247-3173.2017.19.1.20

Abstract: A jet engine is a category of propulsors that can be continuous improved, starting from concept to design and execution to management of thrust and also new approaches regarding maintenance activities. Last decades, the usage of jet engines extended into aeronautical area (UAV, UCAV) as well as into unusual ones (auto-transport, electrical generators). The article wants a review of the F-100 jet engine by exposing a performance analysis using a software tool on an equivalent model.

Keywords: jet engine, Gasturb, F-16 Fighting Falcon, F100-PW220.

Acronims

<i>U(C)AV</i>	<i>Unmanned (Combat) Aerial Vehicles</i>	<i>ATECG</i>	<i>Advanced Turbine Engine Gas Generator</i>
<i>DEEC</i>	<i>Digital Electronic Engine Control</i>	<i>LOD</i>	<i>Light-off Detector</i>
<i>EQ</i>	<i>Equivalent</i>	V_H, V_h	<i>Speed</i>
η	<i>Efficiency</i>	<i>T</i>	<i>Thrust</i>
α	<i>Air coefficient redundance</i>	<i>W</i>	<i>Weight</i>
G_c	<i>Fuel flow per hour</i>	Q	<i>Heat quantity</i>
<i>S</i>	<i>Surface</i>	<i>HPC</i>	<i>High pressure compressor</i>
<i>HPT</i>	<i>High pressure turbine</i>		

1. INTRODUCTION

1.1. F100 general consideration.

The engine was created at the request of United States Army and United States Navy which issued a joint engine request for proposals for the F-14 Tomcat and F-15 Eagle fighters during a program called Advanced Turbine Engine Gas Generator (ATECG) whose goal was to improve thrust and weight to achieve a trust-to-weight ratio of 9. The program awarded Pratt & Whitney company with a contract to produce F100-PW-100 (USAF) and F400-PW-400 (USN) engines, [1, 2, 3], see figures 1 and 2.

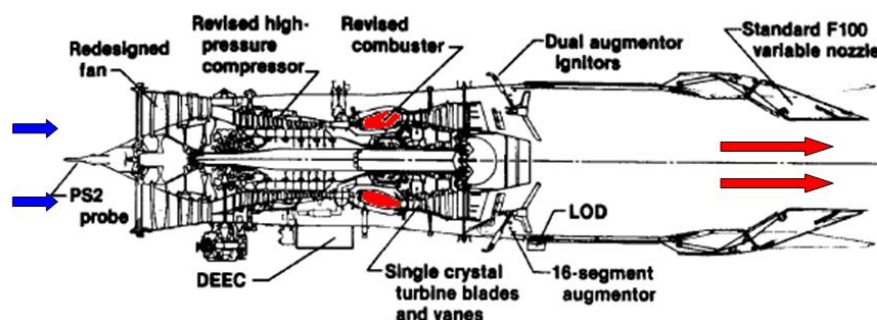


FIG. 1 F100 jet engine diagram, [2, 3]

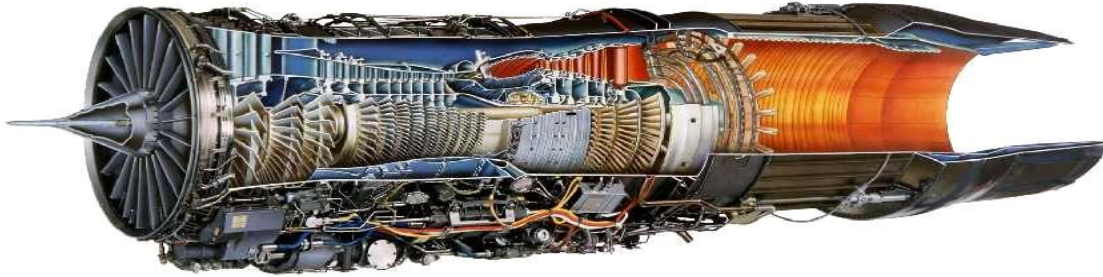


FIG. 2 F100 jet engine [2, 3]

1.2. F100 Versions

The engine is built in more than 7200 pieces, in various versions, and it is currently used in 23 worldwide national air forces, the fiability record being established by the F100-PW-229, [1, 10].

a. F100-PW-100.

The first version is the basic of this engine. The F100-PW-100 first powered the F-15 Eagle in 1972 with a thrust of 106,4 kgf. Numerous problems were encountered in the first days of its use, including high wear, stalling and “hard” afterburner starts. The consequences of these problems caused the large jets of jet fuel to be lit by the engine exhaust resulting in high pressure waves that caused the engine to stall. These problems were solved in an alternate version of this engine, the F-100-PW-F220.

b. F-100-PW-200.

F100-PW-200 engine was the second version of the F100 engine. It was created seeking a way to drive unit costs down. The Alternative Fighter engine program was implemented by USAF in the 1984 and the engine contract was awarded through competition. The F-16C/D Block 30/32 was the first block of planes to use this engine, able to accept the existing engine or the General Electric F110.

c. F100-PW-200/220E

This engine was created due to unsatisfactory reliability, maintenance costs and service life of the F100-PW-100/200. Pratt & Whitney Company was pressured to upgrade the engine to solve these issues; the resulting engine was the F100-PW-220. The engine eliminates stall-stagnations and augments instability as well as doubling the time between depot overhauls. Reliability and maintenance costs were drastically improved and the engine incorporates a digital electronic engine control (DEEC). This engine was released in 1986 and was compatible on either F-15 or F-16. The “220E” name is given to engines which have been upgraded from series 100 or 200 to 220 thus becoming equivalent to 220 specifications.

d. F100-PW-229

The 229 has a thrust of 79,18 kN (dry thrust) and 129,7 kN with afterburner. The late F-16 Fighting Falcon (see figure 3a) and the F-15E Strike Eagle (see figure 3b) are currently powered by this engine. The current production of F100-PW-229 Engine Enhancement package incorporates modern turbine materials, aerodynamics compressor, electronic controls and cooling management [4].



FIG. 3 The applications F100 engine, a. F15E Strike Eagle, b.F16 Fighting Falcon [5, 6]

1.3. Jet engine description.

The F100 jet engine is a two-spool (mixed flow) low by-pass engine, equipped with a high degree compression axial compressor, a post-combustion chamber and a variable geometry nozzle. In table 1 we present the most significant characteristics and performances of the F100 engine family.

Table1. Characteristics and performances

	F100-PW-220	F100-PW-229
Type	Afterburning turbofan	
Length	4900 mm	
Diameter	880 mm inlet, 1180 mm max.	
Dry weight	1,467 kg	1,700 kg
Maximum Thrust	64,9 / 105,7 kN afterburner	79,18 / 129,7 kN afterburner
Pressure ratio	25:1	32:1
Specific consumption	Military thrust (0.73lb/(lbf·h))	Military thrust (0.76lb/(lbf·h)) Full afterburner: 1.94lb/(lbf·h)
Thrust-to-weight ratio	7.4:1	7.8:1

2. THEORETICAL ASPECTS

2.1. Jet engine main functioning parameters.

Main parameters define the operating modes and implicitly the physical and chemical configuration of the flow filed into the jet engine sections, which are: engine rotation (rot/min), specific thrust (T_{sp}), the exit flow temperature (T_3^*), the engine thrust and specific fuel consumption.

The functioning conditions can be: cruising (constant rotation speed, constant fuel flow, constant speed flight, invariable engine interior geometry), transitory (fuel flow, revolution, flight speed, altitude variations in time) and unstable (functioning characteristics constant, but in time, the fuel flow into the engine is unstationary)

2.2.Parameters of the jet engines

Jet engine are defined by a series of specific parameters that give marks regarding global performances of them, [9, 12, 14].

-specific thrust:

$$T_{sp} = \frac{T}{W} \quad \frac{daN \cdot s}{kg} \tag{1}$$

- specific fuel flow:

$$C_{sp} = \frac{G_c}{F_t} \quad \frac{kg}{daN \cdot h} \tag{2}$$

-specific frontal thrust:

$$F_{spf} = \frac{F_t}{S_{\max}} \quad \frac{daN}{m^2} \quad (3)$$

-specific engine weight:

$$W_{sp} = \frac{W_e}{T_t} \quad \frac{kg}{daN} \quad (4)$$

2.3. Jet engines efficiency

Jet engine mainly converts chemical energy into movement mechanical work in mid-air [9].

-global efficiency (the ideal model of engine transformations):

$$\eta_g = \frac{T_{sp} \cdot V}{Q_o} \quad (5)$$

- thermal efficiency of the real engine:

$$\eta_c = \frac{(c_5^2 - V_H^2)}{2 \cdot Q_o} \quad (6)$$

where c_5 -gas exit speed (reactiv nozzle).

Thermodynamic efficiency of the real cycle is $\eta_t=0,25 \div 0,4$ because of the losses of energy (incomplete burn), mechanical and thermal losses into the environment.

-flight efficiency:

$$\eta_F = \frac{T_{sp} \cdot V_h}{\frac{1}{2} \cdot \left(\frac{1 + \alpha \cdot L_0}{\alpha \cdot L_0} \cdot c_5^2 - V_H^2 \right)} \quad (7)$$

where $V_h \neq 0$, α the air excess coefficient and L_0 the theoretic quantity of air required for a complete burn.

3. PW F100 JET ENGINE SOFTWARE ANALYSIS

3.1. Software description.

GasTurb is an engineering software developed by Dr. Joachim Kurzke, firstly in 1991 and the optimization and development of the program continues to the present and future. The latest version of this program and the one we used is GasTurb 12. This software deals with interpretation of engine test results and diagnosis of operational problems, providing control system designers with a simulation of the engine model, providing operators, airframe manufacturers and power station designers with mathematical models and a lot of other functions.

3.2. The case study.

For the case study I chose an F-100-EQ two-spool turbofan (mixed flow) low by-pass engine place in the same category as F-100 engine that equips F-16 Fighting Falcon. The “*basic thermodynamics–cycle design–design point*” analysis has the main parameters highlighted in table 2 in base configuration of the software tool, where we consider zero pressure losses, the exclusion of the turbine to be cooled [7] and specific parameters of the engine, [11].

Table2. Initial main condition

Condition	Value	Condition	Value
Speed	0 km/h	Altitude	0 m
Ext. temperature	288 K	Ext. pressure	101325 kPa
Intake pressure ratio	0,99	Burner exit temperature	1700 K
Mixed efficiency	0,5	Burner pressure ratio	0,99
Design nozzle petal	25 ⁰	Mass flow input	111,5 kg/s
HPC efficiency	0,88	HPT efficiency	0,87
Afterburner	no		

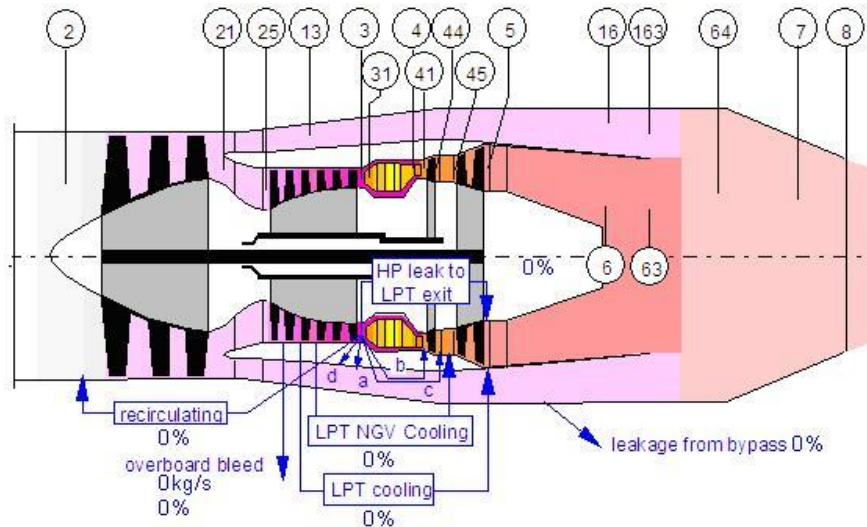


FIG. 4 Total temperature and velocity in jet engine stations, [7]

For Figure 4 jet engine stations: 2-first compressor inlet, 21-inner stream fan exit, 25-high-pressure compressor inlet, 13-outer stream fan exit, 3-last compressor exit, cold side heat exchanger inlet, 31-combustor (burner) inlet, 4-combustor (burner) exit, 41-first turbine stator exit = rotor inlet, 44-high-pressure turbine exit after addition of cooling air, 45-low-pressure turbine inlet, 5-low-pressure turbine exit after addition of cooling air, 6-jet pipe inlet, reheat entry for turbojet, hot side heat, exchanger inlet,16-bypass exit, 63-hot side mixing plane, 163-cold side mixing plane, 64-Mixed flow, reheat entry, 7-reheat exit, hot side heat exchanger exit, 8-nozzle exit, [7].

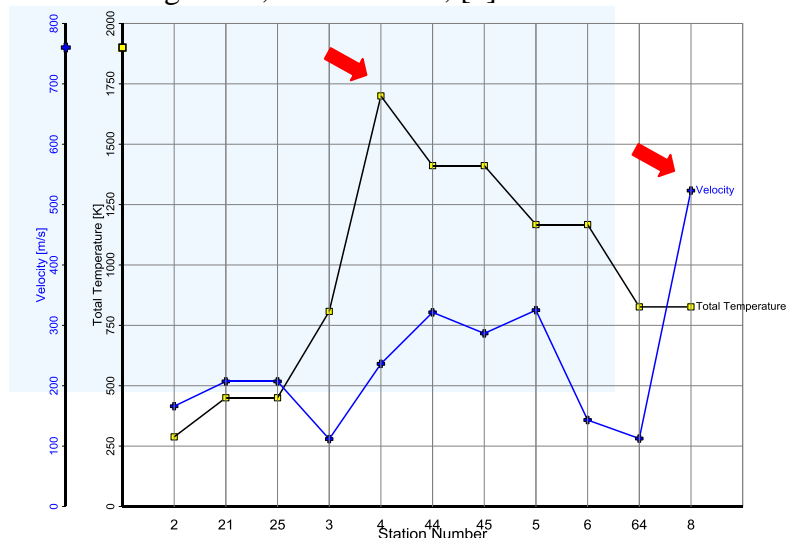


FIG. 5 Total temperature according to velocity in jet engine stations

In figure 5, there can be observed the speed and temperature variations in the engine sections, an accentuated growth of temperature in the burning chamber (sections 3-4) within reaching a maximum of 1700k (section 4) and a obvious speed variation from 100 m/s (section 2) to approximately 1300 m/s (section 8). Also in figure 6 is revealed quasi-identical variation of the entropy according to the total temperature in the engine sections, and the differences of those parameters from section 2 to 8.

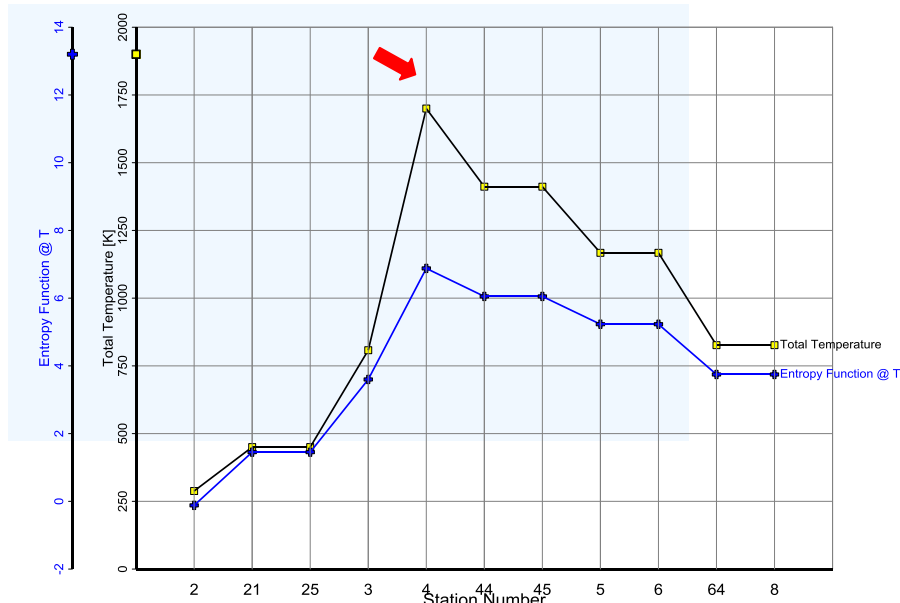


FIG. 6 Entropy function according to total temperature in jet engine stations

In Figure 7 can be observed the variation of the density according to total pressure into the engine sections. To note the values of the 2 parameters in the burning chamber (sections 3-4).

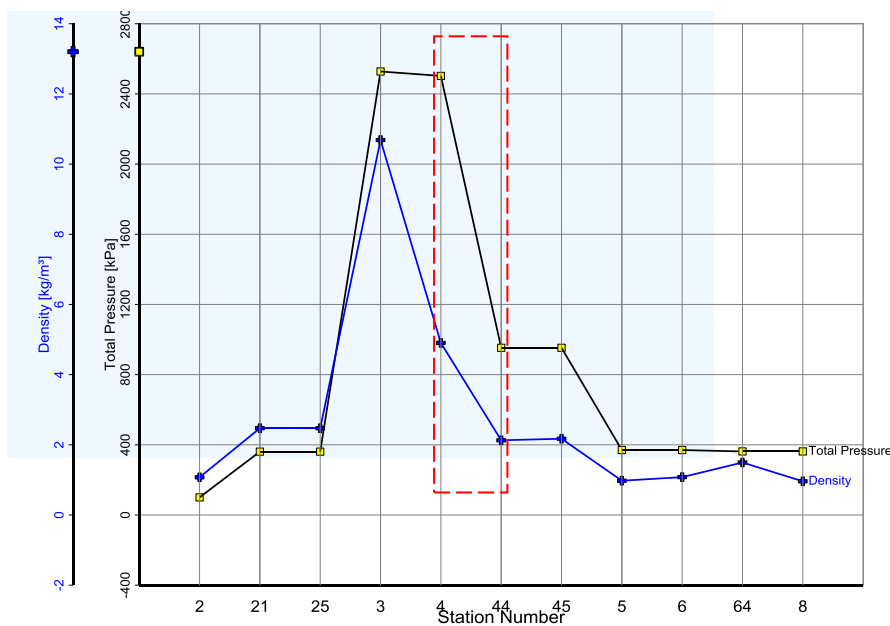


FIG. 7 Density according to total pressure in jet engine stations

In Figure 8 we can observe the limits of the variation of the entropy according to the jet engine functioning temperature gap, and Figure 9 shows the variation of pressure according to the gas volume.

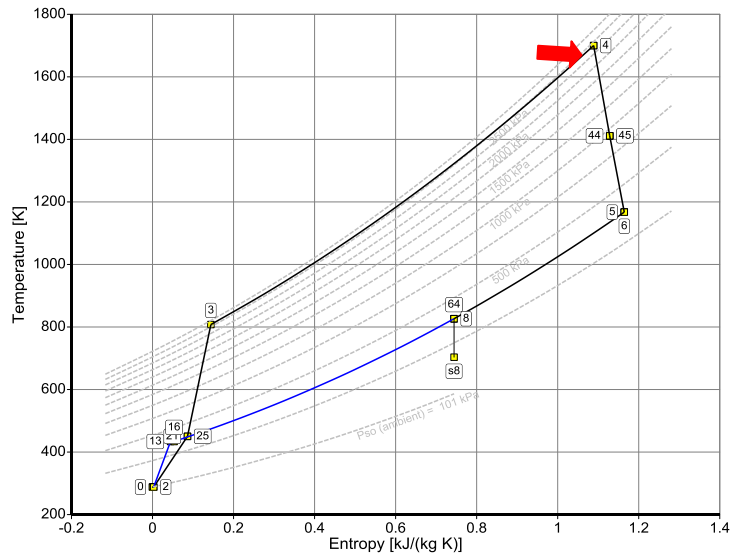


FIG. 8 Entropy according to total temperature

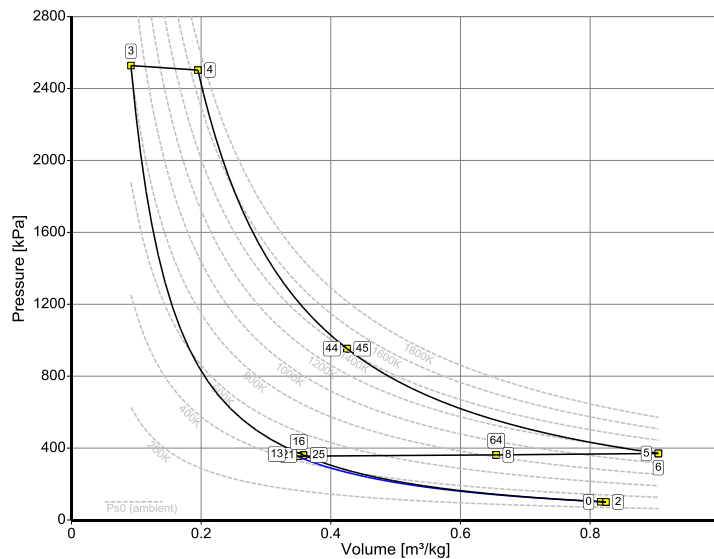


FIG. 9 Pressure according to volume

From the study case resulted a maximum thrust of 78,73kN, which can be compared to the data from the specialty literature (79,18 kN), [11].

4. CONCLUSIONS

Propulsion systems of the aircrafts were and are continuously enhanced and the numerical and simulation methods regarding the optimization of the performances complete the experimental researches that can confirm or not the researchers's previsions.

Software tools used for numerical simulation of propulsion systems performance can approach the aspects of global design goals, optimization options identification, operational problem diagnosis, performance assessment, and interactive teaching methods in the field of propulsion systems.

GasTurb can also be used for teaching gas turbine thermodynamics through graphically exported data of parametric studies that can reveal real figures about how thermal efficiency depends on the pressure ratio and the exit temperature of the combustion chamber.

GasTurb provides assistance to users who need to examine the measured data on a gas turbine in service or in the test stage to confirm the expected performance by creating a precise simulation of a real motor based on typically limited information.

ACKNOWLEDGEMENT

This article has received support from UEFISCDI through national project "TURIST" PN-II-PT-PCCA-2013-4-1187 contract 286/2014.

REFERENCES

- [1] Obaid Younossi, Mark V. Arena, Richard M. Moore Mark Lorell, Joanna Mason, John C. Graser, *Military Jet Engine Acquisition*, ISBN 0-8330-3282-8, RAND 2002, 167p;
- [2] Childre Mark T, McCoy Kevin D. *Flight test of the F100-PW-220 engine in the F-16*, 5/1989, doi: 10.2514/3.23199, Journal of Propulsion and Power, pag.620-625, AIAA, ISSN 0748-4658, <http://dx.doi.org/10.2514/3.23199>;
- [3] <http://www.f-16.net/f-16-news-article3930.html>;
- [4] <http://www.f-15e.info/technology/engines/pw2/pw2.htm>;
- [5] <https://media.defense.gov/2003/Feb/10/2000030380/-1/-1/0/021105-O-9999G-049.JPG>;
- [6] <https://media.defense.gov/2003/Feb/10/2000030393/-1/-1/0/010205-F-1631A-001.JPG>;
- [7] *GasTurb GmbH, GasTurb 12, Design and Off-Design Performance of Gas Turbines*, 2015, 311p. available at www.gasturb.de/Gtb12Manual/GasTurb12.pdf;
- [8] <http://www.globalsecurity.org/military/systems/aircraft/systems/f100.htm>;
- [9] Ciobotea V., *Teoria motoarelor de aviație*, vol. 1, Editura Academiei Militare, București 1978, 412p;
- [10] Frank Camm, *The Development of the F100-PW-220 and F110-GE-100 Engines: A Case Study of Risk Assessment and Risk Management*, RAND 1993, N-3618-AF, 110p;
- [11] A. S. Lee, R. Singh and S. D. Probert, *Modelling of the Performance of a F100-PW229 Equivalent Engine under Sea-level Static Conditions*, 45th AIAA/ASME/SAE/ASEE Joint Propulsion Conference & Exhibit 2 - 5 August 2009, Denver, Colorado, AIAA 2009-5018, p.1-11;
- [12] Pimsner V., *Motoare aeroreactoare*, vol.1, Editura Didactică și Pedagogică, București 1983, 387p.;
- [13] Prisacariu V., Cîrciu I., *Considerations regarding the performance of combustion chambers for turbo-jet engines*, Review of the Air Force Academy No 2 (32) 2016, DOI: 10.19062/1842-9238.2016.14.2.7, ISSN 1842-9238; e-ISSN 2069-4733, p.53-60;
- [14] Rotaru C, Arghiropol, A. Barbu C., Boșcoianu, M., *Some aspects regarding possible improvements in the performances of the aircraft engines*, Proceedings of the 6th IASME/WSEAS International Conference on Fluid Dynamics and Aerodynamics, Greece,2008, SSN: 1790-5095, p196-201;
- [15] Fletcher P., Walsh P.P., *Gas turbine performance*, Second Edition, Wiley, ISBN 0-632-06434-X, 2004;
- [16] Rotaru, C., Sprințu, Iuliana, *State variable modeling of the integrated engine and aircraft dynamics*, AIP Conference Proceedings, vol. 1637, issue 1, p.889-898, 2014.

UNIFORMITY AND STANDARDIZATION OF THE AIR DEFENSE WEAPONS

Marius RĂDULESCU

Electromecanica State Own Company, Ploiești, Romania (marius@elmecph.ro)

DOI: 10.19062/2247-3173.2017.19.1.21

Abstract: *Without any doubt the wide diversity of tactical situations involving the enemy's aerial means requires a certain number of types of AD systems. Some of them are destined to repeal low altitude pinpoint saturation attacks, others aim to face at cruise missiles final approach assault and others must prevent high altitude aircraft evolution at long range (reconnaissance, ELINT/EW, tankers, a.o.). All these requirements cannot be satisfied by a single system but also is uneconomical to spreads too much the number of systems in endowment, especially when the quantity (depending on the Army's size) is small. These considerations impose to search for use the systems very carefully choose and as possible even derivatives of a basic system adapted for mission, conducting to uniformity and standardization. In this case only the cost of life cycle and the replacement spending will be taken under control in small maintenance organizations.*

Keywords: *missile, air defense, system, caliber, maintenance*

1. INTRODUCTION

Today it is not imaginable nor a kind of armed conflict without the use of the air power. The aerial means are intensive used beginning to the preliminary and early stages of modern engagements, either as reconnaissance / lure drones, RECCE / ELINT aircraft, superiority fighters, incursion helicopters, stand-off weapons, cruise missiles, a.o. It can be seen the wide range of threat which air defense must primarily confront and many times simultaneously. Here's why the defensive system must be able to conduct multi-layered air defense (AD) operations, based on centralized multi-spectral sensor network and the cooperation of different fire units, depending on the effective phase of engagement.

A relatively small army usually cannot cover entire area of responsibility, but could try to assure a significant protection for the critical assets, like air / naval bases, important passing points, some special objectives (depots, energy plants, transport hubs), political centres, covering in a same time the bulk of own forces (headquarters, concentrations of mechanized troops, artillery positions, columns).

Even for small sized army (in some limits), it still needs to have a range of AD systems to ensure the two purposes. At a minimum, the types of AD systems generally used in army's endowment are:

- AAG (T) - anti-aerial gun – towed
- SPAAG - self propelled anti-aerial gun
- MANPADS - shoulder fired SAM
- VSHORAD - very short range system, based mainly on SP MANPADS
- SHORAD - short range missile system

- MERAD - medium to extended range missile system
- LRHAAD - long range / high altitude missile system

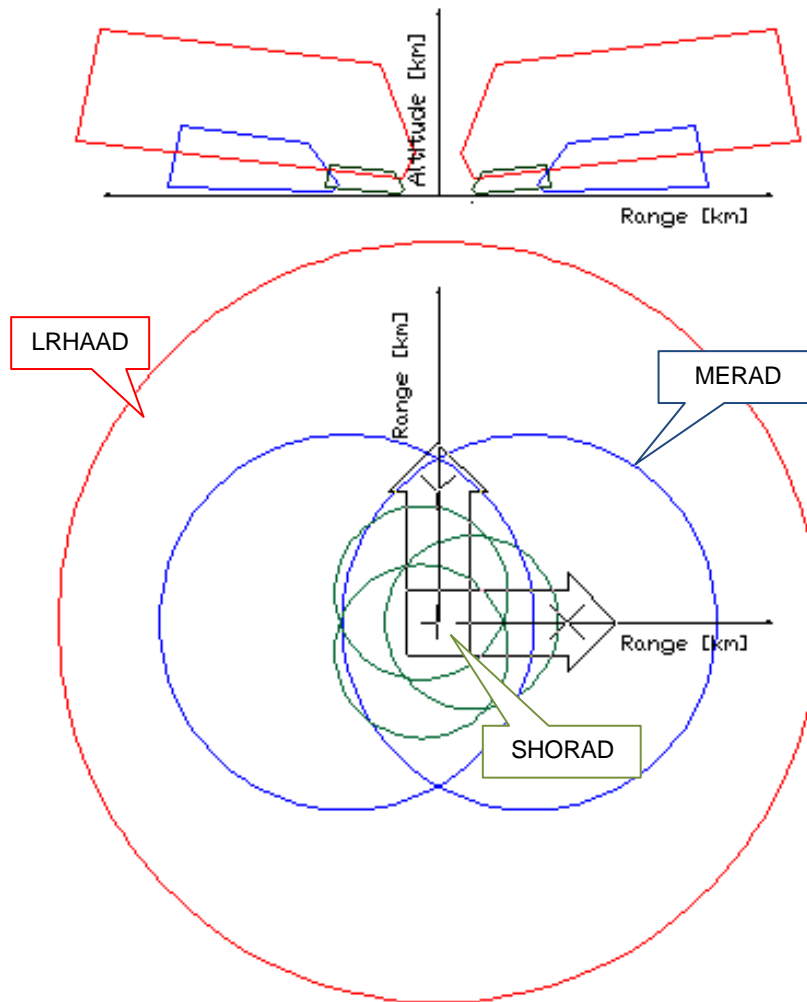


FIG. 1 Multilayer AD diagram

2. SHORT COMMENTS ABOUT PRESENT AD MAIN WEAPONS

In actual structure of the Army the AD weapons are distributed as follows:

Unit / System	AAG (T) 30	AAG (T) 35	SP AAG	AAG 57	CA-94	CA-95	SA-6 Kub	SA-8 OISA	S-75	MIM-23
Mechanized Brigade			X		X	X				
Motor Rifle Brigade	X				X					
Mountain Brigade		X			X					
SAM Regiment						X	X	X		
SAM Brigade									X	X
AFB AD Battalion				X						
Independent Units					X					

At the moment our units uses tree types of AAG (T) and one type of SPAAG:

- A-436 twin 30mm local manufactured
- S-60 57mm Soviet model
- GDF-003 35 mm Swiss-made

The 30mm AAG has little firepower and lack of a modern FCS reduces the utility of this weapon.

The 57mm AAG is reputed inaccurate despite the Radar Fire Control with which is equipped and has a significant weight also, imposing its disposal in fixed positions.

The 35mm twin AAG is relatively useful asset, but needs a good tractor for mobility.

The twin 35mm SPAAG Gepard is a good weapon for the mechanized units close support, mainly combined with a SHORAD.



FIG. 2. The prototype of Gepard SPAAG - mixed VSHORAD at EXPOMIL 2011

Regarding the missile systems available:

The CA-94 MANPADS has some tactical efficacy but the tail-only engagement capability is not enough for the actual battlefield configuration.

The CA-95 is accurate and has a corresponding lethal power, but the range (less 5 km) isn't at the level of a 9 tons SP system.

The SA-8 OSA is developed in little number, without real up-grade solutions and near end of the life-cycle.



FIG. 3. The SA-6 have a certain up-grade potential - here the Polish variant w. RIM-162 ESSM

In a similar situation, SA-6 KUB presents the advantages of a very flexible and reliable chassis and a few NATO-style modernization solutions performed. Both S-75 and MIM-23 systems are now obsolete and must be replaced.

3. PRINCIPLES FOR ENDOWMENT UNIFORMITY

The complete missile range of the Army's equipment includes many other types like:

- Ship borne close AD protection
- Ship borne battle group AD coverage
- Air-to-air dog fight high maneuverable short range missile
- Air-to-air beyond visual range missile

Excepted ground-to-ground, anti-ship and air-to-ground applications, which have another organization and dynamic, parts of other missiles or even entire weapon can be derived in surface-to-air systems. Such a choice could induce some difficulties in the system architecture design but may conduce to great advantages regarding logistics and maintenance.

This permits more flexibility for the resource allocation and allows o concentrate fire power on the threatened directions.

Examples of such development are representing by surface-to-air systems based on the AIM-7 Sparrow, AIM-132 AMRAAM or IRIS-T missiles.



FIG. 4. IRIS-T AAM is directly used in SLS AD derivative -here the Swedish variant

Considering the necessity of replacement/upgrade of totality of actual equipment, the carefully choose of types and models and the limitation of their number appears as mandatory.

A possible schedule of completion to cover the needs of army's structure looks like in the following table:

Unit / System	AAG (T)	SPAAG	MANPAD	VHORAD	SHORAD	MERAD
Mechanized Brigade		X		X		
Motor Rifle Brigade			X			
Mountain Brigade			X			
SAM Regiment					X	
SAM Brigade						X
AFB AD Battalion	X				X	
Independent Units			X			

Accordinging of the size of our Army and of the number and structure of the units, for the moment the 35mm AAG (including SP version) could be the base of barreled AD close range low altitude systems. That may includes ship borne guns and even some primarily ground support guns on vehicle mounts.

Another mandatory item remains a MANPADS, with SP VSHORAD, deck mounting or helicopter-borne self-defense variants.

Considering the capacity to reject the saturation attacks and the wide range of targets which can be engaged a SP SHORAD is necessary; if the weapon (even partially) should assures some ship borne and air-to-air applications, that allows great logistic gain.

A new MERAD system will be necessary to equip the SAM AD Brigade, while a LRHAAD remains to be assured at the NATO Alliance level.

Totally one gun system and three missiles systems, with derivative, could be the backbone of the Romanian AD in the next 20 – 25 years.

4. ADVANTAGES AND COSTS

In the field of logistics, the results of keeping a limited number of AD systems create real advantages regarding:

- depot organization and procedures
- maintenance devices, testers and facilities
- spare parts and auxiliary materials
- transport and maneuver devices and instructions
- personnel training

At the operational level is easier to work using:

- the same symbol code
- the same tactical procedures
- the same efficacy expectations

Considering actual army structure with 5 mechanized and 4 light brigades, 3 SAM regiments, 5 base defense battalions and one SAM brigade the size of the AD equipment is set. Using some market available information it can be estimate, even as a magnitude order, the amount of money that necessary to update the complete AD equipment:

System / Cost	Fire Units	Unitary cost *	Total cost	Comments
Improved AAG	40	20	100	w. 5 radars and TCP's
Improved SPAAG	30	5	150	
MANPAD	60	2.7	162	w. 600 rds
VSHORAD	30	9.5	285	SP systems w. 300 rds
SHORAD	48	10	480	12 Btry w. 480 rds
MERAD	16	350	1400	4 Btry w. 128 rds
Total			2577	

* Estimation mil. USD – for a full package including training, initial spare parts, support equipment, a.o.

These summary looks over a variant of the AD weaponry update process show the complexity and the significant financial effort need for rise an essential branch of Armed Forces, one of the most potent force multiplier and in the same time a real deterrence factor into the hands of political establishment at the opening of a possible conflict.

REFERENCES

- [1] Constantinescu, D., Rădulescu, M., *Euro-Atlantic integration for a high-performance Romanian SHORAD*, Proceedings of the 11th International Scientific Conference „Strategies XXI”, National Defense University „Carol”, Bucharest, April 2 – 3, 2015, ISSN 2285-8318, Vol. 2, p. 59;
- [2] Rădulescu, M., Șandru, V., *Prelungire de resursă, revitalizare și modernizare pentru complexele de rachete antiaeriene*, Revista Gândirea Militară Românească nr. 5 pp. 70–79/2013 ISSN 1454-0460;
- [3] Rădulescu, M., Șandru, V., *SHORAD solutions for the Air Forces systems up-grade*, International Conference of Scientific Paper, AFASES 2015, Vol. 1, p.99, Brașov, 28-30 May 2015;
- [4] ***, *Military equipment guide*, <http://www.military.com/equipment>, accessed April, 2017.

AERIAL PHOTOGRAPHY AND THE USE OF PHOTO CAMERAS ATTACHED TO DRONES

Mihai RADULESCU, Victor VLADAREANU

Institute of Solid Mechanics of the Romanian Academy (mih_rad@yahoo.com)

DOI: 10.19062/2247-3173.2017.19.1.22

Abstract: *In aerial photography performed with the help of the drones, it is advisable to use a recommended camera, which, based on the tests performed on it, proved to be able to get the best photographs. In order to obtain professional aerial photographs using drones, it is necessary to use basic camera settings such as ISO, shutter speed, aperture, focus and measurement together with stabilization of the thorn, which are the most important factors for achieving this goal.*

In this context, some of the most important camera settings used in aerial photography will be presented in this paper. Knowing and implicitly applying these camera settings is imperative in making the most successful and faithful both aerial and land photography.

Using appropriate camera settings that a drone is equipped with will help prevent distortions of photography, such as chromatic aberrations and cylinder distortion. These settings will simplify the image processing tasks required in a host of important applications such as feature extraction, land recognition, and so on. This in turn simplifies the processing tasks required in a number of important applications, such as feature extraction, landmark recognition, etc.

Keywords: *drone aerial photography, ISO, shutter speed, aperture, gimbal stabilization.*

1. INTRODUCTION

An important application of robots is to clarify, limit and combat areas where there is a great danger that staff access is very risky and sometimes impossible. Thus, Kay Daniel [1] presented a project focused on the use of drones in the event of incidents caused by uncontrolled emissions of liquid or gaseous contaminants (e.g. explosive or toxic gases, nuclear, biological or chemical weapons). Another research project - Air Shield [2] - funded by the Federal Ministry of Research and Development German Education in the field of "Civil Security Research", refers to the protection of vital and sensitive infrastructures and population in case of threats to men or natural disasters.

The Air Shield project proposes the use - sometimes partial - of flip-flops (partly autonomous) in order to recognize and support in the anticipation and prevention of emergencies.

The drone can carry several types of cameras. Different remote data levels can be combined to provide some more comprehensive information such as: 15-30 m resolution imaging from space-borne sensors to determine the uniform landscaping; <1 m satellite or aircraft data to evaluate the ecological status model in an area of interest; 5 cm UAV images to measure the gap and patch sizes, as well as the percentage of bare soils and respectively covered with vegetation [3].

One of the aims of this paper was the presentation of those settings of each camera type that are the best in the case of both aerial and landing photography.

Therefore, using in aerial photography an adequate camera and their main specific above-mentioned settings, the distorted photos such as chromatic aberrations and barrel distortion will be avoided [4].

In the case of drone aerial photography, it's important to use a proven and recommended camera to get the best photos every time. Understanding camera settings, such as ISO, shutter speed, aperture, focus and measurement along with thaw stabilization are the most important factors to obtain accurate professional aerial photos.

2. DRONE AERIAL PHOTOGRAPHY CAMERA SETTINGS

The main camera / movie settings used on drones are as follows:

2.1. Optical zoom

Practically all today's digital cameras are equipped with a zoom lens. The zoom lens allows you to control how much of the subject is included in the image without having to change the distance to or from the subject. The zoom range of a digital camera is given according to its 35 mm equivalent. This is because many users are familiar with the 35mm film lens. Zoom is ideal when the original scene looks clustered or has too much distraction [4].

2.2. Shutter-speed

This is probably the most important camera setting for a good aerial shot. The camera shutter commands the amount of time light allowed to reach the CCD (in simple terms, the CCD is the place where digital image pixels are created). Shutter speeds are displayed as multiples of one second. The setting of the shutter speed is a very creative setting to control the movement of an image.

In the case of aerial photography, the depth of field is not a problem, so set your camera on the shutter priority. Select between 1/500th and 1/1000th of a second (1/750th of a second blocks the largest blur with lenses up to 100mm in length on a full-frame camera). Higher trigger speeds (1/500th) tend to freeze the subject's movement, while lower speeds (1/30th) allow to the subject's movement to be recorded as a blur in the image.

2.3. Focus Methods

Digital cameras are connected to an autofocus system (AF). Of course, there are differences from manufacturer to manufacturer. The two basic AF modes are: *Single* and *Continuous*, often referred to as *One-shot* and *Servo*.

Most modern rooms have fast and efficient self-focusing capabilities. *Continuous AF* mode is better for aerial photography and moving targets - such as children playing - because continuous focus is on the subjects.

In the case of static targets on a land or in a stationary vehicle, the *Single AF* mode is used because it will work very well, since autofocus locks on the target when applying a slight push on the trigger button and stays fixed in time hold down the button until you press the button fully to take the shot (picture).

2.4. Stabilization / Vibration

If you purchase a drone from a top manufacturer, you will virtually guarantee that you will get an excelent quality gimbal for stabilizing of the image. Some of the best drones are DJI, 3DR, Walkera, Yuneec, Aerialtronics and Service-Drone. The gimbal holds the drones stable, accessing and adjusting of hundreds of seconds per second to keep the drone in a steady and perfect condition for airshots and aerial photographs. The dampers reduce vibrations. Currently, DJI are world leaders in air technology using gimbal.

The new Phantom 4 Pro, Phantom 3 and Inspire 1 (top-drones), have 4k high-quality cameras. Inspire 1 Pro with the Zenumse X5R gimbal and the Zenumse X5R photo-camera is the world's first aerial camera Micro Four Thirds capable of recording 4K videoclips without losses in RAW.



FIG.1[4] Enchanting Evening Over Chicago's Navy Pier



FIG.2[4] The Inspire 1_Pro with Zenumse X5R Drone

2.5. ISO For Aerial Photos

The ISO setting allows subjects to be photographed in a wider range of lighting conditions. For example, changing to a higher ISO value will allow you to continue taking pictures even when the light is weaker, relatively dark without using the built-in camera flash.

The aerial photographs are strongly correlated with the resolution, so the ISO is lower, the better. Using the lowest ISO settings available with your equipment helps ensure maximum image resolution. It is also recommended not to use the digital ISO settings under the lowest rating of your camera.



Fig.3[4] Heavenly Morning In Historic Spello, Italy

Below are presented some guidelines for different ISO settings:

Low ISO setting (100-200)

Outdoor topics in sunlight. Landscape or static indoor topics using a tripod.

This setting is used when maximum image quality is required.

Medium ISO setting (250-400)

Closed weather scenes. Capturing movements in good light conditions.

In this case are obtained the clear images.

High ISO settings (500-800)

- Scenes with low light, pop concerts and night shots, fast capture of movement in slow or indoor conditions.
- Pop concerts and Night photography
- Capturing fast movement in dull or indoor conditions.

2.6. Diaphragm Aperture

The aperture is one of the three pillars of the photo, the other two being ISO and shutter speed. Undoubtedly, this is the most discussed topic, as the aperture adds a dimension to a photo by blurring the background or by magically inserting all the objects into the lens. An adjustable iris incorporated into a camera lens controls the diaphragm. This iris can be opened or closed to control the amount of light reaching the CCD. The size of the iris hole is marked with f-numbers, written as fractions. For example: f /11, f /5.6 and f /2.8. The higher the number "f", the smaller the iris aperture.

Each lens has a limit on how much or how small the diaphragm size can be varied. If you look at your lens specifications, you'll find out which is the maximum opening (the smallest number "f") and the minimum opening (the largest number "f") of the lens. The maximum aperture of the lens is much more important than the minimum because it shows the shutter speed.



FIG.4[4] Stunning Aerial Photo Of Oahu, Hawaii

2.6.1. Aperture in Aerial Photography

It is known how the diaphragm affects the depth of the field. Unlike the ground photos, the depth of the field is almost a problem in aerial photography because we focus almost infinitely. Set the aperture to the maximum lens sharpness setting. Focus on shutter speed and framing your subject.

You know the f-stop (diaphragm) that gives you maximum clarity for your special purpose. As a general rule for most goals, maximum clarity is generally two downsides to the maximum setting (the widest). For example, a f/2.8 lens will normally achieve maximum clarity at about f/8.

2.7. Metering For Aerial Photography

Metering signifies how your camera determines what the correct shutter speed and aperture should be depending on the amount of light that goes into the camera and the sensitivity of the sensor.

Today, every DSLR has an integrated light meter that automatically measures the reflected light and determines the optimal exposure. The most common metering modes in digital cameras today are:

- Matrix Metering also known as Evaluative Metering and
- Center-weighted Metering; Spot Metering.

In aerial photography use „*Matrix full-frame metering*” rather than “*Spot metering*” mode to reduce exposure issues.



FIG.5[4] Aerial photo over Lake Bled, Slovenia

3. CONCLUSIONS

✚ Using photcameras and settings that are suitable for aerial photography will allow you to avoid distorting photos such as chromatic aberrations and drum distortion. This will in turn provide a much cleaner data stream useful for a wide range of processing tasks such as: features extraction, landmark recognition, various learning applications, and more, which can constitute subsequently the nucleus of more applications like extremely dangerous, autonomous and vital missions that must be intelligently undertaken, including search and rescue military recognition and operation, air inspection, etc. [5]

✚ In the case of the use of aerial drones for aerial photography, it is important to use a camera that was previously tested and certified so that every time the best photographs should be obtained. Camera settings, such as ISO, shutter speed, aperture, focusing, and metering, along with gimbal stabilization, are important factors in the obtaining of clear professional aerial photographs.

✚ Therefore, to obtain an excellent aerial photography, it is necessary to have some excellent piloting skills, a deep knowledge of the principles and parameters which influence the aerial photographs, a vast experience and the best equipment.

REFERENCES

- [1] Kai Daniel, etc „AirShield: MUAV - A system-of-systems remote sensing architecture for disaster response” The 3rd Annual IEEE Systems Conference (2009 Germany)
- [2]Tobias Matschke „Description of the Project AirShield and its results in the final demonstration at Falck RISC Rotterdam” (2012)
- [3] Rango A., Laliberte A., Steele C., etc „Using Unmanned Aerial Vehicles for Rangelands: Current Applications and Future Potentials” *Environmental Practice*, vol.8, no.3, pp.159-168 (2006)
- [4]Fintan Corrigan <https://www.dronezon.com/learn-about-drones-quadcopters/best-lidar-sensors-for-drones-great-uses-for-lidar-sensors/> 4K UHD Video Drones Creating Stunning Aerial Cinematography

DISTANCE LEARNING SYSTEM FOR THEORETICAL TRAINING OF PILOTS

Carmen ȘTEFAN*, Oliver CIUICĂ**

*Romanian Aviation Academy, Bucharest, Romania (carmen.garnita@gmail.com)

**„Henri Coandă” Air Force Academy, Brașov, Romania (oliverciuca@yahoo.com)

DOI: 10.19062/2247-3173.2017.19.1.23

Abstract: *This paper describes a new method used in the pilots training program and discusses the details about content of the distance learning package and about the legal framework. It provides an outline of how to structure and conduct effective distance learning training program.*

The study revealed the fact that distance learning may be an alternative option to the traditional training. It offers a Learning Management System for communication, administration and monitoring students' progress. The legal framework assesses that at least 10% from the total number of hours of each program should be face-to-face training. The ATOs implement the distance learning training due the high demand of the market and due the low costs of implementation. The distance learning could be effective for self-motivated, self-educated students and they might be able to work with new technologies.

The distance learning systems has to help the students to achieve the necessary SKAs to become a pilot.

The study has concluded that the distance learning used in pilots training is a suitable, a modern and an efficient method of training.

Keywords: *distance learning, e-learning, pilots training*

1. INTRODUCTION

Information technology has permeated nearly every aspect of people's lives. Technology is changing the way people and companies present, disseminate, and communicate their messages, creating an ever-present learning environment and an accelerating information society. In an information society, achieving a high level of acquisition and management of knowledge will be one of the key competitive advantages.

In order to decide the deployment of a new type of training, the ATOs should carefully conduct an analysis. For the studied ATO was conducted a PESTLE analysis, a balance score card and there were determined the key performance indicators.

The PESTLE analysis (P for Political, E for Economic, S for Social, T for Technological, L for Legal and E for Environmental) for the specified ATO has revealed the fact that internet and terrorism are main factors that are affecting the training activity. The strength of the analyzed ATO is the human capital, meaning the experienced ground instructors. In order to improve the training activity the analysis emphasized the necessity to implement courses using new technologies. The distance learning program will increase the student number and ATO will be able to offer training programs convenient for the new generations.

Throughout the traditional training or using the distance learning system the ATO has to ensure a high level of SKAs for all students, which is measurable using monitoring students' performance, the feedback from the flight instructors and the feedback from the employers.

The balance score card Fig.1. accentuates the opportunity to use the e-learning system as an alternative to the traditional training.

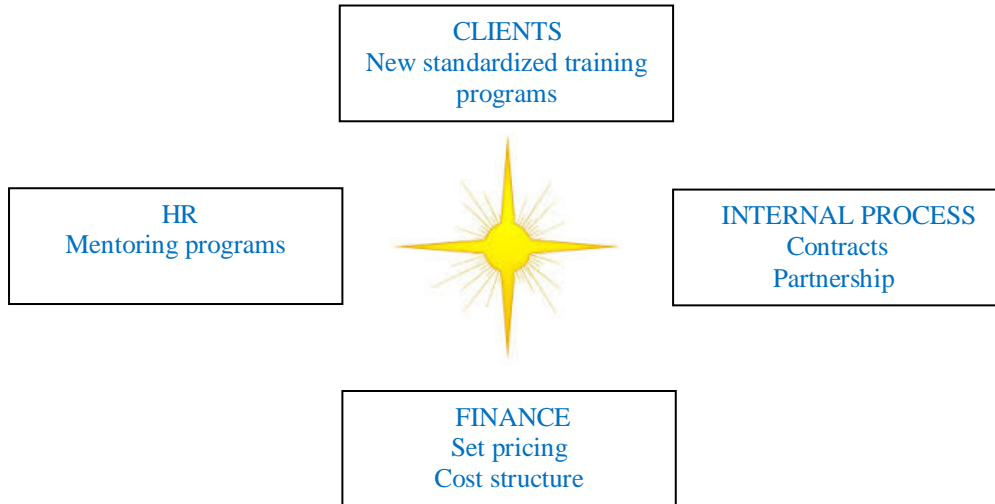


FIG. 1. Balance Score Card

From financial point of view the implementation of a distance learning system is low-priced, because the accreditations' cost are about 1000 euro, the implementation costs are 2250 euro and the revenue is about 16,800 euro for 10 students.

The main advantages of distance learning [5,8] are flexibility, supported study, career changing, low costs and international recognition. This type of training is based on self-study. The study revealed that the compulsory face-to-face training is highly appreciated by the students.

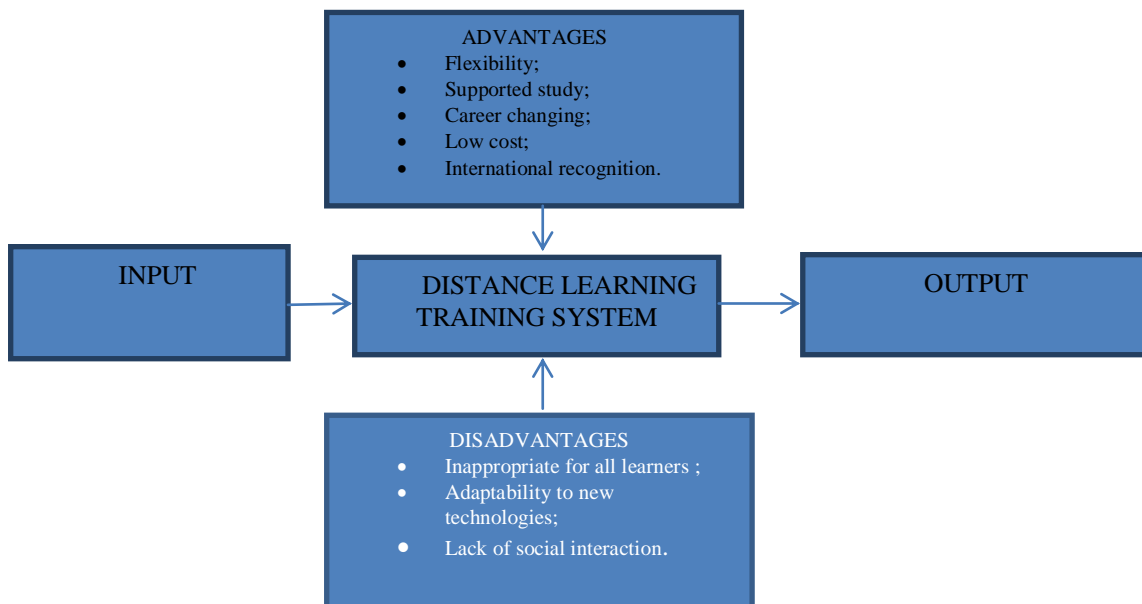


FIG. 2. Advantages and disadvantages of distance learning training system

In the meantime, the disadvantages of distance learning are lack of social interaction, inappropriate type of training for all learners, and the fact that it demands adaptability to the new technologies. Also there may appear a lag between the students' queries and the feedback from the instructor. The advantages and disadvantages of the distance learning system are resumed in fig.2. and it shows the great influence of these particularities on training results.

The student who choose the e-learning system should be self-motivated, self-educated and he needs a high ability to study using new technologies. Due all of these particularities the distance learning training system should be choose only by future-pilots with the specified characteristics features. Only 10% of the future pilots have succeeded to complete the theoretical training in the same period as a traditional training. 30% of the students realize during the training process the fact that the distance learning training program is not suitable for them. The main part of the students manage to complete the training course in a higher period of time than the one attached for the traditional training.

2. THE LEGAL FRAMEWORK

The legal framework of distance learning for pilots training is established by EASA trough Acceptable Means of Compliance (AMC) and Guidance Material (GM) to Part-ORA [3,4] and consist two main point. The first one states that a variety of methods is open to ATOs to present the course material. It is, however, necessary for ATOs to maintain comprehensive records in order to ensure that students make satisfactory academic progress and meet the time constraints laid down in PART-FCL for the completion of modular courses. The ATPL modular course from PPL will be discussed further because it offers the highest qualification in the civil aviation and it has the highest demand on the market.

The second establishes the planning guidelines for ATOs. First of all, the assumption that a student will study for at least 15 hours per week will be used. For that reason it is necessary throughout the course material an indication of what constitutes a week's study. Usually, this is done throughout the guidelines. The e-learning package should include the a recommended course structure. Regarding the progress test it is specified that should be a progressive test for each subject for every 15 hours of study, which should be submitted to ATO for assessment. Additional self-assessed progress test should be completed at intervals of five to ten study hours. The e-learning system should include appropriate contact times throughout the course. The student shall have access to an instructor by telephone, fax, email or the internet.

There should be measurement criteria to determine whether a student has satisfactorily completed the appropriate elements of the course to a standard that, in the judgement of the Head of Training, or Chief Theoretical Knowledge Instructor, will enable them to be entered for the PART-FCL theoretical examinations with a high rate of success.

If the ATO provides the distance learning by help of IT solutions (e.g. internet), the theoretical knowledge instructors should monitor students' progress by appropriate means.

The following pre-requisites should be fulfil before acceptance at a modular ATPL distance learning course:

- Academic:
 - (a) A knowledge of English language proficiency, in accordance with EASA Regulation (Part-FCL 055) or level 4 ICAO Language Proficiency.
 - (b) The student must demonstrate a sufficient knowledge of mathematics and science.

- Hold a PPL(A) issued by an ICAO member state.
- Hold a class 1 medical certificate before starting the course.

The distance learning flowchart for the theoretical course is represented in Fig.3. After getting over the distance learning program the student should attend the face-to-face training and the schools exams. The program is considered to be compliant with international regulations if the student gets at least 75% for each subject. The students' evaluations have to be written and these will be kept for five years.

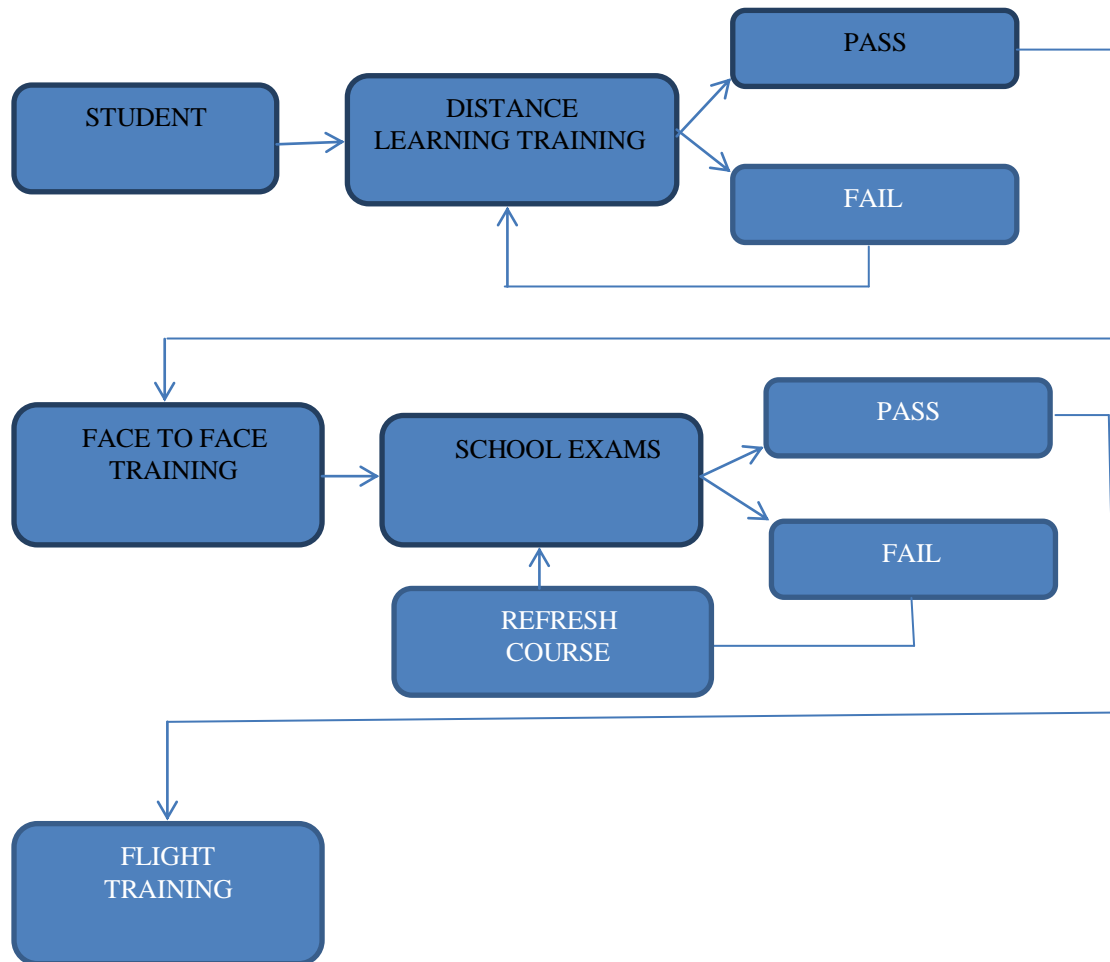


FIG. 3. Distance learning flowchart for theoretical pilots training

3. E-LEARNING PACKAGE CONTENT

There are different types of platforms dedicated to pilots training. Usually, an e-learning package consist of a set of books/e-books in accordance with EASA, Computer Based Training, animations to enhance the learning process, links to relevant web sites and student study guides. For students' evaluation part the e-learning system consists on-line self-assessment tests for each 3 hours of study, on line progress tests after approximately every 15 hours of study, exam reference material (CAP's). The content of an e-learning training package is graphic represented in Fig. 4. The package also includes an online question bank with a few thousands questions. Each theoretical knowledge instructor may add materials and tests for each subject.

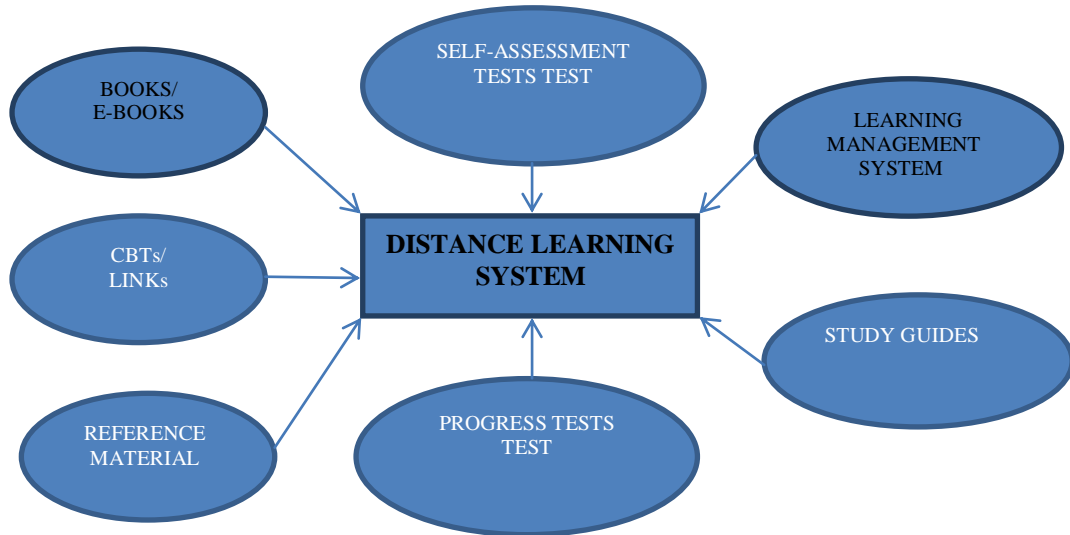


FIG. 4. Distance learning package content

The e-learning system also offer access of ATO management and theoretical knowledge instructors to a Learning Management System for all communication / administration and for monitoring of students’ progress, students’ access to the electronic content, internal email-system and to additional resources and course material that are added by ATO. A Learning Management System is extremely useful both civil and military training schools for pilots[1,2].

The Learning Management System is highly recommended and useful being the key factor used for monitoring students’ progress[4,8]. Also it offers to the theoretical knowledge instructors the possibility to initiate corrective actions as soon as they may consider appropriate. The Learning Management System offers a wide range of reports (e.g. individual reports, class reports, assessment records, assignment reports).

Sometimes there is a supplementary content for the standard e-learning package which may contain an electronic version of the illustration, which will be available for the use of ATO instructors and the student chart manual.

The distance learning system offers an effective management. It helps ATO to improve performance, quality of learning and increases the efficiency of training. Furthermore[6,7], it is cost-effective, it offers a geographical and temporal flexibility, immediate learner feedback and it creates a culture of learning.

CONCLUSIONS

The studied ATO decided to introduce the distance learning system as an alternative option to the traditional training in order to increase the number of courses, students, and revenue. The key performance indicators are students’ performance, feedback from the flight instructors and from their employers. The access to a Learning Management System for communication, administration and monitor the students’ progress is fully compliant with EASA Regulations. The implementation of the distance learning is low-priced and revenue is high.

The distance learning system is not a suitable training program for all future pilots. The distance learning training program is suitable only for students with a specified profile. The students should follow such a learning program only if they are self-motivated, self-educated and they have the ability to work with new technologies.

At the studied ATO in the last year only 25%-30% of the students have chosen the distance learning training. The time assigned for completing the distance learning course is usually double compared to the time assigned for traditional face-to face training. Only a small percent of the future pilots are able to complete the distance learning training program in the minimum specified period of time.

The Learning Management System forms an important part of the e-learning system which ensure the administration part of the training process and it helps the theoretical ground instructors to monitor the students' progress. The Learning Management System gives the status of all assignments in a course.

Theoretical training for pilots may be nowadays delivered using a distance learning system, but this type of training is recommended only for trainees with a specific profile.

REFERENCES

- [1] O. Ciuică and C.Ştefan, *Why safety management system for aeronautical organization*, Buletinul Universitaţii Naţionale de Apărare "Carol I", 2016;
- [2] O. Ciuică, E. Mihai and C.Ştefan, *Flight Safety Introduction for student pilots*, AFASES 2016;
- [3] EASA AMC1 ORA.ATO.300 Annex to ED Decision 2012/007/R
- [4] SSAvC Manual de Instruire Avioane
- [5] <https://le.ac.uk/student-life/distance-learners/benefits>
- [6] <http://www.learninglight.com/aviation-training-elearning/>
- [7] <https://www.webanywhere.co.uk/enterprise/sites/default/files/Webanywhere%20White%20Paper%20Aviation%20Industry.pdf>
- [8] <https://www.thecompleteuniversityguide.co.uk/distance-learning>

AERODYNAMIC DESIGN CONSIDERATIONS OF A FLYING WING TYPE UAV

Cornel STOICA, Dumitru PEPELEA, Mihai NICULESCU, Adrian TOADER

Institutul Național de Cercetări Aeronautice - INCAS București, Romania
(stoica.cornel@incas.ro, pepelea.dumitru@incas.ro, niculescu.mihai@incas.ro,
toader.adrian@incas.ro)

DOI: 10.19062/2247-3173.2017.19.1.24

Abstract: *The UAV field recognizes a full conceptual, technological and applicational maturity, however, a number of national and international scientific references recommend research directions that are insufficiently explored, such as: biological inspiration through the concept of morphing, approaches of the multisystem concept, or optimizations of operating time in hostile environments. For the aerodynamic optimization stage, this paper proposed a tailless / flying wing concept design for the assessment of aerodynamic performance in the flight configuration, by means of experimental tests in a subsonic wind tunnel.*

Keywords: *Flying wing, wind tunnel, INCAS, MASIM.*

1. INTRODUCTION

The UAV field recognizes a full conceptual, technological and applicational maturity, however, a number of national and international scientific references recommend research directions that are insufficiently explored, such as: biological inspiration through the concept of morphing [1, 2, 3], approaches of the multisystem concept [4, 5, 6], or optimizations of operating time in hostile environments [5, 7].

For the aerodynamic optimization stage, this paper proposed a tailless / flying wing concept design for the assessment of aerodynamic performance in the flight configuration, by means of experimental tests in a subsonic wind tunnel [8, 11, 12], as a follow-up of several numerical evaluations [13, 14, 15].

Abbreviations

C_x	-drag coefficient	C_y	-lateral force coefficient
C_z	-lift coefficient	β	-sideslip angle
S	-area	V	-velocity
ρ	-density	K	-turbulence factor
C_m, C_n, C_r	-moment coefficients on the three axes	F_x, F_y, F_z	-aerodynamic forces on the three axes
α	-angle of incidence		

2. AERODYNAMIC TESTS CONCERNING THE PERFORMANCE OF FLYING WING UAV

2.1. Theoretical landmarks and description of the subsonic wind tunnel

The aerodynamic tunnel from INCAS is a Prandtl type, with a closed experimental chamber and octagonal cross section. This wind tunnel provides an ascending cross section channel, having four corners with 90° turning vanes, which direct the airflow from the end of the diffuser towards the collector's entrance.

[X, Y, Z] – Components of the resulting aerodynamic force:

$$C_x = \frac{2 \cdot F_x}{\rho \cdot V^2 \cdot S} \quad (1)$$

$$C_y = \frac{2 \cdot F_y}{\rho \cdot V^2 \cdot S} \quad (2)$$

$$C_z = \frac{2 \cdot F_z}{\rho \cdot V^2 \cdot S} \quad (3)$$

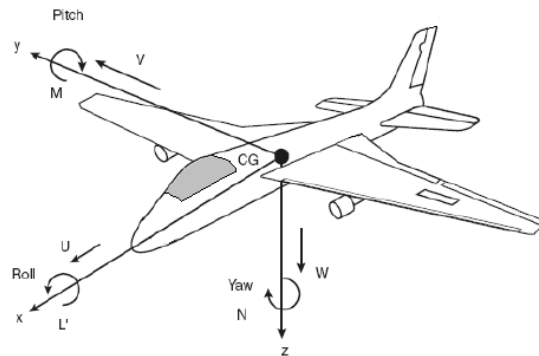


FIG. 1 Model reference system

In Fig.2 such a closed circuit wind tunnel is represented schematically. The term “closed circuit” means that the return of the airflow is done using a single lateral channel [8, 9, 10, 12, 15].

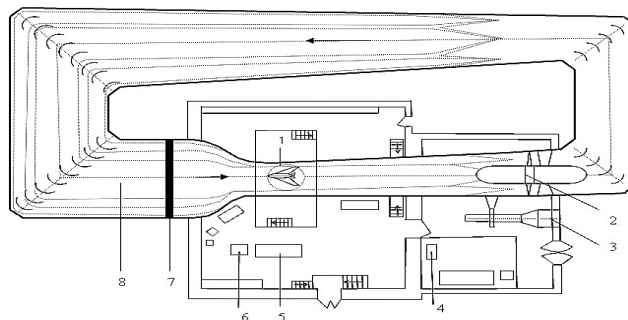


FIG. 2 Prandtl wind tunnel with closed circuit (1.operating room, 2. engine, 3.engine cooling system, 4. power supply panel, 5. control panel, 6. engine control panel, 7. section to minimize turbulence, 8. settling chamber)

In the subsonic wind tunnel from INCAS we find the technical data from Table 1, below. The venue supports testing of aircraft models of up to 1.8 m wing spans.

Table 1. Subsonic wind tunnel technical data

No.	Component	Description
1.	Experimental chamber	2.0 m height x 2.5 m width
2.	Compression ratio	10:1
3.	Experimental chamber dimensions	2 x 2.5 x 6.0 m
4.	Maximum wind speed	110 m/s
5.	Turbulence coefficient	0.2 % (Dryden, at Reynolds No. = 385.000)
6.	Turbulence factor	K = 1.11
7.	Working pressure	atmospheric pressure
8.	Measurement system	external balance, 6 components, of pyramidal type
9.	Accuracy	0.02 % full scale, all axes
10.	Resolution	0.002 % full scale, all axes
11.	Incidence angle	-25....+45 deg. - 1...5 deg/sec
12.	Yaw angle	+/- 180 deg.- 0.5...6 deg/sec

2.3 Experimental setup

The MASIM model was mounted on the three elements of the external balance. The latter is used to measure aerodynamic loads on the model, inside the test section, as seen in Fig. 3.



FIG. 3 Model mounted on the balance inside the subsonic wind tunnel

The balance is located outside the subsonic aerodynamic tunnel and it measures three forces and three moments. It is also used to position the model at different pitch and yaw angles. The position angles are measured with absolute encoders. For all measurements, the incidence varied with one degree step. To determine the aerodynamic parameters of the model, four sets of measurements were taken. The model was positioned on the balance and was considered to be at zero degrees, when the indicator on the control desk measured +7.37 degrees [12].

The first experiment was performed at an incidence angle ranging from -4.53 to 18.37 degrees and yaw angle was constant at 0 degrees. For the next two experiments, the angle of incidence varied from -4.62 to 17.37 degrees, while the yaw angle was constant at -5° and +5° at a time, respectively. For these first three tests, the wind speed inside the experimental chamber was 25 m/s.

The last experiment was performed at a constant yaw angle of 0° , while the incidence angle varied from -2.67 to 17.33 degrees. In this case, the wind speed inside the experimental room was 30 m/s.

2.4 Experimental results

The experimental tests generated a series of results, the most relevant being presented in Fig. 4 (a, b, c, d). The final data is obtained following numerical transformations of the balance measurement units by means of some specific coefficients.

For the speed of 25 m/s, according to Fig.4 we observed a maximum value of the lift coefficient, C_z , at an incidence of 16° for a sideslip angle $\beta=0^\circ$, and of 15° for $\beta=5^\circ$.

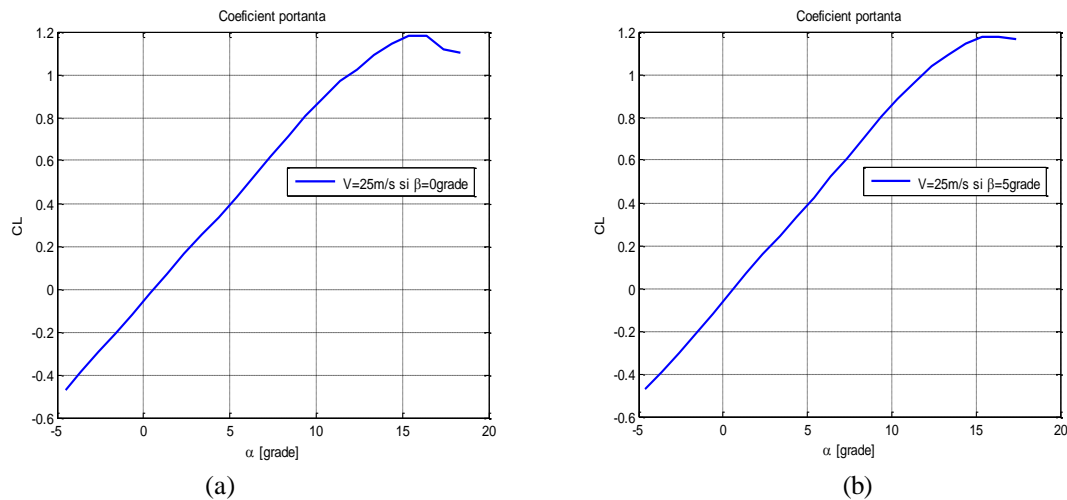


FIG. 4 Lift coefficient, C_z

Drag has a minimum corresponding coefficient, C_D , at 5° incidence (see Fig. 5), and the coefficient of the lateral force F_y grows in absolute value, proportionally (towards -0.03) with flight incidence, but also with the sideslip angle β ($0,005$ for $\beta=0^\circ$ vs $0,025$ for $\beta=5^\circ$), according to the graph in Fig. 6.

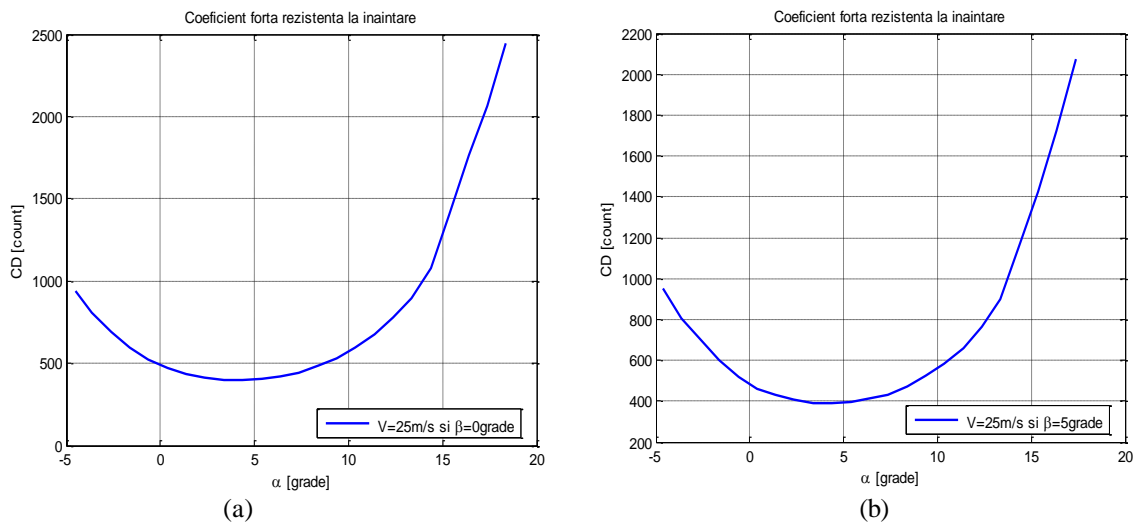


FIG. 5 Drag coefficient, C_D

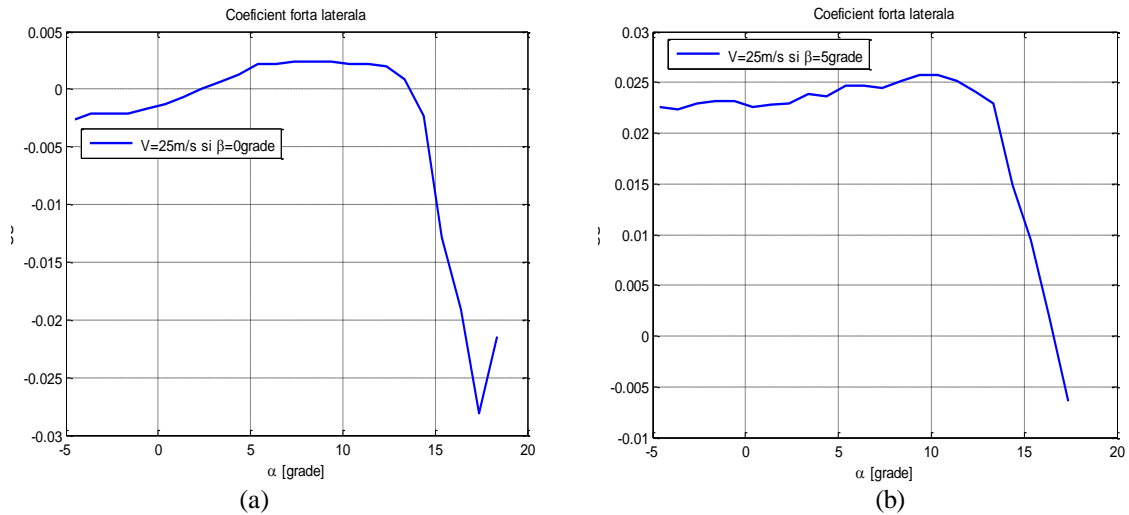


FIG. 6 Coefficient of the side force F_y

The roll coefficient C_r , grows significantly after the incidence of 15° (see Fig.7), having value differences within the incidence range of 0° - 10° .

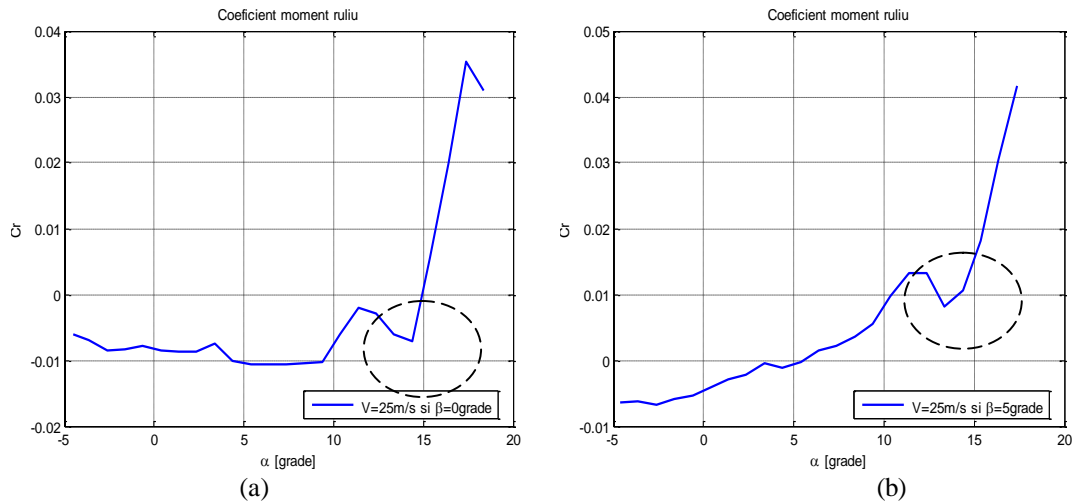


FIG. 7 Rolling moment coefficient

The pitching moment, C_m , versus incidence, for a speed of 25 m/s is highlighted in Fig. 8, with a null C_m , for incidence values around 3° (Fig. 8), for both sideslip angles, β .

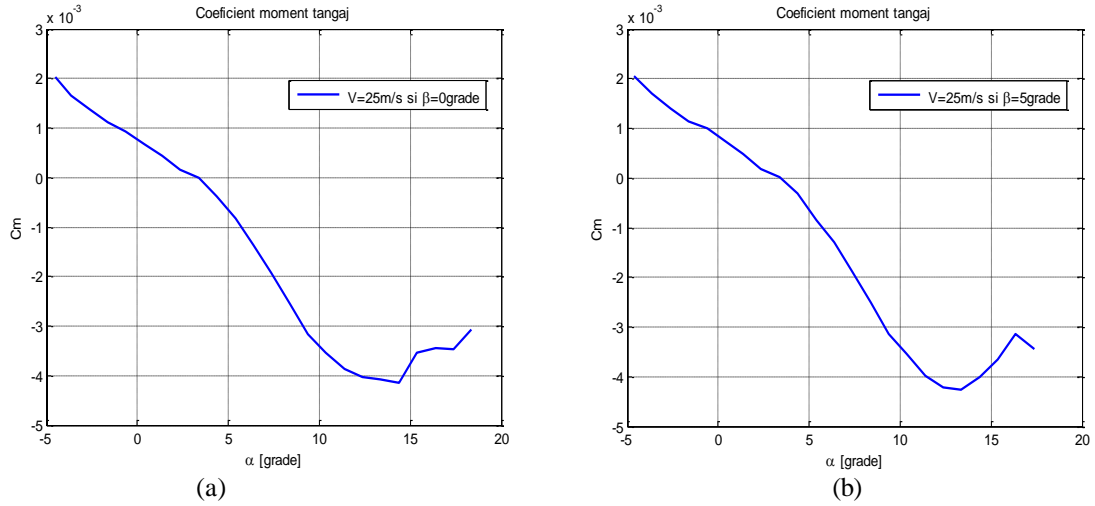


FIG. 8 Pitching moment coefficient

The yawing moment coefficient, C_n , varies significantly after the incidence of 13° , as seen in Fig. 9, having variations in the incidence range of 0° - 10° .

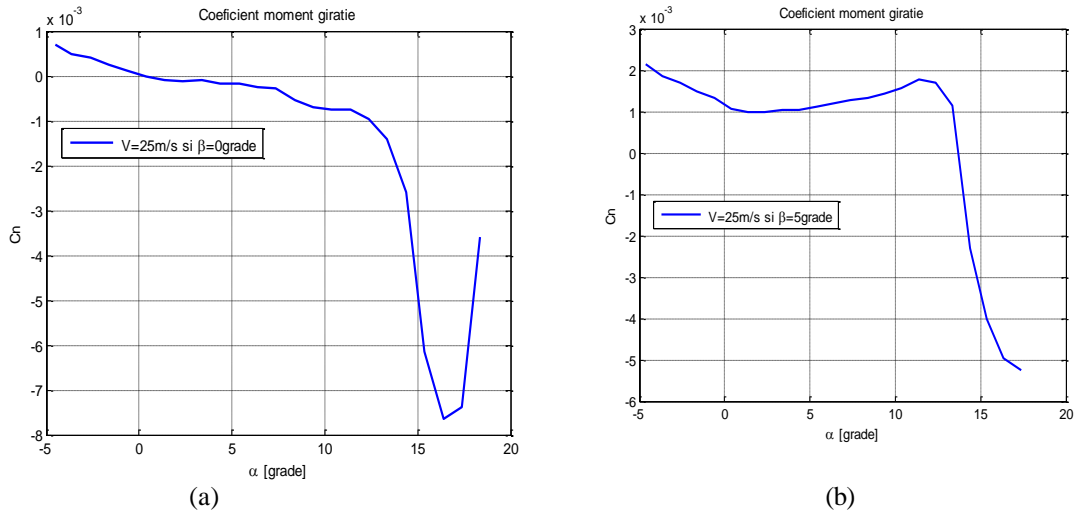


FIG. 9 Yawing moment coefficient

The values of the aerodynamic coefficients are shown in Table 2.

Table 2. Aerodynamic coefficients (left $\beta=0^\circ$, right $\beta=5^\circ$).

V	Incidental	Beta	CL	CD	Cm	CS	Cn	Cr	V	Incidental	Beta	CL	CD	Cm	CS	Cn	Cr
25	7.37	0	0.616138107	0.044525949	-0.0019	0.002147	-0.00033	-0.01079	25	7.37	5	0.610768	0.043713	-0.0019	0.024471	0.00132	0.002485
25	-4.53	0	-0.468694598	0.094089505	0.002028	-0.00258	0.000701	-0.00606	25	-4.63	5	-0.47065	0.094902	0.002049	0.022539	0.002145	-0.00636
25	-3.62	0	-0.389114161	0.080926724	0.001656	-0.00215	0.000495	-0.00691	25	-3.63	5	-0.39107	0.080764	0.001697	0.022324	0.001856	-0.00618
25	-2.62	0	-0.292934124	0.068901468	0.001366	-0.00215	0.000413	-0.00842	25	-2.63	5	-0.30465	0.070201	0.001387	0.022968	0.001691	-0.00679
25	-1.63	0	-0.210424345	0.059476267	0.001118	-0.00215	0.000248	-0.00836	25	-1.63	5	-0.21384	0.059801	0.001138	0.023183	0.001485	-0.00588
25	-0.63	0	-0.116197202	0.052001108	0.000931	-0.00172	0.000124	-0.00782	25	-0.62	5	-0.11717	0.052164	0.000993	0.023183	0.00132	-0.00533
25	0.37	0	-0.018552494	0.046963501	0.000683	-0.00129	0	-0.00855	25	0.37	5	-0.02539	0.046151	0.000745	0.022539	0.001073	-0.00406
25	1.37	0	0.069815966	0.043388425	0.000435	-0.00064	-8.3E-05	-0.00867	25	1.37	5	0.070304	0.043063	0.000497	0.022754	0.00099	-0.00297
25	2.37	0	0.167460674	0.040950873	0.000166	0	-0.00012	-0.00861	25	2.37	5	0.158673	0.040951	0.000186	0.022968	0.00099	-0.00212
25	3.37	0	0.254852688	0.039488341	0	0.000644	-8.3E-05	-0.00752	25	3.37	5	0.244112	0.039163	2.07E-05	0.023827	0.001031	-0.00042
25	4.37	0	0.335409572	0.039650845	-0.00037	0.001288	-0.00017	-0.01	25	4.37	5	0.334433	0.039001	-0.00031	0.023612	0.001031	-0.00121
25	5.37	0	0.429148491	0.040625866	-0.00083	0.002147	-0.00017	-0.01061	25	5.37	5	0.426219	0.039651	-0.00085	0.024686	0.001114	-0.00018
25	6.37	0	0.52142274	0.041925893	-0.00137	0.002147	-0.00025	-0.01061	25	6.37	5	0.523376	0.041113	-0.0013	0.024686	0.001196	0.001576
25	7.37	0	0.617602777	0.044038438	-0.00192	0.002361	-0.00029	-0.01067	25	7.37	5	0.609303	0.043388	-0.00188	0.024471	0.001279	0.002182
25	8.37	0	0.715735709	0.048751039	-0.00255	0.002361	-0.00054	-0.01042	25	8.37	5	0.707436	0.047451	-0.0025	0.025115	0.00132	0.003515
25	9.37	0	0.808498181	0.053301136	-0.00317	0.002361	-0.0007	-0.01018	25	9.37	5	0.801175	0.052489	-0.00315	0.025759	0.001444	0.005515
25	10.37	0	0.887590395	0.059313764	-0.00354	0.002147	-0.00074	-0.006	25	10.37	5	0.888567	0.058339	-0.00354	0.025759	0.001568	0.009819
25	11.37	0	0.972541291	0.067276434	-0.00387	0.002147	-0.00074	-0.00206	25	11.37	5	0.963753	0.066139	-0.00397	0.025115	0.001774	0.013273
25	12.37	0	1.025757656	0.077514152	-0.00404	0.001932	-0.00095	-0.00291	25	12.37	5	1.039428	0.076539	-0.00422	0.024042	0.001691	0.013213
25	13.37	0	1.091179611	0.089539408	-0.00408	0.000859	-0.0014	-0.00606	25	13.37	5	1.090691	0.089864	-0.00426	0.022968	0.001155	0.008122
25	14.37	0	1.146348871	0.107739796	-0.00414	-0.00236	-0.0026	-0.00715	25	14.37	5	1.146837	0.116515	-0.00399	0.014811	-0.00231	0.010607
25	15.38	0	1.182477412	0.140565495	-0.00354	-0.01288	-0.00615	0.005455	25	15.37	5	1.177595	0.142353	-0.00366	0.009445	-0.004	0.018183
25	16.38	0	1.180036295	0.176641264	-0.00344	-0.0191	-0.00763	0.01988	25	16.37	5	1.174178	0.172254	-0.00315	0.001932	-0.00495	0.030486
25	17.38	0	1.119008352	0.206869908	-0.00346	-0.02812	-0.00738	0.03535	25	17.37	5	1.166854	0.207192	-0.00344	-0.00644	-0.00524	0.041638
25	18.37	0	1.104361646	0.244242704	-0.00306	-0.02147	-0.00359	0.030971	25	17.37	5	1.166854	0.207192	-0.00344	-0.00644	-0.00524	0.041638
25	7.37	0	0.607350083	0.043875935	-0.00186	0.001073	-0.00029	-0.01109	25	7.37	5	0.606862	0.043063	-0.00184	0.024686	0.001361	0.002

3. CONCLUSIONS

The experimental steps for the proposed lifting surface were limited procedurally and financially, which led to the strict selection of initial test conditions with minimal implications for the level of confidence of the results. However, some obtained data contain numerical deviations that can be seen in the graphs in Fig.7 regarding the curves of the rolling moment coefficient, C_r , in the incidence range $10^\circ \div 15^\circ$.

Although experimental results depend on a number of parameters from the test chamber (ex. test chamber geometry, airflow quality) [8], tests in the aerodynamic tunnels along with CFD (Computational Fluid Dynamics) simulations can confirm the expectations of the chosen configurations or indicate complete or partial geometric optimization processes.

The paper presents the tests results performed under the MASIM project framework in the INCAS (National Institute for Aerospace Research “Elie Carafoli”) subsonic wind testing facility. The aim of the tests was to obtain the main aerodynamic coefficients for the an flying wing – a member of a formation flying system.

ACKNOWLEDGMENT

This work is supported by the Executive Agency for Higher Education, Research, Development and Innovation Funding (UEFISCDI) under MASIM project (PN-II-PT-PCCA-2013-4-1349).

REFERENCES

- [1] Barbarino S., Bilgen O., Ajaj R.M., Friswell M.I., Inman D. J., A review morphing aircraft, *Journal of intelligent material system and structures*, vol. 22, pp. 823-877, 2011;
- [2] Valasek J., *Morphing aerospace vehicles and structures*, Wiley, ISBN 978-0-470-97286-1, pp. 286, 2012;
- [3] Prisacariu V., Boscoianu M., Cîrciu I., *Morphing wing concept for small UAV*, Applied Mechanics and Materials, Vol. 332 (2013) pp. 44-49, ISSN:1662-7482, © (2013) Trans Tech Publications, Switzerland, doi:10.4028/www.scientific.net /AMM.332.44 OPTIROB 2013;
- [4] Prisacariu V., Cîrciu I., Cioacă C., Boşcoianu M., Luchian A., *Multi aerial system stabilized in altitude for information management*, Review Of The Air Force Academy, 3(27)/2014, Braşov, Romania, ISSN 1842-9238; e-ISSN 2069-4733, pp. 89-94;
- [5] Karen Buondonno, Sarah Gilson, Bina Pastakia, Lacey Sepulvado, *Multi-UAS Operational Assessment: Class D Airspace*, simulation report, DOT/FAA/TC-TN12/45, 2012;
- [6] Ivan Maza, Anibal Ollero, Enrique Casado and David Scarlatti, *Classification of multi-UAV Architectures*, available at <http://www.arcas-project.eu/sites/default/files/Classification%20of%20multi-UAV%20Architectures.pdf> consulted at 02.03.2017;
- [7] Eggers J.W., Draper M.H., *Multi-UAV Control for Tactical Reconnaissance and Close Air Support Missions: Operator Perspectives and Design Challenges*, RTO-HMF-135, 20p, available at <http://public.vrac.iastate.edu/~charding/audio/Eggers%20Paper%2011-06.pdf>, consulted at 03.03.2017;
- [8] Prisacariu V., Cîrciu I., Pop S., *Instruments for the evaluation of the aerodynamic performance of wind tunnels*, International conference, Scientific Research and Education in Air Force – AFASES, 2015 Braşov., ISSN 2247-3173, pp. 93-98;
- [9] Josué Njock Libii, *Wind Tunnels in Engineering Education*, pp. 235-261, in Wind Tunnels and Experimental Fluid Dynamics Research, ISBN 978-953-307-723-2, 2011, 709 p;
- [10] Bapu Joglekar, Rana Manoj Mourya, Design, *Construction and Testing Open Circuit Low Speed Wind Tunnel*, International Journal of Electrical and Electronics Research, ISSN 2348-6988 (online) Vol. 2, Issue 4, pp: 271-285, oct. – dec. 2014, available at: www.researchpublish.com;
- [11] Pepelea D., Cojocaru M.G., Toader A., Niculescu M.L., *CFD analysis for UAV of flying wing*, International conference, Scientific Research and Education in Air Force – AFASES, 2016 Braşov, DOI: 10.19062/2247-3173.2016.18.1.22, ISSN 2247-3173, pp. 171-176;

- [12] Munteanu F., Oprean C., Stoica C., *INCAS subsonic wind tunnel*, INCAS Bulletin, No 1/ 2009, București, DOI: 10.13111/2066-8201.2009.1.1.3, pp. 12-14;
- [13] Prisacariu V., Boșcoianu M., Cîrciu I., Lile Ramona, *Aspects Regarding the Performances of Small Swept Flying Wings Mini UAV-s in Aggressive Maneuvers*, Applied Mechanics and Materials, vol. 811, pp. 157-161, Trans Tech Publications, 10.4028/www.scientific.net/AMM.811.157, ISSN: 1662-7482;
- [14] Prisacariu V., Boșcoianu Corina, Cîrciu I., Boșcoianu M., *The Limits of Downsizing – A Critical Analysis of the Limits of the Agile Flying Wing MiniUAV*, Applied Mechanics And Materials, Vol. 772 (2015) pp 424-429, © (2015) Trans Tech Publications, Switzerland, doi:10.4028/www.scientific.net /AMM.772.424, pp. 424-429;
- [15] *Caiet de sarcini pentru tunel de vant pentru testarea modelelor de turbine eoliene*, available at www.icpe-ca.ro/achizitii-publice/ap2014/tunel-caiet-sarcini.pdf, consulted at 09.03.2017.

THE USE OF ROBOTS IN MILITARY OPERATIONS

Peter SZEGEDI*, Peter KORONVÁRY**, Bertold BÉKÉSI***

*Hungarian Defence Forces Education & Training Directorate (J7), Education Branch,
Hungary (szegeci.peter@hm.gov.hu)

**Faculty of Public Administration, National University of Public Service, Budapest,
Hungary (koronvarty.peter@uni-nke.hu)

***Faculty of Military Science and Officer Training, National University of Public
Service, Budapest, Hungary (bekesi.bertold@uni-nke.hu)

DOI: 10.19062/2247-3173.2017.19.1.25

Abstract: *Technological developments of the past decades made it possible for UAVs to become really effective weapon systems. Autonomic artificial intelligence as weapons can be visualized as humanoid machines of the apocalypse directed by humans who developed them. They may however easily grow over this level as their appearance in the military and non-military operations create new aspects, concepts and needs for the developers to follow. They are present in battle as well as in our cities, in IT and the virtual world, practically everywhere. Their becoming an important factor of future development in military and non-military technology as well as the society, organizations and governance is no fiction but fact.*

The article, with the help of a couple of examples, will try to illustrate how many-folded the use of robots in our societies are, how they can help solve more and more of our problems and tasks, and how they generate newer and newer thoughts in us.

Keywords: *military technology, innovations, weapon systems, military research, UAV, drone*

1. INTRODUCTION

The development of technologies, the application of research results, the appearance of new, more and more complex machines do change our lives from day to day. But they are changing the face of war too. Military robots, the application of semi-independent and (almost fully) independent tools for military purposes is not any more only a fantastic vision in the minds of some sci-fi authors but everyday reality. Unmanned aerial vehicles comprise probably the military equipment of the most versatile use present in the arsenal of modern warfare. It is becoming more and more believable an idea that in the very close future battles, even wars can be fought by robots and mercenaries between not only nation states or their alliances but also but also between irregular groups, terror organisations, international criminals or more traditional political or economic units of all types and levels.

Present research makes it realistic that autonomous systems (drones) will soon be the most widely utilised tools of warfare [4]. Such autonomous complexes, equipped with artificial intelligence and weapon systems, may be very different from the imaginary humanoid machines with a weaponry of apocalyptic effectiveness, construed and directed by mother-born humans. They can take practically any other practical size and form too – they can be wheeled, winged, or tracked, swimming, rolling or flying equipment, of any form and practically of any function.

Even remote control is becoming less and less necessary, even sometimes dangerous if precision is required – fully automated, autonomous, self-directing “intelligence” is practically available or very close to realisation for any purposes and all sizes of machines from giants down to the nano robots capable of executing pre-programmed actions even within the human body. Artificial intelligence is gaining field from medicine to production, from farming to physical exercise, from birth control to mass destruction in human fantasy as well as in the everyday realities of postmodern urban life. It can save and nurture life or destroy the living.

Their utilisation in the military sphere is no longer fiction but fact. They are present in peace keeping as well as in combat action, in urban warfare as well as in the digital battlefield. Such robots comprise an integrated part of the armoury of the modern national and allied forces and provide for much of their capabilities helping to gain the upper edge at battle. They are typically optimised to their tasks all way down to the choice of (in most cases either silicon-based or natural) materials. The existence of such technologies raise not only engineering questions but also those of jurisdiction and utilisation [1][22].

2. ROBOTS IN MILITARY ACTION

The growth of operative speed means that the attacked have less and less time to answer in kind. Defence therefore is more and more forced to apply preventive action to avoid destruction. The application of robot technology may easily lead to the creation of a well-greased on-going mechanistic system aimed at the annihilation of life. Everything can be controlled and monitored, as the context requires rapid and exact decisions as well as precise and effective execution. The development of autonomous wars is further helped by certain tendencies in developed, urban, postmodern societies:

- Technology, due to mass production and miniaturisation is becoming more and more cost-effective.
- A number of cultural developments – among them the mass education and the Internet providing all social layers with knowledge and information, ideas and ideals – strengthen the belief that (biological, i.e. human and non-human) life is valuable, human life being the non plus ultra realisation of value as such.
- It is becoming a core value of democracies that the society is expected to provide the necessary environment and inputs for the individual to live a meaningful life.
- Machines, robots are at least ethically valued to be worth less than human life.
- Machines, due to the rapidly developing IT technology, are faster in sensing, measuring and analysing (in pre-programmed ways) much larger sets of data than those any human being may process, therefore their reaction may follow faster.
- Wear and tear is a lesser problem for well-construed machines than for human beings.
- Machines remain in function under extreme weather conditions or other environmental pressures where human beings could not.
- Machines, unlike people, do not get tired, can handle monotonous processes quite well, do not feel fear or headaches, etc.

In plain English, machines require less and offer more than people. They are also better subordinates, following orders without questioning them (unless programmed otherwise). No wonder that some of the most important projects in defence research are to do with the development of robots and unmanned vehicles. As newer and newer solutions appear, drones are taking over those jobs that used to be done by man or man-run machines, or offer an opportunity to reduce human risks in the execution of dangerous tasks.

The range of possibilities is wider than wide – news speak about robots deactivating bombs, mini unmanned research submarines, reconnaissance planes and helicopters as well as precision attacks executed by unmanned aerial vehicles. All these tools execute their tasks under close human control. Even if their operators do not have to be present in the area of the activities, their active cooperation is needed at the time of action.

All these tools have to be prepared for their tasks. The preparation requires the professional cooperation of engineers and other specialists sharing the room with the tool. The ongoing IT revolution and the appearing new technologies make it possible that unmanned tools are not only becoming cheaper but also widely used. The computers taking over the burden of analysis and programmed decisions are becoming not only faster and smaller, but more and more powerful too – they are able to execute complex computations with an unimaginably huge amount of data in an unimaginably short time. A combination of modern sensor systems, the fast dataflow technology, small sizes and the extremely exact navigation revolutionised automatization by the end of the 20th century.

The development of artificial intelligence that makes the evolution of automated machines into autonomous ones is a trend in military development that is hard to neglect. It is but responsible thinking to try and model what effects they will have on war in the close future and what challenges they may mean to today's national and home defence, and in general security as such. Opportunities of their application from nano systems in the bodies of soldiers informing the command centre about their readiness to automated circular defence systems of warships are practically endless [1][3][4][22].

2.1 PD-100 Black Hornet

A PD-100 Personal Reconnaissance System, that can be smaller than the flat of the hand, is ready for action within a minute and, in fact, the whole equipment consisting of a flying unit and a terminal fits into a pocket-size holder. It looks like some toy but it is much more than that ... due to the micro cameras installed, the 18 gr flying unit is a well-equipped spying tool that can provide crucial visual information about whatever happens behind a corner or a wall. It is quiet, difficult to spot, and relatively fast. The operator can be about 1 km away from the place of action. Its board computer is capable of both directed and independent flight. Various versions of the Hornet are in use in reconnaissance as well as any other type of intelligence operations. It can be used for search, salvage, monitoring, scouting etc. in the open as well as in closed space.



FIG. 1. The Black Hornet [21]

Its use is safe for both people and other aerial vehicles, therefore there is practically never any need for previous air traffic coordination [14][19][20].

2.2 BigDog

The quadruped robot called “Big Dog” looks like a mule (Fig. 2.), approximately 0,91 meters long, 0,76 meters tall and weighs 110 kg. It is developed to provide logistical units where the conventional transport vehicles are not able to operate. The hydraulically operated legs are articulated as other animal’s legs that contain damping elements which absorb the energy of the blows from steps and it recycles them in the next step. The maximum speed is 6.4 km/h and it is able to overcome on a 35-degree slope. The robot is able to go through snow, water, and rocky terrain. Even in rocky terrain it is able to climb muddy natural paths and deliver a maximum 150 kg of additional weight.



FIG. 2. The BigDog [17]

The on-board computer is able to follow its operator from a distance, and control the Big Dog’s movement. The robot’s resource is a two-stroke single-cylinder water-cooled engine. You can find the following sensors which provide the on-board movements: GPS, gyroscope, camera (stereo vision system), LIDAR (follower DPR), engine temperature, speed, hydraulic pressure, temperature, position, dynamometer, battery charge measuring sensors, and so on...



FIG. 3. Modified BigDog [16]

A modified version is equipped with a robot arm (Fig. 3.) in this case it is able to lift up heavy objects. The movement of arms, legs and body is helped by the whole system, like it happens with people and animals [11][12][21].

2.3 Daksh

The Daksh is an electric powered remote controlled vehicle. Its primary function is to secure, localize dangerous objects (eg.: car bombs, lonely suspicious packages), and make easier the handling and destruction of these dangerous objects (Fig. 4.). (This is not the only one device which is developed for these tasks, for example [10] similar purposed robots can be found.)



FIG. 4. The remote controlled vehicle, The Daksh [2]

The device can be remotely controlled from 500 meters distance, its arm is able to extend and remove the IED's (for example: 20 kilograms of hazardous material is possible to remove in the distance of 2.5 meters, and 9 kilograms of hazardous material is possible to remove in the distance of 4 meters.) The robot runs on thick rubber wheels which resist of the air pressure of the explosive charge. The UGV is able to climb stairs, blasts closed doors, get over steep hills, maneuver in tight spaces, and tow suspicious vehicles from busy locations. The vehicle contains water cannon and the robot is able to safely destroy UAVs with it. For the operator it is available an X-Ray machine, which has the option to inspect packages and vehicles. The identification of IED's is based on the X-Ray machine's image processing software. The robot is equipped with a camera, IED control equipment, NBC reconnaissance system, and large-caliber shotgun. From the managing station (MCS Master Control Station) one operator control the Daksh with a remote control. The parts of the equipment are the transport vehicle is, which has been specially designed to Daksh, the managing station, its six main operating personnel, and necessary devices to disarm the bombs, and equipment for the transportation of dangerous goods. There is a separated cabin which has the correct equipment to transport the disarmed bombs [1][2].

2.4 General Atomics MQ-9 Reaper

For the purpose of Air Force the UAVs appeared such as modernized version of Predator called MQ-9 Reaper (Fig. 5.) which is for collecting the information, observing the enemy positions, and perform the Air Force offensive tasks. Or Global Hawk (compared to the performed missions) which replaced the famous U-2 spy aircraft. And the micro,- nano-sized devices appeared too. The MQ-9 Reaper is a medium-altitude, long-range, armed and used for several purposes, without turbo-prop unmanned aircraft, which is capable of both remote controlled and autonomous flights. The significant flight time and onboard a long-range sensors and a multi-mode communications systems and precision weapons provide a unique capability to autonomously perform complete destruction process (search, defining, tracking, target definition, implementation and evaluation). The tasks of those drones, which destroy primary dynamic targets, are intelligence, surveillance (data collection), reconnaissance, ground troops or air support, combat search and rescue tasks, precision strike, convoys surveillance, target designation, flight management stations, etc. Onboard weapons can be: GBU-12 Paveway II laser-guided bombs, AGM-114 Hellfire II air-to-surface missiles, AIM-9 Sidewinder or the GBU-38 JDAM and the future of AIM-92 Stinger can be place to get on-board arsenal.



FIG. 5. The MQ-9 Reaper [6]

The Reaper is part of an UAV system that is more like an airplane. The whole system includes unmanned aircraft with weapons and sensors, a ground control station, (PPSI satellite connection), reserve equipment, and operators and technical personnel up to 24-hour duration of the operations. The basic two-person staff is the ground crew from the pilot and sensor operator who operates the sensors and weapons [1][2][6].

2.5 Global Hawk

The Global Hawk (Fig. 6.) is a high altitude and range unmanned aerial vehicle which provides near real-time reconnaissance, surveillance and intelligence information for the commanders and it has the ability to move over a large geographical area and detect patrols moving target and designate target. Considering the dimensions of a 39.9-meter wingspan, 14.5 meters long, 4.7 meters high, 14 628 kg maximum take-off weight (1360 kg payload) aircraft that can fly a maximum height of 18.3 km, the range is 22780 km.



FIG. 6. Global Hawk [18]

The Global Hawk system allows US forces to dominate from the low level of peace-building operations to high intensity warfare operations. The board placed advanced AN/ZPY type-2 (equipped with phased antenna) radar (independently from the weather) has the ability to observe moving and stationary targets and provide to the leadership real-time information in the struggle [7][18].

2.6 Goalkeeper

Originally developed in 1979 and still today used Goalkeeper is a completely automated weapon system, which is used to protect warships against to the missiles, aircraft and surface swimming vehicles (against any threat of water above the surface). [17] literature shows similar systems.



FIG. 7. The Goalkeeper Defense Weapon System [1]

The system is able to execute detection and monitoring as well as destruction. It uses a dual locator system to identify and prioritize targets and attack the highest priority threat. It is equipped with a GAU-8/A Avenger 30 mm Gatling gun used also on the A-10 Thunderbolt II aircraft. The high precision seven-barrel cannon offers full round defence and is capable of executing 4200 shots per minute [1][17].

3. SHOULD WE HAVE OUR OWN...?!

As the technology is developing, the drones take over sooner or later all of those missions which are operated directly by human powered tools, and help in all those tasks which have great risk in the human life. Nowadays we use robots which are operated by direct human supervision and control; till mini submarines, reconnaissance helicopters operated from boat deck, and active aircrafts which works in high attitude.

The technological developments show some application possibilities where to lead the engineering creativity and knowledge. A few technology obstacles the robots show us raises a few questions with the operations, as:

- Are the robots able to destabilize the military balance, are they warning or encouraging outbreak of war? Does it influence the arms race which are increasing their technological innovation (is it the compulsion to pre-attack, the cheap micro,-nanosystems using for mass, ability for fast action, and so on...)?
- Is it a real danger that these robots can be available for high accuracy/precision planned missions and built tools, or NBC, weapons of mass destruction used by terrorist or Rogue States? (Included in this are threats of individual terrorist attacks or robots carrying weapons of mass destruction used as a vessel against random targets).
- Is there any chance that the belligerent parties or warring parties take obligatory any law, rules?
- Who controls the „daily routine of the battle field”, RoE (Rules of Engagement)? (aggression,)
- Is it possible that the decisions are made by the executors?
- The robot tools remove/dissuade conflicting interest from wars including making warfare cheaper or increase the probability of the outcomes of the conflicts where weapons are used?
- And so on... [21]

All these technologies such as lasers, microwaves, sonic waves, microbiology, genetics, etc... have in general an aim to enhance quality of human life, health, or in contrast technology can be used against human life. Their owners, installation, starting to apply in the military system never be controlled or planned in every part. Nowadays we can say that technology cannot be used anywhere only in a well-equipped laboratory.

This technology works with special tools, devices and/or unordinary big amount of electrical energy.

It is true that forming this developed technology into weapons requires adequate developed industrial and knowledgeable background which today exists; however, limited.

Despite what we think the increasing use of smaller sized weapon autonomous systems decrease the military stability. The evolving application of weapons and its spreading (dissemination) can happen and they will be widely used in the military mission and we have to calculate that it will also be available for terrorist.

Against this background (knowing these) people who are planning future operations and implementing them need to count on "having our own"; principle regardless of dimension of the battlefield (real or virtual space, missile defence system, or "cyber" defence capability, etc). The main factor is related to education and training, which should become an integral part of military service. We do not decide who our enemy is by what kind of means, strategy, preparedness, and qualifications they have. We have the responsibility for our own system design, installation, and operation; to prepare our soldiers to for war. With the improvement of training we should give such opportunities and capabilities into the hands of decision-makers, where well thought out and responsible decisions can be made. For them it should be clear that the future is not just how we solve the problems in the current location, but it is also the possibility to improve their knowledge [1][7][23].

SUMMARY

The developments of the past few years have changed the mode of the use of the armed forces. These instrument systems continue to be used in military technology.

The systems are configured into developmental tools; as a result robots are not intelligent. Their sentient beings of human values, with a silicon shell. They have more advanced computing performance that can provide opportunities that in situations such as prediction, detection, adaptation and decision-making skills which also are significantly increasing.

What is more important, the combat role of robotic powers having to make the decisions over life and death by the press of a button, or substituting the trained soldiers whose health won't be at risk and families won't have to worry? At a glance, a simple and logical step it seems but with the technological barrier it can reduce the armed forces application psychological barrier.

Scientists say maybe in the near future artificial intelligence level of development reaches to the level of the drones. Allowing man to take independent decisions which may have an impact on life and death. Attacks will be decided within fractions of a second, and this type of operation will occur frequently. The learning comes from software and hardware systems, it's important for appropriate authenticity, and accuracy. Even if the technology development level never reached the human level the deficiencies compensated manoeuvrability, pre-programming, and other characteristics. A few random examples can be seen that the engineering ingenuity and knowledge of what it can do in the future. Opportunities and capabilities that give into the hands of decision-makers, which are well thought out and responsible decisions can be made only to those who are in front of the future. It's not just a management problem in the current location, but also the possibility of the development of the knowledge-encompassing responsibility [5].

REFERENCES

- [1] B. Merrill, *Is the Future of War Autonomous?* (online) url: <http://www.makeuseof.com/tag/future-war-autonomous/> (2016.02.06);
- [2] *Army's First Mobile Robot*, (online) url: <http://www.spslandforces.com/story.asp?id=157> (2016.04.01)
- [3] B. Békési and P. Szegedi, *Gondolatok a jövőbeni fegyverek alkalmazási lehetőségeiről*, XIV. Természet-, Műszaki- és Gazdaságtudományok Alkalmazása Nemzetközi Konferencia, Szombathely, Magyarország, 2015.05.16. Nyugat-magyarországi Egyetem (NYME), 2015. pp. 183-188. (ISBN:978-963-359-053-9);
- [4] B. Békési and P. Szegedi, *Napjaink fegyverrendszer fejlesztési trendjei*, *Economica (Szolnok)* 2015. (4/2. szám), pp. 158-168. (2015);
- [5] B. Békési and P. Szegedi, *Napjainkban fejlesztett fegyverrendszerek megjelenése a jövő hadszínterein, tudás alkalmazás és fejlesztés szempontjából*, *Repüléstudományi Közlemények (1997-től)* 2015/3, pp. 105-116. (2015);
- [6] Constantine H. Houppis, Stuart N. Sheldon, *Linear Control System Analysis and Design with MATLAB®*, CRC Press, Sixth Edition, 2014. (online) url: https://books.google.hu/books?id=R07OBQAAQBAJ&pg=PA27&lpg=PA27&dq=buddyaser,+convoy/raid+overwatch&source=bl&ots=gMfQbdnYe5&sig=xHfcR59pB7Z9PhaJc_Kv3GmC3ds&hl=hu&sa=X&ved=0ahUKEwiViNG71ZLLAhVhCpoKHReJAdcQ6AEIjAB#v=onepage&q=buddy-laser%2C%20convoy%20raid%20overwatch&f=false (2016.02.19);
- [7] *Weapons systems Introduced Since Desert Storm (1991) that are available now (2003)*, (online) url: <http://www.iwar.org.uk/military/resources/ndu/systems-for-iraq.pdf> (2016.04.08);
- [8] A.F. Varga, *Robottechnológia és erőalkalmazás*, *Hadmérnök*, VIII. évfolyam, 2. szám, 2013, (online) url: http://www.hadmernok.hu/132_06_vargaaf.pdf (2016.04.08);
- [9] A.L. Barabási, *A hálózatok tudománya*, Libri Kiadó, 2016 ISBN 978 963 310 787 4 p. 446;
- [10] Ministry of Defence, *Latest counter-IED equipment showcased*, (online) url: <https://www.gov.uk/government/news/latest-counter-ied-equipment-showcased> (2016.04.08);
- [11] A. Degeler, *US military's LS3 robotic mule deemed too loud for real-world combat*. (online) url: <http://arstechnica.co.uk/information-technology/2015/12/us-militarys-ls3-robotic-mule-deemed-too-loud-for-real-world-combat/> (2016.04.08);
- [12] O. Solon, *The robot army of the future - from killer drones to cyborg super soldiers* (online) url: <http://www.mirror.co.uk/news/technology-science/technology/robot-army-future---killer-5053344> (2016.04.14);
- [13] N. Friedman, *Unmanned combat air systems. A new kind of carrier aviation*, Naval Institute Press, Annapolis, Maryland, 2010. (ISBN 978-1-59114-285-0);
- [14] *PD-100 Black Hornet Nano Unmanned Air Vehicle*, United Kingdom, (online) url: <http://www.army-technology.com/projects/pd100-black-hornet-nano/> (2016.04.14);
- [15] Boston Dynamics, *BidDog Overview*, (online) url: http://www.bostondynamics.com/img/BigDog_Overview.pdf (2016.04.01);
- [16] E. Ackerman, *BigDog Throws Cinder Blocks with Huge Robotic Face-Arm* (online) url: <http://spectrum.ieee.org/automaton/robotics/military-robots/bigdog-throws-cinder-blocks-with-huge-robotic-facearm> (2016.04.01);
- [17] *Big Dog*, (online) url: <http://www.robthalloffame.org/inductees/12inductees/bigdog.html> (2016.02.19);
- [18] Northrop Grumman, *RQ-4 Block 40 Global Hawk*, (online) url: http://www.northropgrumman.com/Capabilities/GlobalHawk/Documents/Datasheet_GH_Block_40.pdf (2016.04.01);
- [19] M. Nicol, *The Black Hornet - tiny spy drone that can follow enemy targets all the way home* (online) url: <http://www.dailymail.co.uk/news/article-2272590/The-Black-Hornet--tiny-spy-drone-follow-enemy-targets-way-home.html#ixzz2JpyDCbiL> (2016.04.14);
- [20] P. Szegedi, *A pilóta nélküli repüléshez kapcsolódva... Tanulmány a pilóta nélküli légi járművek működésével és üzemeltetésével kapcsolatban*, p.: 80, ISBN 978-963-12-5224-8, 2016 https://m.ludita.uni-nke.hu/repositorium/bitstream/handle/11410/10148/Tanulmany_Szegedi_P%C3%A9ter.pdf?sequence=2&isAllowed=y (2016.04.01);

- [21] B. Békési and P. Szegedi, *A nanotechnológia lehetséges katonai alkalmazásai*, Műszaki tudomány az Észak-Kelet Magyarországi régióban 2016, Debreceni Akadémiai Bizottság Műszaki Szakbizottsága, 2016. 799 p. pp. 592-601. (ISBN:978-963-7064-33-3);
- [22] P. Szegedi and B. Békési, *Sensors on Board of the Unmanned Aerial Vehicles*, Proceedings of 19th International Scientific Conference Transport Means, Kaunas, Litvánia, 2015. 781 p.;
- [23] P. Szegedi, and H. Tircsi: *Nanotechnológia a katonai vezetés új kihívása?* Hadtudományi Szemle, 2017. X. évfolyam, 1. szám pp.: 491-505 (2017.04.06).

CONTROL LAWS FOR AN AIRCRAFT SUPERSONIC INLET WITH MOBILE PANEL

Alexandru Nicolae TUDOSIE

University of Craiova, Craiova, Romania (atudosie@elth.ucv.ro)

DOI: 10.19062/2247-3173.2017.19.1.26

Abstract: *The paper studies a rectangular supersonic inlet for a 2.5 Mach aircraft. Inlet's architecture was chosen in order to assure a wide range of flight regimes (from low regimes of taxi and take-off until high supersonic regime), so it was built with a mobile panel. Applying an algorithm based on inlet's efficiency maximization, the optimal architecture for the most employed flight regime was determined and inlet's characteristics maps for a fixed geometrical configuration were obtained. In order to obtain the flow characteristics improvement, an adjusting law for the mobile panel was imagined and, consequently, some new characteristics maps issued; a complementary law was also described and established. The study is useful for further inlet's automation possibilities analysis and also for combined control law(s) issuing, as well as for similar inlets architecture establishing.*

Keywords: *inlet, control law, ramp, cowl, shock-wave, pressure, supersonic.*

1. INTRODUCTION

Most modern passenger and military aircraft are powered by gas turbine engines (jet engines, turboprops, turbofans, propfans), but several are powered by ramjets. There are lot of different types of aircraft engines, but all these have some parts in common. All engines should have an inlet to bring the air stream inside the engine. For the gas turbine engines, the inlet sits upstream of the compressor and, while the inlet does no work on the flow, there are some important design features of the inlet.

Inlets come in a variety of shapes and sizes with the specifics usually dictated by the speed of the aircraft. Engine's inlet is required to provide the proper quantity and uniformity of air to the engine over a wide range of flight conditions (altitudes and speeds). For aircraft that cannot fly faster than the speed of sound (such as large airliners), inlets' shapes are simple, so a straight, short and low profiled inlet works quite well. A subsonic aircraft has an inlet with a relatively thick lip.

On the other hand, for a supersonic aircraft, the inlet must slow the flow down to subsonic speeds before the air reaches the compressor. An inlet for a supersonic aircraft has a relatively sharp lip. This lip is sharpened to minimize the performance losses from shock waves that occur during supersonic flight. Some supersonic axis-symmetrical inlets use central cones (conical-shaped centerbodies). Other inlets use flat hinged plates or a spike-shaped centerbodies (plan-parallel inlets with rectangular cross section) to shock the flow down to subsonic speeds and to generate the compression through these shock-waves; this kind of inlet is seen on the F-14 and F-15 or on the Mig-29 fighter aircraft. There are other, more exotic inlet shapes used on some aircraft for a variety of reasons.

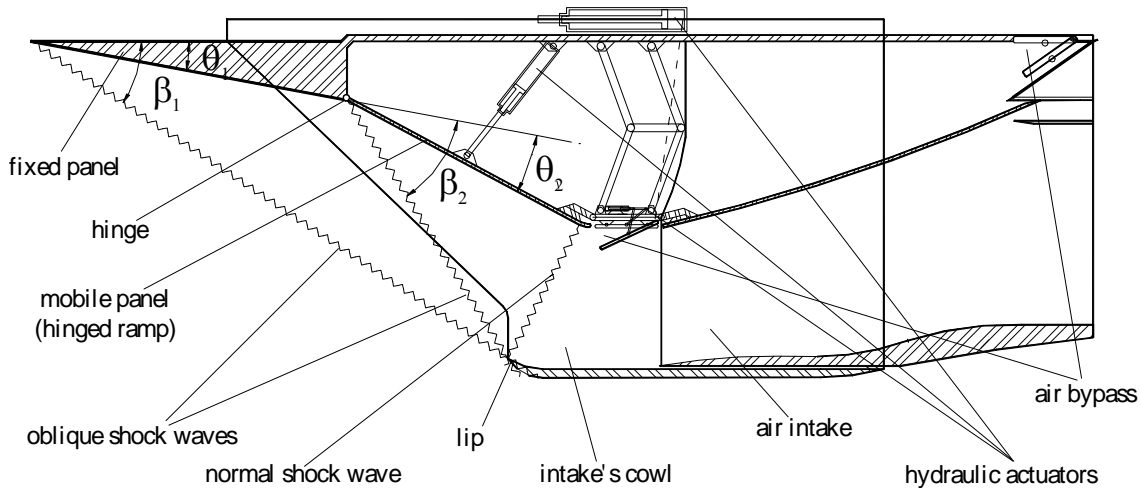


FIG. 1. Supersonic inlet with mobile panel “2+1”-type [12]

An inlet, no matter its architecture, must operate efficiently over the entire flight envelope of the aircraft. At very low aircraft speeds, or when just sitting on the runway, free stream air is “sucked” into the engine by the compressor. Meanwhile, at high speeds, an appropriately designed and manufactured inlet will allow the aircraft to maneuver to high angles of attack and sideslip, without disrupting the air flow to the compressor. It is well known that a loss of 1% from intake’s total air pressure will lead to 0.5÷1.2 % lowering of engine’s thrust, as stated in [4, 6, 9].

Because the inlet is so important to overall aircraft operation, it is usually designed and tested by the airframe company, not by the engine manufacturer; that is the reason because all engine manufacturers also employ aerodynamic engineers for inlet design.

The paper studies a plan supersonic inlet with a single mobile ramp, operating on a supersonic $M_H=2.5$ aircraft, mounted below its wing, as the one in Fig.1.

2. INLET ARCHITECTURE

The inlet in Fig. 1 consists of an air intake (which could have a fixed or a mobile cowl) and a spike-shape body with two different plates (a fixed panel and a hinged panel), assisted by hydraulic actuators. The inlet is mounted below aircraft’s wing; consequently, in supersonic flight, air speed in front of the air intake is less than the airspeed of the airplane, because of two shock waves: the first one is conical and it is triggered by aircraft’s nose, the second one – by aircraft’s wing. Meanwhile, during supersonic operating, the inlet has its own shock wave system, generated by the spike and by cowl’s lip: two oblique shock-waves due to spike’s panels and a final normal shock wave attached to the cowl’s lip.

Mobile panel could have three different positions, as follows: a) for subsonic flights it is completely retracted ($\theta_2 < 0$), offering to the intake the maximum air-breathing cross-section; b) for moderate supersonic flights, the mobile panel is on the fixed one’s direction ($\theta_2 = 0$), extending it; c) for high supersonic flights the mobile panel has variable position ($\theta_2 > 0$, as Fig. 1 shows), according to the air velocity in front of the inlet.

Inlet’s characteristics are: a) the efficiency characteristic (inlet’s total pressure loss σ_i^* versus inlet’s front Mach number) and b) the flow characteristic (inlet’s flow ratio coefficient C_D versus inlet’s front Mach number).

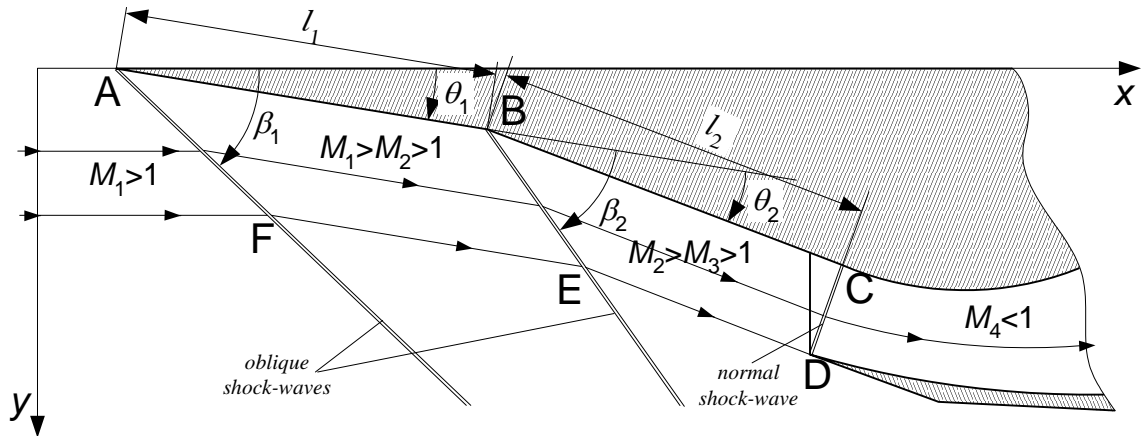


FIG. 2. Supersonic inlet “2+1”-type geometry

Some particular inlets with mobile panels have even the possibility of intake’s blocking, by completely mobile panel’s pull out until it reaches the cowl [10]; this regime characterizes the ground operating (engine’s ground test, aircraft ground maneuvering, low speed take-off running etc.), when the engine’s air breathing is realized through a system of upper flaps, which are automatically open simultaneously with the main intake’s close; main reason for this behavior are connected to engine’s protection against accidental suction into the turbo-engine of small objects on the runway, or on the test platform.

This kind of inlet assures a wide range of aircraft flight regimes (flight altitudes and speeds), as well as the whole range of engine’s operating engines.

For an aircraft designed to reach a flight Mach number of 2.5, air velocity in front of this kind of inlet corresponds to a Mach number of 2.1, because of successive shock down of the air flow through the shock-waves triggered by aircraft’s aerodynamic shape.

3. OPTIMAL INLET CONFIGURATION

Inlet design is an important engineering issue, involving geometric, aerodynamic and energetic grounds. Design methods and algorithms are presented in [6,7,10], different optimization criteria being emphasized.

An algorithm of geometric optimization of an external compression inlet, such as the one in fig. 2 is presented in [7] and is based on inlet’s efficiency maximization. This algorithm aims to determine optimum values of spike’s angles θ_1 and θ_2 , as well as a dimensionless geometry of the inlet; it was also applied for the optimization of the rectangular inlet studied in [12].

Performance criterion for optimization is the maximum inlet efficiency, or else, maximum inlet total pressure loss (or recovery) co-efficient σ_i^* , given by

$$\sigma_i^* = \sigma_{osw1}^* \sigma_{osw2}^* \sigma_{nsw}^* \sigma_d^*, \quad (1)$$

where σ_{osw1}^* , σ_{osw2}^* are total pressure ratios for the oblique shock-waves, σ_{nsw}^* – total pressure ratio for the normal shock-wave and σ_d^* – total pressure ratio into intake’s duct (assumed as constant, no matter the flight regime or the engine regime would be).

Each term in Eq. (1) is given by the aerodynamic and thermodynamic conditions of shock waves, as follows:

- for the oblique shock waves

$$\sin^2 \beta_k = \frac{1}{M_k^2} + \frac{\chi + 1}{2} \frac{\sin \beta_k \cdot \sin \theta_k}{\cos(\beta_k - \theta_k)}, \quad (2)$$

$$M_{k_{av}}^2 = \frac{1}{\sin^2(\beta_k - \theta_k)} \frac{(\chi - 1)M_k^2 \sin^2 \beta_k + 2}{2\chi M_k^2 \sin^2 \beta_k - (\chi - 1)}, \quad (3)$$

$$\sigma_{oswk}^* = \left[\frac{(\chi + 1)M_k^2 \sin^2 \theta_k}{2 + (\chi - 1)M_k^2 \sin^2 \theta_k} \right]^{\frac{\chi}{\chi - 1}} \left[\frac{\chi + 1}{2\chi M_k^2 \sin^2 \theta_k - (\chi - 1)} \right]^{\frac{1}{\chi - 1}}, \quad (4)$$

where $k = \overline{1, 2}$, M_k – Mach number before the shock-wave, $M_{k_{av}}$ – Mach number behind the shock-wave;
 - for the normal shock-wave

$$M_{av}^2 = \frac{(\chi - 1)M_k^2 + 2}{2\chi M_k^2 - (\chi - 1)}, \quad (5)$$

$$\sigma_{nsw}^* = \left[\frac{(\chi + 1)M_k^2}{2 + (\chi - 1)M_k^2} \right]^{\frac{\chi}{\chi - 1}} \left[\frac{\chi + 1}{2\chi M_k^2 - (\chi - 1)} \right]^{\frac{1}{\chi - 1}}, \quad (6)$$

where M_k – Mach number before the shock-wave, M_{av} – Mach number behind the shock-wave, χ – air's adiabatic exponent.

First inlet configuration design issue is the determination of the spike's angles values, starting from the nominal Mach number value in front of the inlet.

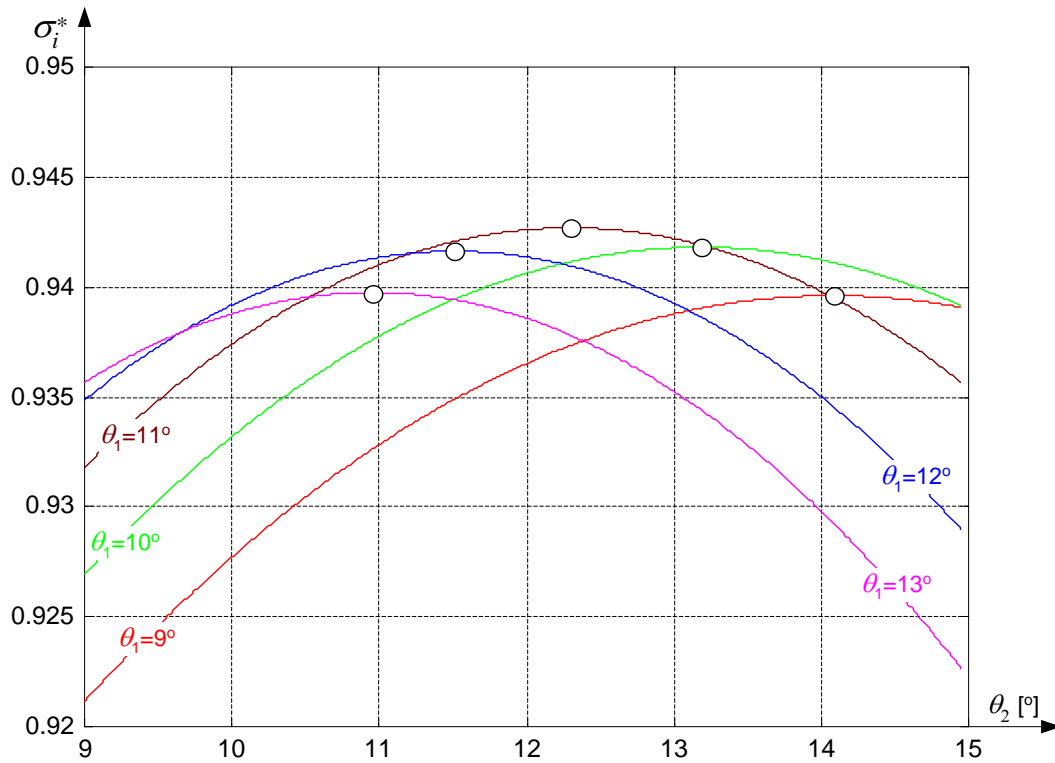


FIG. 3. Total pressure recovery co-efficient versus second panel's angle, for different values for first panel's angle

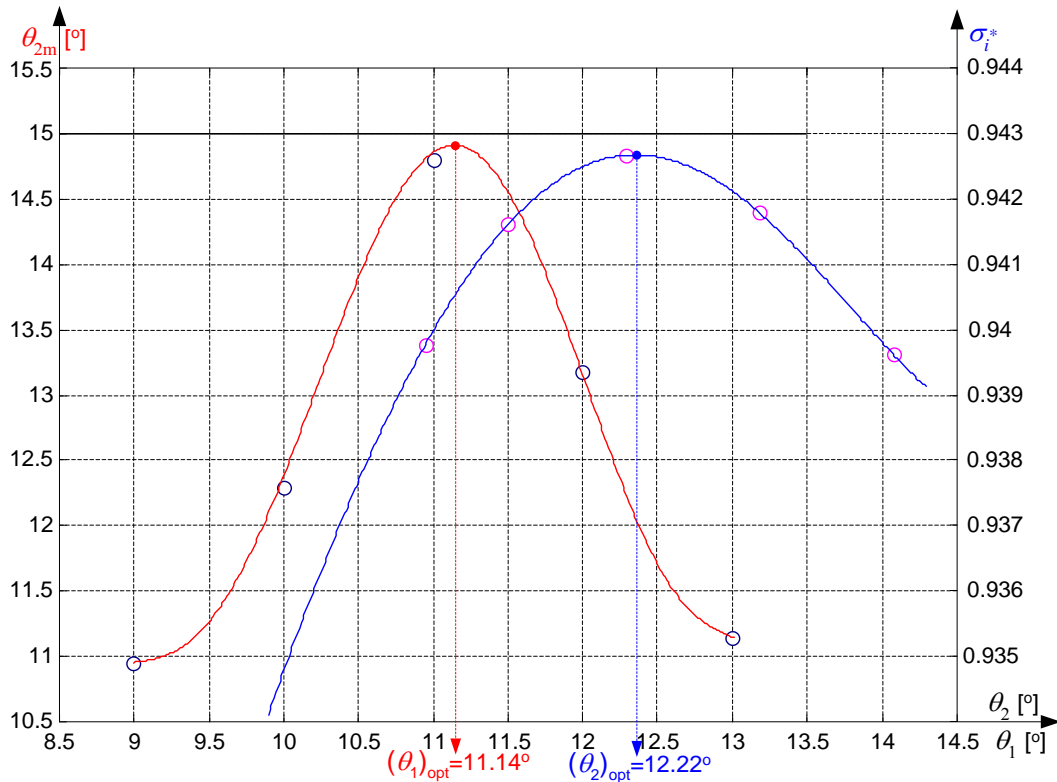


FIG. 4. Panels' angles optimal values determination

For a flight Mach number $M_H = 2.5$, inlet front value M_1 should be around 2.1; starting from this value, one can apply the algorithm, in order to obtain the maximization of σ_i^* . One has to choose intervals of values for θ_1 and for θ_2 and, applying Eqs. (2)...(6), one obtains values for σ_i^* , in fact a family of curves $\sigma_i^* = \sigma_i^*(\theta_2)_{\theta_1}$, as Fig. 3 shows.

Each curve in Fig. 3 has a maximum value point, which correspond to the optimal value of θ_2 -parameter, so one can build the graph $\theta_{2_{opt}} = \theta_{2_{opt}}(\theta_1)$; as Fig. 4 shows, the maximum value of the curve correspond to the optimal value of θ_1 . Consequently, one has obtain both optimal values $\theta_{1_{opt}}$ and $\theta_{2_{opt}}$, which give the maximum value of σ_i^* .

Optimal inlet geometry should be obtained considering the situation when both oblique shock-waves are attached to the cowl's lip (see Fig. 1), or shock focal point is situated on cowl's lip. Considering that cowl's lip point D represents the unitary coordinate ($y_D = 1$), one can determine inlet's dimensionless geometry. With these optimal values of spike's angles one obtains the co-ordinates for the characteristic points in Fig. 2, as follows

$$A(0;0), B(l_1 \cos \theta_{1_{opt}}; l_1 \sin \theta_{1_{opt}}), D\left(\frac{1}{\text{tg} \beta_1(\theta_{1_{opt}})}; 1\right), \tag{7}$$

$$C(l_1 \cos \theta_{1_{opt}} + l_2 \cos(\theta_{1_{opt}} + \theta_{2_{opt}}); l_1 \sin \theta_{1_{opt}} + l_2 \sin(\theta_{1_{opt}} + \theta_{2_{opt}})).$$

where the lengths l_1 and l_2 of the spike panels in Fig. 2 are

$$l_1 = \frac{\operatorname{tg}\beta_1(\theta_{1\text{opt}}) - \operatorname{tg}[\theta_{1\text{opt}} + \beta_2(\theta_{2\text{opt}})]}{\cos\theta_{1\text{opt}} \operatorname{tg}\beta_1(\theta_{1\text{opt}}) \left\{ \operatorname{tg}\theta_{1\text{opt}} - \operatorname{tg}[\theta_{1\text{opt}} + \beta_2(\theta_{2\text{opt}})] \right\}}, \quad (8)$$

$$l_2 = \frac{1}{\cos(\theta_{1\text{opt}} + \theta_{2\text{opt}}) \operatorname{tg}\beta_1(\theta_{1\text{opt}}) \left[1 + \operatorname{tg}^2(\theta_{1\text{opt}} + \theta_{2\text{opt}}) \right]} \left\{ 1 + \operatorname{tg}(\theta_{1\text{opt}} + \theta_{2\text{opt}}) \operatorname{tg}\beta_1(\theta_{1\text{opt}}) - \frac{\operatorname{tg}\beta_1(\theta_{1\text{opt}}) - \operatorname{tg}[\theta_{1\text{opt}} + \beta_2(\theta_{2\text{opt}})]}{\operatorname{tg}\theta_{1\text{opt}} - \operatorname{tg}[\theta_{1\text{opt}} + \beta_2(\theta_{2\text{opt}})]} \left[\operatorname{tg}\theta_{1\text{opt}} \operatorname{tg}(\theta_{1\text{opt}} + \theta_{2\text{opt}}) + 1 \right] \right\}. \quad (9)$$

For a Mach number in front of the inlet $M_1 = M_{1\text{nom}} = 2.1$, one has obtained, for a fixed geometry inlet, the results: $\theta_{1\text{opt}} = 11.14^\circ$, $\theta_{2\text{opt}} = 12.22^\circ$, $l_1 = 0.8849$, $l_2 = 0.7624$ and the coordinates of the characteristic points are A (0,0); B (0.874; 0.142); C (1.569; 0.454); D (1.324; 1).

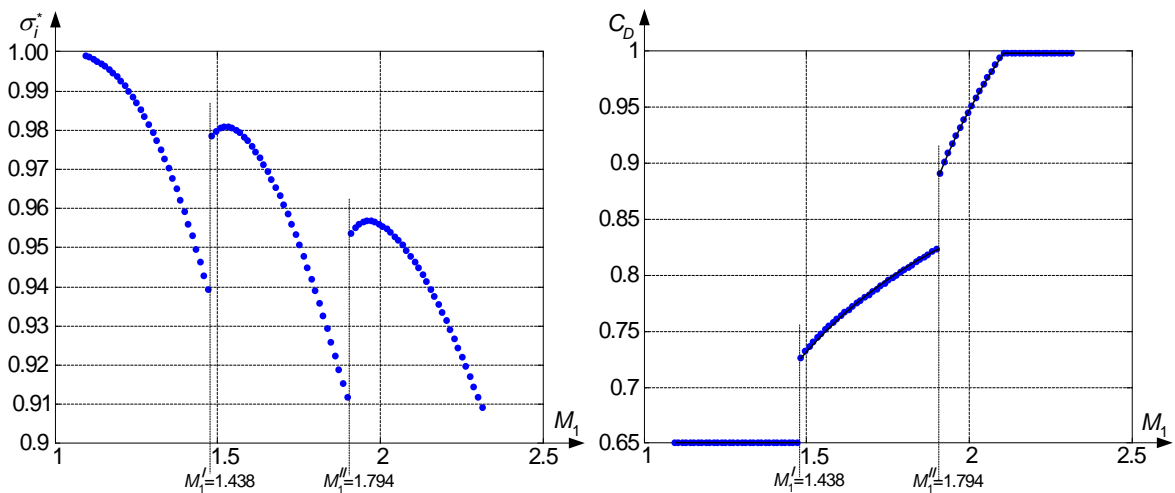
For different M_1 Mach numbers, lower than the design Mach number ($M_1' < M_{1\text{nom}}$), but for fixed inlet geometry, oblique shock-waves are depleting, see Fig. 3, so angles β_1 and β_2 are growing, which means that σ_i^* and C_D are modifying too. While σ_i^* can be calculated with above-mentioned formulas ((1), (4) and (6)), C_D is represented by the inlet's effective air-breathing area A_H / A_I' , which is exactly the co-ordinate y_F in Fig. 3:

$$C_D = \frac{A_H}{A_I'} = \frac{A_H}{(A_H)_{\text{nom}}} = \frac{b \times y_F}{b \times y_D} = \frac{y_F}{y_D} = y_F, \quad (10)$$

E-point and F-point coordinates are:

$$x_E = \frac{y_B - y_D + x_D \operatorname{tg}(\theta_{1\text{opt}} + \theta_{2\text{opt}}) - x_B \operatorname{tg}(\theta_{1\text{opt}} + \beta_2')}{\operatorname{tg}(\theta_{1\text{opt}} + \theta_{2\text{opt}}) - \operatorname{tg}(\theta_{1\text{opt}} + \beta_2')}, \quad (11)$$

$$y_E = y_D + (x_E - x_D) \operatorname{tg}(\theta_{1\text{opt}} + \theta_{2\text{opt}}),$$



a) Inlet efficiency characteristic map

b) Inlet flow rate characteristic map

FIG. 5. Inlet's characteristic maps (fixed geometry architecture)

$$x_F = \frac{y_E - x_E \operatorname{tg} \theta_{1_{\text{opt}}}}{\operatorname{tg} \beta'_1 - \operatorname{tg} \theta_{1_{\text{opt}}}}, \quad y_F = x_F \operatorname{tg} \beta'_1, \quad (12)$$

where values β'_1 and β'_2 are shock-wave's angle values calculated with respect to the new Mach number, but for the same spike angle values: $\beta'_1 = \beta(M'_1, \theta_{1_{\text{opt}}})$, $\beta'_2 = \beta(M'_2, \theta_{2_{\text{opt}}})$.

Inlet's characteristic curves are presented in Fig. 5. One can observe two discontinuities points, which corresponds to oblique shock-waves detaching: a) when $M_1 = 1.438$, which corresponds to a flight Mach number $M_H = 1.7$ and there is only one normal shock-wave in front of the inlet; b) when $M_1 = 1.794$, which corresponds to a flight Mach number $M_H = 2.15$, the spike's first panel generates a first oblique shock wave but the second shock wave is still detached. Only after this Mach number the second shock-wave becomes oblique and the shock-wave system is restored.

4. MOBILE PANEL MOTION LAW

Operation of an inlet with fixed geometry architecture means a lot of losses from air flow rate's point of view, as Fig. 5.b shows; especially for low or medium Mach numbers, flow coefficient C_D is far from the maximum value 1, and it could lead to buzz behavior of the inlet, especially when the engine's regime decreases. In order to grow the C_D -value, an appropriate

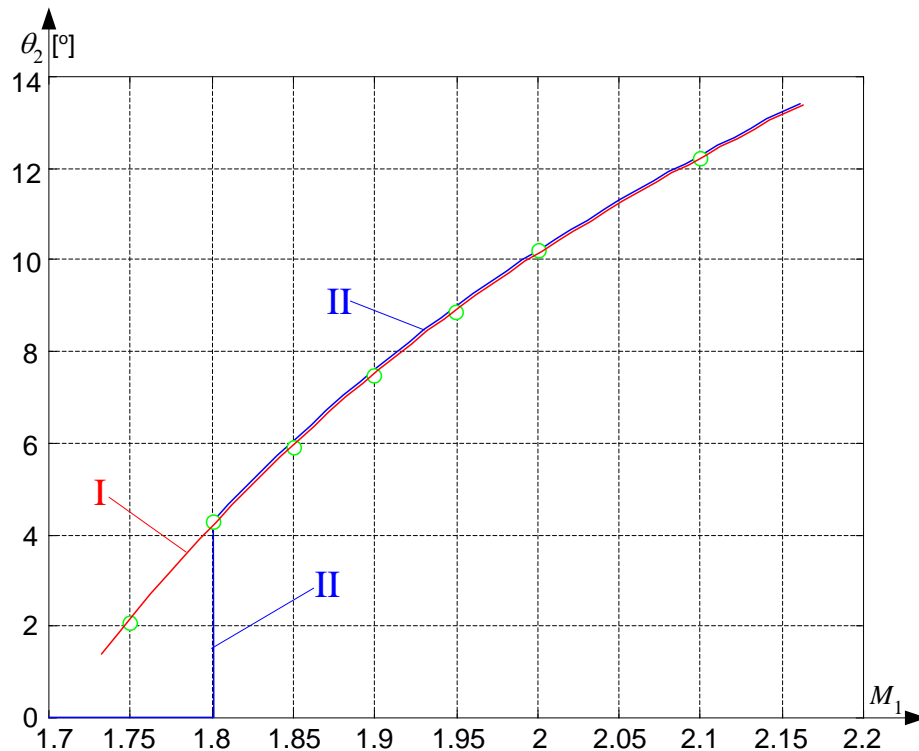


FIG. 6. Inlet's control law (mobile panel's angle versus Mach number in front of the inlet)

solution is to keep the second oblique shock-wave tangent (attached) to the cowl's lip, progressively growing the second spike angle θ_2 , by rotating the mobile panel about its hinge. The condition of attaching the shock-wave is to keep constant the β_2 – angle, which means that one has to find the value of θ_2 which generates such an angle, with respect to the Mach number in front of the inlet; consequently, one has to solve the implicit equation where β_2 is the constant angle value, given by

the position of points B and D in Fig. 2, θ_2 – equation’s argument, M_2 – Mach number behind the first oblique shock-wave and before the second oblique shock-wave, which is given by the value of Mach number in front of the inlet and the spike’s first angle θ_1 . Eventually, one obtains a dependence $\theta_2 = \theta_2(M_1)$, as curve I in Fig. 6 shows, which is a possible motion law for the mobile panel and a theoretical control law for the inlet.

$$\sin^2 \beta_2 = \frac{1}{M_2^2} + \frac{\chi + 1}{2} \frac{\sin \beta_2 \cdot \sin \theta_2}{\cos(\beta_2 - \theta_2)}, \quad (13)$$

The curve in Fig. 6 is a bit non-linear, described by a polynomial expression as:

$$\theta_2(M_1) = 40.07 \cdot M_1^3 - 265.397 \cdot M_1^2 + 603.895 \cdot M_1 - 456.623 \left[^\circ\right]. \quad (14)$$

It should be noted that even if the range of variation for θ_2 could begin at 0° (which correspond to a theoretical Mach number $M_1 = 1.71$), because of second shock-wave’s detachment under air speeds corresponding to $M_1 = 1.794$, it results that the domain of the control law must be restraint. Thus, the variation domain of θ_2 should begin at values bigger than $M_1^{\prime\prime}$, which correspond to a minimum value $(\theta_2)_{\min} = 4.2^\circ$, so the aspect of the control law should be as the curve II in Fig. 6 shows. Moreover, aerodynamics studies have proved that small values for spike angles (under 4°) didn’t generate appropriate oblique shock-waves [6, 10], but detached normal shock-waves, supplementary reason for adopt the modified control law.

According to the above-presented issues, the inlet operates as “1+1” external compression device until the airspeed in front reaches a Mach number $M_1 = 1.8$, because the fixed panel and the mobile one are building a single-flare spike $\theta_2 = 0^\circ$ (see Fig. 7); at $M_1 = 1.8$ the mobile panel moves sudden at $(\theta_2)_{\min} = 4.2^\circ$, then, over this limit $M_1^b = 1.8$ Mach, the inlet behaves like a “2+1” external compression device, but with the second oblique shock-wave tangent to its

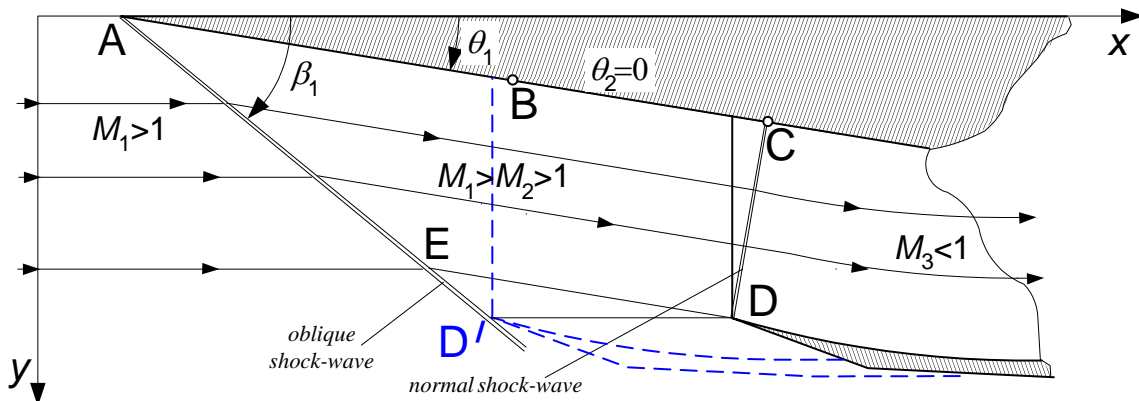


FIG. 7. Inlet's operation as “1+1” external compression device

cowl lip, until the nominal (design) flight Mach number value $(M_1)_{\text{nom}} = 2.1$ is reached.

Inlet’s flow rate characteristics is improved, as shown in Fig. 9; curve I corresponds to inlet totally operation as “1+1” external compression device, while curve II is the flow rate characteristics of the inlet with mobile panel.

4. COMPLEMENTARY MOTION LAW (COWL DISPLACEMENT)

In spite of the above-mentioned improvement, inlet’s behavior may be also improved for the “1+1” operation, from the flow rate characteristics point of view. Thus, in order to assure the maximum value of the flow coefficient C_D , the oblique shock-wave should be tangent to the cowl’s lip, no matter the Mach number in front of the inlet. Since the spike has a fixed single flare, the only adjustment possibility remains intake’s cowl displacement; therefore, a complementary law can be issued, which is intake’s cowl positioning x_{ic} with respect to the Mach number in front of the inlet M_1 .

According to Eq. (2) and as Fig. 7 shows, the oblique shock-wave’s angle β_1 is given by the spike’s angle θ_1 and the Mach number M_1 , while D-point’s co-ordinates are fixed, as determined in chapter 3 of the present paper. Consequently, cowl’s displacement should reduce till cancellation the distance between the cowl’s lip and the oblique the shock-wave, which means that D-point’s new position must be D' in Fig. 7; therefore, one has to determine the complementary law as:

$$x_{ic}(M_1) = x_{D'}(M_1) - x_D = \frac{1}{\text{tg}\beta_1(\theta_1, M_1)} - 1.324. \tag{15}$$

From the intake’s position point of view, when the Mach number in front of the inlet decreases, the cowl must be extended, so its extension should be equal to $|x_{ic}|$.

The front limit of the cowl’s extension is reached for the Mach number M_1' (see Fig. 5), when the first oblique shock wave becomes detached; meanwhile, when M_1 becomes equal to $M_1^b = 1.8$ Mach, the main control law becomes active. Consequently, the domain of applying of this complementary law could be (M_1', M_1^b) , as Fig. 8 shows.

An important observation should be made: if when the Mach number reaches M_1^b – value

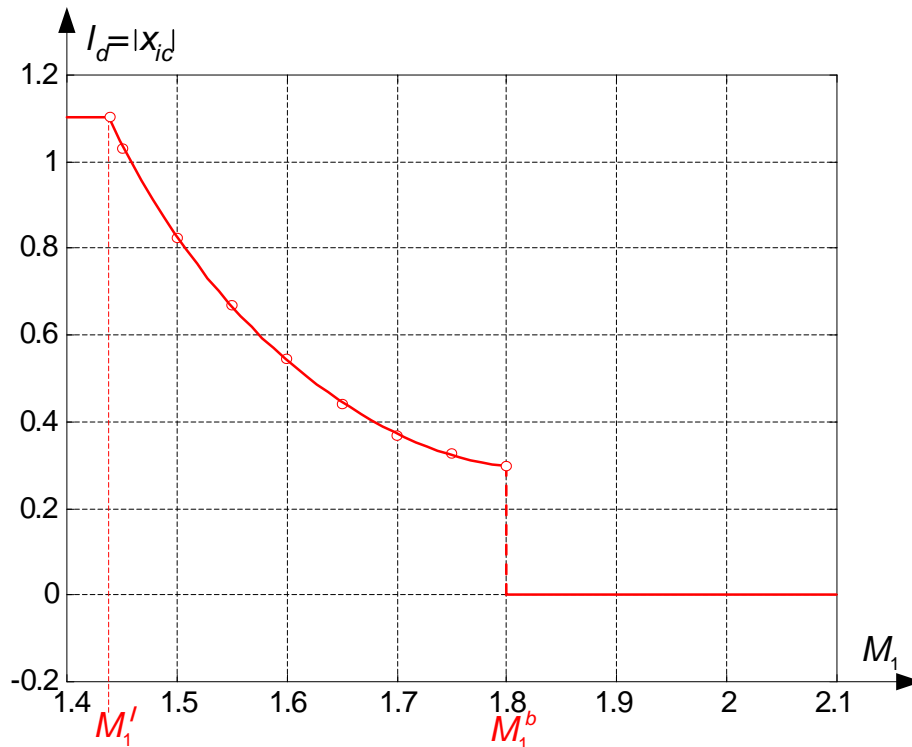


FIG. 8. Inlet’s complementary control law (intake’s cowl displacement)

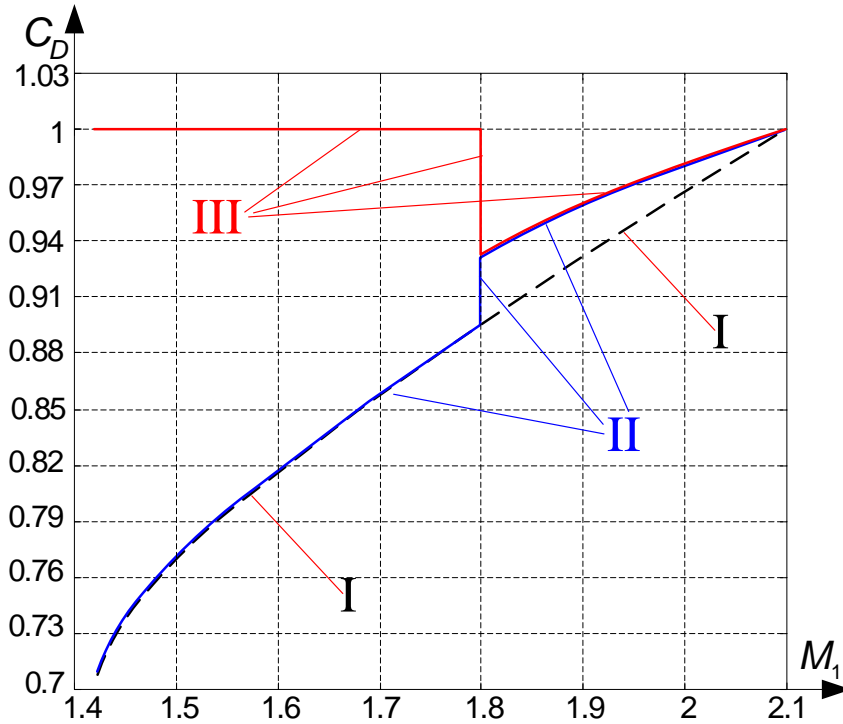


FIG. 9. Inlet's flow rate characteristics maps for different control laws

the cowl remains extended, the new born second oblique shock-wave has a small β_2 – angle and it would be developed inside the intake, which is forbidden (because of reflected shock-waves appearance and flow's speed and pressure fields distortion). Consequently, in order to make possible the main law operation, the cowl must be totally retracted when M_1^b – value is reached, so the point D' in Fig. 7 regains its initial position D.

The complementary law for the intake's cowl displacement is graphically represented in Fig. 8; it has three important zones: a) the first zone, for subsonic and low supersonic airspeeds ($M_1 < M_1^a$), when the cowl is completely extended, b) the second (nonlinear) zone, between M_1^a and M_1^b airspeeds, respectively c) the third high supersonic airspeeds zone ($M_1 > M_1^b$), when the cowl is completely retracted. At $M_1 = M_1^b$ the cowl must be sudden retracted.

As analytical expression, between M_1^a and M_1^b the complementary control law has the form:

$$l_d(M_1) = 29.181M_1^4 - 195.823M_1^3 + 497.021M_1^2 - 566.728M_1 + 245.809. \quad (16)$$

The complementary law applying brings an improvement of the flow rate characteristics, especially for small airspeeds. The curve III in Fig. 9 corresponds to a simultaneously operating of the above-described control laws.

CONCLUSIONS

Supersonic inlets are built in a variety of shapes and sizes which are usually dictated both by the speed of the aircraft and by the position of the inlet on aircraft's airframe.

A plan supersonic inlet with a single mobile ramp, operating on a supersonic aircraft (flying at a Mach number $M_H = 2.5$), mounted below its wing, was studied in this paper. For such a flying Mach number, the airflow in front of the inlet corresponds to a Mach number around 2.1, which was considered the nominal airspeed input, used for the inlet's design.

Inlet's architecture was established using an optimization criterion: the maximization of inlet's efficiency, which means the maximization of overall inlet's total pressure drop σ_i^* . Main geometric elements of the inlet are: centerbody's (spike's) flare angles (θ_1 and θ_2), centerbody's panels' lengths (l_1 and l_2), as well as cowl lip's position. All of these elements were determined for a hypothetical fixed geometry inlet, for a nominal frontal Mach number $M_1 = 2.1$.

Unlike the axially symmetrical inlets (which have conical-shape centerbodies and their control laws are based only on these centerbodies longitudinal displacement), plan (or rectangular) inlets have as control possibilities both spike or cowl longitudinal displacement and spike's second panel's rotation.

Since the studied inlet has a spike-shaped body (with a fixed panel and a hinged mobile panel), its main control law (with respect to the flight regime - altitude and speed), was determined as second panel's angle versus Mach number in front of the inlet. Consequently, the inlet operates in two different situations: a) for $M_1 < 1.8$ the mobile panel is extending the fixed panel, so the inlet works as "1+1"-type; b) for $1.8 \leq M_1 \leq 2.1$, the inlet works as "2+1"-type and the control law $\theta_2 = \theta_2(M_1)$ means a non-linear dependence on M_1 , developed between $(\theta_2)_{\min} = 4.2^\circ$ and $\theta_{2_{\max}} = \theta_{2_{\text{opt}}} = 12.22^\circ$.

Applying the main control law with respect to the flight regime, it assures a better inlet efficiency, but an improper flow rate co-efficient behavior, especially for small airspeed values. Consequently, a complementary control law was issued, in order to improve inlet's behavior at low Mach numbers (air speeds in front of the inlet), concerning the inlet's cowl displacement with respect to the same Mach number M_1 . The complementary law is also non-linear, but its applying grows the flow rate coefficient C_D for low supersonic air speeds, lower than 1.8 Mach.

Both issued motion laws are determined with respect to the flight regime (flight altitude and airspeed, given by the Mach number in front of the inlet). Although, the inlet is sensitive to engine's speed changes too; in fact, engine's regime affects the position of the normal shock-wave in front of the intake [6, 9,10], so other control laws, with respect to aircraft engine's regime, could be issued, but using the same mobile elements (such as intake's cowl).

The paper could be extended with the issuing of such control laws, as well as with control systems architecture studies.

REFERENCES

- [1] Abraham, R. H. *Complex dynamical systems*. Aerial Press, Santa Cruz, California, 1986;
- [2] Aron, I., Tudosie, A., Hydromechanical System For The Supersonic Air Inlet's Channel's Section Control, pp. 266-269, *Proceedings of the International Conference on Applied and Theoretical Electricity*, Craiova, 2000;
- [3] Lungu, R. *Flight apparatus automation*. Publisher Universitaria, Craiova, 2000;
- [4] Mattingly, J. D. *Elements of gas turbine propulsion*. McGraw-Hill, New York, 1996;
- [5] Stevens, B.L., Lewis, E. *Aircraft control and simulation*, John Willey Inc. N. York, 1992;
- [6] Pimsner, V. *Air-breathing jet engines. Processes and characteristics*. Didactical and Pedagogical Publisher, Bucharest, 1984;
- [7] Pimsner, V., Berbente, C. and others, *Flows in turbomachinery*, Tehnica Publishing Bucharest, 1986, ISBN 973-165-4-17;
- [8] Ran, H. and Mavris, D. Preliminary Design of a 2D Supersonic Inlet to Maximize Total Pressure Recovery, pp. 1-11, *Proceedings of AIAA 5th Aviation, Technology, Integration, and Operations Conference (ATIO)*, Arlington, Virginia, USA, 26 - 28 Sept. 2005;
- [9] Rotaru, C., Sprintu, I. State Variable Modeling of the Integrated Engine and Aircraft Dynamics, pp. 889-898, *Proceedings of ICNPAA 2014 (10th International Conference On Mathematical Problems In Engineering, Aerospace And Sciences)*, Narvik, Norway, 15-18 July, 2014.
- [10] Seddon, J. and Goldsmith, E. L. *Intake Aerodynamics*, 2nd edition, AIAA Education Series, 1999.
- [11] Tudosie, A. Shock-waves within plan supersonic inlets, pp. 111-115, *Proceedings of XVth Session of scientific papers*, Naval Academy, Constanta, 5-7th Nov. 1997;

- [12] Tudosie, A. Plan supersonic intake with reflected shock-wave, pp. 229-234, *Proceedings of International Conference on Applied and Theoretical Electricity ICATE'98*, Craiova, 4-5th June 1998.
- [13] Tudosie, A., Dragan, A. Rectangular supersonic air inlet with movable ramp, pp. 453-458, *Proceedings of International Conference on Applied and Theoretical Electricity ICATE 2002*, Craiova, 17-18th Oct. 2002.
- [14] Tudosie, A. *Aerospace propulsion systems automation*, Inprint of University of Craiova, 2005.

AUTOMATIC CONTROL SYSTEM FOR AN AIRCRAFT PLAN SUPERSONIC INLET WITH MOBILE PANEL

Alexandru Nicolae TUDOSIE, Mádálina Luciana PĂUNESCU

University of Craiova, Craiova, Romania (atudosie@elth.ucv.ro,
madalina.paunescu92@yahoo.com)

DOI: 10.19062/2247-3173.2017.19.1.27

Abstract: *The paper deals with a plan supersonic inlet with external compression and mobile panel and studies its control system, based on the second oblique shock-wave positioning and its total pressure ratio recovery. The system’s gas-dynamic conditioning and control criteria are determined. The author has established the system’s non-linear mathematical model and, finally, the linear non-dimensional model; the block diagram with transfer functions description, based on the above-mentioned models was also provided. Some simulations, concerning the system’s stability and quality were performed; furthermore, some conclusions and comment concerning system’s time behavior were issued.*

Keywords: *inlet, supersonic, Mach number, control law, angle, shock-wave, pressure, step input.*

1. INTRODUCTION

The possibilities of the engine’s supersonic inlet’s control, in order to assure the balance of the engine’s necessary air flow rate and the inlet’s delivered air flow rate, are the flow section area’s control by the spike’s positioning or by the inlet’s inner cowl’s positioning [2, 3, 12], as well as the inner minimum cross-section area control by the inner diaphragm’s positioning [11]; the controlled parameter should be the shock-wave’s total pressure ratio (also known as “inlet’s inner perfection co-efficient” or pressure recovery co-efficient), as well as the minimum section pressure ratio. One can observe that the system assures the shock wave’s pressure ratio’s preservation through the shock wave’s positioning, based on the feed back error’s canceling. Formally, a kind of control system’s diagram is presented in Fig.1, similar to the one in [11].

The inlet in Fig. 2 (similar to the one studied in [13] and [14]) has a spike with two disturbance surfaces, which are generating two conic shock waves, so the inner air flow inside the intake remains supersonic; the first body’s disturbance surface is a fixed-one, but the second one has a variable-angle mobile panel.

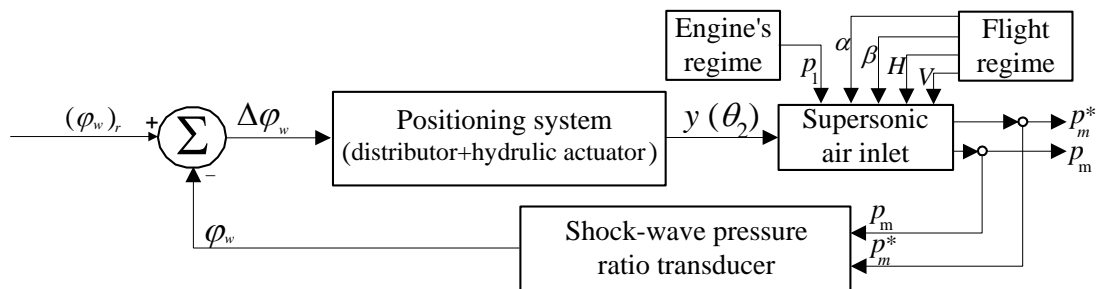


FIG. 1. Supersonic inlet control system’s formal block diagram

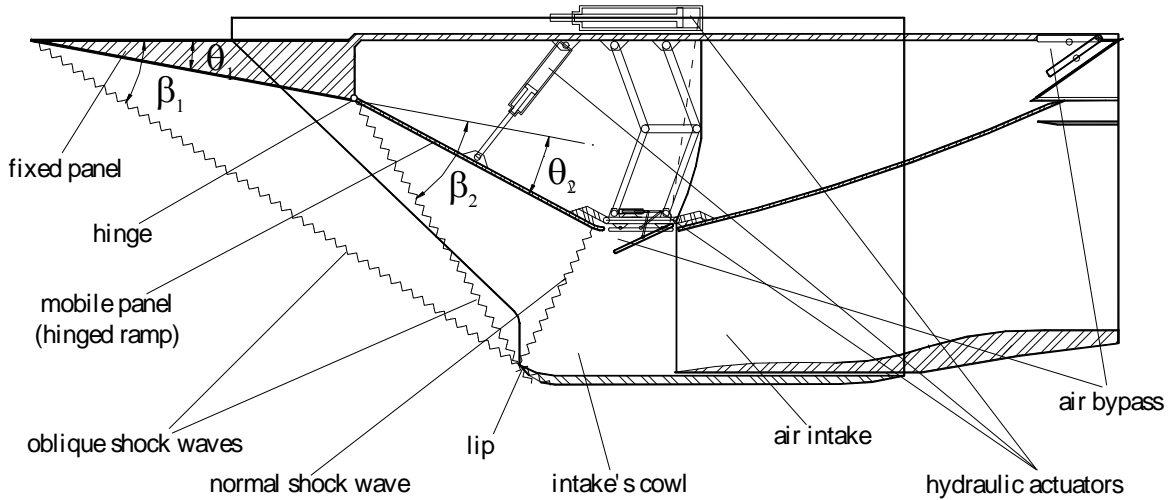


FIG. 2. Supersonic inlet with mobile panel “2+1”-type [13]

The air flow’s speed is decreasing, but the leap supersonic/subsonic is realized by a normal shock wave in the front of the intake (attached to intake’s lip at nominal regime, when Mach number in front of the inlet is the “design Mach number” and engine’s rotational speed is the nominal one- the maximum or the cruise maximum value) [9]. This is the way to assure the gas-dynamic stability against any flow disturbances and also the inlet’s “activation” during transonic flights.

2. CONTROL SYSTEM’S DESCRIPTION

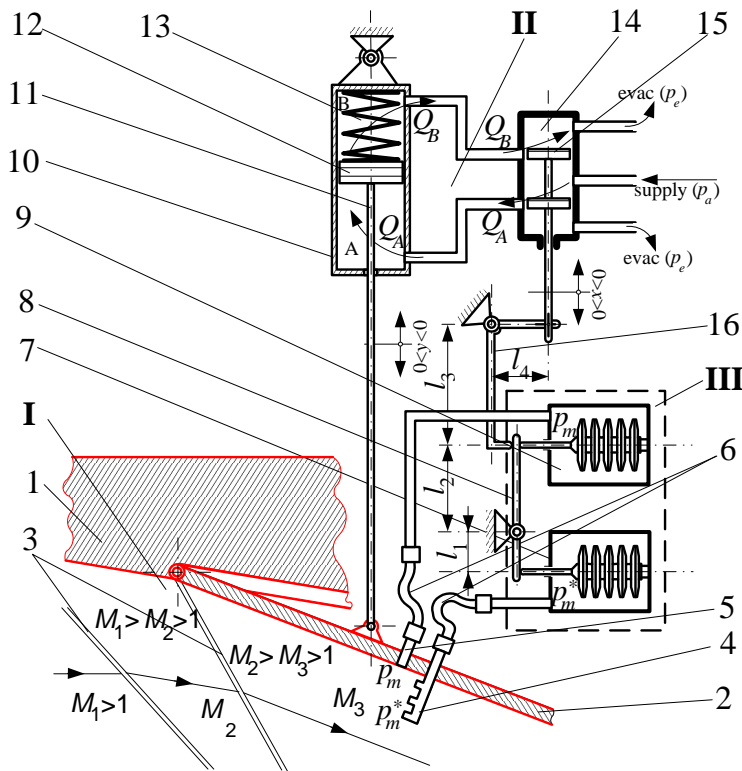
The architecture of the automatic control system is depicted in Fig. 3. It consists of a mobile panel (of the inlet’s spike) with pressure intakes, a pressure sensor (with two capsules, one for the total pressure, the other for the static pressure) and a hydraulic actuator with a slide-valve distributor. System’s main parts are identified in Fig. 3.

Pressure intakes are positioned in order to measure the mean total pressure p_m^* and the mean static pressure p_m behind the second oblique shock-wave. Pressures ratio φ_w , from aerodynamic and thermodynamic points of view, is a function of the Mach number behind the second shock wave M_3 , as follows:

$$\varphi_w = \frac{p_m^*}{p_m} = \left(1 + \frac{\chi - 1}{2} M_3^2 \right)^{\frac{\chi}{\chi - 1}}. \quad (1)$$

Inlet’s control law, with respect to the flight regime, as determined in [15], has a form depending on the Mach number in front of the inlet M_1 . Thus, Mach number(s) behind the shock-wave(s) (M_2 and/or M_3) are depending themselves on M_1 . One may affirm that the pressure ratio behind the oblique shock-wave(s) should be preserved, which involves the panel repositioning with respect to the Mach number.

The inlet operates both as “1+1” and as “2+1” external compression device; for low values of Mach number M_1 , the mobile panel is kept on its initial position (as an extension of the fixed panel of the inlet); after $M_1 = 1.8$ the mobile panel will be positioned with respect to the flight Mach number.



System's main parts:

- I-supersonic inlet;
- II-actuator;
- III-pressure sensor;

- 1-inlet's spike;
- 2-spike's hinged mobile panel;
- 3-oblique shock-waves;
- 4-total pressure intakes ramp;
- 5-static pressure intake;
- 6-flexible pipes;
- 7-total pressure sensor (capsels);
- 8-pressure sensor's lever;
- 9-static pressure sensor (capsels);
- 10-hydraulic actuator;
- 11-actuator's rod;
- 12-actuator's piston;
- 13-actuator's spring;
- 14-distributor;
- 15-distributor's slide-valve;
- 16-rocking lever.

FIG. 3. Automatic control system architecture

Modifying the Mach number means modifying the pressure balance, as well as pressure ratio; when the mobile panel is repositioned, pressure ratio should be restored, in order to assure the same position of the second oblique shock-wave. Positioning law is a non-linear one, but it could be linearised, accepting a mobile panel positioning error and, obviously, a better correlation with the complementary control law (which means the inlet cowl's displacement).

3. SYSTEM'S MATHEMATICAL MODEL

3.1. Non-linear equation system. The system's mathematical model consists of the motion equations for its main parts: static and total pressure's transducer, hydraulic distributor and actuator. These equations are, as follows:

a) pressure ratio's transducer's equation:

$$S_{a1}l_1p_m^* - S_{a2}l_2p_m - \frac{l_2l_4}{l_3} \left(m \frac{d^2x}{dt^2} + \xi \frac{dx}{dt} \right) - (k_{r1}l_1 + k_{r2}l_2)x = 0, \tag{2}$$

where k_{r1}, k_{r2} – transducer's capsule's elastic constants; m – mobile rod and accessories mass; ξ – viscous friction co-efficient; l_1, l_2 – transducer's lever arms length; l_3, l_4 – transducer's rocking lever arms length; S_{a1}, S_{a2} – aneroid capsules surface areas (usually considered as equal $S_{a1} = S_{a2} = S_a$); x – distributor's slide-valve's displacement;

b) actuator's and distributor's equations:

$$Q_A = \mu_a L_d x \sqrt{\frac{2}{\rho_{hf}} \sqrt{p_a - p_A}}, \quad (3)$$

$$Q_B = \mu_a L_d x \sqrt{\frac{2}{\rho_{hf}} \sqrt{p_B - p_e}}, \quad (4)$$

$$Q_A = S_p \frac{d(y_r - y)}{dt} + \beta_{hf} V_{A0} \frac{dp_A}{dt} \quad (5)$$

$$Q_B = S_p \frac{d(y_r + y)}{dt} - \beta_{hf} V_{B0} \frac{dp_B}{dt}, \quad (6)$$

$$S_p (p_A - p_B) = m_p \frac{d^2(y + y_r)}{dt^2} + \xi_f \frac{d(y + y_r)}{dt} + k_{ea} (y_r + y + y_0), \quad (7)$$

where Q_A, Q_B – hydraulic fluid’s flow rates; μ_a – flow rate co-efficient; L_d – distributor’s orifice’s width; p_A, p_B – actuator’s chambers’ pressures; y – actuator’s rod’s displacement; V_A, V_B – transducer’s chambers volume; β_{hf} – hydraulic fluid’s compressibility co-efficient; k_{ea} – actuator’s spring’s elastic constant; m_p – actuator’s mobile rod and accessories mass; ξ_f – viscous friction co-efficient; p_a – hydraulic fluid supplying pressure; p_e – fluid’s pressure in the low pressure circuit (considered negligible, because of its small value, comparing with p_A and p_B).

System’s non-linear mathematical model is described by the equations (2) to (7).

3.2. Linearised mathematical model. The above determined non-linear equation system can be linearised using the small perturbation method, considering formally any variable X as $X = X_0 + \Delta X$ and $\bar{X} = \frac{\Delta X}{X_0}$, where ΔX – deviation, X_0 – steady state regime’s value and

\bar{X} – non-dimensional deviation. One can also make some supplementary hypothesis, considering that the system works nearby a steady state position, thus

$$V_{30} \approx V_{40} = V_0, \quad p_{30} = p_{40} + \frac{k_{ea} y_0}{S_p}, \quad p_{40} \approx p_{30} = \frac{p_a - p_e}{2}.$$

Introducing (3) into (5) and (4) into (6), than adding (4) to (6) it results:

$$S_{a1} l_1 p_m^* - S_{a2} l_2 p_m - \frac{l_2 l_4}{l_3} \left(m \frac{d^2 x}{dt^2} + \xi \frac{dx}{dt} \right) - (k_{r1} l_1 + k_{r2} l_2) x = 0, \quad (8)$$

$$l_1 \Delta p_m^* - l_2 \Delta p_m = \frac{k_{r1} l_1 + k_{r2} l_2}{S_a} \left(T_x^2 \frac{d^2}{dt^2} \Delta x + 2T_x \omega_0 \frac{d}{dt} \Delta x + \Delta x \right), \quad (9)$$

$$\beta_{hf} V_0 \frac{d}{dt} (\Delta p_A - \Delta p_B) + k_{Ap} (\Delta p_A - \Delta p_B) = 2k_{Ax} \Delta x - 2S_p \frac{d}{dt} \Delta y, \quad (10)$$

$$\Delta p_A - \Delta p_B = \frac{k_{ea}}{S_p} \left(T_y^2 \frac{d^2}{dt^2} \Delta y + 2T_y \omega_0 \frac{d}{dt} \Delta y + \Delta y \right), \quad (11)$$

where

$$k_{Ax} = \mu_a L_d \sqrt{\frac{p_a - p_e}{\rho_{hf}}}, T_x = \sqrt{\frac{m l_2 l_4}{(k_{r1} l_1 + k_{r2} l_2) l_3}}, 2T_x \omega_0 = \frac{\xi l_2 l_4}{(k_{r1} l_1 + k_{r2} l_2) l_3}, T_y = \sqrt{\frac{m_p}{k_{ea}}}, \quad (12)$$

$$2T_y \omega_0 = \frac{\xi_f}{k_{ea}}, k_{Ap} = \mu_a L_d x_0 \sqrt{\frac{1}{\rho_{hf} (p_a - p_e)}}.$$

Noting also

$$k_{xs} = \frac{S_a}{k_{r1} l_1 + k_{r2} l_2}, k_{px} = \frac{2k_{Ax}}{k_{Ap}}, \tau_{py} = \frac{2S_p}{k_{Ap}}, \tau_{Ap} = \frac{\beta_{hf} V_0}{k_{Ap}}, k_{py} = \frac{S_p}{k_{ea}}, \quad (13)$$

then, applying the Laplace transforming to the above-presented (8) to (11) equations, one can describe the system by a block diagram, as shown in Fig. 4.

3.3. System non-dimensional linear model and transfer function. Based on the equation system, as well as on the block diagram in fig. 4, one can observe that the model and the transfer functions in the block diagram may be simplified if one assume some new hypothesis: 1) the inertial effects are very small, because of the reduced masses m and m_p , so the time constants T_x and T_y can be considered as null; 2) viscous friction effects can also be neglected, so all the terms in the above equations containing ξ_f or ξ as multipliers are becoming null too; 3) hydraulic fluid’s compressibility is practically null, so the terms where β_{hf} is involved become also null (see τ_{Ap}).

Consequently, the new form of the system’s mathematical model becomes

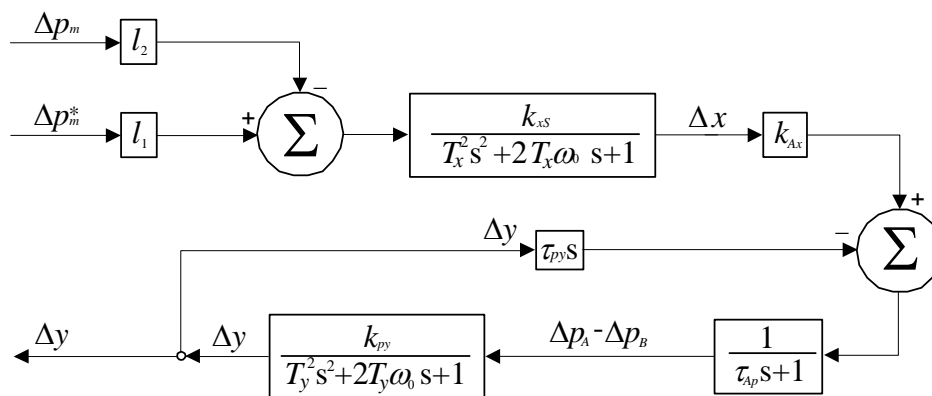


FIG. 4. System’s block diagram

$$k_{mt} \overline{p_m^*} - k_m \overline{p_m} = \overline{x} \quad (14)$$

$$k_x \overline{x} - \tau_y s \overline{y} = (\tau_{Ap} s + 1) (\overline{p_A} - \overline{p_B}) \approx (\overline{p_A} - \overline{p_B}), \quad (15)$$

$$\overline{y} = k_y (\overline{p_A} - \overline{p_B}), \quad (16)$$

with the annotations

$$k_{mt} = \frac{l_1 k_{xs} p_{m0}^*}{x_0}, k_m = \frac{l_2 k_{xs} p_{m0}}{x_0} \approx k_{mt}, k_x = \frac{k_{px} x_0}{p_{A0}}, \tau_y = \frac{\tau_{py} y_0}{p_{A0}}, k_y = \frac{k_{py} p_{A0}}{y_0}. \quad (17)$$

The simplified block diagram is presented in Fig. 5 and the system's restraint model has the following form:

$$k_x k_y (k_{mt} \overline{p_m^*} - k_m \overline{p_m}) = (k_y \tau_y s + 1) \overline{y}, \quad (18)$$

$$\overline{y} = \frac{k_x k_y}{(k_y \tau_y s + 1)} (k_{mt} \overline{p_m^*} - k_m \overline{p_m}) = \frac{k}{(\tau s + 1)} (k_{mt} \overline{p_m^*} - k_m \overline{p_m}). \quad (19)$$

that means a first order system's transfer function, where the time constant τ and the gain co-efficient k are

$$\tau = k_y \tau_y = \frac{2S_p^2 \sqrt{\rho_{hf} (p_a - p_e)}}{k_{ea} \mu_a L_d x_0}, \quad (20)$$

$$k = k_x k_y = \frac{2S_p (p_a - p_e)}{k_{ea} y_0}. \quad (21)$$

System's transfer functions are

$$H_{mt}(s) = \frac{k_x k_y k_{mt}}{(k_y \tau_y s + 1)} \overline{p_m^*} \quad (22)$$

$$H_m(s) = -\frac{k_x k_y k_m}{(k_y \tau_y s + 1)} \overline{p_m}. \quad (23)$$

3.4. Equivalent form of the mathematical model. Based on some considerations, one can obtain a new form of the mathematical model and of system's transfer function, if one make the observation that pressure's ratio $\varphi_w = \frac{P_m^*}{P_m}$ deviation $\Delta\varphi_w$, as well as it non-

dimensional deviation $\bar{\varphi}_w = \frac{\Delta\varphi_w}{\varphi_{w0}}$ may be expressed as:

$$\Delta\varphi_w = \frac{\Delta p_m^* P_m - P_m^* \Delta p_m}{P_m^2} = \frac{\Delta p_m^*}{P_m} - \Delta p_m \frac{P_m^*}{P_m^2}, \quad (24)$$

$$\bar{\varphi}_w = \frac{\Delta\varphi_w}{\varphi_{w0}} = \frac{\frac{\Delta p_m^*}{P_m} - \Delta p_m \frac{P_m^*}{P_m^2}}{\frac{P_{m0}}{P_{m0}^2}} = \bar{p}_m^* - \bar{p}_m. \quad (25)$$

Consequently, the left member of Eq. (18) becomes

$$k_x k_y (k_{m1} \bar{p}_m^* - k_m \bar{p}_m) = k_x k_y k_{m1} (\bar{p}_m^* - \bar{p}_m) = k_x k_y k_{m1} \bar{\varphi}_w, \quad (26)$$

so, considering the above mentioned annotations, a new equivalent form of the simplified mathematical model will be issued, as follows

$$k_x k_y k_{m1} (\bar{\varphi}_r - \bar{\varphi}_w) = (k_y \tau_y s + 1) \bar{y}, \quad (27)$$

where the new term in the above determined equation is $\bar{\varphi}_r$ – the preset reference value of the pressure ratio, given by

$$\bar{\varphi}_r = \frac{P_{m0}^3 l_4 (S_a P_{m0} - l_3 k_{r1}) l_3}{(l_3 k_{r2} - l_3 k_{r1} + S_a P_{m0})^2 S_a (P_{m0}^*)^2}. \quad (28)$$

4. SYSTEM'S STABILITY AND QUALITY

Since transfer functions expressions are first order, as far as one chooses appropriate values for the system's geometric parameters, the above-studied system should be always a stable one. The condition of stability ($k_y \tau_y$ strictly positive) is identically fulfilled if one chooses the values of the lever arms as

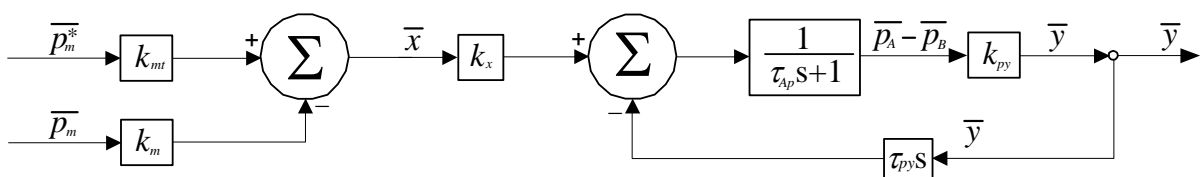


FIG. 5. System's simplified block diagram with transfer functions

$$l_1 = \frac{S_a p_{m0}^2 l_3}{p_{m0}^* (l_3 k_{r2} - l_3 k_{r1} + S_a p_{m0})}, l_2 = \frac{S_a p_{m0}^2 (S_a p_{m0} - l_3 k_{r1})}{p_{m0}^* l_3 k_{r2} (l_3 k_{r2} - l_3 k_{r1} + S_a p_{m0})}. \quad (29)$$

Moreover, if one chooses the aneroid capsules to have identical geometric shape and dimensions ($S_{a1} = S_{a2} = S_a, k_{r1} = k_{r2} = k_r$), the above values of the lever arms become

$$l_1 = \frac{p_{m0}}{p_{m0}^*} l_3, l_2 = \frac{p_{m0} (S_a p_{m0} - l_3 k_r) l_4}{p_{m0}^* k_r l_3}. \quad (30)$$

Based on the above presented mathematical model and coefficient values, some simulations were performed, regarding system's output \bar{y} behavior as time response, considering both situations of step inputs: a) step input of \bar{p}_m^* and constant \bar{p}_m , respectively b) step input of \bar{p}_m and constant \bar{p}_m^* . Results are graphically presented in Fig. 6 a) and b), for both of the studied situations; the curves are represented with continuous line.

In order to improve system's behavior, a rigid feedback between the actuator and the distributor may be used; obviously, the presence of this feedback modifies system's mathematical model and transfer function. First of all, considering feedback's gain as

$\rho_s = \frac{y_0 l_y}{x_0 l_x}$ (where l_x, l_y are feedback's lever's arms length), one obtains new forms for Eqs.

(10) and (15), as follows:

$$\beta_{hf} V_0 \frac{d}{dt} (\Delta p_A - \Delta p_B) + k_{Ap} (\Delta p_A - \Delta p_B) = 2k_{Ax} \Delta x - 2k_{Ax} \frac{l_y}{l_x} \Delta y - 2S_p \frac{d}{dt} \Delta y, \quad (31)$$

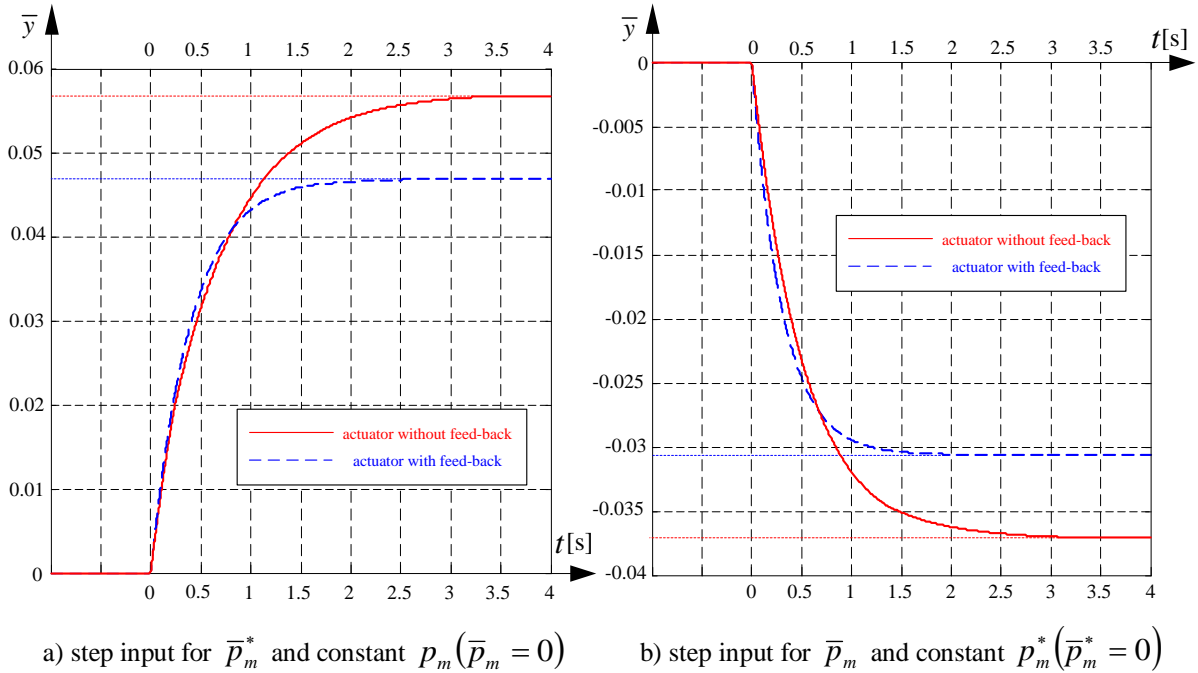


FIG. 6. System's step response for different step inputs

$$k_x \bar{x} - (\tau_y s + \rho_s) \bar{y} = (\tau_{Ap} s + 1) (\bar{p}_A - \bar{p}_B) \approx (\bar{p}_A - \bar{p}_B), \quad (32)$$

so, eventually, the new mathematical model becomes

$$\bar{y} = \frac{k_x k_y}{(k_y \tau_y s + k_y \rho_s + 1)} (k_{mt} \bar{p}_m^* - k_m \bar{p}_m) = \frac{k_1}{(\tau_1 s + 1)} (k_{mt} \bar{p}_m^* - k_m \bar{p}_m), \quad (33)$$

where new values of the time constant and of the gain are becoming smaller, as their next forms are proving:

$$\tau_1 = \frac{k_y}{k_y \rho_s + 1} \tau_y, \quad k_1 = \frac{k_x k_y}{k_y \rho_s + 1}. \quad (34)$$

Based on the new mathematical model, a similar simulation was performed, for both of step input situations. Results are graphically presented in Fig. 6 a) and b), for both of the studied situations, but the curves corresponding to the new model are represented with dashed line.

CONCLUSIONS

Supersonic inlets' automation is one of the most important issues in aircraft engineering. There are a lot of control laws for such inlets, each one of them having its own form and also its own motivation.

In this paper authors have studied a plan supersonic inlet with mobile ramp, as controlled object; an automatic control system was described and mathematically modeled. As controlled parameter the system had the mobile panel's position (more specific: its position angle measured with respect to the spike's fixed panel direction), and as control parameter one has chosen the pressure ratio through the second oblique shock-wave (which is proportional to the flow's Mach number behind this shock).

Control system's most important element is the pressure transducer, which should realize both the sensing task, as well as the comparing with the preset pressure ratio value, imposed by the lever's arm's length choice.

System's mathematical model was linearised and brought to a dimensionless form, in order to be used for studies; one has obtained (after appropriate simplifying) a first order system and its transfer functions were also determined, with respect to the chosen inputs (the total pressure and the static pressure).

From the stability condition the lengths of pressure system's lever arms were determined. An appropriate choosing of pressure system's lever's length assures (even in the phase of control system's pre-design) control system's stability.

Some simulation were performed, for system's time behavior studying, from its output \bar{y} point of view. In fact, y – displacement versus Mach number is non-linear, but it follows properly the control law. The authors have studied two cases, for both pressure (total and static pressure) step inputs. Simulation results, consisting of mobile panel's displacement for both chosen inputs, were graphically represented in Fig. 6. One can observe that in any case, the system has an asymptotically stabile behavior.

For a system with a simple actuator (without inner feedback), the results for both of studied cases show that the system has appropriate stabilization time (around 3.2 seconds for both of cases a) and b)) and, meanwhile, it has static errors (a positive one, 5.5% for \bar{p}_m^* -step input, respectively a negative one, -3.7% for \bar{p}_m -step input).

In order to improve system's time behavior, one has choose to use an actuator with inner feedback (after its rod displacement, as studied in [14]), instead of the basic actuator presented in Fig. 3; as result, system's step response was improved, but not essentially. Thus, the stabilization times were reduced (from 3.2 seconds to 2.0 ÷ 2.5 seconds), which means that the intensity of the command signal was diminished; meanwhile, system's static error were also reduced, but not essentially: from 5.5% to 4.7 % for \bar{p}_m^* -step input, respectively from -3.7% to -3.1 % for \bar{p}_m -step input.

The paper has studied only the main control system of the inlet, the one that acts over the mobile panel; obviously, the paper could be extended with the study of the complementary control law implementation, which means another control system (for the intakes cowl position) which should compulsory operate correlated with the main control system. Moreover, an embedded control system (with correlated architectures) could be described and studied.

REFERENCES

- [1] Abraham, R. H. *Complex dynamical systems*. Aerial Press, Santa Cruz, California, 1986;
- [2] Aron, I., Tudosie, A., Hydromechanical System For The Supersonic Air Inlet's Channel's Section Control, pp. 266-269, *Proceedings of the International Conference on Applied and Theoretical Electricity*, Craiova, 2000;
- [3] Lungu, R., Tudosie, A., Hydromechanical System For The Supersonic Air Intake's Central Corp's Positioning, pp. 266-269, *Proceedings of the International Conference on Applied and Theoretical Electricity*, Craiova, 2000;
- [4] Lungu, R. *Flight apparatus automation*. Publisher Universitaria, Craiova, 2000;
- [5] Mattingly, J. D. *Elements of gas turbine propulsion*. McGraw-Hill, New York, 1996;
- [6] Stevens, B.L., Lewis, E. *Aircraft control and simulation*, John Willey Inc. N. York, 1992;
- [7] Pimsner, V. *Air-breathing jet engines. Processes and characteristics*. Didactical and Pedagogical Publisher, Bucharest, 1984;
- [8] Pimsner, V., Berbente, C. and others, *Flows in turbo-machinery*, Tehnica Publishing Bucharest, 1986, ISBN 973-165-4-17;
- [9] Rotaru, C., Sprintu, I. State Variable Modeling of the Integrated Engine and Aircraft Dynamics, pp. 889-898, *Proceedings of ICNPAA 2014 (10th International Conference On Mathematical Problems In Engineering, Aerospace And Sciences)*, Narvik, Norway, 15-18 July, 2014.
- [10] Seddon, J. and Goldsmith, E. L. *Intake Aerodynamics, 2nd edition*, AIAA Education Series, 1999.
- [11] Tudosie, A. Supersonic Air Inlet's Control System Based On The Inner Normal Shock Wave's Position Stabilisation, pp. 342-349, *Proceedings of International Conference on Military Technologies ICMT 2007*, University of Defense, Brno, Czech Republic, 3-5th May, 2007;
- [12] Tudosie, A. Hydromechanical System for the Supersonic Air Inlet's Central Corp's Positioning, pp. 270-275, *Proceedings of International Conference on Applied and Theoretical Electricity ICATE 2000*, Craiova, 25-26th May, 2000.
- [13] Tudosie, A., Dragan, A. Rectangular supersonic air inlet with movable ramp, pp. 453-458, *Proceedings of International Conference on Applied and Theoretical Electricity ICATE 2002*, Craiova, 17-18th Oct. 2002.
- [14] Tudosie, A. *Aerospace propulsion systems automation*, Inprint of University of Craiova, 2005.
- [15] Tudosie, A. Control Laws For An Aircraft Supersonic Inlet With Mobile Panel, *unpublished*, 2017.

BIODIESEL PRODUCTION USING SOLAR ENERGY

Bogdan Cornel BENEĂ

Transilvania University, Braşov, Romania (b.benea@unitbv.ro)

DOI: 10.19062/2247-3173.2017.19.1.28

Abstract: Due to the decrease of oil reserve it has been searched a new category of energy, obtained from renewable sources. Biodiesel is an attractive replacement for depleting energy sources since it is produced from vegetable oils or animal fats, it is non-toxic and is a renewable resource. To obtain biodiesel is necessary to heat a triglyceride with an alcohol (usually methanol or ethanol). For heating the mixture it is used electricity obtained from fossil resources. In this study is proposed to use the solar energy for heating the mixture using a parabolic reflector. By this method, the emission of carbon dioxide during the biodiesel fabrication process is reduced.

Keywords: biodiesel, solar energy,

1. INTRODUCTION

The world's energy production for vehicles propulsion is based on fossil fuels from coal, crude oils and natural gas. If the global consumption will remain constant, it is estimated that in 30 years the reserve of fossil fuels will be finished [1]. A solution to this problem is that it is needed to use new fuels that are developed from renewable sources. An example of renewable sources is vegetable oil. The crops that are used to obtain the oil can be regenerated periodically. For this reason the vegetable oils can be considerate a renewable fuel sources whose supply will never run out.

Biodiesel is the methyl ester of vegetable oil and is a clean burning, diesel fuel replacement that is an exact substitute for existing compression engine [2]. It can be used in engine as a pure fuel or as a blended mixture with diesel fuel (in any percentage).

The oil can be obtained from various oil plants, with oil production averaging between 5000 kg oil/hectare to 145 kg oil/hectare (Table 1) [3].

Table 1. Oil production averages

Plant	kg oil/hectare
Oil palm	5000
Coconut	2260
Jatropha	1590
Rapeseed	1000
Peanut	890
Sunflower	800
Hemp	305
Corn	145

Some of these plants can be harvested more than once a year, increasing the oil production.

Biodiesel is the alkyl esters that are synthesized from a transesterification reaction on vegetable oils. The transesterification reaction can be catalyzed by either acids or bases the most common means of production is base-catalyzed transesterification. This path has lower reaction times and catalyst cost than those posed by acid catalysis. However, alkaline catalysis has the disadvantage of its high sensitivity to both water and free fatty acids present in the oils. To prepare biodiesel the vegetable oil, alcohol and base have to be mixed together while being heated. Usually, the heating is made using electricity who is generated from fossil fuels. To make the synthetic production of biodiesel more sustainable, alternative heating sources must be developed.

The alcohol used in the transesterification reaction to produce biodiesel is methanol or ethanol. Methanol is produced by destructive distillation of wood. Industrial methanol is produced in a catalytic process directly from carbon monoxide, carbon dioxide and hydrogen. Methanol when drunk is metabolized first to formaldehyde and then to formic acid or formate salts[4]. These are poisonous to the central nervous system and may result in blindness, coma, and death. Ethanol is another alcohol used in the transesterification process. Ethanol is produced by the fermentation of sugars by yeasts or by petrochemical processes. Ethanol is much less poisonous to the central nervous system and is safe for human consumption in moderation at diluted concentrations.

Glycerol is produced in the transesterification process. For every liter of biodiesel produced 125 grams of glycerol is produced [5]. Pure glycerol is used to make products like solvents and preservatives in food industry, pharmaceutical products, personal care products.

This glycerol contains unreacted alcohols, unreacted base, water and salts. For use in industry the glycerol has to be purified. To remove alcohols and water traces the crude glycerol must be heated to boiling. To make this refinement process sustainable must be reduced the amount of energy required to purify the glycerol from the production of biodiesel.

The goal of this study is to make biodiesel without electricity obtained by fossil fuels. A solar reflector was used to heat the biodiesel container and synthesize biodiesel. This reaction was chosen based on its current use in synthesis processes used in industry. Methanol has been used as reaction alcohol. The obtained glycerol is purifying using solar heating.

2. TESTS AND RESULTS

A solar reflector was made using a satellite dish with a diameter of 70 cm. The dish was covered with reflexive paint and transform into a reflexive parabolic mirror that generate heat. The feed horn of the dish was remove and replaced by reaction flasks. The feed horn was placed in the focal point of the mirror and the flask achieve the maximum intensity of sunlight.

To test the viability of the method, two tests were made: one with a 100 ml of vegetable oil and another with 1 liter of vegetable oil.

In the first case (100 ml) was combined 100 ml sunflower oil with 50 ml of methanol and 1 g of sodium hydroxide and swirling the mixture for about four minutes in a 250 ml round flask. The flask was heated by solar radiation for 90 minutes.

In the second case (1 liter) was combined 1 liter of sunflower oil with 500 ml of methanol and 10 g of sodium hydroxide. The mixture was swirling for four minutes in a 2000 ml round flask. The flask was heated by solar radiation for two hours.

In both cases the temperature of mixture was between 70 and 75°C.

After exposure at solar radiation, the flasks was moved and the solutions were cooled at the ambient temperature. During this time it was formed two layers. The top layer was biodiesel and the bottom layer was crude glycerol.

In first case was obtained 95.5 g (94.6%) of biodiesel, and in the second case was obtained 934.3 g (92.5%) of biodiesel.

Data obtained from the synthesis using the heat from solar irradiation concluded that the solar heat source provided an efficient alternative heating source. The biodiesel product yields were similar with the yield obtained in the laboratory (Table 2). These results shows that the heat exchange is equivalent in both methods.

There are some factors that influence the efficiency. On cloudy days is not sufficient solar irradiation to produce enough energy to heat the mixture. The passing clouds affect the process of heating. By increasing the volume of mixture, the larger mass was capable to keep the heat for a longer period of time.

Table 2. Comparison of yields for biodiesel production

Vegetable oil, ml	Yield, %	
	Solar heating	Laboratory
100 ml	94.6	97.3
1000 ml	92.5	95.8

Season and outside temperature had effect about the heating process (Table 3).

Table 3. Seasonal variation

	Spring	Summer	Autumn	Winter
Time to begin reflux	13	4	7	6
Reflux temperature	74°C	77°C	76°C	74°C
Average outside temperature	14°C	28°C	22°C	4°C
Outside conditions	Cloudy	Sunny	Few clouds	Cloudy
Percent yield	91%	96%	95%	92%

Using a small probe of mixture of vegetable oil and methanol were made test to check the yield percent of biodiesel for each season. The colder outside temperature in spring and winter gave the advantage of keeping the condenser cooler than in the summer and autumn. By lower temperature of cooler more of excess methanol was able to be recovered .

No electricity was used during the process of biodiesel production and glycerol purification. All heat used to produce biodiesel and distill methanol from recovered glycerol was generated using the sunlight.

Using a power meter it was determined, in laboratory, the energy (in kWh) used to obtained the biodiesel and to purify the glycerol obtain after the biodiesel process.

It was determined that for heating the mixture up to 70°C it is consumed 0.4 kWh and for purification of glycerol it was used 0.2 kWh. Thus, the total energy used to obtain biodiesel and clear glycerol was 0.6 kWh.

According to “Greenhouse gas reporting” [5] for the production of one kWh is emitted 0.41 kg CO₂. Thus, the 0.6 kWh of energy generates 0.246 kg CO₂. By using the sunlight radiation the greenhouse gas emissions are being eliminated.

The glycerol purification process recovers any trace of alcohol that can be used in subsequent operations. During the glycerol recovery process are generated free fatty acids, which can be used to synthesize more biodiesel.

For drying the biodiesel is used sodium sulfate and is obtained waste. If the biodiesel is stored several days, the water can be removed without sodium sulfate as a drying agent. The water and biodiesel will form two layers, and the water can be removed and the pure biodiesel is obtained.

3. CONCLUSIONS

This work demonstrated that the solar heat source can replace the electric heating source. The outside temperature influences the process of glycerol purification.

Biodiesel was successfully obtained without wastes. Any unreacted alcohol was recovered and the recovered free fatty acid was used to obtain more biodiesel. Waste glycerol was recovered and purified and can be used for another applications.

By using the solar heating no electricity was used, and the greenhouse gas emissions for producing biodiesel and purifying glycerol was 0.

For this dish it can be obtained about 4 liters of biodiesel/day. In the future, plans are to test a larger dish to see if the process can be implemented into industrial reactions.

REFERENCES

- [1] D.L. Klass, *Biomass for Renewable Energy, Fuels and Chemical*, Academic Press, San Diego, 1998;
- [2] G. Knothe, J. Karhl, J. Van Gerpen (Eds), *The Biodiesel Hand Book*, Champaign, AOCS Press, 2005;
- [3] Tickell J, *From the Fryer to the Fuel Take: The Complete Guide to Using Vegetable Oil as an Alternative Fuel*, Ashland, BookMasters, 2003;
- [4] D.G. Barceloux, G.R. Bond, E.P. Krenzelok, Cooper, H; Vale, JA; American Academy of Clinical Toxicology Ad Hoc Committee on the Treatment Guidelines for Methanol, Poisoning (2002);
- [5] Greenhouse gas reporting – Conversion factors 2016 <https://www.gov.uk/government/publications/greenhouse-gas-reporting-conversion-factors-2016>;
- [6] B.M. Agee, G. Mullins, D. J. Swartling, *Use of solar energy for biodiesel production and use of biodiesel waste as a green reaction solvent*, Sustainable Chemical Processes, 2014;
- [7] A. Vale, *Methanol*, Medicine 2007;
- [8] A.A. Kiss, R.M. Ignat, *Enhanced methanol recovery and glycerol separation in biodiesel production – DWC makes It happen*, Appl Energy 2012.

CONSIDERATIONS ABOUT THE INFLUENCE OF CLIMATE CHANGES AT BAIA MARE URBAN SYSTEM LEVEL

Mirela COMAN, Bogdan CIORUȚA

Faculty of Engineering, North University Centre at Baia Mare, Technical University of Cluj-Napoca, Romania (bciorutza@yahoo.com)

DOI: 10.19062/2247-3173.2017.19.1.29

Abstract: *Global warming as a result of climate changes is a phenomenon widely accepted by the international scientific community, already highlighted by analyzing observational data over long periods of time. Simulations made with global climate models indicate that the main factors influencing this phenomenon are both natural and anthropogenic (changes in atmospheric composition due to human activities). But the cumulative effect of the two factors may explain the observed changes in average global temperature over the last 150 years.*

Changes in climate regime in Romania follows the global context, taking into account the regional conditions. Compared to the annual average temperature global increase during 1901-2013 with 0,6°C in Romania the annual average temperature was increased only with 0,3°C. Compared with other regions in the neighborhood, there were differences: a warming more pronounced in the south and east (reaching up to 0,8°C) and non-significant in the intra-Carpathian regions, except the Baia Mare station, where the effect of local anthropogenic activity led to a heating with 0,7°C.

For the present study were performed, using the MS Office Excel and G.S. Surfer program, statistical models to highlight the situation of Baia Mare Urban System, knowing that this region was until recently a hotspot area according to the atmospheric pollution.

Keywords: *climate changes, statistical modeling, vulnerability, Baia Mare*

1. INTRODUCTION

Global warming as a result of climate change is a phenomenon widely accepted by the international scientific community, as already pointed out by analyzing observational data over long periods of time. The simulations made using global climate models indicate that the main factors behind this phenomenon are both natural (variations in solar radiation and volcanic activity) and anthropogenic. The cumulative effect of these factors may explain the observed changes in global mean temperature over the past 150 years.

Increasing greenhouse gas concentrations in the atmosphere [7], especially carbon dioxide (CO₂), the main cause of the global warming, was pronounced in the last 50 years of this century. Global warming is also accepted by the european and romanian scientific community, and as a strategic result major decisions were established for the control and adaptation to the effects of global warming [9, 10].

2. SCENARIOS FOR THE CLIMATE CHANGES

Global average temperature has increased by about 0.74°C over the air in the last 100 years (1906-2005) than 0.6°C during 1901-2000 [1]. Climate Europe experienced a warming of about 1oC in the last century, higher than the global average.

The hydrometeorological recorded data show that precipitation increased significantly in northern Europe, while droughts in southern became increasingly frequent (Fig. 1).

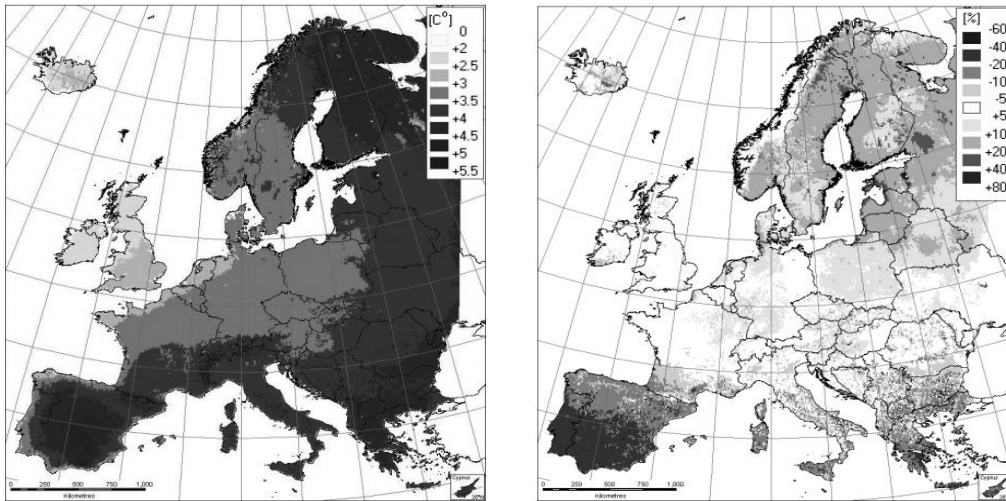


FIG. 1. The evolution trend of average annual temperature and rainfall in the Europe (1900-2050)

Extreme temperatures recorded recently, such as heat wave in the summer of 2003 and especially that of 2007 and 2009 were related to the observed increase in the frequency of extreme events in recent decades, as a consequence of climate change. While single weather events cannot be attributed to a single cause, statistical analyzes have shown that the risk of such events has increased considerably due to climate change. The most vulnerable areas in Europe in terms of the effects of climate change are [1]:

- Southern Europe and the entire Mediterranean Basin - where we meet a deficit due to rising water temperatures and reduced precipitation;
- mountain areas in particular the Alps problems in the water flow regime as a result of melting snow and glaciers volume mitigation;
- coastal areas due to rising sea levels and the risk of extreme weather events;
- densely populated floodplains due to the risk of extreme weather events (as in Fig. 2), rainfall and flash floods, causing major damage to built-up areas and infrastructure.

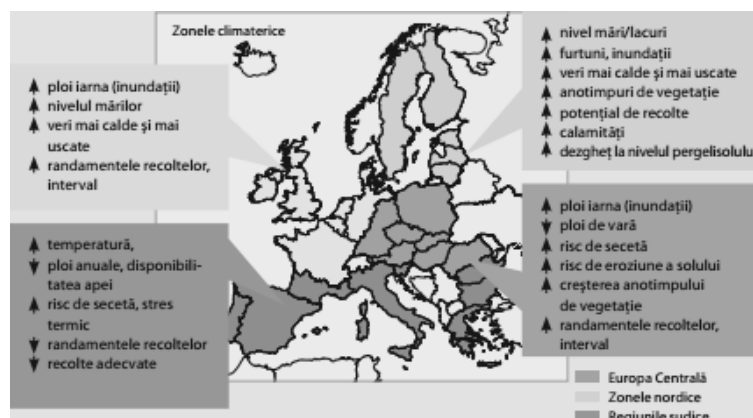


FIG. 2. The early effects of climate changes in different EU regions (2010-2050)

The configuration of these changes is similar to that observed during the 20th century. It is "very likely" that the trend of increase in extreme maximum temperatures and increased frequency of heat waves continue.

The Romania's climate is influenced by the position that it has on the world, as well as its geographical location on the continent. These features give a temperate climate in Romania continental. Compared to the annual global average temperature increase during 1901-2000 $0,6^{\circ}\text{C}$ in Romania the annual average increased by only $0,3^{\circ}\text{C}$.

During 1901-2006 the increase was $0,5^{\circ}\text{C}$ to $0,74^{\circ}\text{C}$ globally (1906-2005), but there were regional differences: a stronger warming in the south and east ($0,8^{\circ}\text{C}$ at stations Bucharest-Filaret and Constanta stations) and significant intra-Carpathian regions, except Baia Mare station, where the effect of anthropogenic activity local heating leading to a $0,7^{\circ}\text{C}$ as presented in Fig. 3 and Fig. 4.

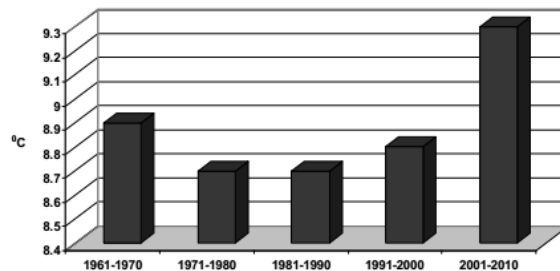


FIG. 3. The mean annual temperature in Romania between 1961-2010

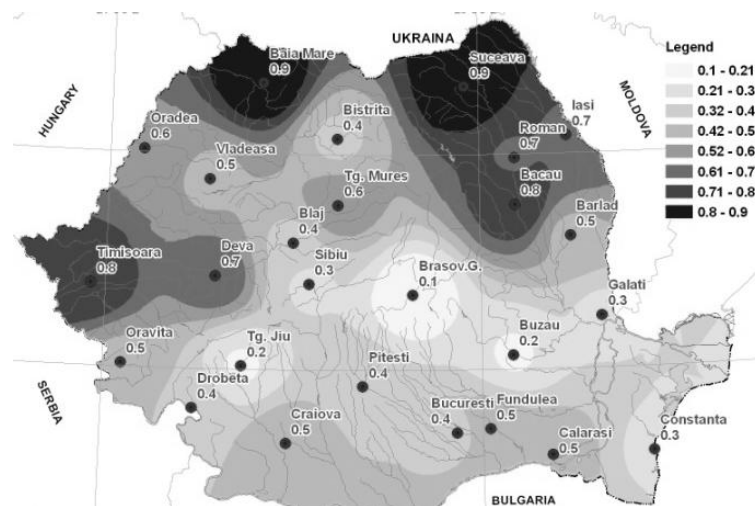


FIG. 4. The temperature increase in Romania between 1961-2010

In terms of rainfall during the period 1901-2010 showed a general trend of decreasing annual rainfall amounts (Fig. 5). Consistent with this result has been increasing the maximum duration of intervals without rainfall in the southwest (winter) and west (summer) [7].

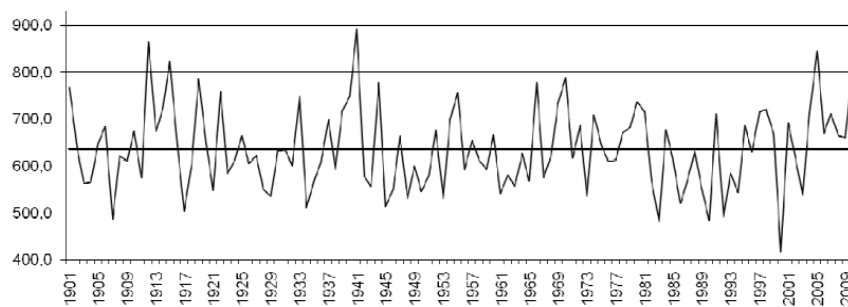


FIG. 5. The mean annual rainfall in Romania between 1901-2010

3. CASE STUDY-EFFECTS AND DISCUSSIONS

Baia Mare Depression climate is characterized by mediteranean influences, in addition morphographical particular conformation generated in contact with the mountain area exposed to the south, meeting the conditions of manifestation of climate shades shelter so that annual average temperatures reaches 9.4-9.6°C Baia Mare, dropping to -8°C in the hilly eastern and southern areas of the basin [4,5]. The average temperature of the summer months is 19.5°C, and the winter months - 2.8°C, with an average annual temperature variation of 20-22°C [2,6], in accordance with the microclimate observations recorded by the meteorological station Oregon Scientific WMR-type 100 (Fig. 6), which operates in the North University Center at Baia Mare, from April 2008.

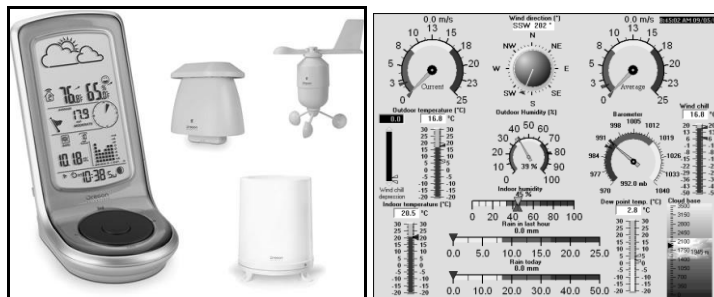


FIG. 6. The meteorological station Oregon Scientific WMR-type 100

Recorded weather variables, displayed on the main console, are: temperature indoor / outdoor, humidity indoor / outdoor, wind speed and direction, average monthly rainfall, daily, annual, atmospheric pressure, dew point temperature, the cooling produced by wind, temperature index and more. Information obtained from the meteorological station, even when measuring small variations - for which the calibration of sensors is automatically implemented by the station's console, is stored as log files containing more than 43,000 rows of data.

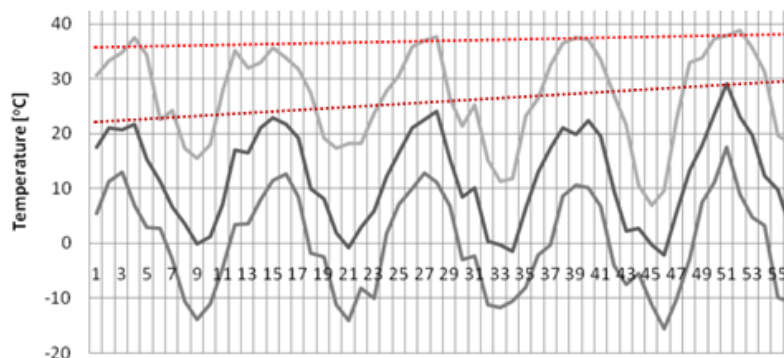


FIG. 7. The evolution of Baia Mare urban area temperature (May 2008-December 2012)

As as it can be observed, in Fig. 7, in terms of the evolution of the maximum temperature recorded in the period 2008-2012 there was an increase of approx. 1°C compared with annual averages temperature's evolution for the same period where growth is more visible - from 22 to 29°C [3].

Another characteristic is the reduced frequency of thermal inversions and a number of days with frost 100-120 days / year. Average relative humidity is at around 80%, favored by the mild climate and wooded areas of northern municipality and numerous green areas of the city administration Baia Mare [2].

According to the Fig. 8, we should mention that since 2009 there have been large fluctuations in terms of atmospheric humidity - with values between 20-80% for average annual humidity [3].

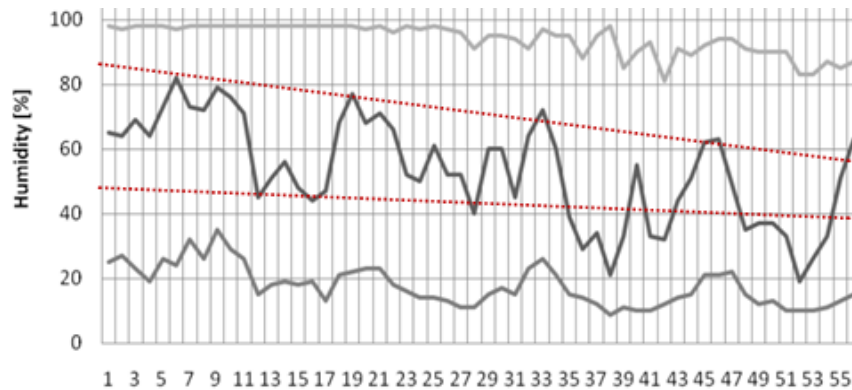


FIG. 8. The evolution of Baia Mare urban area air humidity (May 2008-December 2012)

In addition there has been a certain uniformity (stability) in terms of the evolution of minimum annual atmospheric humidity for which no values were recorded under 10% [2]. The area of Baia Mare depression is also characterized by an increased frequency of rainfall, while the average annual rainfall is increasing from the west (700mm / year) to the south and east (~ 1000mm / year), with an average of 922 mm / year in Baia Mare and the concentration of most of the precipitation in summer season. The number of days with snow increases from west (50 days / year) to the eastern basin (60 days / year) [3,5].

Due to the presence of the Săsar Valley, which crosses the city from east to west lake Firiza approach and developed industrial area of the city, located in the immediate vicinity of the city, misty air rate remains quite high even in the summer months, recorded on average from 13.1 to 16.6 days.

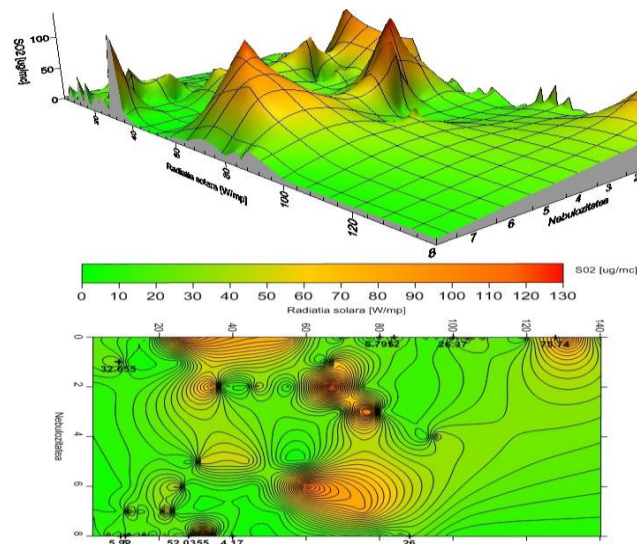


FIG. 9. The variation of CO and SO₂ in relation to nebulosity and solar radiation (Oct. 2010-Feb. 2011)

Changes to the microclimate (2008-2012) observed in the urban area Baia Mare although not seem significant at first, bring to the forefront the progressive growth in terms of temperature and fluctuating decreases in terms of atmospheric humidity, conditions that contribute decisively to the "urban heat islands" - with a significant presence in terms of SO₂ pollution [8].

The horizontal scale - given by the solar radiation (W/m^2) and nebulosity values, both recorded with the meteorological station Oregon Scientific WMR-type 100 - is connected, via the G.S. Surfer 9.0 software model (Fig. 9), to the vertical scale containing SO_2 values - registered, in the same period (oct. 2010 - feb. 2011), on the nearest air quality monitoring local station. According to the correlations made by the G.S. Surfer 9.0 software, there are a few SO_2 peaks highlighted for solar radiation values between 20-80 W/m^2 , which are not increase in frequency during the study or as a result of urbanisation.

Moreover, these effects are felt near industrial or agricultural areas which are still not visibly affected by phenomena such as aridity, soil erosion or intense summer rains followed by devastating floods, but will definitely be affected in the next 10-15 years if microclimate changes continue in the same direction [2].

Another important aspect regarding the evolution of the climate in the Baia Mare area is the decrease in atmospheric inversions appearance, in this sense can lead to maintenance of air pollutants in the lower layers of the atmosphere, with the possibility of acid rain phenomenon, which may enhance the effects of global warming to urban and suburban area of Baia Mare.

CONCLUSIONS

Changes in climate regime in Romania follows the global context, taking into account the regional conditions; a warming more pronounced were identify in the south and east of Romania and in the Baia Mare area, where the effect of local anthropogenic activity led to a heating with 0,7-0,9°C. Baia Mare depression climate is characterized by mediteranean influences, in addition morphographical particular conformation generated in contact with the mountain area exposed to the south, meeting the conditions of manifestation of climate shades shelter so that annual average temperatures reaches 9.4-9.6°C in Baia Mare, dropping to -8°C in the hilly eastern and southern areas of the basin.

Climate changes is expected to have significant negative consequences to human health. It is also possible to have an significant impact heat waves more frequent and intense, especially in "urban heat islands" of cities like Baia Mare along with other extreme weather phenomena with visible effects on sequence plants phenophases, agriculture, forestry and local economy.

REFERENCES

- [1]. Chemery L. *Climate - small Larousse encyclopedia*, Ed. Larousse, București, 2003
- [2]. Cioruța B. *Research regarding the evolution of weather conditions in the Baia Mare urban area (database)* - work in progress, 2017
- [3]. Cioruța B., Iusco I., Pop R. *Considerations regarding the Baia Mare area meteorological conditions in the last 5 years with help of Environmental Informatics*, Conferința "Aerul și apa - componente ale mediului", volum 2013, pag. 524-528, Cluj-Napoca, 2013
- [4]. Coman M. *Research Regarding the Influence of Meteorological Conditions and the Geomorphologic Pollutant Processes on the Baia Mare Depression*, PhD Thesis, Canberra, 2005
- [5]. Coman M. *Baia Mare Depression - environmental protection from sustainable development perspective*, Ed. Risporint, Cluj-Napoca, 2006
- [6]. Coman M., Taro G., Cioruța B. *Application of meteorinformatics for the analysis of weather forecast data*, AFASES International Conference, Brașov, 2011
- [7]. ***Schimbări climatice (Ministerul Mediului), www.anpm.ro/Mediu/schimbari_climatice
- [8]. ***Rețeaua Națională de Monitorizare a Calității Aerului, www.calitateaer.ro
- [9]. ***Strategia Națională privind Schimbările Climatice, www.mmediu.ro/categorie/planul-national-de-actiune-privind-schimbarile-climatice-2016-2020/122
- [10]. ***Planul National de Actiune privind Schimbarile Climatice 2016-2020, www.mmediu.ro/categorie/planul-national-de-actiune-privind-schimbarile-climatice-2016-2020/122

REMOTE DETECTION AND TRACKING OF ALCOHOL CONCENTRATION FOR CAR DRIVERS

Andreea DRĂGHICI, Titus BĂLAN

”Transilvania” University of Braşov, Romania

DOI: 10.19062/2247-3173.2017.19.1.30

Abstract: *As driving under the influence of alcohol is the main cause of fatal vehicle accidents, a reliable method for alcohol testing and data recording, without the possibility to fraud the system is mandatory. Thus, besides the alcohol level measurement, a communication method for remote recording of the test results should be provisioned. This paper describes a microcontroller based implementation with real-time transmission of data, retrieved, modeled and displayed in a chart format, and furthermore securely stored in a record database. In our demonstrator, the code for the microcontroller ATmega328p that controls the data acquisition and transmission is written in C++, while the application created in C# controls all the sensor received information for calibration, verification and metrology testing. The system implementation uses low cost components with high performance.*

Keywords: *Real-time communications, ATmega328p, breathalyzer, remote measurement, SQL*

1. INTRODUCTION

Alcohol consumption under no control and monitoring increases the number of car accidents and the traffic accidents victims. Methods to test and record the alcohol level - BAC (blood alcohol concentration) in the body can reduce the risks of traffic accidents. From statistical point of view only a few drivers have BACs higher than 0.15. Yet a much, much higher proportion have fatal crashes. The average BAC among fatally injured drinking drivers is about twice the legal limit [1]. BAC monitoring can be used also in different working environments for employee testing as the senses of perception and the possibilities to have coordinated moves are affected by alcohol.

In 1927 the breath analyzer took shape, represented by a football bladder, followed by the ethanol percentage analyses for the air in the football bladder that concluded that a man was “50 per cent drunk”, as it was presented as court evidence in a trial. The portable device for breath analyze was introduced by Parry Jones in 1972, as a consequence of the decision of the British government, introduced in 1957 the Road Safety Act, which defined the maximum level of alcohol that a person should have in his body while driving an auto vehicle. The company that Parry Jones began the examination of possibilities to develop a fuel cell alcohol sensor based of a more reliable screening instrument which help the police to test drivers much easier and it removes the test of urine and blood. [2]

Though monitored by police officers via breath analyses, the measurement must be tracked and stored, thus possible fraud or test changes are eliminated, and measurements can be considered as reliable evidence in a court of law.

What makes the difference between our demonstration for a breathalyzer and the other implementations [3][4] is that we have developed a method for the police to have a good trace of the people that will be tested in traffic.

Thus, we have included a method for the wireless transmission of measured information. Furthermore, a graphical display of results and integration with a SQL database, possibly extended Secure Storage in the Cloud, is part of the implementation. The Atmel AVR microcontroller performance makes the difference in case of the wireless transmission because the analog-to-digital conversion (ADC) speed is much faster and thus it brings efficiency for producing a real-time diagram. The microcontroller AVR it is used mostly for multi-processing on a common bus.

By adding the wireless to our implementation (though also mobile network like 3G-LTE could be an option [5]), data is transmitted in real time, captured and processed much faster, the measurement can be time-stamped, thus becoming evidence, data cannot be erased or modified. This kind of integrated communication uses a low-cost technology that can be implemented in any type of device and it provides flexibility and opens the borders in any area of interest.

2. SYSTEM COMPONENTS AND IMPLEMENTATION SCENARIO

The scenario that we have implemented is considering a portable alcohol tester that is connected via the wireless interface the police car, where data is automatically tracked and stored in a database, and furthermore it could be shared to a to a cloud database and a secure storage element. The system architecture is depicted in figure 1. The alcohol sensor takes 10 bits of data and transmits them to the police car through a wireless connection.

For an increased usability, the breathalyzer has a LED-based local indication of the measured alcohol level. When the sensor indicates a low alcohol, vapors level the green LED will light, when is medium the orange one will light, and the red LED is used for high sense of alcohol vapors. In the same time, the captured data are read by an application in C# that filters according to the calculation of BAC and help building a graphic. The application has a build-in database where data is recorded, searched or displayed.

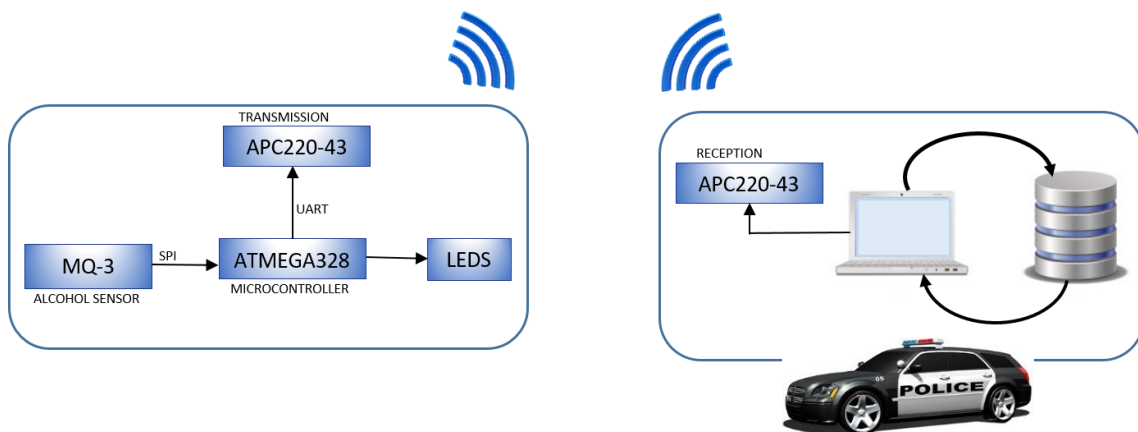


FIG. 1. Scenario for remote alcohol concentration testing for car drivers

3. HARDWARE IMPLEMENTATION

ATmega328P is a high-performance microchip pico-Power 8-bit AVR RISC-based microcontroller that combines a 32KB ISP flash memory with read-write capabilities, 1024 EEPROM, 2KB SRAM, 23 general purpose I/O lines, 32 general working registers, three flexible timer/counters with compare modes, internal and external interrupts, serial programmable USART, a byte-orientated 2-wire serial interface, SPI serial port, a 6-channel 10-bit A/D converter, programmable watchdog timer with internal oscillator, and five software selectable power saving modes. The device operates between 1.80-5.5 volts. By executing powerful instructions in a single clock cycle, the device achieves throughput approaching 1 MIPS per MHz, balancing power consumption and processing speed. [6]

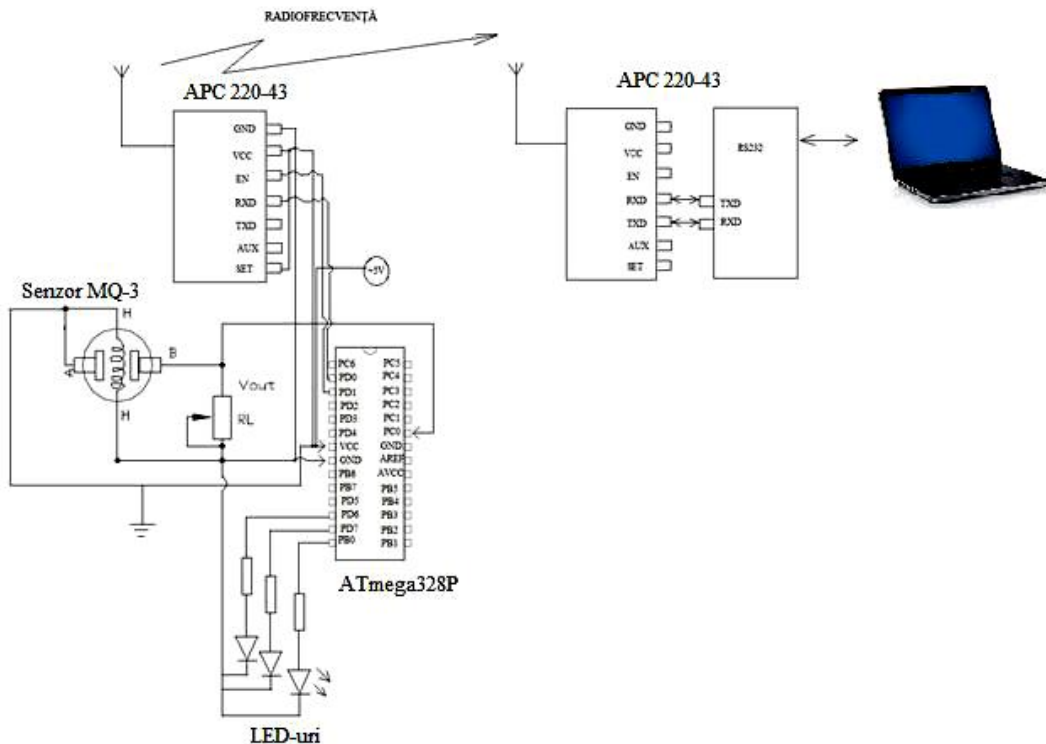


FIG. 2. The system block diagram

The sensor MQ-3 has a relatively simple 6-pin configuration, but there are used only 4 of them. Two are for the heat system, they are called H, and the other two are for voltage and ground. Inside the sensor exists a tiny tube that represents the heating system consisting of aluminum oxide and tin dioxide. Part of this tube is coil in which it is practically produced the heat. The sensor provides an analog resistive output based on the alcohol concentration and the drive circuit is represented by one resistor.

APC 220-43 is a highly integrated semi-duplex low power transceiver module, with high speed MCU. This equipment is using high efficiency forward error correction; it transmits transparent data with large data buffer zone and it provides more than 100 channels. Via the COM serial port or directly in software a user can set up the UART parameters. This wireless module can communicate with the other devices at about 1km distance with 2400 bps, the output power is 20 mW, the frequency 418MHz to 455MHz, uses for GFSK modulation, the interface is UART/TTL.[7] So for our implementation scenario, the transmission distance from the portable alcohol sensor to the police car should be sufficient.

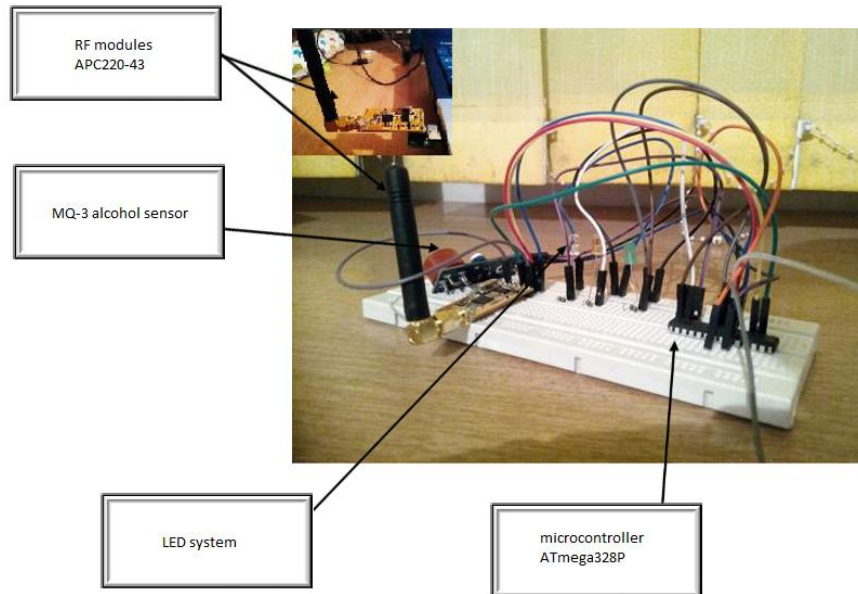


FIG. 3. The hardware components of the system

4. SOFTWARE IMPLEMENTATION

The tools used for the software implementation are AVR Studio 6.0 for implementing the C++ code on the microcontroller that it can perform the required tasks related to the project requirements, and Visual Studio Express to create an environment for the user, for this the code used is C#.

The code sequence that connects COM1 serial port is the following:

```
private void Make_Serial(string port, int boudrate, Parity parity, int
data_bit, StopBits stop_bit)
{
Serial_Port = new SerialPort(port, boudrate, parity, data_bit,
stop_bit);
try
{
Serial_Port.Open();
Serial_Port.DataReceived += new
SerialDataReceivedEventHandler(Serial_catch_data);
}
catch (Exception e)
{
MessageBox.Show(e.ToString(), "This is a error", MessageBoxButtons.OK,
MessageBoxIcon.Warning);
}
}
```

We have considered a real-time data acquisition form the sensor, so more values are recorded from the sample driver. Subsequent samples could help reduce one-time measurement errors and the need for retests. The user interface designed in C# presents in a graphical format these subsequent values.

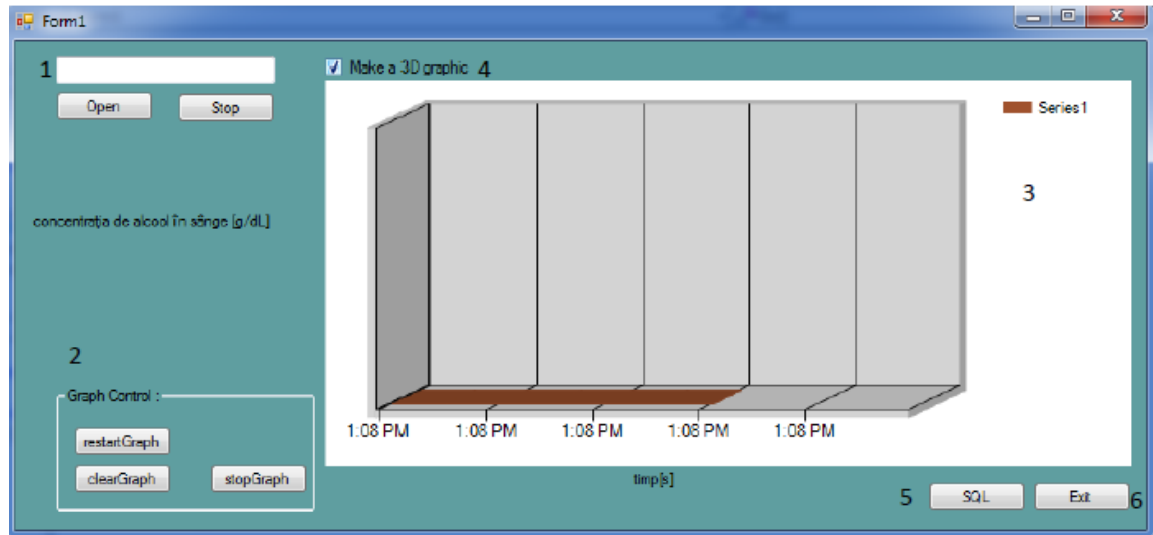


FIG. 3. The graphic displaying subsequent alcohol level sample reads.

The system has an SQL Server 2008 and all data displayed in the C# graphical interface is synchronized with the SQL Server. As visible in figure 4, from C# we have included some functions to search or display records from the SQL database.

To manage the massive information, the database is synchronized to an enterprise data warehouse, via the extraction, transformation and loading (ETL) tool from Informatica PowerCenter [8]. Thus, by using integration connectors data can be retrieved and manipulated, as Informatica PowerCenter can support an entire data integration lifecycle.

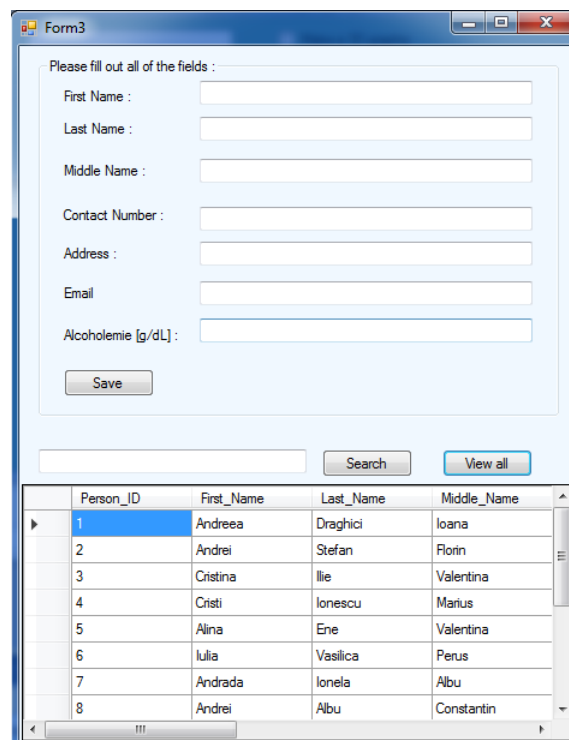


FIG. 4. The database interface and methods to search for previous records

5. CONCLUSIONS AND FUTURE WORK

The project aims to develop a new type of alcohol-test, more efficient and portable, including a method to prevent the fraud of the police check measurement and a method that helps storing the data and linking the data acquisition records to profile of the tested driver.

Another advantage of the structure and the malleability of the alcohol tester is the extension of the applicability domain, not only in police institutes, but also to other institutions or as a self-check for the driver itself, some automated systems coupling the breathalyzers to the car electronic, making it impossible for the driver to start the engine in case his alcohol vapor level is not proper. Using a microcontroller minimizes the dimension and reduces the cost of the system compared to using single board computers (SBC) like Arduino, Raspberry Pi, that are more expensive implementations.

The project may change in the future through a more comprehensive approach by introducing a LCD that will be able to see the values transmitted by the sensor in real-time. The radio frequency module used can be replaced by a mobile 3G/LTE one, thus extending the data acquisition area.

Other enhancement for the current system would be having an encrypted wireless transmission so that the information can't be retrieved by an unwanted person or have any kind of interferences that could corrupt the measured data. We chose the AES key-length 128 bit [9] to encrypt and decrypt the data using the Crypto-avr-lib, a set of implementations of different cryptographic primitives [10]. Due to the special limitations of microcontrollers (very little space, RAM and flash are ranging from a few bytes to a few KiB) reference implementations of encryption algorithms are not usable with their latest improvements, but Crypto-avr-lib offers adapted methods for microcontrollers. As AES is a symmetric-key algorithm, the same cryptographic keys for both encryption of plaintext and decryption of cyphertext will be used for protecting the data communication. This encryption of the communication should be doubled by the database encryption and a Cloud distributed database back-up, so that data is securely replicated and stored in different locations.

REFERENCES

- [1] Natl Highway Traff Safe Ad (NHTSA) Impaired Driving. 2016;
- [2] The Telegraph: Tom Parry Jones. Retrieved 16 January 2013, <http://www.telegraph.co.uk/news/obituaries/9803707/Tom-Parry-Jones.html>;
- [3] A. Jonsson, B. Hok and M. Ekstrom, Development of a Breath Alcohol Analyser for use on Patients in Emergency Care, World Congress on Medical Physics and Biomedical Engineering, Munich, Germany, September 7 - 12, 2009, 84-87;
- [4] L. M. Barba-Maza and C. Sánchez-López, "Development of a breathalyzer for car drivers," 2016 IEEE International Autumn Meeting on Power, Electronics and Computing (ROPEC), Ixtapa, 2016, pp. 1-4;
- [5] J. Shao Q.J. Tang C. Cheng Z.Y. Li Y.X. Wu "Remote detection of alcohol concentration in vehicle based on TDLAS", Symp. Photon. Optoelectron, vol. 1 pp. 1-4 2010;
- [6] "ATmega328P". Retrieved 2016-07-14, Available at <http://www.atmel.com/devices/atmega328p.aspx>;
- [7] ***, APC Series Transparent Transceiver Module APC220-43, Available at http://image.dfrobot.com/image/data/TEL0005/APC220_Datasheet.pdf;
- [8] Informatica Powercenter <https://www.informatica.com/products/data-integration/powercenter.html>;
- [9] <http://www.axantum.com/AxCrypt/etc/seagate128vs256.pdf> "Advanced Encryption Standard (AES)" Retrieved March 9, 2015;
- [10] AVR cryptolib <https://wiki.das-labor.org/w/AVR-Crypto-Lib/en>.

STUDY AND CONSTRUCTION OF AN AMPEROMETRIC POTENTIOSTAT SUITABLE FOR USE IN ENVIRONMENTAL MONITORING

Laura Mihaela LELUȚIU, Marius Dan BENȚA

Transilvania University of Brasov, Romania, Dep. of Electrical and Engineering
(lelutiulaura@gmail.com, marius.bentea@unitbv.ro)

DOI: 10.19062/2247-3173.2017.19.1.31

Abstract: *The paper presents some new requirements and trends concerning applications of amperometric biosensors and some practical problems for the environmental monitoring. The goal of this work was to build and study an amperometric potentiostat suitable for use in environmental monitoring. The amperometric potentiostat is an interface circuit which can adapt the biosensor for detection of pesticides in actual water samples. A rapid, simple, and sensitive amperometric potentiostat for direct total micro analysis measurement was developed. The large purpose of our work is creation of fast chemical test-systems with quite enough low detection limits and enough high selectivity. This paper presents some experimental studies of this apparatus.*

Keywords: *biosensors, amperometric, potentiostat, environmental, monitoring*

1. INTRODUCTION

In the last years the need for analytical devices to be used for environmental, industrial or medical controls has been growing very quickly. Today, the capability of sensors is a decisive factor in determining whether a system is of practical use or not. The development of new sensors for monitoring the complex matrix of physical, chemical, and biological entities is critical to our ability to deal with evolving environmental problems. Recently, pollution of environmental water and soil by pesticides has received much attention due to the use of large amounts of pesticides in agriculture and related activities. Small concentrations of such eco toxicants in soil and food products are the reason for many diseases in the population. Because similar compounds were produced as possible nerve poisons, a further area of application is in the military [1]. The application of enzymes as catalysts in organic solvents has led to the important development of organic-phase biosensors. However, the use of pure organic solvents leads to many problems, such as the incompatibility with enzyme, substrates and supports. The activity of enzymes is strongly dependent on their hydration layer, which is essential for their conformational flexibility. Therefore, an enzyme activity is influenced by the presence of organic solvents that interact with the aqueous layer around the enzyme molecule. Organic solvents can induce extensive changes in enzyme activity and specificity.

This is because the enzyme structure and activity depend on several non-covalent interactions, such as hydrogen bonding, ionic, hydrophobic, and Van der Waals interactions [2].

Therefore, important aspects of biosensors are the immobilization procedure for the enzyme on the electrode surface, and the selection of the solvent and electron communication between the electrode and the enzyme. Environmental monitoring involves three basic steps: collection of a representative environmental sample; extraction, separation, other sample pre-treatment; and finally, chemical analysis to determine the identity and quantity of material present in the sample.

2. CONSIDERATIONS ABOUT APPARATUS

Environmental monitoring involves three basic steps: collection of a representative environmental sample; extraction, separation, other sample pre-treatment; and finally, chemical analysis to determine the identity and quantity of material present in the sample. For an amperometric measurement a defined potential is applied at a working electrode with respect to a reference electrode while the circuit is closed by means of a counter electrode. Most electrochemical work with an electrochemical cell is achieved using what is called a potentiostat. Potentiostats are amplifiers used to control a voltage between two electrodes, a working electrode and a reference electrode, to a constant value. Both electrodes are contained in an electrochemical cell. Some designs have been proposed for VLSI potentiostats. Each of these designs amplifies smaller currents to the μA range and then measures the input current by calibrating their design at higher current range. By converting input current directly into time we eliminate amplifying circuitry, avoid matching problems and save on area and power consumption [3].

We have designed a potentiostat circuit that accepts an electrical signal, proportional to current flowing through the electrolyte (in the electrochemical cell) and measure the time it takes to charge or discharge a capacitor. For construction of suitable potentiostat we must study a simplified one. We can be seen below a simplified schematic of a potentiostat. A potentiostat is an electronic device that controls the voltage difference between a working electrode and a reference electrode. The potentiostat implements this control by injecting current into the cell through an auxiliary electrode. In almost all applications, the potentiostat measures the current flow between the working and auxiliary electrodes. The controlled variable in a potentiostat is the cell potential and the measured variable is the cell current. A potentiostat typically functions with an electrochemical cell containing three electrodes and that is true for both field probes and lab cells:

- Working Electrode: Electrochemical reactions being studied occur at the working electrode. This is analogous to testing using weight loss coupons. The working electrode can be bare metal or coated.
- Reference Electrode: A reference electrode is used in measuring the working electrode potential. A reference electrode should have a constant electrochemical potential as long as no current flows through it.
- Auxiliary Electrode: The Auxiliary electrode is a conductor that completes the cell circuit. The auxiliary (counter) electrode in lab cells is generally an inert conductor like platinum or graphite. In field probes it's generally another piece of the working electrode material [4].

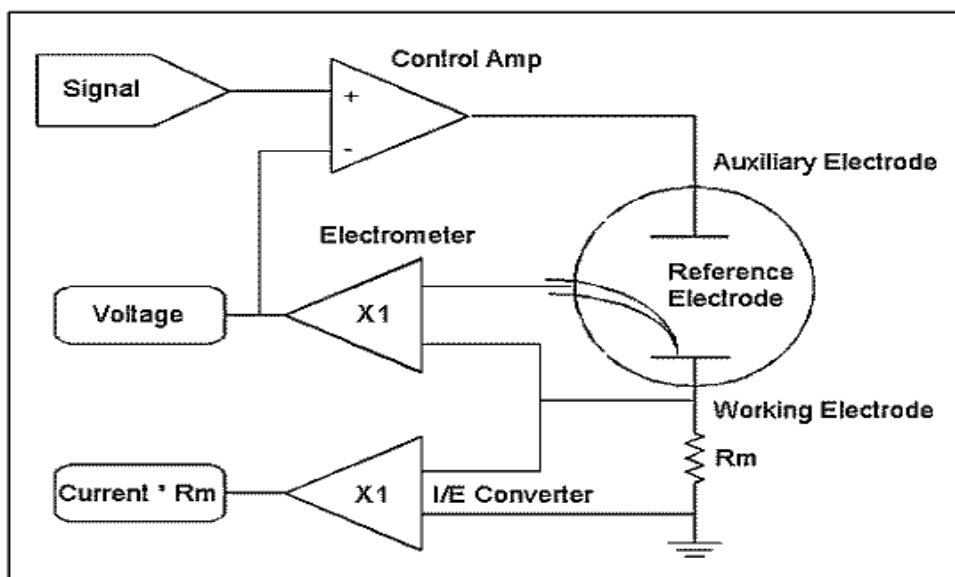


FIG. 1. A schematic diagram of a Potentiostat

Additional components are:

- **Electrometer:** The electrometer circuit measures the voltage difference between the reference and working electrodes. Its output has two major functions: it is the feedback signal in the potentiostat circuit and it is the signal that is measured whenever the cell voltage is needed. An ideal electrometer has zero input current and infinite input impedance.
- **I/E Converter:** The Current to Voltage (I/E) converter in the simplified schematic measures the cell current. It forces the cell current to flow through a current measurement resistor. The voltage drop across that resistor is a measure of the cell current.
- **Control Amplifier:** The control amplifier is a servo amplifier. It compares the measured cell voltage with the desired voltage and drives current into the cell to force the voltages to be the same. Under normal conditions, the cell voltage is controlled to be identical to the signal source voltage.
- **The Signal:** The signal circuit is a computer controlled voltage source. It is generally the output of a Digital to Analog (D/A) converter that converts computer generated numbers into voltages.
- **Galvanostats and Zero Resistance Ammeters (ZRAs):** Most laboratory grade potentiostats can also be operated as galvanostats or ZRAs (Zero Resistance Ammeter). Galvanostat is an electronic instrument that controls the current through an electrochemical cell at a preset value, as long as the needed cell voltage and current do not exceed the compliance limits of the galvanostat. Also it is called "amperostat." [5].

An interesting application is when the coupling current between two nominally identical electrodes is measured.

If both electrodes were identical then very little coupling current would flow. In real situations these electrodes will be slightly different, one being more anodic or cathodic than the other and a small coupling current will exist.

In an electrochemical cell, any change in the potential of the cathodic electrode, results in a flow of current in the electrolyte so the potential of the electrode is maintained. It is a fact that the biosensors require low-power electronics for providing the interface between biological electrode and signal processing devices (Fig. 2). The amperometric potentiostat is suitable for the above presented direct interfacing [6].

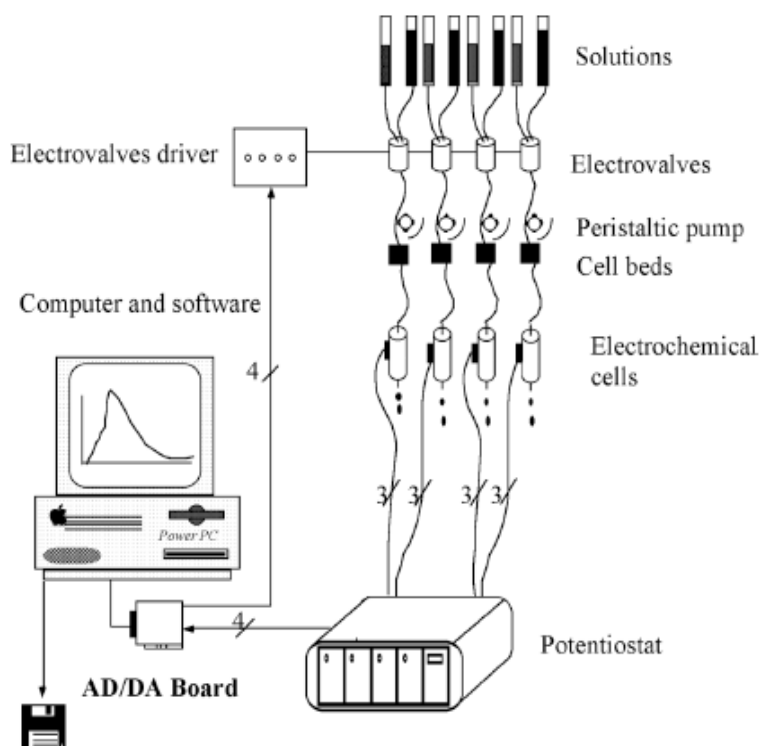


FIG. 2. The interface between biological electrode and signal processing devices

Basal incubating solutions or chemical stimuli are selected by the electro-valves. These valves can be manually operated or by a TTL signal generated by a computer digital output. A four-channel peristaltic pump is continuously perfusing the cell chambers or adrenal glands.

The emanating fluid is passed through the electrochemical cells for catecholamine detection. The potentiostats send the analogic signal (± 12 V) to a computer through a 12-bit AD/DA board.

3. CONSTRUCTION OF THE AMPEROMETRIC POTENTIOSTAT

Our presented amperometric potentiostat exhibits good linearity in the current range up to 200 nA when calibrated with highly stable thick-film resistors, with a detection limit of approximately 3 nA. In the embodiment tested, a sensitivity of just over 3 Hz/nA was achieved. The potentiostat was able to control the working electrode potential with respect to the counter electrode with a regulation of better than $\pm 2\%$ under various complex load impedances. The circuit consumes 500 μ W of power, achieved through the careful use of low-power CMOS amplifiers in the circuit design, and minimal quiescent current drain, and is therefore suitable for operation from standard 3 V Lithium coin cells. In fact, we developed a current-to-frequency converter circuit. This apparatus has been designed by us for implementing the function of an amperometric potentiostat with a minimum number of components. The specific unique qualities of this current-to-frequency converter that make it particularly suited to this type of application are high input impedance, necessary to obtain accurate amperometric measurements, and the direct production of a pulsed digital output, compatible with low-voltage CMOS logic gates, using only a few components [7].

4. EXPERIMENTAL DETERMINATIONS

The experimental measurements were accomplished using physical methods of conductivity and potentiometry. For low current densities, the error arising from the dependence of the potential from the cell current may be neglected and a two-electrode set-up is

sufficient for amperometric investigations. The constructed converter exhibits good linearity in the nanoampere current range that is relevant for many chemical and biosensor electrodes.

This particular design has a very low-power consumption, and may easily be adapted to meet the requirements of different electrode-based amperometric sensors. Our aim was to obtain the calibration curve for the potentiostat. It was measured the dependency between the current and frequency and the results obtained are shown in Table 1.

f [Hz]	15	20	40	60	90	120	150	200
I [nA]	50	65	120	180	270	340	420	620

We processed the experimental data by making use of a tblcurve and orrigin soft. in figures 3, 4 and 5 there is represented the dependency between the current-to-frequency calibrations curves obtained for the potentiostat. different currents were sequentially set with high-ohmic thick-film resistors connected across the working and counter electrode terminals of the potentiostat. the current value was calculated from the ratio of the measured electrode potential difference to the measured value of the applied resistance.

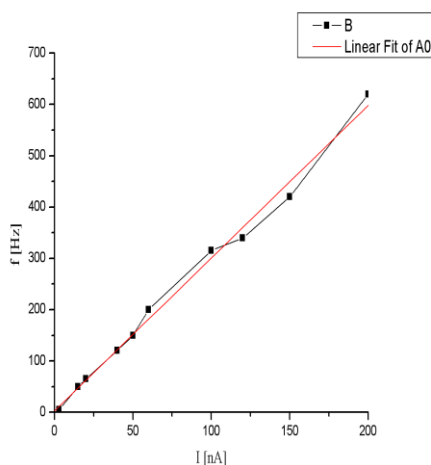


FIG. 3. The current-to-frequency calibration curve of the potentiostat. obtained by making use of a ORRIGIN SOFT-(a) Linear current range

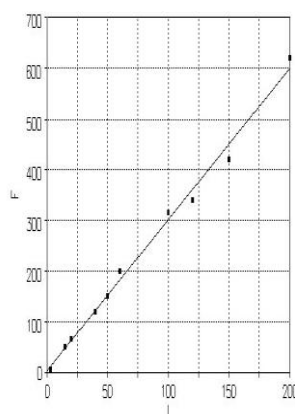


FIG. 4. The current-to-frequency calibration curve of the potentiostat obtained by making use of a TBLCURVE SOFT, with resistive loading to the electrode terminals.

By processing the experimental data by making use of a TBLCURVE and ORRIGIN SOFT there was established the equation of the curve of dependency of the current-to-frequency. The Figure 4 show that the current-to-frequency transfer function is linear between approximately 4 and 200 nA, and extends up to currents of 700 nA. In the linear region, after processing the experimental data, the output frequency there was obtained by the the following equation:

$$f_{\text{out}} = 2.8472 + 2.9769 I_{\text{cell}} \quad (1)$$

where I_{cell} is the electrode current in nA. We find that the zero offset of the converter is 2.8472 nA, and the sensitivity is 2.9769 Hz/nA.

5. CONCLUSIONS

The above constructed potentiostat exhibits good linearity in the nanoampere current range that is relevant for many chemical and biosensor electrodes. This apparatus has been designed by us for implementing the function of an amperometric potentiostat with a minimum number of components. This particular design has a very low-power consumption, and may easily be adapted to meet the requirements of different electrode-based amperometric sensors. The requirements for environmental monitoring are not easily satisfied, but step by step the aim is to establish more reliable and rational sensors. Important challenges remain in the area of environmental sensing. The scope of these challenges ranges from monitoring global atmospheric phenomena to detecting alternations in the structure of DNA. To be effective, the measurement, electronics and control components, and sub-systems, in particular sensors and sensors systems have to be developed in parallel as part of computer-controlled manufacturing systems. Adequate solutions have been found for most practical measurement problems, but there are applications where the available solutions are not fully satisfactory. Still, a few general environmental sensing trends can be identified. In assessing the risks to human health from chemical hazards, increasing emphasis is being placed on measuring individual exposures, with personal monitors or through analysis of biological fluids. New instruments and methods being developed show promise for continuous, in situ monitoring of toxic compounds. The environmental analytical community continues to search for portable analytical techniques that can give reliable, on-site results for a variety of matrices and a host of analytes. New technology, new principles for reliable sensors are expected to be developed. To meet both present and anticipated requirements, new and improved methods are needed. It is now recognized that these methods must be based on the powerful techniques employing computer-assisted information systems and production methods.

REFERENCES

- [1] Rab, L.: *Applications of sensors in environmental monitoring* In: In Proceedings of International Conference on materials science and engineering, Bramat-2001, Brasov, ISBN 973-8124-15-8, pp.176-179.
- [2] Florescu M., Rab, L.: Biosensors as warning devise for enviromental measurements In: In Proceedings of International Conference on materials science and engineering, Bramat-2005, Brasov, ISBN 937-635-454-7, Romania, pp.176-179.
- [3] Popescu, A.: *Fundamentele biofizicii medicale,, vol II*. București, Editura Didactică și Pedagogică, 1994.
- [4] Stanciu, D.: *Senzori. Prezent și perspectiva*, București, Editura Tehnică , 1987.
- [5] Gopel, W.: *Sensors, vol II*. , New York, Ed.by T.Grandke, 1989.
- [6] Gopel, W.: *Sensors, vol IV*. , New York, Ed.by T.Grandke, 1989.
- [7] Leluțiu, L.M. – *Senzori utilizați în măsurarea și controlul mărimilor specifice calității mediului*, Ed. Universității Transilvania din Brașov, 2010, ISBN 978-973-598-820-3

DETERMINING THE CAPACITY CONDENSER VALUE AT SINGLE-PHASE MOTOR SPEED CHANGE

Valentin MÜLLER, Monica SZABO

University “Aurel Vlaicu”, Arad, Romania (valentinmuller7@yahoo.com,
szabomonica@yahoo.com)

DOI: 10.19062/2247-3173.2017.19.1.32

Abstract: This paper determines the value of capacitor connected in series with the auxiliary phase for a single-phase induction machine. Capacitance of the capacitor is determined by a certain gap between the main and auxiliary phase of the machine, having variable speed.

Keywords: Single phase induction motor, capacitance of the capacitor.

1. INTRODUCTION

Considering a single-phase asynchronous machine type with a capacitive booster phase having the lag angle θ between the axis of the main phase (A) and the axis of the booster phase (B), (figure 1).

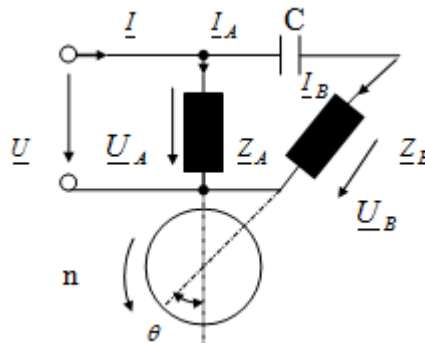


FIG.1. Asynchronous machine with capacitive booster phase.

It applies the method of symmetrical components in the general case, the different electrical parameters of the main and auxiliary phase.

The stator magnetic range is an elliptical range, it is in two parts, the forward and the reverse, and the impeller featuring the same range components as a result of the reaction of the rotor range. The homopolar component of the stator coil current is different from zero, which determines a magnetic range the same size as the dispersion range, because the range lines approach to the homopolar flux close through low magnetic permeability environments. The homopolar component of the rotor flux is of no value, having no place to enwrap.

2. THE MATHEMATICAL MODEL

As a reference axis for writing equations A axis is chosen to which we have all the electrical quantities from stator and rotor.

Considering asynchronous machine analysis with split phase in symmetrical components [1,2,4] and for a gap of $\pi/2$ between the main and auxiliary phase shows the following:

$$\underline{U}_A = \underline{Z}_1 \underline{I}_A + \underline{Z}_2 \underline{I}_B \quad (1)$$

$$\underline{U}_B = -\underline{Z}_2 \underline{I}_A + \underline{Z}_3 \underline{I}_B \quad (2)$$

$$\underline{U}_A = \underline{U} \quad (3)$$

$$\underline{U}_B = \underline{U} - \underline{I}_B \underline{Z} \quad (4)$$

$$\underline{Z}_1 = \frac{1}{3} (\underline{Z}_{e2Ad} + \underline{Z}_{e2Ai} + 2\underline{Z}_A + \underline{Z}_{A0}) \quad (5)$$

$$\underline{Z}_2 = \frac{j}{K} (\underline{Z}_{e2Ai} - \underline{Z}_{e2Ad}) \quad (6)$$

$$\underline{Z}_3 = \frac{1}{3} \left(\frac{\underline{Z}_{e2Ad} + \underline{Z}_{e2Ai}}{K^2} + 2\underline{Z}_B + \underline{Z}_{B0} \right) \quad (7)$$

$$\underline{Z} = \frac{-j}{\omega_1 C} \quad (8)$$

$\underline{Z}_A = R_A + jX_A$ - the main phase impedance;

$\underline{Z}_B = R_B + jX_B$ - the auxiliary phase impedance;

$\underline{Z}_{A0} = R_A + j\alpha X_A$ - the main phase of the monopolar impedance;

$\underline{Z}_{B0} = R_B + j\alpha X_B$ - the auxiliary phase of the monopolar impedance;

$\underline{Z}_{Am} = R_{Am} + jX_{Am}$ - the magnetization impedance;

$\underline{Z}'_{2Ad} = \frac{R'_{2A}}{s} + jX'_{2A}$ - the direct sequence rotor impedance relative to the main phase;

$\underline{Z}'_{2Ai} = \frac{R'_{2A}}{2-s} + jX'_{2A}$ - the reverse sequence rotor impedance relative to the main phase;

$K = \frac{N_A k_{bA}}{N_B k_{bB}}$ - the conversion factor of voltages between the main and auxiliary phase;

$$\underline{Z}_{e2Ad} = \frac{\underline{Z}_{Am} \underline{Z}'_{2Ad}}{\underline{Z}_{Am} + \underline{Z}'_{2Ad}} \quad (9)$$

$$\underline{Z}_{e2Ai} = \frac{\underline{Z}_{Am} \underline{Z}'_{2Ai}}{\underline{Z}_{Am} + \underline{Z}'_{2Ai}} \quad (10)$$

The main and auxiliary phase currents using equations (1.1-1.4):

$$\underline{I}_A = \underline{Y}_{eA} \underline{U} \quad (11)$$

$$\underline{I}_B = \underline{Y}_{eB} \underline{U} \quad (12)$$

Where equivalent admittance of the main and auxiliary phase have the expressions:

$$Y_{eA} = \frac{\underline{Z}_3 + \underline{Z} - \underline{Z}_2}{\underline{Z}\underline{Z}_1 + \underline{Z}_2^2 + \underline{Z}_1\underline{Z}_3} \quad (13)$$

$$Y_{eB} = \frac{\underline{Z}_1 + \underline{Z}_2}{\underline{Z}\underline{Z}_1 + \underline{Z}_2^2 + \underline{Z}_1\underline{Z}_3} \quad (14)$$

The reverse component of the electromagnetic torque is canceled for $\underline{I}'_{2Ai} = 0$, meaning [3]:

$$KY_{eA} + jY_{eB} = 0 \quad (15)$$

where you obtain the condenser capacity value, depending on the power supply frequency in the form:

$$C = \frac{3K^2}{2\pi f_1 \left[(4\underline{Z}_{e2Ad} - 2\underline{Z}_{e2Ai})(1 + jK) + 2jK\underline{Z}_A + \underline{jKZ}_{A0} + 2K^2\underline{Z}_B + K^2\underline{Z}_{B0} \right]} \quad (16)$$

The equivalent impedances corresponding to direct sequence \underline{Z}_{e2Ad} and reverse \underline{Z}_{e2Ai} shown in relations (9,10), are depending of sliding and machine speed.

Condenser capacity value for different frequencies is determined at rated slip s_N of the machine.

3. CASE STUDY

It is considered a single-phase asynchronous motor with auxiliary phase power $P_N=370W$ and RPM $n=1500\text{rot}/\text{min}$ at $C=20\mu F$, with electrical parameters: $R_A=7,47\Omega$; $R_B=11,97\Omega$; $L_A=0,039H$; $L_B=0,07H$; $M_A=0,345H$; $M_B=0,448H$; $R_2=1,6 \cdot 10^{-4}\Omega$; $L_2=4,4 \cdot 10^{-7}H$

Table 1 shows the values for voltage and capacity condenser at different machine speeds having stator phase angle difference of $\theta=90^\circ$.

Table 1

f=25Hz	$U_A=130V$	$C=90\mu F$	$n_N=660\text{rot}/\text{min}$
f=40Hz	$U_A=176V$	$C=40\mu F$	$n_N=1056\text{rot}/\text{min}$
f=50Hz	$U_A=220V$	$C=25\mu F$	$n_N=1320\text{rot}/\text{min}$
f=70Hz	$U_A=220V$	$C=16\mu F$	$n_N=1848\text{rot}/\text{min}$
f=100Hz	$U_A=220V$	$C=10\mu F$	$n_N=2640\text{rot}/\text{min}$

Table 2 shows the values for gap between stator phases of $\theta = 30^0$.

Table 2

f=25Hz	$U_A=130V$	$C=90\mu F$	$n_N=660\text{rot/min}$
f=40Hz	$U_A=176V$	$C=40\mu F$	$n_N=1056\text{rot/min}$
f=50Hz	$U_A=220V$	$C=25\mu F$	$n_N=1320\text{rot/min}$
f=70Hz	$U_A=220V$	$C=16\mu F$	$n_N=1848\text{rot/min}$
f=100Hz	$U_A=220V$	$C=10\mu F$	$n_N=2640\text{rot/min}$

Table 3 shows the values for gap between stator phases $\theta = 120^0$.

Table 3.

f=25Hz	$U_A=130V$	$C=210\mu F$	$n_N=660\text{rot/min}$
f=40Hz	$U_A=176V$	$C=100\mu F$	$n_N=1056\text{rot/min}$
f=50Hz	$U_A=220V$	$C=70\mu F$	$n_N=1320\text{rot/min}$
f=70Hz	$U_A=220V$	$C=40\mu F$	$n_N=1848\text{rot/min}$
f=100Hz	$U_A=220V$	$C=25\mu F$	$n_N=2640\text{rot/min}$

Table 4 shows the values for gap between stator phases $\theta = 150^0$

Table 4.

f=25Hz	$U_A=130V$	$C=148\mu F$	$n_N=660\text{rot/min}$
f=40Hz	$U_A=176V$	$C=65\mu F$	$n_N=1056\text{rot/min}$
f=50Hz	$U_A=220V$	$C=75\mu F$	$n_N=1320\text{rot/min}$
f=70Hz	$U_A=220V$	$C=25\mu F$	$n_N=1848\text{rot/min}$
f=100Hz	$U_A=220V$	$C=16\mu F$	$n_N=2640\text{rot/min}$

CONCLUSIONS

The optimal capacity of the capacitor is determined by the condition of reverse component of the electromagnetic torque cancellation.

From the tables is observed that the value of the capacitor power decreases with increasing RPM.

A gap θ between auxiliary and main phase other than $\frac{\pi}{2}$ determinates a considerable increase in the output capacitor, especially at low motor speed.

The capacitor power value can be adjusted using electronic devices connected in parallel with the capacitor of fixed value.

REFERENCES

- [1] M. Babescu, *Maşini electrice monofazate*, Editura Tehnică Bucureşti, 1992;
- [2] V. Müller, *Motorul asincron monofazat cu fază auxiliară*. Studiu. Performanţe, Editura Politehnica Timişoara, 2002;
- [3] V.Müller, *Maşina asincronă monofazată cu fază auxiliară în sisteme de reglare automată*, Editura Politehnica Timişoara, 2004;
- [4] T.M. Lettenmaier, D.W. Novotny, T.A. Lipo, *Single-Phase Induction Motor with an Electronically Controlled Capacitor*, Conference Record of the IEEE Industry Applications Society Annual Meeting, Vol. 1, pp. 169-174, 1988.

STUDYING THE POSSIBILITY OF INCREASING THE FLIGHT AUTONOMY OF A ROTARY-WING MUAV

Cristian VIDAN*, Daniel MĂRĂCINE**

*Military Technical Academy, Bucharest, Romania (vidan.cristian@yahoo.com)

**Politehnica University, Bucharest, Romania (dani.maracine@gmail.com)

DOI: 10.19062/2247-3173.2017.19.1.33

Abstract: *In the last few years, many researchers wrestle with the challenge to increase the flight autonomy of mUAVs. All these efforts were conclude in some results in term of fixed wing mUAV, where the flight autonomy has increased significantly, but for the rotary wing mUAV, the improvements are still pending. This paper approaches the idea of increasing autonomy for a quad rotor mUAV, by implementing a hydrogen PEM fuel cell alongside two lithium batteries. The idea behind this concept is to charge a battery from the PEM fuel cell, while using another battery to power the system. To test different configurations, simulations of the charging and discharging process were realized using Simulink and represent the main subject of this paper. The theoretical mUAV model used in the simulation, makes use of state of the art components, available on the market, to achieve great efficiency.*

Keywords: *flight autonomy, PEM cell, rotary wing, quadcopter, battery.*

1. INTRODUCTION

The UAV domain is in a continuous expansion from the point of view of both the manufacturing process and the missions that can be accomplished by those. A great interest was built in the military and civilian around the unmanned aircraft thanks to a great number of successful military missions performed by drones.

Advances in technology and the use of intelligent materials allow for more and more challenging and interesting UAV projects to emerge.

At this time, multi-rotor MUAVs are continuously researched and developed. Manufacturers keep introducing new hardware such as cameras, gimbals, sensors, tanks and sprays for agriculture and also new software functions, including subject capabilities, preset path, automatic return, automatic landing, autonomous flight, mapping, obstacle detection, flight management, battery management.

The development and implementation of all these features implies an increasing energy consumption. In this paper a method of increasing flight autonomy is approached, and as a reference model was chosen a rotary-wing UAV, in this case a quadcopter.

The method consists in implementing a hybrid power system which is made up of two batteries, alternately charged during flight by a hydrogen fuel cell.

To demonstrate this method, a Matlab - Simulink model was designed, in which two batteries are charged by aid of a constant voltage source (21V), representing the PEM (Proton Exchange Membrane) fuel cell, and between these two components is connected a high rate battery charger.

Simulating a possible implementation of this system will notice an increase in flight autonomy for the particular quadcopter case.

2. SYSTEM DESCRIPTION

Quadcopter has received considerable attention from researchers as the complex phenomena of the quadcopter has generated several areas of interest. The basic dynamical model of the quadcopter is the starting point for all of the studies but more complex aerodynamic properties has been introduced as well.[1,2]

As a reference model we used a Tarot F650 Ironman quadcopter (fig. 1.) which is equipped with four LD Power Motors M2810-720KV with 12x5.5” propellers, single battery powered, with a total mass approximated to 2.2kg and a total power onboard consumption measured in different operating modes as it is depicted in the following table:

Table 1:measurements of a power consumption of a Tarot F650 Ironman

Mode	Power(W)	Current(A)	Electric Charge(Ah)
Stand-by	5.8-5.9	0.38	15×10^{-3}
Idle	14.4	1	32×10^{-3}
50%	210	15	14×10^{-2}
100%	700	50	48×10^{-2}

The reference hydrogen subsystem is composed of a fuel cell stack, a hydrogen tank and auxiliary components.

Fuel cells are inherently modular and therefore lend themselves to a wide range of applications, from large stationary power plants to small portable power packs.[3]

The fuel cell stack has the following electrical characteristics: 200W rated output power of 21V nominal voltage, and 9.52A output current. It weighs about 600g and measures 130mm in length, 85mm in width and 68mm in height.



FIG. 1. Tarot F650 Ironman quadcopter

The output of a PEM Fuel Cell is an electric energy, with water and heat as the only by-products. Efficiency can be high due to the absence of a Carnot cycle. From the electrical point of view, the cell can be seen as a voltage source where the output impedance presents a highly nonlinear dependence to operating conditions such as temperature, electric current, partial pressure and humidity levels of the incoming gases. [4].

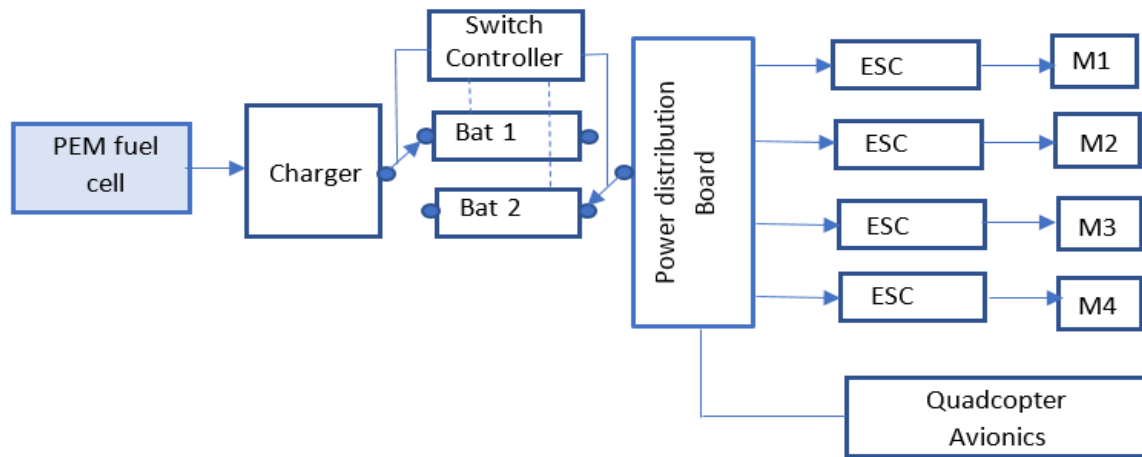


FIG. 2. Block diagram of a hybrid power system

At the time of take-off, it is assumed that the batteries are already charged 100% and the onboard consumers are powered by a single battery, the fuel cell and the charger are in stand-by.

When the first battery reaches 10%, estimating that this will happen after approximately 13 minutes, the switch controller switches the load on to the 2nd battery, and at the same time the fuel cell and the charger start charging the first battery at an initial charge rate About 16 A.

The second battery will also reach 10%, which is the minimum preset value at which switching between batteries is performed. Flight time with the 2nd battery reaches 13 minutes. In the 13-minute operation of a battery, the charger managed to charge the first battery, bringing it to a value of 35%, which means another 5 minutes of extra flight.

After 3 switching between batteries, you can reach a 30-minute flight time, which means 5 minutes longer than a flight using 2 parallel-connected batteries.

3. SIMULATION

In the Simulink model, the fuel cell stack is represented as a constant voltage source connected to a DC-DC buck converter to which we have implemented a feedback controller to allow CC/CV(constant current/ constant voltage) charging. The batteries are connected to the charger via individual switches operated by a controller. The same controller switches the load (esc, motors, autopilot, auxiliary devices) between the batteries, allowing one battery to be charged and the other discharged in parallel.

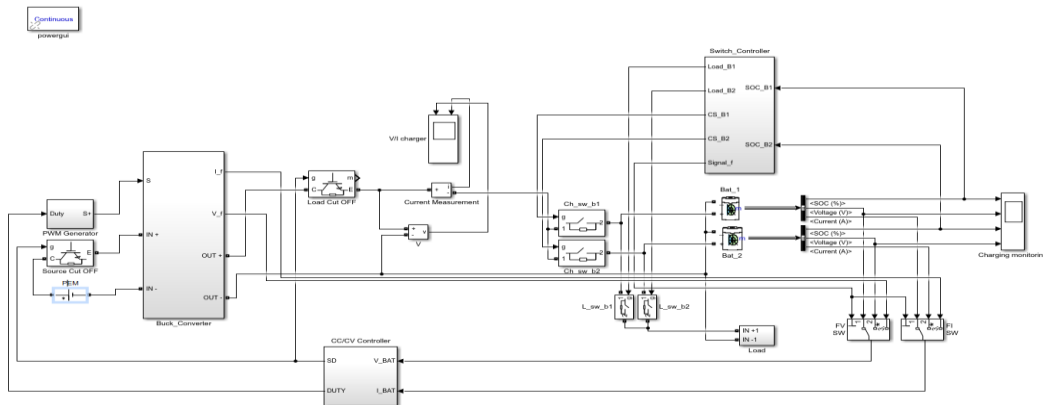


FIG. 3. Model Simulation in Simulink – MatLab

The designed model implements two separate circuits, one charging circuit and one for discharge. The charging circuit starts with a PEM fuel cell, implemented as a constant voltage source (21V), which feeds directly to a Buck DC-DC converter with a feedback controller for output regulation.

The buck converter steps down with high efficiency, the voltage of 21 V to 12.6 V, regulated by the feedback controller, through a PWM signal.

The feedback controller ensures the CC / CV charging mode so that until the battery reaches the maximum voltage of 12.6V, it is charged with constant current. After reaching the maximum voltage, the controller switches to CV mode and gradually decreases the battery power while keeping the voltage at 12.6V.

The two batteries are charged in an alternative way. This process of switching is ensured by the switch controller, which is based on an editable threshold representing the minimum state of charge accepted, disconnects the battery and connects the other. The same controller connects the load to the battery disconnected from the charging circuit and switches between the signals fed to the feedback controller.

4. RESULTS

Figure 4 shows the simulation result of the hybrid power system. In the first graph you can see the battery status number 1 represented in percentages and reaching the 10% threshold. Graph 2 accompanies graph number 1 and represents the battery number 1 voltage during the process of discharging and then the process of charging.

In graphs 3 and 4 the same features are represented, but for battery number 2. By comparing the two batteries represented in figure 4, it is noticeable that while the first battery is being charged, the second one is discharged by feeding the consumers on board of the mUAV and vice versa.

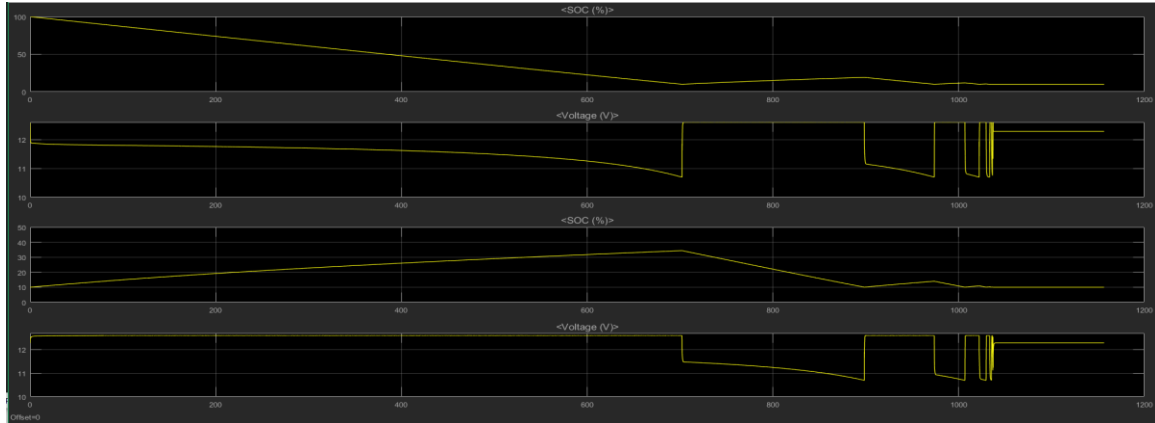


FIG. 4. Graphical representation of the evolution of batteries

Following the implementation of this hybrid power system, we have estimated the following flight times according to different power system configurations, as shown in the following table:

Table 2: Estimated flight times on different configurations of power systems

Power system	Estimated flight time	MTOW
One battery	17 min	2.2 kg
Two batteries	25 min	2.7 kg
Hybrid system	33 min	3.5 kg

5. CONCLUSION

Hoping for a future development of fuel cell technology by decreasing weight and improving performance. This hybrid power system can become an alternative solution for increasing flight autonomy for both rotary-wing mUAVs and fixed-wing mUAV.

Even if the implementation of this system can reach several thousand euros, the security and intervention structures (Firefighters Department, Police etc.) can take advantage of it, especially as when a droning operation is used, each minute with which the autonomy is extended flight can be decisive in saving human lives.

In this paper we have demonstrated that there are alternative sources of power supply for MUAVs others than LiPo batteries. It is also possible to consider creating a power system consisting exclusively PEM fuel cell stack.

7. FUTURE WORK

As future improvements to the system implemented in this paper, we thought about the following:

Integration of a method of supplying the consumers and using the PEM fuel cell in parallel with the first battery, starting with the take-off time until the first battery is discharged. This can lead to an increase in the duration of the first battery discharge from 13 minutes to approximately 20 minutes.

Implement a failsafe function that, if both batteries are fully downloaded, can feed the system directly from the PEM fuel cell.

REFERENCES

- [1] G. M. Hoffmann, H. Huang, S. L. Waslander, and C. J. Tomlin, "Quadrotor helicopter flight dynamics and control: Theory and experiment," Proceedings of the AIAA Guidance, Navigation and Control Conference and Exhibit, Aug. 2007.
- [2] H. Huang, G. M. Hoffmann, S. L. Waslander, and C. J. Tomlin, "Aerodynamics and control of autonomous quadrotor helicopters in aggressive maneuvering," IEEE International Conference on Robotics and Automation, pp. 3277–3282, May 2009.
- [3] "Fuel Cell Technology", College of the Desert, December 2001.
- [4] C. Kunusch et al., Sliding-Mode Control of PEM Fuel Cells, Advances in Industrial Control, Springer-Verlag London Limited 2012

A STUDY ON THE VEHICLE EVALUATION METHODS IN JUDICIAL TECHNICAL EXPERT REPORTS

Cornel ARAMĂ*, Lavinia ARAMĂ**, Mariana ARAMĂ*

*"Henri Coandă" Air Force Academy, Braşov, Romania (aramis5791@gmail.com)
**freelancer (lavinia_ana@yahoo.com)

DOI: 10.19062/2247-3173.2017.19.1.34

Abstract: *The judicial technical expert reports in automotive and traffic is a sensitive area. Few people are aware of their existence until they need one, and only then do they realize that the judge's final ruling depends on the expert's decisions. In this paper we are going to refer to the Civil Code judicial expert reports. More precisely, we are going to analyze some aspects about the litigation reports between the insurance firms and their insurants for some due compensation. One of the most sensitive problems in this situation is the evaluation of second-hand vehicles market value. We are going to suggest some methods of second-hand cars evaluation values.*

Keywords: *judicial technical expert, reports, evaluation, second-hand vehicles values ...*

1. INTRODUCTION

The judicial technical expert reports in automotive and traffic is a sensitive area. Few people are aware of their existence until they need one, and only then do they realize that the judge's final ruling depends on the expert's decisions.

Practice has proven that the majority of automotive and traffic judicial expert reports fall under the Penal and Civil Code areas. The first includes the analysis of different kinds of tragically traffic accidents with a lot of damages, loss of human lives and serious wounds. The majority of the analyzed situations in the Civil Code refer to different litigations between insurance firms and their insurants.

Generally, the traffic accident reconstruction has taken a big step forward, first of all due to the dedicated IT programs which make the work of traffic accident reconstruction specialists much easier. Unfortunately, these programs are very expensive and Romanian experts cannot afford to buy them. On the other hand, the demo versions of these programs allow the specialists to model different situation.

Secondly, a lot of tests have been made that take into consideration almost all the situations that can be met in traffic accidents and this thing has allowed to establish a lot of apparently abstract formulas, but which can lead to simplified and accurate calculi.

In this paper we are going to refer to the other kind of judicial expert reports: the Civil Code provisions. More precisely, we are going to analyze some aspects about the litigation reports between the insurance firms and their insurants for some due compensation. One of the most sensitive problems is the evaluation of second-hand vehicles market value.

2. STATE OF ART

From the point of view of mandatory vehicle insurance (RCA-type), until 01.01.2015 the algorithm was clear because the Order CSA no. 14/2011 stipulated a rigid system of calculating the market value for a second-hand vehicle. This algorithm was based on the wear coefficients presented in the annexes to the order.

The current order, CSA no. 23/06.11.2014, entered into force in 01.01.2015 and it no longer states clearly how vehicles must be evaluated. As written down in Art. 52/CSA23/2014: “(1) The value of the vehicle at the time of the traffic accident is established on the base of the market study taking into consideration the market values of similar vehicles with the same manufacturer, type, model, technical characteristics, technical equipment, manufacturing year, the same number of kilometers and state of maintenance. (2) The vehicles market value must be established on the base of specialty systems for the evaluation of the vehicles permanently registered in Romania and on the base of any documents presented by the injured party which can prove the prejudice.”

As one can easily infer, establishing the second-hand vehicles market value could be a permanent source of evaluator’s subjectivism, especially as far as CASCO insurance is concerned, where the insurants, who are not specialists in this field, can fail to notice very important details included in the insurance contract.

The Romanian Evaluators National Association (ANEVAR) supports its members by developing evaluation standards and guides, but these are difficult to access by the experts who are not ANEVAR members.

However, as long as there is no legal obligation to comply with some evaluation methods, technical experts have the duty to develop more or less original techniques to get closer to the real value.

3. SUGGESTED METHODS OF EVALUATING VEHICLES (example)

Evaluated vehicle:

Table 1. Evaluated vehicle characteristics

Manufacturer	Skoda
Model	Octavia II A5
Generation	Octavia II (facelift 2009)
Factory	Skoda Czech Republic- Mladá Boleslav
Engine type	1.6 MPI (102 HP)
Door number	5
Engine power	102 HP /5600 rot/min
Manufacturing year	2011
Body type	Hatchback
Engine type	Otto
Ecological standard	EURO IV
Date of the event	28.11.2014
Odometer	Unknown

The odometer is very important in order to evaluate the car as accurately as possible, taking into account that we do not know the on board kilometres we have to evaluate. So:

- the odometer on 29.05.2014 (date when the CASCO insurance was signed): 128.875 km;

- the date of first car registration: 10.11.2011 → the vehicle circulated until the insurance was signed, 29.05.2014, approximately 30,5 months;

- the average of kilometres circulated monthly:

$$M = \frac{128875}{30,5} = 4225 \text{ km/month} \quad (1)$$

- the car is very likely to have circulated from the moment when the insurance was signed, 29.05.2014, until the date of accident, 28.11.2014:

$$\begin{aligned} KM \text{ rolling till the date of accident} &= 6 \text{ months} \times 4225 \frac{\text{km}}{\text{month}} \\ &= 25350 \text{ km} \end{aligned} \quad (2)$$

- so, very probably the Skoda Octavia had an odometer on the date of the accident, 28.11.2014:

$$KM \text{ presumptiv odometer} = 128875 + 25350 = 154225 \text{ km} \quad (3)$$

CONCLUSION: The car evaluation on the date of the accident will be done taking into account 154.225 kilometres on board!

A. The evaluation based on CSA 14/2011 algorithm

The acquisition value of the new Skoda Octavia, based on acquisition invoice, was 56.163 lei.

The leu/euro exchange rate in 28.10.2011 was 4,3150 lei/1 euro.

So, the car value in 28.10.2011 was:

$$V_{\text{euro}} = \frac{56163 \text{ lei}}{4,3150} = 13015,75 \text{ euro} \quad (4)$$

It results that the value for a new car was:

$$V_{\text{Skoda}} = 56163 \text{ lei} = 13015,75 \text{ euro} \quad (5)$$

→ Accordingly, the calculi for establishing the real value on the date of the accident are going to be made starting from the new car price of 13.015,75 euro.

The date of the first registration of Skoda Octavia, according to the Registration Licence, is 10.11.2011. It results that the exploitation time on the date of the accident was 3 years and 1 month.

According to the calculi made on the 2.3.1 part, at that moment the odometer was 154.225 km.

→ **The establishment of wear coefficient:**

The average number of kilometres per month:

$$Km_{\text{per month}} = \frac{154225}{37} = 4168 \text{ km} \quad (6)$$

Kilometres per year:

$$Km_{\text{per year}} = 4168 * 12 = 50019 \text{ km} \quad (7)$$

The correction of the wear coefficient:

$$C_{\text{wear coefficient}} = \frac{50019 - 15000}{1000} * 0,5 = 17,50\% \quad (8)$$

The calculus of temporarily wear coefficient:

$$U = 37 + 17,50 = 54,50\% \quad (9)$$

The wear coefficient of Skoda Octavia is adopted for the date 28.11.2014:

$$U_r = 45\%$$

→ It results that the value of Skoda Octavia in 28.11.2014 was:

$$V_{Skoda} = A * U_r = 13015,75 \text{ euro} * (100 - 45)\% = 7158,66 \text{ euro} \quad (10)$$

Taking into account the exchange rate leu/euro in 28.11.2014 the value of Skoda Octavia will be:

$$V_{Opel} = 7158,66 * 4.4247 = 31674,93 \text{ lei} \quad (11)$$

B. The establishment of the real value based on online market study of sites specialised in second-hand vehicles commercialization

Investigation factors:

Manufacturer - Skoda

Model - Octavia II (facelift 2009)

Engine type - 1.6 MPI (102 HP), gasoline

Body type – 3 volumes

Manufacturing year – 2011

Odometer – aprox. 155.000

Table 2. www.olx.ro

According to: https://www.olx.ro/						
No.	Manufacturer, type, model	Engine capacity [cm ³]	Manufacturing year	Odometer	Required price [euro]	Comments
1	Skoda Octavia 1.6 MPI	1600	2012	150000	7000	

Table 3. www.autovit.ro

According to: https://www.autovit.ro						
No.	Manufacturer, type, model	Engine capacity [cm ³]	Manufacturing year	Odometer	Required price [euro]	Comments
1	Skoda Octavia 2	1595	2012	122700	6555	+ 202 euro stamp tax
2		1600	2012	145000	6280	
3		1598	2010	119000	5487	

Table 4. lajumate.ro

According to: https://lajumate.ro						
No.	Manufacturer, type, model	Engine capacity [cm ³]	Manufacturing year	Odometer	Required price [euro]	Comments
1	Skoda Octavia 2 1.6 MPI	1600	2011	119000	7100	with GPL system
2		1595	2010	101000	7899	

Table 5. www.bestauto.ro

According to: http://www.bestauto.ro						
No.	Manufacturer, type, model	Engine capacity [cm ³]	Manufacturing year	Odometer	Required price [euro]	Comments
1	Skoda Octavia 2	1595	2011	81000	8250	
2		1400	2011	155.355	7900	
3		1400	2011	169.000	5600	

In order to evaluate the average price required by the sellers, the method of balanced average cost, CMP, is going to be applied, as it follows:

$$\begin{aligned}
 CMP &= \frac{\sum_1^n (\text{required price})_n}{n} \\
 &= \frac{7000 + 6757 + 6482 + 5689 + 7100 + 7899 + 8250 + 7900 + 5600}{9} \quad (12) \\
 &= 6964 \text{ euro}
 \end{aligned}$$

After that, a negotiation decrease coefficient in value of 17% will be applied and the final price will be:

$$PF = 6964 \text{ euro} \times 83\% = 5780 \text{ euro} \quad (13)$$

Justification: when we appreciated the negotiation decrease coefficient, we took into account, as decreasing factors, that the evaluated car was used by a firm and 4168 km/month is a very high value for a car rolling in Romania. It is clear that the vehicle was used intensively. Also, as increasing factors, we took into account that the exploitation working time was short, the maintenance state was good and the general aspect was good, too.

C. The establishment of the real value based on the online market study of sites specialised in vehicles evaluation

Table 6. www.autotrader.co.uk

Accordingly to: http://www.autotrader.co.uk environmental stamp: http://www.4tuning.ro
3350 pounds sterling ≈ 3970 euro + TVA → 4764 euro + 202 euro (stamp tax) = 4966 euro

Table 7. www.eurotax.nl

Accordingly to : http://www.eurotax.nl environmental stamp: http://www.4tuning.ro/
6070 euro + 202 euro (stamp tax) = 6272 euro

Table 8. www.vezicatface.ro

Accordingly to : http://www.vezicatface.ro/
7112 euro

In order to evaluate the average price appreciated by the specialised sites in vehicles evaluation, the method of balanced average cost, CMP, is going to be applied, as it follows:

$$CMP = \frac{\sum_1^n (\text{evaluated cost})_n}{n} = \frac{4966 + 6272 + 7112}{3} = 6117 \text{ euro} \quad (14)$$

CONCLUSIONS

Taking into account the increase of serious traffic accidents, it is very important to elaborate more and more abstract and accurate methods, without possibilities of interpretation, in order to decrease the huge expenses resulted from these types of events.

Unfortunately, the calculi systems used to evaluate the second-hand vehicles or the wrecked bodies resulted from the traffic accidents are not very accurate and they could be very subjective. Accordingly, the establishment of some very accurate calculus methods is absolutely necessary in order not to let the results be at the hand of the investigator's subjectivism.

Using the mass media in order to evaluate vehicles involved in traffic accident is not a very accurate method especially when we have to apply the results on judicial reports. For example, the sites specialised in vehicles commercialization cannot foresee the normal negotiation between sellers and buyers and the algorithm used by the sites specialised in evaluation are unknown to the public.

Otherwise, in case of the wrecked bodies resulted from the traffic accidents, the subjectivism of the evaluators is more significant because, sometimes, the judge's request for evaluations based on the parts which have not been destroyed in the accident. This situation is very difficult for the specialist because the UR laws forbid dismantling the wrecked bodies. Only specialised firms are allowed to do so. The unknown points in this situation are so many that it is almost impossible for the specialist to come up with a clear evaluation.

REFERENCES

- [1] N. Cordoş, I. Rus and N. Burnete, *Automobile. Construcție, uzare, evaluare*, Todesco Publishing House, Cluj-Napoca, 2005;
- [2] R. Gaiginschi, *Reconstrucția și expertiza accidentelor rutiere*, Tehnică Publishing House, București, 2009;
- [3] H. Braess, U. Seiffert, *Handbook of Automotive Engineering*, SAE order no. R-312, ISBN 0-7680-0783-6;
- [4] Ghid de evaluare ANEVAR GEV-620, *Evaluarea bunurilor mobile (mașini, echipamente, instalații și stocuri)*, Standarde de evaluare ANEVAR.

EXPERIMENTAL RESEARCH ON POWDER PROPERTIES RESULTING IN BEARING RECTIFYING

Ion DINESCU

“Henri Coanda” Air Force Academy of Brasov, Brasov, Romania
(dinescuion@yahoo.com)

DOI: 10.19062/2247-3173.2017.19.1.35

Abstract: *This paper presents some results obtained as the consequence of researches in the powder obtained by processing the bearings properties. The studied parameters values are correlated with the values of the same specific parameters of other powders, produced by other methods.*

Keywords: *powder, steel, bearing, rectifying, properties.*

1. INTRODUCTION

The metallic powders and the products which are made from these are useful for a large scale in machine building industry, in aeronautical industry, electrotechnics, chemistry industry and other domains [1,3,4].

The metallic powders are useful either in pure stage (the initial stage) or in mixture of different composition depending on the characteristics of the sintered product.

As a result of processing the bearings, a large quantity of sludge is collected. This sludge obtained by rectifying process contains mostly steel powder. Besides this steel powder, it can be found also small mineral particles of grinding stone.

This paper presents the results obtained as consequence of researches regarding this powder, which have the purpose of establish a procedure for recycling this powder

2. POWDER OBTAINING

The studied powder is obtained by the rectifying process the bearings. The sludge resulted here contains, besides basic powder, impurities like:

- rectifying stone particles – by major rectifying they exist in a proportion of 14-16%, and by fine rectifying they can be found in a proportion of 10-12%;
- binder particles from the rectifying stone;
- oil and water from the stone and object cooling emulsion.

The granules of this powder are plasticity deformed, because the hard particles of the rectifying stone are splintering the object with major distinct angles [2].

The powder is, sometime, rosted on its surface because of the high temperature produced in the moment of splinter detachment from the rectified object.

For the research purpose, the sludge was processed this way:

1. Drying: was made both in laboratory ovens and simply, in atmosphere;
2. Softening baking and/or softening reduction: was made with the purpose of softening the splinter and rejecting the oxides formed at the object surface; there was applied a thermic treatment, with cyclogram presented in figure 1.

All our performed researches have shown us that the controlled atmosphere, high temperature and maintenance time lead to power reduction and softening (initially, the granules had an extreme high hardness: 350...500 HV).

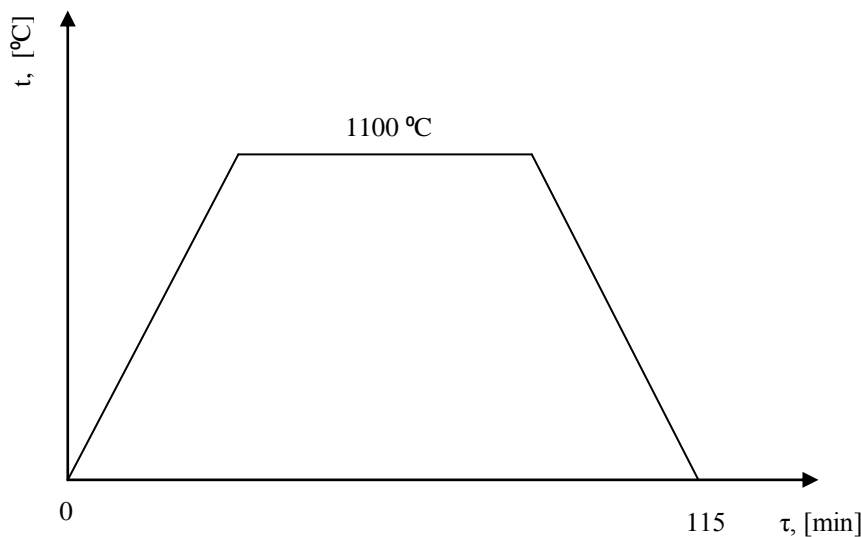


FIG. 1. Thermal treatment's cyclogram

3. Powder enrichment by magnetic separation: by separation can be partially reject the impurities, but still there remain 1...2% of them.

Mention: during the researches it was used both enriched and not enriched powder.

3. CHARACTERIZATION OF POWDER

Taking and preparing the evidences for the determination of the metallic powders properties must be assure a real representation of the lot and this is fulfil in keeping with STAS.

The attempt's results can be more and more better if you take the next aspects into account:

- to decrease to minimum the possibility influence of the possible segregation;
- to avoid the oxidation;
- to avoid the growth of humidity.

If the evidence must be keep with a view determination of their characteristic, the keep must be make in a way what guarantees the initial state of the powders.

The evidences what make the object of this investigations have processed of the powder, result from the processing of bearings. This powder has been washed for the removing of the oils and the other impurities which appear at the cooling of the parts and the tools of the mechanics processing [1,5].

The physics property which made the object of this investigations were:

1. *the granule's form;*
2. *the border structure of the granules;*
3. *the granule's micro hardness;*
4. *the size of the granules and their granulometric repartition.*

1. The granule's form in general is determinate in the process of the manufacture of the powder, but, it can be modificate (improvement) afterwards with different proper treatments. The powders can have spherical granules, ovoide, lamellar, acicular, lensical etc.

The investigate powder was looked at many type of microscope: biological, metallographic, stereoscopic. In all this case it has been used the size 100X. The granules of this powder have an acicular form (in general), but there are lensical and lamellare form too.

Because of the rectifying method, the powder granules haven't the same size and shape; some of the blades are longer, other are bended.

From the quantitative point of view, the granule shape is expressed by using the shape coefficient: *n* (length coefficient) and *m* (breadth coefficient).

For the studied powder the coefficient is medium – sized: $n/m = 0.188/0.055 = 3.4$

2. The border structure of the granules can be dense or porous spongy. For the resultant powder from the process of bearings the border structure is determinate with the metallographic microscope help.

The powder have included in a synthetic resin (plastics) after this, the evidences which have been obtaining have been polished and attacked with a metallographic reagent. At the and of these operations have ascertained that the granules of this powder have a complet structure, but it have been observed too porous spongy granules with traces of oxide.

3. The granule's micro hardness are dependent on the chemical composition of the powder's material and on the proceeding how was made the powder.

The micro hardness have been determined with the metallographic evidence which were used the determination of the boarder structure of the granules.

The investigate powder presents a big micro hardness, understandable with the way for obtain the powder.

For enlarge the duration of the press moulds and the improvement of the powder's property, is recommend a For a longer period of time, the pressure molds and the improvement of the powder's property are recommended a reducing protective atmosphere to reduce the oxide layer.

4. The size of the granules and their granulometricchal repartition present a decisive influence on the technological properties of the powder and on the properties of the products and sintered products.

The granulometricchal repartition of the result of powder from the processing of the bearings, have been determined with the analysis sifting, and using un set of sieves in accordance STAS. For this determination have used two type of powder prepared in different mood (write down 1 and 2).

The results of this analysis of sift are dates in tables number 1 and 2.

Table 1. Granulometric analysis for type 1 powder

The class of granulation, [mm]	The weight of the granulometricchal, [g]	The accumulation crossing, [%]
> 0.595	9.50	100.00
0.595 – 0.297	8.66	90.50
0.297 – 0.149	15.34	81.84
0.149 – 0.125	7.80	66.50
0.125 – 0.088	7.80	58.70
< 0.088	50.90	50.90

Table 2. Granulometric analysis for type 2 powder

The class of granulation, [mm]	The weight of the granulometric, [g]	The accumulation crossing, [%]
> 0.595	7.80	100.00
0.595 – 0.297	7.00	92.20
0.297 – 0.149	13.00	85.20
0.149 – 0.125	5.50	72.20
0.125 – 0.088	7.30	66.70
< 0.088	59.40	59.40

4. CONCLUSIONS

The powder which are have obtained in the mechanical processing of bearings present some important physics properties: the form and the boarder structure of the granules, the powder's fineness and the granulometric repartition.

These properties present an important interest in the utility of this powder for the obtaining of products with the metallurgical technologies of powder.

The utility of this powder is determinate too both way of obtain and the nature (steel of bearings) and the not negligible amount.

This investigations permit the stabilization of some technology for the powder which was obtained in the mechanics processing of the bearings.

REFERENCES

- [1] I. Dinescu, s.a., *Theoretical and Practical Researches concerning New Recycling Technologies for Steel Powder from the Sludge Obtained after Rectifying Bearings Elements*, Second International Conference on THE RECYCLING OF METALS, organized by the European Council of ASM International Europe and its Recycling Division, Amsterdam, Netherlands, 19-21 October 1994, pp. 295-304;
- [2] I. Dinescu, *Researches Regarding the Powder resulted by the processing of Bearings*, Bulletin of the Transilvania University of Brasov, vol. 1 (36) – New Series, Series A, Published by Transilvania University Press, Brasov, Romania, 1994, ISSN 1223-9631, pp. 179-184;
- [3] I. Dinescu, *Tehnologia materialelor, Materiale tehnologice*, Editura Academiei Aviatiei si Apararii antiaeriene "Henri Coanda", Brasov, Romania, 2000, ISBN 973-99808-4-8, p. 256;
- [4] I. Dinescu, M. Smeada, M. Stoicanescu, *Materiale modern utilizate in tehnica militara*, Editura Academiei Fortelor Aeriene "Henri Coanda", Brasov, Romania, 2012, ISBN 978-606-8356-05-1, p. 144;
- [5] M. Smeada, I. Dinescu, M. Stoicanescu, *Materiale metalice si nemetalice utilizate in tehnica militara*, Editura Academiei Fortelor Aeriene "Henri Coanda", Brasov, Romania, 2012, ISBN 978-606-8356-06-8, p. 185.

DYNAMICS OF RECOIL SIMULATION DEVICE POWERED BY CARBON DIOXIDE

Linh DO DUC^{*}, Vladimír HORÁK^{*}, Tomáš LUKÁČ^{*}, Vladimír KULISH^{**}

^{*}University of Defence, Brno, Czech Republic (duclinh.do@gmail.com, vladimir.horak@unob.cz, tomas.lukac@unob.cz)

^{**}School of Mechanical & Aerospace Engineering, Nanyang Technological University, Singapore (mvvkulish@ntu.edu.sg)

DOI: 10.19062/2247-3173.2017.19.1.36

Abstract: *The paper is focused on the dynamics of the recoil simulation device powered by the carbon dioxide (CO₂). The objective is to formulate a mathematical model simulating the cylinder pressurization, and the displacement of the recoil simulation device moving part. The CO₂ is considered as the real gas. The speed of sound in a two-phase saturation is taken into account for the determination of the critical gas flow rate from the CO₂ pressure tank into the cylinder. The problem is solved using the MATLAB environment and results of the theoretical solution are verified experimentally.*

Keywords: *recoil, recoil simulation, gas gun, carbon dioxide, discharge, speed of sound*

1. INTRODUCTION

Employing virtual shooting range has become a solution to increase the safety and effectiveness of shooting and tactical training, at the same time to reduce the cost of training, and the toxic wastes produced by shooting with blank or live ammunition. Recoil simulation becomes an integral part of simulated training weapons used in the virtual shooting ranges.

The recoil simulation devices use the energy of compressed gas from an external source instead of the traditional powder charge to propel the moving part. A positive advantage gained from using CO₂ as a propellant is that a small volume of liquid can convert to a large volume of pressurized gas, thus, the carbon dioxide tanks tend to be smaller and lighter compared to high-pressure air tanks while yielding the same or more shots per fill. Carbon dioxide was the first propellant used in paintball and airsoft technology and due to its low cost, the carbon dioxide has been being widely utilized as a power gas for gas guns and for a recoil simulation.

There is a number of commercial recoil simulation devices on the market, for example [1-3], but there is almost no available literature on dynamics of the recoil simulation device. There are several related publications have been appeared in the last few years documenting the study of phase behavior of carbon dioxide as the power gas for gas guns [4], the simulation of the sound effect of RPG-7 anti-tank grenade launcher for shooting training [5], and the possibility to develop an advanced non-equilibrium model of depressurization in CO₂ two-phase fluids [6].

In this paper, a novel mathematical model simulating the recoil simulation device dynamics is formulated. In order to verify the model, an experimental apparatus is also established.

2. PRINCIPLE OF CO₂ POWERED RECOIL SIMULATION DEVICE OPERATION

Figure 1 shows the basic concept of a CO₂ powered recoil simulation device consisting of a piston, a control valve system, and a return spring. The cylinder is connected with the pressure tank through the control valve system that controls the amount of CO₂ discharged from the pressure tank into the cylinder.

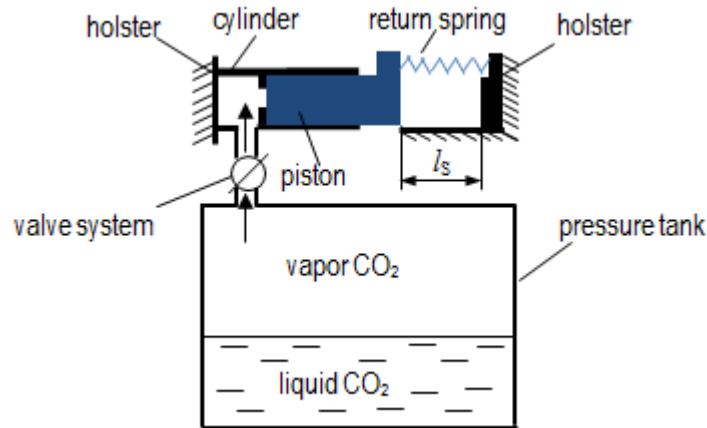


FIG. 1. Schematic of the recoil simulation device powered by CO₂

When the valve is opened by the trigger, a certain amount of CO₂ vapor discharges out of the pressure tank through the valve into the cylinder, in which the pressure increases rapidly, acts on the front of the piston and causes the piston to move backward. At the moment, when the piston reaches its working stroke, it reaches the impact velocity and collides with the device holster on the back position resulting in generating the impact force. After that, the piston returns to the initial position by the return spring force. Then, it collides with the gun holster on the front position and generates the impact force. The resultant force of impact forces and the return spring force is transmitted from the device to the mount and causes the recoil effect.

3. MATHEMATICAL MODEL

3.1. Description and bases of the mathematical model

The above schematic of the CO₂ powered recoil simulation device can be replaced by the thermodynamic system shown in Fig. 2.

Depending upon the initial temperature and pressure within the pressure tank, the CO₂ can exist in the form of single- or two-phase fluid. In the case of single phase CO₂ can exist in the form of vapor if it is superheated, or in liquid form, if the pressure tank is supercharged. In this work, we assume that in the pressure tank CO₂ exists in a liquid-vapor equilibrium, in which the vapor phase occupies the upper part of the tank and the bottom tank portion is occupied by the liquid phase. There exists an interface between the two phases. The change in volume dV/dt is caused by the displacement of the moving part, i.e. the piston.

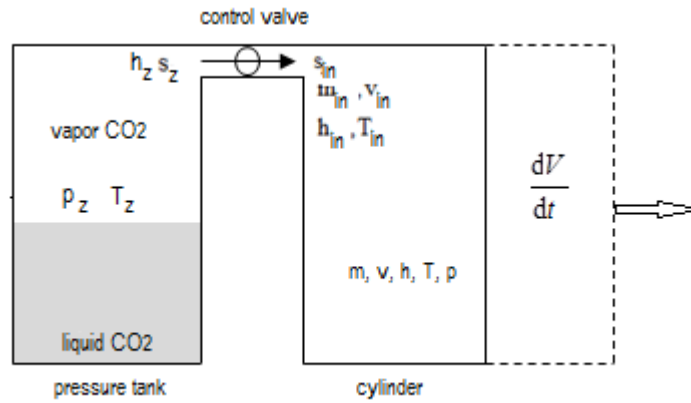


FIG. 2. Open thermodynamic system

3.2. Assumptions

The mathematical model is developed on the basis of the following assumptions:

- Open thermodynamic system.
- Carbon dioxide is considered as a real gas.
- The one-dimensional flow of heterogeneous fluid.
- Two-phase or single phase fluid in the thermal equilibrium.
- In two-phase thermal equilibrium: specific enthalpy, specific volume, density and specific capacities of each phase are functions of temperature or pressure. In the case of single-phase: specific enthalpy and specific capacities are functions of temperature and pressure.
- The isentropic expanding flow of CO₂ through the discharge orifice of the control valve.
- No heat transfer between the fluid within the tank and its walls.
- Control valve opening/closing is immediate, i.e. without any time delay.
- No gas leakage.

The study of the phase behavior of thermodynamic quantities (i.e. pressure, temperature, mass, etc.) within the pressure tank is not the goal of this paper. The comprehensive study of the thermodynamic quantities can be found in [4]. In this paper, we consider the constant values of the thermodynamic quantities inside the pressure tank.

3.3. Equations of the mathematical model

The exchange of mass and energy within the cylinder takes place in the open thermodynamic system. During the unsteady-state processes, when the state quantities of a system vary in time and also the state and the amount of incoming and outgoing fluid can vary in time, the first law of thermodynamics acquires the common differential rate form with respect to a time-lag dt [7]

$$\sum \frac{dH}{dt} = \frac{dU}{dt} + p \frac{dV}{dt}. \quad (1)$$

The change in enthalpy appearing in Eq. (1) is given by the specific enthalpy, h_{in} , and the mass flow rate, \dot{m}_{in} , that are incoming from the pressure tank into the cylinder

$$\sum \frac{dH}{dt} = \dot{m}_{in} h_{in}. \quad (2)$$

The change in the internal energy within the cylinder appearing in Eq. (1) is given by

$$\frac{dU}{dt} = \frac{d(um)}{dt} = m \frac{du}{dt} + u \frac{dm}{dt}, \quad (3)$$

where m and u account for the mass of CO₂ and the specific internal energy within the cylinder, respectively.

There is the only incoming CO₂ mass flow rate \dot{m}_{in} . Thus, the change in mass of CO₂ inside the cylinder is given by

$$\frac{dm}{dt} = \dot{m}_{in}, \quad (4)$$

The change in the specific internal energy in the above equation can be determined using the following formula [7]:

$$\frac{du}{dt} = c_v \frac{dT}{dt} - \left[T \left(\frac{\partial p}{\partial T} \right)_v - p \right] \frac{dv}{dt}. \quad (5)$$

The specific heat capacity at constant volume c_v for gaseous CO₂ appearing in the above equation is given by the difference of the specific heat capacity at constant pressure c_p and the specific gas constant r . The values of c_p are available in [8].

The thermodynamic quantities in the output of the valve depend on the pressure p in the cylinder. We consider the phenomena occurring at the beginning of the process, as the first amount of gaseous phase flows into the cylinder. Assuming that the initial pressure p equals to the pressure of the surrounding environment, thus, the mixture appearing at the output of the valve includes dry ice in the form of small solid particles and vapor of CO₂. At the valve output, the mixture temperature T^* is a function of the cylinder pressure p and it is interpolated from the saturation curves. After entering to the cylinder, this two-phase fluid expands to whole cylinder volume, where its equilibrium state is broken due to the change in temperature T within the cylinder. The initial temperature T is assumed to be the surrounding temperature. It causes that the most of the dry ice particles sublimate. Hence, the mixture in the cylinder is in metastable state until the temperature and pressure conditions of the two-phase mixture are met. Therefore, the presence of residual dry ice particles within the cylinder can be neglected. Then, it is possible to describe the thermodynamic state of the gas inside the cylinder by using the van der Waals equation of state [7] that can be written in form

$$p = \frac{rT}{v-b} - \frac{a}{v^2}, \quad (6)$$

where r is the CO₂ specific gas constant, constant a provides a correction for the intermolecular forces and the constant b represents a correction for finite molecular size. The values of constants a , b may be obtained by the theorem of corresponding states [7] using the CO₂ critical point conditions.

From Eq. (6), we obtain the partial derivative appearing in Eq. (5) as

$$\left(\frac{\partial p}{\partial T} \right)_v = \frac{r}{v-b}. \quad (7)$$

The time change in the specific volume appearing in Eq. (5) is given as

$$\frac{dv}{dt} = \frac{1}{m} \frac{dV}{dt} - \frac{V}{m^2} \frac{dm}{dt}, \quad (8)$$

where V is the total volume of the cylinder and its change in time is given by the chamber cross-sectional area A_p and the velocity v_p of the moving part as bellow

$$\frac{dV}{dt} = -v_p A_p \quad (9)$$

Introducing Eq. (7) and Eq. (8) into Eq. (5) yields

$$\frac{du}{dt} = c_v \frac{dT}{dt} - \frac{1}{m} \left(\frac{a}{v^2} \frac{dV}{dt} + \frac{a}{v} \frac{dm}{dt} \right). \quad (10)$$

The internal energy of the cylinder is given by

$$u = h - pv. \quad (11)$$

The specific enthalpy h is a function of pressure p and temperature T within the cylinder:

$$h = h(p, T). \quad (12)$$

By introducing Eq. (4), Eq.(10) and Eq. (11) into Eq. (3), then introducing Eq. (2) and Eq. (3) into Eq. (1), and by rearranging we obtain the time change in temperature within the cylinder in form

$$\frac{dT}{dt} = \frac{1}{mc_v} \left[\dot{m}_{in} \left(h_{in} - h - \frac{a}{v} + pv \right) + \left(\frac{a}{v^2} - p \right) A_p v_p \right]. \quad (13)$$

At the control valve output, carbon dioxide exists in the two-phase mixture in solid – vapor or liquid – vapor equilibrium. The specific volume v_{in} , specific enthalpy h_{in} , specific entropy s_{in} and the density ρ_{in} of the two-phase mixture at the valve output are determined as

$$v_{in} = \gamma v_{in}'' + (1 - \gamma) v_{in}', \quad (14)$$

$$h_{in} = \gamma h_{in}'' + (1 - \gamma) h_{in}', \quad (15)$$

$$s_{in} = \gamma s_{in}'' + (1 - \gamma) s_{in}', \quad (16)$$

$$\rho_{in} = \gamma \rho_{in}'' + (1 - \gamma) \rho_{in}', \quad (17)$$

where $v_{in}' = v_{in}'(p)$, $v_{in}'' = v_{in}''(p)$, $h_{in}' = h_{in}'(p)$, $h_{in}'' = h_{in}''(p)$, $s_{in}' = s_{in}'(p)$, $\rho_{in}'' = \rho_{in}''(p)$,

$\rho_{in}' = \rho_{in}'(p)$ are functions of the cylinder pressure p .

The γ is the quality of the outgoing two-phase fluid that can be calculated by assuming that CO₂ expands from the pressure tank through the valve orifice to the cylinder isentropically. This assumption means that $s_z = s_{in}$, where s_z represents the specific enthalpy of CO₂ in front of the control valve input opening (Fig. 2).

By introducing $s_z = s_{in}$ into Eq. (16) and by rearranging yields

$$\gamma = \frac{s_z - s_{in}'}{s_{in}'' - s_{in}'}, \quad (18)$$

The mass flow rate \dot{m}_{in} from the pressure tank through the control valve of the cross-sectional area A_o into the cylinder is given by

$$\dot{m}_{in} = \mu A_o \frac{w_{in}}{v_{in}}, \quad (19)$$

where μ is the discharge coefficient, it is usually assumed that the discharge coefficient is between 0.45-0.61. w_{in} (m/s) is the discharge flow velocity that can be defined as

$$w_{in} = \min \left\{ \sqrt{2(h_z - h_{in})}, a_{sonic} \right\}, \quad (20)$$

where h_z is the specific enthalpy of CO₂ in front of the control valve input opening (see Fig. 2) and a_{sonic} (m/s) is the speed of sound in the CO₂ two-phase fluid that is defined by the fluid $p-v-T$ behavior using the following formula [4]

$$a_{\text{sonic}} = \left[\rho_2 \left(\frac{\Theta_{12}}{\rho_{12}'' a_G^2} + \frac{1 - \Theta_{12}}{\rho_{12}' a_{\text{SL}}^2} \right) \right]^{\left(-\frac{1}{2}\right)} \quad (21)$$

Here: $\Theta_{\text{in}} = \gamma v_{\text{in}}'' / v_{\text{in}}$ accounts for the void fraction, a_G is the speed of sound in the gaseous phase and a_{SL} denotes the speed of sound in solid or liquid phase. Values of speeds of sound a_G and a_{SL} for CO₂ are also functions of pressure p .

We apply the Newton's Second Law of motion for the piston backward and forward. There are three forces acting on the piston during its moving backward: the return spring force F_{sp} , pressure force F_p and the friction force F_f .

The return spring force is generally given by the return spring constant c and the working stroke that is equal to the piston displacement x_p . It is necessary to take also the return spring preload into consideration. In this case, the return spring is initially compressed. Hence, we can express the spring force in the form

$$F_{\text{sp}} = F_{\text{ini}} + cx_p, \quad (22)$$

where the force F_{ini} is the initial compression spring force corresponding the initial spring compression, which is determined by the summation of the working and spring preload.

The pressure force F_p is given by the difference of the compression cylinder pressure and the atmospheric pressure behind the piston:

$$F_p = A_p (p - p_a). \quad (23)$$

The friction force F_f between the compression chamber internal surfaces and the contact surface of the piston seal A_f can be determined as

$$F_f = A_f f (p - p_a), \quad (24)$$

where f is the piston friction coefficient. Its value depends upon both the material, the thickness of the piston sealing and quality of the compression chamber internal surface.

The equation of motion of the piston while moving backward is

$$\left(m_p + \frac{1}{3} m_{\text{sp}} \right) \frac{dv_p}{dt} = F_p - F_{\text{sp}} - F_f, \quad (25)$$

where m_p and m_{sp} represent the piston and return spring mass, respectively.

There only two forces acting on the piston while moving forward: the return spring force and the friction force.

$$\left(m_p + \frac{1}{3} m_{\text{sp}} \right) \frac{dv_p}{dt} = -F_{\text{sp}} - F_f, \quad (26)$$

4. RESULTS OF SOLUTION

The mathematical model describing the piston dynamics includes five variables, i.e. the cylinder temperature T given by Eq.(13) , the pressure p given by Eq. (6), the total CO₂ mass m given by Eq.(4), then specific volume v given by Eq.(8) and the piston velocity is given by Eq. (25) and Eq. (26).The above-described problem was solved by numerical integration with MATLAB using the explicit fourth-order Runge-Kutta method.

Mathematical model considers a range of input data parameters and boundary conditions (i.e. the initial cylinder volume, the initial temperature, the pressure tank's specific enthalpy and entropy of CO₂, the mass of the piston, the return spring constant, the discharge coefficient, etc.). In order to present results of the solution, we selected the input data parameters and boundary conditions shown in Tab. 1 that correspond to the design parameters of the breechblock of AKM gas-operated automatic rifle [9]. Results of the solution of the developed mathematical model for this given example are presented in Fig. 3 and Fig. 4.

Table 1. Initial data parameters and boundary conditions

Quantity	Value	Quantity	Value
Initial cylinder volume (ml)	1.5	Return spring constant (N/m)	290
Cylinder diameter (mm)	30	Return spring mass (kg)	0.026
Piston mass (kg)	0.55	Control valve diameter (mm)	4
Piston working stroke (mm)	118	Initial cylinder temperature (K)	288
Discharge coefficient	0.7		

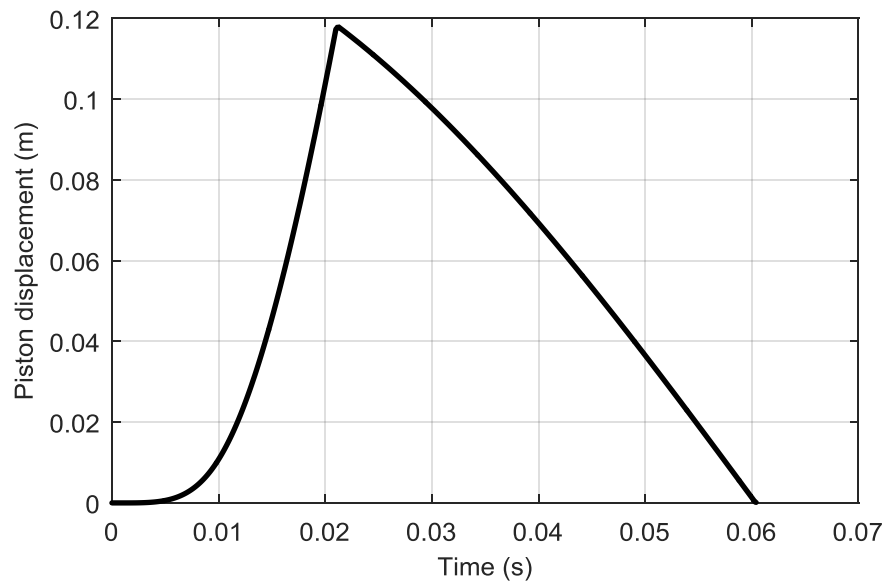


FIG. 3. Piston displacement vs. time

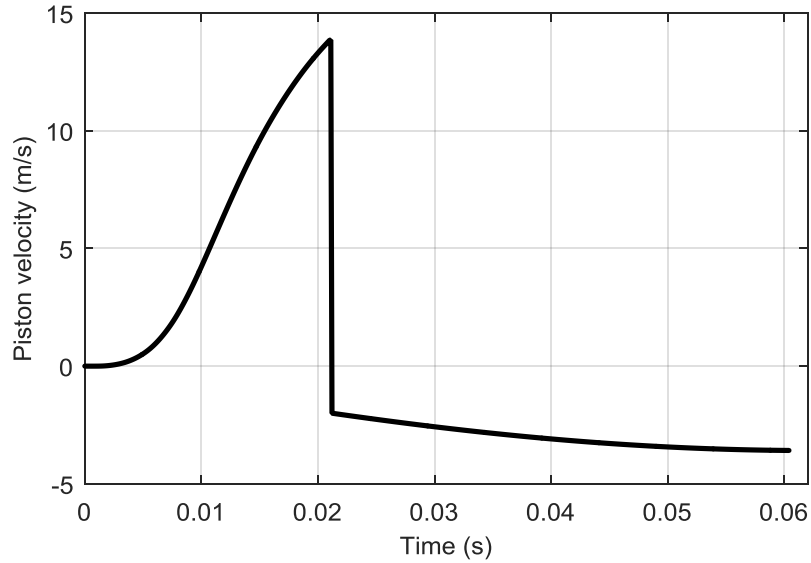


FIG. 4. Piston velocity vs. time

The dynamics of the recoil simulation device is clearly shown in Fig. 3. In the first phase of operation, the piston is accelerated backward by the pressure force. When the piston reaches its working stroke, it reaches the impact velocity $v_{\text{imp/b}} = 13.85$ m/s. After the collision with the device holster, it starts moving forward by the return spring force. The impact velocity on the front position is $v_{\text{imp/f}} = 3.58$ m/s (Fig. 4). The time course of the cylinder pressure in the first phase of operation is shown in Fig. 5. It can be seen that the maximum value of the pressure is 1.3 MPa.

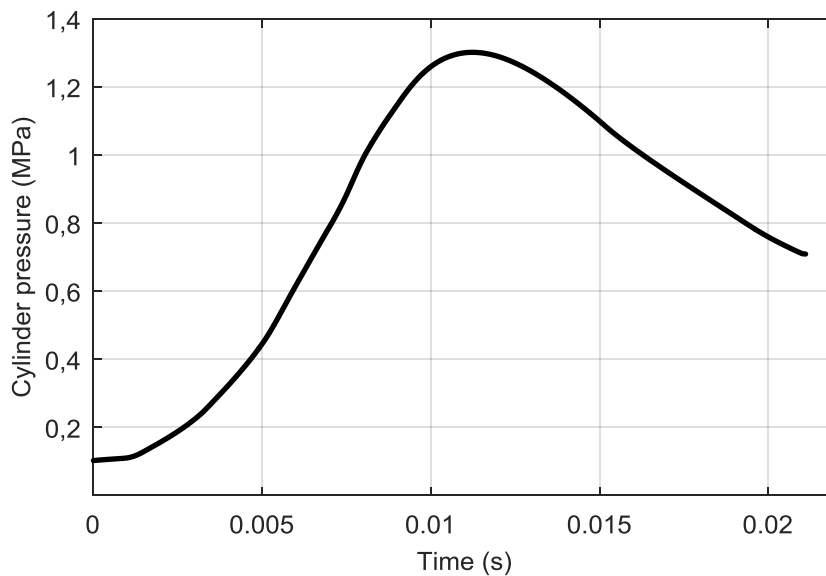


FIG. 5. Time change in cylinder pressure

5. VERIFICATION OF THE MATHEMATICAL MODEL

Results of solution of the piston impact velocity in the back position are compared with the measured values. The view of the experimental device is shown in Fig. 5.

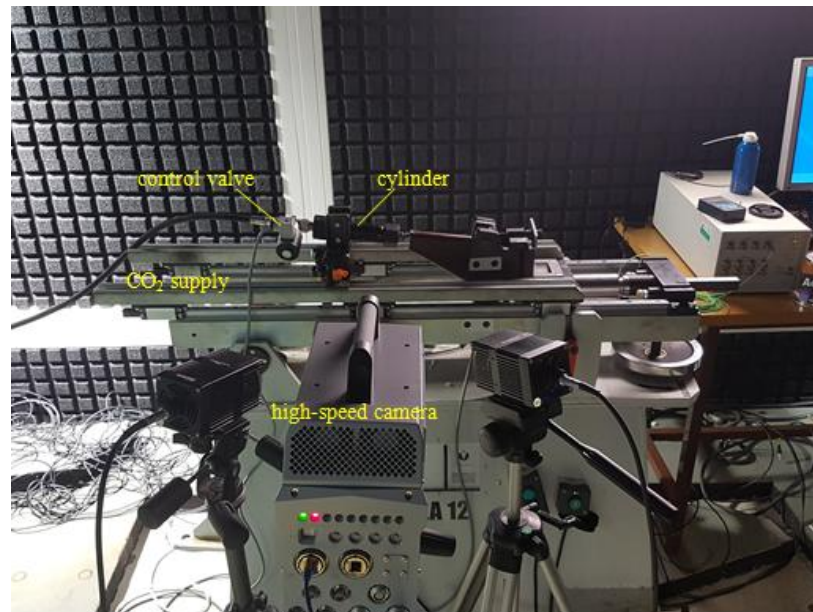


FIG. 6. View of experimental device

Here we use two types of the piston of different masses (0.309 kg and 0.240 kg). The constant of return spring is 550 N/m, the cylinder diameter is 30 mm, and the piston working stroke is 67.5 mm. A high-speed camera is used in order to measure the piston displacement. Taking differential of the measured piston displacement with respect to time yields the piston velocity. The comparison of calculated and experimentally obtained values of the piston impact velocity in the back position is shown in Tab. 2, from that we can conclude a quite good agreement between the results of the mathematical model and experimentally obtained values.

Table 2. Piston impact velocity in the back position comparison

Piston mass (kg)	Piston impact velocity in the back position (m/s)		Difference (%)
	Experiment	Model	
0.309	8.10	8.56	5.67
0.240	9.16	9.64	5.24

CONCLUSIONS

In this paper, the mathematical model for the study of the dynamics of the recoil simulation device has been formulated. The problem has been solved numerically using the Runge-Kutta method in MATLAB environment. The mathematical model is verified by the measurement of the piston impact velocity using the high-speed camera. The model provides good agreement with measured data. Obtained results enable us to analyze various influences of changes in several design parameters.

As the future improvement of the experimental device, the range of piston mass will be wider and the flow area size of the control valve can be changed.

ACKNOWLEDGMENT

The work presented in this paper has been supported by the institutional funding DZRO K 201 "VÝZBROJ" and by the specific research project of Faculty of the Military Technology SV16-216.

REFERENCES

- [1] Dvorak Product listing and descriptions, TRS Firearms training systems. Available from http://www.stressvest.com/pdfs/dvorak_tetherless.pdf [online, retrieved 24/4/2016].
- [2] VirTra, Standard recoil kits – Weapons Simulator. Available from: <http://www.virtra.com/tethered-recoil-kits/> [online, retrieved 24/4/2016].
- [3] Recoil simulation equipment. Available from: <http://eli.ee/products/1/recoil-simulation-equipment.html> [online, retrieved 24/4/2016].
- [4] L. Do Duc, V. Horák, T. Lukáč, Q. H. Mai, *Study of Phase Behavior of Carbon Dioxide as the Power Gas for Gas Guns*. In KRIVANEK, V. (ed.) *International Conference on Military Technologies, Proceedings ICMT'15*, Brno: University of Defence, p. 29-36, 2015;
- [5] Q.H. Mai, V. Horák, L. Do Duc, Sound Effect of RPG-7 Antitank Grenade Launcher for Shooting Training, *Advances in Military Technology*, vol. 9, no. 2, p. 49-60. 2014;
- [6] L. DO DUC, V. HORÁK; V. KULISH, T. LUKÁČ. *On the possibility to develop an advanced non-equilibrium model of depressurisation in two-phase fluids*. In: *11th International Conference on Mathematical Problems in Engineering, Aerospace and Sciences, ICNPAA 2016*. La Rochelle: American Institute of Physics Inc., 2017, p. 1-5.
- [7] V. Horák and V. V. Kulish, „Thermodynamics“, Brno, University of Defence, 2011, 102 p.
- [8] L. Do Duc, *Software for thermodynamic and design calculation of gas guns*, Thesis, University of Defence, 2015.
- [9] T. S. Ngo, *Design analysis and comparison of gas operated automatic rifles Sa-58 and AKM*, Thesis, University of Defence, 2011.

THE MAGNETIC PROPERTIES OF MATERIALS AND NEW MILITARY APPLICATIONS OF THEM

Daniela Georgiana GOLEA*, Lucian Ștefan COZMA**

*"Mihai Viteazul" National Academy of Intelligence, Bucharest, Romania
(kolerdaniela@yahoo.com)

** Faculty of Physics, University of Bucharest, Romania (lucian.stefan@yahoo.fr)

DOI: 10.19062/2247-3173.2017.19.1.37

Abstract: *The technological development of the last decades has brought to light more and more important possibilities for improving the technologies applied in aviation. Among other things, the low-speed aircrafts can be in the near future equipped with electric engines of a totally new type. But for this, we must first establish theoretically how the direct conversion of the magnetic energy can be done and also, we have to study the properties of the magnetic materials and how they can be used in the design of a new type of a prime mover. Aviation should be one of the first areas that would benefit from the results of this research and development activity.*

Keywords: *magnetic energy, prime movers, electric engine.*

INTRODUCTION

The idea and the desire to build vehicles (including aircrafts) driven by electric (or magnetic) engine is very old. But the multitude of problems that have arisen has prevented and still hindered the large-scale development of such (electric) vehicles and if they are still realized, they have extremely high price, often inaccessible so that we do not discuss these cases. We will therefore see if there are technological solutions that can overcome this deadlock.

1. THE MAGNETIC AND THE ELECTRIC ENERGY

While it is inappropriate to review the definition of electric energy, which is widely known and used at present, we will still focus our attention on the magnetic energy, much less known and rarely directly applied: *the magnetic energy is a physical size that shows the capacity of a physically system corresponding to the magnetic circuits to store the energy consumed by the mechanical work of an electric current, but also the ability to perform a mechanical work at the transition from the given state to the reference state, its value depending only on the magnetic field strength and the permeability of the environment, i.e. the magnetic properties of the matter; also representing a potential function with the function of state function for the physical system corresponding to the magnetic circuit.*

By such a definition, we try to make a preamble of presenting the practical aspects of the use of magnetic energy in the case of prime movers, which are also applicable to motor-powered terrestrial vehicles and aircrafts.

Naturally, there are physical and mathematical instruments of calculating the magnetic energy whose determination as a self-standing notion has been mentioned before, urging physicists and engineers to pay more attention to the study and the theoretical determination of all aspects regarding this form of energy. A form of energy that, although recognized by the scientific world, is insufficiently studied and most often treated very superficially in the works of art, which at best barely consecrates a few rows.

As we can see from the bibliography research in this area, often, there are not clear and complete definitions about the magnetic energy, considering that the magnetic energy would be a sort of accessory to electricity. Nothing more fake! In spite of the indisputable complementarity of electricity and magnetism, as well as the fact that without electricity the magnetism phenomenon could not exist, the magnetic energy is, however, a separate concept, directly and strongly related to the magnetic properties of the material, but also to its size and configuration, because the magnetic material acts as *an energy storage environment*, the value of which depends on the dimensions of that "reservoir".

In the case of a bobbin, the calculation of the magnetic energy that is lost when the supply to the circuit is interrupted is done when the circuit is closed or when the source is disconnected. In order to obtain a current increase, it is necessary that the electromotive force of the source be operated in accordance with Lenz's law, ie against the self-inductive automotive voltage, because during the current increases, the electromotive voltage of the source performs a mechanical work against the self-induction and so, we can consider that the time interval due to the increase of the current through the circuit will pass an amount of electricity equal to:

$$dQ = Idt \tag{1}$$

where dt is the aforementioned time interval, and the mechanical work against the electromotive voltage of self induction is given by the expression

$$dA = -E_{ind} Idt \tag{2}$$

knowing that

$$E_{ind} = -\frac{d\Phi}{dt} \tag{3}$$

and obtaining

$$dA = I \frac{d\Phi}{dt} dt = Id\Phi \tag{4}$$

where we have the transformation into the magnetic energy of the energy from the source, the increase of energy being

$$dW = Id\Phi \tag{5}$$

for which, considering the Biot-Savart-Laplace Law, we have an induction that depends on the current in a linear fashion, and how-

$$\Phi = BS = LI \tag{6}$$

then it follows that,

$$dW = ILdI \quad (7)$$

but in order to obtain the total value of magnetic energy, we have to sum up practically all the elementary mechanical works transformed into magnetic energy, which we can do by integrating-

$$W_{mag} = \int_0^I ILdt = L \int_0^I Idt \quad (8)$$

Therefore

$$W_{mag} = \frac{1}{2} LI^2 \quad (9)$$

Thus, we see that similarly to the electric field, the magnetic field is accompanied by an energy. As mentioned above, a mechanical work must be consumed for the production of this field, which, in practice, in the case of electromagnets (as used by the magnetic engine shown in the present paper), it is carried out by the current i that induces into the excitation coil windings a voltage u . It has been assumed for the above relationships that L inductance and magnetic permeability μ are constant throughout the process described. This gives us the validity of relationships especially for the massive magnetic cores and for air.

Considering, however, that-

$$L = \frac{n^2 \mu_0 \mu_r S}{l} \quad (10)$$

where S is the field surface of section, l is the length of proceeding lines of force (in the air gap), n the number of windings and

$$I = \frac{Hl}{n} \quad (11)$$

therefore obtaining another way to write the expression (9) namely

$$W_{mag} = \frac{1}{2} H^2 \mu_0 \mu_r l S [Joule]_{SI} \quad (13)$$

also for μ with constant value, and from the above expression it can easily be observed that virtually the magnetic energy is contained in the volume

$$V = l \cdot S \quad (14)$$

and from all the above, we can conclude *that the magnetic energy carrier is the magnetic field*, since in the volume V in which the field operates, there is magnetic material, its value μ_r can no longer be considered as constant, since it starts from the initial expression

$$dW = nid\Phi \quad (15)$$

above mentioned, which becomes

$$dW = HlSdB \quad (16)$$

where it ultimately results

$$W = V \int HdB \quad (17)$$

an integral that can not be calculated exactly because the intensity H is not an analytical function of the induction B but is related to it by the magnetization curve given by the hysteresis cycle. However, the intensity may be conveniently graphically determined. For example, the mechanical work required to pass the hysteresis loop can only be performed if this loop is considered to be cut into very narrow (infinitesimal) horizontal "slices" of the height dB and the width H . In this way, the above integral will represent the surface area of the hysteresis cycle, and in this case it is sufficient to measure this area in order to obtain the value of the mechanical work on the unit of volume of the magnetic core.

In applications, however, we are interested in how this magnetic energy can be converted into kinetic energy so that the (electro)magnet used can exert on a certain technical component, a force of the highest value. From this perspective, we draw particular attention to the relatively high value of the force that a (electro)magnet can develop, with low energy consume, compared to the rather poor performance of electric cars, plus the high costs and technological complications, as well as relatively high electricity consumption.

We will see the force of a classical electromagnet, and then we will try to move to the case of the electromagnet with rotating armature to get closer to the magnetic machine model to which the present work actually refers.

We assume that in front of the poles of an electromagnet there is an iron armature which is attracted to an F force, but the volume $V = l \cdot S$ of the air gap, which contains a part of the total magnetic field, holds in it the magnetic energy given by the relationship-

$$W_{mag} = \frac{H^2 \mu_0 l S}{2} \quad (18)$$

in the air gap we consider that $\mu_r = 1$, but knowing that $\mu_0 H = B$, we will have

$$W_{mag} = \frac{B l S}{2 \mu_0} \quad (19)$$

and after applying the armature on the electromagnet poles, this part of the magnetic field and the corresponding energy cease to exist. Instead, it will be performed a mechanical work equivalent to $W = Fl$. As 1 Joule = Newton meter, we have

$$F = \frac{B^2 S}{2\mu_0} \text{ [Newton]}_{SI} \quad (20)$$

or

$$F = \frac{B^2 \cdot 10^{-8} \cdot S \cdot 10^{-4}}{2 \cdot 1,256 \cdot 10^{-6} \cdot 9,80665} \cong \left(\frac{B}{5000} \right)^2 S [\text{Kgf}]_{MKS} \quad (21)$$

From the above relationships, we can easily see that an electromagnet can easily develop important forces with relatively low energy consumption. For example, we will take an electromagnet from ferromagnetic material, cut into U-shape, for which we will consider the two polar surfaces of 5 cm^2 , knowing its magnetization curve; if it is excited by 1000 amper-turns, for a total length of 0,5 m of force lines, we find that the electromagnet will develop a bearing force:

-for the field intensity of $H = \frac{1000 \text{ Amperi}}{0,5 \text{ metri}} = 2000 \frac{A}{m}$;

-according the magnetization curve (appling thea graphic method) we will have a induction of about 15000 Gs;

-and having two pole faces, $S = 10 \text{ cm}^2$ aşadar $F = \left(\frac{15000 \text{Gs}}{5000} \right) \cdot 10 \text{cm}^2 = 30 \text{Kgf}$.

From this small example, you can see how a small device with a very simple structure is able to develop important forces. However, it is a matter of adapting the classic magnetic circuits so that they can develop a continuous force on a rotating mobile element.

Practically, the example below is with 3 pairs of annular electromagnets which form a group of forces in which the electrical energy is first transformed into magnetic energy in order to subsequently convert the desired magnetic energy into kinetic energy .

2. THE MAGNETIC PRIME MOVER - A POSSIBLE SOLUTION IN LIGHT AVIATION

There is the possibility of building prime movers based on the transformation of magnetic energy into mechanical energy, with low energy consumption. These prime movers would operate in more advantageous regimes than any of the currently known electric engines. On this occasion, the authors also proposed a series of reconsiderations in the terminology used in physics and electrotechnics, pointing to the misuse or inappropriate use of sme terms. A comparative presentation between the electric/ *the magnetic motor*:

- the electric engine requires large-scale polar parts, which are very heavy; *a well-designed electromagnet must not be large in size to develop a considerable bearing force*;
- the electric engine often requires massive windings, which lead to increased weight and higher the overall costs; *a correctly designed electromagnet will match the number of turns to the current value by choosing the optimum values for the maximum bearing force*;

- in the electric engine, the magnetic field lines do not close tightly in the yokes, most often only partly within the yokes and permanently subjected to the "stretching" and "breaking" phenomena of the field lines caused by the movement of the armature in which the lines of the field should close; *the magnetic engine shows the correct way of closing the field lines;*

-in the electric engine, in order to drive the rotor it is induced by a current, this phenomenon being accompanied by large losses due to the Joule-Lenz effect and the Foucault currents, as well as due to imperfections related to the configuration of the engine parts; *the correct interaction must be the only the direct interaction between the (electro)magnets, whether it be between the opposing sign poles or the same sign; therefore, no inductor, no induced;*

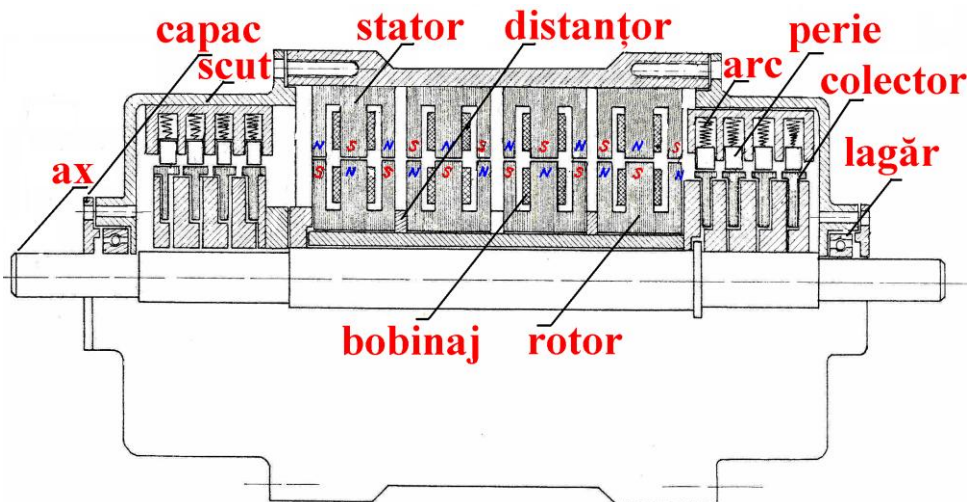


FIG.1 Magnetic prime mover with brushes.

- the electric engine, once the induction is made, induces the phenomenon of self-induction, which leads to other losses, and as soon as the magnetic flux registers variations and the parts move, there is the phenomenon of hysteresis and the action of the counter-electromagnetic forces caused in large part by the application of the Law of Lenz; *an appropriate design of a pair of electromagnets placed on the stator and rotor using a fixed magnetic field configuration interacts through the force lines without inducing induction phenomena in the magnetic core or the occurrence of phenomena occurring in the power electrical machine;*

-in the case of an electric engine, the actual drive of the mobile component (the rotor) is mainly due to the Lenz force which, due to the circuit losses, is much weaker than the direct magnetic interaction; *a magnet engine, takes over the magnet interaction model and adapts it to a magnetic circuit of ring or circular configuration;*

-in the electric engines, for the continuous drive of the rotor, the electrical machines require complex switching, which raises technological problems, including cost problems, not removed in latest years by the various improvements; *a pair of annular electromagnets can perform sequential polarity changes by means of a rudimentary switching apparatus;*

-there is known that the electric machines have great technological problems when they have to vary the speed and the power regime; requiring sometimes the existence of saturation regimes and the application of high frequencies in the feed circuit; *a magnetic motor, does not require any of this, ranging in high speed (from 500 to 15,000 rpm) but keeping the power supply parameters unchanged, and still in direct current;*

-the known electric machines require high energy consume because they do not judiciously use the magnetic properties of the ferromagnetic material; emphasizing the quantity, not the quality and making waste of magnetic core and copper winding; a magnetic engine for the same developed power has much smaller dimensions and much smaller quantities of Fe-Si material and copper;

-the electric power engines use electricity to convert it into mechanical energy or vice versa; this process is indirect (except in the case of electrostatic engines or other types of engines which use the electric fields) and is accompanied by large losses, so that, a poor yield; a magnetic engine will directly convert the magnetic energy into mechanical energy at a better efficiency.

So we can identify the differences between the electric and magnetic engine:

-in terms of applied phenomena (***operating principle***), the electric motor uses the magnetic induction between (at least) an inductor and (at least) an induced and therefore, the electromagnetic interaction established as a result of the application of the self induction phenomena, the appearance of the Lenz Force and Laplace Force, amid the general phenomena of hysteresis and the action of the Foucault currents, while *the magnetic motor uses the simple interaction between magnetic fields formed around (electro) magnets;*

-from the point of view of ***the magnetic field configuration***, in the electric engine the field lines suffer a series of alterations due to the imperfection of the magnetic circuit which fails to close well the field lines, breaking them both because of the defective configuration and especially because of the use of the rotary magnetic field, while the magnetic motor does not have any rotary magnetic field but a fixed configuration of the magnetic field as tightly closed and interacting only at the level of the air gap, eliminating the induction phenomena within the magnetic cores;

-regarding ***the configuration of the pole pieces***, the electric engine has a wide variety of possible geometries, at which the poles are visible, shielded, drowned, etc., characterized by a wide variety of magnetic spectra they can create; in the magnetic motor for driving a rotor, the polar parts are annular, with small semicircular (not radial!) excitation coils;

- in terms of ***structure and composition***, the electric engine must be formed at least by a stator and a rotor, one of which has the inductor function, the other one to be induced; besides these, there are also the auxiliary components necessary to assemble the main components or to ensure their operation; whereas the magnetic motor is only compulsorily made of pairs of annular (electro)magnets, which can either be divided into the stator and the rotor, or both of them as stator components, but separated by an air gap in which a non-winding rotor is disposed;

-according ***the principle applied to the drive***, the electric motor is generally based on the Lenz Force; while the magnetic motor applies the interaction between magnetic fields of the opposite sign or the same sign, that can be exerted directly between (electro)magnets or on a reactive discoidal Fe-Si element, placed in the air gap between the electromagnets provided with sequential polarity change.

On the basis of the above, one of the authors has already proposed the adoption of the term „*the magnetic field motor in a polar alternating stationary field*”, being a technical system using the magnetic energy the carrier of which is the magnetic field, by which magnetic attraction forces are applied and simultaneous and synchronous with repulsion forces within the circumference of a circular mobile device. The magnetic prime mover is a modular system, consisting of pairs arranged and running on the same shaft. Each stator-rotor pair can operate independently and has its own sequential switch-gear. Each pair is separate from the others in mechanical and electrical terms. It is the situation that when a pair fails, the others continue to work.

CONCLUSIONS

Following the analysis of the possibilities of direct use of magnetic energy in power machinery, the following conclusions were drawn:

-although the electromagnet is defined as a temporary magnet intended to transform the electric energy into mechanical energy through the magnetic energy, we can state that under certain conditions (magnetic interactions only between magnetic fields) the electromagnet allows ***the direct transformation of magnetic energy into mechanical energy***;

-the magnetic materials (with good magnetic permeability) also allow ***the storage of energy*** but also its amplification due to the magnetic qualities of the material used; that is why the magnetic induction of a given current becomes much higher when it is exerted on an environment with good magnetic properties; this gives rise to the possibility for prime movers to develop big forces;

-given the ability of the magnetic material to store the electric energy at high values and within a relatively small volume, its ability to transfer energy in the form of mechanical energy results in higher efficiency values than the transfer of electric energy to mechanical energy (made in the "electrostatic" motors or the engines which apply the Laplace or Lenz forces - as is the case of the most current electric motors);

-the above mentioned facts require the introduction of a clear distinction in typologies, between the electric prime movers and the magnetic prime movers, just as the magnetic energy is separately defined and introduced in the known typology; the energy forms (mechanical, thermal, nuclear, electric, chemical, magnetic) correspond each to a specific prime mover, therefore the magnetic energy must correspond to the magnetic prime mover; so that, the electromagnet is not a simple intermediate in the transformation between electrical and mechanical energy, because by the intervention of its magnetic properties and corresponding its dimensions (volume, the area of the section traversed by the magnetic force lines, etc.) it has the ability to amplify a received energy; regarding these aspects, we consider that the real energy transfer is actually applied between the magnetic and the mechanical energy, so it is necessary to introduce in the typology the concept of *the magnetic prime mover*;

-regarding the applications in the field of engines, it is appropriate to abandon the inductor-induced pair and generally, the principle of induction; we also consider erroneous to apply at the engines the Force of Lenz, because it (along with the phenomenon of induction) gives rise to negative effects such as the occurrence of counter-electromotive forces, the Foucault currents etc .;

-it is also appropriate to use the direct magnetic interaction between the force lines of two concentric annular (electro)magnets each having only two notches, they have semi-circular polar parts forming circular arcs describing angles of 165° ;

-the annular configuration of (electromagnets) and the existence of each of them only two notches (correspondingly only two polar pieces, one on each half-circumference) makes the area of the active section of the pole pieces the maximum (describing in total an angle of 330° of the total 360° of the circle) and the magnetic flux is therefore very high; at the same time, the magnitude of the magnetic interaction is greatest, being achieved at almost the entire circumference of the circle;

-an optimal magnetic circuit, is the one that closes the field lines very well and does not allow the interference of parasitic fields or the occurrence of magnetic spectrum distortions, as is the case of the rotary magnetic field and generally the case of today induction motors.

Therefore, the optimal magnetic circuit is that which uses a stable (immobile) magnetic spectrum, well-closed in the configuration of the pole and yoke. According to the above, it results the possibility of creating prime movers with performances beyond all the known and applied prime movers.

REFERENCES

- [1] US381968- (Nikola Tesla) Motor electromagnetic;
- [2] FR1502811- (J. Jarret) Motor cu reluctanță variabilă;
- [3] US4154200- (J. Jarret) Motor cu pistoane libere;
- [4] US4260926- (J. Jarret) Motor reluctant cu poli progresiv saturați;
- [5] FR2314614- (J. Jarret) Alternator cu excitație în impulsuri;
- [6] FR2109144- (J. Jarret) Motor cu reluctanță variabilă;
- [7] RO87074- (Dan Teodorescu) Cuplaj electromagnetic de inducție reglabil, cu rotor disc și câmp magnetic axial;
- [8] FR1503668- (Dan Teodorescu) Motor de inducție cu turație înaltă, alimentat la frecvența de rețea;
- [9] US3191077- (A.M. Marks) Sistem de conversie a energiei;
- [10] GB640889- (Charles George Smith) Perfecționări la sursele electrochimice secundare;
- [11] FR551882- (Jules Guillot) Aparat de captare a curenților electrici din atmosferă;
- [12] US2021177- (A. di Angelo) Motor-generator;
- [13] US2876368- (A. Thomas) Baterie nucleară (betavoltaică) cu electreți;
- [14] US3510730- (Dan Teodorescu) Servomecanism electromagnetic;
- [15] E. Cazacu, *Levitația electromagnetică*, Editura Electra, București 2004;
- [16] E. Cazacu, M. Stănculescu, *Bazele electrotehnicii. Teoria circuitelor electrice și aplicații*, vol.1 și 2, Editura Cartea Universitară, București 2003;
- [17] E. Cazacu, I. V. Nemoianu, *Dispozitive magnetice speciale. Elemente de teorie și calcul*, Editura Matrix Rom, București 2008;
- [18] Horia Gavrilă, Horia Chiriac, Petru Ciureanu, Valentin Ioniță, Arthur Yelon, *Magnetism tehnic și aplicat*, Ed. Academiei Române, București, 2000;
- [19] Horia Gavrilă, Valentin Ioniță, *Metode experimentale în magnetism*, Ed. Universitară “Carol Davila”, București, 2003;
- [20] E. Lefter, *Alimentarea cu energie electrică a automobilelor*, Editura Mediamira, 2006;
- [21] A. Simion, *Mașini electrice vol. I-II*, Editura Gh. Asachi, Iași, 2003;
- [22] Augustin Moraru, *Bazele electrotehnicii. Teoria cimpului electromagnetic*, Editura Matrix Rom, București, 2002;
- [23] Emil Cazacu, Iosif Vasile Nemoianu, *Dispozitive magnetice speciale. Elemente de teorie și calcul*, Editura Matrix Rom, București, 2008;
- [24] A. Tomescu, F. M. G. Tomescu, *Bazele electrotehnicii. Circuite electrice*, Editura Matrix Rom, București, 2005;
- [25] Alina Machedon, *Masini electrice folosite in transporturi*, Editura Matrix Rom, București 2005;
- [26] F. M. G. Tomescu, Anca Tomescu, *Bazele electrotehnicii. Cimp electromagnetic*, Editura Matrix Rom, București, 2006;
- [27] Anca Tomescu, I. B. L. Tomescu, F. M. G. Tomescu, *Electrotehnica. Cimp electromagnetic. Circuite electrice*, Editura: Matrix Rom, București, 2007;
- [28] Anca Tomescu, I. B. L. Tomescu, F. M. G. Tomescu, *Conversiunea directă a energiei*, Editura Matrix Rom, București, 2008;
- [29] Constantin Ghiță, *Mașini electrice*, Editura Matrix Rom, București, 2005;

- [30] Ștefan Procopiu, *Electricitate și magnetism* vol.I și II, Editura Laboratorului de Electricitate din cadrul Politehnicii Gheorghe Asachi, Iași, 1942;
- [31] M.A.Liubcik, *Electromagneți de curent continuu și alternativ. Calcul și proiectare*, Editura tehnică, București, 1963;
- [32] Emil Burzo, *Fizica fenomenelor magnetice* vol.I și II, Editura Academiei RSR, București, 1979;
- [33] Emil Burzo, *Magneți permanenți* vol.I și II, Editura Academiei RSR, București, 1986;
- [34] Ion Spânulescu, *Electricitate și magnetism*, Editura Victor, București, 2001;
- [35] Mircea Crișan, *Teoria cuantică a magnetismului*, Editura Dacia, Cluj-Napoca, 1977;
- [36] Arsene Rădoi, *Electromobilul*, Editura Tehnică, București, 1981;
- [37] Ion Boldea, *Vehicule pe pernă magnetică*, Editura Academiei RSR, București, 1981.

DYNAMICAL ANALYSIS OF THE GAS POWERED IMPULSE GENERATOR

Tomáš LUKÁČ, Roman VÍTEK, Linh DO DUC, Vladimír HORÁK

Faculty of Military Technology, University of Defence, Brno, Czech Republic
(tomas.lukac@unob.cz, roman.vitek@unob.cz, duclinh.do@gmail.com,
vladimir.horak@unob.cz)

DOI: 10.19062/2247-3173.2017.19.1.38

***Abstract:** The paper presents the 3D design, results of the theoretical calculation of the force generated by the experimental carbon dioxide powered recoil force and impulse generator and comparison with the experimental measurement on the manufactured origin. The approximate calculation of the resultant generated force was performed with the kinetic energy loses method. The comparison with the measured real firearm recoil force and impulse is also presented.*

***Keywords:** recoil simulation, assault rifle, impulse, force diagram*

1. INTRODUCTION

Presented experimental, carbon dioxide powered, impulse generator was designed to provide an experimental data for the purpose of the research and development of the device for the gun's recoil simulation. The main idea for the design and development is to acquire the force and impulse diagrams and compare them with the earlier obtained diagrams of the commercial carbon dioxide training recoil adapters. The generator was designed in the CAD environment of the SolidWorks 2015 and subsequently manufactured. The part of design was an approximate calculation of the impact speed of the piston on the buffer and the generated force size. At the end the experimental measurement was also performed.

2. 3D DESIGN

The origin of the carbon dioxide powered recoil force generator was designed in the CAD environment of the SolidWorks 2015. The mechanical drawings of the components were exported after the design completion and next the functional origin was manufactured.

2.1 Design description. Whole mechanism is located in the cylinder with the inner diameter of 30 mm. The cylinder allows the moving of the movable piston from the front to the rear position. The piston is forced to move by the expansion of the injected pressurized carbon dioxide. The dimension tolerance between the cylinder inner diameter and the piston diameter is minimal and with the lubricant provides the sufficient tightness. For the purpose of the measurement, two pistons with different masses were manufactured. The weight of the heavier piston is 309 g and in the case of the lighter piston it is 240 g. The aperture in the rear part of the cylinder provides the discharge of the air in front of the piston and the aperture in the middle of the cylinder provides the discharge of the pressurized carbon dioxide after the acceleration of the piston.

The threads on the both ends of the cylinder are for the closing nuts. In the rear of the cylinder a case with the buffer is inserted and it's directly connected with a firearm stock.

A bronze was chosen as a material for the slip edges, due its better slip properties. The recoil spring provides the piston transfer back to the front position. The spring stiffness is 550 N.m^{-1} . The view of the mechanical part arrangement of the generator is shown in Fig. 1.

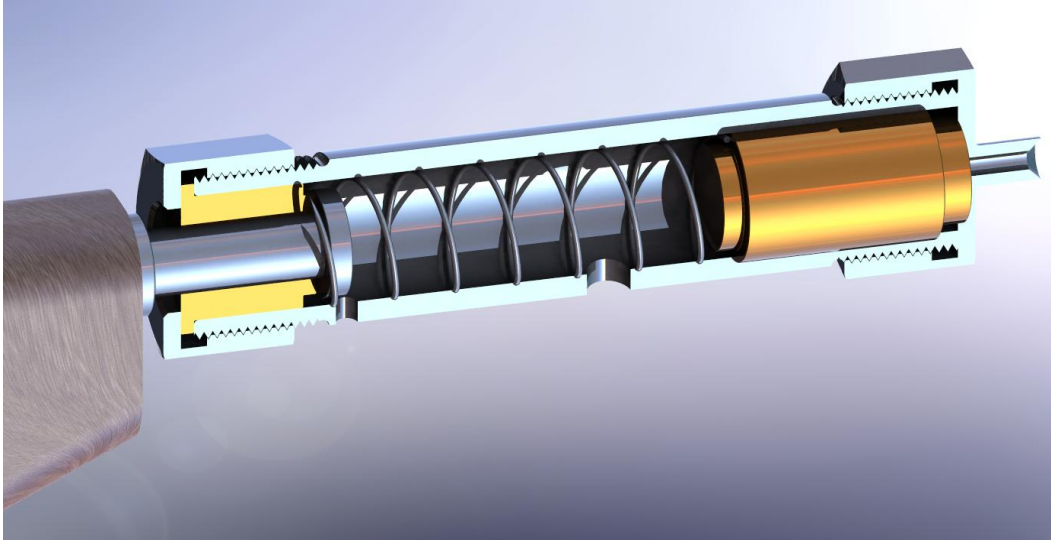


FIG. 1 Inner arrangement of mechanical parts

2.2 Function principle. The pressurized carbon dioxide is injected under the piston in the cylinder. The mass of the injected carbon dioxide is controlled by the electromagnetic valve GSR Type 46, driven by the time relay ElkoEP PDR-2. The parameters are closely presented in [1]. The carbon dioxide begins to expand and force the piston to move. The piston begins to move immediately after the pressure rises to the sufficient level. The recoil spring is also pressed by the piston during its move in to the rear position and when the rear edge of the piston get through the aperture in the cylinder, the discharge of the carbon dioxide from the cylinder begins. After that the piston moves freely to the rear position, where impacts the buffer. This way a recoil force is generated and transferred through the stock to the ballistic mount or the shooter's arm. When the carbon dioxide is fully discharged, the recoil spring forces the piston to move to the initial position.

Fig. 2. shows the view of the designed and manufactured generator system.



FIG. 2 View of the system

3. CALCULATION OF THE IMPACT SPEED

The input data for the calculation are given in the Tab. 1. The maximum pressure in the cylinder depends on the pressure losses in the valve, inlet port cross-section, initial volume and the mass of the injected carbon dioxide and substantially differs from the pressure in carbon dioxide tank. The approximate initial value of the pressure around 2 MPa was obtained from the Matlab calculation model, see [2]. The calculation was realized on the basis of the kinetic energy losses in the each phase.

Table 1. Input data

Mass of the piston	0.309 kg
Mass of the recoil parts	0.314 kg
Stiffness of the recoil spring	550 N.m ⁻¹
Initial force of the recoil spring	2 N
Maximal force of the recoil spring	48.37 N
Pressure	1,5 MPa
Total stroke of the piston	84.3 mm
Section lengths	67.5; 10; 3.5 mm

3.1 Calculation of the phases of motion. In the first phase, the initial energy is given to the piston by the pressurized carbon dioxide. The piston starts to move before the pressure rises to the maximum magnitude and then the maximal pressure is smaller. During the motion in this phase, the small amount of the energy is spent by the recoil spring. The length of the first phase is 67.5 mm. The second phase length is 10 mm and due to the simplicity, the calculation in this phase expects the immediately depressurization, so in this section, the piston moves freely with the initial velocity and energy.

Cross-section of the piston:

$$S_p = \frac{\pi \cdot d^2}{4} = \frac{\pi \cdot 0.03^2}{4} = 0.0007065 \text{ m}^2$$

Where S_p – cross-section of the piston,
 d – diameter of the piston.

Maximal force provided by the carbon dioxide on the piston:

$$F_{HP} = p \cdot S_p = 1500000 \cdot 0.0007065 = 1060 \text{ N}$$

Where F_{HP} – maximal force acting to the piston,
 p – acting pressure.

Recoil spring force on the end of the phase:

$$F_{675} = F_{p1} + (c_{pp} \cdot x_1) = 2 + (0.55 \cdot 67.5) = 39.125 \text{ N}$$

Where F_{675} – force at the end of the phase,
 F_{p1} – initial force of the recoil spring,
 c_{pp} – stiffness of the recoil spring,
 x_1 – length of the phase.

The force acting on the piston at the end of the phase:

$$F_{res} = F_{HP} - F_{675} = 1060 - 39.125 = 1020.875 \text{ N}$$

Where F_{res} – resulting force at the end of the phase.

Piston acceleration:

$$a_p = \frac{F_{res}}{m_{pp}} = \frac{1020.875}{0.31} = 3285.27 \text{ m.s}^{-2}$$

Where a_p – acceleration of the piston.

Time of the movement in the phase:

$$t_{675} = \sqrt{\frac{2 \cdot x_1}{a_p}} = \sqrt{\frac{2 \cdot 0.0675}{3285.27}} = 0.0064 \text{ s}$$

Where t_{675} – whole time of the motion in the phase.

The piston velocity at the end of the phase:

$$v_{p1} = a_p \cdot t_{675} = 3285.27 \cdot 0.0064 = 21.06 \text{ m.s}^{-1}$$

Where v_{p1} – resulting velocity of the piston at the end of the phase.

Energy spent by the recoil spring:

$$A = \frac{F_{p1} + F_{675}}{2} \cdot x_1 = \frac{2 + 39.125}{2} \cdot 0.0675 = 1.388 \text{ J}$$

Where A – Energy spent by the recoil spring during the pressing.

Kinetic energy at the end of the phase:

$$E_{p1} = \frac{1}{2} m_{p\check{c}} \cdot v_{p1}^2 - A = \frac{1}{2} \cdot 0.31 \cdot 21.06^2 - 1.388 = 67.5 \text{ J}$$

Where E_{p1} – resulting energy of the piston after the first phase.

Analogically the next two phases were calculated and the maximum final calculated recoil force, transferred to the arm, was 4 363 N.

4. VERIFICATION MEASUREMENT

The measurement was realized for the both used pistons in the firing rest STZA 12 equipped by the Kistler 9051A annular force-sensor. As a ballistic computer, the Dewetron DEWE 5000 was used. Several free runs were realized before the measurement due to the device stabilization in the firing rest. The impact speed of the piston on the buffer was evaluated from the hi-speed camera record.

After the initial stabilization, the 5 cycles were performed, the data from the ballistic computer were processed and the obtained force diagram for the five runs with the heavier piston is shown in Fig. 3.

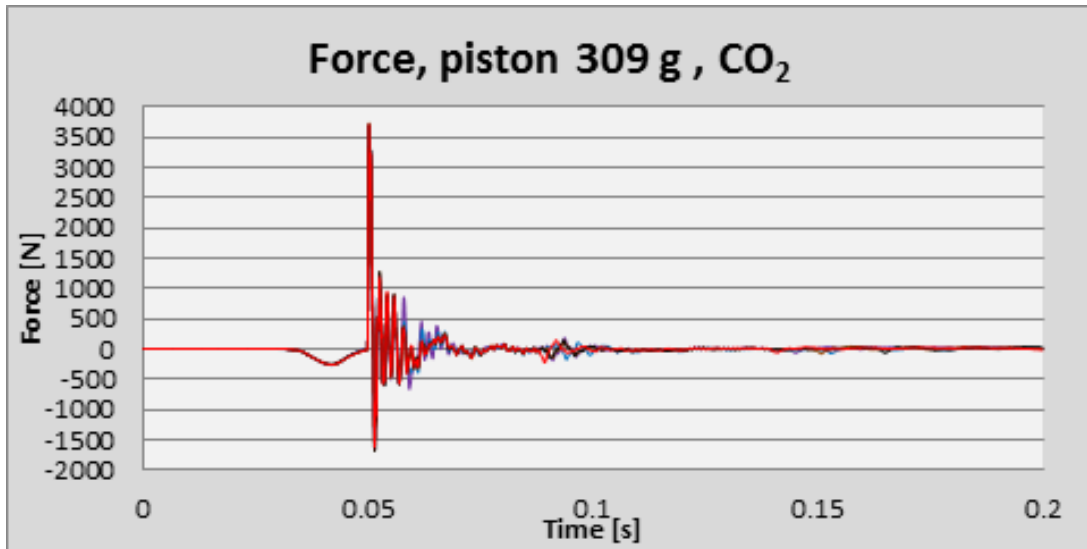


FIG. 3 Force diagram for the 309g piston

The small negative spike at the motion beginning is caused by the acceleration of the the piston after its release. During the forced motion of the piston to the rear position, the whole device is forced by the pressurized gas to move in the opposite direction.

The main force peak is caused by the piston impact and it's in the range from 3 600 to 3 750 N. This is around the 70% of the real maximum recoil force peak. This is caused by a non-absolute stiffness of the firing rest recoil system and the previous measurements in this firing rest configuration shows that it's around 70%. The real recoil force peak is then in the range between 5 100 and 5 400 N.

Impulse diagram was obtained by the numerical integration from the measured data in the table processor. The impulse courses for the each measurement are shown in Fig. 4.

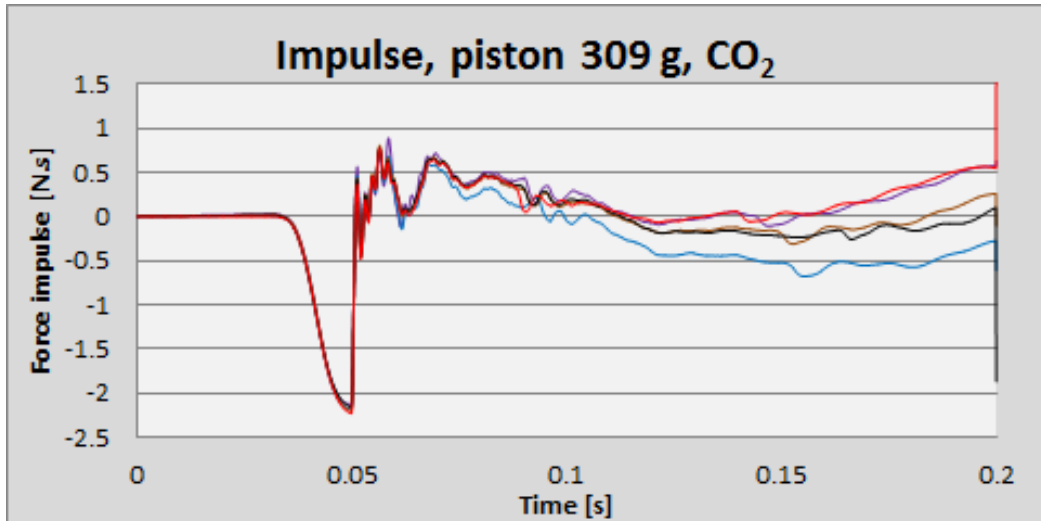


FIG. 4 Impulse diagram for the 309g piston

The obtained time courses of the force and impulse are almost identical, what makes this measurement representative and repeatable.

The next diagram in the Fig. 5 shows the force time courses in case of the lighter, 240g piston.

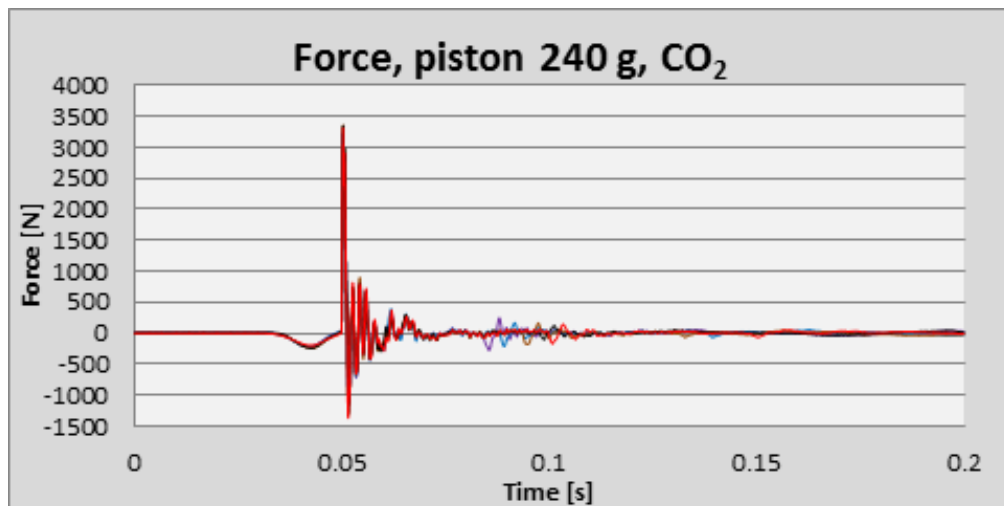


FIG. 5 Force diagram for the 240g piston

The time course is very similar and the measured main force peak is in the range between 4 300 and 5 000 N. It's evident, the piston with the smaller mass generates the smaller force and impulse at the impact in the rear position. The corresponding impulse diagram is shown in the Fig. 6.

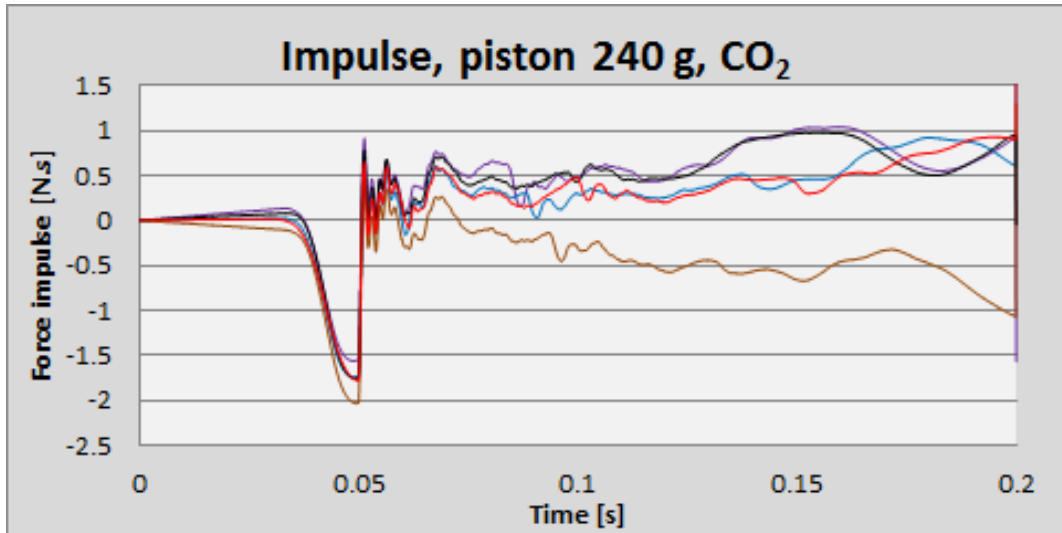


FIG. 6 Impulse diagram for the 240g piston

5. COMPARISON WITH COMMERCIAL RECOIL ADAPTER

The part of the research was also focused on the measurement of the force generated by the commercial recoil training adapters, provided by Eli Military Simulations, see [2]. Measurement of the recoil force and impulse of the automatic rifle vz.58, see[3]. The measurement was performed on the available adapters for the AK47 and AR-15 based rifles. The next table shows the results of the measurement and the comparison with the results of the measurement during the shooting with a live and blank ammunition.

Table 1. Comparison of measured parameters

	Force [N]			Impulse [N.s]		
	Live	Blank	Adapter	Live	Blank	Adapter
AK47	5 700	3 000	2 100	10-11	2.85-3.15	1.42
SA58	4 600	-	-	10-11	-	-
PAR Mk3	1 700- 2 000	-	1 700	5.7-7	-	2.6
CO2 impulse generator	-	-	5 100 (4 300)	-	-	1.3 (1.1)

CONCLUSIONS

The presented impulse generator is the part of the the research and development of the device for gun’s recoil simulation. In this phase, the 3D model of the generator was created, subsequently was the generator manufactured. The verification of the calculated parameters was realized by an experimental measurement. The measurement shows that the generated force and impulse are comparable with force and impulse provided by a real firearm during the shooting with the live ammunition, and are higher than a force and impulse provided by an commercially used recoil adapters. In the next steps of the development, the reduction of the mass and eventually the dimensions will be realized.

ACKNOWLEDGMENT

The work presented in this paper has been supported by the institutional funding DZRO K201 “VÝZBROJ” and by the specific research support project of the Faculty of Military Technology SV16-216.

REFERENCES

- [1] LUKÁČ, Tomáš; HORÁK, Vladimír; DO DUC, Linh; ROZEHNAL, Dalibor. Experimental Setup for Studying Properties of Power Gases. In: *The 17th INTERNATIONAL CONFERENCE AFASES 2015*. Brasov, Rumunsko: Publishing House of “Henri Coanda” Air Force Academy, 2015, p. 429-436. ISSN 2247-3173
- [2] DO DUC, Linh; HORÁK, Vladimír; LUKÁČ, Tomáš; VÍTEK, Roman; MAI, Quang Huy. Dynamics of Knock-Open Valve for Gas Guns Powered by Carbon Dioxide. In: *Scientific Research and Education in the Air Force - AFASES 2016*. Brasov: Publishing House of “Henri Coanda” Air Force Academy, 2016, p. 323-330. ISSN 2247-3173
- [2] LUKÁČ, Tomáš; DO DUC, Linh; HORÁK, Vladimír; PILCH, Ondrej. EXPERIMENTAL ANALYSIS OF THE RECOIL FORCE OF REAL FIREARM AND ITS RECOIL SIMULATION SYSTEM. In: *Armament and Technics of Land Forces 2016*. Liptovský Mikuláš: Akadémia ozbrojených síl generála M. R. Štefánika, 2016, p. 121-127. ISBN 978-80-8040-537-3
- [4] LUKÁČ, Tomáš; VÍTEK, Roman; DO DUC, Linh; HORÁK, Vladimír. Experimental Mechanical Device for Recoil Simulation. In: *Scientific Research and Education in the Air Force - AFASES 2016*. Brasov: Publishing House of “Henri Coanda” Air Force Academy, 2016, p. 337-343. ISSN 2247-3173

DERIVATION OF MASS, STIFFNESS AND DAMPING MATRICES OF A MODEL WING FROM EXPERIMENTAL MODAL DATA

Ionel POPESCU, Lică FLORE, Albert ARNAU CUBILLO

Institute for Theoretical and Experimental Analysis of Aero-Astronautical Structures
STRAERO S.A., Bucharest, Romania (ionel.popescu@straero.ro, lica.flore@straero.ro,
albert.acubillo@gmail.com)

DOI: 10.19062/2247-3173.2017.19.1.39

***Abstract:** This paper presents the results of the experimental modal analysis of a wing structure along with the derivation of full mass, damping and stiffness matrices from modal parameters. Using the derived matrices, the natural frequencies of the structure were computed and compared with the experimentally determined ones. Very good correlation was found, which confirms the validity of the method.*

***Keywords:** experimental modal analysis, mass, stiffness, damping, mode shapes, frequencies*

1. INTRODUCTION

The specialized systems for experimental modal analysis do not usually provide mass, stiffness and damping matrices in spatial coordinates but the ones in the modal space. While the modal matrices are very useful in a large number of engineering applications, there are cases in which matrices in spatial coordinates are preferred. Such a case is the active control of aeroelastic oscillations and flutter phenomena in which it would be difficult to express the aerodynamic forces in the modal space. To avoid such complications and to use the measured modal data, a method of deriving these matrices in spatial coordinates from the ones in modal space is needed. Such a method is well presented in [2] and is applied in our study on experimental modal data obtained for a model wing aimed for flutter control experiments in aerodynamic wind tunnel.

More than the derivation of mass, stiffness and damping matrices in spatial coordinates from modal data, this paper aims to validate the obtained matrices. To accomplish that, the natural frequencies of the free undamped wing structure are computed by using the derived mass and stiffness matrices. Very good correlation is found between the computed and the experimentally determined natural frequencies.

2. EQUIPMENT USED AND TEST CONFIGURATION

The Prodera installation is a modal analysis equipment that uses up to 16 unidirectional accelerometers simultaneously to determine the vibration parameters of a structure. Its software features pre, real-time and post processing tools that allow to prepare and perform impulse and harmonic vibration tests and to calculate modal parameters using specific methods (power complex method, quadrature method). This system also provides graphical representation during and after tests. The equipment is pictured in Fig. 1 with a general view of the data acquisition, control and computing cabinet in (a) and electromechanical shaker connected to the test specimen in (b).

The studied structure is a model wing developed in the frame of a research project for active control of flutter phenomena. The wing has a 1.2m span, a 0.3m chord and is equipped with a piezoelectric-actuated control surface. For the purpose of the vibration test, the control surface has been blocked in the neutral position. The wing has been mounted vertically by clamping it to a very rigid steel base on the ground and excited with an electromechanic shaker mounted in the horizontal direction, as detailed in Fig.1 (b).



FIG. 1. (a) Prodera equipment, (b) Mechanical link between exciter and wing structure

The wing structure is instrumented with 11 acceleration transducers which are positioned on the wing surface according to Fig. 2 (a), (b) and table 1.

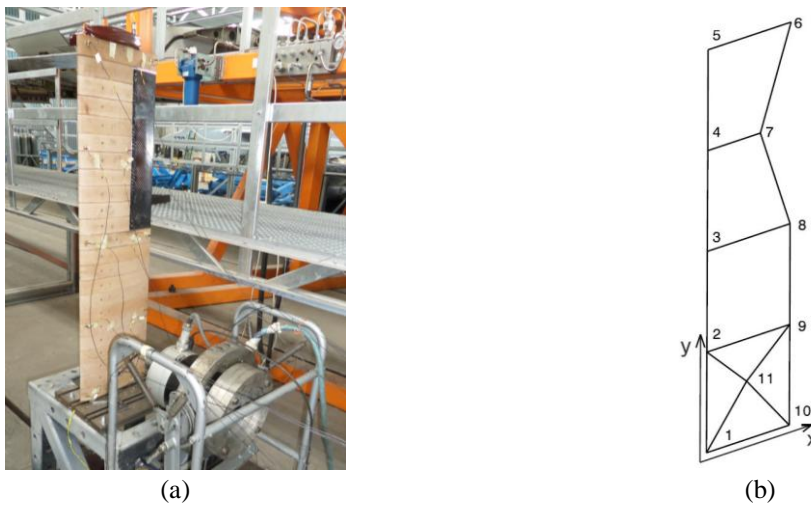


FIG. 2. (a) Test configuration, (b) Geometry of digitized structure

Table 1. Position of Transducers and Shaker

Point No.	Coord. in x [mm]	Coord. in y [mm]	Comment
1	20	20	Transducer 1
2	20	296	Transducer 2
3	20	572	Transducer 3
4	20	848	Transducer 4
5	20	1124	Transducer 5
6	280	1124	Transducer 6
7	185	848	Transducer 7
8	280	572	Transducer 8

Point No.	Coord. in x [mm]	Coord. in y [mm]	Comment
9	280	296	Transducer 9
10	280	20	Transducer 10
11	145	180	Transducer 11 and Shaker

3. TEST PROCEDURE AND RESULTS

The experimental procedure aimed to identify the modal parameters of the wing structure in three phases, based on phase excitation technique.

Firstly, the structure has been excited from 0 to 50Hz with a 0.1Hz step, and a stabilizing time of 10 seconds. The mode indicator function (MIF), which is based on the fact that at resonance real part of the FRF is zero, was applied on the acquired data. This provided a general view of the number and location of natural frequencies in the interest range 0-50Hz.

Secondly, the structure has been excited around each of these frequencies, in separate tests, in a narrow range (+/- 0.3Hz), with a step of 0.001Hz, and adequate force excitation and stabilizing time. The mode indicator function has been again applied to accurately identify the natural frequencies.

The third phase was mainly automated and consisted in the excitation of the structure around each natural frequency with automatically selected range, step and other parameters. The methods used by Prodera [1] were: automatic complex power (computes natural frequency, modal damping, mass and stiffness associated to the studied mode), automatic logarithmic decrement (computes modal damping), readout of the mode shape (computes mode shape), and phase index (computes the real and imaginary part of the acceleration for the selected frequency).

The test results used for the purpose of this paper are presented in table 2. The mode shapes are graphically represented in Fig.3. The modal mass, damping and stiffness matrices are assembled in tables 3, 4 and 5.

Table 2. Experimental Modal Data

	Mode 1	Mode 2	Mode 3	Mode 4	Mode 5
Frequency [Hz]	5.865	14.463	23.137	41.850	49.413
Modal damping	0.00418	0.00108	0.00555	0.00308	0.00847
Modal mass [Kg*m ²]	1.336	4.346	2.181	0.725	3.824
Modal stiffness [Kg*m ² /s ²]	1813.559	35887.128	46094.437	50126.386	368594.781
Transducer	Mode shapes (not normalized)				
1	0.000365	5.24E-5	2.89E-5	9.06E-6	3.81E-5
2	0.000987	-8.43E-5	0.001289	-0.00018	0.000708
3	0.002122	-0.00043	0.002048	-0.00034	0.00024
4	0.004253	-0.00053	0.001161	-0.00011	-0.0003
5	0.006077	-0.00071	-0.00077	0.000317	0.0001
6	0.00829	0.001028	-0.00322	-0.00035	0.000624
7	0.005248	0.000396	0.00083	-0.00011	-0.00075
8	0.002785	0.000793	0.00317	0.000383	-0.00062
9	0.000788	0.00016	0.002479	0.000342	0.000778
10	-5.80E-5	6.17E-6	1.61E-5	4.88E-6	2.87E-5
11	0.000464	-1.03E-6	0.000887	2.16E-5	0.000714

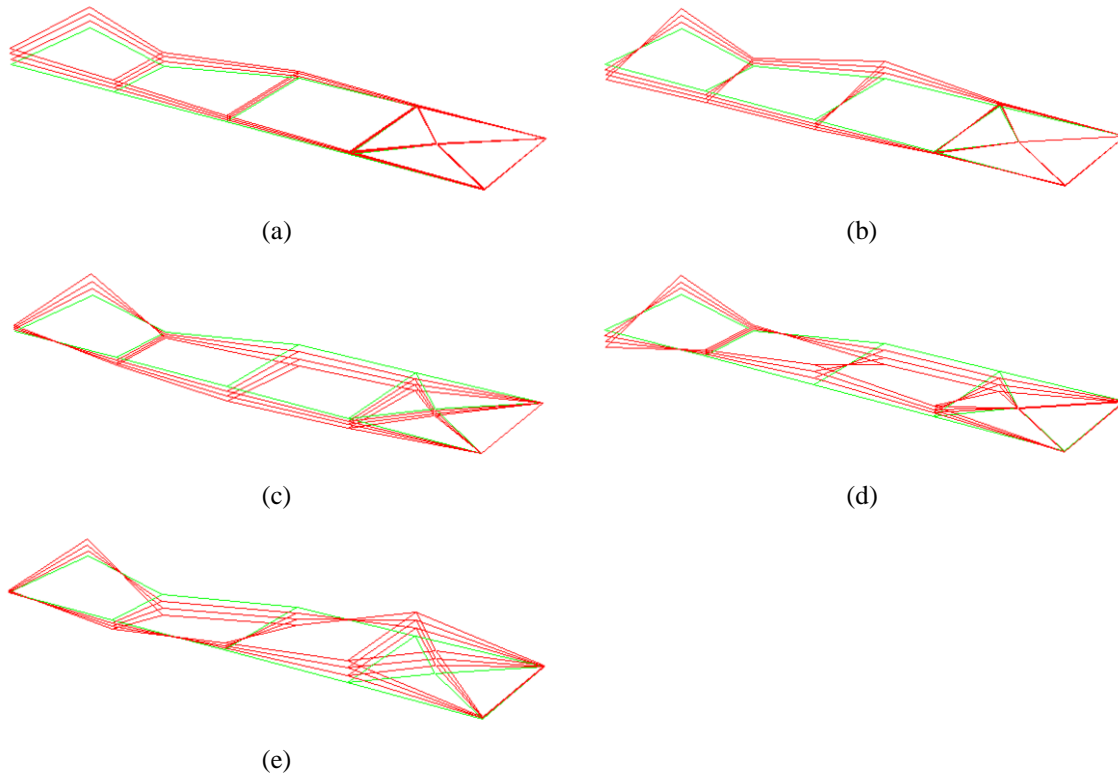


FIG. 3. Mode shapes: (a) Mode 1, (b) Mode 2, (c) Mode 3, (d) Mode 4, (e) Mode 5

Table 3. Modal Mass Matrix

1.336	0	0	0	0
0	4.346	0	0	0
0	0	2.181	0	0
0	0	0	0.725	0
0	0	0	0	3.824

Table 4. Modal Damping Matrix

0.00418	0	0	0	0
0	0.00108	0	0	0
0	0	0.00555	0	0
0	0	0	0.00308	0
0	0	0	0	0.00847

Table 5. Modal Stiffness Matrix

1.81355945E+03	0	0	0	0
0	3.58871289E+04	0	0	0
0	0	4.60944375E+04	0	0
0	0	0	5.01263867E+04	0
0	0	0	0	3.68594781E+05

4. DERIVATION OF [M], [C], [K] MATRICES FROM EXPERIMENTAL MODAL DATA

Once a set of modal data has been measured for the wing structure, it is possible to compute the full mass, stiffness and damping matrices (matrices in spatial coordinates). Formulas derived from the relationship between the time domain differential equations of motion and the transfer function matrix model of the structure are provided in [2]:

$$[M] = ([\Phi]^T)^{-1} [m][\Phi]^{-1} \tag{1}$$

$$[C] = ([\Phi]^T)^{-1} [c][\Phi]^{-1} \tag{2}$$

$$[K] = ([\Phi]^T)^{-1} [k][\Phi]^{-1} \tag{3}$$

where

- $[\Phi] = [\{u_1\}, \{u_2\}, \dots, \{u_m\}]$ - mode shape matrix
- $[m], [c], [k]$ - modal mass, damping and stiffness matrices (4)
- $[M], [C], [K]$ - full mass, damping and stiffness matrices

The direct use of these equations is prohibitively difficult, especially when using experimental modal data, since the mode shape matrix $[\Phi]$ is usually not square (in our case is 11x5).

To overcome this problem, an assumption can be made [2]: if the mode shape vectors are assured to be orthogonal with respect to one another (and are also normalized to unit magnitudes), then the mode shape matrix has the following properties:

$$[\Phi]^T [\Phi] = [I] = [\Phi]^{-1} [\Phi] \Rightarrow [\Phi]^T = [\Phi]^{-1} \tag{5}$$

To take advantage of this properties we used classical Gram-Schmidt algorithm to orthonormalize the mode shape matrix of the wing structure. The result is presented in the next table.

Table 6. Mode Shape Matrix normalized with Gram-Schmidt algorithm

	Mode 1	Mode 2	Mode 3	Mode 4	Mode 5
DOF 1	0.028355	2.48E-02	9.25E-03	1.30E-02	2.44E-02
DOF 2	0.076688	-7.15E-02	0.215205	-0.31529	0.381528
DOF 3	0.164976	-0.30742	0.325731	-0.55954	0.075313
DOF 4	0.330597	-0.40826	0.177782	-0.15961	-0.20987
DOF 5	0.472374	-0.55461	-0.15215	0.563064	0.07069
DOF 6	0.644439	0.463578	-0.45139	-0.18477	0.279941
DOF 7	0.40793	0.137127	0.181038	-0.15417	-0.44512
DOF 8	0.216532	0.429949	0.590723	0.312044	-0.2448
DOF 9	0.061222	0.082489	0.429535	0.298114	0.533291
DOF 10	-4.51E-03	4.95E-03	2.88E-03	4.67E-03	1.79E-02
DOF 11	0.036089	-9.97E-03	0.150844	-2.55E-02	0.421877

Checking orthogonality yields very good results:

$$[\Phi]^T [\Phi] = \begin{bmatrix} 1 & 5.93E-17 & -3.73E-17 & 5.35E-17 & 1.56E-17 \\ 5.93E-17 & 1 & -4.16E-17 & 8.19E-17 & 2.34E-17 \\ -3.73E-17 & -4.16E-17 & 1 & -3.56E-17 & -5.55E-17 \\ 5.35E-17 & 8.19E-17 & -3.56E-17 & 1 & 2.43E-17 \\ 1.56E-17 & 2.34E-17 & -5.55E-17 & 2.43E-17 & 1 \end{bmatrix} \square [I] \quad (6)$$

Because the inverse of the mode shape matrix is now equal to its transpose, the formulas for full mass, stiffness and damping matrices are straightforward [2]:

$$[M] = [\Phi][m][\Phi]^T \quad (7)$$

$$[C] = [\Phi][c][\Phi]^T \quad (8)$$

$$[K] = [\Phi][k][\Phi]^T \quad (9)$$

The resulted matrices are presented in tables 7, 8 and 9:

Table 7. Mass Matrix in spatial coordinates

0.006341	3.22E-02	-1.86E-02	-4.90E-02	-3.31E-02	0.0897	-0.00914	0.046552	0.072513	0.002137	0.04251
3.22E-02	7.60E-01	5.03E-01	-2.55E-02	1.24E-01	0.160713	-0.53003	-0.26269	0.892146	0.024403	0.698933
-1.86E-02	5.03E-01	0.927163	7.49E-01	5.29E-01	-0.64242	-0.03033	-0.30413	0.241087	-0.0023	0.260285
-4.90E-02	-2.55E-02	7.49E-01	1.126217	1.01E+00	-0.91619	0.382137	-0.27781	-0.41526	-0.02456	-0.24351
-3.31E-02	1.24E-01	5.29E-01	1.01E+00	1.934379	-0.56065	-0.31642	-1.0345	-0.03688	-0.00899	0.100368
0.0897	0.160713	-0.64242	-0.91619	-0.56065	2.257634	-0.00659	0.167238	0.326983	0.021785	0.317522
-0.00914	-0.53003	-0.03033	0.382137	-0.31642	-0.00659	1.150406	0.989282	-0.68893	-0.02936	-0.64195
0.046552	-0.26269	-0.30413	-0.27781	-1.0345	0.167238	0.989282	1.926845	0.293468	-0.00404	-0.21454
0.072513	0.892146	0.241087	-0.41526	-0.03688	0.326983	-0.68893	0.293468	1.58895	0.041624	0.995513
2.14E-03	2.44E-02	-2.30E-03	-2.46E-02	-8.99E-03	0.021785	-0.02936	-0.00404	0.041624	0.001393	0.02931
0.04251	6.99E-01	0.260285	-2.44E-01	0.100368	0.317522	-0.64195	-0.21454	0.995513	0.02931	0.732868

Table 8. Damping Matrix in spatial coordinates

1.01E-05	8.46E-05	2.12E-05	-1.24E-05	7.05E-05	0.000116	-3.70E-05	2.94E-05	0.000154	3.64E-06	9.80E-05
8.46E-05	1.83E-03	1.25E-03	-1.73E-04	-3.06E-04	0.000716	-0.00095	-0.00035	0.00196	5.49E-05	0.001581
2.12E-05	1.25E-03	0.001817	8.26E-04	-6.90E-04	-2.85E-05	0.000545	0.000381	0.000618	3.83E-06	0.000614
-1.24E-05	-1.73E-04	8.26E-04	0.001264	3.45E-04	-0.00017	0.001549	0.000974	-0.00062	-3.97E-05	-0.00053
7.05E-05	-3.06E-04	-6.90E-04	3.45E-04	0.002412	0.001223	3.66E-05	6.58E-05	0.000545	4.52E-06	0.000158
0.000116	0.000716	-2.85E-05	-0.00017	0.001223	0.003868	-0.00025	-0.00144	0.000225	2.29E-05	0.000729
-3.70E-05	-0.00095	0.000545	0.001549	3.66E-05	-0.00025	0.002649	0.001801	-0.0016	-7.38E-05	-0.00137
2.94E-05	-0.00035	0.000381	0.000974	6.58E-05	-0.00144	0.001801	0.00314	0.000683	-2.50E-05	-0.00038
0.000154	0.00196	0.000618	-0.00062	0.000545	0.000225	-0.0016	0.000683	0.00373	9.13E-05	0.00225
3.64E-06	5.49E-05	3.83E-06	-3.97E-05	4.52E-06	2.29E-05	-7.38E-05	-2.50E-05	9.13E-05	2.94E-06	6.53E-05
9.80E-05	1.58E-03	0.000614	-5.34E-04	0.000158	0.000729	-0.00137	-0.00038	0.00225	6.53E-05	0.001641

Table 9. Stiffness Matrix in spatial coordinates

2.56E+02	3.26E+03	1.88E+02	-2.26E+03	4.69E+02	2653.935	-3.89E+03	-1.36E+03	5256.299	1.70E+02	3.84E+03
3.26E+03	6.10E+04	2.35E+04	-2.41E+04	1.02E+03	36710.03	-58659.5	-34571.1	74342.57	2.46E+03	61258.56
1.88E+02	2.35E+04	26116.03	5.92E+03	-9.85E+03	1.25E+03	-6704.87	-11356.9	12000.22	3.53E+02	14812.64
-2.26E+03	-2.41E+04	5.92E+03	25148.67	-2.81E+03	-30281.9	35385.82	15111.85	-41291.1	-1.47E+03	-31027.4
4.69E+02	1.02E+03	-9.85E+03	-2.81E+03	30244.51	-3429.85	-1.96E+04	-1.01E+04	17707.6	4.76E+02	9443.556
2653.935	36710.03	1.25E+03	-30281.9	-3429.85	48454.39	-45510.2	-33034.6	44773.21	1.82E+03	40505.5
-3.89E+03	-58659.5	-6704.87	35385.82	-1.96E+04	-45510.2	76708.61	44957.64	-85764.4	-2.93E+03	-67783.1
-1.36E+03	-34571.1	-11356.9	15111.85	-1.01E+04	-33034.6	44957.64	49773.19	-30464	-1.39E+03	-34498
5256.299	74342.57	12000.22	-41291.1	17707.6	44773.21	-85764.4	-30464	118038.4	3.66E+03	85507.52
1.70E+02	2.46E+03	3.53E+02	-1.47E+03	4.76E+02	1.82E+03	-2.93E+03	-1.39E+03	3.66E+03	1.21E+02	2.80E+03
3.84E+03	6.13E+04	14812.64	-3.10E+04	9443.556	40505.5	-67783.1	-34498	85507.52	2.80E+03	66690.13

5. VALIDATION OF [M], [C], [K] MATRICES

In absence of damping and external load, the equation of motion in matrix form for a given structure is [3]:

$$[M]\{\ddot{q}\} + [K]\{q\} = 0 \quad (10)$$

which, for solving, we assume a harmonic solution of the form:

$$\{q\} = \{u\} \sin \omega t \quad (11)$$

Through differentiation and substitution in equation 10, the following is obtained:

$$-\omega^2 [M]\{u\} \sin \omega t + [K]\{u\} \sin \omega t = 0 \quad (12)$$

which after simplifying becomes:

$$([K] - \omega^2 [M])\{u\} = 0 \quad (13)$$

This reduces to an eigenvalue problem of the basic form:

$$[A - \lambda I]x = 0 \quad (14)$$

By solving the eigenvalues problem we find the eigenvalues and eigenvectors associated to the structure. The i^{th} eigenvalue λ_i is related to the i^{th} natural frequency f_i as follows:

$$f_i = \frac{\omega_i}{2\pi}, \quad \omega_i = \sqrt{\lambda_i} \quad (15)$$

The natural frequencies f_i have been computed using mass [M] and stiffness [K] matrices, previously derived for the wing structure, and the results are presented in the next table along with the experimentally determined frequencies. Very good correlation is found.

Table 10. Computed and experimental frequencies

No.	Computed frequencies	Experimental frequencies	No.
1	5.86384930583323	5.865	1
2	14.4625418258649	14.463	2
3	16.1181473527133	-	
4	21.5627768416534	-	
5	23.1375067594382	23.137	3
6	35.1286393566203	-	
7	37.3453361756750	-	
8	41.8489271158046	41.850	4
9	45.8132201895832	-	
10	49.4123809131585	49.413	5
11	49.7003108389488	-	

CONCLUSIONS

The experimentally determined frequencies are all found through the numerical procedure with very good accuracy. This confirms that [M] and [K] matrices accurately describe the wing structure (up to the fifth vibration mode). This also confirms that [C] matrix, which was neglected in equation 10, is indeed negligible, in line with the small values presented in table 8.

As can be seen in table 10, the computed frequencies no. 3,4,6,7,9 and 11 do not have correspondence in the set of experimental frequencies. The experimental modal analysis was performed in a very accurate manner and no other natural frequency has been found between the experimental frequencies listed above. The values of these additional (computed) frequencies vary with the quality of the mode shape matrix orthonormalization (for example by using classical Gram-Schmidt or modified Gram-Schmidt methods) and are a direct consequence of constructing 11x11 mass, stiffness and damping matrices from experimental modal data gathered from only 5 modes of vibration.

ACKNOWLEDGMENT

This work was financially supported by UEFISCDI within the frame of the research project “AFDPA - Anti flutter Demonstrator with Piezoelectric Actuation”, contract no. 289/2014.

The test specimen was provided by INCAS - National Institute for Aerospace Research "Elie Carafoli", the coordinator of the aforementioned project.

The tests were performed at STRAERO facilities.

REFERENCES

- [1] K. Dijkstra, B. Marinez Vasquez, *Modal Analysis Methods*, Prodera Manual, 2002.
- [2] M. H. Richardson, *Derivation of Mass, Stiffness and Damping Parameters From Experimental Modal Data*, Hewlett Packard Company, Santa Clara Division, June, 1977.
- [3] SIEMENS, NASTRAN NX, *Basic Dynamic Analysis User's Guide / Chapter 4: Real Eigenvalue Analysis (SOL 103) / 4.3 Overview of Normal Modes Analysis*. Available at https://docs.plm.automation.siemens.com/data_services/resources/nxnastran/10/help/en_US/tdocExt/pdf/basic_dynamics.pdf, accessed on 9 May 2017.

NEW COMPOSITE SANDWICH WITH ALUMINUM CORE

Horatiu TEODORESCU-DRAGHICESCU*, Mariana Domnica STANCIU*, Florin TEODORESCU-DRAGHICESCU**

*Transilvania University of Brasov, Braşov, Romania

(draghicescu.teodorescu@unitbv.ro, mariana.stanciu@unitbv.ro)

**Politehnica University, Bucharest, Romania (florin.teodorescu@ltpc.pub.ro)

DOI: 10.19062/2247-3173.2017.19.1.40

Abstract: *This paper presents a new developed ultra-lightweight composite sandwich with very good mechanical properties suitable for aerospace and defense applications. The 13.8 mm thick structure has a 3003 aluminum honeycomb core with 5.2 mm cell size and two opposite skins made of woven glass fabric reinforced epoxy resin laminates. Very good stiffness and mechanical work have been obtained during three-point bend tests. Samples have been subjected to load at break and up to 50 mm deflection. More compact values of mechanical properties have been obtained at break than at 50 mm deflection.*

Keywords: *sandwich, aluminum honeycomb core, composite skins, stiffness, mechanical work*

1. INTRODUCTION

Sandwich structures present a wide range of applications. Basically, a sandwich has a continuous or discontinuous core made of lightweight materials providing mechanical stiffness [1, 2, 3]. This core with more or less thickness is bonded with similar or dissimilar opposite skins to form a load-bearing structure. The quality of interface between core and skins will depend the subsequent mechanical behavior of the sandwich structure. Therefore, this interface plays a major role in determining the structure's mechanical properties. It is essential that the core should be as lightweight as possible taking loads only perpendicular to its surface [4]. To avoid skins buckling in compression loadings, the core must have a satisfactory stiffness. Skins can be metal sheets or polymer matrix composite laminates based on thermoplastic or other resins [5]. Polyester and epoxy reinforced composite laminates are usually used in a wide range of composite structures. As reinforcement, glass fibers in form of chopped strand mats and roving fabrics of various specific weights are commonly used. To choose a material for a specific application is quite a challenging task. The user should consult the supplier for detailed mechanical property data on current materials, together with wider databases required for other property data (e.g. electrical, thermal, fire properties, surface finish, etc.), process information (e.g. gel time, working life, curing temperature, cure time, mold release temperature, etc.), as well as material or process costs [6]. For composite applications, most design procedures, whether simple or sophisticated, will be based initially on stiffness data and will often relate to strain or deflection limits design [7, 8]. Consequently, Young's modulus values are normally required for the main in-plane directions of a composite laminate using orthogonal axes [9, 10, 11, 12]. Young's modulus is an important feature of any kind of material since represents its stiffness [13, 14, 15].

In addition, many applications of composites are based on thin-walled structures (e.g. thin pultruded profiles, skins of sandwich structures, etc.) [16, 17, 18, 19, 20, 21].

2. MATERIAL AND EXPERIMENTAL SET-UP

Following new lightweight composite sandwich has been designed and developed presenting this architecture (Fig. 1): two skins (0.55 mm thickness) composite laminates based on two layers of 380 g/m² specific weight woven glass fabric impregnated with epoxy resin and a 3003 aluminum honeycomb core with 5.2 mm cell size (12.7 mm thickness). These skins have been separately cured and glued to core using high performance epoxy adhesive film. From a panel (1250x380x13.8 mm), ten samples with following dimensions have been cut: samples length: 280 mm; samples width: 30 mm; samples thickness: 13.8 mm. The sample width is measured with an accuracy of 0.1 mm in its central section, then three thickness measurements with 0.02 mm accuracy are performed and the arithmetic mean of these measurements is used for subsequent calculations. The test speed is determined in the following manner:

- For material's characterization, the speed value is equal to half the value of the specimen thickness;
- For common tests, the speed is set to 10 mm/min.

The sample is put symmetrically with respect to the parallel supports ensuring that the sample length is perpendicular to them. The central crosshead is positioned exactly at the middle of the span and a load is applied with uniform speed avoiding shocks. To determine the Young's modulus of bending, the load/deflection values are read simultaneously. The machine software is able to draw a true load-deflection distribution. The experimental set-up and details of three-point bend tests are shown in Figs. 2-4.



FIG. 1. Sandwich with 5.2 mm cell size

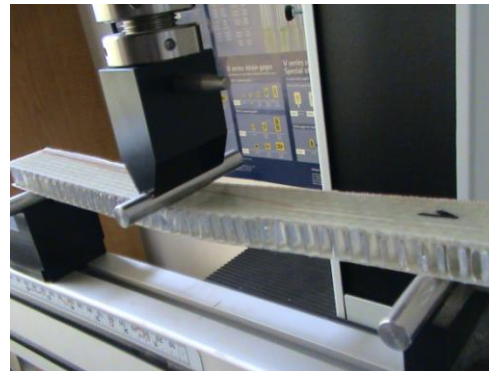


FIG. 2. "LR5K Plus" materials testing machine

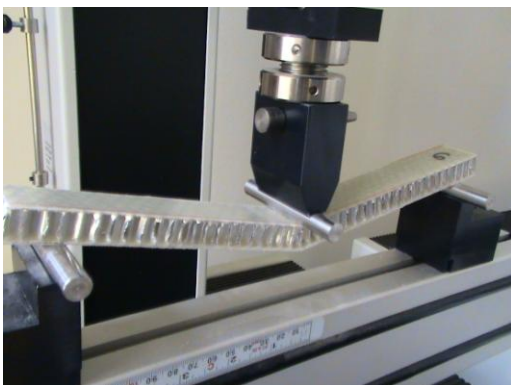


FIG. 3. Sample on three-point bend device



FIG. 4. Loading detail

3. RESULTS

From total number of samples, half of them have been subjected to three-point bend tests up to break and half to 50 mm maximum deflection on a “LR5K Plus” Lloyd Instruments materials testing machine. The three-point bend test characteristics are: testing direction: compression; test speed: 10 mm/min; test method: three-point bending; span between supports: 240 mm. Load-deflection distributions up to break of five sandwich samples with 3003 aluminum honeycomb core (5.2 cell size) have been experimentally determined using “Nexygen Plus” materials testing machine software developed by Lloyd Instruments (Fig. 5). Distributions up to break of Young’s modulus of bending versus stiffness as well as work to maximum load versus work to maximum deflection are shown in Figs. 6-7. To see the subsequent behavior of the composite, other bending tests have been carried out on five samples up to 50 mm deflection. These distributions are presented in Figs. 8-10 and a comparison between distributions at break and at 50 mm deflection are shown in Figs. 11-12.

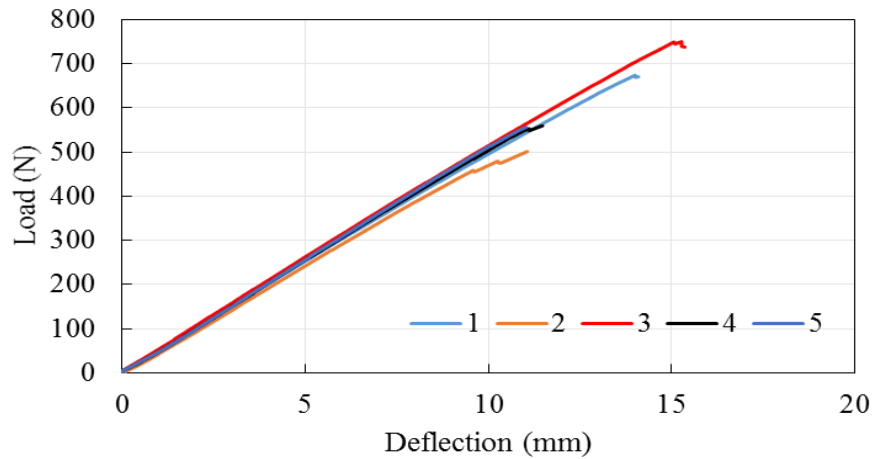


FIG. 5. Five load-deflection distributions up to break

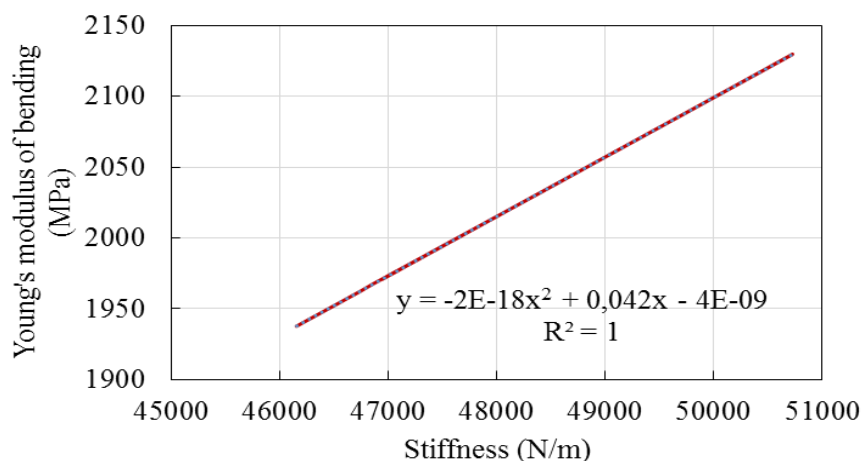


FIG. 6. Distribution up to break of Young’s modulus of bending versus stiffness

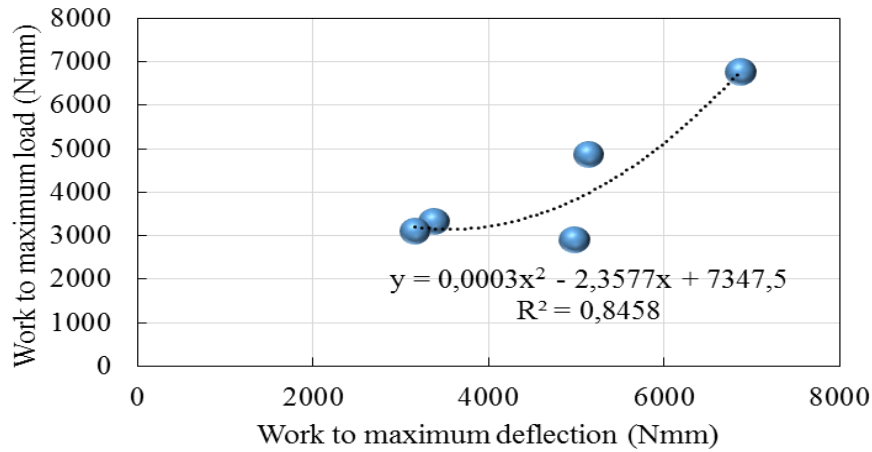


FIG. 7. Distribution up to break of work to maximum load/deflection

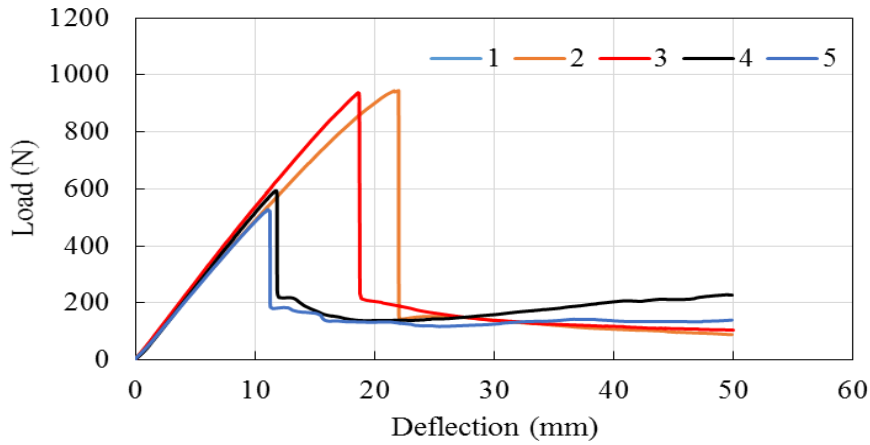


FIG. 8. Five load-deflection distributions up to 50 mm deflection

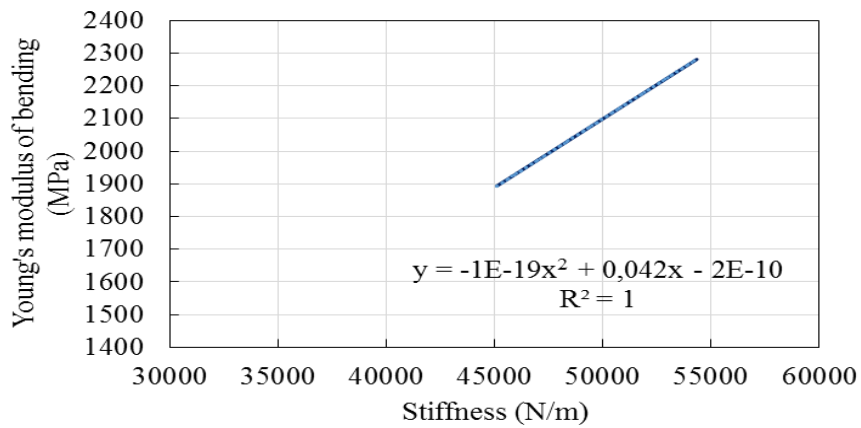


FIG. 9. Distribution up to 50 mm deflection of Young's modulus of bending versus stiffness

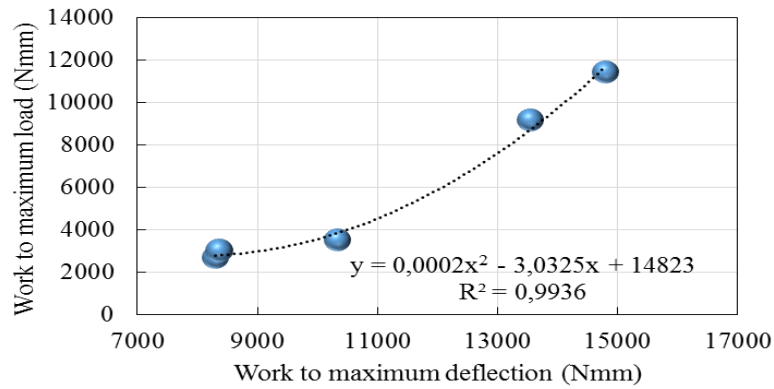


FIG. 10. Distribution up to 50 mm deflection of work to maximum load/deflection

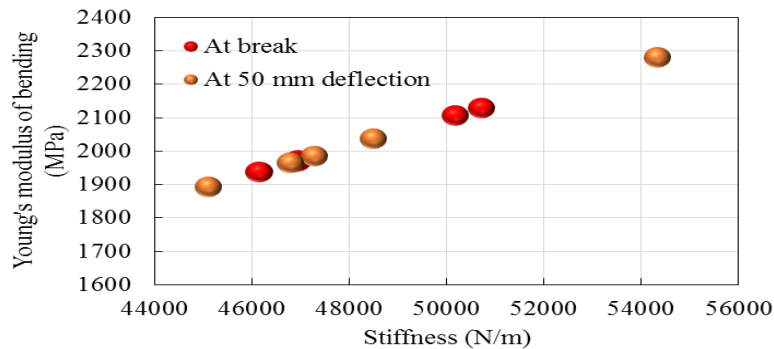


FIG. 11. Young's modulus of bending versus stiffness at break and 50 mm deflection

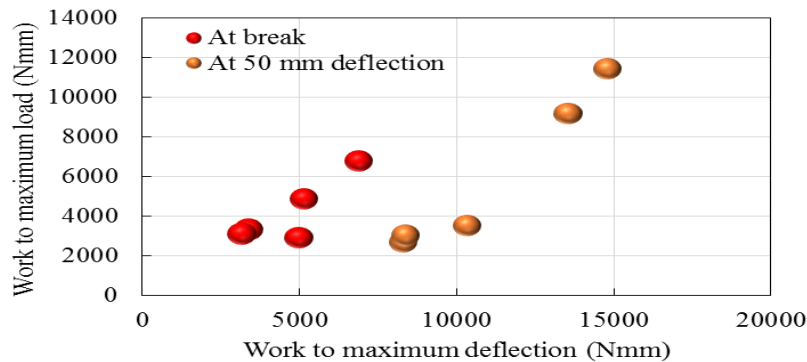


FIG. 12. Distributions of work to maximum load/deflection at break and 50 mm deflection

4. CONCLUSIONS

Load-deflection distributions of sandwich samples present a load variation between 500 - 950 N until irreversible damage occur. It can be noticed that the deflection that caused irreversible damage (drop of load) inside the composite material varies between 10.5 mm and 22 mm. Frequent deflection value at which irreversible damage has occurred was 10.5 mm. The developed sandwich of 3003 aluminum honeycomb core with 5.2 mm cell size, bonded with two layers of 380 g/m² specific weight woven glass fabric impregnated with epoxy resin presents low weight (under 10 kg for a panel with dimensions 2500x1200x13.8 mm) and high stiffness. These unique characteristics make this structure suitable especially for aerospace and defense applications, like shelters, doors, floors and other specific panels with maximum temperatures range up to 80°C.

REFERENCES

- [1] D. B. Miracle and R. L. Donaldson, *ASM Handbook Volume 21: Composites*, ASM International, 2001;
- [2] I. M. Daniel and O. Ishai, *Engineering of Composite Materials*, Oxford University Press, 2nd ed., 2005;
- [3] J. R. Vinson, *Plate and Panel Structures of Isotropic, Composite and Piezoelectric Materials, Including Sandwich Construction*, Springer, 1st ed., 2005;
- [4] L. C. Bank, *Composites for Construction: Structural Design with FRP Materials*, Wiley, 2006;
- [5] D. G. Lee and N. P. Suh, *Axiomatic Design and Fabrication of Composite Structures: Applications in Robots, Machine Tools, and Automobiles*, Oxford University Press, 2005;
- [6] A. B. Strong, *Fundamentals of Composites Manufacturing: Materials, Methods and Applications*, Society of Manufacturing Engineers, 2nd ed., 2007;
- [7] B. F. Backman, *Composite Structures, Design, Safety and Innovation*, Elsevier Science, 2005;
- [8] J. R. Vinson and R. L. Sierakowski, *The Behavior of Structures Composed of Composite Materials*, Springer, 2008;
- [9] H. Teodorescu-Draghicescu and S. Vlase, Homogenization and Averaging Methods to Predict Elastic Properties of Pre-Impregnated Composite Materials, *Computational Materials Science*, vol. 50, no. 4, pp. 1310-1314, 2011;
- [10] H. Teodorescu-Draghicescu, S. Vlase, M. L. Scutaru, L. Serbina and M. R. Calin, Hysteresis Effect in a Three-Phase Polymer Matrix Composite Subjected to Static Cyclic Loadings, *Optoelectronics and Advanced Materials – Rapid Communications*, vol. 5, no. 3, pp. 273-277, 2011;
- [11] S. Vlase, H. Teodorescu-Draghicescu, D. L. Motoc, M. L. Scutaru, L. Serbina and M. R. Calin, Behavior of Multiphase Fiber-Reinforced Polymers Under Short Time Cyclic Loading, *Optoelectronics and Advanced Materials – Rapid Communications*, vol. 5, no. 4, pp. 419-423, 2011;
- [12] S. Vlase, H. Teodorescu-Draghicescu, M. R. Calin and L. Serbina, Simulation of the Elastic Properties of Some Fibre-Reinforced Composite Laminates Under Off-Axis Loading System, *Optoelectronics and Advanced Materials – Rapid Communications*, vol. 5, no. 4, pp. 424-429, 2011;
- [13] H. Teodorescu-Draghicescu, A. Stanciu, S. Vlase, M. L. Scutaru, M. R. Calin and L. Serbina, Finite Element Method Analysis Of Some Fibre-Reinforced Composite Laminates, *Optoelectronics and Advanced Materials – Rapid Communications*, vol. 5, no. 7, pp. 782-785, 2011;
- [14] A. Stanciu, H. Teodorescu-Draghicescu, S. Vlase, M. L. Scutaru and M. R. Calin, Mechanical Behavior of CSM450 and RT800 Laminates Subjected to Four-Point Bend Tests, *Optoelectronics and Advanced Materials – Rapid Communications*, vol. 6, no. 3-4, pp. 495-497, 2012;
- [15] S. Vlase, H. Teodorescu-Draghicescu, M. R. Calin and M. L. Scutaru, Advanced Polylyte composite laminate material behavior to tensile stress on weft direction, *Journal of Optoelectronics and Advanced Materials*, vol. 14, no. 7-8, pp. 658-663, 2012;
- [16] H. Teodorescu-Draghicescu, M. L. Scutaru, D. Rosu, M. R. Calin and P. Grigore, New Advanced Sandwich Composite with twill weave carbon and EPS, *Journal of Optoelectronics and Advanced Materials*, vol. 15, no. 3-4, pp. 199-203, 2013;
- [17] A. Modrea, S. Vlase, H. Teodorescu-Draghicescu, M. Mihalca, M. R. Calin and C. Astalos, Properties of Advanced New Materials Used in Automotive Engineering, *Optoelectronics And Advanced Materials – Rapid Communications*, vol. 7, no. 5-6, pp. 452-455, 2013;
- [18] S. Vlase, R. Purcarea, H. Teodorescu-Draghicescu, M. R. Calin, I. Szava and M. Mihalca, Behavior of a new Heliopol/Stratimat300 composite laminate, *Optoelectronics And Advanced Materials – Rapid Communications*, vol. 7, no. 7-8, pp. 569-572, 2013;
- [19] T. Heitz, H. Teodorescu-Draghicescu, S. Lache, A. Chiru and M. R. Calin, Advanced T700/XB3585 UD carbon fibers-reinforced composite, *Journal of Optoelectronics and Advanced Materials*, vol. 16, no. 5-6, pp. 568-573, 2014;
- [20] H. Teodorescu-Draghicescu, S. Vlase, M. D. Stanciu, I. Curtu and M. Mihalca, Advanced Pultruded Glass Fibers-Reinforced Isophthalic Polyester Resin, *Materiale Plastice*, vol. 52, no. 1, pp. 62-64, 2015;
- [21] M. L. Scutaru, H. Teodorescu-Draghicescu, S. Vlase and M. Marin, Advanced HDPE with increased stiffness used for water supply networks, *Journal of Optoelectronics and Advanced Materials*, vol. 17, no. 3-4, pp. 484-488, 2015.

GAS TURBINE ENGINE COMBUSTORS AND THE ESTIMATION OF THEIR PRESSURE LOSS

Béla VARGA, Gyula ÓVÁRI, László KAVAS

National University of Public Service, Budapest, Hungary (varga.bela@uni-nke.hu, ovari.gyula@uni-nke.hu, kavas.laszlo@uni-nke.hu)

DOI: 10.19062/2247-3173.2017.19.1.41

Abstract: *The combustor is a crucial component of the gas turbine engines through which the chemical energy of the fuel is converted into thermal energy preferably with minimal pressure loss and maximal burner efficiency meanwhile the emitted harmful pollutants and the deposit must be minimised. That condition can be achieved through highly turbulent flow which description with numerical methods is difficult even today. In accordance with it the design of combustor is based more empiricism collected from the previous experiences and tests. In this paper we deal with the pressure loss in the combustors examining what kind of methods, empirical equations can be used to predict the estimated value of pressure loss. Using the Fanno and Rayleigh line flow we tried to determine the pressure loss in the combustor of TV2-117A turboshaft engine built in Mi-8 helicopter.*

Keywords: *gas turbine engine, combustor, pressure loss, Fanno line flow, nonisentropic irreversible flow, Rayleigh line flow, heat drag.*

1. HISTORIC REVIEW

By the end of World War II aircraft with traditional propulsion system (piston engine with propeller) practically achieved their limits. The flying speed of fighters approached 750 km/h and the flying altitude 12 km, meanwhile some special reconnaissance aircraft could reach 14 km. These limits considering the aerodynamics of aircraft and their propulsion systems were well known even before the war but that time the aircraft performance of participated countries were well below to the above mentioned limits. However, there was no strong intention in any country to find new revolutionary way of aircraft propulsion some inventors tried find new solutions. One of them was the British Frank Whittle whose work in this field unchallenged. His gas turbine (Fig 1.) in late 1930s had every element a modern gas turbine today has.

The first operational gas turbine, *Heinkel HE S3*, built in aircraft, was invented and built by Hans von Ohain, a German scientist. It was built in a Heinkel HE 178 aircraft, which maiden flight was made in August 27, 1939 and become the first ever aircraft propelled by gas turbine engine. In the 1940s the gas turbine engines became more and more frequently used in different aircraft, for example the German Messerschmitt Me 262, Arado 234, or the British Gloster Meteor (however this last one didn't take part in the air battles at the end of the war).

The early gas turbine engines suffered still numerous children's illnesses because of the lack of appropriate materials and technologies. The inventors practically were in the dark.

The problems emerged again and again had to be solved without any cooperation because before and during the WW II there was no any cooperation even within the Allied Forces. Every component of the gas turbine engine had its own problems. Very low compressor pressure ratio (2-3), and turbine inlet temperature due to the weak heat resistance of turbine blades and the lack of turbine cooling, meanwhile the component efficiencies were also very low, but the most serious problem was to create a heat resistant but efficient combustor. It proved to be a formidable task for both groups and, in Whittle's case, combustion problems dominated the first three years of engine development. Considering the isolated developing processes quite many different shapes, sizes, structures, vaporization solution appeared (Fig. 2.) that time.

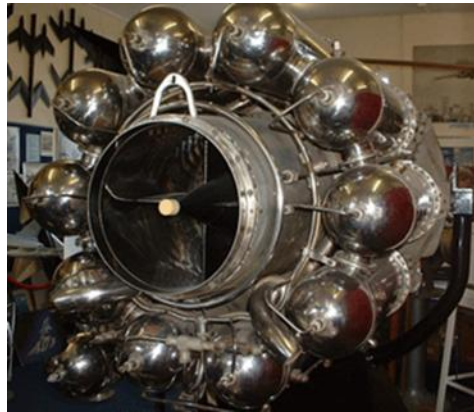


FIG. 1. Frank Whittle's gas turbine engine [1]

In the 1950s the gas turbines irrevocably conquered the aviation. By that time, the development work carried out in the UK, Germany, and the United States had established the basic design features of aero-engine combustors that have remained largely unchanged. The main components are a diffuser for reducing the compressor outlet air velocity to avoid high-pressure losses in combustion, a liner (or flame tube) that is arranged to be concentric within the outer combustor casing, means for supplying the combustion zone with atomized or vaporized fuel and, with tubular liners, interconnectors (or cross-fire tubes) through which hot gases can flow from a lighted liner to an adjacent unlighted liner.

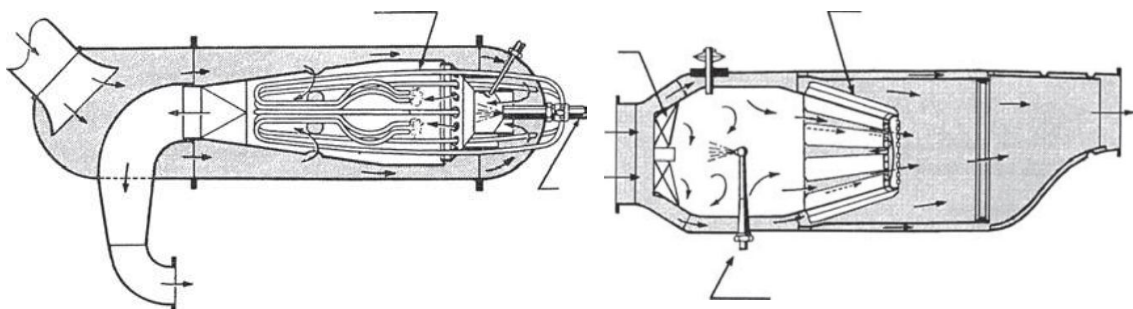


FIG. 2. To the left Frank Whittle's combustor, to the right combustor of JUMO 004 engine [5]

Since that the development has been continuous but without major breakthrough. Until the 1970s the designers of combustors were fully occupied with providing stable operation, low pressure loss and high burner efficiency, however, unfortunately, the last two are in antagonistic relation with each other.

Until 1980, little attention was paid to pollution, but since that time different ICAO regulations (ICAO '86, CAEP2-tól CAEP-8-ig) have pressed the manufacturers to decrease the emitted pollutants continuously and today that is the main aspect of developments.

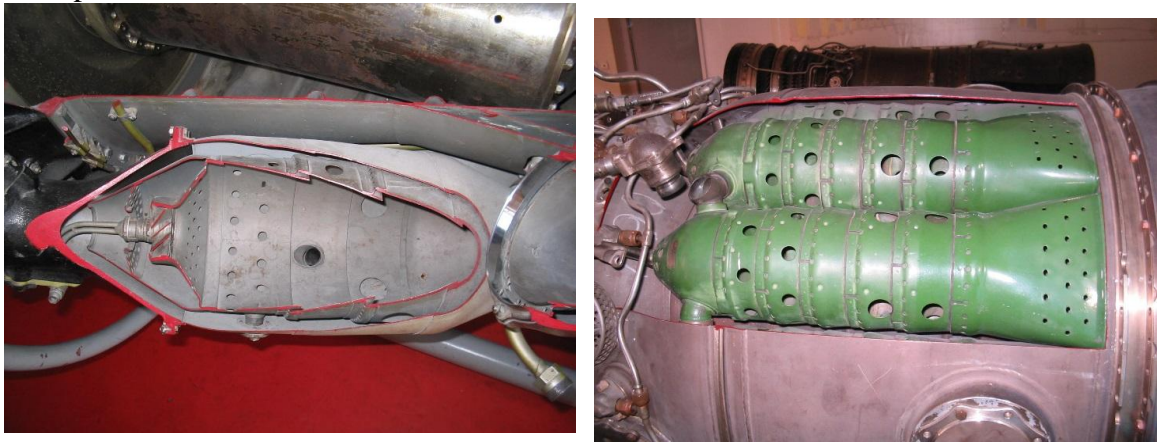


FIG. 3. To the left can (or tube) type, to the right tuboannular combustor [own photo]

In the last 70 years three different types of combustor layout have become widespread, namely the can or tube type, tuboannular (Fig. 3) and annular combustors (Fig. 4). Practically the first two due to their disadvantages are not used today. From the 1960s the annular combustors and their modifications have become generally used. In this type, an annular liner is mounted concentrically inside an annular casing. In many ways it is an ideal form of chamber, because its clean aerodynamic layout resulted a compact unit, lower weight and lower pressure loss (<5%) than other combustor types and in addition in the inlet section of the turbine they provide uniform flame temperature.



FIG. 4. To the left annular combustor, to the right an annular liner [own photo]

Nevertheless, the combustors had to be adapted to the continuously increasing performance of other gas turbine engine components. The combustor inlet temperature changed from at about 450 K to 900 K and the exit temperature from 1100 K to 1800 K or more (difficult to find correct data). The pressure changed from 5 bar to 50 bar.

Driven by the increased temperatures of the gas turbines and the need for improved emission control, significant development efforts have been made to advance the combustion hardware, by way of adopting sophisticated materials and processes. Traditionally combustor components have been fabricated out of sheet nickel-base superalloys.

Hastelloy X, a material with higher creep strength was used from 1960s to 1980s. Nimonic 263 was subsequently introduced and has still higher creep strength. As firing temperatures further increased in the newer gas turbine models, HA-188, a cobalt based superalloy has been recently adopted for some combustion system components for improved creep rupture strength. In addition to designing with improved materials, combustion liners and transition pieces of advanced and uprated machines involving higher temperatures are given a thermal barrier coating (TBC). The coating serves to provide an insulating layer and reduces the underlying base metal temperature [8].

Due to the above mentioned improvements some hundreds hour operational time of early gas turbine combustors has increased to some tens of thousands operational hours.

2. MAIN REQUIREMENTS IN THE DESIGN OF COMBUSTOR

The designer of gas turbine combustors has to face numerous hardships to meet the multiple requirements a combustor have to perform. The most important of them are bellow.

- Complete combustion to avoid the waste of fuel and to provide high burner efficiency;
- Minimal total pressure loss;
- The combustion must take place in turbine and never in turbine;
- The deposit creation on the liner must be avoided, because it can cause further pressure loss, hot spots, and they are signs of insufficient burning;
- Easy ignition and relight;
- Long lives, without any cracks and failure, because it can cause fatal accident;
- The exit temperature must be uniform both in space and time avoiding the heat stress;
- Stable flame in any operating conditions, air mass flow rate, flow speed and pressure;
- The flame in the combustor shouldn't be prone to flame out;
- Minimal weight and volume [7].

Minimal pressure loss is one of the basic requirements of any gas turbine combustor. The pressure loss is due to two different reasons. First effect is the friction of the working fluid flows through the combustor, while the second is the nonisentropic and irreversible heating in the combustor. None of them can be eliminated totally, what is more improving the mixing of air and fuel the necessary turbulence increases the pressure loss, consequently the turbulence shouldn't be any higher than necessary to ensure the good mix.

The two effects can be analyzed with two different methods, which are the Fanno and Rayleigh line flow models. These flow models have many analytical uses, most notably involving aircraft engines, for instance, the combustion chambers, which usually have a constant area and the fuel mass addition is negligible. The Fanno line flow is suitable to examine flow with friction but without heat addition, meanwhile the Rayleigh line flow is suitable to determine the pressure loss of flow with heat addition, but without friction.

3. FANNO LINE FLOW

Fanno line curve represents the relationship between the entropy and temperature of fluid flow in $S=S(T)$ coordinate system when the irreversible velocity change due to friction is associated with entropy change.

Fanno flow refers to adiabatic, steady ideal gas flow through a constant (or near constant) area duct where the effect of friction is considered. The change of entropy can be deducted using the energy conservation, mass conservation and ideal gas law, while the friction can be taken into consideration through the impulse momentum theory. The above mentioned equations can be used to plot the Fanno line, which represents a locus of states for given Fanno flow conditions on an T-S diagram.

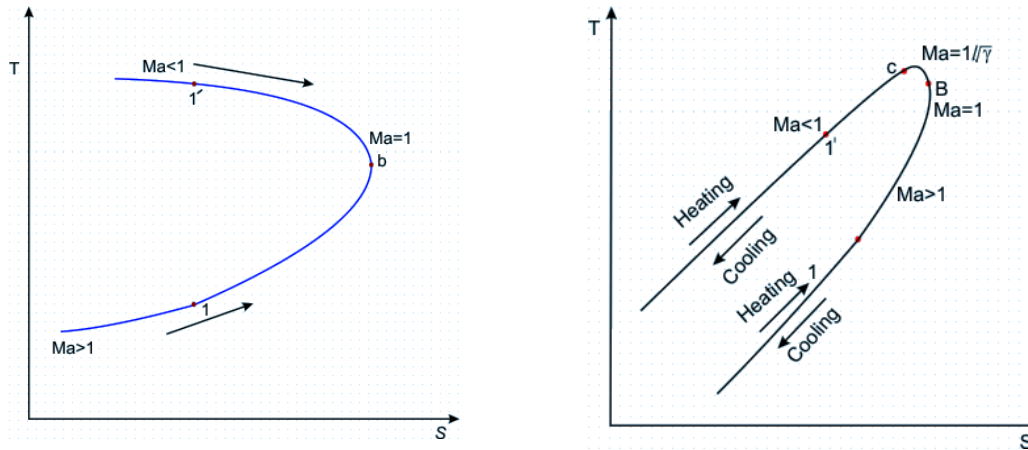


FIG. 5. To the left the Fanno line curve, to the right the Reyleigh line curve [3]

In Fig. 5. left side, the Fanno line reaches maximum entropy at point “b” and the flow is choked, $Ma=1$ (Ma : Mach number). According to the second law of thermodynamics, entropy must always increase for Fanno flow. This means that a subsonic flow entering a duct with friction will have an increase in its Mach number and if the duct is long enough, the flow is choked (with increasing length the working point moves from point $1'$ to b). Conversely, the Mach number of a supersonic flow will decrease until the flow is choked (with increasing length the working point moves from point 1 to b). In accordance with it each point on the Fanno line corresponds with a different Mach number, and the movement to choked flow [2;3].

For any initial (inlet section) state, duct geometry and friction coefficient (factor) the final (exit section) state can be determined easily using an online calculator called *Compressible Aerodynamics Calculator* [4], or an Android based smart phone application called *Compressible Flow Calculator*.

During the examination of the chosen combustor we used the above mentioned *Compressible Aerodynamics Calculator*. Using the known initial parameters in the inlet section of combustor, the combustor geometry and friction we can calculate the parameters in the final section (practically how much the working point $1'$ moves on the process curve to point b).

4. RAYLEIGH LINE FLOW

Rayleigh flow refers to frictionless, non-adiabatic flow through a constant (or near constant) area duct where the effect of heat addition or rejection is considered. Rayleigh line curve represents the relationship between the entropy and temperature of fluid flow in $S=S(T)$ coordinate system when the heat transfer is associated with entropy change.

In Fig. 5. right side, the Rayleigh line reaches maximum entropy at point “B” and the flow is choked, $Ma=1$. A subsonic flow entering a duct with heat addition will have an increase in its Mach number and at last the flow is choked.

Conversely, the Mach number of a supersonic flow will decrease with heat addition until the flow is choked at the same point. In accordance with it each point on the Rayleigh line corresponds with a different Mach number, and the movement to choked flow [2;3]. The maximum static temperature of the flow (point C), where $Ma=1/\gamma^{1/2}$.

In the same way we can presume the initial (inlet section) state is point 1' and with the heat addition the working point moves closer to point C. We can use the same *Compressible Aerodynamics Calculator* [4], like we used at Fanno line flow.

5. USING FANNO LINE FLOW TO CALCULATE THE FRICTION CAUSED PRESSURE LOSS OF TV2-117A ENGINE COMBUSTOR

The chosen rate of power is the take-off power. Earlier one of the authors made the thermodynamic cycle calculation and the analyses of the compressor stages. According to the analyses the total pressure, temperature, Mach number and adiabatic exponent (here gamma) respectively 662070 Pa, 523 K, 0,1744, 1,384 [6]. The total temperature in the exit section is 1148 K [6]. Length and the effective diameter of the chosen combustor are respectively 0.34 m and 0.086 m. The estimated friction coefficient is 0.04 [7].

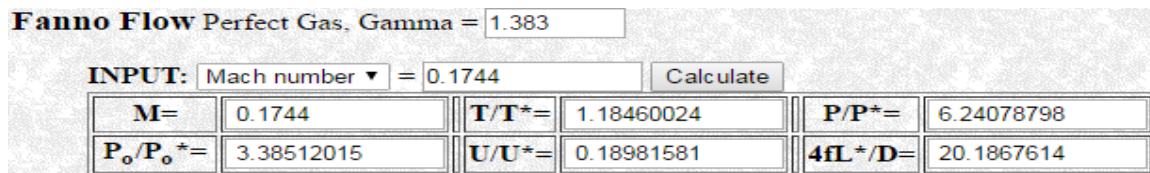


FIG. 6. Fanno variables at the inlet section of the combustor [4]

Filling the table with the necessary input data for the inlet section (Mach number and adiabatic exponent) we get the ratios of different variables, see Fig. 6.

Where: T, P, U, M : temperature, pressure, internal energy, Mach number respectively;

P_0 : the total pressure;

$T^* \dots U^*$: the value of the variables when the flow is choked ($M = 1$), the most right side point of Fanno Line curve;

P_0^* : the total pressure when the flow is choked ($M = 1$);

$4fL^*/D$: nondimensional length to diameter parameter;

f : Fanno friction factor ($1/4 \cdot$ Darcy friction factor);

L : length of the combustor;

D : effective diameter of the combustor;

σ_{sur} : pressure loss due to the friction in combustor (practically the ratio of exit and inlet total pressure).

As a next step is to modify the inlet $\left[\frac{4fL^*}{D} \right]_1$ factor (equation 1.) with the data of

examined stream tube (combustor) and insert it in the next round as input data and we get the ratios of different variables for the exit section, see Fig. 7.

$$\left[\frac{4fL^*}{D} \right]_1 = 20.1867 \quad \left[\frac{4fL^*}{D} \right]_{1-2} = \frac{4 \cdot 0.04 \cdot 0.34}{0.086} = 0,6325 \quad \left[\frac{4fL^*}{D} \right]_2 = 20.1867 - 0.6325 = 19.5542 \quad (1)$$

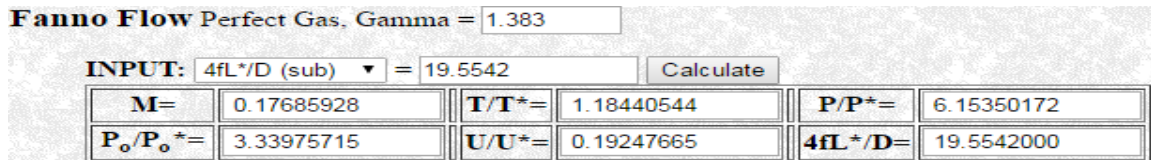


FIG. 7. Fanno variables at the exit section of the combustor [4]

We are interested in the ratio of exit total pressure and inlet total pressure. Since P_0^* refers to the total pressure when the flow is choked ($M = 1$) and that is unchanged we can create the equation 2 to determine the combustor pressure loss due to the friction.

$$\sigma_{friction} = \frac{P_{0(inlet)} / P_0^*}{P_{0(exit)} / P_0^*} = \frac{3,3397}{3,3851} \approx 0.9865 \quad (2)$$

The result of the calculation gave 0.9865 friction pressure loss, which is a normal value for that gas turbine combustor.

6. USING RAYLEIGH LINE FLOW TO CALCULATE THE HEAT TRANSFER CAUSED PRESSURE LOSS OF TV2-117A ENGINE COMBUSTOR

In this case we examine the combustor pressure loss due to temperature raise caused by the heat addition using the Rayleigh flow. This model can be applied to cases where the heat transfer is significant and the friction can be ignored.

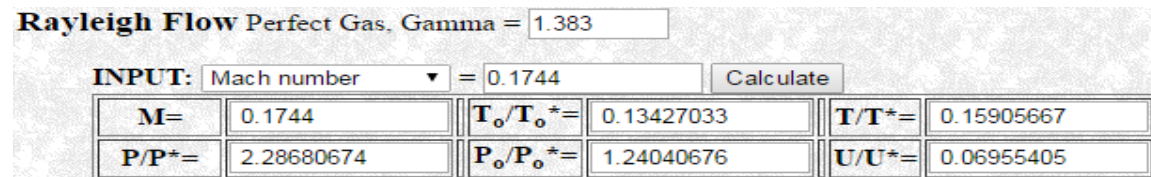


FIG. 8. Rayleigh variables at the inlet section of the combustor [4]

$$T_0^* = \frac{523K}{0,1342} = 3897K \quad p_0^* = \frac{662070Pa}{1,2404} = 533755Pa \quad \frac{T_{0out}}{T_0^*} = \frac{1148K}{3897K} = 0,2945 \quad (3)$$

Substituting the combustor inlet Mach number, we get the ratios of total variables and choked condition total variables (temperature and pressure). With these ratios we can calculate the choked condition total temperature and pressure for this combustor and the new temperature ratio for the exit section (T_{0out}/T_0^*), see equation 3. It is used in the next round of calculation as input data.

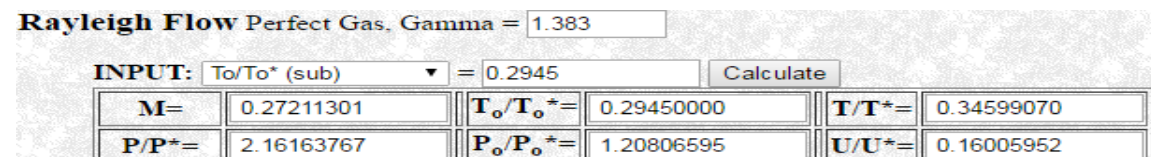


FIG. 9. Rayleigh variables at the exit section of the combustor [4]

From the new pressure ratio of total pressure and choked total pressure (p_0/p_0^*) the exit total pressure (p_{0exit}) can be calculated. Creating again the ratio of exit and inlet total pressure ratio we get the pressure loss (σ_{heat}) of the combustor due to the heat addition. Multiplying the two pressure losses with each other the total pressure loss can be calculated (σ_{Σ}).

$$p_{0_{exit}} = 1,2080 \cdot 533755 Pa = 644776 Pa \quad \sigma_{heat} = \frac{644776 Pa}{662070 Pa} \approx 0,9738 \quad \sigma_{\Sigma} \approx 0,9865 \cdot 0,9738 = 0,9607 \quad (4)$$

I used four decimal digits offered by the software, but of course in this case due to the other uncertainties it is less reasonable, but the final ~4% pressure loss is presumably close to correct considering the average pressure loss is at about 3-5%. Usually those are the values we use calculating the gas turbine thermodynamic cycles.

CONCLUSIONS

In gas turbine combustors basically two different losses can be defined. The first one is originated from the insufficient burning, which can be describe with the burning efficiency. The other one is the pressure loss, which is the main subject of our paper. The second loss also can be divided for two subtypes, namely the pressure loss caused by the friction and the pressure loss caused by the heat addition and temperature raise. However, we can also mention the fact that due to the specific nature of combustors increasing burner efficiency usually goes hand in hand with higher friction pressure loss. Considering this problem, the designer always has to make compromise to make the flow in the combustor only the necessarily turbulent providing good burner efficiency but keep the pressure loss as low as possible. Other pressure loss comes from the heat addition called heat drag. The result of this examination proved that 1/3 of the pressure loss is the friction loss while the other 2/3 is caused by the heat addition.

REFERENCES

- [1] url: http://it.wikipedia.org/wiki/File:Whittle_Jet_Engine_W2-700.JPG, (2013.07.15.).
- [2] url: http://www.ara.bme.hu/oktatas/letolt/1ljegyzet/GD_05p.htm, (2017.01.01.).
- [3] url: http://nptel.ac.in/courses/112104118/ui/Course_home-12.htm, (2017.01.01.).
- [4] url: <http://www.dept.aoe.vt.edu/~devenpor/aoe3114/calc.html>, (2017.01.01.).
- [5] A. H. LEFEBVRE, D. R. BALLAL, Gas Turbine Combustion, Alternative Fuels and Emissions, Taylor and Francis Group, 2010.
- [6] B. VARGA, A TV2-117A hajtómű termikus matematikai modellje, Diploma munka, Budapesti Műszaki Egyetem, 1990.
- [7] R. D. FLACK, Fundamentals of Jet Propulsion with Applications, Cambridge University Press, Cambridge, 2005.
- [8] url: <http://cdn.intechweb.org/pdfs/22905.pdf>, Materials for Gas Turbines–Overview, Nageswara Rao Muktinutalapati, VIT University, India, (2017.03.01.).

This work was supported by the European Regional Development Fund (GINOP 2.3.2-15-2016-00007, “Increasing and integrating the interdisciplinary scientific potential relating to aviation safety into the international research network at the National University of Public Service - VOLARE”). The project was realised through the assistance of the European Union, and co-financed by the European Regional Development Fund.



TRANSITION PROBABILITY MODELING FOR QUANTUM OPTICS

Alexandra BĂLUȚĂ, Diana ROTARU, Mihaela ILIE, Dragoș FĂLIE, Eugen VASILE

„Politehnica” University from Bucharest, Romania (alexandraa.baluta@gmail.com, evasevas@yahoo.com)

DOI: 10.19062/2247-3173.2017.19.1.42

Abstract: *The phenomenon of stimulated optical transition in anisotropic crystals that has been experimentally studied in our quantum lab; both its mathematical modeling and numerical simulation are approached. In order to evaluate the stimulated transition probability a revision of the perturbation theory equations is performed. For these equations the states spectrum of a quantum system being perturbed by an other system (in the frame of the quantum physics Hilbert space) is considered. Our formalization acts in accordance with the formal framework of information theory (characterized by: entropy, conditional entropy and mutual information) applied to two sources that interact, one being a perturbation of the other. In order to perform the numerical simulation the analytical relations are systematized. Some particular temporal patterns of the perturbation (e.g. (quasi) -rectangular or (envelope) -sinus, mono-pulse) and their corresponding transition probabilities are analyzed, then normalized and afterwards graphically represented using MathCAD.*

Keywords: *Quantum Optics, transition probability, MathCAD*

1. INTRODUCTION

The mathematical modeling and computer numerical simulation are necessary steps in the design of engineering quantum optics applications for quantum information processing.

But [1] “*these subjects follow either a semi-classical approach (often oversimplified), or a full quantum approach (often too difficult)*”. This is the motivation for this revised physical modeling based on mathematical rigorous description.

In order to numerically evaluate the stimulated transition probability of a system when interacting with an other system (in the frame of the quantum physics Hilbert space [2]) a revision of the perturbation theory equations is performed in agreement with the requirements of our software tool (mathCAD).

This formalization is in accordance with the formal framework of the information theory applied to the interaction of two sources, one of each being the perturbation of the other. The entropy, conditional entropy and mutual information are described.

In the case of quantum optics applications, when one desires to transmit information using “photons” *it is unrealistic to work with planar harmonic waves, requiring "wave packets" delimited in time and space* [3]. Instead, the impulsive waveforms are used, enabling the study of the temporal behaviour of both perturbation and light stimulated atoms.

Thus, the modeling and simulation succeeds to overcome the previously encountered difficulties as follows: a) to understand the treatment with real and complex signal representation (Fourier) for engineering applications; b)-to solve the equations complicated due to too many qualitative and quantitative approximations; c)- to be in agreement with the software requirements.

2. THE EVOLUTION OF STIMULATED QUANTUM SYSTEMS

Qualitative considerations

We perform a qualitative analysis with C^∞ class functions, as follows:

- a a stimulated quantum system: $a_t : [t_\alpha, t_\beta] \rightarrow \mathcal{Q}$
- ζ a perturbing quantum system (e.g. electromagnetic field): $\zeta_{t,\eta} : [t_\alpha, t_\beta] \times \mathcal{R} \rightarrow \mathcal{K}$

$$\zeta_{t,\eta} := \begin{cases} \neq \emptyset & t \in (t_0, t_*) \subseteq (t_\alpha, t_\beta) \\ = \emptyset & t \in [t_\alpha, t_\beta] - (t_0, t_*) \end{cases}; \quad \zeta_{t_0,\eta} \equiv \emptyset \equiv \zeta_{t_*,\eta}$$

$$\lim_{\eta \rightarrow 0} \zeta_{t,\eta} = \zeta_{t,0} = \emptyset$$

- the Taylor formal series after the control parameter $\eta \in \mathcal{R}$

$$\zeta_{t,\eta} = \zeta_{t,0} + \frac{\eta}{1!} \cdot \left(\frac{\partial \zeta_{t,\eta}}{\partial \eta} \right)_{\eta=0} + \frac{\eta^2}{2!} \cdot \left(\frac{\partial^2 \zeta_{t,\eta}}{\partial \eta^2} \right)_{\eta=0} + \dots; \quad \frac{1}{r!} \cdot \left(\frac{\partial^r \zeta_{t,\eta}}{\partial \eta^r} \right) =: \zeta_{t,\eta}^{<r>}$$

$$\zeta_{t,\eta} = \zeta_{t,0}^{<0>} + \eta \cdot \zeta_{t,0}^{<1>} + \eta^2 \cdot \zeta_{t,0}^{<2>} + \dots; \quad \zeta_{t,\eta}^{<0>} = \zeta_{t,\eta}, \quad \zeta_{t,0}^{<0>} = \zeta_{t,0} = \emptyset$$

$$\zeta_{t,\eta} = \eta \cdot \zeta_{t,0}^{<1>} + \eta^2 \cdot \zeta_{t,0}^{<2>} + \dots \text{ so for } \eta \rightarrow 0, \text{ asymptotically } \zeta_{t,\eta} \cong \eta \cdot \zeta_{t,0}^{<1>}$$

We emphasize the following *algebraic structuring*:

- intensive composition of a disjoint systems $a \in \mathcal{A}$ & $b \in \mathcal{B}$, disjoint $a \cap b = \emptyset = b \cap a$:
 $c = a \oplus b : \mathcal{A} \times \mathcal{B} \rightarrow \mathcal{C}$ binary composition law, (“superposition” by interaction),
intensive in the sense that any event $\omega_{a \oplus b}$ in the compound system $a \oplus b$ is defined by $\omega_{a \oplus b} := \omega_a \wedge \omega_b$, the intensive composition of an event ω_a in the system a with an event ω_b in the system b ; we have $a \oplus b = b \oplus a$, $a \oplus \emptyset = \emptyset \oplus a = a$.

- hybrid composition ($\lceil a \rceil$ and $\lfloor \zeta \rfloor$ isolated systems) as a limiting case of *integrated* compound case: $a \& \zeta = \lim_{a \rightarrow \lceil a \rceil, \zeta \rightarrow \lfloor \zeta \rfloor} (a \oplus \zeta)$, $\zeta \& a = \lim_{\zeta \rightarrow \lfloor \zeta \rfloor, a \rightarrow \lceil a \rceil} (\zeta \oplus a)$.

- absence of perturbation in composition (at $\eta := 0$ or $t := t_0$ or $t := t_*$):

$$(a \oplus \zeta)_{t,0} \equiv (a \oplus \emptyset)_t \equiv a_t \quad (\zeta \oplus a)_{t,0} \equiv (\emptyset \oplus a)_t \equiv a_t$$

$$(a \oplus \zeta)_{t_0,\eta} \equiv (a \oplus \emptyset)_{t_0} \equiv a_{t_0} \quad (\zeta \oplus a)_{t_0,\eta} \equiv (\emptyset \oplus a)_{t_0} \equiv a_{t_0}$$

$$(a \oplus \zeta)_{t_*,\eta} \equiv (a \oplus \emptyset)_{t_*} \equiv a_{t_*} \quad (\zeta \oplus a)_{t_*,\eta} \equiv (\emptyset \oplus a)_{t_*} \equiv a_{t_*}$$

- interaction reduces non-interaction: $\zeta \oplus a \subseteq \zeta \& a \equiv a \& \zeta \supseteq a \oplus \zeta$ and we define:
protocol (agreement) subsystems:

$$\underline{a \perp \zeta} \equiv a \perp \zeta = \zeta \& a - \zeta \oplus a \quad \zeta \text{ by } a, \quad \underline{\zeta \perp a} \equiv \zeta \perp a := a \& \zeta - a \oplus \zeta \quad a \text{ by } \zeta$$

$$a \perp \zeta = \emptyset \Leftrightarrow \zeta \oplus a = \zeta \& a \quad \zeta \perp a = \emptyset \Leftrightarrow a \oplus \zeta = a \& \zeta$$

$$(a \perp \zeta)_{t,\eta} = \zeta_{t,\eta} \& a_t - \zeta_{t,\eta} \oplus a_t \quad (\zeta \perp a)_{t,\eta} = a_t \& \zeta_{t,\eta} - a_t \oplus \zeta_{t,\eta}$$

and we have $(a \perp \zeta) = (\zeta \perp a)$, that is the protocol is mutual.

- the protocol is disjunctively filled with the composition

$$(a \perp \zeta) \cap (\zeta \oplus a) = \emptyset, \quad (a \perp \zeta) \cup (\zeta \oplus a) = \zeta \& a, \quad \zeta \oplus a = (\zeta \& a) - (a \perp \zeta)$$

$$(\zeta \perp a) \cap (a \oplus \zeta) = \emptyset, \quad (\zeta \perp a) \cup (a \oplus \zeta) = a \& \zeta, \quad a \oplus \zeta = (a \& \zeta) - (\zeta \perp a)$$

- the absence of perturbation abolishes the protocols:
 $(a \perp \zeta)_{t,0} \equiv a_t \perp \emptyset \equiv a_t \& \emptyset - a_t \oplus \emptyset \equiv a_t - a_t \equiv \emptyset$; $a_t \perp \zeta_{t,0} \equiv \zeta_{t,0} \perp a_t \equiv \emptyset$
 $(a \perp \zeta)_{t_0,\eta} \equiv a_{t_0} \perp \emptyset = a_{t_0} \& \emptyset - a_{t_0} \oplus \emptyset = a_{t_0} - a_{t_0} = \emptyset$
 $(a \perp \zeta)_{t_s,\eta} \equiv a_{t_s} \perp \emptyset = a_{t_s} \& \emptyset - a_{t_s} \oplus \emptyset = a_{t_s} - a_{t_s} = \emptyset$; $a_{t_s} \perp \zeta_{t_s,\eta} \equiv \zeta_{t_s,\eta} \perp a_{t_s} \equiv \emptyset$
- conditioning:
 $\underline{\zeta | a} \equiv \zeta | a$, $(\zeta | a)_{t,\eta} = \zeta_{t,\eta} | a_t$ the perturbing ζ under conditions imposed by a
 $\underline{a | \zeta} \equiv a | \zeta$, $(a | \zeta)_{t,\eta} = a_t | \zeta_{t,\eta}$ the chosen system a under conditions imposed by ζ

"imposed conditions" \equiv "constitutive laws" of the interaction

- the absence of perturbation abolishes conditionalities:
 $(a | \zeta)_{t,0} \equiv a_t | \emptyset \equiv \emptyset$ $(a | \zeta)_{t_0,\eta} \equiv a_{t_0} | \emptyset \equiv \emptyset$ $(a | \zeta)_{t_s,\eta} \equiv a_{t_s} | \emptyset \equiv \emptyset$
 $(\zeta | a)_{t,0} \equiv \emptyset | a_t \equiv \emptyset$ $(\zeta | a)_{t_0,\eta} \equiv \emptyset | a_{t_0} \equiv \emptyset$ $(\zeta | a)_{t_s,\eta} \equiv \emptyset | a_{t_s} \equiv \emptyset$
- conditionalities are disjunctively complemented by protocols
 $(a | \zeta) \cap (a \perp \zeta) = \emptyset$, $a = (a | \zeta) \& (a \perp \zeta)$, $a \perp \zeta = a - (a | \zeta)$
 $(\zeta | a) \cap (\zeta \perp a) = \emptyset$, $\zeta = (\zeta | a) \& (\zeta \perp a)$, $\zeta \perp a = \zeta - (\zeta | a)$
- conditionalities determine the compositions (**general relations of interactions**)
 $a \oplus \zeta = (a \& \zeta) - (\zeta \perp a) = a \& \zeta - [\zeta - (\zeta | a)] = [(a \& \zeta) - \zeta] \& (\zeta | a) = a \& (\zeta | a)$
 $\zeta \oplus a = (\zeta \& a) - (a \perp \zeta) = \zeta \& a - [a - (a | \zeta)] = [(\zeta \& a) - a] \& (a | \zeta) = \zeta \& (a | \zeta)$
 $a \& (\zeta | a) = a \oplus \zeta = \zeta \oplus a = \zeta \& (a | \zeta)$, $a \& (\zeta) = a \& \zeta = \zeta \& a = \zeta \& (a)$

These relationships, about the idea of of interaction system vs. perturbation, are in agreement with the formal framework of information theory: regarding: state vs probability / entropy, protocol vs mutual information / transinformation, interaction vs conditional probability / conditional entropy.

3. QUANTITATIVE OPERATOR CONSIDERATIONS

According to quantum physics we have the self-adjoint operators:

- ω temporal pulse operator (ω_{a_t} , $\omega_{\zeta_{t,\eta}}$, $\omega_{(a \oplus \zeta)_{t,\eta}}$)
- \mathbf{H} hamiltonian operator (\mathbf{H}_{a_t} , $\mathbf{H}_{\zeta_{t,\eta}}$, $\mathbf{H}_{(a \oplus \zeta)_{t,\eta}}$)
- the quantum temporal condition (operator format): $\mathbf{H} = \hbar \cdot \omega$
- the total time derivation of an operator \mathbf{A} using the Hamiltonian commutator:
 $d\mathbf{A} / dt = \partial\mathbf{A} / \partial t + [\mathbf{H}, \mathbf{A}]$ so that $d\mathbf{H} / dt = \partial\mathbf{H} / \partial t + [\mathbf{H}, \mathbf{H}] = \partial\mathbf{H} / \partial t$

The general relationships of the quantitative form of interaction are:

- \oplus - integrated composition: $\mathbf{H}_{a_t} + \mathbf{H}_{(\zeta|a)_{t,\eta}} = \mathbf{H}_{(a \oplus \zeta)_{t,\eta}} = \mathbf{H}_{(\zeta \oplus a)_{t,\eta}} = \mathbf{H}_{\zeta_{t,\eta}} + \mathbf{H}_{(a|\zeta)_{t,\eta}}$
- $\&$ - hybrid composition ($\zeta | a = \zeta$): $\mathbf{H}_{a_t} + \mathbf{H}_{\zeta_{t,\eta}} = \mathbf{H}_{(a \& \zeta)_{t,\eta}} = \mathbf{H}_{(\zeta \& a)_{t,\eta}} = \mathbf{H}_{\zeta_{t,\eta}} + \mathbf{H}_{a_t}$

For the isolated (unperturbed - time stationary) system a we have $\partial a_t / \partial t = \emptyset$ and the time flows uniformly ($\partial \mathbf{H}_{a_t} / \partial t = \mathbf{0}$), so that $d\mathbf{H}_{a_t} / dt = \partial \mathbf{H}_{a_t} / \partial t = \mathbf{0}$; $\mathbf{H}_{a_t} \equiv \mathbf{H}_a$.

- the equations with eigen states and values are: $\mathbf{H}_a \cdot \mathbf{s}_n = E_n \cdot \mathbf{s}_n$, $\omega_a \cdot \mathbf{s}_n = \omega_n \cdot \mathbf{s}_n$; with $E_n = \hbar \cdot \omega_n$ & spectral differences: $E^{p,m} := E_m - E_p$, $\omega^{p,m} := \omega_m - \omega_p$; $E^{p,m} = \hbar \cdot \omega^{p,m}$.
- the orthonormal basis $\{\mathbf{s}_n | n \in \mathbb{S}\}$ of eigenstates has the properties:
 $\langle \mathbf{s}_p | \mathbf{s}_m \rangle = \langle \mathbf{s}_p | \cdot | \mathbf{s}_m \rangle = \delta_p^m = \overline{\delta_p^m} = \overline{\langle \mathbf{s}_p | \cdot | \mathbf{s}_m \rangle}$, $\langle \mathbf{s}_p | \cdot | \mathbf{s}_n \rangle \cdot \overline{\langle \mathbf{s}_n | \cdot | \mathbf{s}_m \rangle} = \delta_p^n \cdot \delta_n^m$,

$$\sum_n \langle \mathbf{s}_p | \cdot \langle \overline{\mathbf{s}_n} | \cdot \langle \overline{\mathbf{s}_n} | \cdot | \mathbf{s}_m \rangle = \sum_n \delta_p^n \cdot \delta_n^m, \sum_n \langle \overline{\mathbf{s}_n} | \cdot \langle \overline{\mathbf{s}_n} | = [\mathbf{I}] = \sum_n | \mathbf{s}_n \rangle \cdot \langle \mathbf{s}_n |$$

▪ the quantum state of (isolated) a_t , in general format, is a linear combinations

$$\Psi_{a_t} = \sum_n c_{a_t}^n \cdot \mathbf{s}_n \quad \& \quad c_{a_t}^n / c_{a_0}^n = e^{-i\omega_n \cdot (t-t_0)} \quad (\text{Schrödinger eq.}) \quad \text{hence} \quad \Psi_{a_t} = \sum_n c_{a_0}^n \cdot e^{-i\omega_n \cdot (t-t_0)} \cdot \mathbf{s}_n$$

where usually $t_0 := t_0 := 0$.

We analyze the state for hybrid system $a \& \zeta = \zeta \& a$ vs. for composed system $a \oplus \zeta$; so $\mathbf{H}_a + \mathbf{H}_\zeta = \mathbf{H}_{a\&\zeta} = \mathbf{H}_{\zeta\&a} = \mathbf{H}_\zeta + \mathbf{H}_a$ and we have two formats:

▪ *format: $a \oplus \zeta = a \& \zeta - (\zeta \perp a) = \zeta \& a - (a \perp \zeta) = \zeta \oplus a$*

$$\mathbf{H}_a + \mathbf{H}_\zeta - \mathbf{H}_{\zeta \perp a} = \mathbf{H}_{a \oplus \zeta} = \mathbf{H}_{\zeta \oplus a} = \mathbf{H}_\zeta + \mathbf{H}_a - \mathbf{H}_{a \perp \zeta}$$

$$\mathbf{H}_{\zeta \perp a} := \mathbf{H}_a + \mathbf{H}_\zeta - \mathbf{H}_{a \oplus \zeta} \quad \mathbf{H}_{a \perp \zeta} := \mathbf{H}_\zeta + \mathbf{H}_a - \mathbf{H}_{\zeta \oplus a}$$

$$\mathbf{H}_a + \mathbf{H}_\zeta = \mathbf{H}_{a \oplus \zeta} = \mathbf{H}_{\zeta \oplus a} = \mathbf{H}_\zeta + \mathbf{H}_a \Leftrightarrow \mathbf{H}_{\zeta \perp a} = \mathbf{0} = \mathbf{H}_{a \perp \zeta},$$

▪ *format: $a \& (\zeta | a) = a \oplus \zeta = \zeta \oplus a = \zeta \& (a | \zeta)$, $\mathbf{H}_a + \mathbf{H}_{\zeta|a} = \mathbf{H}_{a \oplus \zeta} = \mathbf{H}_{\zeta \oplus a} = \mathbf{H}_\zeta + \mathbf{H}_{a| \zeta}$*

$$\mathbf{H}_{\zeta|a} := \mathbf{H}_{a \oplus \zeta} - \mathbf{H}_a \quad (\text{perturbant hamiltonian}) \quad \mathbf{H}_{a| \zeta} := \mathbf{H}_{\zeta \oplus a} - \mathbf{H}_\zeta \quad (\text{perturbed hamiltonian})$$

$$\mathbf{H}_a + \mathbf{H}_\zeta = \mathbf{H}_{a \oplus \zeta} = \mathbf{H}_{\zeta \oplus a} = \mathbf{H}_\zeta + \mathbf{H}_a \Leftrightarrow \zeta | a \equiv \zeta \quad \& \quad a | \zeta \equiv a$$

We describe perturbing action in the format $\mathbf{H}_{a \oplus \zeta} = \mathbf{H}_a + \mathbf{H}_{\zeta|a}$, as follows:

▪ the quantum system state $a \oplus \zeta$ (general format) is $\Psi_{a_t \oplus \zeta_{t,\eta}} = \sum_n c_{a_t \oplus \zeta_{t,\eta}}^n \cdot \mathbf{s}_n$ where

$$c_{a_t \oplus \zeta_{t,\eta}}^n \neq c_{a_t}^n, \text{ because } a \text{ interacts with } \zeta; \quad c_{a_t \oplus \zeta_{t,0}}^n = c_{a_t}^n, \quad \Psi_{a_t \oplus \zeta_{t,0}} \equiv \Psi_{a_t}, \quad c_{a_0 \oplus \zeta_{t_0,\eta}}^n = c_{a_0}^n,$$

$$\Psi_{a_0 \oplus \zeta_{t_0,\eta}} \equiv \Psi_{a_0}, \quad \Psi_{a_0 \oplus \zeta_{t_0,\eta}} = \sum_n c_{a_0 \oplus \zeta_{t_0,\eta}}^n \cdot \mathbf{s}_n.$$

▪ we practice a double coefficient relativization $\frac{c_{a_t \oplus \zeta_{t,\eta}}^n}{c_{a_t}^n / c_{a_0}^n} = \frac{c_{a_t \oplus \zeta_{t,\eta}}^n}{e^{-i\omega_n \cdot (t-t_0)}} =: \gamma_{a_t \oplus \zeta_{t,\eta}}^n$ so that:

$$\gamma_{a_t \oplus \zeta_{t,\eta}}^n := c_{a_t \oplus \zeta_{t,\eta}}^n \cdot e^{i\omega_n \cdot (t-t_0)}, \quad c_{a_t \oplus \zeta_{t,\eta}}^n = \gamma_{a_t \oplus \zeta_{t,\eta}}^n \cdot e^{-i\omega_n \cdot (t-t_0)}, \quad \gamma_{a_t \oplus \zeta_{t,0}}^n = c_{a_t \oplus \zeta_{t,0}}^n \cdot e^{i\omega_n \cdot (t-t_0)},$$

$$\gamma_{a_t}^n := c_{a_t}^n \cdot e^{i\omega_n \cdot (t-t_0)}, \quad \gamma_{a_0}^n = c_{a_0}^n, \quad c_{a_t \oplus \zeta_{t,0}}^n = \gamma_{a_t \oplus \zeta_{t,0}}^n \cdot e^{-i\omega_n \cdot (t-t_0)}, \quad c_{a_t}^n = \gamma_{a_t}^n \cdot e^{-i\omega_n \cdot (t-t_0)},$$

$$c_{a_0}^n = \gamma_{a_0}^n, \quad \gamma_{a_0 \oplus \zeta_{t_0,\eta}}^n = c_{a_0 \oplus \zeta_{t_0,\eta}}^n = c_{a_0}^n = \gamma_{a_0}^n$$

▪ the state vectors are:

$$\Psi_{a_t \oplus \zeta_{t,\eta}} = \sum_n c_{a_t \oplus \zeta_{t,\eta}}^n \cdot \mathbf{s}_n = \sum_n \gamma_{a_t \oplus \zeta_{t,\eta}}^n \cdot e^{-i\omega_n \cdot (t-t_0)} \cdot \mathbf{s}_n, \quad \Psi_{a_0} = \sum_n c_{a_0}^n \cdot \mathbf{s}_n = \sum_n \gamma_{a_0}^n \cdot \mathbf{s}_n \quad \text{where}$$

$$\Psi_{a_0 \oplus \zeta_{t_0,\eta}} \equiv \Psi_{a_0 \oplus \emptyset} = \Psi_{a_0}$$

▪ If $\Psi_{a_0}^p = \sum_n c_{a_0}^{n|p} \cdot \mathbf{s}_n \equiv \sum_n c_{a_0 \oplus \zeta_{t_0,\eta}}^{n|p} \cdot \mathbf{s}_n$ then $\Psi_{a_t \oplus \zeta_{t,\eta}}^p = \sum_{n'} c_{a_t \oplus \zeta_{t,\eta}}^{n'|p} \cdot \mathbf{s}_{n'}$, and the probability

$$P_{\Psi_{a_0}^p \mapsto \Psi_{a_t \oplus \zeta_{t,\eta}}^m} \equiv P_{\eta,t|t_0}^{m|p} \quad \text{to find } a \text{ in the state } \Psi_{a_t \oplus \zeta_{t,\eta}}^m = \sum_{n''} c_{a_t \oplus \zeta_{t,\eta}}^{n''|m} \cdot \mathbf{s}_{n''} \text{ represent the probability}$$

that the system a to perform in the temporal interval $[t_0, t]$ transition from state $\Psi_{a_0}^p$ in the state $\Psi_{a_t \oplus \zeta_{t,\eta}}^m$ or otherwise, from state $\Psi_{a_0 \oplus \zeta_{t_0,\eta}}^p$ in the state $\Psi_{a_t \geq t_0 \oplus \zeta_{t \geq t_0,\eta}}^m$ is:

$$\begin{aligned}
 P_{\eta,t|t_0}^{m|p} &= P_{\Psi_{a_0}^p \mapsto \Psi_{a_t \oplus \zeta_{t,\eta}}^m} = \left| \left\langle \Psi_{a_t \oplus \zeta_{t,\eta}}^p \left| \Psi_{a_t \oplus \zeta_{t,\eta}}^m \right. \right\rangle \right|^2 = \left| \left\langle \sum_{n'} c_{a_t \oplus \zeta_{t,\eta}}^{n'|p} \cdot \mathbf{s}_{n'} \left| \sum_{n''} c_{a_t \oplus \zeta_{t,\eta}}^{n''|m} \cdot \mathbf{s}_{n''} \right. \right\rangle \right|^2 \\
 &= \left| \sum_{n'} \sum_{n''} c_{a_t \oplus \zeta_{t,\eta}}^{n'|p} \cdot \overline{c_{a_t \oplus \zeta_{t,\eta}}^{n''|m}} \cdot \langle \mathbf{s}_{n'} | \mathbf{s}_{n''} \rangle \right|^2 = \left| \sum_{n'} \sum_{n''} c_{a_t \oplus \zeta_{t,\eta}}^{n'|p} \cdot \overline{c_{a_t \oplus \zeta_{t,\eta}}^{n''|m}} \cdot \delta_{n',n''} \right|^2 = \left| \sum_n c_{a_t \oplus \zeta_{t,\eta}}^{n|p} \cdot \overline{c_{a_t \oplus \zeta_{t,\eta}}^{n|m}} \right|^2
 \end{aligned}$$

$$\text{We have also: } P_{\eta,t|t_0}^{m|p} = \left| \sum_n \gamma_{a_t \oplus \zeta_{t,\eta}}^{n|p} \cdot e^{-i \cdot \omega_n \cdot (t-t_0)} \cdot \overline{\gamma_{a_t \oplus \zeta_{t,\eta}}^{n|m}} \cdot e^{-i \cdot \omega_n \cdot (t-t_0)} \right|^2 = \left| \sum_n \gamma_{a_t \oplus \zeta_{t,\eta}}^{n|p} \cdot \overline{\gamma_{a_t \oplus \zeta_{t,\eta}}^{n|m}} \right|^2$$

We proceed to perturbation series expansion of interaction hamiltonian:

$$\blacksquare \mathbf{H}_{\zeta_{t,\eta}|a_t} = \mathbf{H}_{\zeta_{t,0}|a_t} + \frac{\eta}{1!} \cdot \left(\frac{\partial \mathbf{H}_{\zeta_{t,\eta}|a_t}}{\partial \eta} \right)_{\eta=0} + \frac{\eta^2}{2!} \cdot \left(\frac{\partial^2 \mathbf{H}_{\zeta_{t,\eta}|a_t}}{\partial \eta^2} \right)_{\eta=0} + \dots$$

$$\blacksquare \text{ but } \forall t, \lim_{\eta \rightarrow 0} \mathbf{H}_{\zeta_{t,\eta}|a_t} = \mathbf{H}_{\zeta_{t,0}|a_t} = \mathbf{H}_{\emptyset|a_t} = \mathbf{H}_{\emptyset} = \mathbf{0}, \text{ so}$$

$$\blacksquare \mathbf{H}_{\zeta_{t,\eta}|a_t} = \frac{\eta}{1!} \cdot \left(\frac{\partial \mathbf{H}_{\zeta_{t,\eta}|a_t}}{\partial \eta} \right)_{\eta=0} + \frac{\eta^2}{2!} \cdot \left(\frac{\partial^2 \mathbf{H}_{\zeta_{t,\eta}|a_t}}{\partial \eta^2} \right)_{\eta=0} + \dots \equiv \eta \cdot \mathcal{H}_{\zeta_{t,\eta}|a_t}$$

$$\blacksquare \mathcal{H}_{\zeta_{t,\eta}|a_t} := \mathbf{H}_{\zeta_{t,\eta}|a_t} / \eta \text{ is the parametric Hamiltonian perturbation mean density:}$$

$$\mathcal{H}_{\zeta_{t,\eta}|a_t} \equiv \mathcal{H}_{\zeta_{t,0}|a_t} + \eta \cdot \mathcal{R}_{\zeta_{t,\eta}|a_t}, \quad \mathcal{H}_{\zeta_{t,0}|a_t} \equiv \left(\frac{\partial \mathbf{H}_{\zeta_{t,\eta}|a_t}}{\partial \eta} \right)_{\eta=0}, \quad \mathcal{R}_{\zeta_{t,\eta}|a_t} \equiv \sum_{r=2}^{\infty} \frac{\eta^{r-2}}{r!} \left(\frac{\partial^r \mathbf{H}_{\zeta_{t,\eta}|a_t}}{\partial \eta^r} \right)_{\eta=0}$$

$$\mathcal{H}_{\zeta_{t,0}|a_t} = \lim_{\eta \rightarrow 0} \mathcal{H}_{\zeta_{t,\eta}|a_t} = \lim_{\eta \rightarrow 0} \frac{\mathbf{H}_{\zeta_{t,\eta}|a_t}}{\eta} = \left(\frac{\partial \mathbf{H}_{\zeta_{t,\eta}|a_t}}{\partial \eta} \right)_{\eta=0} \neq \mathbf{0}$$

$$\mathbf{H}_{\zeta_{t,\eta}|a_t} \equiv \eta \cdot \mathcal{H}_{\zeta_{t,0}|a_t} + \mathcal{O}(\eta^2), \text{ for } \eta \rightarrow 0, \text{ asymptotic: } \mathbf{H}_{\zeta_{t,\eta}|a_t} \cong \eta \cdot \mathcal{H}_{\zeta_{t,0}|a_t}$$

$$\mathbf{H}_{\zeta_{t,\eta} \oplus a_t} = \mathbf{H}_{a_t} + \mathbf{H}_{\zeta_{t,\eta}|a_t} \equiv \mathbf{H}_{a_t} + \eta \cdot \mathcal{H}_{\zeta_{t,\eta}|a_t} \cong \mathbf{H}_{a_t} + \eta \cdot \mathcal{H}_{\zeta_{t,0}|a_t}$$

• The Schrödinger equation [2] for the system is:

$$i \cdot \hbar \cdot \frac{d\psi(t)}{dt} = \mathbf{H} \cdot \psi(t) \text{ or in matriceal form: } i \cdot \hbar \cdot \frac{\partial}{\partial t} |\psi(t)\rangle = [\mathbf{H}] \cdot |\psi(t)\rangle \text{ and we apply:}$$

$$i \cdot \hbar \cdot \frac{\partial \Psi_{a_t \oplus \zeta_{t,\eta}}}{\partial t} = \mathbf{H}_{a_t \oplus \zeta_{t,\eta}} \cdot \Psi_{a_t \oplus \zeta_{t,\eta}} = \mathbf{H}_{a_t} \cdot \Psi_{a_t \oplus \zeta_{t,\eta}} + \eta \cdot \mathcal{H}_{\zeta_{t,0}|a_t} \cdot \Psi_{a_t \oplus \zeta_{t,\eta}},$$

$$i \cdot \hbar \cdot \frac{\partial}{\partial t} |\Psi_{a_t \oplus \zeta_{t,\eta}}\rangle = [\mathbf{H}_{a_t \oplus \zeta_{t,\eta}}] \cdot |\Psi_{a_t \oplus \zeta_{t,\eta}}\rangle, \quad i \cdot \hbar \cdot \frac{\partial}{\partial t} |\Psi_{a_t \oplus \zeta_{t,\eta}}\rangle = [\mathbf{H}_{a_t \oplus \zeta_{t,\eta}}] \cdot |\Psi_{a_t \oplus \zeta_{t,\eta}}\rangle$$

we project this equation on an eigenstates \mathbf{s}_m of $\mathbf{H}_{a_t} \equiv \mathbf{H}_a$:

$$i \cdot \hbar \cdot \frac{\partial \langle \Psi_{a_t \oplus \zeta_{t,\eta}} | \mathbf{s}_m \rangle}{\partial t} = \langle \mathbf{H}_{a_t} \cdot \Psi_{a_t \oplus \zeta_{t,\eta}} | \mathbf{s}_m \rangle + \eta \cdot \langle \mathcal{H}_{\zeta_{t,0}|a_t} \cdot \Psi_{a_t \oplus \zeta_{t,\eta}} | \mathbf{s}_m \rangle \text{ with:}$$

$$\Psi_{a_t \oplus \zeta_{t,\eta}} = \sum_n c_{a_t \oplus \zeta_{t,\eta}}^n \cdot \mathbf{s}_n = \sum_n \gamma_{a_t \oplus \zeta_{t,\eta}}^n \cdot e^{-i \cdot \omega_n \cdot (t-t_0)} \cdot \mathbf{s}_n$$

$$\langle \Psi_{a_t \oplus \zeta_{t,\eta}} | \mathbf{s}_m \rangle = \left\langle \sum_n c_{a_t \oplus \zeta_{t,\eta}}^n \cdot \mathbf{s}_n \left| \mathbf{s}_m \right. \right\rangle = \sum_n c_{a_t \oplus \zeta_{t,\eta}}^n \cdot \langle \mathbf{s}_n | \mathbf{s}_m \rangle = \sum_n c_{a_t \oplus \zeta_{t,\eta}}^n \cdot \delta_n^m = c_{a_t \oplus \zeta_{t,\eta}}^m$$

$$\langle \mathbf{H}_{a_t} \cdot \Psi_{a_t \oplus \zeta_{t,\eta}} | \mathbf{s}_m \rangle = \langle \Psi_{a_t \oplus \zeta_{t,\eta}} | \mathbf{H}_{a_t}^\dagger \cdot \mathbf{s}_m \rangle = \langle \Psi_{a_t \oplus \zeta_{t,\eta}} | \mathbf{H}_{a_t} \cdot \mathbf{s}_m \rangle = \langle \Psi_{a_t \oplus \zeta_{t,\eta}} | E_m \cdot \mathbf{s}_m \rangle$$

$$= E_m \cdot \left\langle \sum_n c_{a_t \oplus \zeta_{t,\eta}}^n \cdot \mathbf{s}_n \left| \mathbf{s}_m \right. \right\rangle = E_m \cdot \sum_n c_{a_t \oplus \zeta_{t,\eta}}^n \cdot \langle \mathbf{s}_n | \mathbf{s}_m \rangle = E_m \cdot \sum_n c_{a_t \oplus \zeta_{t,\eta}}^n \cdot \delta_n^m = E_m \cdot c_{a_t \oplus \zeta_{t,\eta}}^m$$

$$\begin{aligned} \langle \mathcal{H}_{\zeta_{t,0}|a_t} \cdot \Psi_{a_t \oplus \zeta_{t,\eta}} | \mathbf{s}_m \rangle &= \langle \Psi_{a_t \oplus \zeta_{t,\eta}} | \mathcal{H}_{\zeta_{t,0}|a_t}^\dagger \cdot \mathbf{s}_m \rangle = \langle \Psi_{a_t \oplus \zeta_{t,\eta}} | \mathcal{H}_{\zeta_{t,0}|a_t} \cdot \mathbf{s}_m \rangle \\ &= \langle \Psi_{a_t \oplus \zeta_{t,\eta}} | \cdot \overline{[\mathcal{H}_{\zeta_{t,0}|a_t}]} \cdot \overline{|\mathbf{s}_m\rangle} \rangle = \langle \Psi_{a_t \oplus \zeta_{t,\eta}} | \cdot [\mathbf{I}] \cdot \overline{[\mathcal{H}_{\zeta_{t,0}|a_t}]} \cdot \overline{|\mathbf{s}_m\rangle} \rangle \\ &= \langle \Psi_{a_t \oplus \zeta_{t,\eta}} | \cdot \left(\sum_n \overline{|\mathbf{s}_n\rangle} \cdot \overline{\langle \mathbf{s}_n|} \right) \cdot \overline{[\mathcal{H}_{\zeta_{t,0}|a_t}]} \cdot \overline{|\mathbf{s}_m\rangle} \rangle \\ &= \sum_n \langle \Psi_{a_t \oplus \zeta_{t,\eta}} | \cdot \overline{|\mathbf{s}_n\rangle} \cdot \overline{\langle \mathbf{s}_n|} \cdot \overline{[\mathcal{H}_{\zeta_{t,0}|a_t}]} \cdot \overline{|\mathbf{s}_m\rangle} \rangle = \sum_n \langle \Psi_{a_t \oplus \zeta_{t,\eta}} | \mathbf{s}_n \rangle \cdot \overline{\langle \mathbf{s}_n|} \cdot \overline{[\mathcal{H}_{\zeta_{t,0}|a_t}]} \cdot \overline{|\mathbf{s}_m\rangle} \rangle \end{aligned}$$

and with the notation $\langle \mathbf{s}_n | \cdot \overline{[\mathcal{H}_{\zeta_{t,0}|a_t}]} \cdot \overline{|\mathbf{s}_m\rangle} \rangle = \mathcal{H}^{n,m}(t)$, after some elementary calculations in Schrödinger equation we obtain:

$$i \cdot \hbar \cdot \frac{\partial \gamma_{a_t \oplus \zeta_{t,\eta}}^m}{\partial t} = \eta \cdot \sum_n \overline{\mathcal{H}^{n,m}(t)} \cdot e^{i \cdot \omega^{n,m} \cdot (t-t_0)} \cdot \gamma_{a_t \oplus \zeta_{t,\eta}}^n$$

In this equation we develop $\gamma_{a_t \oplus \zeta_{t,\eta}}^n$ as a power series in η ,

$$\gamma_{a_t \oplus \zeta_{t,\eta}}^n = \gamma_{a_t \oplus \zeta_{t,0}}^n + \frac{\eta}{1!} \cdot \left(\frac{\partial \gamma_{a_t \oplus \zeta_{t,\eta}}^n}{\partial \eta} \right)_{\eta=0} + \frac{\eta^2}{2!} \cdot \left(\frac{\partial^2 \gamma_{a_t \oplus \zeta_{t,\eta}}^n}{\partial \eta^2} \right)_{\eta=0} + \dots, \zeta_{t,r}^n := \frac{1}{r!} \cdot \left(\frac{\partial^r \gamma_{a_t \oplus \zeta_{t,\eta}}^n}{\partial \eta^r} \right)_{\eta=0}$$

$$\zeta_{t,0}^n := \gamma_{a_t \oplus \zeta_{t,0}}^n \equiv \gamma_{a_t}^n, \gamma_{a_t \oplus \zeta_{t,\eta}}^n = \zeta_{t,0}^n + \eta \cdot \zeta_{t,1}^n + \eta^2 \cdot \zeta_{t,2}^n + \dots, \zeta_{t,0}^n = \gamma_{a_t}^n, \zeta_{t_0,0}^n = \gamma_{a_{t_0}}^n = c_{a_{t_0}}^n$$

$$\gamma_{a_t \oplus \zeta_{t,\eta}}^m = \zeta_{t,0}^m + \eta \cdot \zeta_{t,1}^m + \eta^2 \cdot \zeta_{t,2}^m + \dots, \zeta_{t,0}^m = \gamma_{a_t}^m, \zeta_{t_0,0}^m = \gamma_{a_{t_0}}^m = c_{a_{t_0}}^m, \gamma_{a_{t_0} \oplus \zeta_{t_0,\eta}}^n \equiv c_{a_{t_0} \oplus \zeta_{t_0,\eta}}^n \equiv c_{a_{t_0}}^n$$

$$\gamma_{a_{t_0} \oplus \zeta_{t_0,\eta}}^n \equiv \zeta_{t_0,0}^n + \eta \cdot \zeta_{t_0,1}^n + \eta^2 \cdot \zeta_{t_0,2}^n + \dots, c_{a_{t_0}}^n \equiv c_{a_{t_0}}^n + \eta \cdot \zeta_{t_0,1}^n + \eta^2 \cdot \zeta_{t_0,2}^n + \dots$$

$$0 \equiv \eta \cdot \zeta_{t_0,1}^n + \eta^2 \cdot \zeta_{t_0,2}^n + \dots, 0 = \zeta_{t_0,1}^n = \zeta_{t_0,2}^n = \dots$$

$$i \cdot \hbar \cdot \frac{\partial}{\partial t} [\zeta_{t,0}^m + \eta \cdot \zeta_{t,1}^m + \eta^2 \cdot \zeta_{t,2}^m + \dots] = \eta \cdot \sum_n \overline{\mathcal{H}^{n,m}(t)} \cdot e^{i \cdot \omega^{n,m} \cdot (t-t_0)} \cdot [\zeta_{t_0,0}^n + \eta \cdot \zeta_{t_0,1}^n + \eta^2 \cdot \zeta_{t_0,2}^n + \dots]$$

and by identifying the coefficients, we obtain the system of differential equations:

$$i \cdot \hbar \cdot \frac{d \zeta_{t,0}^m}{dt} = 0, i \cdot \hbar \cdot \frac{d \zeta_{t,1}^m}{dt} = \sum_n \overline{\mathcal{H}^{n,m}(t)} \cdot e^{i \cdot \omega^{n,m} \cdot (t-t_0)} \cdot \zeta_{t_0,0}^n,$$

$$i \cdot \hbar \cdot \frac{d \zeta_{t,2}^m}{dt} = \sum_n \overline{\mathcal{H}^{n,m}(t)} \cdot e^{i \cdot \omega^{n,m} \cdot (t-t_0)} \cdot \zeta_{t_0,1}^n, \dots, i \cdot \hbar \cdot \frac{d \zeta_{t,r}^m}{dt} = \sum_n \overline{\mathcal{H}^{n,m}(t)} \cdot e^{i \cdot \omega^{n,m} \cdot (t-t_0)} \cdot \zeta_{t_0,r-1}^n$$

which can be solved *iteratively*.

4. TRANSITION PROBABILITY

We consider the possibility of transitions $s_p \mapsto s_m$ (type $m|p$) with probability

$$P_{\eta,t|t_0}^{m|p} = |c_{a_t \oplus \zeta_{t,\eta}}^{m|p}|^2, \text{ where } c_{a_t \oplus \zeta_{t,\eta}}^{m|p} = \gamma_{a_t \oplus \zeta_{t,\eta}}^{m|p} \cdot e^{-i \cdot \omega_n \cdot (t-t_0)} \text{ and:}$$

- $\gamma_{a_t \oplus \zeta_{t,\eta}}^{n|p} = \zeta_{t,0}^{n|p} + \eta \cdot \zeta_{t,1}^{n|p} + \eta^2 \cdot \zeta_{t,2}^{n|p} + \dots, \zeta_{t,0}^{n|p} = \gamma_{a_t}^{n|p}, \zeta_{t_0,0}^{n|p} = \gamma_{a_{t_0}}^{n|p} = c_{a_{t_0}}^{n|p} = \delta_p^n,$
- $\gamma_{a_{t_0} \oplus \zeta_{t_0,\eta}}^{n|p} \equiv \zeta_{t_0,0}^{n|p} + \eta \cdot \zeta_{t_0,1}^{n|p} + \eta^2 \cdot \zeta_{t_0,2}^{n|p} + \dots, \gamma_{a_{t_0}}^{n|p} \equiv \zeta_{t_0,0}^{n|p} + \eta \cdot \zeta_{t_0,1}^{n|p} + \eta^2 \cdot \zeta_{t_0,2}^{n|p} + \dots,$
- $\gamma_{a_{t_0}}^{n|p} \equiv \gamma_{a_{t_0}}^{n|p} + \eta \cdot \zeta_{t_0,1}^{n|p} + \eta^2 \cdot \zeta_{t_0,2}^{n|p} + \dots, 0 \equiv \eta \cdot \zeta_{t_0,1}^{n|p} + \eta^2 \cdot \zeta_{t_0,2}^{n|p} + \dots, 0 = \zeta_{t_0|1}^{n|p} = \zeta_{t_0|2}^{n|p} = \dots$
- $c_{a_t \oplus \zeta_{t,\eta}}^{n|p} = (\zeta_{t,0}^{n|p} + \eta \cdot \zeta_{t,1}^{n|p} + \eta^2 \cdot \zeta_{t,2}^{n|p} + \dots) \cdot e^{-i \cdot \omega_n \cdot (t-t_0)}$
- $c_{a_t \oplus \zeta_{t,\eta}}^{m|p} = (\zeta_{t,0}^{m|p} + \eta \cdot \zeta_{t,1}^{m|p} + \eta^2 \cdot \zeta_{t,2}^{m|p} + \dots) \cdot e^{-i \cdot \omega_m \cdot (t-t_0)}$

$$\begin{aligned}
 & \bullet \quad i \cdot \hbar \cdot \frac{d\zeta_{t,0}^{m|p}}{dt} = 0 \Rightarrow \forall t, \zeta_{t,0}^{m|p} = \zeta_{t_0,0}^{m|p} = \gamma_{a_0}^{m|p} = c_{a_0}^{m|p} = \delta_p^m, \quad \zeta_{t,0}^{n|p} = \delta_p^n \\
 & \quad \text{for } m \neq p \text{ and } 0 \neq \eta \rightarrow 0 \text{ we have } c_{a_t \oplus \zeta_{t,\eta}}^{m|p} \cong \eta \cdot \zeta_{t,1}^{m|p} \cdot e^{-i \cdot \omega_m \cdot (t-t_0)}, \\
 & i \cdot \hbar \cdot \frac{d\zeta_{t,1}^{m|p}}{dt} = \sum_n \overline{\mathcal{H}^{n,m}(t)} \cdot e^{i \cdot \omega^{n,m} \cdot (t-t_0)} \cdot \zeta_{t,0}^{n|p}, \quad i \cdot \hbar \cdot \frac{d\zeta_{t,1}^{m|p}}{dt} = \sum_n \overline{\mathcal{H}^{n,m}(t)} \cdot e^{i \cdot \omega^{n,m} \cdot (t-t_0)} \cdot \delta_p^n, \\
 & \frac{d\zeta_{t,1}^{m|p}}{dt} = \frac{e^{-i \cdot \omega^{p,m} \cdot t_0}}{i \cdot \hbar} \cdot \overline{\mathcal{H}^{p,m}(t)} \cdot e^{i \cdot \omega^{p,m} \cdot t} \text{ and by integration } \int_{t_0}^t \dots dt' \text{ with } t_0 \leq t \leq t_* \text{ result:} \\
 & \zeta_{t,1}^{m|p} - \zeta_{t_0,1}^{m|p} = \frac{e^{-i \cdot \omega^{p,m} \cdot t_0}}{i \cdot \hbar} \cdot \int_{t_0}^t \overline{\mathcal{H}^{p,m}(t')} \cdot e^{i \cdot \omega^{p,m} \cdot t'} \cdot dt' \text{ with } 0 = \zeta_{t_0,1}^{m|p} \text{ and } \omega^{p,m} = \omega_m - \omega_p \text{ so:} \\
 & \zeta_{t,1}^{m|p} = \frac{e^{-i \cdot \omega^{p,m} \cdot t_0}}{i \cdot \hbar} \cdot \int_{t_0}^t \overline{\mathcal{H}^{p,m}(t')} \cdot e^{i \cdot \omega^{p,m} \cdot t'} \cdot dt'; \text{ with: } c_{a_t \oplus \zeta_{t,\eta}}^{m|p} \cong \eta \cdot \zeta_{t,1}^{m|p} \cdot e^{-i \cdot \omega_m \cdot (t-t_0)} \text{ we have:} \\
 & c_{a_t \oplus \zeta_{t,\eta}}^{m|p} \cong \frac{\eta \cdot e^{-i \cdot (\omega_m \cdot t - \omega_p \cdot t_0)}}{i \cdot \hbar} \cdot \int_{t_0}^t \overline{\mathcal{H}^{p,m}(t')} \cdot e^{-i \cdot \omega^{p,m} \cdot t'} \cdot dt' \text{ and the transition probability is:} \\
 & P_{\eta,t|t_0}^{m|p} = |c_{a_t \oplus \zeta_{t,\eta}}^{m|p}|^2 \cong \left(\frac{\eta}{\hbar} \right)^2 \cdot \left| \int_{t_0}^t \overline{\mathcal{H}^{p,m}(t')} \cdot e^{-i \cdot \omega^{p,m} \cdot t'} \cdot dt' \right|^2
 \end{aligned}$$

For the entire duration of the perturbation ($t := t_* = t_0 + T$):

$$\begin{aligned}
 c_{a_{t_*} \oplus \zeta_{t_*,\eta}}^{m|p} & \cong \frac{\eta \cdot e^{-i \cdot (\omega_m \cdot t_* - \omega_p \cdot t_0)}}{i \cdot \hbar} \cdot \int_{t_0}^{t_*} \overline{\mathcal{H}^{p,m}(t)} \cdot e^{-i \cdot \omega^{p,m} \cdot t} \cdot dt \\
 P_{\eta,t_*|t_0}^{m|p} & = |c_{a_{t_*} \oplus \zeta_{t_*,\eta}}^{m|p}|^2 \cong \left(\frac{\eta}{\hbar} \right)^2 \cdot \left| \int_{t_0}^{t_*} \overline{\mathcal{H}^{p,m}(t)} \cdot e^{-i \cdot \omega^{p,m} \cdot t} \cdot dt \right|^2
 \end{aligned}$$

Introducing the complex representation:

$$\begin{aligned}
 \underline{\mathcal{H}}_{t_0,t_*}^{p,m}(\omega) & := \int_{t_0}^{t_*} \overline{\mathcal{H}^{p,m}(t)} \cdot e^{-i \cdot \omega \cdot t} \cdot dt, \quad \overline{\underline{\mathcal{H}}}_{t_0,t_*}^{p,m}(-\omega) := \int_{t_0}^{t_*} \mathcal{H}^{p,m}(t) \cdot e^{-i \cdot \omega \cdot t} \cdot dt \text{ we have:} \\
 c_{a_{t_*} \oplus \zeta_{t_*,\eta}}^{m|p} & \cong \frac{\eta \cdot e^{-i \cdot (\omega_m \cdot t_* - \omega_p \cdot t_0)}}{i \cdot \hbar} \cdot \overline{\underline{\mathcal{H}}}_{t_0,t_*}^{p,m}(-\omega^{p,m}) \quad P_{\eta,t_*|t_0}^{m|p} = |c_{a_{t_*} \oplus \zeta_{t_*,\eta}}^{m|p}|^2 \cong \left(\frac{\eta}{\hbar} \right)^2 \cdot |\underline{\mathcal{H}}_{t_0,t_*}^{p,m}(-\omega^{p,m})|^2
 \end{aligned}$$

5. TEMPORAL PERTURBATION – MONOPLS

In this case the perturbant hamiltonian is $\mathbf{H}_{\zeta_{t,\eta}|a_t} := \eta \cdot \mathcal{W} \cdot h(t)$ where \mathcal{W} is a structural (atemporal) operator, and $h(t) := \begin{cases} u(t) & t \in (t_0, t_*) \subseteq (t_\alpha, t_\beta) \\ 0 & t \in [t_\alpha, t_\beta] - (t_0, t_*) \end{cases}$ with a temporal form factor $|u(t)| \leq 1$; we define: $\varphi_t \equiv \varphi(t) := \text{Arccos}[u(t)]$ the temporal phase of perturbation, so $u(t) := \cos(\varphi_t)$, $\theta_u := \varphi_{t_*} - \varphi_{t_0} = \omega_0 \cdot T$; $T := t_* - t_0$ is the duration of perturbation. Particular forms of general relations are:

$$\mathcal{H}_{\zeta_{t,0}|a_t} = \left(\frac{\partial \mathbf{H}_{\zeta_{t,\eta}|a_t}}{\partial \eta} \right)_{\eta=0} = \frac{\partial \mathbf{H}_{\zeta_{t,\eta}|a_t}}{\partial \eta} = \mathcal{W} \cdot h(t) \quad \langle \mathbf{s}_p | \cdot [\mathcal{W}] \cdot | \mathbf{s}_m \rangle =: \mathcal{W}^{p,m} \equiv \hbar \cdot \omega^{p,m}$$

$$\mathcal{H}^{p,m}(t) = \langle \mathbf{s}_p | \cdot [\mathcal{H}_{\zeta_{r,0}|a_r}] \cdot | \mathbf{s}_m \rangle = \langle \mathbf{s}_p | \cdot [\mathcal{W}] \cdot | \mathbf{s}_m \rangle \cdot h(t) = \mathcal{W}^{p,m} \cdot h(t) = \hbar \cdot \omega^{p,m} \cdot h(t)$$

$$\underline{\mathcal{H}}_{t_0,t_*}^{p,m}(\omega) = \hbar \cdot \omega^{p,m} \cdot \int_{t_0}^{t_*} u(t) \cdot e^{-i \cdot \omega \cdot t} \cdot dt = \hbar \cdot \omega^{p,m} \cdot \underline{u}_{t_0,t_*}(\omega), \quad \underline{u}_{t_0,t_*}(\omega) := \int_{t_0}^{t_*} u(t) \cdot e^{-i \cdot \omega \cdot t} \cdot dt$$

$$c_{a_i \oplus \zeta_{i,\eta}}^{m|p} \cong \frac{\eta \cdot e^{-i \cdot (\omega_m \cdot t - \omega_p \cdot t_0)}}{i \cdot \hbar} \cdot \int_{t_0}^t \overline{\mathcal{H}^{p,m}(t')} \cdot e^{-i \cdot \omega^{p,m} \cdot t'} \cdot dt' = -i \cdot \eta \cdot e^{-i \cdot (\omega_m \cdot t - \omega_p \cdot t_0)} \cdot \overline{\omega^{p,m}} \cdot \underline{u}_{t_0,t}(\omega^{p,m})$$

the transition probability is:

$$P_{\eta,t|t_0}^{m|p} \cong |c_{a_i \oplus \zeta_{i,\eta}}^{m|p}|^2 \cong |\eta \cdot \omega^{p,m}|^2 \cdot |\underline{u}_{t_0,t}(\omega^{p,m})|^2, \quad P_{\eta,t_*|t_0}^{m|p} \cong |\eta \cdot \omega^{p,m}|^2 \cdot |\underline{u}_{t_0,t_*}(\omega^{p,m})|^2; \text{ we calculate}$$

$$\underline{u}_{t_0,t_*}(\omega) = \frac{e^{-i \cdot \omega \cdot t_0}}{2 \cdot i} \cdot \left\{ \left[\frac{e^{i \cdot (\theta_u - \theta)}}{\varphi'_{t_*} - \omega} - \frac{1}{\varphi'_{t_0} - \omega} \right] \cdot e^{i \cdot \varphi_{t_0}} - \left[\frac{e^{-i \cdot (\theta_u + \theta)}}{\varphi'_{t_*} + \omega} - \frac{1}{\varphi'_{t_0} + \omega} \right] \cdot e^{-i \cdot \varphi_{t_0}} \right\} \quad (1)$$

$$\text{for: } \varphi_0 := \pi / 2 \text{ result } \underline{u}_{t_0,t_*}(\omega) = \frac{e^{-i \cdot \omega \cdot t_0}}{2} \cdot \left\{ \left[\frac{e^{i \cdot (\theta_u - \theta)}}{\varphi'_{t_*} - \omega} - \frac{1}{\varphi'_{t_0} - \omega} \right] + \left[\frac{e^{-i \cdot (\theta_u + \theta)}}{\varphi'_{t_*} + \omega} - \frac{1}{\varphi'_{t_0} + \omega} \right] \right\}$$

6. TIME PERTURBATION - RECTANGULAR MONOPLS

In this case the “temporal perturbation - monopuls“ has $u(t) \equiv 1$, $\varphi_t := \text{Arccos}(1) \equiv 0$, $u(t) \equiv \cos(0) = 1$, $0 = \theta_u := \varphi_{t_0+T} - \varphi_{t_0} = \omega_0 \cdot T$ and the width of the time window of the perturbation is timed with a own **clock, locked** $\omega_0 := \theta_u / T = 0$; $\theta(\omega_0, T) \equiv \theta_{\omega_0, T} \equiv \theta_u = 0$ & $\theta / \theta_u = \omega / \omega_0 = \infty$. In the relation (1) we have $\varphi' = 0$ and by direct calculation

(including the prolongation by continuity) we obtain $\underline{u}_{t_0,t_*}(\omega) = T \cdot e^{-i \cdot (\omega t_0 + \frac{\theta}{2})} \cdot \text{sinc}\left(\frac{\theta}{2}\right)$; so

$$P_{\eta,t_*|t_0}^{m|p} \cong |\eta \cdot \omega^{p,m}|^2 \cdot |\underline{u}_{t_0,t_*}(\omega^{p,m})|^2 \cong |\eta \cdot \omega^{p,m}|^2 \cdot (T/2)^2 \cdot \mu_T^\Pi(\omega^{p,m}) \equiv P_{\eta,T}^{m|p}$$

$$\mu^\Pi(\theta) = 4 \cdot \left[\text{sinc}\left(\frac{\theta}{2}\right) \right]^2, \quad \mu_T^\Pi(\omega) := 4 \cdot \left[\text{sinc}\left(\omega \cdot \frac{T}{2}\right) \right]^2, \quad \mu_{\Pi}(f, T) := 4 \cdot [\text{sinc}(\pi \cdot f \cdot T)]^2$$

▪ The transition probability, with some versions, is:

$$P_{\eta,T}^{m|p} \cong |\eta \cdot \omega^{p,m}|^2 \cdot g_T(\omega^{p,m}), \quad g_T(\omega) := \left[T \cdot \text{sinc}\left(\omega \cdot \frac{T}{2}\right) \right]^2, \quad g(f, T) \equiv T \cdot \chi(f, T)$$

$$\chi(f, T) := T \cdot [\text{sinc}(\pi \cdot f \cdot T)]^2 \text{ where } \int_{-\infty}^{+\infty} \chi(f, T) \cdot df \equiv 1 \text{ \& } \lim_{T \rightarrow \infty} \chi(f, T) = \delta(f)$$

The approximation with δ -Dirac distribution is often used in qualitative analyzes. We have MathCAD representations (fig. 1) for the laser THz domain. For a given frequency the transition probability varies periodically with the duration of perturbation (fig. 2).

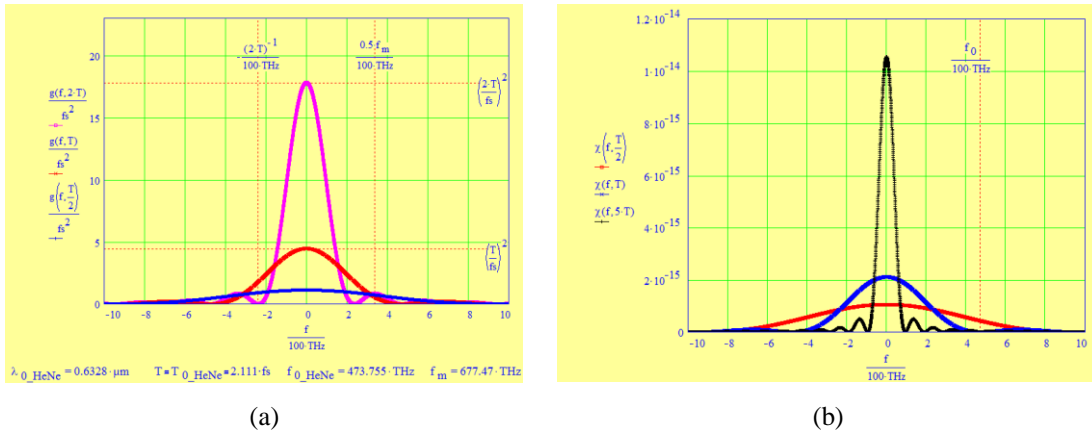


FIG. 1. Rectangular perturbation mono-pulse case: (a) transition probability factor in our laser frequencies domain frequency for different durations of perturbation; (b) δ -Dirac approximation

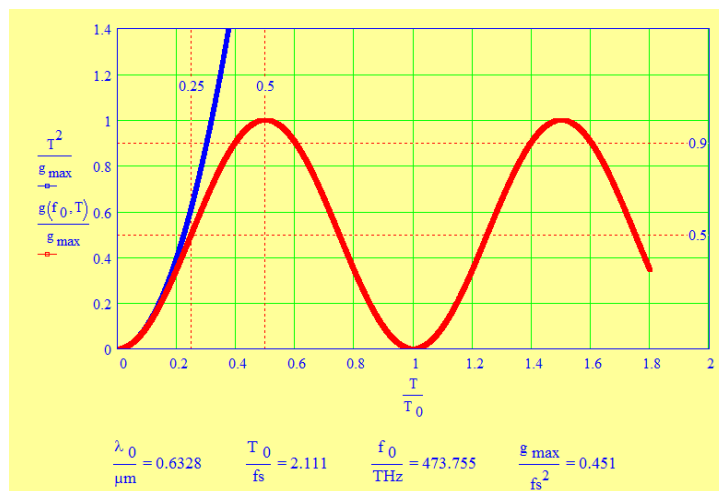


FIG. 2. Rectangular perturbation mono-pulse case: transition probability factor (for a given laser frequency) vs duration duration of perturbation

7. TIME PERTURBATION – SINUSOIDAL MONOPULS

In this case we have $u(t) := \cos(\varphi_t)$, $\varphi_t := \omega_0 \cdot (t - t_0) + \varphi_0$; $\omega_0 = 2 \cdot \pi \cdot f_0$, $T_0 := 1/f_0$, $\theta_u := [\omega_0 \cdot (t_* - t_0) + \varphi_0] - \varphi_0 = \omega_0 \cdot T$, $\theta := \omega \cdot T$ and the width of the time window of the perturbation is timed with a own **clock** $\omega_0 := \theta_u/T$ & $\theta/\theta_u = \omega/\omega_0$. In the relation (1) $\varphi'_t = \omega_0$ and by direct calculation (including the prolongation by continuity) we obtain:

$$\underline{u}_{t_0, t_*}(\omega) = \frac{T}{2} \cdot \frac{e^{-i \cdot \omega_0 \cdot t_0}}{i} \cdot \begin{cases} \frac{e^{i \cdot (\theta_u - \theta)} - 1}{(\theta_u - \theta) \cdot e^{-i \cdot \varphi_0}} - \frac{e^{-i \cdot (\theta_u + \theta)} - 1}{(\theta_u + \theta) \cdot e^{i \cdot \varphi_0}} & |\omega| \neq \omega_0 \\ \frac{i}{e^{-i \cdot \varphi_0}} - \frac{e^{-i \cdot 2 \cdot \theta_u} - 1}{2 \cdot \theta_u \cdot e^{i \cdot \varphi_0}} & \omega = \omega_0, \quad \theta := \omega \cdot T \\ \frac{e^{i \cdot 2 \cdot \theta_u} - 1}{2 \cdot \theta_u \cdot e^{-i \cdot \varphi_0}} + \frac{i}{e^{i \cdot \varphi_0}} & \omega = -\omega_0, \quad \theta_u := \omega_0 \cdot T \end{cases}$$

▪ The transition probability, with some universal functions, is:

$$P_{\eta, t/t_0}^{mlp} \cong |\eta \cdot \omega^{p,m}|^2 \cdot |\underline{u}_{t_0, t_*}(\omega^{p,m})|^2 \cong |\eta \cdot \omega^{p,m}|^2 \cdot (T/2)^2 \cdot \mu_T^S(\omega^{p,m}, \omega_0, \varphi_0) \equiv P_{\eta, T}^{mlp}$$

where, in complex format we have

$$\mu_T^S(\omega, \omega_0, \varphi_0) := \mu^S(\omega \cdot T, \omega_0 \cdot T, \varphi_0), \quad \mu^S(\theta, \theta_u, \varphi_0) := \left| \frac{u_{f_0, f_u}(\omega)}{T/2} \right|^2$$

$$\mu_S(f, T, f_0, \varphi_0) := \begin{cases} \frac{1}{4 \cdot \pi^2 \cdot T^2} \cdot \left| \frac{e^{i2\pi(f_0-f)T} - 1}{(f_0 - f) \cdot e^{-i\varphi_0}} - \frac{e^{-i2\pi(f_0+f)T} - 1}{(f_0 + f) \cdot e^{i\varphi_0}} \right|^2 & |f| \neq f_0 \\ \left| \frac{e^{i4\pi f_0 T} - 1}{4 \cdot \pi \cdot f_0 \cdot T \cdot e^{-i\varphi_0}} + \frac{i}{e^{i\varphi_0}} \right|^2 & |f| = f_0 \end{cases}$$

or in real format

$$\mu_S(f, T, f_0, \varphi_0) := [\text{sinc}(\pi \cdot (f_0 - f))]^2 + [\text{sinc}(\pi \cdot (f_0 + f))]^2 + 2 \cdot \text{sinc}(\pi \cdot (f_0 - f)) \cdot \text{sinc}(\pi \cdot (f_0 + f)) \cdot \cos(2 \cdot (\pi \cdot f_0 \cdot T + \varphi_0))$$

This sinusoidal monopuls is an ideal approximation of a more realistic case (MathCAD represented in fig. 3). With reduced notation $\mu_S(f, T, f_0, \pi/2) \equiv \mu(f, T)$ we have (fig. 4) the frequency spectrum in the approximate idealized rectangular envelope for sinusoidal perturbation.

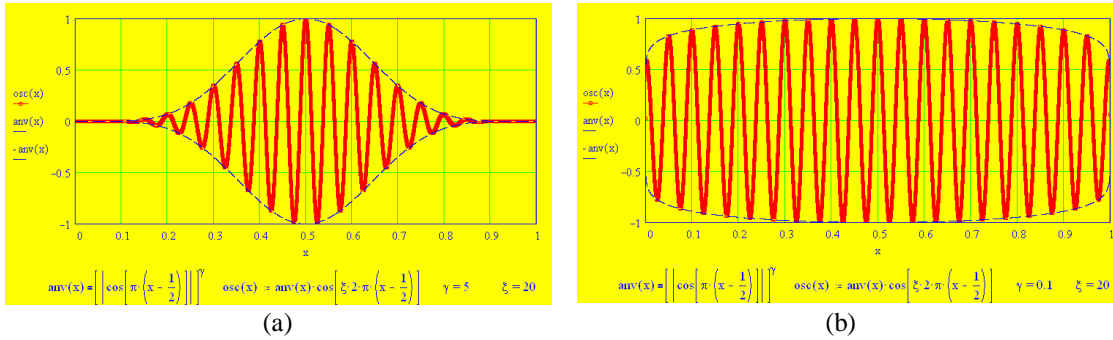


FIG. 3. Sinusoidal perturbation mono-puls case: (a) realistic sinusoidal envelope; (b) idealized rectangular envelope

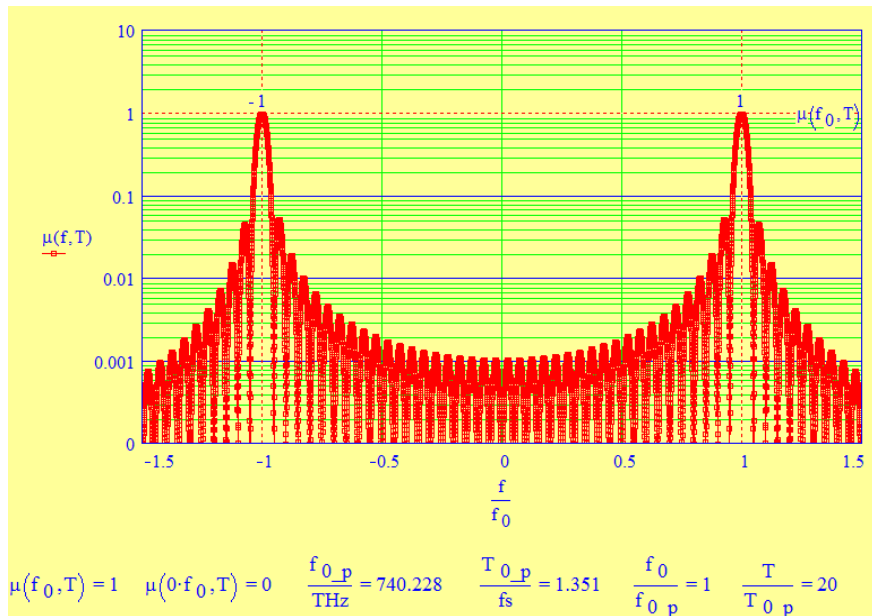


FIG. 4. The frequency spectrum sinusoidal perturbation mono-puls case, idealized rectangular envelope

8. ON THT SECOND-ORDER APPROXIMATION

If the initial s_p & final s_m states ($p \neq m$) are not directly coupled by perturbation Hamiltonian $\mathbf{H}_{\zeta_{t,\eta}|a_t} \cong \eta \cdot \mathcal{H}_{\zeta_{t,0}|a_t}$ (1^{st} - order approximation !) because $\mathcal{H}^{p,m}(t) \equiv 0$, but if s_p & s_m are indirectly coupled via a states s_n we evaluate (2^{nd} - order approximation !) ($s_p \mapsto s_m$) = $\sum_n (s_p \mapsto s_n \mapsto s_m)$ in the context of the superposition principle of quantum physics states, as follows:

$$P_{\eta,t|t_0}^{m|p} = |c_{a_t \oplus \zeta_{t,\eta}}^{m|p}|^2 = |\overline{c_{a_t \oplus \zeta_{t,\eta}}^{m|p}}|^2, c_{a_t \oplus \zeta_{t,\eta}}^{m|p} = \gamma_{a_t \oplus \zeta_{t,\eta}}^{m|p} \cdot e^{-i \cdot \omega_m \cdot (t-t_0)}, \gamma_{a_t \oplus \zeta_{t,\eta}}^{m|p} \cong \eta^2 \cdot \zeta_{t,2}^{m|p} \text{ and}$$

$$i \cdot \hbar \cdot \frac{d\zeta_{t,2}^{m|p}}{dt} = \sum_{n \neq m} [e^{-i \cdot \omega^{n,m} \cdot t_0} \cdot \overline{\mathcal{H}^{n,m}(t)} \cdot e^{i \cdot \omega^{n,m} \cdot t} \cdot \zeta_{t,1}^{n|p}], 2^{nd} \text{ - order approximation, based on:}$$

$$\zeta_{t,1}^{n|p} = \frac{e^{-i \cdot \omega^{p,n} \cdot t_0}}{i \cdot \hbar} \cdot \int_{t_0}^t \overline{\mathcal{H}^{p,n}(t')} \cdot e^{i \cdot \omega^{p,n} \cdot t'} \cdot dt' \neq 0 \text{ } 1^{st} \text{ - order approximation; by integration:}$$

$$\zeta_{t,2}^{m|p} = \frac{e^{-i \cdot \omega^{p,m} \cdot t_0}}{(i \cdot \hbar)^2} \cdot \sum_n \left[\int_{t_0}^t dt'' \cdot \int_{t_0}^{t''} dt' \cdot \overline{\mathcal{H}^{p,n}(t')} \cdot \mathcal{H}^{n,m}(t'') \cdot e^{i \cdot (\omega^{p,n} \cdot t' + \omega^{n,m} \cdot t'')} \right]$$

$$P_{\eta,t_*|t_0}^{m|p} \cong \left(\frac{\eta}{\hbar} \right)^4 \cdot \left[\sum_{p \neq n \neq m} \left[\int_{t_0}^{t_*} dt'' \cdot \int_{t_0}^{t''} dt' \cdot \overline{\mathcal{H}^{p,n}(t')} \cdot \mathcal{H}^{n,m}(t'') \cdot e^{-i \cdot (\omega^{p,n} \cdot t' + \omega^{n,m} \cdot t'')} \right] \right]^2$$

The approximate calculation of this iterated integration has led (for example in the rectangular monopuls, single intermediate energy level at $\varepsilon = 50 \cdot \%$) to the relationship:

$$P_{\eta,t_*|t_0}^{m|p} \cong \eta^4 \cdot |w^{p,n} \cdot w^{n,m}|^2 \cdot |J_{\Pi}|^2, J_{\Pi}(f, T, \varepsilon) := \frac{2 \cdot \sin(\pi \cdot f \cdot T)}{i \cdot \varepsilon^2 \cdot (2 \cdot \pi \cdot f)^2} \cdot e^{i \cdot \pi \cdot f \cdot T}$$

The maximization of the transition does not coincide with the laser frequency (fig. 5).

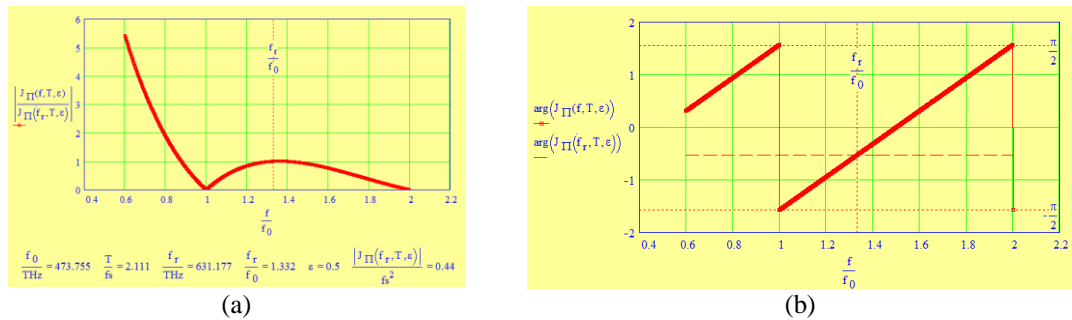


FIG. 5. Second order approximation factor (of transition probability) frequency analysis rectangular perturbation mono-pulse case: (a) normalized modulus; (b) phase of factor

9. CONCLUSIONS

- Both mathematical modeling and numerical simulation of stimulated transition probabilities for quantum optics have been performed.
- Revised perturbation theory equations in the states spectrum of a quantum system have been established in order to evaluate the stimulated transition probability (in the quantum physics Hilbert space).

- The formalization is in accordance with the formal framework of information theory (regarding: entropy, conditional entropy and mutual information adapted to the Hamiltonian Formalism).
- The operatorial relationships have been used distinctly from matrix-type relationships (Dirac formalism with “bra” and “ket”) and have been intended exclusively for the numerical simulation.
- Analytical relations have been rewritten and systematized
- Particular temporal patterns, (quasi)-rectangular or (envelope)-sinusoidal, mono-pulse of the perturbation and corresponding transition probabilities were analyzed and represented normalized by MathCAD.

ACKNOWLEDGMENTS

The authors acknowledge the Romanian Space Agency for the financial support of the 3 Photons - project 2013-2016.

REFERENCES

- [1] Gilbert Grynberg, Alain Aspect, Claude Fabre, *Introduction to Quantum Optics (From the Semi-classical Approach to Quantized Light)*, Cambridge University Press, 2010
- [2] George C. Moisil, *Physics for Engineers, vol I & II*, Editura Tehnică, București, 1968
- [3] Ion M. Popescu, *Electromagnetic macroscopic theory of light*, București, Editura Științifică și Enciclopedică, 1986
- [4] PTC MathCAD Software, <https://www.ptc.com/en/mathcad-software>

AUTOPILOT DESIGN FOR THE LATERAL-DIRECTIONAL MOTION OF AN UAV

Costin ENE, Adrian-Mihail STOICA, Petrisor-Valentin PARVU

University “Politehnica” of Bucharest, Faculty of Aerospace Engineering, Bucharest, Romania (ene.costin27@gmail.com, adrian.stoica@upb.ro, parvupv@gmail.com)

DOI: 10.19062/2247-3173.2017.19.1.43

Abstract: *The aim of the paper is to present a design procedure for the lateral-directional autopilot of an unmanned aerial vehicle (UAV) using a modified loop-shaping based control configuration. The design objectives include besides robust stability properties, the tracking of a reference model chosen such that maneuverability performances are accomplished. A reduced order autopilot is obtained solving an H_∞ norm minimization problem with imposed structure of the controller. The proposed design methodology is illustrated and validated by a case study in which the performances of the lateral autopilot are analyzed for various flight conditions.*

Keywords: *UAV, Lateral-Directional dynamics, loop shaping, robust stability, ideal model tracking, H_∞ norm minimization, Hinfstruct*

1. INTRODUCTION

Unmanned Air Vehicle's (UAV's) are widely used in several domains of activity including the military domain. Some of the advantages for these types of aircraft are that their structure is usually of small dimensions, which makes them light, have great autonomy and able to reach places that pose danger for humans. They can also be used in reconnaissance or surveillance missions. There exist several types of UAV from which the flying wing configuration has the main advantage of having reduced drag and energy consumption. A drawback of these types of UAV is that their dynamics are usually unstable, thus they require automatic control in order to obtain the desired maneuverability qualities. In order to ensure stability several control techniques have been proposed in the available literature such as PID control [1], dynamic inversion and μ -Synthesis [2], LQR and LQG control [3,4], L_1 norm based techniques [5], H_∞ norm minimization [7]. All these methods require ensuring a trade-off between their achievable performance and the robustness requirements. The actual applications require a wide spectrum of performances including not only the stabilization of the aircraft but also robustness with respect to modeling uncertainties and flying conditions changes, time response performances and reduced sensitivity to disturbances and measurement errors. H_∞ control theory is well suitable to handle control design specifications and create an environment that allows for systematic handling of performance and robustness objectives. Practice, however, shows that numerical issues can arise when dealing with flexible and high dimensional control problems. The resulting controllers from the synthesis procedure usually have a high order because H_∞ design is a full-order method which provides controllers of the same order as the weighted synthesis model which is the sum of the order of the controlled plant and the order of the used weightings.

Also different hardware or software constrains (given by the computational power for example) can impose post-design truncation procedures in order to reduce the controller dimension.

The aim of this paper is to present a reduced order H_∞ design based on structured μ -Synthesis developed in [8] for the Heading Hold (HH) autopilot of the flying wing configuration Hirus UAV. This UAV was designed and manufactured by a private Romanian company in collaboration with academics from Faculty of Aerospace Engineering of University "Politehnica" of Bucharest. In [7] the design approach is based on a modified version of the so-called two degrees of freedom (2 DOF) H_∞ loop-shaping and it's able to accomplish simultaneously several objectives as robustness stability, model tracking and disturbances attenuation requirements. A comparison between the full order controller and the reduced order controller obtained through truncation using a balanced realization procedure [7] and the reduced order controller using structured μ -Synthesis is provided.

The paper is organized as follows: in the second section, the design objectives, the design model of the UAV and the Simulink model of the heading hold autopilot are presented. The third section provides some insight on the structured μ -Synthesis controllers, but more details can be found in [8]. Simulation results, for the Hirus UAV, that include atmosphere turbulences are provided in section four as a comparison between three controllers: the full eight-order controller and its truncated fifth-order version obtained in [7] and the structured μ -Synthesis controller which is only second-order. The paper ends with some concluding remarks.

2. DESIGN MODELS AND AUTOPILOT SYNTHESIS OBJECTIVES

The Hirus platform illustrated in Fig. 1 has a flying wing configuration with the wingspan 3.2 m, length 1.2 m, maximum takeoff weight 6.5 kg, maximum cruising speed of 80 km/h and with a maximum payload of 1 kg.

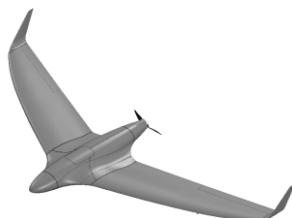


FIG.1. Hirus UAV [6]

The lateral-directional dynamics of the UAV is approximated by the following linearized nominal model:

$$\begin{aligned} \dot{x}(t) &= Ax(t) + B\delta(t) \\ y(t) &= Cx(t) + D\delta(t), \end{aligned} \tag{1}$$

where $x(t) = [v(t); p(t); r(t); \phi(t); \psi(t)]$ is the state vector with components sideslip velocity v , roll rate p , yaw rate r , roll angle ϕ and the heading angle ψ respectively. The control input $\delta(t)$ denotes the elevon deflection, while $y(t) = [r(t); \phi(t); \psi(t)]$ denote the measured outputs. For the nominal flight conditions $V = 14.8277 \text{ m/s}$ and the cruising altitude $h = 1000 \text{ m}$, the state matrix A , the control matrix B and the output matrices C and D are given by:

$$A = \begin{bmatrix} -0.0742 & 0.1174 & -14.7871 & 9.81 & 0 \\ -0.8443 & -19.2893 & 3.7078 & 0 & 0 \\ 0.2689 & -1.1721 & -0.1960 & 0 & 0 \\ 0 & 1 & 0 & 0 & 0 \\ 0 & 0 & 1 & 0 & 0 \end{bmatrix}; B = \begin{bmatrix} 0.1419 \\ 8.6676 \\ -0.3126 \\ 0 \\ 0 \end{bmatrix}; C = \begin{bmatrix} 0 & 0 & 1 & 0 & 0 \\ 0 & 0 & 0 & 1 & 0 \\ 0 & 0 & 0 & 0 & 1 \end{bmatrix}; D = \begin{bmatrix} 0 \\ 0 \\ 0 \end{bmatrix}. \quad (2)$$

The above flight condition is unstable in the absence of an automatic flight control system, fact which can be seen by computing the eigenvalues of the state matrix $\lambda_A = \{0; -19.1207; -0.2597 \pm 2.2877i; 0.0805\}$.

The design objectives for the HH autopilot are:

(DO1) Stabilization of the lateral-directional dynamics;

(DO2) Zero steady state value for the tracking error $\psi_{com} - \psi(t)$ for piecewise constant values of the commanded heading angle ψ_{com} ;

(DO3) Coordinated turns implying accomplishing the condition ([10])

$$r = \frac{g}{V} \tan(\phi); \quad (3)$$

(DO4) Reduced sensitivity with respect to low frequency measurement errors and robust stability with respect to modeling uncertainties.

These design objectives are achieved using a 8-th order optimal H_∞ controller. The controller architecture can be found in [7], where the authors also used a balanced realization technique in order to reduce the order of the controller from 8 to 5.

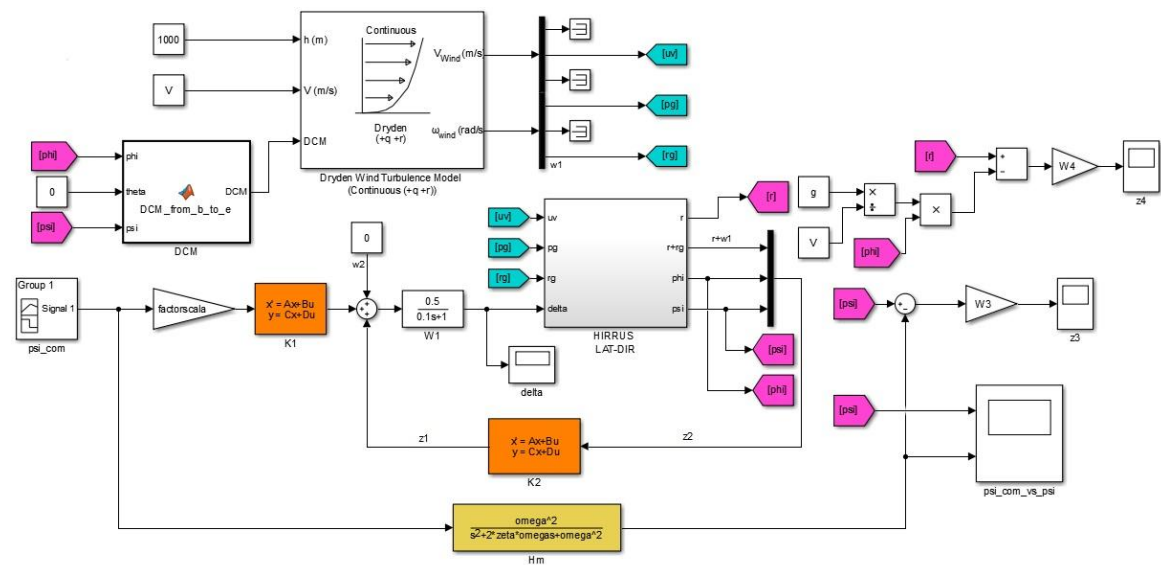


FIG.2. HIRRU control configuration with 2DOF autopilot

In Fig.2 The control problem is finding $K = [K_1 \ K_2]$ that stabilizes the system given by (1,2) and minimizes the H_∞ norm of the mapping $u_1 \rightarrow y_1$ where

$$u_1 = \begin{bmatrix} \psi_{com} \\ w_1 \\ w_2 \end{bmatrix} \text{ and } y_1 = \begin{bmatrix} z_1 \\ z_2 \\ z_3 \\ z_4 \end{bmatrix} \quad (4)$$

In the above configuration the reference model H_m has $\omega_m = 0.6 \text{ rad/s}$ and $\zeta_m = 0.7$, $W_3 = 100$ and $W_4 = 10$.

The only modification is $W_1(s) = \frac{0.5}{0.1s+1}$ instead of the value $W_1(s) = \frac{100}{0.1s+1}$ used in [7] because if sensitivity is pushed down in the low frequency range (i.e, good load disturbance rejection and reference tracking), it increases by an equal amount at others frequencies amplifying for instance control command or noise propagation. Thus using 0.5 instead of 100 for W_1 will still keep the sensitivity acceptable for low frequency range disturbances while providing a reasonable values for the control input, the elevon deflection δ .

The aim of this paper is to replace the 8-th order controller $K = [K_1 \ K_2]$ obtained in [7] with a reduced order one obtained using the structured μ -Synthesis design.

3. STRUCTURED - SYNTHESIS DESIGN

Consider the interconnected synthesis scheme of Fig. 3 where the weighting functions W_1, W_2, W_3 and W_4 are introduced to shape the closed loop system responses according to the robust performance and stability margin requirements. The trimmed plant dynamics is represented by $P_0(s)$. The uncertain system is modeled as $G(s) = P_0(s)(I + W_c(s)\Delta_c)$, where Δ_c belonging to some known set, represents the uncertain dynamics with unit peak gain and $W_c(s)$ is a stable, minimum-phase shaping filter that adjusts the amount of uncertainty at each frequency. One can notice that even though the problem formulation here is not exactly the same as in Fig. 2, it has some similarities. In Fig. 2 w_1 and w_2 represent the same type of additive uncertainties as d_1 and d_2 . Also the case from Fig. 2 does not include the multiplicative uncertainties given by Δ_c and in Fig. 3 one doesn't use a reference model in order to shape the output y neither split the controller K into two controllers K_1 and K_2 . However, adjustments were made in order to solve the control problem from Fig. 2 using the μ -Synthesis design.

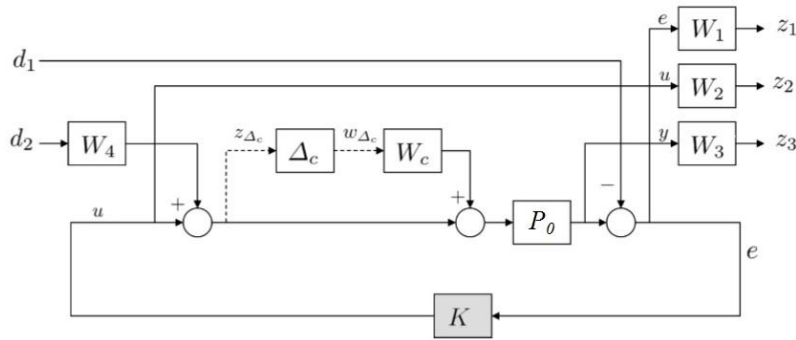


FIG.3. Closed loop interconnected structure of the μ -Synthesis design

This system in Fig. 3 can be rearranged as a generalized μ -Synthesis design as shown in Fig. 4. Considering the open loop interconnection \tilde{P} (the partition matrix of P) one must find a stabilizing controller $K(s)$ such that the peak value μ_Δ of the closed loop transfer function $L(s) = F_l(\tilde{P}, K)$ is minimized:

$$\min_{K(s)} \max_{\omega} \mu_\Delta F_l(\tilde{P}(j\omega), K(j\omega)), \quad (5)$$

where $\Delta := \text{diag}(\Delta_c, \Delta_p)$. Δ_p is introduced to close the loops between the input and output channels associated to the performance criterion and $L(j\omega) = F_l(\tilde{P}(j\omega), K(j\omega)) = \tilde{P}_{11} + \tilde{P}_{12}K(I - \tilde{P}_{22}K)^{-1}\tilde{P}_{21}$.

Thus the resulting partitioned matrix $\tilde{L}_{ij}, (i, j) := 1: 2$ is given by:

$$\begin{bmatrix} z_{\Delta_c} \\ z_1 \\ z_2 \\ z_3 \end{bmatrix} = W_a \begin{bmatrix} -T & | & KS & S \\ -GS & | & S & -GS \\ -T & | & KS & -T \\ GS & | & T & GS \end{bmatrix} W_b \begin{bmatrix} \omega_{\Delta_c} \\ d_1 \\ d_2 \end{bmatrix}, \quad (6)$$

where $S = (I + GK)^{-1}$ and $T = GK(I + GK)^{-1}$ denote the output sensitivity and the complementary sensitivity functions and $z_{\Delta_c} = \Delta_p \omega_{\Delta_c}$. The control design objectives are shaped by the weighting functions given by $W_a = \text{diag}(W_c, W_1, W_2, W_3)$ and $W_b = \text{diag}(I_2, W_4)$.

These filters are designed in order to limit the undesired effects of the off diagonal elements, thus resulting in a less conservative solution. Typos on how to tune these weighting functions can be found in [8].

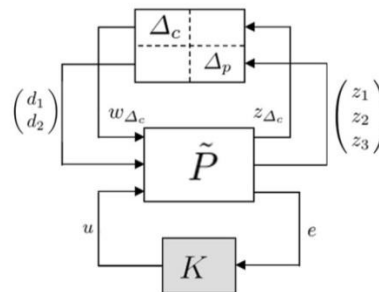


FIG.4. Closed loop interconnected design for the generalized μ -Synthesis

The main idea for obtaining a solution with reduced order is to approximate the μ -function by its upper bounds which remains an optimally scaled maximum singular value:

$$\mu_{\Delta}(L) \leq \inf_{D \in \Lambda} \bar{\sigma}(D \tilde{P} D^{-1}) \quad (7)$$

where D is the set of scaling matrices commuting with Δ and belonging to the set Λ

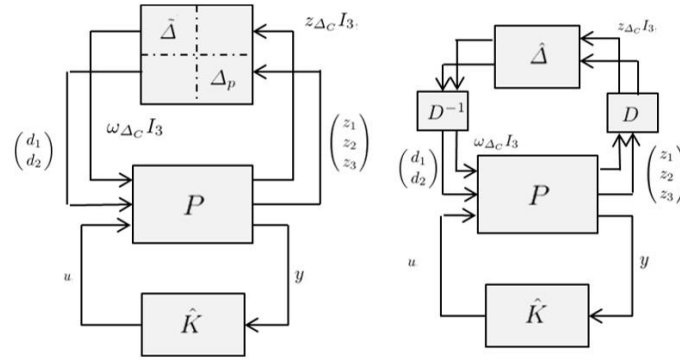
$$\Lambda = \{D = D^T > 0 : \forall \Delta, \Delta D = D \Delta\} \quad (8)$$

Thus the minimization problem in (5) is reformulated into

$$\min_{K(s)} \min_{D \in \Lambda} \left\| D(j\omega) F_l(\tilde{P}(j\omega), K(j\omega)) D^{-1}(j\omega) \right\|_{\infty}, \quad (9)$$

which can be solved using procedures from [9].

The structured μ -synthesis problem is formulated as a systematic Multi-Model control design problem. The control design objectives are decomposed into three main interconnection schemes that is S , GS and GK , in order to avoid interactions between control objectives. In the structured design those closed-loop transfer functions are shaped using the weighting functions W_1, W_2 and W_3 .


 FIG.5. Closed loop interconnected design for structured μ -Synthesis

In Fig. 5 one can see the general interconnection scheme for structured μ -Synthesis where $\hat{K} = \text{diag}(K, K, K)$ and $\tilde{\Delta} = \text{diag}(\Delta_e, \Delta_e, \Delta_e)$. Thus the block $\tilde{\Delta} = \text{diag}(\tilde{\Delta}, \Delta_p)$ is constructed with the help of scaling matrices D . For that end, consider $\tilde{D}(s) = D(s) - I$ such that $\tilde{D}(j\omega)\tilde{\Delta} = \tilde{\Delta}\tilde{D}(j\omega)$ with $D(j\omega) \in \Lambda$. With the new scalings one obtains:

$$D(j\omega)F_l(\tilde{P}(j\omega), \tilde{K}(j\omega))D^{-1}(j\omega) = F_l\left(\tilde{P}(s), \begin{bmatrix} \tilde{K}(s) & 0 & 0 \\ 0 & \tilde{D}(s) & 0 \\ 0 & 0 & \tilde{D}(s) \end{bmatrix}\right). \quad (10)$$

Thus the structured μ -synthesis becomes the non-smooth program with block diagonal controller $K(s) = \text{diag}(\tilde{K}(s), \tilde{D}(s), \tilde{D}(s))$

$$\begin{cases} \text{minimize}_{K(s)} \sup_{\omega} \bar{\sigma}(\tilde{P}(s), K(s)) \\ K(s) := \begin{bmatrix} \tilde{K}(s) & 0 & 0 \\ 0 & \tilde{D}(s) & 0 \\ 0 & 0 & \tilde{D}(s) \end{bmatrix}, \tilde{D}(s) \in \Lambda, \end{cases} \quad (11)$$

and can be solved with the Hinfstruct function from MATLAB toolbox.

4. PERFORMANCE ANALYSIS

This chapter presents the simulation results of the above method and compares the resulted reduced order μ -Synthesis controller with the results from [7]

The controller order is chosen to be 2 and following using the procedure Hinfstruct one obtains the controller $K_\mu = [K_{1\mu} \ K_{2\mu}]$ ($K_{1\mu}$ uses $B_{K_\mu}(:, 1)$, while $K_{2\mu}$ uses $B_{K_\mu}(:, 2:4)$):

$$\begin{aligned} A_{K_\mu} &= \begin{bmatrix} -0.6423 & -6.812 \\ 0.6387 & -110.4 \end{bmatrix}; B_{K_\mu} = \begin{bmatrix} 0.7759 & 1.313 & 0.6676 & -0.5121 \\ 2.195 & 9.48 & 19.73 & 16.25 \end{bmatrix}; \\ C_{K_\mu} &= [-0.8693 \quad 10.97]; D_{K_\mu} = [0.9277 \quad -0.4702 \quad -3.34 \quad -3.975]. \end{aligned} \quad (12)$$

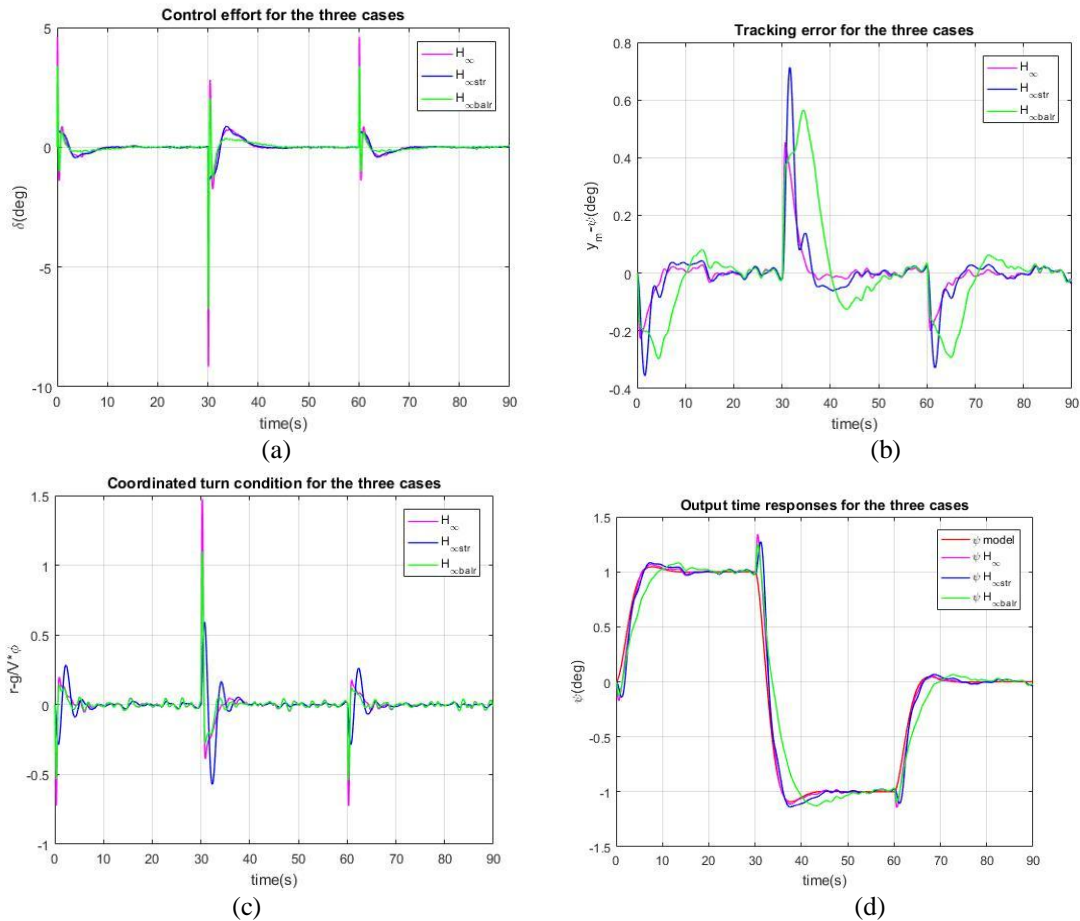


FIG.6. Performance analysis in turbulent atmosphere of HIRRUS UAV for the three proposed cases

Fig. 6 illustrates the performance analysis given by the control configuration in Fig. 2, in which the controllers $[K_1 K_2]$ have been replaced corresponding to the three proposed controllers. The first one is the full eight-order H_{∞} controller (magenta line color) obtained in [7] the second one is the structured μ -Synthesis second-order controller (blue line color) obtained in (12) and the third is the reduced fifth-order H_{∞} controller obtained through a truncating balanced realization technique obtained also in [7] (green line color). One can see that the full order controller achieves the best tracking error Fig.6 (b,d) with respect to the reference model, while the fifth-order one has the worst tracking error. The second order controller, although it has the biggest spike at tracking error, because of the doublet type command, it recovers quicker than the fifth-order one. In terms of control deflection Fig.6 (a) the full order controller has the biggest spike of approximately 9 deg., while the second order is deflected for about 2 deg. Also one obtains the H_{∞} norm for the second-order controller to be $\gamma_{min} = 136.25$, while for the full eight-order one $\gamma_{min} = 76.491$. The coordinated turn requirement Fig.6 (c) in (DO3) is best achieved by the fifth order controller, closely following the full order controller, but without the spike.

CONCLUSIONS

From the performance analysis chapter one can conclude that the structured μ -Synthesis second-order controller gives better results than the fifth order one obtain through truncating the full order one. Even tough is only a second order controller it achieves good performances with respect to the full eight-order one.

ACKNOWLEDGMENT

This paper has been supported by MEN-UEFISCDI, Program Partnerships, Projects PN-II-PT-PCCA- 2013-4-1349.

REFERENCES

- [1] G. Stenfelt and U. Ringertz, *Lateral Stability and Control of Tailless Aircraft Configuration*, Journal of Aircraft, vol. 46, no. 6, pp. 2161-2164, 2009.
- [2] A.D. Ngo, W.C. Reigelsperger and S.S. Banda, *Tailless Aircraft Control Law Design Using Dynamic Inversion and m -Synthesis*, Proceedings of the 1996 IEEE International Conference on Control Applications, September 15-18, 1996, Dearborn, MI, pp. 107-112, 1996.
- [3] M. Voskuijl, G. La Rocca and F. Dircken, *Controllability of Blended Wing Body Aircraft*, Proceedings of the 26th International Congress of the Aeronautical Sciences (ICAS), USA, 2008.
- [4] V.G. Nair, M.V. Dileep and V.I. George, Aircraft yaw control system using LQR and fuzzy logic controller, *International Journal of Computer Applications*, vol. 45, no. 9, pp. 25-30, 2012.
- [5] A.-M. Stoica: L_1 Controller Design for a Flying Wing Unmanned Aerial Vehicle, Proceedings of ICMERA, 24-27 October 2013, Bucharest, Romania, 2013.
- [6] User Guide for mini UAS Hirus v1.2, Autonomous Flight Technology, 2015.
- [7] A. M. Stoica, P. V. Parvu, M. Bivolaru, *An H_∞ Design Approach for the Heading Hold Autopilot of a Flying Wing UAV*, Applied Mechanics and Materials, Vol. 841, pp. 315-322, 2016
- [8] A. Falcoz, C.Pittet, S.Bennani, A. Guignard, B. Frapard, *Systematic design methods of robust and structured controllers for satellite: Application to the refinement of Rosetta's orbit controller*, CEAS space journal, vol. 7, n3, pp. 319-334, 2015
- [9] G. Balas, J. Doyle, K. Glover, A. Packard, R. Smith, *μ -analysis and synthesis toolbox*, MUSYN Inc. and The MathWorks Inc., Natick MA (1991)
- [10] D. McLean, *Automatic Flight Control Systems*, Prentice Hall International, 1990.

SOLUTIONS FOR SECURITY ENHANCEMENTS IN DIGITAL NETWORKS

Bogdan GOHOREANU, Florin SANDU, Dan-Nicolae ROBU

“Transilvania” University, Brasov, Romania (bogdan.gohoreanu@gmail.com,
sandu@unitbv.ro, robu.dan@unitbv.ro)

DOI: 10.19062/2247-3173.2017.19.1.44

***Abstract:** The paper is approaching a subject that is sensitive nowadays - security vulnerabilities and protection methods that can be implemented to prevent a cyber-attack. In this scope, we studied Telnet and SSH network protocols using Wireshark and made a comparative assessment regarding the safety mechanisms that each has when the data is transmitted. We proposed security enhancements dedicated to Wireless Networks because they are very popular these days and it is well known the specific high risk of a security breach. In the Internet applications sphere there are presented the most known security breaches and there are proposed some methods to fight against them.*

***Keywords:** security, digital communication networks, web applications, network protocols, SQL Injection*

1. INTRODUCTION

Considering the technology progress, cyber security is an area which is developing fast. The big companies and government institutions are investing more and more resources in network security. Training their employees to identify cyber-attacks is an important part of this process.

This domain is continuously growing, involving major changes in a short time because the attackers are very inventive and the traditional preventive methods do not give efficiency always as expected. This kind of problems causes financial loses in amount of billions of dollars and the average cost of a security incident is about \$12 million. Every year, the authorities have knowledge about millions of cyber-attacks, some of them being successful, but others not so much [1].

2. SECURITY ASPECTS IN DIGITAL NETWORKS AND WEB APPLICATIONS

2.1 Network Protocols

Considering the importance of working “remotely” nowadays, this paper is presenting the main advantages and disadvantages of the Telnet protocol and which is the alternative solution that satisfies also the security criteria – the SSH protocol.

Telnet is a protocol used for remote connection to a server. Client – server connections are established using the TCP protocol. After this stage, Telnet server and client are negotiating the resources that will be supported by each of them during the connection [2].

This protocol doesn't have security mechanisms for data transmission and that is why all information is transmitted in plain text, including passwords [3]. Another safety measure that is not implemented is authentication and the consequence can be communication interception and changing the source computer with another that is pretending to be the real source.

Another protocol that is serving the same purpose as Telnet, but doesn't have obvious security vulnerabilities is SSH (Secure Shell). Using SSH, data is encrypted and for authentication this protocol is using a public key [4].

A domain that is continuously developing nowadays is IoT (Internet of Things) and one of the standard protocols is MQTT (Message Queueing Telemetry Transport). Secure communications can be implemented by using MQTT [5]. MQTT implementations provide a security certificate mode that can be achieved with the Java Paho library [6, 7].

2.2 Web Applications

Statistics show that 61% of the USA companies are the target of "web-based" attacks. This type of attacks is motivated by the current state of web applications: 55% have at least one high severity vulnerability, 84% have at least one medium severity vulnerability and 35% of the web-sites have certificates based on SHA-1 [8].

The main "web-based" threats are:

- Brute Force Attack;
- Malware – Spyware/Key logger;
- SQL Injection;
- Social – Phishing.

The most known, but still present in 25% of the cases is SQL Injection. A type of SQL Injection can be altering the Connection String parameters.

Connection Strings are used to connect the application with the database.

E.g. `connectionString = "Data Source=ServerName;Initial Catalog=DataBaseName;User Id=Username; Password=pwd";`

SQL Injection consequences:

- Loss of data confidentiality;
- Loss of data integrity;
- Data loss;
- Compromise the entire network.

Methods to prevent SQL Injection [9]:

- Using Firewall to filter malicious data;
- Using reduced privileges accounts for database connections - administrator account to be used if necessary;
- Using parameterized queries or stored procedures instead of dynamic SQL.

2.3 Wireless Networks

Wi-Fi networks are very popular nowadays because the majority of people installed this type of Internet home connections.

The main Wi-Fi advantages:

- Low cost;
- Easy to deploy;
- Radio technology with high performance that doesn't depend on the building physical parameters.

These characteristics are also big vulnerabilities. In case of an attack on this type of network the attacker is very difficult to be found. Main types of attacks that can happen are the following:

- Brute Force Attack on the AP password;
- WEP/WPA key crack;
- “Denial of Service” attack;
- “Man-in-the-middle” attack.

There are Linux distributions (e.g. Kali Linux) that are more suitable to test attacks on the wireless networks. The following two programs are popular for testing network security: Reaver and Pixiewps. An attacker can be focused to crack the WPS, rather than the WPA key. If a device will connect via WPS, it will receive also a WPA key.

3. PRACTICAL SOLUTIONS AND EXPERIMENTAL VALIDATIONS

3.1. Telnet security vulnerabilities

Network protocols security was tested using Wireshark by capturing data packets sent when connecting to a remote server from a computer running the Windows 7 operating system.

It can be seen in the screenshots of Fig.1 that, using Telnet, the information is being sent in plain text. Even login credentials (username and password) are transmitted in plain text (“password: 123”).

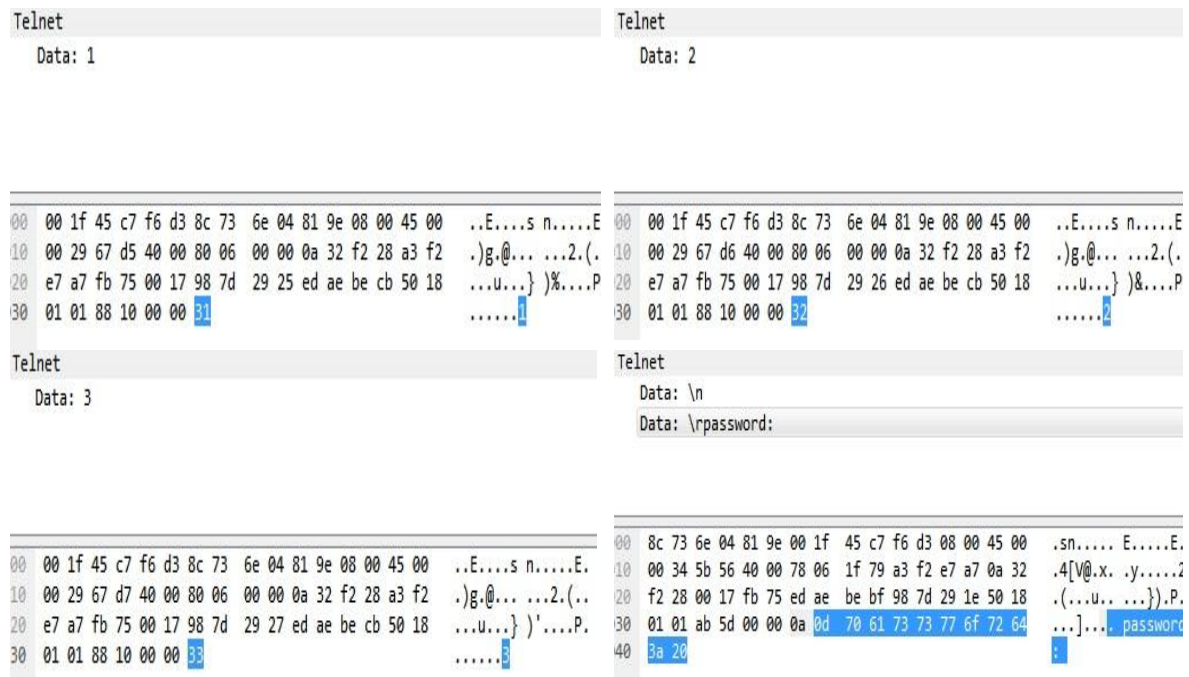


FIG. 1. Telnet packets - data transmitted in plain text

3.2. SQL Injection

Most of the sites give users the possibility to subscribe for receiving newsletters via e-mail. We have proven specific site vulnerabilities by programming an example of a wrong subscribing form (Fig.2).

FIG. 2. Example of subscribing form

Such an application is vulnerable to SQL Injection because of the form processing. Saving the e-mail address in the database is done using the following C# code:

```
private void btnSubmit_Click(object sender, EventArgs e)
{
    string queryString = "insert into table_name values(' + textBoxEmail.Text+' )";
    SqlConnection connection = new SqlConnection(connectionString);
    SqlCommand command = new SqlCommand(queryString, connection);
    command.Connection.Open();
    command.ExecuteNonQuery();
}
```

Instead of a valid e-mail address, an attacker can enter the following text that will be interpreted as an SQL command and executed:

```
user1@domain.com');insert into newsletter values('user2@domain.com
```

As a consequence, in the database there will be introduced two e-mail addresses:

[user1@domain.com](#) and [user2@domain.com](#)

These types of mistakes are developer's faults. In the above-presented case, the consequences do not have a vital impact, but it can be introduced malicious code that will affect the functionality of the application (e.g. removing the database).

This kind of breach can be fixed in several ways:

- Introducing code to validate the format of an e-mail address;
- Using a parameterized stored procedure for database insertion.

3.3. Securing the Wireless Networks

For a better securing of wireless home networks, it exists the possibility to hide the network name or, in technical terms, the network SSID. By doing this, the network will be invisible to a potential attacker.

The majority of wireless routers used for home Wi-Fi can be configured very easily to hide the SSID. The steps for doing this configuration on a TP-Link router are the following: the user opens an Internet browser and connects to the router using its web interface; in the section "Wireless > Wireless settings" he/she will deactivate the option "Enable SSID Broadcast" (Fig. 3) [10].

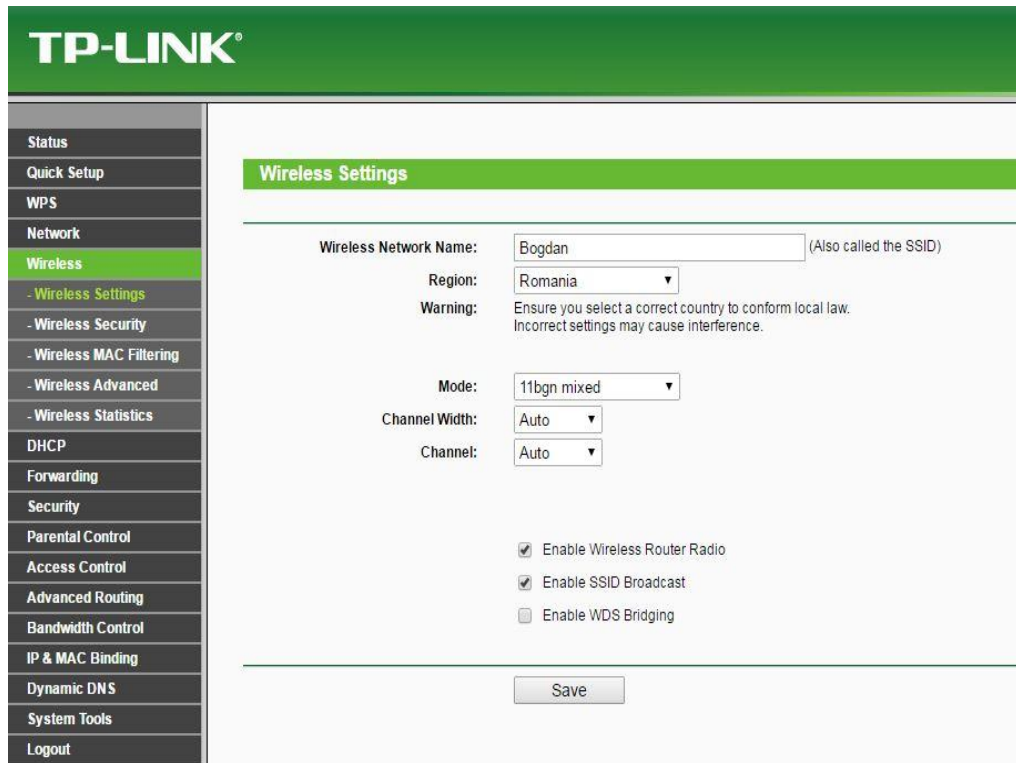


FIG. 3. Deactivating SSID Broadcast

Using Kali Linux and Pixiewps, we assessed the security of wireless networks facing a brute force attack.

With a few commands, there can be displayed the neighbour networks and some of their parameters like: channel, signal power (RSSI), the WPS version (fig.4).

Configuring the router in such a way that the network and its parameters will be invisible, the software will not detect the existence of the network (fig.5).

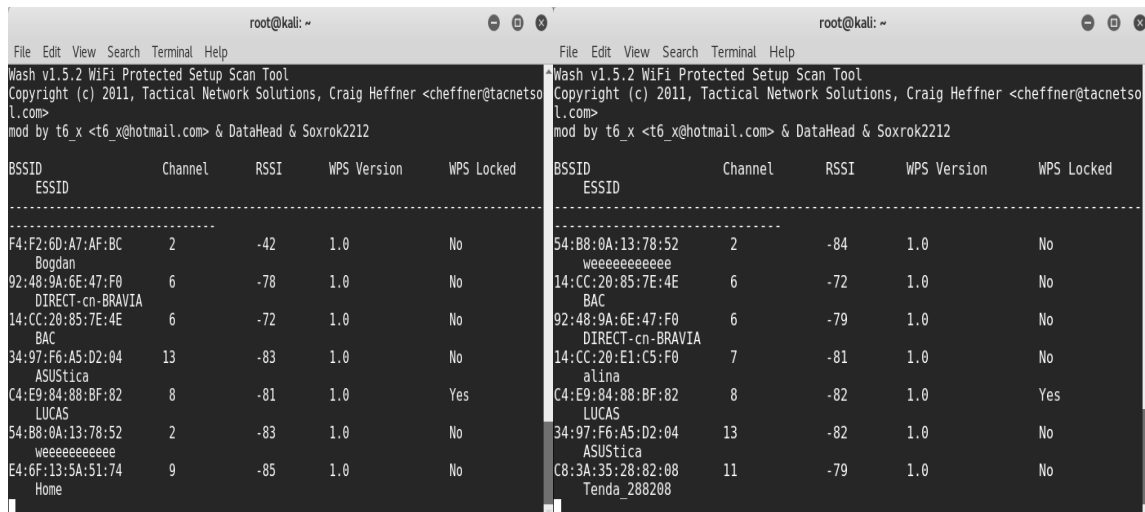


FIG. 4. "Bogdan" network visible; SSID Broadcast enabled

FIG. 5. "Bogdan" network hidden; SSID Broadcast deactivated

Disabling the WPS will further increase the security of the network, by closing the way an attacker could receive a valid WPA/WPA2 key.

4. CONCLUSIONS

Some practical solutions have been proposed in this paper, together with the specific test environments, appropriate operating systems and special security breach scenarios.

The Telnet protocol is recommended to be used in private networks (with lower exposure to intruders), not in public networks where attackers can take advantages of a security breach. For public networks, it can be used the SSH.

To avoid attacks based on SQL Injection, application developers and testers must conduct test scenarios for this type of security breach before the application is released.

To enhance the security of a wireless network, the router must be configured with different settings than the default ones (WPA/WPA2) and the password should be strong, at least 15 characters including small and capital letters, numbers and special characters – the strength of a longer password was demonstrated using Kali Linux. Also the highest supported security setting should be used, that is supported by all the necessary devices in the network (e.g. if all devices support WPA/WPA2 with AES, then WPA/WPA2 with TKIP should be disabled to avoid the fallback to a weaker security mode). Also the WPS should be disabled in order to maximize the security of the network.

5. REFERENCES

- [1] <http://www.csoonline.com/article/3153707/security/top-5-cybersecurity-facts-figures-and-statistics-for-2017.html>, accessed on March 19, 2017;
- [2] Javvin Technologies, *Network Protocols Handbook*, Second Edition, ISBN 0-9740945-2-8, 46;
- [3] <http://www.differencebetween.net/technology/internet/difference-between-telnet-and-ssh/>, accessed on February 7, 2017;
- [4] J. Gilmore et al, *Using Raw Public Keys in Transport Layer Security (TLS) and Datagram Transport Layer Security (DTLS)*, RFC7250, 2014;
- [5] Sorin Zamfir, Titus Balan, Florin Sandu, Iulian Iliescu, *A Security Analysis on Standard IoT Protocols*, Applied and Theoretical Electricity (ICATE), 2016 International Conference;
- [6] Eclipse Paho, <http://www.eclipse.org/paho/>, accessed on February 11, 2017;
- [7] Eclipse Californium, <http://www.eclipse.org/californium/>, accessed on February 11, 2017;
- [8] OpenSSL, <https://www.openssl.org/>, accessed on February 10, 2017;
- [9] <http://www.enterprisenetworkingplanet.com/netsecur/article.php/3866756/10-Ways-to-Prevent-or-Mitigate-SQL-Injection-Attacks.htm>, accessed on February 9, 2017;
- [10] <http://www.tp-link.ro/faq-417.html>, accessed on March 10, 2017.

THE MANAGAMENT OF BALLISTIC OPERATIONS USING MATLAB SOFTWARE

Cosmin-Constantin IACOB, Gabriel BORSOS, Gavrilă CALEFARIU

Transylvania University, Braşov, Romania (cosmin.iacob@unitbv.ro)

DOI: 10.19062/2247-3173.2017.19.1.45

Abstract: *The purpose of this paper is based on the analysis of military products performances between the interests of the company and customer's requirements achieved by using MATLAB software method in exterior ballistics calculation.*

I have started with a few notions related to the method in order to understand exactly how it applies continuing with generic drawings and descriptions of product in order to protect the company interests, and finally the proper analysis by numerical modeling through MATLAB.

Keywords: *exterior ballistics, illuminating bombs, trajectory, aerodynamics*

1. INTRODUCTION

Exterior ballistics is a branch of mechanics that studies the laws of motion of a heavy body thrown at an angle to the horizontal plane.

By definition characteristics of illuminating bomb aims to bomb the center of mass motion until initiation system operation.

For the proper functioning of bomb, and increased accuracy, aims to determine all elements bomb trajectory: maximum range, arrow trajectory, total flight time [5].

Bombs are equipped with a stabilization system disposed at the rear of the body; in this case the center of pressure is behind the center of mass.

Behavior bomb while flying along the trajectory is defined by movement around the center of mass bomb [10].

Because the bomb hasn't its own rotational motion, movement around its center of mass is given by movement around its longitudinal axis [8].

2. FORCES AND MOMENTS ACTING ON THE BOMB TRAJECTORY

2.1 The stability of bomb along trajectory. When leaving the launcher bomb is committed outside longitudinal movement, in a swirling motion around an axis passing through the center of gravity C_g (figure 1) and perpendicular to the axis of symmetry of the bomb, the movement characterized by initial angular velocity ω_0 [4].

Longitudinal displacement is determined as a result of the action of the initial velocity V_0 and initial lateral velocity ω_0 .

The initial conditions of the movement of rotation of the bomb is determined by the size and direction of the angular displacement φ_0 and the speed of rotation ω_0 [9].

On leaving the launcher, due to inertia, the bomb will tend to rotate around its center of gravity. Appears but the force of air resistance (R), the point of application (C_p) is set to stabilizer behind the center of gravity. The timing of that force relative to the center of gravity gives it a bomb that opposes the rotation speed ω_0 .

If when resistance force fails to stop at a certain time (characterized by the angle of rotation φ_{0max}) the rotation bomb, then it will tip over losing stability [1].

In reality however, the parameters change from blowing to blowing and so the bomb trajectory oscillations will differ from the bomb to bomb, which is one of the important causes of spreading blowing. To improve scattering have acted on building the bomb to achieve value for ω_0 and a greater ability to quickly absorb bomb trajectory oscillations.

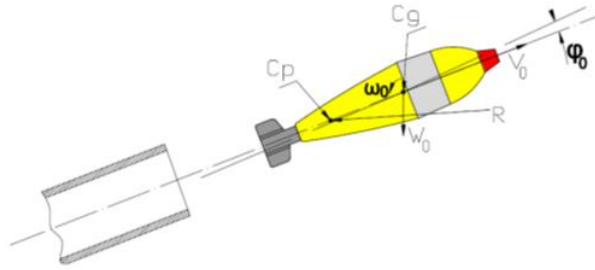


FIG. 1. The initial conditions of the motion trajectory bomb

On bomb the force of gravity acting on the trajectory and force of air resistance. The size and direction of the resultant of the air resistance depends on the velocity of the center of gravity of the bomb, the angle of inclination of the axis of symmetry of the bomb, to the tangent to the trajectory, the speed, and the construction of the pivoting movement of the stabilizer body and the bomb [1].

As a result of the inclination of the axis of symmetry of the bomb to the direction of action of the resultant of the air flow (figure 2) direction of air resistance R does not overlap with the direction of air flow V_{aer} . Therefore decomposition of air resistance force into two components: one noted R_x directed in the direction of center of gravity speed and reverse it, and another noted R_y after normal to the direction of travel of the bomb [1].

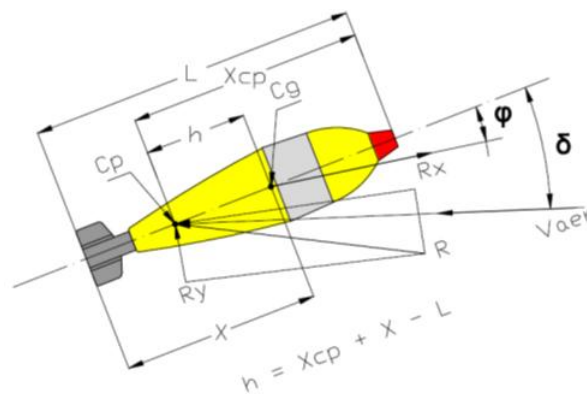


FIG. 2. Air resistance force components

R_x component is called the frontal resistance and R_y component ascending power. The frontal resistance R_x has the expression:

$$R_x = C_x \cdot v^2 \cdot \rho \cdot S \tag{2.1}$$

when :

- C_x – Front aerodynamic resistance
- ρ – air density
- S – maximum transverse surface action bomb
- v – velocity of the center of gravity of the bomb

Front aerodynamic resistance characteristic size depends on the angle of attack δ and can be calculated with a sufficiently good approximation formula:

$$C_x = C_{xc} \cdot (1 + k \cdot \delta^2) \tag{2.2}$$

when :

- C_{xc} – is the characteristic of front air resistance for $\delta=0$;
- k – a coefficient based on the construction of the bomb
- C_x - aerodynamic characteristic graph of variation depending on the angle of attack δ is shown in figure 3 showing that for angles from 0^0 to 3^0 , $C_x=ct$.

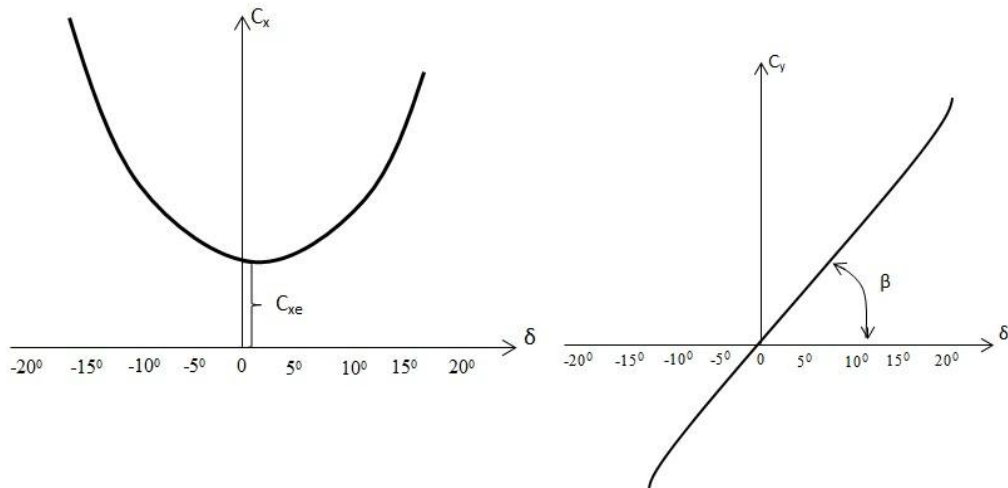


FIG. 3. Graphs C_x and C_y aerodynamics changes depending on the angle δ .

For angles $\delta = \pm 10^\circ$, C_x increase by 50%, and $\delta = \pm 15^\circ$ with 110 %.
The component ascending power R_y has the expression:

$$R_y = C_y \cdot v^2 \cdot \rho \cdot S \tag{2.3}$$

when:

C_y is the aerodynamic characteristic of ascending power .

Variation graph of C_y depending on δ angle is shown in fig. 3 which results in:

- a) The value and characteristic sign is the value and sign of the angle δ
- b) For $\delta=0$, $C_y=0$
- c) For $\delta = \pm 15^\circ$, C_y is proportional with δ : $C_y = C'_y \cdot \delta$ where C'_y is the coefficient of slope of the curve $C_y=f(\delta)$.

The force of air resistance R gives a moment which in turn decomposes to stabilizer moment M_s and amortization moment M_a . [3].

Stabilizer moment is composed of front resistance moment (M_x) and ascending force moment (M_y).

From figure 2 results:

$$M_x = R_x \cdot h \cdot \sin(\delta) \quad (2.4)$$

$$M_y = R_y \cdot h \cdot \cos(\delta) \quad (2.5)$$

when:

h is the distance between the center of gravity and center of pressure.

$$M_s = M_x + M_y \quad (2.6)$$

$$M_s = \left(C_x + \frac{C_y}{\delta} \right) \cdot v^2 \cdot \rho \cdot S \cdot h \cdot \delta \quad (2.7)$$

$$M_s = (C_x + C'_y) \cdot v^2 \cdot \rho \cdot S \cdot h \cdot \delta \quad (2.8)$$

Noting

$$C_x + C'_y = C_m$$

Result

$$M_s = C_m \cdot v^2 \cdot \rho \cdot S \cdot h \cdot \delta \quad (2.9)$$

Stabilizing moment is proportional to the angle δ and transverse surface moment ($S \cdot h$). The maximum value of the stabilizing moment occurs when the maximum angle δ value. When overlapping axis tangent to the trajectory bombs, the stabilizer moment is null. In conclusion when motion stabilizer angle δ acts to tilt the axis of symmetry of the bomb to the tangent to the trajectory [2].

M_s stabilizing moment fails to achieve damping of oscillations. Depreciation is actuated through oscillation damping moment (M_a) of the force of air resistance. Moment oscillation damping occurs as a result of the bomb trajectory, being proportional to the angular velocity of the bomb oscillations around its center of gravity and moment of cross-sectional area ($S \cdot h$).

$$M_a = C_a \cdot v \cdot S \cdot h^2 \cdot \frac{d\delta}{dt} \quad (2.10)$$

Maximum damping moment is obtained for $\delta = 0$, when the angular velocity is maximum. When $\delta = \delta_{\max}$ the amortization moment is null because $d\delta/dt = 0$. In this way moment M_a tends to decrease the speed of oscillation, making this move a amortized oscillation [3].

In aerodynamic the aerodynamic characteristics above are determined in relation to the factor $\frac{\rho \cdot v^2}{2}$ and the entire length of the bomb (L).

3. NUMERICAL MODELING BOMB TRAJECTORY MATLAB PROGRAM

The purpose of studying the movement of the center of mass of bomb consists mainly trajectory calculation and thus determining the change of speed, time, motion and tilt speed along the trajectory [7].

The trajectory calculation is done in the following assumptions [6]:

- Longitudinal axis of the bomb is almost tangent to the trajectory
- Weather conditions are normal ground (standard), and the variation with altitude meteorological parameters normal law-abiding
- Ballistic conditions are normal (standard) for bomb mass, form and its dimensions mass and temperature load flinging.
- The acceleration of the weight is constant in size and direction, being parallel to the plumb line from the origin of the trajectory.

To determine the outer ballistic trajectory, that is the relationship between Flight (x) and Height (y), the system (3.1) must be integrated.

$$m \frac{d^2 x}{dt^2} = -F_{rao} \frac{\frac{dx}{dt}}{\left(\frac{dx}{dt}\right)^2 + \left(\frac{dy}{dt}\right)^2} \tag{3.1}$$

$$m \frac{d^2 y}{dt^2} = -(G + F_{rao}) \frac{\frac{dy}{dt}}{\left(\frac{dx}{dt}\right)^2 + \left(\frac{dy}{dt}\right)^2}$$

Where:

m – the mass of the projectile;

G – Weight

F_{rao} – It is the pressure force exerted by the air on the head of the ogive.

$$F_{rao} = 0,55 \rho A_o c_d \left[\left(\frac{dx}{dt}\right)^2 + \left(\frac{dy}{dt}\right)^2 \right] \tag{3.2}$$

Where:

ρ – air density;

A₀ – the area of the maximum section of the ogive;

C_d – a coefficient comprised between 0 and 0.6 depending on the speed.

The model described above can be more effective if the air resistance is considered to be on the bomb wings and horizontal deviation due to lateral wind (if any).

Although the system is nonlinear, solving it does not pose problems when it comes to numerical computation.

The integration of differential equations was performed using ode23 function of the Matlab software, customized for illuminating bombs.

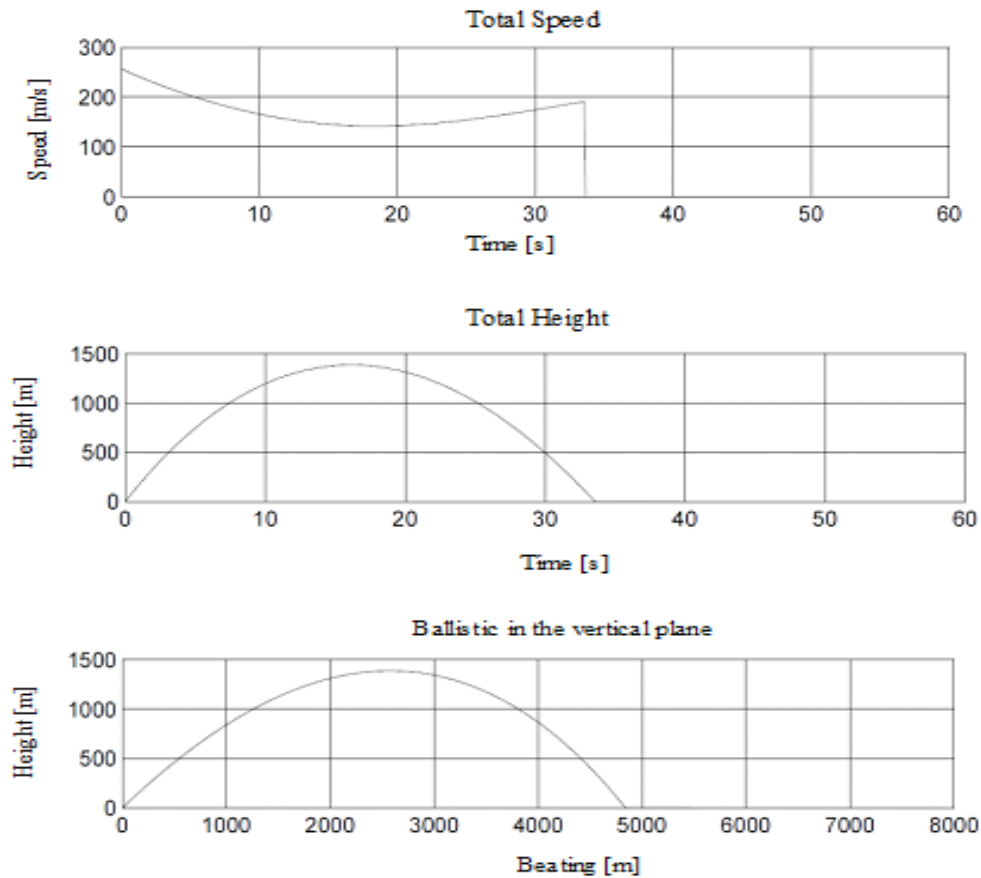


FIG. 4. Trajectory speed variation graph, the graph height versus time and trajectory chart.

The main benefit of the method presented above is the considerable costs decreasing. Currently, for each bomb load, it is necessary to test hundreds of projectiles for a statistical determination of precision. This is very expensive in terms of time and money.

Our purposed method allows to optimize the batches size and to decrease the resources consumptions.

Transposed in money, this means notable savings (see table 3.1):

Table 3.1 Benefits of the proposed method

Actual method			Proposed method			Saving
1	2	3	4	5	6	(3) –(6)
Pieces tested	Unit Value [€]	Total Value [€]	Pieces tested	Unit Value [€]	Total Value [€]	105000
110	1000	110000	5	1000	5000	

CONCLUSIONS

Following the analysis made using the integration of differential equations performed in Matlab software, a correlation has been achieved, between customer requirements of high standards quality of military products performances and business interests.

In a competitive economy environment on a short market the most important criteria for the company are customers satisfaction and maintaining it as well as the reducing the production costs.

The company wants to improve the criteria listed above in order to be able to achieve its objectives on everything related to service quality, improving customer relationships and possible national and international expansion, in other words to gain a competitive advantage in the market.

In this paper has developed a knowledgebase of ballistics analysis customized for illuminating bombs in a nonflexible manufacturing system that adapts knowledge into product development where the major objectives were to provide decision support to help economic field, according the utilization of best-know knowledge, minimize costs, achieve quality assurance and shorten time to product.

Product development activities must be structured in such a way that any engineering decisions taken are based on proven knowledge and experience.

REFERENCES

- [1] I. Antonescu, Bazele Proiectării bombelor de aruncător, Academia Militară, București 1976, pag.188-205;
- [2] T.V. Chelaru, *Dinamica zborului, îndrumar de laborator*, Ed. Politehnică Press, ISBN 978-606-515-445--2, București, 2013;
- [3] T.V. Chelaru, *Dinamica zborului, note de curs*, Ed. Politehnică Press, ISBN 978-606-515-059-1, București, 2009;
- [4] H. Deconinck, E. Dick, "Computational Fluid Dynamics", Proceedings of the Fourth International Conference on Computational Fluid Dynamics, ICCFD 4, Ghent, Belgium, 10-14 July 2006;
- [5] M.J. Nusca, Army Ballistic Research Lab Aberdeen Proving Ground MD., " *Supersonic/Hyper-sonic Aerodynamics and Heat Transfer for Projectile Using Viscous-Inviscid Interaction*", Defense Technical Information Center, 1990;
- [6] L. A. Pars, *A Treatise on Analytical Dynamics*, London 1965;
- [7] J.M. Sidi, *Spacecraft dynamic & control - a practical engineering approach*, Cambridge University Press, New York, NY 1003-2473, USA;
- [8] M. J. Spearman, "The Aerodynamics of Some Guided Projectiles", N.A.S.A, 1984;
- [9] Sir Geoffrey Ingram Taylor, "Aerodynamics and the mechanics of projectile and explosions", University Press, California, USA, 1963;
- [10] V. Titică, *Balistică interioară și exterioară* vol I și II.

ANALYTIC-NUMERIC METHODS IN THE VALIDATION OF ANY FLOW REGIMES IN HYDRO-AERODYNAMICS

Mircea LUPU*, Gheorghe RADU**, Cristian-George CONSTANTINESCU**

*"Transilvania" University, Faculty of Mathematics and Computer Science, Braşov, Romania (m.lupu@unitbv.ro)

Member of The Academy of Romanian Scientists

**"Henri Coandă" Air Force Academy, Braşov, Romania (gh.radu@gmail.com, c.g.constantinescu@gmail.com)

DOI: 10.19062/2247-3173.2017.19.1.46

Abstract: In this paper there are studied two kinds of problems about a fluid flow or a hot transfer regime. The first problem refers to a parabolic type of a laminar or viscous fluid flow or a hot transfer in a plane or cylindrical domain. It is considered an inverse problem: knowing the data on the boundary of the domain, a method to find the viscosity coefficient or the hot transfer coefficient is given. The best numerical results may be obtained when the number of measurements is increased. The second problem refers to the free boundary flow in the presence of a curvilinear symmetrical obstacle. There are considered the Helmholtz problem when the fluid is unlimited and the Rethi-Jacob scheme when a jet of fluid is forked by a symmetrical obstacle. The problems were studied using singular integral equations and the shapes of the maximal drag obstacle are obtained.

Keywords: parabolic equations, the trapeze formula, viscosity coefficient, inviscid jets, nonlinear operator, optimal design.

1. DETERMINING THE COEFFICIENT FROM THE PARABOLIC TYPE EQUATION

The mathematical modeling of viscous fluid flows, the heating and cooling problems, metal melting, ice melting, wood drying, dispersion or aggregated, mass and heat transfer lead to partial derivate equations of a parabolic type. The viscosity coefficients appear in these equations, humidity coefficients or dispersion – they can be both constant and variable. We present a method to determinate these coefficients when they are not stationary, in the plane case or cylindrical, having input data regarding the speed or the tension on the boundary, or the temperature and the thermal flow changed with the exterior, [8] [3].

A. We consider the parabolic equation:

$$k(t) \frac{\partial w}{\partial t} = \frac{\partial^2 w}{\partial x^2} + F(x, t), w = w(x, t), x \in [0, l], t \geq 0 \quad (1)$$

Representing the plane flow between two plates or the thermal process delimited by the $x=0$, $x=h$ plates. For start we will consider the homogeneity case $E(x, t)=0$ and assume that we have the following information $w(x, t)$:

$$w(x, t = 0) = f(x) \tag{2}$$

$$w(x = 0, t) = g(t), w(x = l, t) = h(t) \tag{3}$$

$$\left. \frac{\partial w}{\partial x} \right|_{x=0} = G(t), \left. \frac{\partial w}{\partial x} \right|_{x=l} = H(t) \tag{4}$$

The conditions (2)-(4) are actually Sturm-Liouville type conditions and have physical meanings related to the according studied problems: so, viscous fluids the conditions (3) of Couette type [3] show the mobility of the plates with speeds $g(t), h(t)$ and the relation (4) shows the tensions that emerge between the fluid and the plates. For the caloric problem, w is the temperature, (3) the walls heating, (4) the caloric flow between the inside and the outside trough the walls.

Having these data we will present methods to find the coefficient $k(t)$ with the conditions (2)-(4) or by weakening them. In order to perform calculations in these continuous environments we impose the non polarity conditions for data, meaning:

$$g(0) = f(0), h(0) = f(l), G(0) = f'(0), H(0) = f'(l) \tag{5}$$

along with the continuity of the simple and partial derivates.

We integrate the equation (1) with respect to x

$$k(t) \int_0^l \frac{\partial w}{\partial t} dx = \int_0^l \frac{\partial}{\partial x} \left(\frac{\partial w}{\partial x} \right) dx = \left. \frac{\partial w}{\partial x} \right|_{x=l} - \left. \frac{\partial w}{\partial x} \right|_{x=0} = H(t) - G(t) \tag{6}$$

We apply in the integral the trapeze formula and together with (3) we have:

$$k(t) \frac{l}{2} \left[\left(\frac{\partial w}{\partial t} \right)_{x=l} + \left(\frac{\partial w}{\partial t} \right)_{x=0} \right] = k(t) \frac{l}{2} [h'(t) + g'(t)] \approx H(t) - G(t) \tag{7}$$

$$k(t) \approx \frac{2[H(t) - G(t)]}{l[h'(t) + g'(t)]} \tag{8}$$

If in (1) appears also $F(x, t)$ then besides H-G we add $U = \int_0^l F(x, t) dx$. We notice that $k(t)$ is

retrieved and we have not use (2) $f(x)$ – although, this will definitely be used if $w(x, t)$ is numerically determined in (8) we notice the validity condition $H \neq G$ meaning the plates are not moving parallel with Ox simultaneous with constant speed. The formula (8) will be correct as much as in order to apply the trapeze formula we will consider on $[0, l]$ multiple nodes having $x_i = i \frac{l}{n}, i = 0, 1, \dots, n$ with $w(x, t) = h(x, t), h'(x_i, t) = \frac{\partial w(x_i, t)}{\partial t}$.

In the end results, with these data, applying the trapeze formula,

$$k(t) \approx \frac{H(t) - G(t)}{\frac{l}{n} \left[\frac{h'(t) + g'(t)}{2} + \sum_{i=1}^{n-1} h'_i(x_i, t) \right]} \tag{9}$$

Lets' obtain $k(t)$ if one information, either $H(t)$ or $G(t)$ is missing – the case when $G(t)$ is missing from (3), (4); we apply the same operations:

$$h(t) - g(t) = w(l,t) - w(0,t) = \int_0^l \frac{\partial w}{\partial x}(s,t) ds \quad (10)$$

$$\int_{\xi}^l \frac{\partial^2 w}{\partial x^2} dx = \int_{\xi}^l W(s,t) ds = \frac{\partial w}{\partial x}(l,t) - \frac{\partial w}{\partial x}(\xi,t) \quad (11)$$

$$\frac{\partial w}{\partial x}(\xi,t) = H(t) - \int_{\xi}^l W(s,t) ds, \frac{\partial^2 w}{\partial x^2} = W(x,t) = k(t) \frac{\partial w}{\partial t} \quad (12)$$

We replace (12) in (10) and we will apply the Dirichlet formula for the iterate integral

$$\int_a^b d\xi \int_a^{\xi} W(s,t) ds = \int_a^b ds \int_s^b W(s,t) d\xi = \int_a^b (b - \xi) W(s,t) ds$$

$$h(t) - g(t) = lH(t) - \int_0^l (l - s) W(s,t) ds \approx lH(t) - \frac{l^2}{2} W(0,t) \quad (13)$$

$$h(t) - g(t) \approx lH(t) - k(t) \frac{l^2}{2} \frac{\partial w}{\partial t} \Big|_{x=0} = lH(t) - k(t) \frac{l^2 g'(t)}{2} \quad (14)$$

$$k(t) \approx \frac{2[lH(t) - h(t) + g(t)]}{l^2 g'(t)} = k_H(t) \quad (15)$$

In (13) we applied the trapeze formula, formulas (2) and (3), obtaining (15) comparable with (8); the trapeze formula can be applied on more nodes obtaining a formula comparable with (9). If $G(t)$ is present and $H(t)$ missing the reasoning in identical obtaining:

$$k(t) \approx \frac{2[h(t) - g(t) - lG(t)]}{l^2 g'(t)} = k_G(t) \quad (16)$$

It can be noticed that the formulas (8) (15) (16) are not identical; for a greater precision we must use the (9) type formulas; because of the data structure and presentation we can build an optimal control problem to exactly determine $k(t)$ [1]: Determine the k control that minimizes the functional $I(k)$

$$I(k) = \int_0^T \left[\left(\frac{\partial w}{\partial x}(0,t) - G(t) \right)^2 + \left(\frac{\partial w}{\partial x}(l,t) - H(t) \right)^2 \right] dt \rightarrow \min \quad (17)$$

With the restrictions (1) (2) (3) if minimum is zero then w is the solution satisfying (1) (2) (3).

B. The case of cylindrical coordinates (coaxial cylinders with radius $r_1 < r_2$) or the circular crown domain; it is studied considering the equation and conditions [3] [8] for Couette type movements or with gravity and pressure difference trough $F(r,t)$

$$k(t) \frac{\partial w}{\partial t} = \frac{1}{r} \frac{\partial}{\partial r} \left(r \frac{\partial w}{\partial r} \right) + F(r,t), w = w(r,t), r_1 < r < r_2 \quad (18)$$

$$w(r,t=0) = f(r) \quad (19)$$

$$w(r_1,t) = g_1(t), w(r_2,t) = g_2(t) \quad (20)$$

$$\left. \frac{\partial w}{\partial r} \right|_{r=r_1} = G_1(t), \left. \frac{\partial w}{\partial r} \right|_{r=r_2} = G_2(t) \quad (21)$$

Using the same rationale we get $k(t)$: we apply the trapeze formula after we integrate with respect to r (18).

$$rk(t) \frac{\partial w}{\partial t} = \frac{\partial}{\partial r} \left(r \frac{\partial w}{\partial r} \right); k(t) \int_{r_1}^{r_2} \rho \frac{\partial w}{\partial t}(\rho, t) d\rho = r_2 G_2 - r_1 G_1 \quad (22)$$

$$k(t) \frac{r_2 - r_1}{2} \left[r_1 \frac{\partial w}{\partial t}(r_1, t) + r_2 \frac{\partial w}{\partial t}(r_2, t) \right] \approx r_2 G_2(t) - r_1 G_1(t) \quad \text{meaning}$$

$$k(t) \approx \frac{2}{r_2 - r_1} \frac{r_2 G_2(t) - r_1 G_1(t)}{r_1 g_1'(t) + r_2 g_2'(t)} \quad (23)$$

For a greater precision we split the interval $[r_1, r_2]$ in n parts with $r_i = i \frac{r_2 - r_1}{n}$ and the integral from (22) we apply the trapeze formula, obtaining a type (9) formula

$$k(t) \approx \frac{2n}{r_2 - r_1} \frac{r_2 G_2(t) - r_1 G_1(t)}{r_1 g_1'(t) + r_2 g_2'(t) + 2 \sum_{i=1}^{n-1} r_i g_i'(t)} \quad (23')$$

If in (18) appears $F(r,t)$ then in formulas (23)(23')(25) U is added the upper side of the fraction $r_2 G_2 - r_1 G_1 + U(r,t)$ where $U(r,t) = \int_{r_1}^{r_2} r F(r,t) dr$ and $G_2(t) = \frac{1}{R} \int_0^R r F(r,t) dr$. It can be noticed that in (23)(23') we have the validity condition for the experimental case so that $r_2 G_2(t) \neq r_1 G_1(t)$.

If we have the circular cylinder of radius R , $r_1 = 0, r_2 = R$ and $G_1(t)$ is missing, we integrate (18) and apply the trapeze formula on the interval $[0,R]$ obtaining $k(t)$:

$$k(t) \int_0^R r \frac{\partial w}{\partial t}(r,t) dr = r \left. \frac{\partial w}{\partial r} \right|_{r=0}^{r=R} = R G_2(t)$$

$$k(t) \approx \frac{2}{R} \frac{G_2(t)}{g_1(t)} \quad (24)$$

Since the approximation is wide, we split $[0,R]$ in n parts with $r_i = i \frac{R}{n}$ obtaining with data $w(r_i,t) = g_i(t)$

$$k(t) \approx \frac{G_2(t)}{\frac{R}{2n} \left[2 \sum_{i=1}^{n-1} r_i g_i'(t) + R g_R'(t) \right]} \quad (25)$$

In an analog manner we can formulate the optimal control problem for the determination of $k(t)$: Determine the control $k(t)$ which minimize the functional $I[k]$ [1]:

$$I(k) = \int_0^T \left[\left(\frac{\partial w}{\partial r}(r_1, t) - G_1(t) \right)^2 + \left(\frac{\partial w}{\partial r}(r_2, t) - G_2(t) \right)^2 \right] dt \rightarrow \min$$

with the restriction (18) (19) (20). The method can be applied numerical and experimental in biology, thermal processes, drying, melting, diffusion etc. with practical data observable on measure machines, determining this way the coefficient $k(t)$.

2. THE STUDY OF POTENTIAL PLANE FLOWS WITH STREAM LINES FOR INCOMPRESSIBLE FLUIDS IN THE PRESENCE OF SYMMETRICAL CURVILINEAR PROFILES

We consider the potential plane flows, with free lines, for incompressible fluids in the presence of symmetrical profiles in two cases: first case – curvilinear obstacle in free unlimited stream (based on Helmholtz schema) [9] and the second case – fluid streams, upstream delimited by the height h , forked by a symmetrical obstacle, the stream lines at infinity having the asymptotic angle γ (the Rethi-Jacob model) [2].

The obstacles have the same length L and in each situation we'll have three sub-cases: 1st case – curvilinear obstacle convex toward downstream, 2nd case – straight perpendicular plate and 3rd case – curvilinear obstacle convex toward upstream (fig. I1, I2, I3) [6] and for the second situation we have the same obstacles in the presence of the limit stream with γ , asymptotic angle (fig. II1, II2, II3).

The studies we made [4], [5] considered the as helping canonical domain – the half plane $\zeta = \xi + i\eta, \eta \geq 0$ and the Jukovski function $\omega(\zeta) = t + i\theta = \ln \frac{V^0}{V} + i\theta, V < V^0$ where V^0 is the fluid speed on the free lines, V is the speed modulus $|w| = V, \bar{w} = u - iv = \frac{df}{dz}$, $\theta = \arg w, \bar{w} = V^0 e^{-i\theta}$. We'll consider the physical domain D_z, D_f the potential domain, D_ω the hodographic domain and D_ζ the canonical domain, where:

$$f(z) = \varphi(x, y) + i\psi(x, y), \quad \bar{w} = \frac{df}{dz} = V e^{-i\theta} \quad (26)$$

the complex potential were determined $f = f(\zeta)$ for the two situations $f_I(\zeta) = A\zeta, f_{II}(\zeta) = \frac{q}{2\pi} \ln(\zeta - a) + \frac{iq}{2}$ where A, a are the parameters $a > 1$ and q is the stream debit of width h . We determine $\omega = \omega(\zeta)$ and so $W = W(\zeta)$; in this manner, from

$\frac{df}{dz} = \frac{df}{d\zeta} \frac{d\zeta}{dz}$ we get $z = z(\zeta)$ and the correspondent D_z, D_f, D_ω, D_w with D_ζ conformal transformations, and through transitivity $f=f(z), w=w(z)$.

$$\omega(\zeta) = \frac{\sqrt{1-\zeta}}{\pi} \int_{-1}^1 \frac{\theta(s)}{\sqrt{1-s}} \frac{ds}{s-\zeta}, \quad \omega(\zeta) = \frac{\sqrt{\zeta+1}}{i\pi} \int_{-1}^1 \frac{t(s)}{\sqrt{s+1}} \frac{ds}{s-\zeta}$$

The singular integral equations resulted from determining $\omega(\zeta)$ which links dual $\theta(\xi)$ with $t(\xi)$, $\xi \in (-1,1)$ are, for the two situations the followings [4] [5] [6] (obtained with Sohotski – Plemelj formula)

$$t(\xi) = \frac{\sqrt{1-\xi}}{\pi} \int_{-1}^1 \frac{\theta(s)}{\sqrt{1-s}} \frac{ds}{s-\xi}, \quad \theta(\xi) = -\frac{\sqrt{\xi+1}}{\pi} \int_{-1}^1 \frac{t(s)}{\sqrt{s+1}} \frac{ds}{s-\xi} \tag{27}$$

For the 1st situation the upstream asymptotic angle is $\gamma \equiv 0$ and for the 2nd situation:

$$\gamma(a) = \frac{\sqrt{a+1}}{\pi} \int_{-1}^1 \frac{t(s)}{\sqrt{s+1}} \frac{ds}{a-s}; \quad k = \frac{L}{h} = \frac{1}{\pi} \int_{-1}^1 \frac{V^0}{V(\xi)} \frac{d\xi}{a-\xi} = \frac{1}{\pi} \int_{-1}^1 \frac{e^{t(\xi)}}{a-\xi} d\xi \tag{28}$$

where k is the connection report from which we find the values for a parameter, knowing k and the speed distribution on the profile $V = V(\xi)$ or $t = t(\xi), \xi \in (-1,1)$.

The formulas (27) allow solving reverse problems, with $t(\xi)$ or $\theta(\xi)$ given on the profile, the profile shape is determined, for cases (26), (28), $V = V(\xi)$ will be given and $\theta(\xi)$ determined, and for (27) of the plate $\theta = \pi/2$ is determined $V = V(\xi), t = t(\xi)$.

The aero dynamical and geometric parameters for the presented 6 cases are represented in the tables below [4] [5] [6].

Cases I1, I2, I3 based on Helmholtz schema [6]:

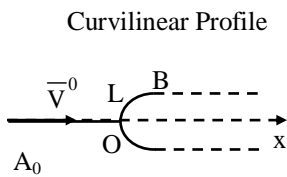


Fig. I1

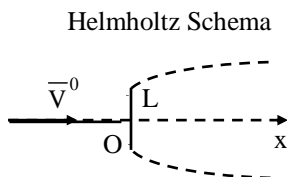


Fig. I2

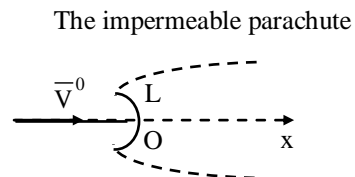


Fig. I3

Parameters in $f = f(\zeta)$ will be:

$$f(\zeta) = A\zeta, A = \frac{LV^0}{4}$$

$$f(\zeta) = A\zeta, A = \frac{2LV^0}{\pi + 4}$$

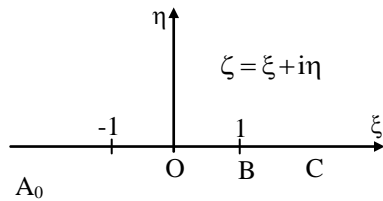
$$f(\zeta) = A\zeta, A = \frac{LV^0}{4e}$$

The speed distribution on the profile:

$$V_1 = V^0 \sqrt{\frac{1+\xi}{2}}; \quad V_2 = V^0 \left(\frac{\sqrt{2}-\sqrt{1-\xi}}{\sqrt{2}+\sqrt{1-\xi}} \right)^{1/2} \approx \frac{V_0}{2} \sqrt{\frac{1+\xi}{2}}; \quad V_3 = \frac{V^0}{e} \sqrt{\frac{1+\xi}{2}}.$$

The curvilinear obstacle's tangent angle:

$$\theta_1 = \frac{\pi}{2} - T \left[\sqrt{\frac{1+\xi}{2}} \right] < \frac{\pi}{2}; \quad \theta_2 = \frac{\pi}{2}; \quad \theta_3 = \frac{\pi}{2} + \frac{1}{\pi} \ln \frac{\sqrt{2}+\sqrt{1+\xi}}{\sqrt{2}-\sqrt{1-\xi}} - T \left[\sqrt{\frac{1+\xi}{2}} \right] > \frac{\pi}{2}.$$



Pressures resultant:

$$P_1 = \frac{\rho V^0{}^2 L}{\pi}; \quad P_2 = \frac{\rho V_0^2 L}{2} \frac{2\pi}{\pi+4}; \quad P_3 = \frac{\rho V^0{}^2 L}{2} J[t] \quad \text{with} \quad J[t] = \frac{\left(\int_{-1}^1 \frac{t(s)}{\sqrt{1+s}} ds \right)^2}{\int_{-1}^1 e^{t(s)} ds}.$$

The distribution V_3 was obtained by extending $J[t]$ with the Jensen inequality for

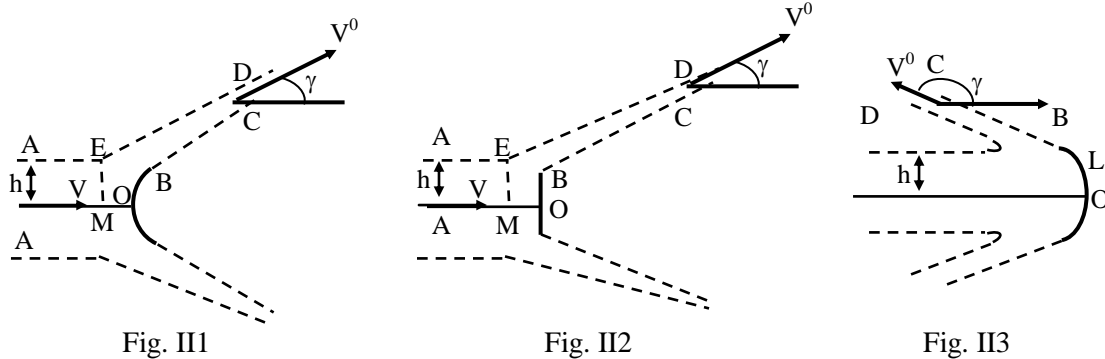
$$t_3 = 1 + \ln \sqrt{\frac{2}{1+\xi}} \quad [5].$$

The resistance coefficient:

$$C_x^1 = \frac{2}{\pi} \cong 0,637; \quad C_x^2 = \frac{2\pi}{\pi+4} \cong 0,87980; \quad C_x^3 = \frac{8}{\pi e} \cong 0,936797;$$

$$C_x = \frac{2P}{\rho V^0 L}, C_x^1 < C_x^2 < C_x^3 (\text{maximal}).$$

Cases II1, II2, II3 limited stream of width h , forked by obstacle:



$$V_1 = V^0 \sqrt{\frac{1+\xi}{2}}; \quad V_2 = V^0 \left(\frac{\sqrt{2}-\sqrt{1-\xi}}{\sqrt{2}+\sqrt{1-\xi}} \right)^{1/2} \approx \frac{V_0}{2} \sqrt{\frac{1+\xi}{2}}; \quad V_3 = \frac{V^0}{e} \sqrt{\frac{1+\xi}{2}}; \quad V_1 < V_2 < V_3.$$

The value of angle θ on the profile:

$$\theta_{1h} = \frac{\pi}{2} - T \left[\sqrt{\frac{1+\xi}{2}} \right] < \frac{\pi}{2}; \quad \theta_{2h} = \frac{\pi}{2}; \quad \theta_{3h} = \frac{\pi}{2} + \frac{1}{\pi} \ln \frac{\sqrt{2} + \sqrt{1+\xi}}{\sqrt{2} - \sqrt{1-\xi}} - T \left[\sqrt{\frac{1+\xi}{2}} \right] > \frac{\pi}{2};$$

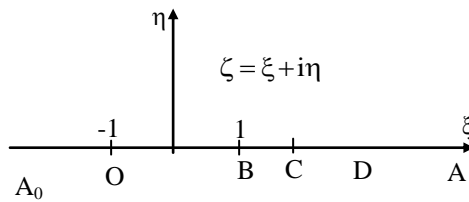
$$T[u] = \frac{1}{\pi} \int_0^u \ln \frac{1+u}{1-u} \frac{du}{u}, \quad u \in [0,1], \quad \frac{\partial T}{\partial u} > 0.$$

The asymptotic angle $\gamma(h)$ downstream:

$$\gamma_{1h}(a) = T \left[\sqrt{\frac{2}{a+1}} \right]; \quad \gamma_{2h}(a) = \arctg \sqrt{\frac{2}{a-1}}; \quad \gamma_{3h}(a) = T \left[\sqrt{\frac{2}{a+1}} \right] + \frac{1}{2} \ln \frac{\sqrt{a+1} + \sqrt{2}}{\sqrt{a+1} - \sqrt{2}}.$$

$\gamma_h(a)$ is descendant with respect to h and ascendant for $\theta(\xi)$ [6] [7].

$$\gamma_{1h} < \gamma_{2h} < \gamma_{3h} = \gamma_{\max}; \quad 0 < \gamma_1 < \frac{\pi}{4}; \quad 0 < \gamma_2 < \frac{\pi}{2}; \quad 0 < \gamma_3 < \pi.$$



With $\lim_{h \rightarrow \infty, a \rightarrow \infty} \gamma(h(a)) = 0$ we get case I from II.

If the reports $k = \frac{L}{h}$ are given is found and then a^* :

$$k_1^{(u)} = \frac{1}{\pi} u \ln \frac{u+1}{u-1}; \quad k_2^{(u)} = 1 - \sqrt{1-u^2} + \frac{1}{\pi} u \ln \frac{u+1}{u-1}; \quad k_3^{(u)} = \frac{e}{\pi} u \ln \frac{u+1}{u-1}.$$

$$k = \frac{L}{h} \Rightarrow k_1 < k_2 < k_3 \quad \text{with} \quad u^* = \sqrt{\frac{2}{a+1}} < 1. \quad \text{Given} \quad k \Rightarrow u = u^* \Rightarrow a = a^*.$$

$$C_x^1(h) = \frac{2[1 - \cos \gamma_1(h(a^*))]}{k_1}; \quad C_x^2(h) = \frac{2[1 - \cos \gamma_2(h(a^*))]}{k_2}; \quad C_x^3(h) = \frac{2[1 - \cos \gamma_3(h(a^*))]}{k_3};$$

$$C_x^1(h) < C_x^2(h) < C_x^3(h).$$

For k and L fixed we get: $\gamma_1(h) < \gamma_2(h) < \gamma_3(h)$. We can notice that $C_x(h)$ is ascendant with respect to $\gamma(h)$, $\frac{\partial C_x(h)}{\partial \gamma(h)} > 0$, meaning $C_x(h)$ is ascendant in h and, if $h \rightarrow \infty$, $\frac{\partial C_x(h)}{\partial \gamma(h)} > 0$ then

$$\lim_{h \rightarrow \infty} C_x(h) = C_x.$$

$$C_x^1(h) \xrightarrow{h \rightarrow \infty} C_x^1 = \frac{2}{\pi}; \quad C_x^2(h) \xrightarrow{h \rightarrow \infty} \frac{2\pi}{\pi + 4}; \quad C_x^3(h) \xrightarrow{h \rightarrow \infty} \frac{8}{\pi e}.$$

As a result we obtain a way to go from 2nd case, trough flow's width enlargement $u \rightarrow \infty, h \rightarrow \infty$, to the 1st situation – obstacle in unlimited fluid (Helmholtz version) [7] [6].

We represent $C_x(h)$ with the help of the asymptotic angle γ : $\gamma = \gamma(u) \Rightarrow u = f^{-1}(\gamma)$.

$$\gamma_1(h) = T(u) = f_1(u); \quad \gamma_2(h) = \arctg \frac{u}{\sqrt{1-u}} = f_2(u); \quad \gamma_3(h) = T(u) + \frac{1}{2} \ln \frac{1+u}{1-u} = f_3(u);$$

$$u = f_1^{-1}(\gamma_1); \quad u = f_2^{-1}(\gamma_2) \quad u = f_3^{-1}(\gamma_3)$$

$$C_x^1(h) = \frac{2[1 - \cos f_1(u)]}{k_1(u)}; \quad C_x^2(h) = \frac{2[1 - \cos f_2(u)]}{k_2(u)}; \quad C_x^3(h) = \frac{2[1 - \cos f_3(u)]}{k_3(u)}.$$

$$C_x^1(h) = C_x^1(\gamma_1); \quad C_x^2(h) = C_x^2(\gamma_2) = \frac{2}{1 + \frac{2}{\pi} \text{ctg} \frac{\gamma}{2} \ln \text{tg} \left(\frac{\gamma}{2} + \frac{\pi}{4} \right)} \quad C_x^3(h) = C_x^3(\gamma_3).$$

We've got the general case $C_x(h) = C_x(\gamma)$ including the C. Iacob formula for $C_x^2(h) = C_x(h) = C_x^2(\gamma)$.

Analyzing the values of $C_x(h), C_x(k)$ for the plate, obtained by C. Iacob [2], S. Popp [9], and the tables of $C_x(h)$ for the curvilinear obstacle $C_x h(\gamma)$ [4], in the last situation II3 there is a case where $L=1$ when $\gamma \rightarrow \pi$; in this case $\gamma(a^*) = \pi \Rightarrow a^* = 1,005; k^* = 6,412$ and $h^* = 1/k^* = 0,156$. We get the following conclusions regarding the movement behavior and validity conditions for $C_x(h)$ with respect to C_x (unlimited stream), the optimal deflector for maximal resistance [4].

If :

- a) $0 < h < h^* \Rightarrow C_x^h = 2h(1 - \cos \gamma_3)$;
- b) $k \rightarrow k^* \cong 6,412 \Rightarrow C_x^h \rightarrow C_x^{h^*} = 4h^* \cong 0,623; \gamma \rightarrow \pi (h \rightarrow h^*)$;
- c) $h > h^*$ and $h \rightarrow \infty \Rightarrow C_x(h) \uparrow C_x^3 = \frac{8}{\pi e} \cong 0,936$; in this case $h > 0,156L$.

Table 1

K	2.245	3	4	5	6.142k ₀	7
γ	1.571	1.1871	2.251	2.623	3.142	3.359
a*	1.494	1.219	1.074	1.024	1.005	1.002
C _x	0.891	0.864	0.814	0.747	0.624	0.565

Table 2

K	$\frac{\pi}{6}$	$\frac{\pi}{4}$	$\frac{\pi}{3}$	$\frac{\pi}{2}$	$\frac{2\pi}{3}$	$\frac{3\pi}{4}$	$\frac{5\pi}{6}$	$\frac{11\pi}{12}$	π
γ	0.287	0.623	1.088	2.245	3.584	4.282	4.989	5.700	6.412
a*	11.747	5.217	2.974	1.494	1.116	1.054	1.024	1.011	1.005
C _x	0.933	0.928	0.919	0.891	0.837	0.797	0.748	0.690	0.624

REFERENCES

- [1] V. Barbu, *Metode matematice în optimizarea sistemelor diferențiale*, Editura Academiei, București, 1989;
- [2] C. Iacob, *Introduction mathématique a la mécanique des fluides*, Editions Gautier Villars, Paris, 1959;
- [3] D. Ionescu, *Introducere în mecanica fluidelor*, Editura Tehnică, București, 2004;
- [4] M. Lupu and E. Scheiber, *Analytical method for airfoils optimization in the case of nonlinear problems in jet aerodynamics*, In: Mathematical Reports, Romanian Academy, no. 1, p. 33-43, 2001;
- [5] M. Lupu and E. Scheiber, *Exact solution for an optimal impermeable parachute problem*, In: Journal of Computational and Applied Mathematics, Elsevier, vol. 147, p. 277-286, 2002;
- [6] M. Lupu and F. Isaia, *Utilizarea problemelor la limită inverse la optimizarea operatorilor neliniari în hidroaerodinamică*, In Bulletin of the Transilvania University of Brașov, p. 133-142, 2003;
- [7] M. Lupu, Gh. Radu, Șt. Nedelcu and M. Boșcoianu, *New Methods of Optimization Shape for Maximal Drag or Lift Force Airfoils*, Review of the Air Force Academy, The Scientific Informative Review, No. 2(17), pp. 55-62, 2010;
- [8] T. Oroveanu, *Mecanica fluidelor vâscoase*, Editura Academiei, București, 1967;
- [9] S. Popp, *Mathematical models in cavity flow theory*, Editura Tehnică, București, 1985.

APPLICATION OF THE CHAUVENET CRITERION TO DETECTION OF THE ABERRANT DATA OBTAINED IN THE INDUSTRIAL PROCESSES

Ioan MILOSAN

Transilvania University, Brasov, Romania (milosan@unitbv.ro)

DOI: 10.19062/2247-3173.2017.19.1.47

Abstract: *In scientific research, there are cases of experimental errors that can cause problems in interpreting the results. Different statistical criteria are used to identify and correct these errors. In this paper, experimental hardness results of a heat treated Cr-Cu cast iron, are analyzed using the Chauvenet criterion.*

Keywords: *Chauvenet criterion, aberrant data, cast iron, heat treatment, hardness*

1. INTRODUCTION

Statistical verification of experimental data in any area of research is one of the researchers' priorities.

Experimental data to be used in mathematical modulation may also contain abnormal results (errors, disparate results, aberrant results, etc.) that, if not identified and removed, can lead to mathematical models that do not correspond to reality and That is, different tests for the validation of experimental data, tests that fall within the field of statistical processing of experimental data, are used.

One of the most criterion for the validation of experimental data is the Chauvenet criterion. The Chauvet abnormal outcomes criterion is based on the consideration that any value whose probability of occurrence is less than a limit value that depends on the "n" number of results, should be eliminated [1, 2, 4, 5, 7, 8].

This paper presents the main steps in the correct application of the detection of abnormal results and their removal from the experimental data base.

2. APPLICATION OF THE CHAUVENET CRITERION

Application of the Chauvenet criterion to detection and eliminating aberrant results obtained in the industrial processes, is carried out with the help of the statistical processing of the research results, as follows [1, 5, 8]:

- (1) Data grouping is performed and extreme values are determined: the minimum (x_{\min}) and maximum (x_{\max}) of data experimental values;
- (2) Arithmetic average is calculated [2]:

$$\bar{x} = \frac{1}{n}(x_1 + x_2 + \dots + x_n) = \frac{1}{n} \sum_{i=1}^n x_i \quad (1)$$

(3) Dispersion is calculated [2]:

$$s^2 = \frac{1}{n-1} [(x_1 - \bar{x})^2 + \dots + (x_n - \bar{x})^2] = \frac{1}{n-1} \sum_{i=1}^n (x_i - \bar{x})^2 \quad (2)$$

(4) Standard deviation is calculated [2]:

$$s = \sqrt{\frac{1}{n-1} \sum_{i=1}^n (x_i - \bar{x})^2} \quad (3)$$

(5) Standard deviation from the mean for all suspected outliers is calculated [2]:

$$\tau_{sus} = \frac{|x_{sus} - \bar{x}|}{s} \quad (4)$$

(6) Choosing the critical value of the Chauvenet criterion (τ_{crit}), according to the coefficient of statistical confidence level (α) and the number of determinations (n);

(7) Comparing the number of standard deviation of Chauvenet criterion for the suspect outliers (τ_{sus}), with the critical value (τ_{crit}) of the Chauvenet criterion.

where:

n = number of experimental data;

\bar{x} = arithmetic average of the experimental data;

x_{sus} = the suspected date to be abnormal (outlier) from the experimental determinations;

s^2 = the dispersion of the experimental data;

s = the standard deviation of the experimental data;

τ_{sus} = the number of standard deviation from the mean for all suspected outliers;

τ_{crit} = the critical value (limit value) of the Chauvenet criterion, that depends on the "n" number of results [3];

α = the confidence coefficient; $\alpha = 0.95$ [7];

After comparing the two values, there may be two Chauvenet criterion specific situations:

(a) If $\tau_{sus} > \tau_{crit}$, the values of the x_{sus} is affected by aberrant errors, that value is eliminated from the sample (x_{sus} is an outlier);

In this care, we recalculate the values of the average (\bar{x}) and standard deviation (s) for the remained values and we start again with verifying the (a) condition, the algorithm is applied until that condition is no longer verified for any of the two external values of the sample (x_{min} or x_{max}).

b) If $\tau_{sus} < \tau_{crit}$, the values of the x_{sus} it is a noticeable value for the experimental data set.

3. MATERIALS AND RESULTS

3.1. Materials

The material on which experimental research has been performed has the following chemical composition: 3.61 %C; 2.22 %Si; 0.44 %Mn; 0.012%P; 0.003 %S; 0.06 %Mg; 0.42 %Cr and 0.21 %Cu.

The specific parameters of the heat treatment applied were:

- the austenizing temperature, $t_A = 900$ [°C];
- the maintained time at austenizing temperature, $\tau_A = 60$ [min];
- the temperature at isothermal level, $t_{iz} = 300$ [°C] for lot A and 400[°C] for lot B;

- the maintained time at the isothermal level, $\tau_{iz} = 60$ [min], corresponding to the first stage for obtaining bainitic structure.

Isothermal maintenance was carried out in a salt bath (55% KNO_3 +45% $NaNO_3$), subsequent cooling was done in the air.

From this material, 2 typical test specimens for hardness (HB) (100x10x10mm) were done: 1 for lot A and 1 for lot B.

3.2. Results

In table 1 are presented the mechanical results.

Table 1. Mechanical results of hardness [HB] values

Lot	t_A [°C]	τ_A [min]	t_{iz} [°C]	τ_{iz} [min]	Hardness [HB] (parallel determinations)
A	900	60	300	60	404; 426; 415; 398; 363; 390; 420;415;
B			400		331; 323; 302; 331; 315; 375; 315; 302;

It is noted that it is the structure that determines the values of the mechanical properties, specific to each thermal treatment parameter [3, 6]:

- specific to lot A ($t_{iz} = 300$ °C), is the structure consisting of inferior bainite, residual austenite and martensite, constituents that determine higher values of hardness (HB);

- specific to lot B ($t_{iz} = 400$ °C), is the structure consisting of superior bainite, and residual austenite, constituents that determine low values of hardness (HB);

- together with increasing the level of the isothermal maintenance temperature inside the structure will appear the superior bainite and the martensite will disappear (lot B).

4. APPLICATION OF THE CHAUVENET CRITERION TO DETECTION OF THE ABERRANT DATA

Experimental data of hardness (HB) with sixth parallel determinations of each experimental lots (A and B), presented in table 1, are checked using Chauvenet criterion [1, 2, 4, 5, 7, 8]. Chauvenet criterion for data sets are presented in table 2.

Table 2. Chauvenet criterion for data sets

Lot	Parallel determination [HB]	n	X	\bar{x}	s^2	s	τ_{sus}	τ_{crit}	Values remains Yes/No
A	404; 426; 415; 398; 363; 390; 420; 415;	8	$x_{max}=426$	403.875	413.554	20.336	1.088	1.863	Yes
			$x_{min}=363$				2.010		No
	404; 426; 415; 398; 390; 420; 426	7	$x_{max}=426$	409.714	164.238	12.816	1.271	1.803	Yes
			$x_{min}=390$				1.538		Yes
B	331; 323; 302; 331; 315; 375; 315; 302;	8	$x_{max}=375$	324.250	547.071	23.389	2.169	1.863	No
			$x_{min}=302$				0.951		Yes
	331; 323; 302; 331; 315; 315; 302;	7	$x_{max}=331$	317.000	147.667	12.152	1.152	1.863	Yes
			$x_{min}=302$				1.234		Yes

Comparing the τ_{sus} with the critical value τ_{crit} and analyzing the results for the Chauvenet criterion, two situations can occur:

(a) If $\tau_{\text{sus}} < \tau_{\text{crit}}$, the values of the x_{sus} it is a noticeable value for the experimental data set and in table 2 it is noted with "Yes";

(b) If $\tau_{\text{sus}} > \tau_{\text{crit}}$, the values of the x_{sus} is affected by aberrant errors, in table 2 it is noted with "No" and that value is eliminated from the sample (x_{sus} is an outlier);

In this case, we recalculate the values of the average (\bar{x}) and standard deviation (s) for the remained values and we start again with verifying the (a) condition, the algorithm is applied until that condition is no longer verified for any of the two external values of the sample (x_{min} or x_{max}).

A general remark comes from studying the data presented in table 2: with "YES", note the values that are experimental results accepted by the criterion and with "NO" note the that that are rejected by the criterion:

- the value of $x_{\text{min}} = 363$, from the lot A with 8 number of the parallel determinations, $\tau_{\text{sus}} = 2.010$, $\tau_{\text{crit}} = 1.863$ so $\tau_{\text{sus}} > \tau_{\text{crit}}$. In this care $x_{\text{min}} = 363$ is an outlier, so we recalculate the values of

the average (\bar{x}) and standard deviation (s) for the 7 remained values. Criterion Chauvenet was recalculated, and all values were found to be noticeable values for the experimental data.

- the value of $x_{\text{max}} = 375$, from the lot B with 8 number of the parallel determinations, $\tau_{\text{sus}} = 2.169$, $\tau_{\text{crit}} = 1.863$ so $\tau_{\text{sus}} > \tau_{\text{crit}}$. In this care $x_{\text{max}} = 375$ is an outlier, so we recalculate the values

of the average (\bar{x}) and standard deviation (s) for the 7 remained values. Criterion Chauvenet was recalculated, and all values were found to be noticeable values for the experimental data.

CONCLUSIONS

(a) It is the structure that determines the values of the mechanical properties, specific to each thermal treatment parameter;

(b) Application of the Chauvenet criterion to detection and eliminating aberrant results obtained in the industrial processes, is carried out with the help of the statistical processing;

(c) After identifying and removing abnormal values, the Chauvenet criterion is again applied until abnormal values are no longer found;

(d) With Chauvenet's criterion you can be sure that your experimental research are free of aberrant data.

REFERENCES

- [1] L. Lin and P.D. Sherman, *Cleaning Data the Chauvenet Way*, SESUS proceedings, Paper SA11, pp. 1-11, Available at <http://analytics.ncsu.edu/sesug/2007/SA11.pdf>, accessed on 24 April 2017;
- [2] M. R. Costescu, *Identifying Data Affected by Aberrant Errors. Applied Program*, Economic Informatics, vol. 12, no. 1, pp. 52 - 22, 2008;
- [3] M. Mărușteri, *Biostatistică, 2005*, Available at http://sorana.academicdirect.ro/pages/doc/Doc2012/_materiale/Biostatistica_curs.pdf, accessed on 24 April 2017;
- [4] *** STATISTICS HOW TO, *Chauvenet's Criterion*, Practically Cheating Statistics Handbook, Available at <http://www.statisticshowto.com/chauvenets-criterion/>, accessed on 20 April 2017;
- [5] N. M. Halfina, *Applications of the Chauvenet Test to Detection of Overliers in Observations Connected into a Homogeneous Markov Chain*, Journal of Mathematical Sciences, vol. 118, no. 6, pp. 5667–5672, 2003, Available at <http://link.springer.com/article/10.1023/A:1026159026782>, accessed on 20 April 2017;
- [6] S. Sabade and D. M. H. Walker, *Evaluation of statistical outlier rejection methods for IDDQ limit setting*, Conference Paper, pp. 1-7, 2002, ResearchGate, Available at https://www.researchgate.net/profile/Sagar_Sabade/publication/3943191_Evaluation_of_statistical_outlier_rejection_methods_for_IDDQ_limit_setting/links/5408775f0cf23d9765b2dab8/Evaluation-of-statistical-outlier-rejection-methods-for-IDDQ-limit-setting.pdf, accessed on 20 April 2017;
- [7] R.A. Harding, *The production, properties and automotive applications of austempered ductile iron*. Kovove Materialy, vol. 45, pp.1-16, 2007;
- [8] A. Rimmer, *ADI solutions aid vehicle design*, The Foundry Trade Journal, vol. 2, pp. 54-56, 2004.

REGARDING A CONTINUOUSLY DIFFERENTIABLE FRICTION MODEL USED FOR CONTROL OF DYNAMIC SYSTEMS DESIGN

Bogdan CIORUȚA

Faculty of Engineering, North University Centre at Baia Mare, Technical University of Cluj-Napoca, Romania (bciorutza@yahoo.com)

DOI: 10.19062/2247-3173.2017.19.1.49

Abstract: This paper analyzes several models that have been useful to characterize friction in motion control systems, where for high-performance of different engineering systems, model-based controllers are required to accommodate for the system nonlinearities. Unfortunately, according to the dynamical systems theory, developing accurate models for friction has been historically challenging, because typical models were either discontinuous or only piecewise continuous. Motivated by the fact that discontinuous and piecewise continuous friction models are problematic for the development of high-performance continuous controllers, a new model for friction is considered and analysed in this paper. This simple continuously differentiable friction model represents a foundation that captures the major effects existed in the friction modeling area of applied mathematics and physics.

Keywords: motion control systems, friction, dynamic models, optimal control systems.

1. INTRODUCTION

The dynamical systems theory [1] provide us many dynamical systems (physical, chemical, economical, ecological etc) [2] that can be modeled by different mathematical relations. In this context, we relate to stochastic differential and/or difference equations [3]. As their name suggest, these mathematical systems change with time or any other independent parameters according to the dynamical relations.

In this case, a mathematical model (as presented in **Fig. 1a**) is a precise representation of a system's dynamics used to answer questions via numerical analysis and computers simulation, describing, at the same time, the input/output behavior of systems [13].

The input given to the system corresponding to this best situation is called "optimal" control [4]. For high-performance engineering systems, model-based controllers are typically required to accommodate for the system nonlinearities [14].

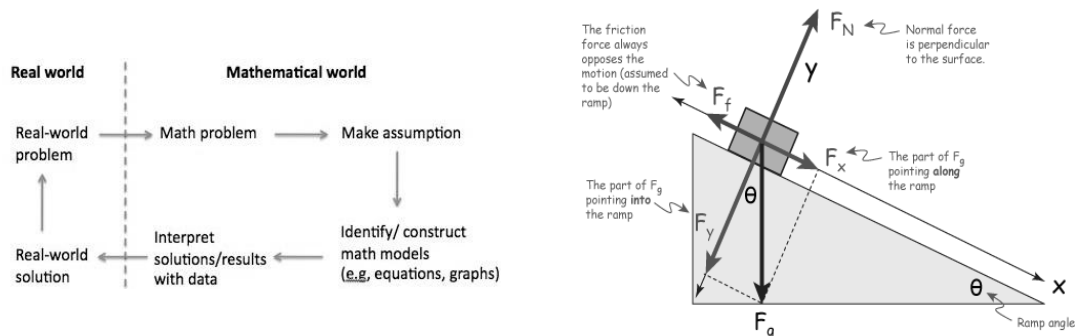


FIG. 1. a) Mathematical models as a bridge between real and mathematical world; b) The description of the friction behavior (source: math4teaching.com/mathematical-modeling/ / www.dracruz.com/friction.html)

Unfortunately, developing accurate models for friction is difficult. Typical models are either discontinuous and many other models are only piecewise continuous [12]. Friction is generally described as the resistance to motion [9], when two surfaces slide against each other. On the other hand friction can also cause undesirable effects. For high precision mechanical motion systems for example, friction can deteriorate the performance of the system, so the possible unwanted consequences caused by friction appear to be: *tracking errors, limit cycling and hunting* [7]. In motion control a possible way to minimize the influences of friction is to compensate for it (**Fig. 1b**).

2. FRICTION MODELS: PROPERTIES AND CLASSIFICATION

Motivated by the desire to develop an accurate representation of friction in systems, various control researchers have developed different analytical models. In general, the dominant friction components that have been modeled include: *static friction* (the torque that opposes the motion at zero velocity), *Coulomb friction* (the constant motion opposing torque at non-zero velocity), *viscous friction* (when full fluid lubrication exists between the contact surfaces), *asymmetries* (different friction behavior for different directions of motion), *Stribeck effect* (at very low speed, when partial fluid lubrication exists, contact between the surfaces decreases and thus friction decreases exponentially from stiction), *position dependence* (oscillatory behavior of the friction torque due to small imperfections on the motor shaft and reductor centres, as well as ball bearings elastic deformation).

For situations where the starting friction is higher than friction at a nonzero velocity "static" friction force (F_s) can be distinguished as in **Fig. 2a-c**. For the most common situations the friction decreases with increasing velocity for a certain velocity regime. This is called the Stribeck effect and is shown in **Fig. 2d**.

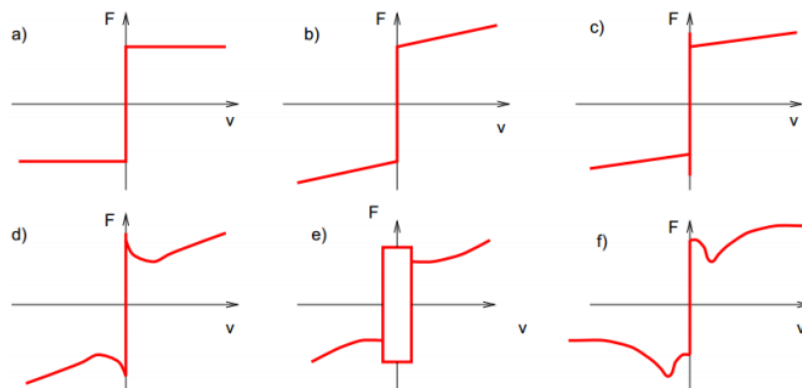


FIG. 2. The representation of the basic static friction force effects [9]: a) Coulomb; b) Coulomb + viscous; c) Coulomb + viscous + stiction; d) Stribeck effect; e) Karnopp; f) Hess and Soom Armstrong.

These basic models describe a static relationship between the friction force and velocity. At rest where the velocity is zero, the friction force cannot be described as a function of velocity alone. For practical high accurate positioning systems however other frictional properties have to be considered for a satisfying model.

The models described so far are all empirical-based models. An other branch of friction models is the so called *physics-motivated friction models*. These describe friction on three different physical levels namely on *atomic-molecular* [6], *asperity-scale* [10] and at *tectonic-plate level* [15,16].

Although the physics-based models are capable of capturing all friction-induced phenomena that are observed so far, they are much too complicated for online control purposes, or for the optimal control.

3. THE ANALYSIS OF THE DYNAMIC SYSTEMS DESIGN USING A CONTINUOUSLY DIFFERENTIABLE FRICTION MODEL

The scientific literature that we consulted provide us a few options available for characterizing the friction models, such as:

- *adaptive compensation* with differential filter & fuzzy controller (full-states & position measurements);
- characterization of the limit cycles caused by friction (*stick-slip*, "*jump*" motion);
- identification and stability analysis of friction using *Lyapunov's method*;
- modeling and simulation of the dynamic behavior of systems with friction, using *continuously differentiable model* (6 terms parameterizable form with tanh).
- optimal control and friction estimation using LQR (linear quadratic regulator), PID (proportional-integral-derivative), SVM (support vector machine) and AAD (adaptive anti-disturbance);

Starting from the last one and according to the general Euler-Lagrange dynamic system, which is following the nonlinear dynamic model characteristics, we can considered - in accordance with [12] - that the friction behavior could be model by a friction term $f(q')$ that is assumed to have the following non-linear parameterizable form:

$$f(q') = \gamma_1(\tanh(\gamma_2 q') - \tanh(\gamma_3 q')) + \gamma_4(\tanh(\gamma_5 q')) + \gamma_6 q' \quad (1)$$

where γ_i denote unknown positive constants.

The above friction model (1) has the following properties (as resulted from **Fig. 3**):

- is symmetric about the origin and the static coefficient of friction can be approximated by $\gamma_1 + \gamma_4$;
- the term $\tanh(\gamma_2 q') - \tanh(\gamma_3 q')$ captures the Stribeck effect where the friction coefficient decreases from the static coefficient of friction with increasing slip velocity near the origin;
- the Coulombic friction coefficient is present in the absence of viscous dissipation and is modelled by the term $\gamma_4(\tanh(\gamma_5 q'))$, and a viscous dissipation term is given by $\gamma_6 q'$.

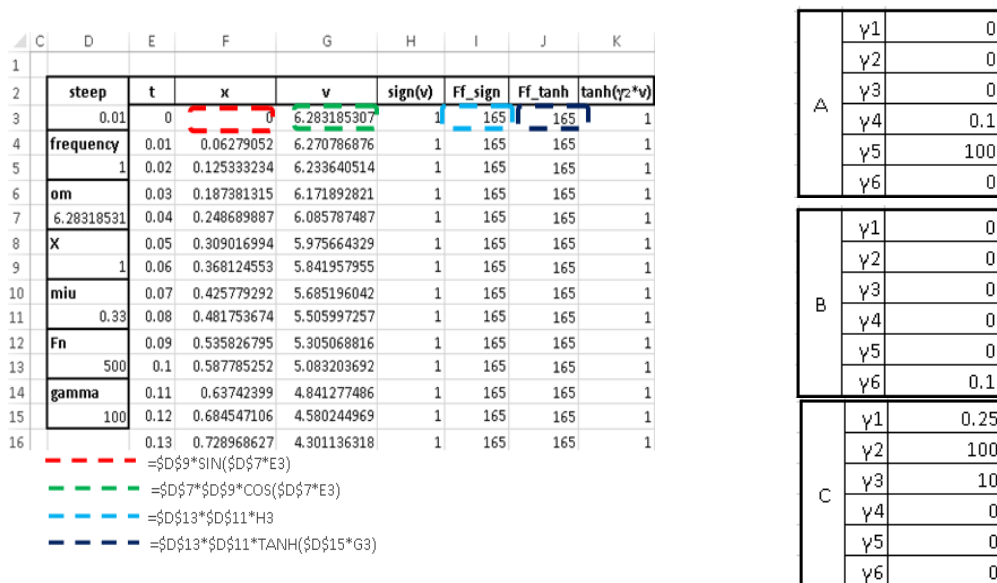


FIG. 3. The representation of the non-linear parameterizable friction model construction

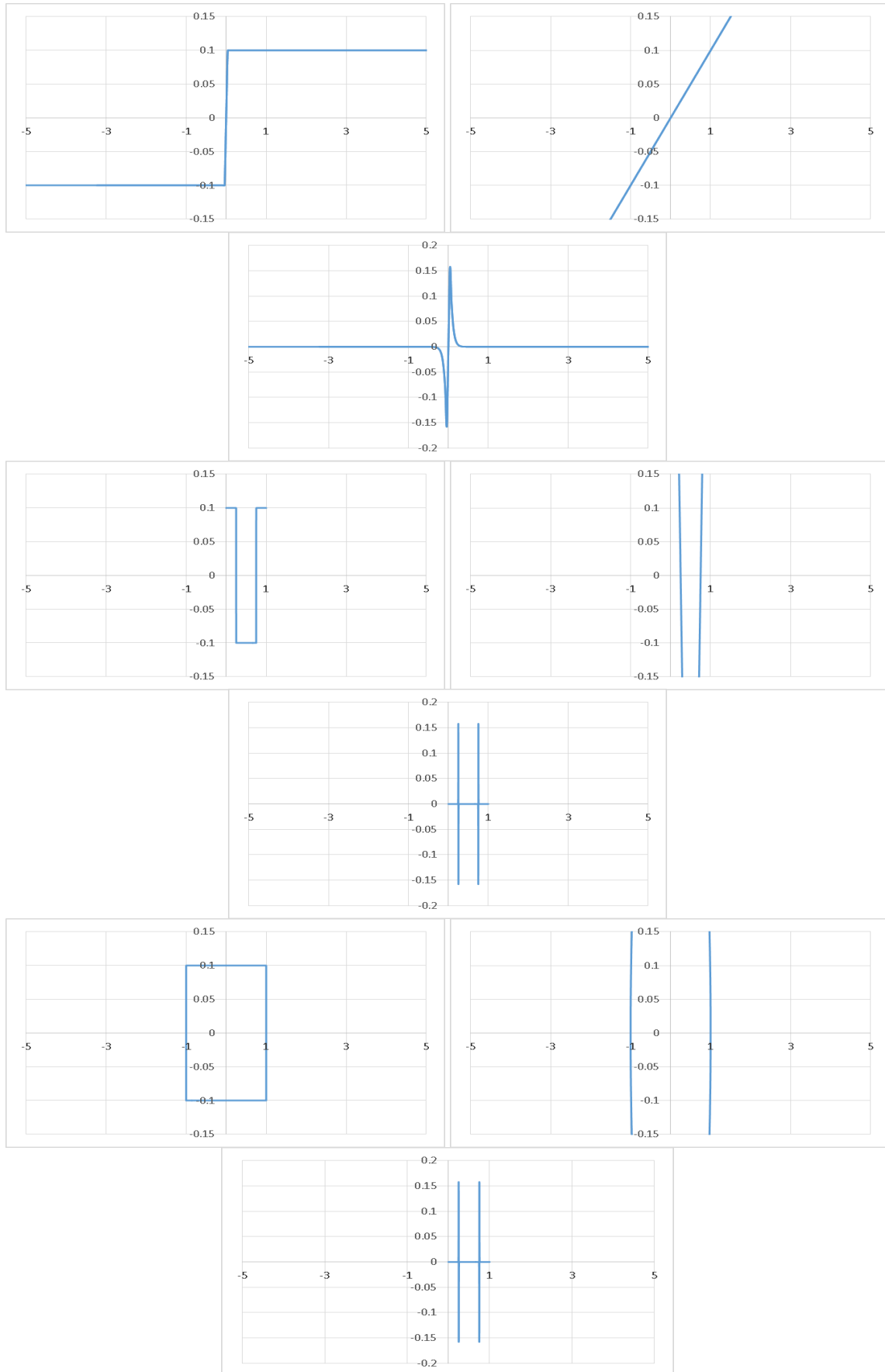


FIG. 4. The representation of $F_r(A,B,C)$ vs. speed (v) / time (t) / displacement (x) - case no. 1: steep (0.001), frequency (1), displacement - x (1)

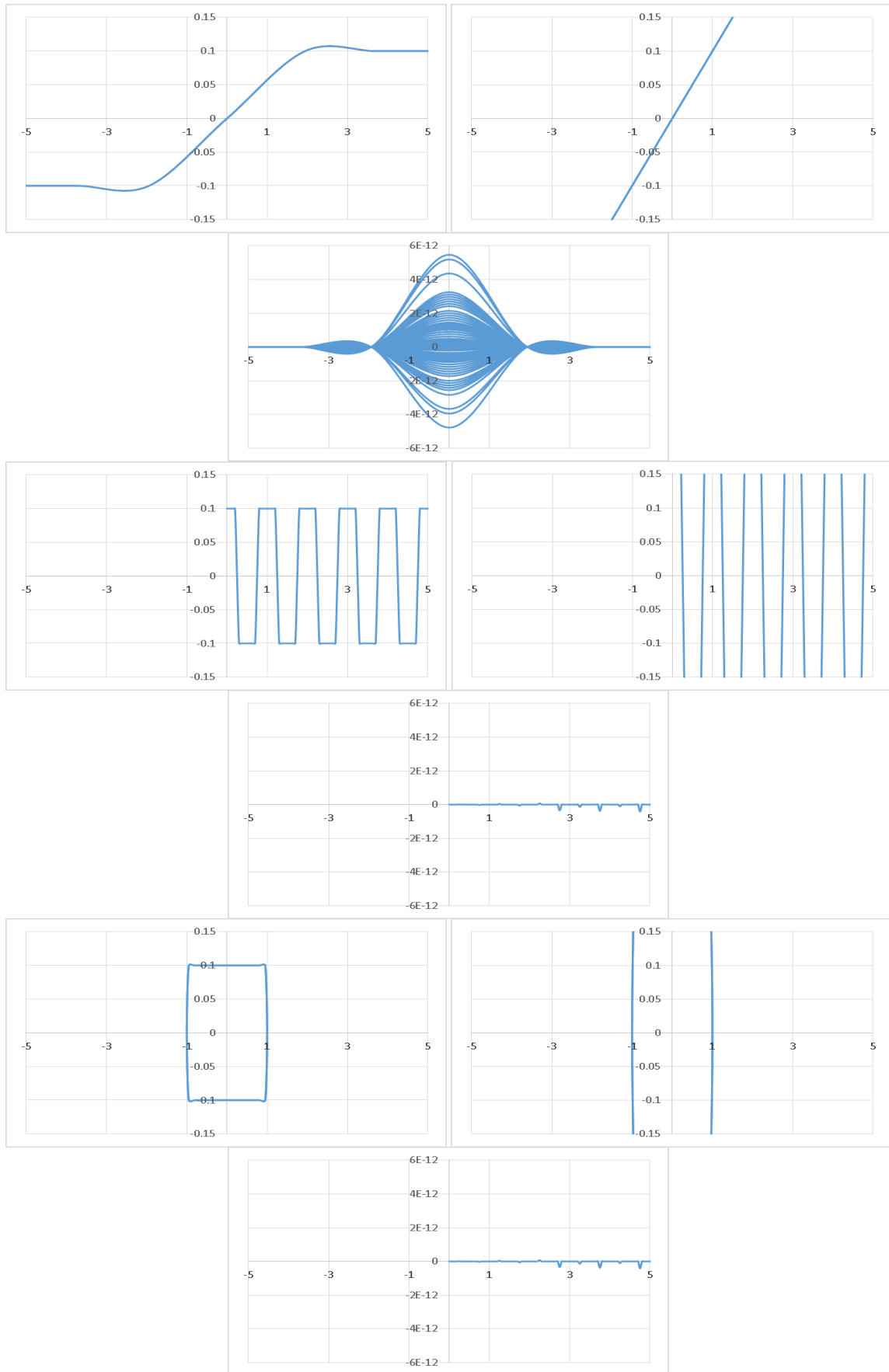


FIG. 5. The representation of $F_r(A,B,C)$ vs. speed (v) / time (t) / displacement (x) - case no. 2: steep (0.05), frequency (1), displacement – x (1)

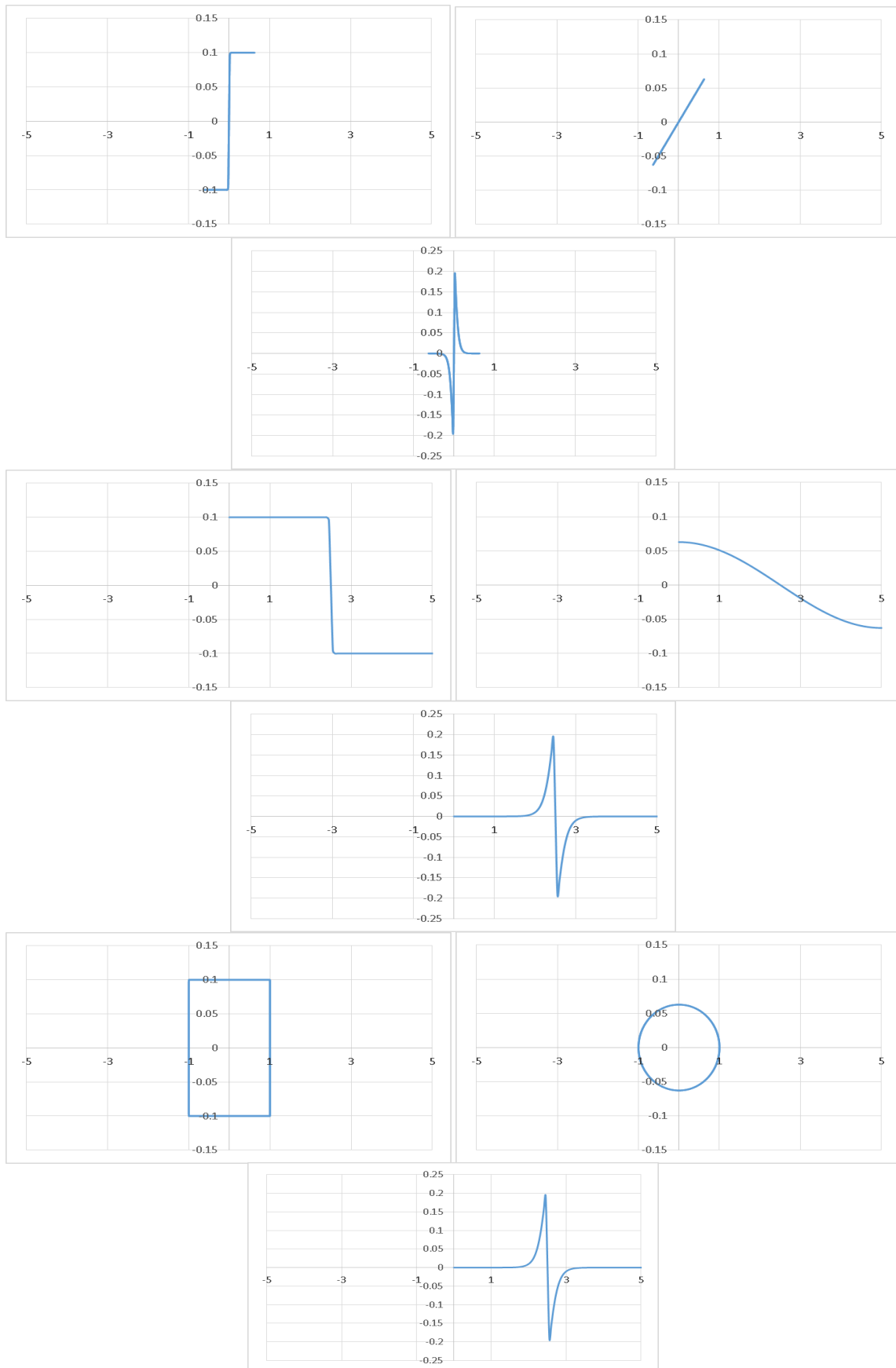


FIG. 6. The representation of $F_r(A,B,C)$ vs. speed (v) / time (t) / displacement (x) - case no. 2*: **steep (0.05), frequency (0.1), displacement – x (1)**

CONCLUSIONS

The friction phenomenon is not considered in system modeling and controller design; however, it has many damaging effects on operation of systems and controllers. Hence, a friction compensation is needed. It is possible to steer these systems from one state to another state by the application of some type of external inputs or controls. If there are different ways of doing the same task, then there may be one way of doing it in the "best" way. This best way can be minimum time to go from one state to another state, or maximum thrust developed by a rocket engine.

The input given to the system corresponding to this best situation is called "optimal" control. For high-performance engineering systems, model-based controllers are typically required to accommodate for the system nonlinearities.

In the present paper we focus on the representation of the non-linear parameterizable friction model construction, so we present the friction force $F_f(A,B,C)$ vs. speed (v) / time (t) / displacement (x) and 3 cases as follow:

- case no. 1: steep (0.001), frequency (1), displacement – x (1);
- case no. 2: steep (0.05), frequency (1), displacement – x (1);
- case no. 2*: steep (0.05), frequency (0.1), displacement – x (1).

with some notable results under computational representation.

REFERENCES

- [1]. *** https://en.wikipedia.org/wiki/Dynamical_systems_theory;
- [2]. *** https://en.wikipedia.org/wiki/Dynamical_system;
- [3]. *** https://en.wikipedia.org/wiki/Differential_equation;
- [4]. *** https://en.wikipedia.org/wiki/Optimal_control;
- [5]. *** <https://en.wikipedia.org/wiki/Friction>;
- [6]. Braun O.M., Kivshar Y.S., *Nonlinear dynamics of the frenkel-kontorova model*, *Physics Report*, 306(1): 1–108, 1998;
- [7]. Canudas C., Olsson H., Astrom K., Lischinsky P., *New model for control of systems with friction*, *IEEE Transactions on Automatic Control*, 40(3): 419–425, 1995 www.control.lth.se/.../1995/can+95.pdf;
- [8]. Farid A., *Fundamentals of friction modeling*, American Society for Precision Engineering, 2010 aspe.net/publications/spring_2010/spr10ab/1010albender.pdf;
- [9]. Geffen V., *A study of friction models and friction compensation*, Technische Universiteit Eindhoven, Eindhoven, 2009 www.mate.tue.nl/11194.pdf;
- [10]. Haessig D., Friedland B., *On the modeling and simulation of friction*, *Journal of Dynamic Systems, Measurement and Control, Transactions of the ASME*, 113(3): 354–362, 1991;
- [11]. Iwata K., Osakada K., Terasaka Y., *Process Modelling of Orthogonal Cutting by the Rigid Plastic Finite Element Method*, *J. Engng. Ind., Trans. ASME*, Vol. 106, pp. 132-138, 1984;
- [12]. Makkar, C., Dixon, W. E., Sawyer, W. G., Hu G., *A New Continuously Differentiable Friction Model for Control Systems Design*, *Proceedings of the International Conference on Advanced Intelligent Mechatronics*, 24-28 July 2005, Monterey, California nersp.osg.ufl.edu/~wsawyer/AIM2005.PDF;
- [13]. Murray, R., *Analysis and Design of Feedback Systems*, *Computing and Mathematical Sciences (CMS) Department, California Institute of Technology*, pg. 31-60, 2012 www.cds.caltech.edu/~murray.pdf;
- [14]. Naidu, D.S., *Optimal control systems*, *Electrical engineering textbook series, CRC PRESS LLC*, 2003 dl.offdownload.ir/optimal_control_systems.pdf;

- [15]. Swevers J., Al-Bender F., Ganseman.G., Prajogo T., *An integrated friction model structure with improved presliding behavior for accurate friction compensation*, IEEE Transactions on Automatic Control, 45(4): 675–686, 2000;
- [16]. Swevers J., Al-Bender F., Lampaert V., *A novel generic model at asperity level for dry friction force dynamics*, Tribology Letters, 16(1-2): 81–94, 2004.